TABLE OF CONTENTS

Section	Page	
1.0 SUMMARY	1	1/C1
2.0 INTRODUCTION	3	1/C3
3.0 TEST APPARATUS AND PROCEDURES	5	1/C5
3.1 FACILITIES	5	1/C5
3.1.1 General Electric Jet Engine Noise Outdoor Test Stand (JENOTS) Description	6	1/C6
3.1.1.1 **Acoustic Arena**	6	1/C6
3.1.1.2 Coannular-Flow System	6	1/C6
3.1.1.3 Coannular Frame Section	10	1/C12
3.1.1.4 Plenum Instrumentation Section	10	1/C12
3.1.1.5 Facility Acoustic Validation	12	1/C14
3.1.2 FluiDyne Aerodynamic-Performance Test Facility Description	12	1/C14
3.2 JENOTS INSTRUMENTATION SYSTEMS	16	1/D5
3.2.1 Acoustic Instrumentation Systems	16	1/D5
3.2.2 Laser Velocimeter System	18	1/D8
3.2.2.1 General Arrangement	18	1/D8
3.2.2.2 LV Actuator and Seeding	21	1/D13
3.2.2.3 Signal Processing and Recording	21	1/D13
3.3 DATA REDUCTION METHODS	21	1/D13
3.3.1 Acoustic Data Reduction	22	1/D14
3.3.1.1 JENOTS Data Reduction Systems	22	1/D14
3.3.1.2 Air-Attenuation Corrections	22	1/D14
3.3.1.3 Data-Scaling Procedure	30	1/E12
3.3.1.4 Data Corrections to a Free-Field Environment	30	1/E12
3.3.1.5 Power Level Calculation	30	1/E12
3.3.1.6 Acoustic Measurement Errors, Electronic Noise Floor	30	1/E12
3.3.2 Laser Velocimeter Data Reduction	33	1/F3
3.3.2.1 Basic Idea for LV rms Measurements	33	1/F3
3.3.2.2 The Histogram	36	1/F6
3.3.2.3 Mean Velocity	36	1/F6
3.3.2.4 Turbulent Velocity	37	1/F7
3.3.2.5 Statistical Errors for LV Mean and Turbulent Velocity Measurements	37	1/F7

TABLE OF CONTENTS (continued)

Section Page

3.3.3 Aerodynamic-Performance Test Data Reduction 37 1/F7
3.3.3.1 Flow Rates 39 1/F9
3.3.3.2 Discharge Coefficients 39 1/F9
3.3.3.3 Nozzle Throat 39 1/F9
3.3.3.4 Thrust Coefficient 40 1/F10
3.3.3.5 FluiDyne Force Balance Calibration 40 1/F10
3.3.3.6 Pressure and Temperature Data 41 1/F11
3.3.3.7 Data Quality 41 1/F11

4.0 MODEL DESCRIPTION AND DEFINITION OF TEST MATRICES 44 1/F14

4.1 MODEL DESIGN - SYSTEM EVOLUTION 44 1/F14
4.2 DESCRIPTION OF TEST MODELS 48 1/G6
4.3 ACOUSTIC TEST MATRIX 52 1/G12
4.4 LASER VELOCIMETER TEST MATRIX 56 2/A7
4.5 AERODYNAMIC-PERFORMANCE TEST MATRIX 61 2/B1
4.6 DATA SECTION 61 2/B1

5.0 DISCUSSION OF ACOUSTIC TEST RESULTS 63 2/B3

5.1 ESTABLISHMENT OF GROUND RULES FOR ACOUSTIC COMPARISONS AND DATA ILLUSTRATIONS 63 2/B3

5.1.1 Synthesized Baseline 63 2/B3
5.1.2 Average Conical Nozzle Noise Baseline 64 2/B4
5.1.3 Density Normalization and Presentation of Results 64 2/B4
5.1.3.1 Density Normalization Factors 64 2/B4
5.1.3.2 Presentation of Results 70 2/B13

5.2 UNSUPPRESSED COANNULAR NOZZLES 71 2/B14

5.2.1 High Core-Flow Test Results 71 2/B14
5.2.1.1 Overall Power Level Test Results 71 2/B14
5.2.1.2 Power Spectra Test Results 71 2/B14
5.2.1.3 Perceived Noise Level Test Results 71 2/B14
5.2.1.4 Perceived Noise Level Directivity Test Results 75 2/C6
5.2.1.5 Sound Pressure Level Spectra Test Results 75 2/C6
5.2.2 Low Core-Flow Test Results 75 2/C6
5.2.3 Acoustic Correlations 84 2/D5
5.2.4 Summary Remarks 84 2/D5

5.3 MULTIELEMENT FAN-SUPPRESSOR NOZZLES 88 2/D11

5.3.1 High Core Flow Test Results 88 2/D11
5.3.1.1 Overall Power Level Test Results 88 2/D11
5.3.1.2 Power Spectra Test Results 97 2/E11

TABLE OF CONTENTS (continued)

Section Page

5.3.1.3 Perceived Noise Level Test Results 97 2/E11
5.3.1.4 Sound Pressure Level Spectra Test Results 98 2/E12
5.3.2 Low Core-Flow Test Results 98 2/E12
5.3.3 Comparisons with Unsuppressed Coannular Nozzles 98 2/E12
5.3.4 Summary Remarks 104 2/F9

5.4 MULTIELEMENT FAN-SUPPRESSOR NOZZLES WITH EJECTORS 104 2/F9

5.4.1 Hardwall Ejector Effects 107 2/F12
5.4.1.1 Overall Power Level Test Results 107 2/F12
5.4.1.2 Power Spectra Test Results 107 2/F12
5.4.1.3 Perceived Noise Level Test Results 107 2/F12
5.4.1.4 Sound Pressure Level Test Results 111 2/G2
5.4.2 Treated Ejector Effects 111 2/G2
5.4.2.1 Overall Power Level Test Results 111 2/G2
5.4.2.2 Power Spectra Test Results 115 2/G6
5.4.2.3 Perceived Noise Level Test Results 115 2/G6
5.4.2.4 Sound Pressure Level Test Results 120 2/G11
5.4.3 Inlet Lip Geometry Effects on the Hardwall Ejector 120 2/G11
5.4.3.1 Power Level Test Results 120 2/G11
5.4.3.2 Perceived Noise Level Test Results 124 3/A8
5.4.3.3 Sound Pressure Level Test Results 124 3/A8
5.4.4 Summary Remarks 124 3/A8

5.5 EVALUATION OF A PARTIAL MECHANICAL SHIELD 130 3/B1

5.5.1 Perceived Noise Level Test Results 130 3/B1
5.5.2 Sound Pressure Level Spectra Results 134 3/B6
5.5.3 Summary Remarks 134 3/B6

6.0 DISCUSSION OF AERODYNAMIC-PERFORMANCE TEST RESULTS 140 3/C1

6.1 THRUST COEFFICIENTS 140 3/C1

6.1.1 Unsuppressed Coannular Nozzle with Plug 140 3/C1
6.1.2 Multichute Fan-Suppressor Nozzle 143 3/C5
6.1.3 Multichute Fan-Suppressor Nozzle with Hardwall Ejector with Sharp Lip 143 3/C5
6.1.4 Multitube Fan-Suppressor Nozzle 150 3/C12
6.1.5 Multitube Fan-Suppressor Nozzle with Hardwall Ejector with Sharp Lip 150 3/C12

6.2 EFFECT OF HOT EXHAUST FLOW ON THE THRUST COEFFICIENT OF THE MULTITUBE FAN-SUPPRESSOR NOZZLE WITH HARDWALL EJECTOR WITH SHARP LIP 156 3/D7

TABLE OF CONTENTS (continued)

Section Page

6.3 FLOW COEFFICIENTS 161 3/D14

6.3.1 Unsuppressed Coannular Nozzle with Plug 161 3/D14
6.3.2 Multichute Fan-Suppressor Nozzle 165 3/E6
6.3.3 Multichute Fan-Suppressor Nozzle with Hardwall Ejector with Sharp Lip 165 3/E6
6.3.4 Multitube Fan-Suppressor Nozzle 169 3/E10
6.3.5 Multitube Fan-Suppressor Nozzle with Hardwall Ejector with Sharp Lip 169 3/E10

7.0 DISCUSSION OF LASER VELOCIMETER TEST RESULTS 173 3/E14

7.1 LASER VELOCIMETER PLUME MEASUREMENTS FOR THE UNSUPPRESSED COANNULAR NOZZLE WITH PLUG 173 3/E14

7.1.1 Axial Mean-Velocity Distributions 173 3/E14
7.1.2 Mean-Velocity, Radial-Profile Distributions 176 3/F5
7.1.3 Axial Turbulent-Velocity, Radial-Profile Distributions 176 3/F5

7.2 LASER VELOCIMETER PLUME MEASUREMENTS FOR THE FAN-SUPPRESSED NOZZLES 176 3/F5

7.2.1 Axial Mean-Velocity Distributions 176 3/F5
7.2.2 Mean- and Turbulent-Velocity, Radial-Profile Distributions 180 3/F12
7.2.2.1 Multichute Fan Suppressor 180 3/F12
7.2.2.2 Multitube Fan Suppressor 180 3/F12

7.3 SUMMARY OF OBSERVATIONS 180 3/F12

8.0 DISCUSSION OF ACOUSTIC/AERODYNAMIC-PERFORMANCE CORRELATIONS 186 3/G8

8.1 EVALUATION OF NOISE CANDIDATES FOR DUCT-BURNING TURBOFAN ENGINES 186 3/G8
8.2 LOW CORE-FLOW COMPARISONS 191 4/A6

9.0 CONCLUSIONS AND RECOMMENDATIONS 196 4/A12

9.1 CONCLUSIONS 196 4/A12
9.2 RECOMMENDATIONS 197 4/A13

TABLE OF CONTENTS (concluded)

Section	Page	
APPENDIX A - GENERAL ELECTRIC AIR-ATTENUATION MODEL	199	4/B1
APPENDIX B - POWER LEVEL CALCULATION PROCEDURE	210	4/C1
APPENDIX C - DETAILED DESCRIPTION OF TEST MODELS	214	4/C5
APPENDIX D - ACOUSTIC TEST MATRIX FOR ALL DBTF MODELS AND EXAMPLE DATA PRINT OUT SHEETS	221	4/D3
APPENDIX E - FAN PLUG PRESSURE DISTRIBUTIONS FOR AERODYNAMIC MODEL 5	240	4/F13
APPENDIX F - MODEL 7 AXIAL-VELOCITY PROFILES	249	5/A8
APPENDIX G - MODEL 7 AXIAL-VELOCITY PROFILES WITH NO CORE FLOW	270	5/D7
APPENDIX H - MODEL 7 AXIAL-VELOCITY PROFILES WITH NO FAN FLOW	286	5/F10
APPENDIX I - MODEL 1 AXIAL-VELOCITY PROFILES	295	5/G13
APPENDIX J - MODEL 2 AXIAL-VELOCITY PROFILES	303	6/B5
APPENDIX K - NOMENCLATURE	313	6/C11
REFERENCES	317	6/D1

AUG 1 4 1978

NASA Contractor Report 2966

COMPLETED
ORIGINAL

Acoustic Tests of Duct-Burning Turbofan Jet Noise Simulation

P. R. Knott, E. J. Stringas, J. F. Brausch,
P. S. Staid, P. H. Heck, and D. Latham

CONTRACT NAS3-18008
JULY 1978

NASA

349

NASA Contractor Report 2966

Acoustic Tests of Duct-Burning Turbofan Jet Noise Simulation

P. R. Knott, E. J. Stringas, J. F. Brausch,
P. S. Staid, P. H. Heck, and D. Latham
General Electric Company
Cincinnati, Ohio

Prepared for
Lewis Research Center
under Contract NAS3-18008

NASA
National Aeronautics
and Space Administration

Scientific and Technical
Information Office

1978

Blank

Page

LIST OF ILLUSTRATIONS

Figure		Page
1.	Schematic of Jet Engine Noise Outdoor Test Stand (JENOTS) Facility Acoustic Arena.	7
2.	Jet Engine Noise Outdoor Test Stand (JENOTS), Acoustic Arena.	8
3.	High Temperature Coannular Plenum Chamber.	9
4.	Coannular Frame and Instrumentation Sections.	11
5.	Example of Acoustic Facility Noise Validation Test Series; Core Flow at High Temperature Using Coannular Design.	13
6.	FluiDyne Channel 11 Aerodynamic Performance Facility Layout.	14
7.	FluiDyne Force Balance Station Notations for Aerodynamic Model Tests.	15
8.	JENOTS Acoustic Data Acquisition System.	17
9.	Laser Velocimeter Optics Package.	19
10.	Laser Velocimeter Set Up at General Electric's JENOTS Facility.	20
11.	Acoustic Data Reduction System.	23
12.	Comparison of Alternate Air-Attenuation Models.	25
13.	Comparison of Alternate Air-Attenuation Factors.	26
14.	PWL Spectra Comparison Between DBTF Data Utilizing GE Correction Factors and Extrapolated SAE Correction Factors.	27
15.	SPL Spectra Comparison Between DBTF Data Utilizing GE Correction Factors and Extrapolated SAE Correction Factors.	28
16.	PNL Vs. Angle Comparison Between DBTF Data Utilizing GE Correction Factors and Extrapolated SAE Correction Factors.	29

LIST OF ILLUSTRATIONS (Continued)

Figure		Page
17.	Scale-Model and Full-Scale Data Reduction Operations.	31
18.	Typical Electronic Noise Floor Spectra for Electronic System at JENOTS.	34
19.	Schematic of Laser Velocity Measurements.	35
20.	Comparison of Measured and Predicted Thrust and Flow Coefficients for Various ASME Nozzle Setups at FluiDyne Test Facility.	43
21.	Schematic of Engine Propulsion Nozzle System Utilizing Dual-Flow Plug Design.	45
22.	Schematic of Model Propulsion Nozzle System Adapted to Test Facility.	47
23.	Acoustic Test Matrix, Fan and Core Aerodynamic Test Conditions Interrelating V_f, V_c, and V_f/V_c.	54
24.	Acoustic Test Matrix, Fan and Core Aerodynamic Test Conditions Interrelating $(T_T)_{f,c}$; $(P_T/P_o)_{f,c}$; and $V_{f,c}$.	55
25.	Definition of Data Planes for Models 1, 2, and 7.	60
26.	Synthesized Baseline Noise Level Determination.	65
27.	Comparison of Unsuppressed Coannular Nozzle with Plug Noise levels Vs. Synthesized Baseline Noise Levels.	66
28.	Comparison of Various Scaled-Up or Full-Size Conical Nozzle Maximum Perceived Noise Levels.	67
29.	Variation of Density Correction Factor with Ideal Jet Velocity and Temperature.	69
30.	Effect of Fan Jet Velocity on Normalized Overall Sound Power Level of Unsuppressed Coannular Nozzles.	72
31.	One-Third-Octave Sound Power Spectral Characteristics of Unsuppressed Coannular Nozzles.	73
32.	Effect of Fan Jet Velocity on Normalized Maximum Perceived Noise Level on Unsuppressed Coannular Nozzles.	74

LIST OF ILLUSTRATIONS (Continued)

Figure		Page
33.	PNL Directivity Characteristics of Unsuppressed Coannular Nozzles.	76
34.	Unsuppressed Coannular Nozzle SPL Spectra Comparisons at V_f = 1800 ft/sec (548.6 m/sec) and V_c = 1200 ft/sec (365.8 m/sec).	77
35.	Unsuppressed Coannular Nozzle SPL Spectra Comparisons at V_f = 2400 ft/sec (731.5 m/sec) and V_c = 1200 ft/sec (365.8 m/sec).	78
36.	Unsuppressed Coannular Nozzle SPL Spectra Comparisons at V_f = 2800 ft/sec (853.4 m/sec) and V_c = 1400 ft/sec (426.7 m/sec).	79
37.	Effect of Fan Jet Velocity on Unsuppressed Coannular Nozzles During Low Core-Flow Operation.	80
38.	Effect of Core Flow and Fan Velocity on Normalized Perceived Noise Level on the Unsuppresed Coannular Nozzle with Plug (Model 7).	81
39.	Core/Fan Weight-Flow Ratio Effect on Maximum Perceived Noise Level on the Unsuppressed Coannular Nozzle with Plug (Model 7).	82
40.	Effect of Core Flow on PNL Directivity on the Unsuppressed Coannular Nozzle with Plug (Model 7).	83
41.	Effect of Core Flow on Unsuppressed Coannular Nozzle with Plug (Model 7) SPL Spectra.	85
42.	Effect of Fan to Core Velocity Ratio on Normalized Overall Sound Power Level of Unsuppressed Coannular Nozzle without Plug (Model 8).	86
43.	Effect of Fan to Core Velocity Ratio on Normalized Overall Sound Power Level of Unsuppressed Coannular Nozzle with Plug (Model 7).	87
44.	Effect of Fan to Core Velocity Ratio on Normalized Overall Sound Power Level of Multichute Fan Suppressor Nozzle (Model 1).	89

LIST OF ILLUSTRATIONS (Continued)

Figure		Page
45.	Effect of Fan to Core Velocity Ratio on Normalized Overall Sound Power Level of Multitube Fan Suppressor Nozzle (Model 2).	90
46.	Effect of Fan Jet Velocity on Normalized Overall Sound Power Level of Multielement Fan Suppressor Nozzles.	91
47.	One-Third-Octave Sound Power Spectral Characteristics of Multielement Fan Suppressor Nozzles.	92
48.	Effect of Fan Jet Velocity on Normalized Maximum Perceived Noise Level of Multielement Fan Suppressor Nozzles.	93
49.	PNL Directivity Characteristics of Multielement Fan Suppressor Nozzles.	94
50.	Multielement Fan Suppressor Nozzle SPL Spectra Comparisons at V_f = 1800 ft/sec (548.6 m/sec) and V_c = 1200 ft/sec (365.8 m/sec).	95
51.	Multielement Fan Suppressor Nozzle SPL Spectra Comparisons at V_f = 2400 ft/sec (731.5 m/sec) and V_c = 1200 ft/sec (365.8 m/sec).	96
52.	Multielement Fan Suppressor Nozzle SPL Spectra Comparisons at V_f = 2800 ft/sec (853.4 m/sec) and V_c = 1400 ft/sec (426.7 m/sec).	99
53.	Effect of Core Flow and Fan Velocity on Normalized Maximum Perceived Noise Level of the Multitube Fan Suppressor Nozzle (Model 2).	100
54.	Core/Fan Weight-Flow Ratio Effect on Maximum Perceived Noise Level of the Multitube Fan Suppressor Nozzle (Model 2).	101
55.	Effect of Core Flow on PNL Directivity of the Multitube Fan Suppressor Nozzle (Model 2).	102
56.	Comparison of Normalized Maximum Perceived Noise Levels Vs. Fan Jet Velocity for Unsuppressed Coannular Nozzles and Multielement Fan Suppressor Nozzles.	103
57.	PNL Directivity Comparisons Between Unsuppressed Coannular Nozzles and Multielement Fan Suppressor Nozzles.	105

LIST OF ILLUSTRATIONS (Continued)

Figure		Page
58.	SPL Spectra Comparisons Between Unsuppressed Coannular Nozzles and Multielement Fan Suppressor Nozzles.	106
59.	Effect of Hardwall Ejectors on Multielement Fan Suppressor Nozzle Normalized Overall Sound Power Level.	108
60.	Effect of Hardwall Ejectors on Multielement Fan Suppressor Nozzle One-Third-Octave Sound Power Spectra.	109
61.	Effect of Hardwall Ejectors on Multielement Fan Suppressor Nozzle Normalized Maximum Perceived Noise Level.	110
62.	Effect of Hardwall Ejectors on Multielement Fan Suppressor Nozzle PNL Directivity.	112
63.	Effect of Hardwall Ejector on Multitube Fan Suppressor Nozzle SPL Spectra.	113
64.	Effect of Hardwall Ejector on Multichute Fan Suppressor Nozzle SPL Spectra.	114
65.	Comparison of Overall Sound Power Level from Multielement Fan Suppressor Nozzles with Hardwall and Treated Ejectors.	116
66.	Comparison of One-Third Sound Power Spectra from Multielement Fan Suppressor Nozzles with Hardwall and Treated Ejectors.	117
67.	Comparison of Normalized Maximum Perceived Noise Level from Multielement Fan Suppressor Nozzles with Hardwall and Treated Ejectors.	118
68.	Comparison of PNL Directivity from Multielement Fan Suppressor Nozzles with Hardwall and Treated Ejectors.	119
69.	Comparison of SPL Spectra from Multitube Fan Suppres-Nozzle with Hardwall and Treated Ejectors SPL Spectra.	121
70.	Comparison of SPL Spectra from Multichute Fan Suppressor Nozzle with Hardwall and Treated Ejectors.	122
71.	Effect of Ejector Lip Geometry on Multichute Fan Suppressor Nozzles with Hardwall Ejector Normalized Overall Power Level.	123

LIST OF ILLUSTRATIONS (Continued)

Figure		Page
72.	Effect of Ejector Lip Geometry on Multichute Fan Suppressor Nozzles with Hardwall Ejector One-Third-Octave Sound Power Spectra.	125
73.	Effect of Ejector Lip Geometry on Multichute Fan Suppressor Nozzles with Hardwall Ejector Normalized Maximum Perceived Noise Level.	126
74.	Effect of Ejector Lip Geometry on Multichute Fan Suppressor Nozzles with Hardwall Ejector PNL Directivity.	127
75.	Effect of Ejector Lip Geometry on Multichute Fan Suppressor with Hardwall Ejector SPL Spectra on Maximum PNL Noise Angle.	128
76.	Effect of Ejector Lip Geometry on Multichute Fan Suppressor Nozzle with Hardwall Ejector SPL Spectra.	129
77.	Model Scale Spectral Comparisons of Measured Data at Two Microphone Heights for the Multichute Fan Suppressor with a Treated Ejector.	131
78.	Model Scale Spectral Comparisons of Measured Data at Two Microphone Heights for the Multichute Fan Suppressor with a Treated Ejector.	132
79.	Maximum PNL for the Multichute Fan Suppressor with a Partial Shield Compared to the Multichute Fan Suppressor Alone and the Hardwall Ejector.	133
80.	PNL Directivity for the Multichute Fan Suppressor with A Partial Shield Compared to a Hardwall Ejector and the Multichute Fan Suppressor Alone.	135
81.	PNL Directivity for the Multichute Fan Suppressor with a Partial Shield Compared to a Hardwall Ejector and the Multichute Fan Suppressor Alone.	136
82.	Spectral Comparisons of Multichute Fan Suppressor with a Partial Shield in the Sideline and Overhead Positions.	137
83.	Spectral Characteristics of the Multichute Fan Suppressor with a Partial Shield Compared to a Hardwall Ejector and the Multichute Fan Suppressor Alone.	138

LIST OF ILLUSTRATIONS (Continued)

Figure		Page
84.	Spectral Characteristics of the Multichute Fan Suppressor with a Partial Shield Compared to a Hardwall Ejector and the Multichute Fan Suppressor Alone.	139
85.	Thrust Coefficients for the Unsuppressed Coannular Nozzle with Plug (Model 7).	141
86.	Core Plug Pressure Distributions, Unsuppressed Coannular Nozzle with Plug (Model 7).	142
87.	Fan Plug Pressure Distributions, Unsuppressed Coannular Nozzle with Plug (Model 7).	142
88.	Integrated Plug Pressure Forces, Unsuppressed Coannular Nozzle with Plug (Model 7).	144
89.	Thrust Coefficients for the Multichute Fan Suppressor Nozzle (Model 1).	145
90.	Chute Base Pressure Distributions, Multichute Fan Suppressor (Model 1).	146
91.	Chute Average Base Pressure and Base Drag, Multichute Fan Suppressor (Model 1).	146
92.	Thrust Coefficients for the Multichute Fan Suppressor Nozzle with Hardwall Ejector with Sharp Lip (Model 9).	147
93.	Chute Base Pressure Distributions, Multichute Fan Suppressor Nozzle with Hardwall Ejector with Sharp Lip (Model 9).	147
94.	Fan Plug Pressure Distributions, Multichute Fan Suppressor Nozzle (Model 1).	148
95.	Fan Plug Pressure Distributions, Multichute Fan Suppressor Nozzle with Hardwall Ejector with Sharp Lip (Model 9).	148
96.	Core Plug Pressure Distributions, Multichute Fan Suppressor Nozzle (Model 1).	149
97.	Core Plug Pressure Distributions, Multichute Fan Suppressor with Hardwall Ejector with Sharp Lip (Model 9).	149
98.	Ejector Pressure Distributions, Multichute Fan Suppressor Nozzle with Hardwall Ejector with Sharp Lip (Model 9), $(P_T/P_o)_c = 1.3$.	151

LIST OF ILLUSTRATIONS (Continued)

Figure Page

99. Ejector Pressure Distributions, Multichute Fan Suppressor Nozzle with Hardwall Ejector with Sharp Lip (Model 9), $(P_T/P_o)_c = 1.9$. 151

100. Integrated Model Surface Pressure Forces, Multichute Fan Suppressor Nozzle (Model 1) and Multichute Fan Suppressor Nozzle with Hardwall Ejector with Sharp Lip (Model 9). 152

101. Thrust Coefficients for the Multitube Fan Suppressor Nozzle (Model 2). 153

102. Tube Baseplate Pressure Distributions, Multitube Fan Suppressor Nozzle (Model 2). 153

103. Tube Baseplate Average Base Pressure and Base Drag, Multitube Fan Suppressor Nozzle (Model 2). 154

104. Thrust Coefficients for the Multitube Fan Suppressor Nozzle with Hardwall Ejector with Sharp Lip (Aerodynamic Model 5). 155

105. Tube Baseplate Pressure Distributions, Multitube Fan Suppressor Nozzle with Hardwall Ejector with Sharp Lip (Aerodynamic Model 5). 155

106. Ejector Pressure Distributions, Multitube Fan Suppressor Nozzle with Hardwall Ejector with Sharp Lip (Aerodynamic Model 5). 157

107. Integrated Model Surface Pressure Forces, Multitube Fan Suppressor Nozzle (Model 2) and Multitube Fan Suppressor Nozzle with Hardwall Ejector with Sharp Lip (Aerodynamic Model 5). 158

108. Thrust Coefficients for Hot and Cold Flow Tests on the Multitube Fan Suppressor Nozzle with Hardwall Ejector with Sharp Lip (Aerodynamic Model 5). 159

109. Comparison of Hot and Cold Flow Ejector Pressure Distributions, Multitube Fan Suppressor Nozzle with Hardwall Ejector with Sharp Lip (Aerodynamic Model 5). 160

110. Comparison of Hot and Cold Flow Integrated Pressure Forces, Multitube Fan Suppressor Nozzle with Hardwall Ejector with Sharp Lip (Aerodynamic Model 5). 162

LIST OF ILLUSTRATIONS (Continued)

Figure Page

111. Comparison of Hot and Cold Flow Total Integrated Pressure Forces, Multitube Fan Suppressor Nozzle with Hardwall Ejector with Sharp Lip (Aerodynamic Model 5). 163

112. Fan Duct Flow Coefficients for the Unsuppressed Coannular Nozzle with Plug (Model 7). 164

113. Core Duct Flow Coefficients for the Unsuppressed Coannular Nozzle with Plug (Model 7). 166

114. Fan and Core Duct Flow Coefficients for the Multichute Fan Suppressor Nozzle (Model 1). 167

115. Fan and Core Duct Flow Coefficients for the Multichute Fan Suppressor Nozzle with Hardwall Ejector with Sharp Lip (Model 9). 168

116. Fan and Core Duct Flow Coefficients for the Multitube Fan Suppressor Nozzle (Model 2). 170

117. Fan and Core Duct Flow Coefficients for the Multitube Fan Suppressor Nozzle with Hardwall Ejector with Sharp Lip (Aerodynamic Model 5). 171

118. Hot Flow Fan and Core Duct Flow Coefficients for the Multitube Fan Suppressor Nozzle with Hardwall Ejector with Sharp Lip (Aerodynamic Model 5). 172

119. Comparison of Laser Velocimeter Measured Axial Peak Mean Velocity Distributions Between an Unsuppressed Coannular Nozzle with Plug and a Typical Conical Nozzle. 174

120. Comparison of Laser Velocimeter Measured Axial Peak Mean Velocity Distributions for an Unsuppressed Coannular Nozzle with Plug; Fan-Alone Flow and Core-Alone Flow. 175

121. Laser Velocimeter Measured Mean Velocity Radial Profiles at Several Axial Stations for the Unsuppressed Coannular Nozzle with Plug (Model 7). 177

122. Laser Velocimeter Measured Local Turbulence Velocity Radial Profiles at Several Axial Stations for the Unsuppressed Coannular Nozzle with Plug (Model 7). 178

LIST OF ILLUSTRATIONS (Continued)

Figure		Page
123.	Comparison of Laser Velocimeter Measured Axial Peak Mean Velocity Distributions for the Multitube and Tube Fan Suppressor, the Unsuppressed Coannular Nozzle with Plug, and a Typical Conical Nozzle.	179
124.	Laser Velocimeter Measured Mean Velocity Radial Profiles at Several Axial Stations for the Multichute Fan Suppressor Nozzle (Model 1).	181
125.	Laser Velocimeter Measured Local Turbulence Velocity Radial Profiles at Several Axial Stations for the Multichute Fan Suppressor Nozzle (Model 1).	182
126.	Laser Velocimeter Measured Mean Velocity Radial Profiles at Several Axial Stations for the Multitube Fan Suppressor Nozzle (Model 2).	183
127.	Laser Velocimeter Measured Local Turbulence Velocity Radial Profiles at Several Axial Stations for the Multitube Fan Suppressor Nozzle (Model 2).	184
128.	Acoustic Suppression Relative to Synthesized Baseline for Conditions Typical of DBTF Engines at Takeoff.	187
129.	Aerodynamic Performance Summary Relative to Unsuppressed Coannular Nozzle with Plug for Conditions Typical of DBTF Engines at Takeoff.	189
130.	Acoustic/Aerodynamic Performance Relative to Unsuppressed Coannular Nozzle with Plug for Conditions Typical of DBTF Engines at Takeoff.	190
131.	Single-Stream Annular Nozzle Inherent Suppression Correlation.	193
132.	Correlations of PNL Suppression for Potential Unsuppressed/Suppressed Annular Nozzles with Low Core Flow Relative to Synthesized Baseline Data.	195
133.	JENOTS Data: SPL Spectra, FSDR Program Calculation.	200
134.	JENOTS Data: SPL Spectra, FSDR Program Calculation.	201
135.	Revised Atmospheric Correction Factors.	202
136.	Revised Atmospheric Absorption.	203

LIST OF ILLUSTRATIONS (Continued)

Figure		Page
137.	Atmospheric Attenuation Factors.	204
138.	Total Absorption of Sound in Air as a Function of Frequency.	205
139.	Spherical Strip Area Calculation, Definition of Geometry.	212
140.	Multichute Fan Suppressor Nozzle Schematic (For Models 1, 3, 4, 9, and 11).	215
141.	Multitube Fan Suppressor Nozzle Schematic (for Models 2, 5, and 6).	216
142.	Unsuppressed Coannular Nozzle with Plug Schematic (Model 7).	217
143.	Unsuppressed Coannular Nozzle without Plug Schematic (Model 8).	218
144.	Multielement Fan Suppressor Nozzle with Hardwall/Treated Ejector Schematic (Models 4 and 6, Treated Ejectors; Models 3, 5, and 9, Hardwall Ejectors).	219
145.	Multichute Fan Suppressor Nozzle with Partial Mechanical Shield Schematic.	220
146.	Definition of Parameters Utilized in Tables XII through XXII.	222
147.	Comparison of Hot and Cold Flow Fan Plug Pressure Distributions, Multitube Fan Suppressor Nozzle with Hardwall Ejector (Sharp Lip); Aerodynamic Model 5, $P_T/P_o)_f = 2.25$.	241
148.	Comparison of Hot and Cold Flow Plug Pressure Distributions, Multitube Fan Suppressor Nozzle with Hardwall Ejector (Sharp Lip); Aerodynmaic Model 5, $P_T/P_o)_f = 3.2$.	242
149.	Comparison of Hot and Cold Flow Fan Plug Pressure Distributions, Multitube Fan Suppressor Nozzle with Hardwall Ejector (Sharp Lip); Aerodynamic Model, $(P_T/P_o)_f = 4.0$.	243

LIST OF ILLUSTRATIONS (Continued)

Figure | Page

150. Comparison of Hot and Cold Flow Core Plug Pressure Distributions, Multitube Fan Suppressor Nozzle with Hardwall Ejector (Sharp Lip); Aerodynamic Model 5, $(P_T/P_o)_f$ = 2.25. 244

151. Comparison of Hot and Cold Flow Core Plug Pressure Distributions, Multitube Fan Suppressor Nozzle with Hardwall Ejector (Sharp Lip); Aerodynamic Model 5, $(P_T/P_o)_f$ = 3.25. 245

152. Comparison of Hot and Cold Flow Core Plug Pressure Distributions, Multitube Fan Suppressor Nozzle with Hardwall Ejector (Sharp Lip); Aerodynamic Model 5, $(P_T/P_o)_f$ = 4.00. 246

153. Comparison of Hot and Cold Flow Tube Baseplate Pressure Distributions, Multitube Fan Suppressor Nozzle with Hardwall Ejector (Sharp Lip); Aerodynamic Model 5, $(P_T/P_o)_f$ = 2.25 and 3.25. 247

154. Comparison of Hot and Cold Flow Tube Baseplate Pressure Distributions, Multitube Fan Suppressor Nozzle with Hardwall Ejector (Sharp Lip); Aerodynamic Model 5, $(P_T/P_o)_f$ = 4.0. 248

155. Laser Velocimeter Velocity Profile and Turbulence Measurement; Unsuppressed Coannular Nozzle with Plug (Model 7) at X/D_{Ref} = -0.52. 250

156. Laser Velocimeter Velocity Profile and Turbulence Measurement; Unsuppressed Coannular Nozzle with Plug (Model 7) at X/D_{Ref} = -0.167. 251

157. Laser Velocimenter Velocity Profile and Turbulence Measurement; Unsuppressed Coannular Nozzle with Plug (Model 7) at X/D_{Ref} = 0. 252

158. Laser Velocimeter Velocity Profile and Turbulence Measurement; Unsuppressed Coannular Nozzle with Plug (Model 7) at X/D_{Ref} = 0.167. 253

159. Laser Velocimeter Velocity Profile and Turbulence Measurement; Unsuppressed Coannular Nozzle with Plug (Model 7) at X/D_{Ref} = 0.332. 254

LIST OF ILLUSTRATIONS (Continued)

Figure Page

160. Laser Velocimeter Velocity Profile and Turbulence Measurement; Unsuppressed Coannular Nozzle with Plug (Model 7) at $X/D_{Ref} = 0.5$. 255

161. Laser Velocimeter Velocity Profile and Turbulence Measurement; Unsuppressed Coannular Nozzle with Plug (Model 7) at $X/D_{Ref} = 0.67$. 256

162. Laser Velocimeter Velocity Profile and Turbulence Measurement; Unsuppressed Coannular Nozzle with Plug (Model 7) at $X/D_{Ref} = 0.83$. 257

163. Laser Velocimeter Velocity Profile and Turbulence Measurement; Unsuppressed Coannular Nozzle with Plug (Model 7) at $X/D_{Ref} = 1.025$. 258

164. Laser Velocimeter Velocity Profile and Turbulence Measurement; Unsuppressed Coannular Nozzle with Plug (Model 7) at $X/D_{Ref} = 1.35$. 259

165. Laser Velocimeter Velocity Profile and Turbulence Measurement; Unsuppressed Coannular Nozzle with Plug (Model 7) at $X/D_{Ref} = 1.68$. 260

166. Laser Velocimeter Velocity Profile and Turbulence Measurement; Unsuppressed Coannular Nozzle with Plug (Model 7) at $X/D_{Ref} = 2.17$. 261

167. Laser Velocimeter Velocity Profile and Turbulence Measurement; Unsuppressed Coannular Nozzle with Plug (Model 7) at $X/D_{Ref} = 2.34$. 262

168. Laser Velocimeter Velocity Profile and Turbulence Measurement; Unsuppressed Coannular Nozzle with Plug (Model 7) at $X/D_{Ref} = 2.61$. 263

169. Laser Velocimeter Velocity Profile and Turbulence Measurement; Unsuppressed Coannular Nozzle with Plug (Model 7) at $X/D_{Ref} = 3.34$. 264

170. Laser Velocimeter Velocity Profile and Turbulence Measurement; Unsuppressed Coannular Nozzle with Plug (Model 7) at $X/D_{Ref} = 3.67$. 265

171. Laser Velocimeter Velocity Profile and Turbulence Measurement; Unsuppressed Coannular Nozzle with Plug (Model 7) at $X/D_{Ref} = 4.17$. 266

LIST OF ILLUSTRATIONS (Continued)

Figure | Page

172. Laser Velocimeter Velocity Profile and Turbulence Measurement; Unsuppressed Coannular Nozzle with Plug (Model 7) at X/D_{Ref} = 4.61. 267

173. Laser Velocimeter Velocity Profile and Turbulence Measurement; Unsuppressed Coannular Nozzle with Plug (Model 7) at X/D_{Ref} = 5.52. 268

174. Laser Velocimeter Velocity Profile and Turbulence Measurement; Unsuppressed Coannular Nozzle with Plug (Model 7) at X/D_{Ref} = 6.67. 269

175. Laser Velocimeter Velocity Profile and Turbulence Measurement for the Unsuppressed Coannular Nozzle with Plug (Model 7) (Fan Stream Flowing, Core Stream Set for No Flow); X/D_{Ref} = -0.53. 271

176. Laser Velocimeter Velocity Profile and Turbulence Measurement for the Unsuppressed Coannular Nozzle with Plug (Model 7) (Fan Stream Flowing, Core Stream Set for No Flow); X/D_{Ref} = -0.08. 272

177. Laser Velocimeter Velocity Profile and Turbulence Measurement for the Unsuppressed Coannular Nozzle with Plug (Model 7) (Fan Stream Flowing, Core Stream Set for No Flow); X/D_{Ref} = 0. 273

178. Laser Velocimeter Velocity Profile and Turbulence Measurement for the Unsuppressed Coannular Nozzle with Plug (Model 7) (Fan Stream Flowing, Core Stream Set for No Flow); X/D_{Ref} = 0.17. 274

179. Laser Velocimeter Velocity Profile and Turbulence Measurement for the Unsuppressed Coannular Nozzle with Plug (Model 7) (Fan Stream Flowing, Core Stream Set for No Flow); X/D_{Ref} = 0.33. 275

180. Laser Velocimeter Velocity Profile and Turbulence Measurement for the Unsuppressed Coannular Nozzle with Plug (Model 7) (Fan Stream Flowing, Core Stream Set for No Flow); X/D_{Ref} = 0.50. 276

181. Laser Velocimeter Velocity Profile and Turbulence Measurement for the Unsuppressed Coannular Nozzle with Plug (Model 7)(Fan Stream Flowing, Core Stream Set for No Flow); X/D_{Ref} = 0.67. 277

LIST OF ILLUSTRATIONS (Continued)

Figure Page

182. Laser Velocimeter Velocity Profile and Turbulence Measurement for the Unsuppressed Coannular Nozzle with Plug (Model 7)(Fan Stream Flowing, Core Stream Set for No Flow); $X/D_{Ref} = 0.83$. 278

183. Laser Velocimeter Velocity Profile and Turbulence Measurement for the Unsuppressed Coannular Nozzle with Plug (Model 7)(Fan Stream Flowing, Core Stream Set for No Flow); $X/D_{Ref} = 1.05$. 279

184. Laser Velocimeter Velocity Profile and Turbulence Measurement for the Unsuppressed Coannular Nozzle with Plug (Model 7)(Fan Stream Flowing, Core Stream Set for No Flow); $X/D_{Ref} = 1.33$. 280

185. Laser Velocimeter Velocity Profile and Turbulence Measurement for the Unsuppressed Coannular Nozzle with Plug (Model 7) (Fan Stream Flowing, Core Stream Set for No Flow); $X/D_{Ref} = 2.0$. 281

186. Laser Velocimeter Velocity Profile and Turbulence Measurement for the Unsuppressed Coannular Nozzle with Plug (Model 7) (Fan Stream Flowing, Core Stream Set for No Flow); $X/D_{Ref} = 2.61$. 282

187. Laser Velocimeter Velocity Profile and Turbulence Measurement for the Unsuppressed Coannular Nozzle with Plug (Model 7) (Fan Stream Flowing, Core Stream Set for No Flow); $X/D_{Ref} = 3.67$. 283

188. Laser Velocimeter Velocity Profile and Turbulence Measurement for the Unsuppressed Coannular Nozzle with Plug (Model 7) (Fan Stream Flowing, Core Stream Set for No Flow); $X/D_{Ref} = 4.61$. 284

189. Laser Velocimeter Velocimeter Profile and Turbulence Measurement for the Unsuppressed Coannular Nozzle with Plug (Model 7) (Fan Stream Flowing, Core Stream Set for No Flow); $X/D_{Ref} = 6.70$. 285

190. Laser Velocimeter Velocity Profile and Turbulence Measurement for the Unsuppressed Coannular Nozzle with Plug (Model 7) (Core Stream Flowing, Fan Stream Set for No Flow); $X/D_{Ref} = 0.03$. 287

LIST OF ILLUSTRATIONS (Continued)

Figure Page

191. Laser Velocimeter Velocity Profile and Turbulence Measurement for the Unsuppressed Coannular Nozzle with Plug (Model 7) (Core Stream Flowing, Fan Stream Set for No Flow); $X/D_{Ref} = 0.2$. 288

192. Laser Velocimeter Velocity Profile and Turbulence Measurement for the Unsuppressed Coannular Nozzle with Plug (Model 7) (Core Stream Flowing, Fan Stream Set for No Flow); $X/D_{Ref} = 0.5$. 289

193. Laser Velocimeter Velocity Profile and Turbulence Measurement for the Unsuppressed Coannular Nozzle with Plug (Model 7) (Core Stream Flowing, Fan Stream Set for No Flow); $X/D_{Ref} = 1.025$. 290

194. Laser Velocimeter Velocity Profile and Turbulence Measurement for the Unsuppressed Coannular Nozzle with Plug (Model 7) (Core Stream Flowing, Fan Stream Set for No Flow); $X/D_{Ref} = 1.67$. 291

195. Laser Velocimeter Velocity Profile and Turbulence Measurement for the Unsuppressed Coannular Nozzle with Plug (Model 7) (Core Stream Flowing, Fan Stream Set for No Flow); $X/D_{Ref} = 2.61$. 292

196. Laser Velocimeter Velocity Profile and Turbulence Measurement for the Unsuppressed Coannular Nozzle with Plug (Model 7) (Core Stream Flowing, Fan Stream Set for No Flow); $X/D_{Ref} = 4.62$. 293

197. Laser Velocimeter Velocity Profile and Turbulence Measurement for the Unsuppressed Coannular Nozzle with Plug (Model 7)(Core Stream Flowing, Fan Stream Set for No Flow); $X/D_{Ref} = 6.67$. 294

198. Laser Velocimeter Velocity Profile and Turbulence Measurements for the Multichute Fan Suppressor Nozzle (Model 1) at $X/D_{Ref} = 0.02$. 296

199. Laser Velocimeter Velocity Profile and Turbulence Measurments for the Multichute Fan Suppressor Nozzle (Model 1) at $X/D_{Ref} = 1.05$. 297

200. Laser Velocimeter Velocity Profile and Turbulence Measurements for the Multichute Fan Suppressor Nozzle (Model 1) at $X/D_{Ref} = 2.67$. 298

LIST OF ILLUSTRATIONS (Continued)

Figure | Page

201. Laser Velocimeter Velocity Profile and Turbulence Measurements for the Multichute Fan Suppressor Nozzle (Model 1) at $X/D_{Ref} = 4.92$. 299

202. Laser Velocimeter Velocity Profile and Turbulence Measurements for the Multichute Fan Suppressor Nozzle (Model 1) at $X/D_{Ref} = 1.77$. 300

203. Laser Velocimeter Velocity Profile and Turbulence Measurements for the Multichute Fan Suppressor Nozzle (Model 1) at $X/D_{Ref} = 2.67$. 301

204. Laser Velocimeter Velocity Profile and Turbulence Measurements for the Multichute Fan Suppressor Nozzle (Model 1) at $X/D_{Ref} = 4.92$. 302

205. Laser Velocimeter Velocity Profile and Turbulence Measurements for the Multichute Fan Suppressor Nozzle (Model 2) at $X/D_{Ref} = 0.03$. 304

206. Laser Velocimeter Velocity Profile and Turbulence Measurements for the Multitube Fan Suppressor Nozzle (Model 2) at $X/D_{Ref} = 1.09$. 305

207. Laser Velocimeter Velocity Profile and Turbulence Measurements for the Multitube Fan Suppressor Nozzle (Model 2) at $X/D_{Ref} = 1.58$. 306

208. Laser Velocimeter Velocity Profile and Turbulence Measurements for the Multitube Fan Suppressor Nozzle (Model 2) at $X/D_{Ref} = 1.64$. 307

209. Laser Velocimeter Velocity Profile and Turbulence Measurements for the Multitube Fan Suppressor Nozzle (Model 2) at $X/D_{Ref} = 3.52$. 308

210. Laser Velocimeter Velocity Profile and Turbulence Measurements for the Multitube Fan Suppressor Nozzle (Model 2) at $X/D_{Ref} = 0$. 309

211. Laser Velocimeter Velocity Profile and Turbulence Measurements for the Multitube Fan Suppressor Nozzle (Model 2) at $X/D_{Ref} = 1.058$. 310

21 Laser Velocimeter Velocity Profile and Turbulence Measurements for the Multitube Fan Suppressor Nozzle (Model 2) at $X/D_{Ref} = 1.55$. 311

LIST OF ILLUSTRATIONS (Concluded)

Figure | Page
213. Laser Velocimeter Velocity Profile and Turbulence Measurements for the Multitube Fan Suppressor Nozzle (Model 2) at $X/D_{Ref} = 3.56$. 312

LIST OF TABLES

Table No.		Page No.
I	JENOTS Ground Reflection Corrections (Δ dBs to be added to SPL's).	32
II	Estimated Percent Error in the LV Measurement of Mean Velocity with 95% Confidence.	38
III	Estimated Percent Error for LV Turbulent Velocity Measurements with 95% Confidence.	38
IV	Description of Test Models and Test Types.	49
V	Acoustic Test Matrix, Aerodynamic Test Conditions (Nominal Values).	53
VI	Acoustic Test Schedule.	57
VII	Laser Velocimeter Test Matrix, Aerodynamic Test Conditions (Nominal Values).	58
VIII	Laser Velocimeter Data Planes.	59
IX	Aerodynamic Test Matrix.	62
X	Conical and Convergent-Divergent Nozzle Data Sources.	68
XI	Listing of the GE Air-Attenuation Correction Computer Program.	206
XII	Acoustic Test Matrix, Aerodynamic Test Conditions, DBTF Model 1.	223
XIII	Acoustic Test Matrix, Aerodynamic Test Conditions, DBTF Model 2.	225
XIV	Acoustic Test Matrix, Aerodynamic Test Conditions, DBTF Model 3.	227
XV	Acoustic Test Matrix, Aerodynamic Test Conditions, DBTF Model 4.	228
XVI	Acoustic Test Matrix, Aerodynamic Test Conditions, DBTF Model 5.	229
XVII	Acoustic Test Matrix, Aerodynamic Test Conditions, DBTF Model 6.	230

LIST OF TABLES Concluded

Table No.		Page No.
XVIII	Acoustic Test Matrix, Aerodynamic Test Conditions, DBTF Model 7.	231
XIX	Acoustic Test Matrix, Aerodynamic Test Conditions, DBTF Model 8.	233
XX	Acoustic Test Matrix, Aerodynamic Test Conditions, DBTF Model 9.	234
XXI	Acoustic Test Matrix, Aerodynamic Test Conditions, DBTF Model 10.	235
XXII	Acoustic Test Matrix, Aerodynamic Test Conditions, DBTF Model 11.	235
XXIII	Full-Scale Data Reduction Format.	236
XXIV	Scale-Model Acoustic Data.	237
XXV	Scaled (Full Size) Acoustic Data.	238
XXVI	Extrapolated, Scaled (Full Size), Acoustic Data.	239

1.0 SUMMARY

This report, along with the companion comprehensive data report under separate cover (NASA CR 135236), summarizes results of a one-year, static acoustic and aerodynamic-performance test program performed at the General Electric Company on coannular unsuppressed and fan-suppressed coannular nozzle configurations under NASA-Lewis sponsorship. The nozzle configurations selected were applicable to dual-stream exhaust systems with the high velocity and high temperature stream on the outside, e.g. the duct-burning turbofan cycle.

In all, eleven dual-stream models were tested acoustically and aerodynamically. The models tested consisted of unsuppressed coannular nozzles, multielement fan-suppressed coannular nozzles, and multielement fan-suppressed coannular nozzles with hardwall and treated ejectors. Additionally, aerodynamic performance measurements were performed to evaluate the differences between hot-flow and cold-flow testing, and a series of laser velocimeter measurements was performed to study the detailed mean-velocity and turbulent-velocity exhaust plume characteristics of several of the models investigated.

Very significant interaction benefits were found for the coannular acoustic nozzles when the high velocity jet stream exhausts as the outer stream. Compared to noise levels that are predicted by simply summing the noise of two independent and equivalent jet streams (no interaction effects) the following static acoustic results were obtained:

- For the unsuppressed coannular plug nozzle, at fan to core velocity ratios greater than 1.5 and at a fan to core area ratio of 0.65, noise reductions of 10 PNdB were found.

- A coannular, coplanar nozzle at a smaller fan-stream radius ratio yielded 2 PNdB less noise reduction than the unsuppressed, coannular, plug nozzle. These results imply that a high radius ratio may be important to the observed noise reduction levels.

- 15 PNdB noise reduction was observed with either the 36-chute or the 69-tube fan-suppressed coannular nozzles.

- 17 to 18 PNdB noise reduction was observed for treated ejector arrangements on the fan-suppressed, coannular-flow nozzles.

- When either the unsuppressed or the fan-suppressed nozzles were tested with low core flows large noise reductions were still observed.

The static, scale-model, aerodynamic-performance test results showed high thrust coefficient levels. Thrust coefficients, C_T, of up to 0.972

were measured for the unsuppressed coannular nozzle with plug. For the multichute and the multitube fan-suppressor nozzles, thrust coefficients were measured that were only 1.2% and 1.7% lower than the unsuppressed coannular nozzle with plug. The addition of a hardwall ejector with a sharp lip onto the fan-suppressed coannular nozzles improved the measured basic fan-suppressor nozzle static performance by 2% for the multitube fan suppressor and 0.5% for the multichute fan-suppressor nozzle. These performance improvements, however, will be substantially negated due to thrust losses attributed to acoustic liners (2 to 5% relative to hardwall ejectors), as well as the effect of flight relative to static performance degradation (estimated at 2 to 4%).

The exhaust-plume velocity measurements made with a laser velocimeter on the unsuppressed and the fan-suppressed coannular-flow nozzles showed a very rapid mean-velocity decay compared to a typical conical nozzle. These velocity-decay measurements also point to the importance of a high radius ratio design for the high velocity efflux gas stream. Phenomonologically this rapid decay in mean velocity is associated with a reduction in turbulent mixing noise which in part is responsible for the observed jet noise reduction.

2.0 INTRODUCTION

During 1973 the NASA-Lewis Research Center initiated an exploratory scale-model acoustic and aerodynamic-performance test program to obtain parametric data measurements of separate-flow unsuppressed and fan-suppressed coannular nozzles. The program was directed toward the development of high velocity jet noise technology for Advanced Supersonic Transport (AST) application. The essential features of this program were: (1) Dual-flow nozzle systems with the high velocity and high temperature jet in the fan stream (which is the reverse of conventional bypass engines). (2) The study of the effectiveness of adding suppressor elements to the flow stream only. (3) The performance of a systematic, static, aerodynamic-performance study of unsuppressed and fan-suppressed coannular flow nozzles. (4) Obtain, for the first time, detailed velocity-field surveys of the mixing streams of high velocity and high temperature coannular-flow nozzles. (5) Presentation of the acoustic results at large scale factors to simulate actual jet engine noise conditions.

The composition of this technical report is as follows:

Sections 1.0 and 2.0 are the Summary and Introduction Sections.

Section 3.0 deals with a description of the acoustic and aerodynamic-performance facilities, the acoustic and laser velocimeter measurement systems, and data reduction procedures employed for the measurements obtained in this program.

Section 4.0 describes the models tested and the test-matrix definitions for all of the acoustic, aerodynamic performance, and laser velocimeter measurements performed on this program.

Section 5.0 reports on the series of model-scale acoustic test results for unsuppressed and multielement fan-suppressed coannular nozzles; this section illustrates all the main acoustic spectral directivity characteristics of the tested configurations. The test results show systematic noise reduction trends for the fan-suppressed configurations as well as the unsuppressed coannular-nozzle configurations when the noise levels are compared to predicted levels of the simple sum of two independent but equivalent jet nozzles without any assumed interaction benefits (a synthesized jet noise baseline).

Section 6.0 describes the model-scale, aerodynamic-performance measurements conducted on the selected nozzles; test results are presented for cold flow tests and for hot flow tests. The reported results show relatively high levels of static thrust coefficient for the unsuppressed and the fan-suppressed coannular nozzles. It is also shown that, at most, the heated-flow performance tests were 1% lower than the cold flow tests.

Section 7.0 is devoted to a description of laser velocimeter measurements performed on some of the tested models. The results show a rapid decay in the axial mean-velocity distributions which tend to substantiate the noise reduction levels observed and reported in Section 5.0.

Section 8.0 presents a discussion of preliminary acoustic and aerodynamic-performance correlations; the section concludes with a geometry related correlation scheme for collapsing the low core-flow, coannular-nozzle, acoustic test results.

Section 9.0* presents the major conclusions of the performed work efforts and presents recommendations for future exploratory work efforts.

All the acoustic data obtained under this study are presented under separate cover in the companion Comprehensive Data Report, NASA CR-135236.

---

*Author's Note: The results presented in this report represent work performed during the 1973-1975 time period. Since this time additional work has been performed under Contract NAS3-19777 to parametrically study the unsuppressed, coannular, plug nozzle. Section 9 contains a brief preview of some of the results observed from the new measurements and data analyses.

3.0 TEST APPARATUS AND PROCEDURES

This section includes a comprehensive description of the acoustical and aerodynamic performance facilities, the acoustic and laser velocimeter measuring systems, and the acoustic, aerodynamic performance, and laser velocimeter data reduction procedures employed for the measurements obtained in this program.

Section 3.1 describes the General Electric Jet Exhaust Noise Outdoor Test Site (JENOTS) located at Evendale, Ohio and the FluiDyne Engineering Corporation Aerodynamic Laboratory facility located in Medicine Lake, Minnesota. Considerable detail is given in this section, particularly in describing the coannular-flow acoustic system. This detailed description is given because the facility for this program was designed to operate at fan and core flow temperature conditions of 1960° R (1089 K); the details of such a facility system design are not common knowledge and it was felt that these descriptions would be helpful to any future investigators.

Section 3.2 describes the basic acoustic and laser velocimeter instrumentation systems developed for General Electric outdoor acoustic and aerodynamic plume testing and used for the tests conducted on this program. Since one of the goals of the program was to provide acoustic measurements up to 80 kHz, it was again necessary to describe in some detail the acoustic instrumentation and setup.

Section 3.3 describes the key elements of the data reduction techniques used for acoustic, laser velocimeter, and aerodynamic-performance tests. Because the acoustic test site was outdoors and the goal was to obtain accurate acoustic measurements up to 80 kHz, this section includes descriptions of air-attenuation corrections developed, typical data-scaling procedures, ground-reflection corrections used, and an evaluation of the acoustic system electronic-noise floor. Additionally, descriptions of the laser velocimeter data reduction methods and the aerodynamic performance test data reduction procedures are included.

3.1 FACILITIES

The General Electric Jet Exhaust Noise Outdoor Test Site (JENOTS) located at Evendale, Ohio (used for acoustic tests) and the FluiDyne Engineering Corporation Aerodynamic Laboratory located at Medicine Lake, Minnesota (used for aerodynamic-performance tests) are described in this section.

3.1.1 General Electric Jet Engine Noise Outdoor Test Stand (JENOTS) Description

3.1.1.1 The Acoustic Arena

The scale-model, acoustic test facility is shown schematically in Figure 1 and pictorially in Figure 2. The nozzle centerline is 55 inches (1.4 m) above the ground plane. The acoustic measurement arena is composed of concrete to a radius of 20 feet (6.1 m) from the nozzle exit and then crushed rock to a radius of 40 feet (12.2 m); a grassy field exists beyond the acoustic arena. Specially designed acoustic barriers are located 60 feet (18.3 m) from the sound field to protect the neighboring community from the high sound levels. The control room is located 100 feet (30.5 m) from the sound field.

The outdoor arena is subject to ambient weather conditions. The barometric pressure, along with wet and dry bulb temperatures, are recorded throughout a test; this information is used to correct the sound data to standard day. The wind speed and direction are also recorded. All acoustic testing is performed, during daytime, when the weather conditions are such that there is no rain, snow, or winds over 10 mph (16 km/h).

3.1.1.2 Coannular-Flow System

The coannular-flow facility at JENOTS is shown schematically in Figure 1 and pictorially in Figure 3. Air for the core and fan streams is supplied from the Evendale central air supply system through 10-inch (25.4 cm) and 16-inch (40.6 cm) air lines, respectively. The plenum chamber to which the test models are attached is also shown schematically in Figure 3. It serves a two-fold purpose: giving the flow a uniform velocity profile and eliminating any high frequency system noise through the use of acoustically treated baffles located in the fan and core streams.

Flow conditions for the fan and core streams are controlled separately; the airflows are measured using an orifice-plate system coupled with pressure and thermocouple rakes. Rig instrumentation data are converted to digital punched tape and displayed in engineering units through the use of a time-sharing computer program. Burner systems located in the air supply lines prior to the plenum chamber provide heated streams. The range of conditions under which the facility operated for this program was:

Bypass Ratio	0 - 15
Fan Temperature	ambient to 1960° R (1089 K)
Core Temperature	ambient to 1960° R (1089 K)
Fan Pressure Ratio	1.05 to 4.0

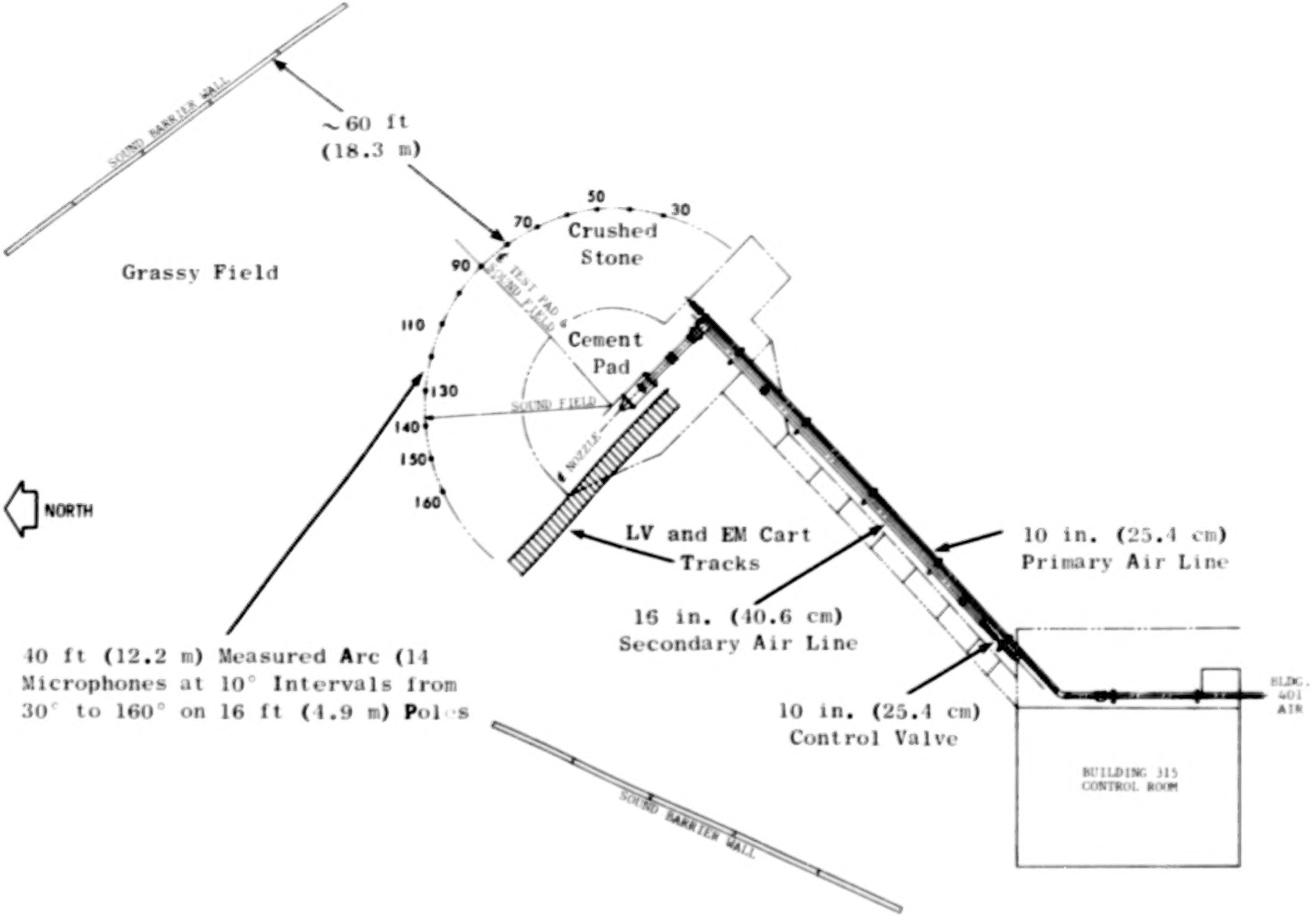
SOUND BARRIER WALL
~60 ft
(18.3 m)
50
30
70
Crushed
Stone
90
TEST PAD
SOUND FIELD
Grassy Field
110
Cement
Pad
130
SOUND FIELD
140
NOZZLE
150
160
NORTH
LV and EM Cart
Tracks
10 in. (25.4 cm)
Primary Air Line
16 in. (40.6 cm)
Secondary Air Line
40 ft (12.2 m) Measured Arc (14
Microphones at 10° Intervals from
30° to 160° on 16 ft (4.9 m) Poles
10 in. (25.4 cm)
Control Valve
BLDG.
401
AIR
BUILDING 315
CONTROL ROOM
SOUND BARRIER WALL

Figure 1. Schematic of Jet Engine Noise Outdoor Test Stand (JENOTS) Facility Acoustic Arena.

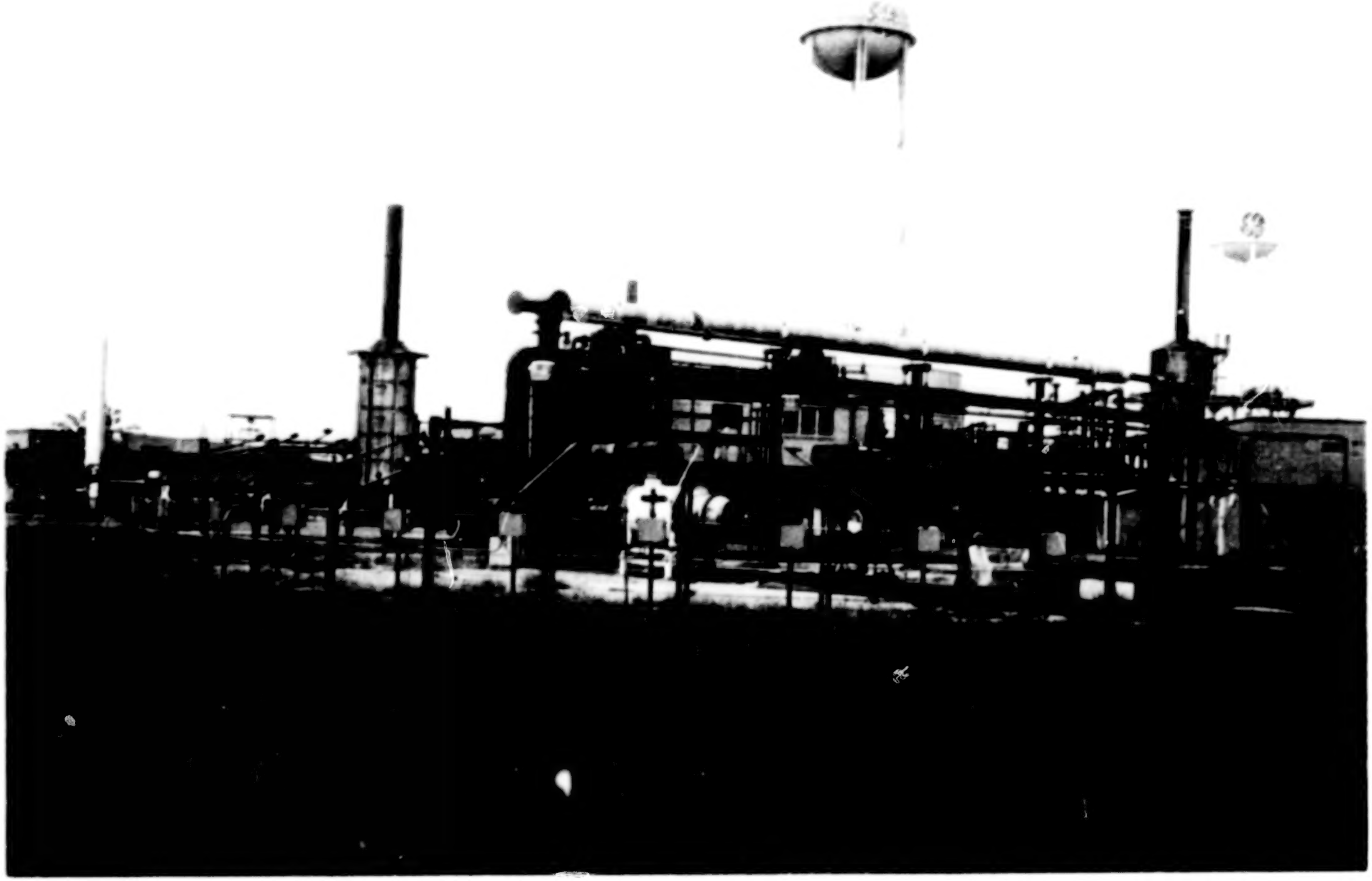

Figure 2. Jet Engine Noise Outdoor Test Stand (JENOTS), Acoustic Arena.

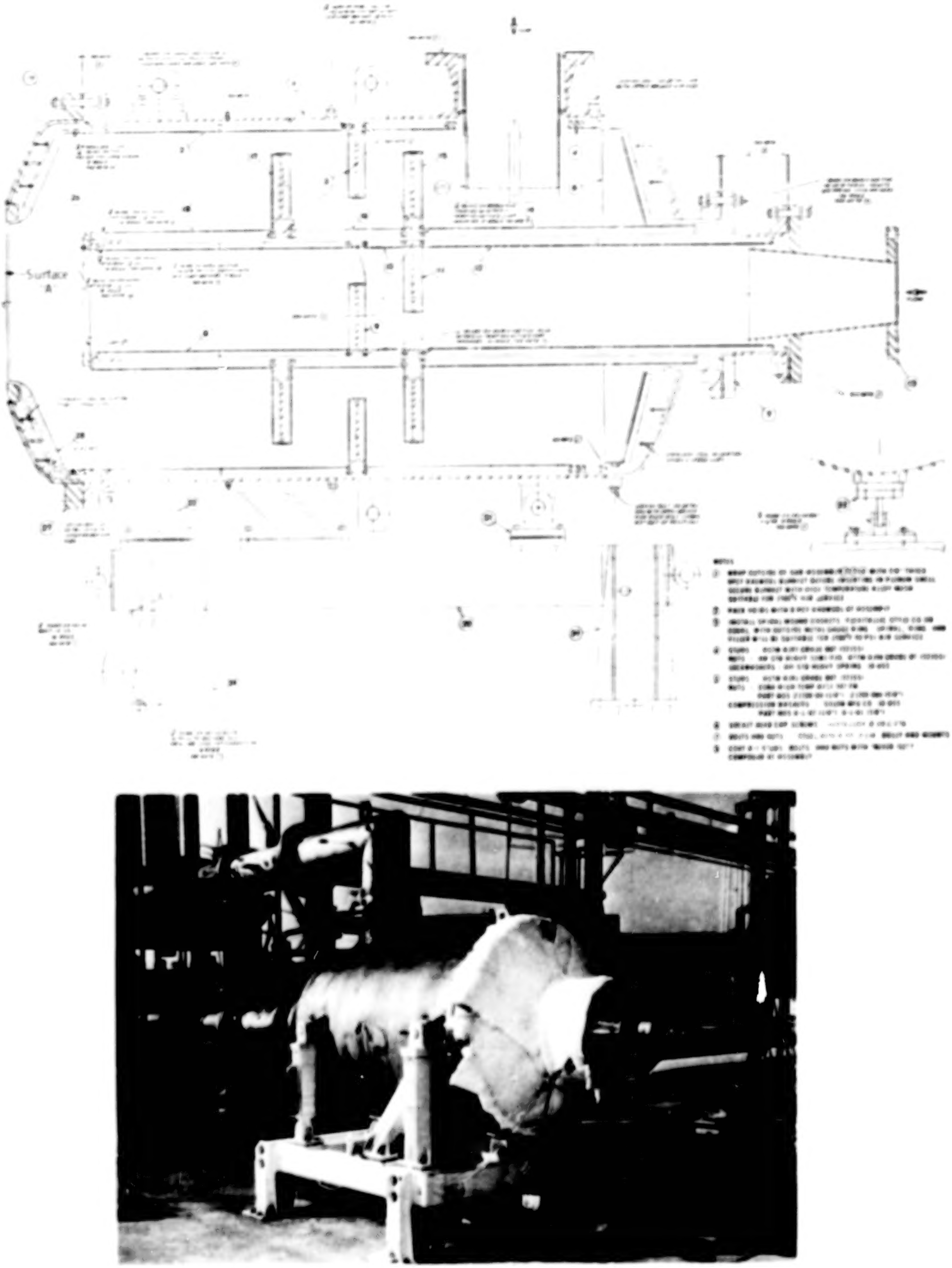

Figure 3. High Temperature Coannular Plenum Chamber.

Core Pressure Ratio	1.05 to 3.0
Fan Weight Flow	0 to 50 lbm/sec (22.7 kg/sec)
Core Weight Flow	0 to 30 lbm/sec (13.6 kg/sec)

3.1.1.3 Coannular Frame Section

The design of the plenum (and the model hardware) to meet the various usage intents was a major task. Since the model hardware was exposed to large temperature gradients between the core and the fan streams, $\Delta T = T_f - T_c$ to 1000° R (556 K), allowances for differential radial and axial thermal-growth rates were provided within the plenum frame section used to connect the instrumentation section to the plenum chamber. A schematic of this frame hardware with the unsuppressed coannular nozzle with plug model is shown in Figure 4. Independent core and fan stream frames were designed and interconnected at the core outside diameter (O.D.) and fan stream inside diameter (I.D.) flowpaths with a flexing wishbone structure. The wishbone absorbs deflection due to differential thermal growth, thus eliminating high stress concentrations. The fan stream frame section adapts to the coannular plenum through a cylindrical outer frame support and a conical transition piece. Thus the fan stream outer shell supports the entire model and frame assembly. Core O.D. and fan I.D. sliding transition pieces complete the inner flowpaths from the frames to the plenum. Sealing mechanisms are provided to eliminate leakage between streams at the interface of the core frame and coannular plenum inner supply pipe. Differential axial growth from the frame section aft through the model hardware is provided by a sliding interface between the core O.D. and fan I.D. hardware pieces at the exit plane. Compensation for differential radial growth is also provided for at the same exit-plane interface. Sufficient radial gap is allowed such that: when operating the core hot, at 1960° R (1089 K), and the fan at ambient the core O.D. will grow radially into the fan I.D. hardware but will not overstress due to buckling; when operating the fan hot, at 1960° R (1089 K) and core at ambient the gap will be increased due to faster fan-hardware radial growth.

3.1.1.4 Plenum Instrumentation Section

As seen in the photographs in Figure 4, an instrumentation section is positioned aft of the frames for measuring the flow conditions at the nozzle exit plane. Instrumentation within the flow-metering section consists of two combination total pressure and total temperature (P_T/T_T) rakes plus four static pressure taps in each of the two streams. The schematic of the instrumentation layout presented in Figure 4 shows the P_T/T_T rakes located midway between the wakes of the upstream struts within the core and fan streams. The static pressure taps are located just to the side of each rake to assure that any flow disturbance from the rake body does not interfere with the measurements. Each P_T/T_T rake is an integral part of a removable pad such that, when inserted within the stream, no

- Frame Section (Attaches to Surface "A" of Figure 3)

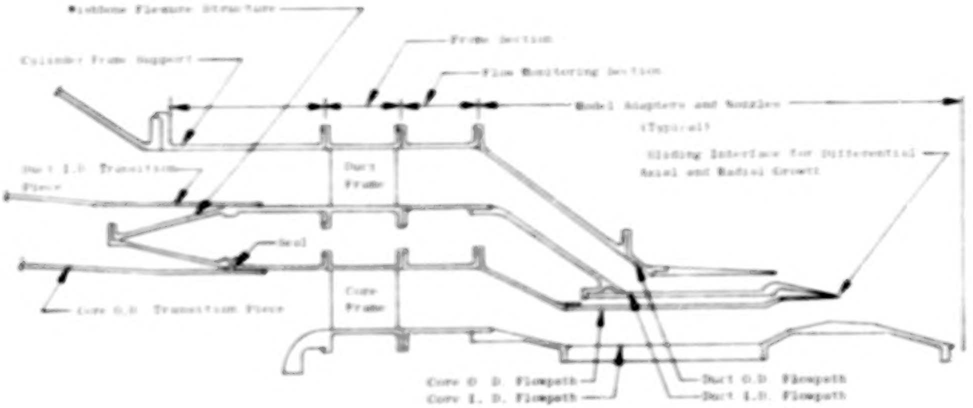
Wishbone Flexure Structure
Cylinder Frame Support
Frame Section
Flow Monitoring Section
Model Adapters and Nozzles (Typical)
Sliding Interface for Differential Axial and Radial Growth
Duct I.D. Transition Piece
Duct Frame
Seal
Core O.D. Transition Piece
Core Frame
Core O. D. Flowpath
Core I. D. Flowpath
Duct O.D. Flowpath
Duct I.D. Flowpath

- Frame and Instrumentation Assemblies

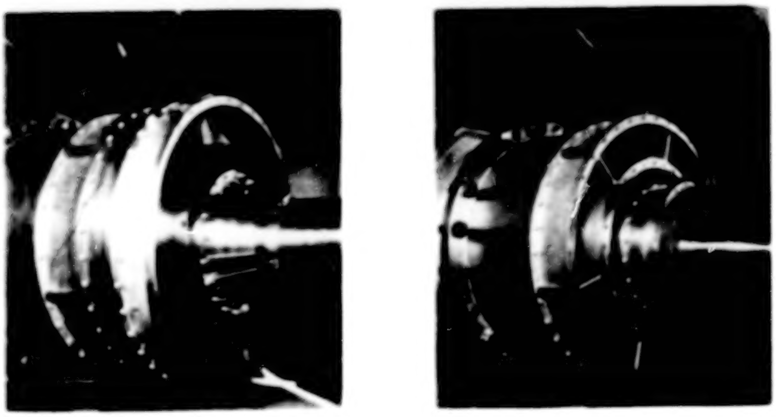
Instrumentation

Frame

- Instrumentation Section

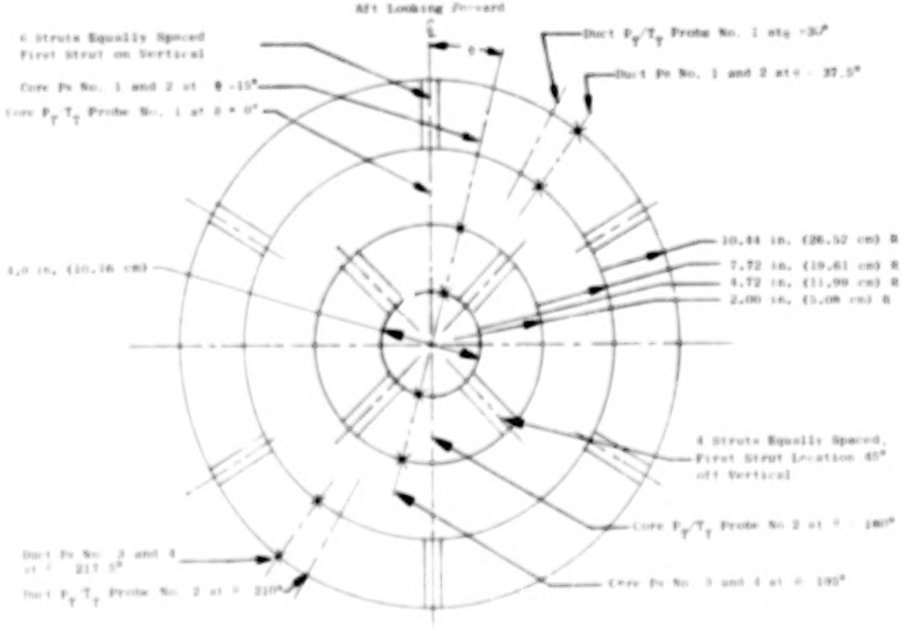
Aft Looking Forward
℄
θ
6 Struts Equally Spaced First Strut on Vertical
Core Ps No. 1 and 2 at θ = 15°
Core P_T/T_T Probe No. 1 at θ = 0°
Duct P_T/T_T Probe No. 1 at θ = 30°
Duct Ps No. 1 and 2 at θ = 37.5°
10.44 in. (26.52 cm) R
7.72 in. (19.61 cm) R
4.72 in. (11.99 cm) R
2.00 in. (5.08 cm) R
4.0 in. (10.16 cm)
4 Struts Equally Spaced, First Strut Location 45° off Vertical
Core P_T/T_T Probe No 2 at θ = 180°
Duct Ps No. 3 and 4 at θ = 217.5°
Duct P_T/T_T Probe No. 2 at θ = 210°
Core Ps No. 3 and 4 at θ = 195°

Figure 4. Coannular Frame and Instrumentation Sections.

discontinuity in internal flowpath is seen other than the probe body. All internal static pressure tap leads are routed up through slots in the frame struts. The use of a common flow-monitoring section between acoustic and aerodynamic testing provides for consistency of measurements among all test models.

3.1.1.5 Facility Acoustic Validation

Two precautions were taken to eliminate extraneous facility type noise sources: all air-supply pipe lines were wrapped with sheet lead to preclude piping noise from air leakage at the pipe flanges; all elbows in the lines were lined internally with acoustically absorbent material to minimize the internal pipe flow-noise propagation. To validate the precautions a pretest checkout of the facility system was conducted; the checkout consisted of running velocity variations along constant temperature lines. The normalized overall sound pressure level at the 90° station was compared to the eighth-power law as shown in Figure 5. The guideline used was that variations of less than 1 dB were accepted as uncontaminated jet noise data. The data used in the facility validation (as well as all the program data) were corrected for ground reflections by the method described in Section 3.3.1. The density normalization used was that of Hoch, et al. (Reference 1). The result of the facility validation tests was that the high temperature coannular facility provides clean jet noise down to approximately 500 ft/sec (150 m/sec).

3.1.2 FluiDyne Aerodynamic-Performance Test Facility Description

The aerodynamic-performance tests were conducted at FluiDyne Engineering Corporation's Medicine Lake Aerodynamic Laboratory. Channel 11 at the facility (a two-flow, static-thrust stand with the capability of heating one of the two air supplies) was utilized for the test; the general arrangement of Channel 11 is shown in Figure 6.

The two airflows are obtained from the facility high-pressure, dry-air storage system. Air for the cold passage is throttled, metered through a long-radius ASME nozzle, ducted to the cold passage of the test nozzle, and then exhausted to atmosphere. Air for the hot passage is throttled, passed through a regenerative storage heater, mixed with unheated bypass flow to achieve a desired temperature, metered through a long-radius ASME nozzle, ducted to the hot passage of the test nozzle, and finally exhausted to atmosphere. The air heater used for the hot flow contains alumina pebbles preheated to approximately 1710° R (950 K) with a combustion heater. For cold-flow-only tests, the pebbles are simply left unheated.

The nozzle thrust is determined from force measurements made with a strain gage force balance which supports the model assembly. The metric (model) portion of the assembly is isolated from the nonmetric facility piping portion by two elastic seals (Figure 7). Calibration of the balance and seals is described in Section 3.3.3.5.

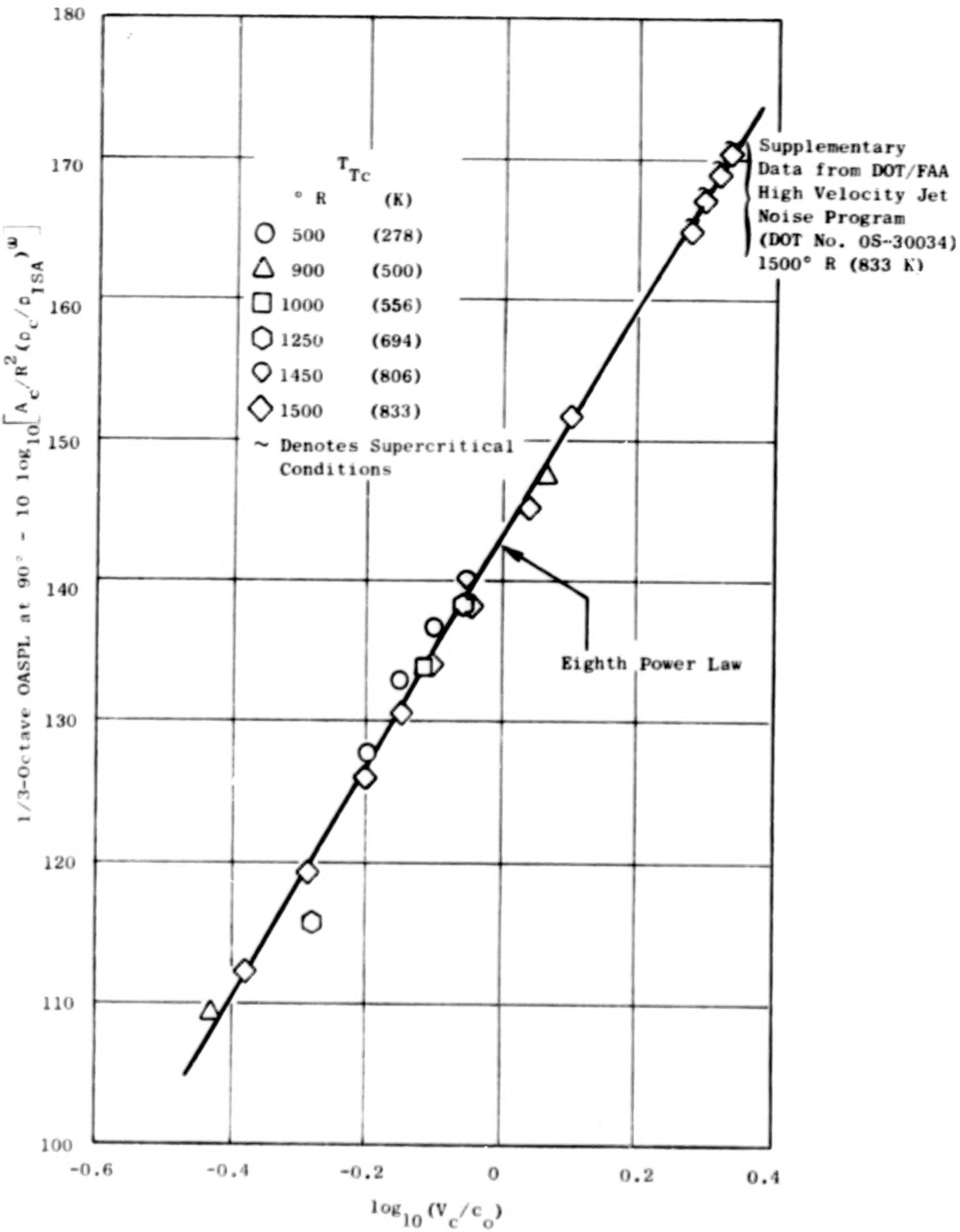

Figure 5. Example of Acoustic Facility Noise Validation Test Series; Core Flow through Core (only) Nozzle of Model 8.

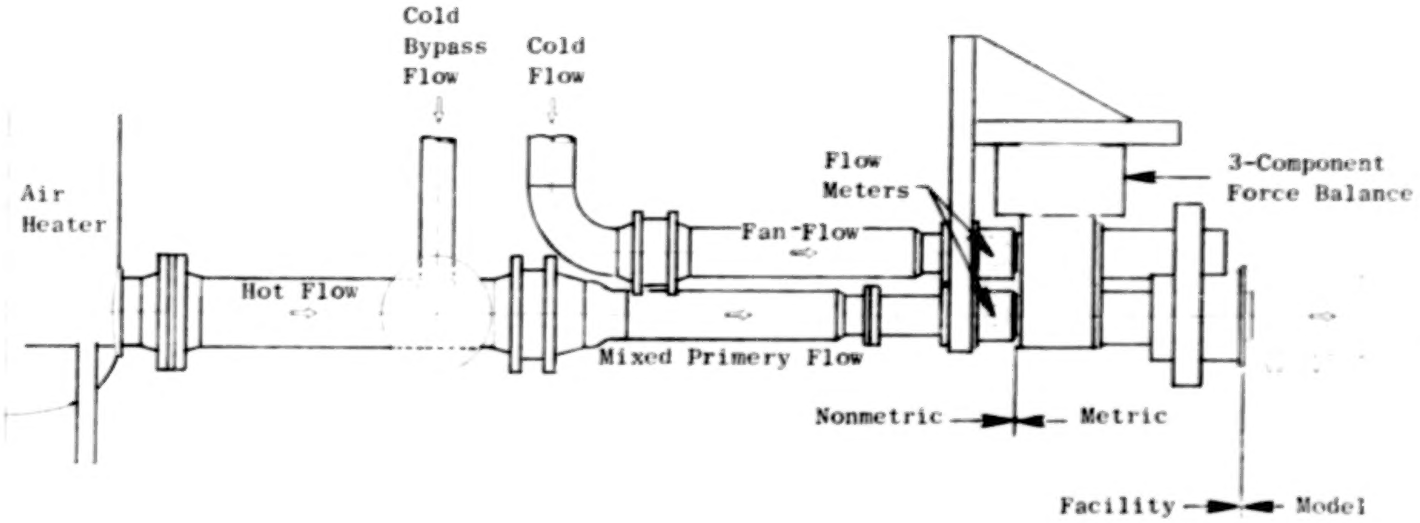
Cold
Bypass
Flow
Cold
Flow
Air
Heater
Hot Flow
Flow
Meters
Fan Flow
Mixed Primery Flow
3-Component
Force Balance
Nonmetric
Metric
Facility
Model

Figure 6. FluiDyne Channel 11 Aerodynamic Performance Facility Layout.

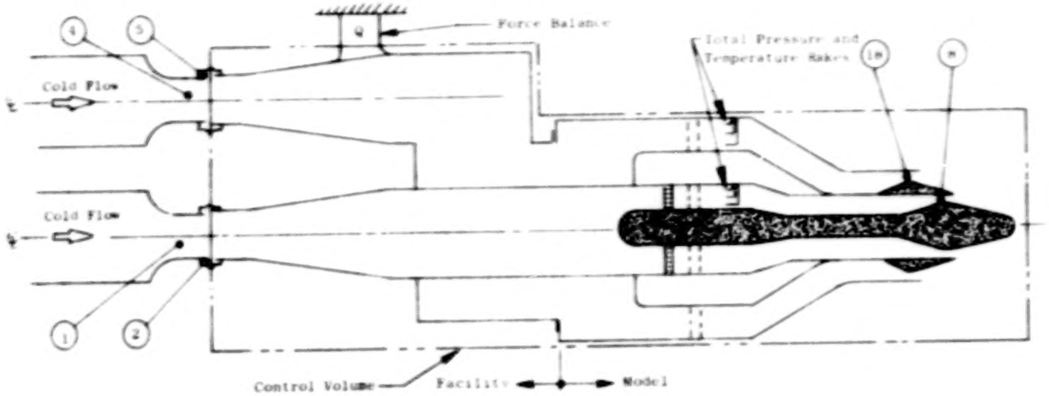
Force Balance
Q
4
5
Cold Flow
℄
Total Pressure and Temperature Rakes
18
8
Cold Flow
℄
1
2
Control Volume
Facility
Model

Station	Description
1	ASME Meter Throat (Core Flow)
2	Flexible Seal (Core Flow)
4	ASME Meter Throat (fan flow)
5	Flexible Seal (Fan Flow)
8	Core Nozzle
18	Fan Nozzle

a) Cold Flow Model Tests

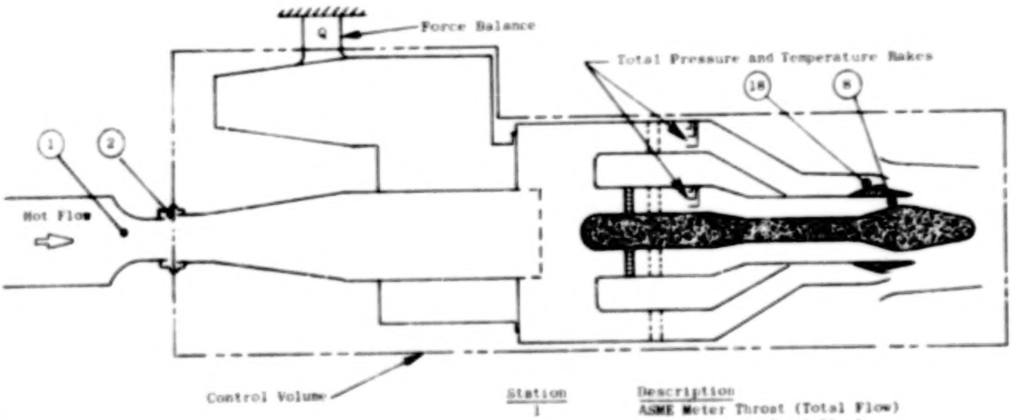
Force Balance
Q
Total Pressure and Temperature Rakes
18
8
1
2
Hot Flow
Control Volume

Station	Description
1	ASME Meter Throat (Total Flow)
2	Flexible Seal (Total Flow)
8	Core Nozzle
18	Fan Nozzle

b) Hot Flow Model Tests

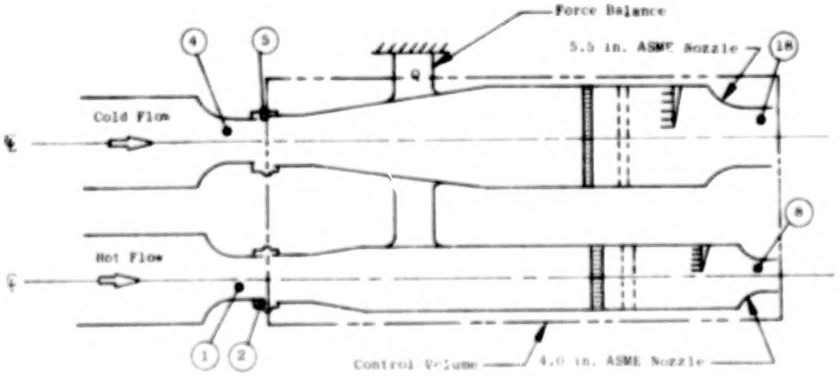
Force Balance
4
5
Q
5.5 in. ASME Nozzle
18
Cold Flow
℄
8
Hot Flow
℄
1
2
Control Volume
4.0 in. ASME Nozzle

Station	
1	ASME Meter Throat (Core Flow)
2	Flexible Seal (Core Flow)
4	ASME Meter THROAT (Fan Flow)
5	Flexible Seal (Fan Flow)
18	5.5 in. Cold ASME Nozzle Throat
8	4.0 in. Hot ASME Nozzle Throat

c) ASME Checkout Tests

Figure 7. FluiDyne Force Balance Station Notations for Aerodynamic Model Tests.

The ASME meter at Station 1 is water cooled to protect the elastic seal from thermal effects. Since the cooling water is confined to the upstream (i.e., nonmetric) hardware only, no tare forces are introduced by the water supply lines.

Pressure data were recorded with Polaroid photographs of gages and manometer boards. Temperature and force balance data were recorded with digital printers.

3.2 JENOTS INSTRUMENTATION SYSTEMS

3.2.1 Acoustic Instrumentation Systems

The acoustic data collection system at JENOTS is shown schematically in Figure 8. It is composed of a B&K microphone/cathode follower, powered and conditioned by a B&K 2801 power supply, followed by three feet (0.914 m) of line to a specially designed, 10-dB, fixed-gain preamplifier which drives 150 feet (45.7 m) of cable terminating at the variable-gain, differential-input amplifiers to the Sangamo Sabre IV tape recorder. The signal is recorded on tape for future playback in the data reduction room.

The free-field microphones utilized for these tests were B&K 4135, 1/4-inch (0.635 cm) with grid caps removed. The cathode follower used was the B&K 2615 preamplifier powered by a B&K 2801 power supply which is operated in the direct output mode to avoid sensitivity loss. The frequency response of the various preamplifiers is not influenced by the power supply when used in this position.

The fixed 10-dB amplifier for driving the signal to the tape recorder amplifier was designed by the General Electric Aircraft Engine Group (AEG) Electronic Instrumentation Group and built from high quality components by Random Electronics, a Cincinnati firm. In anticipation of the low sound levels experienced at high frequency, the circuitry was designed with a frequency response that "preemphasized" the high frequency signals such that it has a 3-dB increase at 40 kHz and an additional 3-dB increase between 40 kHz to 80 kHz.

A two-conductor, shielded wire was chosen for the 150 feet (45.7 m) of lead from the line driver to the tape recorder amplifier. The amplifier at the tape recorder was designed by GE and built by Random Electronics. The amplifiers are flat within 5% from 5 Hz to 100 kHz. Each amplifier has an adjustable vernier attenuator which can give any desired measure of attenuation between 0 and 10 dB. During test calibration this vernier is usually adjusted to make the 124 dB pistonphone calibration signal the full-scale (1.4 volts rms) input to the tape recorder. The 10-dB steps in the tape recorder amplifier then directly correspond to 10-dB steps in OASPL, (overall sound pressure level) from 124 dB. The vernier can be moved to the fixed position, in which case the signal goes directly into the 10-dB-step tape recorder amplifier. The output of each amplifier

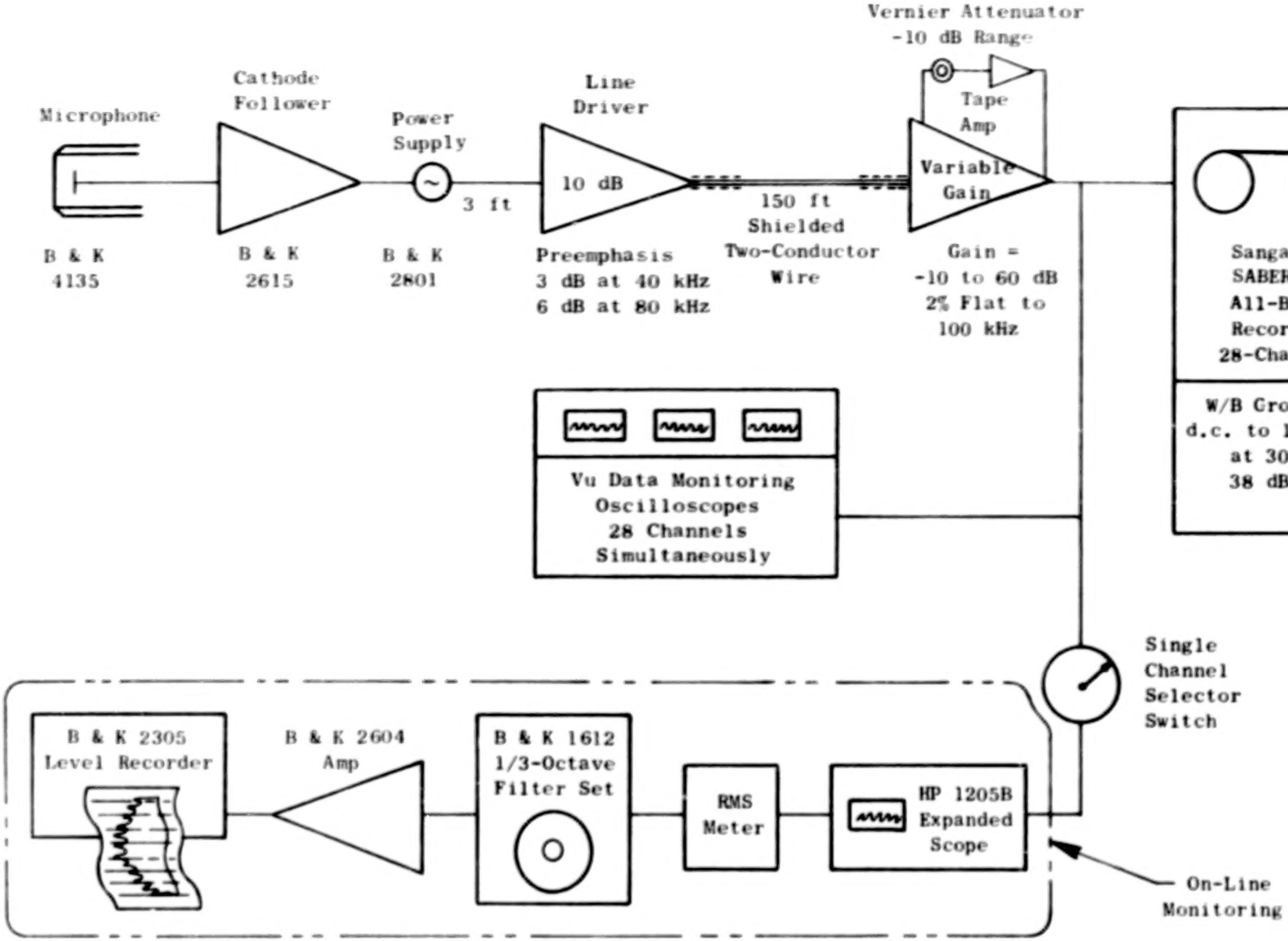

Vernier Attenuator
-10 dB Range
Microphone
Cathode Follower
Power Supply
Line Driver
Tape Amp
Variable Gain
10 dB
3 ft
150 ft
Shielded
Two-Conductor
Wire
B & K
4135
B & K
2615
B & K
2801
Preemphasis
3 dB at 40 kHz
6 dB at 80 kHz
Gain =
-10 to 60 dB
2% Flat to
100 kHz
Sangamo
SABER IV
All-Band
Recorder,
28-Channel
W/B Group II
d.c. to 125 kHz
at 30 ips
38 dB S/N
Vu Data Monitoring
Oscilloscopes
28 Channels
Simultaneously
Single
Channel
Selector
Switch
B & K 2305
Level Recorder
B & K 2604
Amp
B & K 1612
1/3-Octave
Filter Set
RMS
Meter
HP 1205B
Expanded
Scope
On-Line
Monitoring

Figure 8. JENOTS Acoustic Data Acquisition System.

channel has a Vu-Data monitoring oscilloscope for continual inspection of all signals for any clipping or deterioration of the signal due to excessive crest factor (peak value/rms).

The Sangamo Sabre IV 4930 magnetic tape recorder/reproducer has IRIG (Inner-Range Instrumentation Group)wideband and FM (frequency modulated) wideband Group I and II capability. JENOTS data are all recorded on one-inch (2.54 cm) tape in wideband Group II at 30 in./sec (0.762 m/sec) which has a flat frequency response in excess of 100 kHz when used in conjunction with the B&K 4135 microphone. The voice channel is recorded direct.

The JENOTS recorder was modified to record 28 tracks and to improve its signal-to-noise dynamic range from the normal 32 dB to 39 dB over all frequencies. This lower noise floor was obtained by individual channel tuning by the Sangamo Electric Company at the factory.

On-line data display during testing at JENOTS was obtained by utilizing a single-channel selector switch which can route any microphone signal parallel to the tape recorder for expanded waveform presentation on an HP 1205 B oscilloscope, as shown in Figure 8. The signal is then passed through a B&K 1612 band-pass filter set, amplified by a B&K 2604 amplifier, and recorded on a B&K 2305 level recorder. The filter set can be dialed to one-third-octave frequencies from 12.5 Hz to 40 kHz, octave frequencies from 16 Hz to 31.5 kHz, or linear, "A," "B," and "C" weighted networks from 20 Hz to 45 kHz.

3.2.2 Laser Velocimeter System

3.2.2.1 General Arrangement

The laser velocimeter (LV) arrangement used at JENOTS for measuring jet plume mean velocity and turbulent velocity levels is a system developed under a USAF/DOT sponsored program and reported in detail in Reference 2 and Reference 3. The general features of the system are described below.

The basic optics system is a differential Doppler, backscatter, single-package arrangement that has the proven feature of ruggedness for the rather severe JENOTS environment. Figure 9 shows a schematic arrangement of the laser package used on this program. The laser beams are projected from below the lens, forming an angle that keeps the major axis of the control volume ellipsoid to a minimum. The dimensions of the control volume are 0.25 inch (0.636 cm) for the major axis and 0.020 inch (0.508 cm) for the minor axis. The range of the LV control volume from the laser hardware was 85 inches (2.16 m); at this distance from the jet a protective enclosure is not necessary. The three steering mirrors and the beam splitter are mounted on adjustable supports, all of the same aluminum alloy, which eliminates temperature-alignment problems. Figure 10 shows a photograph of the laser velocimeter setup at JENOTS. This LV setup is used only for exhaust plume surveys and is removed during acoustic tests.

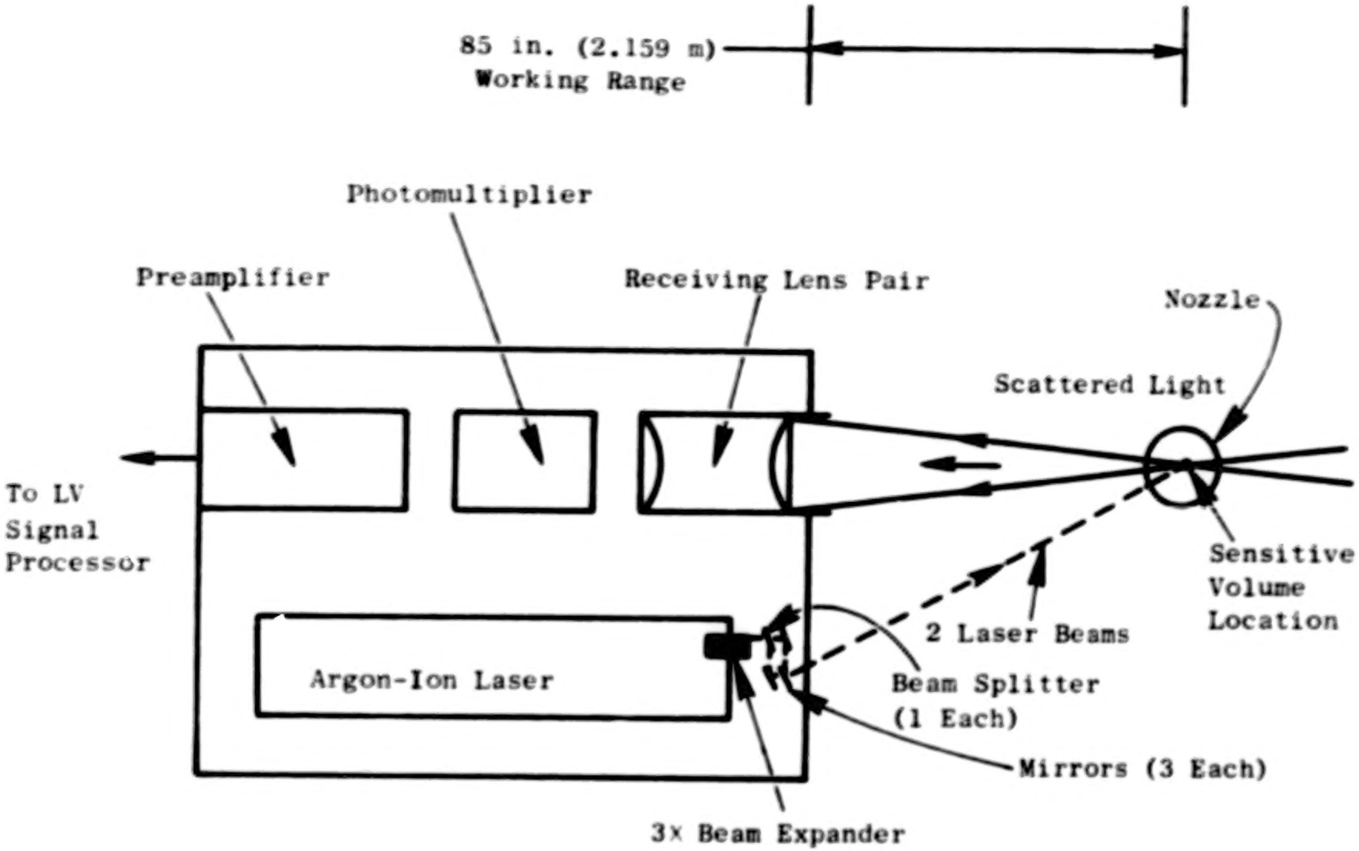
85 in. (2.159 m)
Working Range
Photomultiplier
Preamplifier
Receiving Lens Pair
Nozzle
Scattered Light
To LV
Signal
Processor
Sensitive
Volume
Location
2 Laser Beams
Argon-Ion Laser
Beam Splitter
(1 Each)
Mirrors (3 Each)
3× Beam Expander

Figure 9. Laser Velocimeter Optics Package.

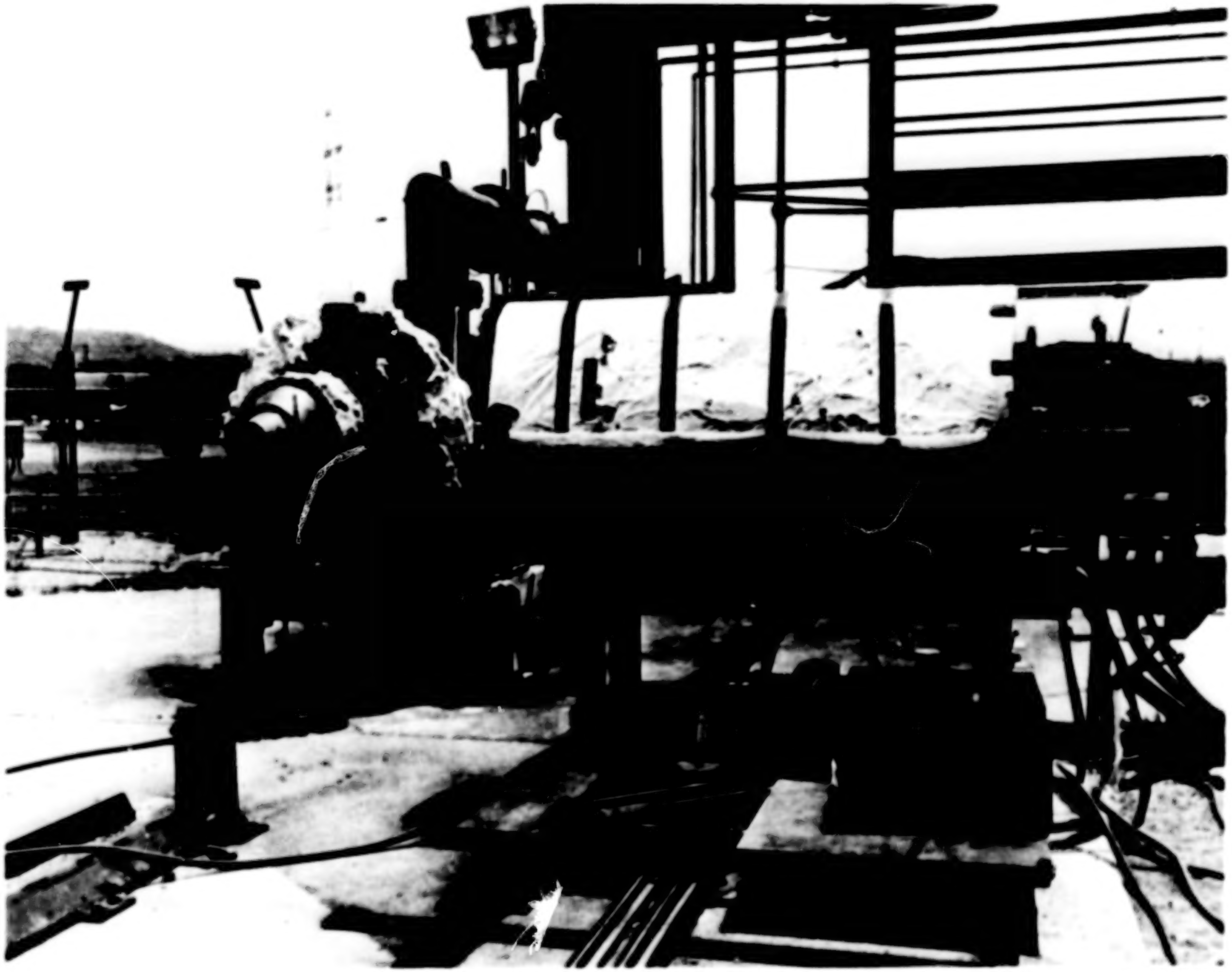

Figure 10. Laser Velocimeter Set Up at General Electric's JENOTS Facility.

The range of 85 inches (2.16 m) presented two problems. The first was the increased sensitivity to temperature gradients in the air intervening between the package and the sensitive volume. This causes a small decrease in accepted-data rate in cold weather, when convection gradients occur right at the front of the package where the laser beams emerge. The data rate is estimated to drop by 20% to 30% when the outdoor temperature is 25° F (269 K). The package temperature is usually held between 60° F (288.6 K) and 80° F (299.7 K) by a thermostat. The second problem caused by the range extension was a reduction in the return light power. This occurs because a six-inch (0.152 m) diameter lens was used at a greater distance (smaller solid angle of light collection). The reduction in light power collected was partly compensated for by increasing the electrical gain of the photomultiplier through use of higher supply voltage; however, this resulted in greater shot (light quantum) noise reaching the LV processor. As a result, the percentage of laser Doppler bursts validated dropped by a factor of perhaps two.

3.2.2.2 LV Actuator and Seeding

A remotely actuated platform is used which allows motion in three directions: vertical, horizontal, and axial. Travel capabilities are 32 inches (0.813 m), 32 inches (0.813 m) and 240 inches (6.1 m), respectively. Resolution was ±1/16 inch (0.1588 cm) for each axis except for the last 208 inches (5.28 m) of axial travel, which has a resolution of ±1/8 inch (0.3175 cm).

Seeding is by injection of aluminum oxide (Al_2O_3) powder, nominal one-micron diameter, into the supply air to the burner and into the region of the nozzle so as to seed the entrained air. The powder-feeder equipment used is reported in Reference 2, Chapter V, Section 3, except that the fluidized bed column supply air was heated to about 250° F (394.1 K) to prevent powder aggregation by moisture absorption.

3.2.2.3 Signal Processing and Recording

The laser velocimeter signal processor used is a direct-counter (time-domain) type similar to that reported in Reference 2, Chapter V, but with some improvements. These improvements result in a lowered rate of false validations and improved linearity and resolution. Turbulent velocity probability distributions (histograms) were recorded by a NS633 pulse-height Analyzer, 256-channel, and dumped into an X-Y plotter.

3.3 DATA REDUCTION METHODS

This section describes the key elements of the data reduction techniques used for acoustic, LV, and aerodynamic-performance data including operating procedures, corrections, analysis procedures, and data ouput formats.

3.3.1 Acoustic Data Reduction

3.3.1.1 JENOTS Data Reduction Systems

Standard data reduction is conducted in the General Electric Instrumentation and Data Room (IDR), as illustrated in Figure 11. During acoustic testing a tone is inserted on the tape recorder to mark the point on the tape where recording of the microphone signal for a given acoustic test point is initiated. During the data-reduction phase a tape control unit automatically shuttles the tape, initiating an integration-start signal to the analyzer at this tone as the tape moves in its forward motion. This motion continues until an integration-complete signal is received; then the tape control unit switches to the next channel, the tape rewinds, and process is repeated. When all channels are complete, the tape moves forward to the next data point on the magnetic tape.

All one-third-octave analyses are performed on a General Radio 1921 one-third-octave analyzer. Normal integration time is set for 32 seconds to ensure good integration for the low frequency content. The analyzer has a one-third-octave filter set for 12.5 Hz to 100 kHz and has a rated accuracy of ± 1/4 dB in each band. Each data channel is passed through an interface to the GEPAC 30 computer where the data are corrected for the frequency response of the microphone and the data acquisition system and corrected to Standard Day (59° F, 70% relative humidity) atmospheric attenuation conditions per References 4 and 5 (SAE ARP866 Standards) to 8 kHz and per GE corrections (see Section 3.3.1.2) from 10 kHz to 80 kHz. The output of the computer is passed to a Terminet 300 console where the corrected SPL (sound pressure level) can be printed out on sheets for "quick look" analysis. For calculation of acoustic power, corrections for ground reflections to free field, scaling to other nozzle sizes, or extrapolations to different far-field distances the data are sent to the Honeywell 6000 computer for data processing where the data are processed through the full-scale data reduction (FSDR) program, and the appropriate calculations are performed. The data printout is accomplished on a high speed "remote" terminal. A magnetic tape is also written for CALCOMP plotting of the data.

3.3.1.2 Air-Attenuation Corrections

Testing outdoors is subject to changes in the ambient air temperature and humidity from day to day, and the attenuation of sound over the distance from the jet source to the microphone will change with the environment due to differences in atmospheric absorption. It is common practice to attempt to account for these differences by either correcting the data for air attenuation from the measured day values to a "standard day" of 59° F (288 K) and 70% relative humidity, or by removing all the air attenuation from the data. These corrections have been calculated using References 4 and 5. This work extended the experimental data of Reference 6 (Harris) taken at 68° F (293 K) to other temperatures using the theoretical work of Reference 7 (Knesner). Reference 6 experiments, however, were only

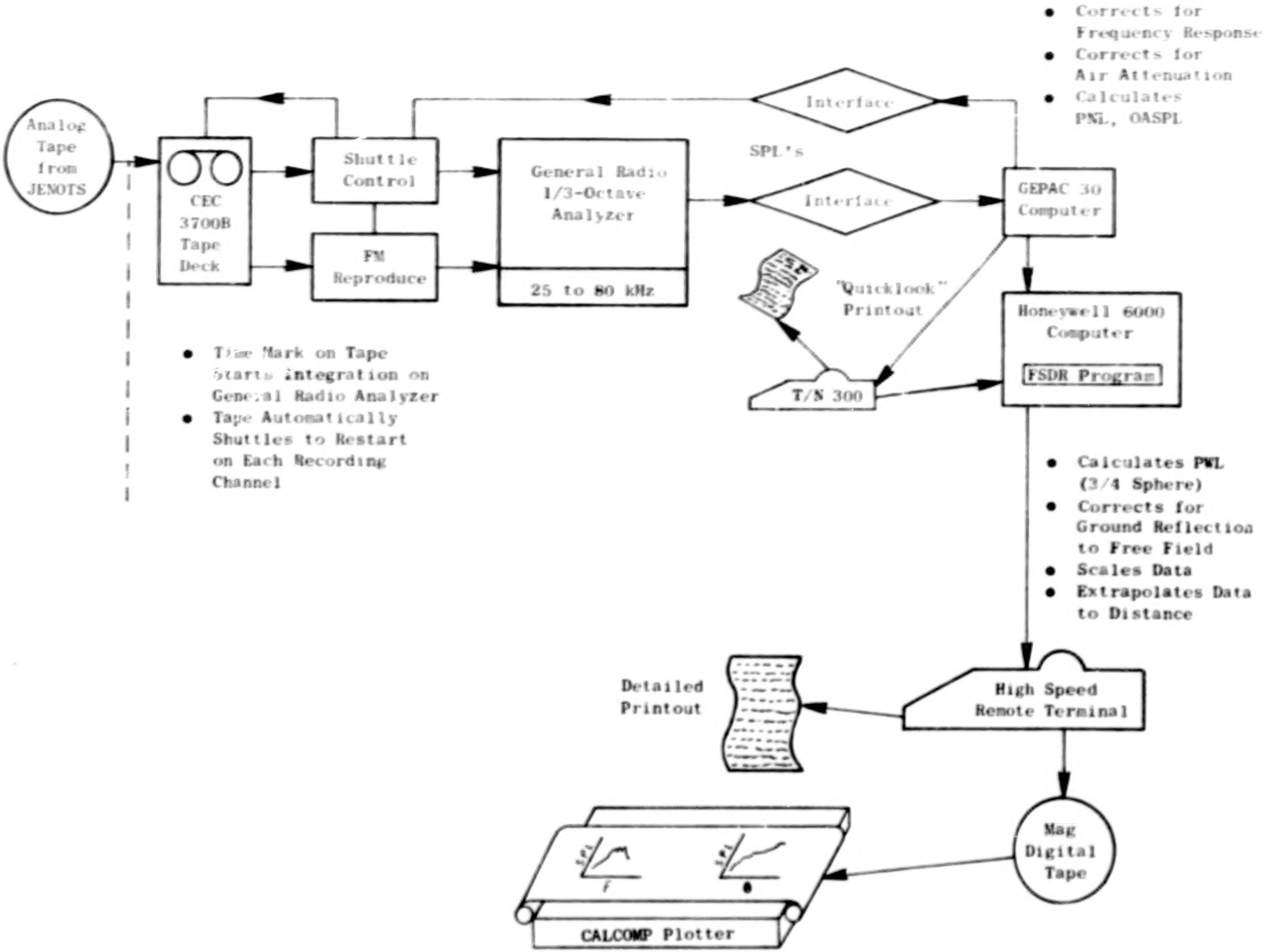
Analog Tape from JENOTS
CEC 3700B Tape Deck
Shuttle Control
FM Reproduce
General Radio 1/3-Octave Analyzer
25 to 80 kHz
SPL's
Interface
Interface
GEPAC 30 Computer
• Corrects for Frequency Response
• Corrects for Air Attenuation
• Calculates PNL, OASPL
"Quicklook" Printout
T/N 300
Honeywell 6000 Computer
FSDR Program
• Time Mark on Tape Starts Integration on General Radio Analyzer
• Tape Automatically Shuttles to Restart on Each Recording Channel
• Calculates PWL (3/4 Sphere)
• Corrects for Ground Reflection to Free Field
• Scales Data
• Extrapolates Data to Distance
High Speed Remote Terminal
Detailed Printout
Mag Digital Tape
SPL
f
SPL
θ
CALCOMP Plotter

Figure 11. Acoustic Data Reduction System.

performed to the 12.5 kHz narrowband, and its corrections are limited to the 8 kHz one-third-octave band. The need for corrections at higher frequencies led to an extension to 80 kHz (Reference 8). These corrections were developed by extrapolations of the Reference 4 and 5 (ARP866) curves, tempered by the continual experience of comparing scaled jet spectra of nozzles ranging from 1 inch (2.54 cm) to 4 feet (1.219 m) in diameter. Reference 7 does not give an adequate description of the entire problem since, at frequencies well below the maximum absorption, there is a distinct systematic deviation from single-relaxation theory. To reconcile this discrepancy, References 9 and 10 recently developed a model for predictions at 68° F (293 K) for frequencies up to 100 kHz (but they do not recommend that the model be extrapolated to temperatures beyond a 5° spread).

The Reference 8 air-attenuation model as used in this program is discussed in Appendix A, including a listing of the computer program used to generate the high frequency factors. The air-attenuation correction is calculated using the dry and wet bulb temperatures recorded during the test. Figure 12 shows a comparison of the Reference 8 high frequency correction factors and the Reference 9 and 10 predicted factors, while Figure 13 compares the Reference 9 and 10 factors to the extrapolated Reference 4 and 5 (SAE/ARP866) corrections. The Reference 8 model tends to underpredict, and the extrapolated Reference 4 and 5 model generally overpredicts the attenuation factors relative to References 9 and 10. The differences between the three approaches are sufficiently large that significant errors could result, depending on how the model data is scaled up and the distance to which it is extrapolated. The proper air attenuation model for frequencies above 10 kHz is expected to be resolved by current NASA-Lewis-sponsored investigations at the University of Mississippi (NASA CR-2760).

Figures 14 through 16 show measured noise levels for the unsuppressed, coannular nozzle with plug model recorded at JENOTS at the 40-foot (12.2 m) microphone distance corrected to standard day and free-field conditions (see Section 3.3.1.4), scaled up 8:1 (full size to model-size diameter ratio), and extrapolated from the 320-foot (97.5 m) arc to a distance of 2400 feet (731.5 m). The results were then corrected according to Reference 8, and according to References 4 and 5, in order to evaluate the impact of one technique versus the other. The acoustic range selected corresponds to about the maximum noise level to be monitored at the FAR part 36 sideline location, e.g. 2128 feet (648.6 m) with the aircraft at an altitude of 1110 feet (338.8 m). Figure 14 presents the comparison of one-third-octave band power level spectra, and Figure 15 presents comparisons of one-third-octave band sound pressure level at inlet angles (θ_I) of 50°, 90°, and 130° respectively. Although this figure shows differences in the high frequency region, their Noy weighting as reflected in the perceived noise level (PNL) directivity plot of Figure 16 is seen to have no impact on the resulting PNL. Since all the scale-model data taken in the program exhibited spectral characteristics similar to those discussed above, the air-attenuation model applied (Appendix A) was considered sufficient for all practical purposes.

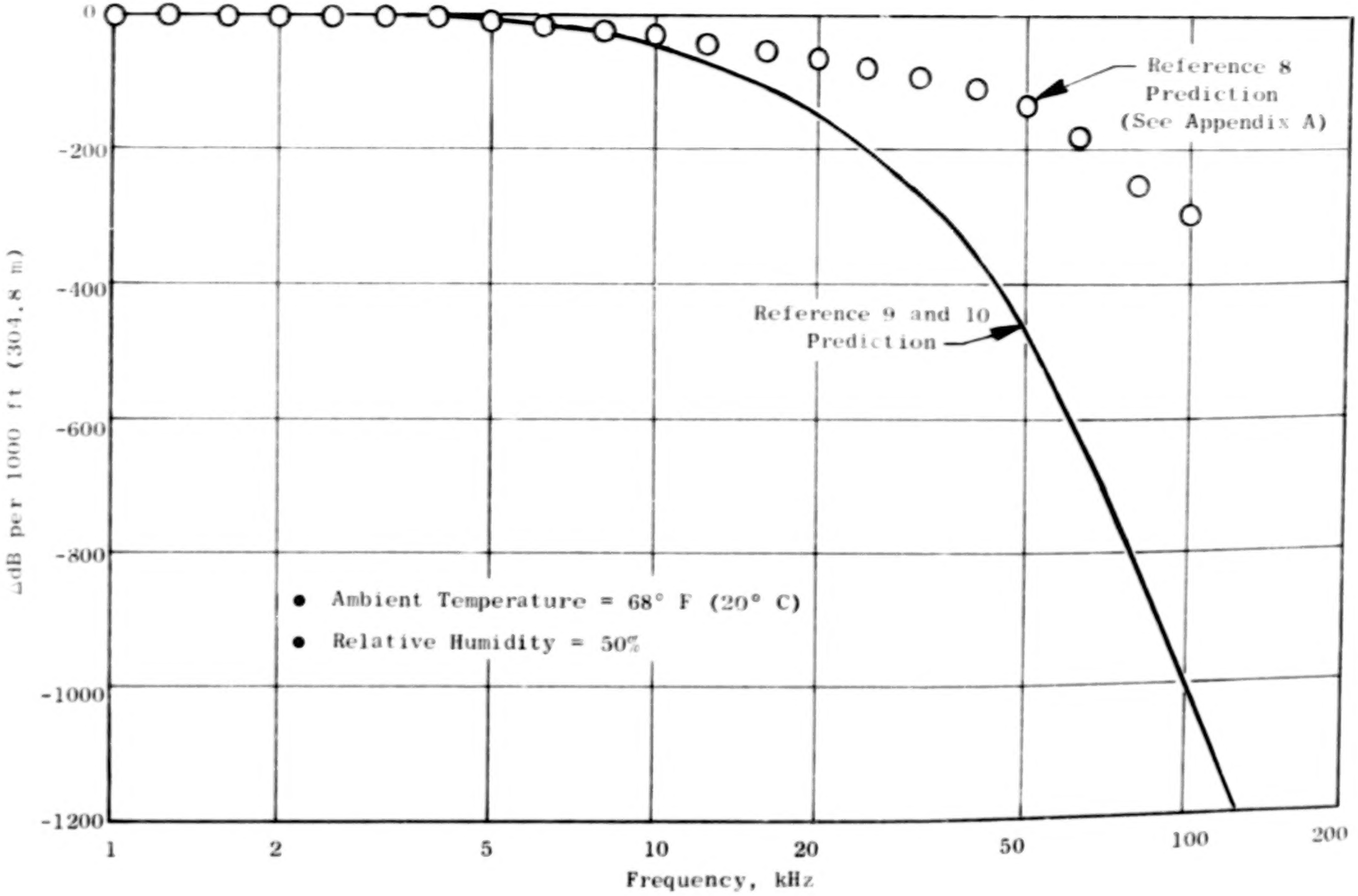

Figure 12. Comparison of Alternate Air-Attenuation Models.

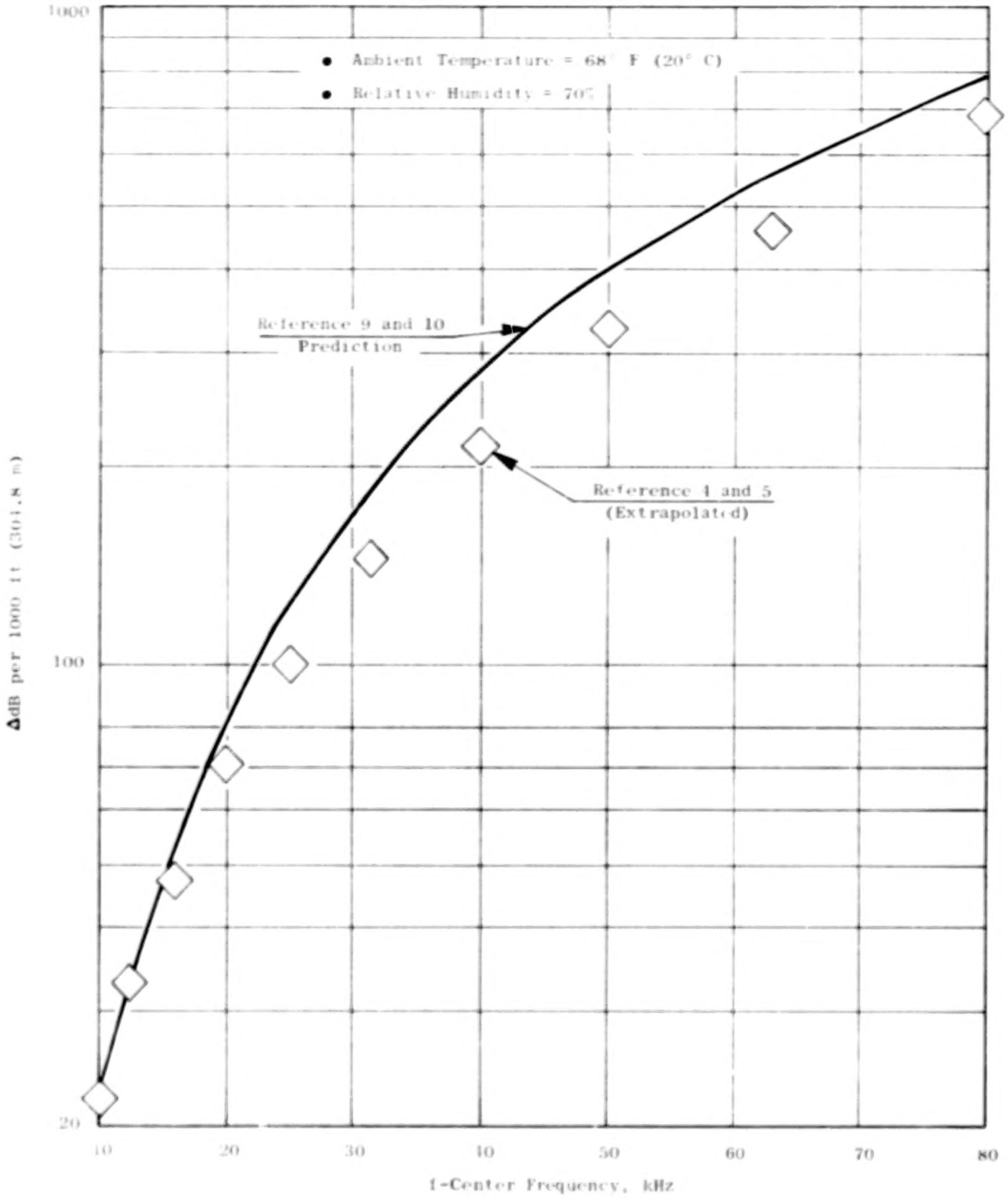

Figure 13. Comparison of Alternate Air-Attenuation Factors.

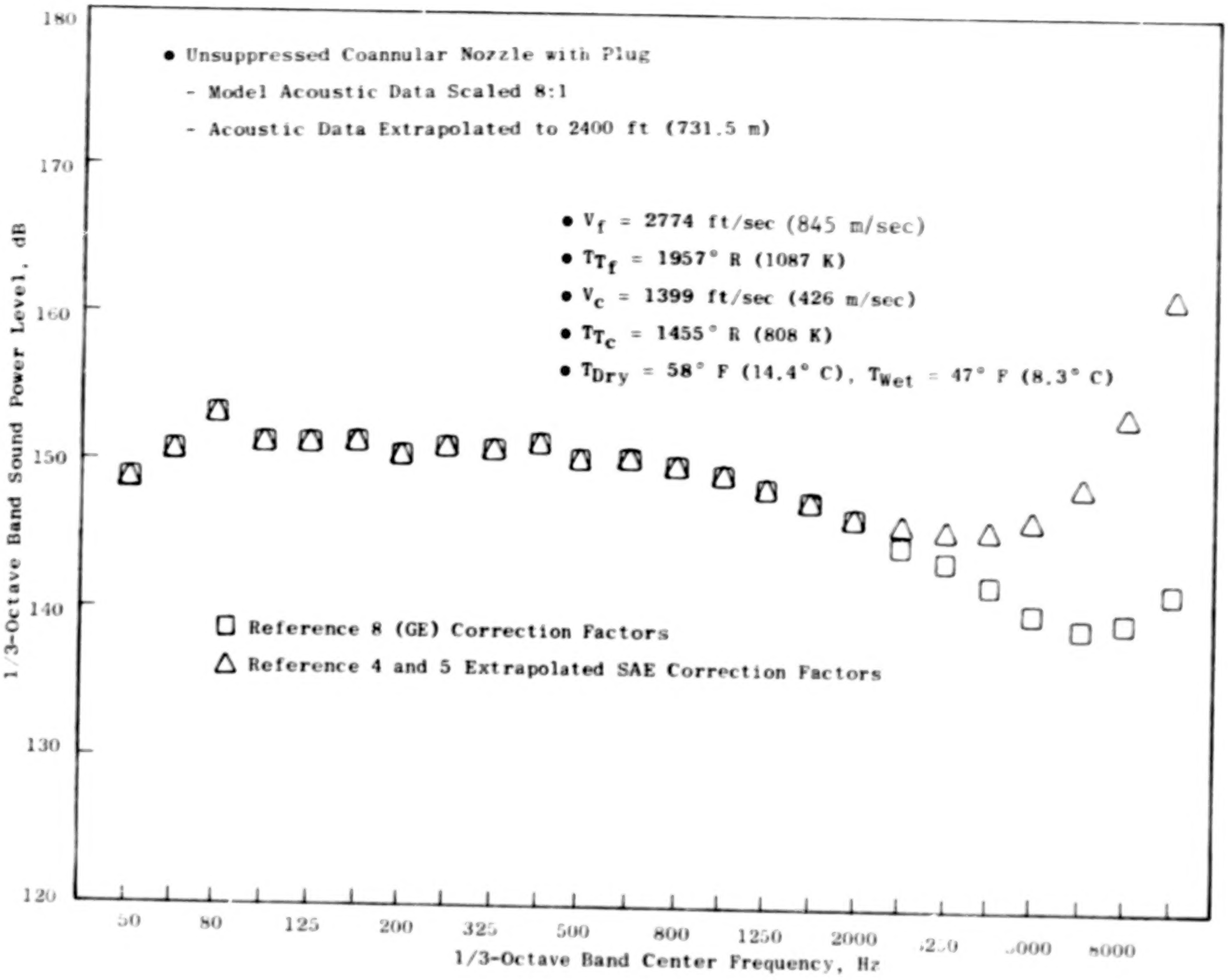

Figure 14. PWL Spectra Comparison Between DBTF Data Utilizing GE Correction Factors and Extrapolated SAE Correction Factors.

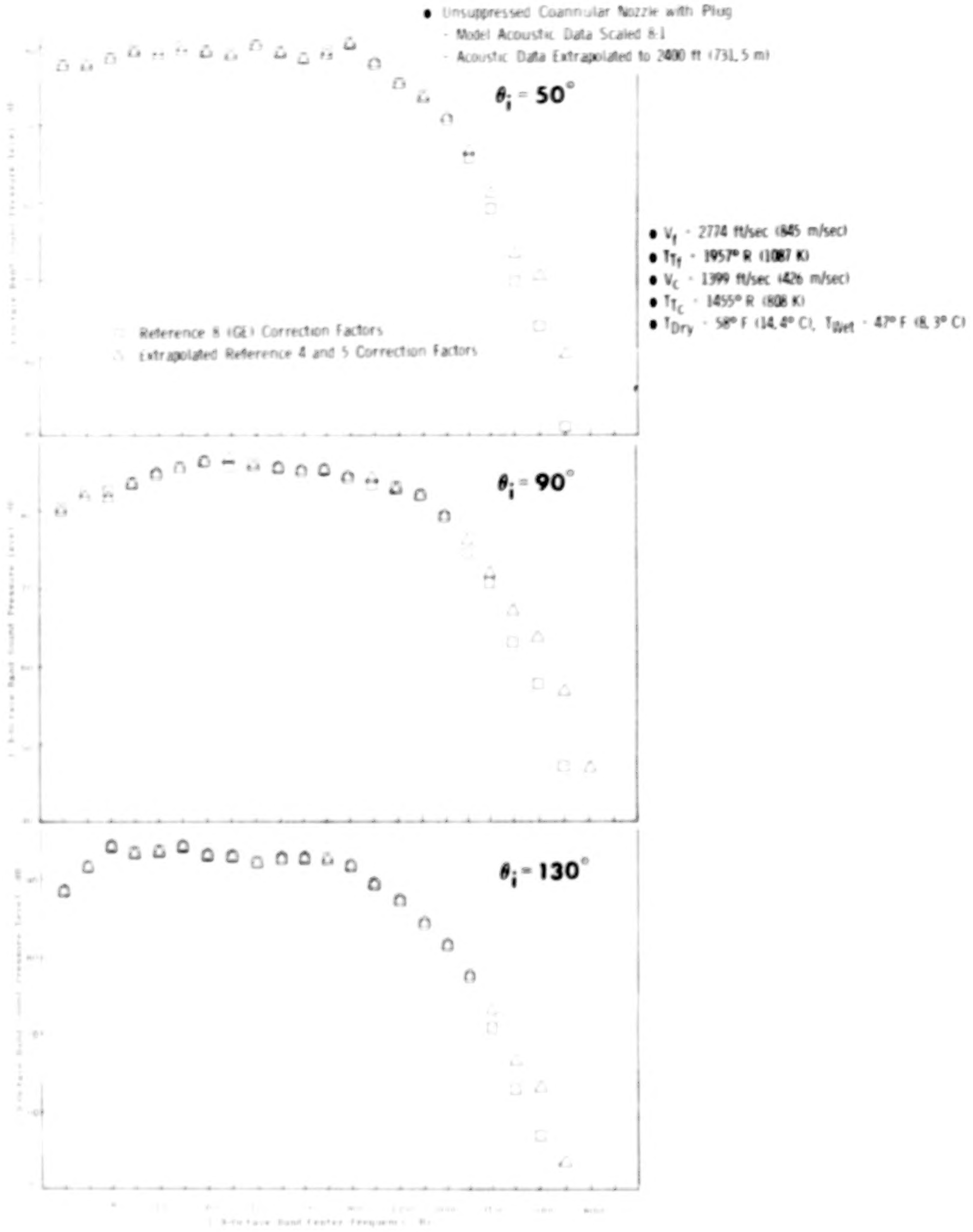

Figure 15. SPL Spectra Comparison Between DBTF Data Utilizing GE Correction Factors and Extrapolated SAE Correction Factors.

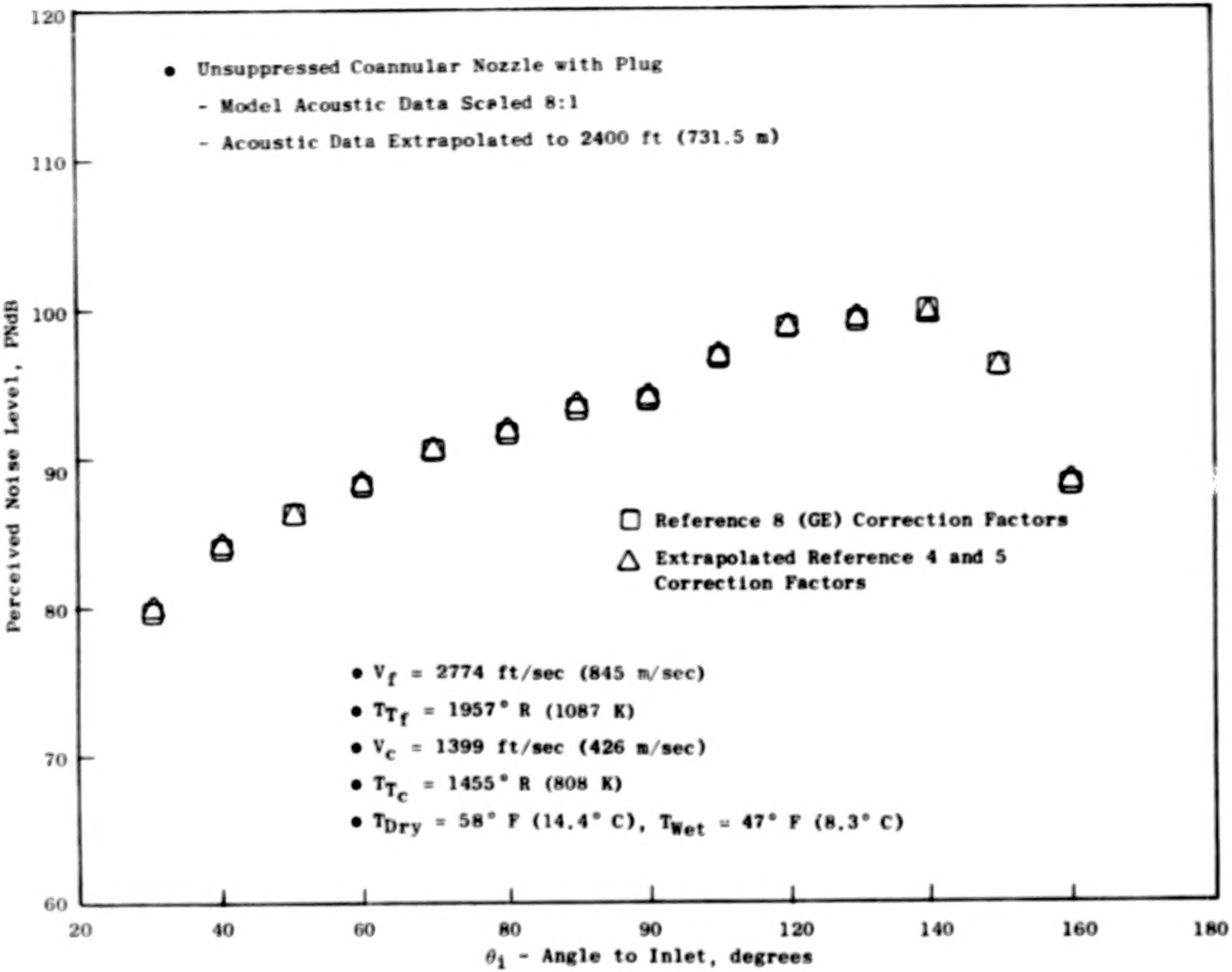

Figure 16. PNL Vs. Angle Comparison Between DBTF Data Utilizing GE Correction Factors and Extrapolated SAE Correction Factors.

3.3.1.3 Data-Scaling Procedure

The primary function of a scaling procedure is to present test data in a useful form for engineering evaluation. Prior to scaling, the model SPL's are conditioned as described in Section 3.3.1.1 (e.g. adjusted for test calibration factors and corrected to standard day). These model SPL's are then corrected to the source by removal of air attenuation (Reference 8) and extra ground attenuation (EGA), Reference 11.

Ground reflections are also removed from all data prior to scaling, as will be described in Section 3.3.1.4. The resultant spectrum frequencies are shifted on a one-third-octave basis as a function of nozzle diameter ratio (e.g., $(\lambda_{full\ scale}/\lambda_{model\ scale})$. Absolute level is adjusted by the weight flow ratio (which is assumed equal to the square of the diameter ratio). The resultant spectrum is extrapolated to the desired sideline or flyover path using the inverse square law (20 log distance) and atmospheric absorption. EGA was not used in the scaling subroutine. Figure 17 schematically shows how the model-scale data is processed for scaling.

3.3.1.4 Data Corrections to a Free-Field Environment

The presence of ground at JENOTS affects the propagation of noise reflection/absorption. The approach taken to convert the measured noise data to the "free field" was based on theoretical analysis of the ideal case of an infinitely hard surface, a point source of broadband noise, and a stable homogeneous medium (Reference 12). The analysis was modified by a series of tests and parametric studies conducted in Task 1 of the FAA High Velocity Jet Noise Source Location and Reduction Program, Contract DOT-OS-30034 (Reference 13). This involved the determination of the ground impedance phase factor and reflection coefficient, an estimate of the scattering phenomenon, and a correction for the distributed source effects of the jet. The results of the calculations are shown in Table 1. These values were incorporated into the data reduction program as standard ground reflection corrections for all JENOTS data.

3.3.1.5 Power Level Calculation

The method used to calculate sound power levels from the corrected SPL's is to integrate sound pressure levels assigned to strip areas based on the input microphone radius and acoustic angles of interest. The method used in the computer program is detailed in Appendix B **for a three-quarter sphere. All data presented herein has been adjusted up by 1.3 dB to represent full-scale spherical radiation.**

3.3.1.6 Acoustic Measurement Errors, Electronic Noise Floor

There are some limitations of the data acquisition and reduction systems which are attributable to electronic noise. An investigation of electronic

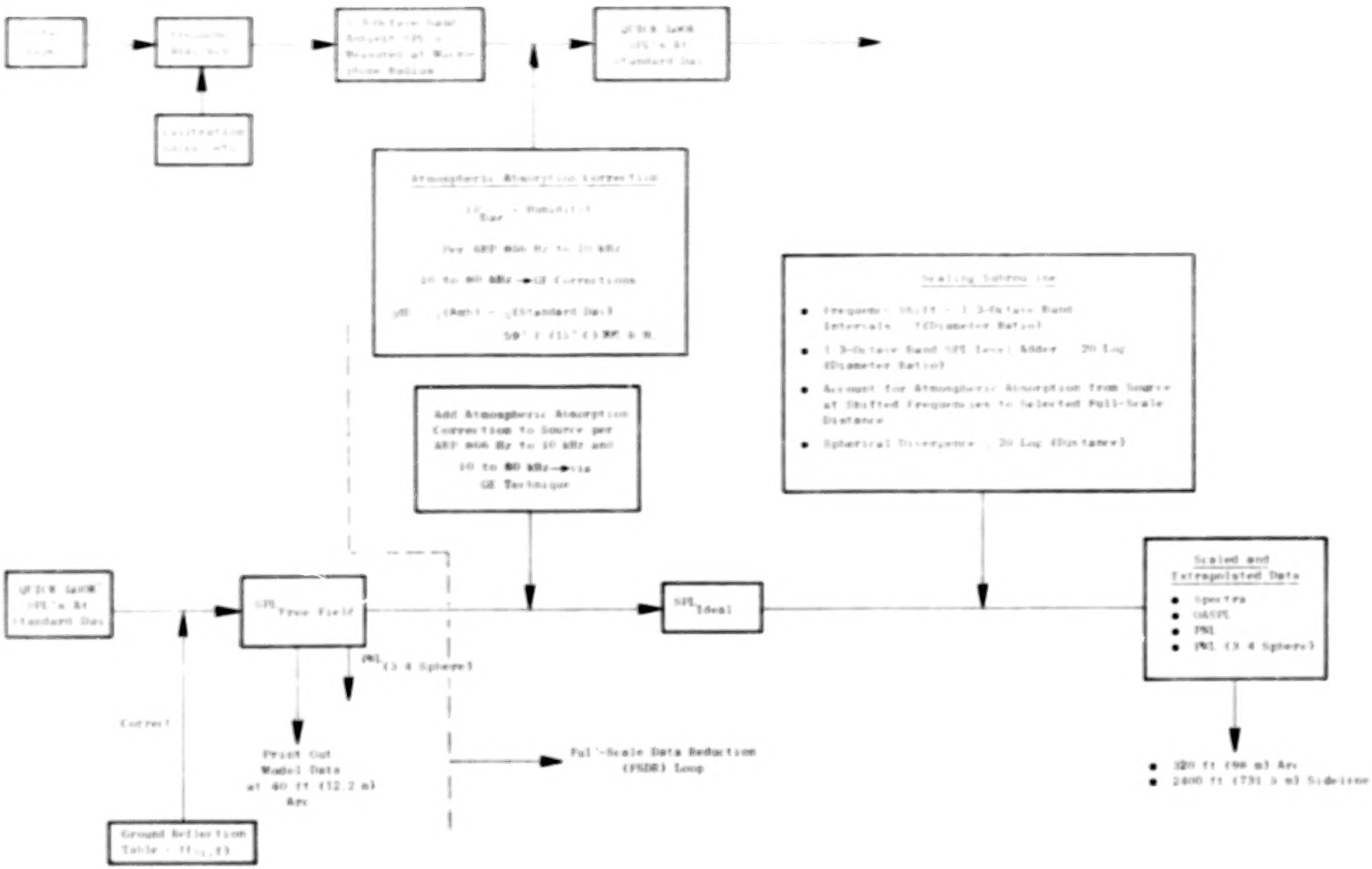
Data Tape
Frequency Analysis
Calibration Signals, etc.
1/3-Octave Band Analyzed SPL's Measured at Microphone Radius
QUICK LOOK SPL's At Standard Day
Atmospheric Absorption Correction
(T_Dew - Humidity)
Per ARP 866 Hz to 10 kHz
10 to 80 kHz → GE Corrections
ΔdB = α(Amb) - α(Standard Day)
59° F (15° C) 70% R.H.
Scaling Subroutine
Frequency Shift = 1/3-Octave Band Intervals = f(Diameter Ratio)
1/3-Octave Band SPL Level Adder = 20 Log (Diameter Ratio)
Account for Atmospheric Absorption from Source at Shifted Frequencies to Selected Full-Scale Distance
Spherical Divergence = 20 Log (Distance)
Add Atmospheric Absorption Correction to Source per ARP 866 Hz to 10 kHz and 10 to 80 kHz → via GE Technique
QUICK LOOK SPL's At Standard Day
SPL Free Field
SPL Ideal
PNL (3/4 Sphere)
Correct
Print Out Model Data at 40 ft (12.2 m) Arc
Ground Reflection Table = f(θi, f)
Full-Scale Data Reduction (FSDR) Loop
Scaled and Extrapolated Data
Spectra
OASPL
PNL
PNL (3/4 Sphere)
320 ft (98 m) Arc
2400 ft (731.5 m) Sideline

Figure 17. Scale-Model and Full-Scale Data Reduction Operations.

Table I. JENOTS Ground Reflection Corrections (ΔdB's to be added to SPL's).

Frequency (Hz)	Angle to Inlet, degrees													
	30	40	50	60	70	80	90	100	110	120	130	140	150	160
50	-4.99	-4.97	-4.93	-4.88	-4.82	-4.75	-4.66	-4.55	-4.41	-4.24	-4.03	-3.77	-3.46	-3.1
63	-4.45	-4.41	-4.35	-4.29	-4.21	-4.1	-3.98	-3.82	-3.64	-3.42	-3.16	-2.86	-2.52	-2.19
80	-4.0	-4.0	-3.34	-3.23	-3.1	-2.95	-2.76	-2.53	-2.27	-1.96	-1.61	-1.22	-0.83	-0.47
100	-4.0	-4.0	-3.0	-3.0	-3.0	-2.0	-0.7	-0.34	-0.07	0	0	1.6	2.11	2.54
125	-3.5	-4.0	-3.5	-2.0	-2.5	-0.5	1.7	1.0	1.0	2.0	2.0	2.9	3.8	2.8
160	0	-1.5	-2.5	-0.5	-1.0	1.5	2.7	1.5	3.0	3.0	2.0	3.0	3.2	2.2
200	-2.0	-1.5	-1.5	-1.0	-1.0	0.5	0	0	0.5	1.0	-0.17	-0.65	-1.03	0
250	0	0	0	-0.5	-1.5	-1.5	-2.5	-2.5	1.5	-1.0	-2.0	-4.48	-4.58	-2.39
315	1.5	0	-1.5	-1.5	-1.5	-1.8	-4.0	-1.5	-3.0	-3.0	-3.0	-4.9	-5.09	-2.0
400	-2.0	-4.2	-4.1	-3.5	-2.5	-3.2	-3.1	-2.34	-1.85	-1.34	-4.9	-0.37	-0.7	-4.3
500	-1.0	-1.0	0	-1.3	-1.1	-1.2	-1.1	-1.35	-1.14	-1.87	-2.1	+1.8	-0.5	-0.5
630	-1.64	-1.5	-1.0	-2.5	-2.0	-3.2	-2.1	-2.09	-2.03	-3.5	-3.5	-1.64	-1.3	-0.9
800	-1.55	-1.35	-1.12	-1.0	-1.0	-2.0	-2.1	-0.88	-1.22	-0.5	-1.05	-0.5	-0.8	+2.2
1000	-1.0	-2.44	-1.3	-2.36	-2.3	-2.13	-1.9	-1.72	-1.47	-1.22	-2.1	-1.9	-0.71	-0.8
1250	-1.97	-2.03	-2.10	-2.17	-2.24	-2.28	-2.3	-2.28	-2.24	-2.18	-2.12	-2.08	-2.04	-2.2
1600	-2.17	-1.5	-2.06	-1.98	-1.90	-1.83	-1.8	-1.83	-1.93	-2.07	-2.23	-2.36	-2.45	-2.5
2000	-0.74	-2.0	-2.8	-0.92	-1.11	-1.37	-1.7	-1.90	-2.05	-2.10	-2.06	-1.97	-1.88	-1.8
2500	-1.5	-2.0	-1.8	-2.84	-2.70	-2.52	-2.35	-2.29	-2.31	-2.37	-2.45	-2.51	-2.54	-2.56
3150	-2.57	-2.57	-2.60	-2.66	-2.78	-2.93	-3.1	-3.14	-3.07	-2.91	-2.75	-2.65	-2.6	-2.59
4000	-2.80	-2.78	-2.74	-2.66	-2.58	-2.55	-2.60	-2.67	-2.72	-2.72	-2.72	-2.72	-2.72	-2.71
5000	-2.69	-2.72	-2.77	-2.84	-2.90	-2.85	-2.60	-2.41	-2.36	-2.44	-2.52	-2.56	-2.58	-2.59
6300	-2.70	-2.68	-2.64	-2.59	-2.56	-2.64	-2.90	-2.97	-2.85	-2.72	-2.68	-2.66	-2.66	-2.66
8000	-2.76	-2.76	-2.75	-2.73	-2.67	-2.60	-2.70	-2.80	-2.78	-2.74	-2.72	-2.71	-2.7	-2.7
10000	-2.69	-2.69	-2.68	-2.67	-2.67	-2.71	-2.80	-2.70	-2.60	-2.63	-2.65	-2.65	-2.65	-2.65
12500	-2.70	-2.70	-2.71	-2.69	-2.69	-2.70	-2.70	-2.70	-2.66	-2.66	-2.66	-2.66	-2.66	-2.66
16000	-2.61	-2.61	-2.61	-2.60	-2.58	-2.56	-2.70	-2.60	-2.57	-2.57	-2.57	-2.57	-2.57	-2.57
20000	-2.63	-2.63	-2.63	-2.62	-2.61	-2.61	-2.70	-2.56	-2.60	-2.60	-2.59	-2.59	-2.59	-2.59
2500	-2.71	-2.71	-2.71	-2.70	-2.70	-2.69	-2.70	-2.68	-2.68	-2.68	-2.67	-2.67	-2.67	-2.66
31500	-2.74	-2.73	-2.73	-2.73	-2.72	-2.72	-2.70	-2.71	-2.71	-2.70	-2.70	-2.69	-2.69	-2.69
40000	-2.71	-2.71	-2.71	-2.71	-2.70	-2.70	-2.70	-2.69	-2.68	-2.68	-2.68	-2.67	-2.67	-2.67
50000	-2.73	-2.73	-2.73	-2.73	-2.72	-2.72	-2.70	-2.71	-2.70	-2.70	-2.70	-2.69	-2.69	-2.69
63000	-2.70	-2.70	-2.70	-2.69	-2.69	-2.68	-2.70	-2.68	-2.67	-2.67	-2.66	-2.66	-2.66	-2.65
80000	-2.72	-2.72	-2.72	-2.71	-2.71	-2.71	-2.70	-2.70	-2.69	-2.69	-2.68	-2.68	-2.68	-2.68

noise-floor spectral shape was undertaken, and typical results are shown in Figure 18. One of plots in Figure 18 represents the frequency distribution of the electronic noise floor for the JENOTS electronic system; it was obtained by removing the microphone from the cathode follower and replacing it with a shorting cap.

Several distinct characteristics are apparent. The first is the relatively constant level from 50 Hz to 400 Hz and from 1600 Hz to 10 kHz. The fact that this flat region shifts uniformly with the 10-dB gain steps and vanishes at the highest setting indicates that this portion of the spectra is associated with the tape recorder electronics. The second characteristic is the peculiar peaks occuring in the bands from 500 Hz to 1250 Hz. The fact that the shape is maintained and shifted uniformly with amplifier gain, and that it tends to "sink into the mud" at the highest gain, implies that the phenomenon is associated with the tape recorder electronics. The third spectral characteristic is the 6-dB-per-octave ramp occurring at high frequency. As the tape recorder gain is increased, more of this ramp is uncovered and the upswing occurs at an earlier frequency. This is believed to be electronic noise from the cathode follower, power supply, and line drivers responding to the preemphasis built into the line driver frequency response. Of the three sources, the cathode follower is the noisiest. In a similar test, B&K 4135 1/4-inch (0.635 cm) microphones were left on the cathode follower and the microphones were covered by a pistonphone calibrator; similar characteristics were observed (see Figure 18). The low frequency portion of the spectra is dominated by ambient acoustic signals which are leaking into the pistonphone.

Given the nominal values for noise floor quoted in the equipment specifications, it is apparent that the tape recorder 38-dB dynamic range is the limiting floor at most gain settings for jet noise measurements. In the course of acquiring data in this test program, several test points were inadvertently taken where a higher gain setting should have been used. This deterioration of the dynamic range was reflected in the spectrum level above 50 kHz. No attempt was made to correct the acoustic results presented herein since the error associated with this loss in dynamic range causes a change in sound power level of less than 0.5 dB on an overall basis.

3.3.2 Laser Velocimeter Data Reduction

3.3.2.1 Basic Idea for LV rms Measurements

The concept of using laser velocimeter measurements for obtaining routine mean- and turbulent-velocity profiles may be described in the following simple fashion. Two beams of monochromatic light intersect at a point in space and set up a fringe pattern of known spacing (see Figure 19). The flow is seeded with small particles which pass through the measuring volume; the light scattered from the particles is collected, and the laser signal processor measures the time it takes for the particles to pass through each fringe. Knowing the distance and time for each validated

• Microphone System with Shorted Cathode Follower

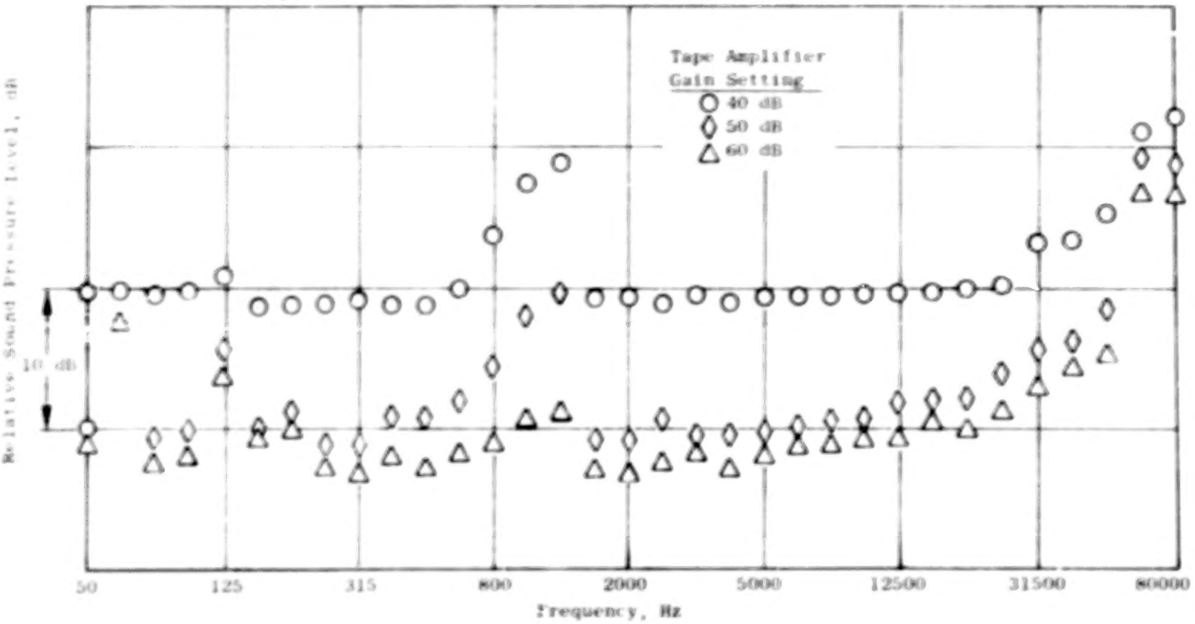

• Microphone Covered by Piston-Phone

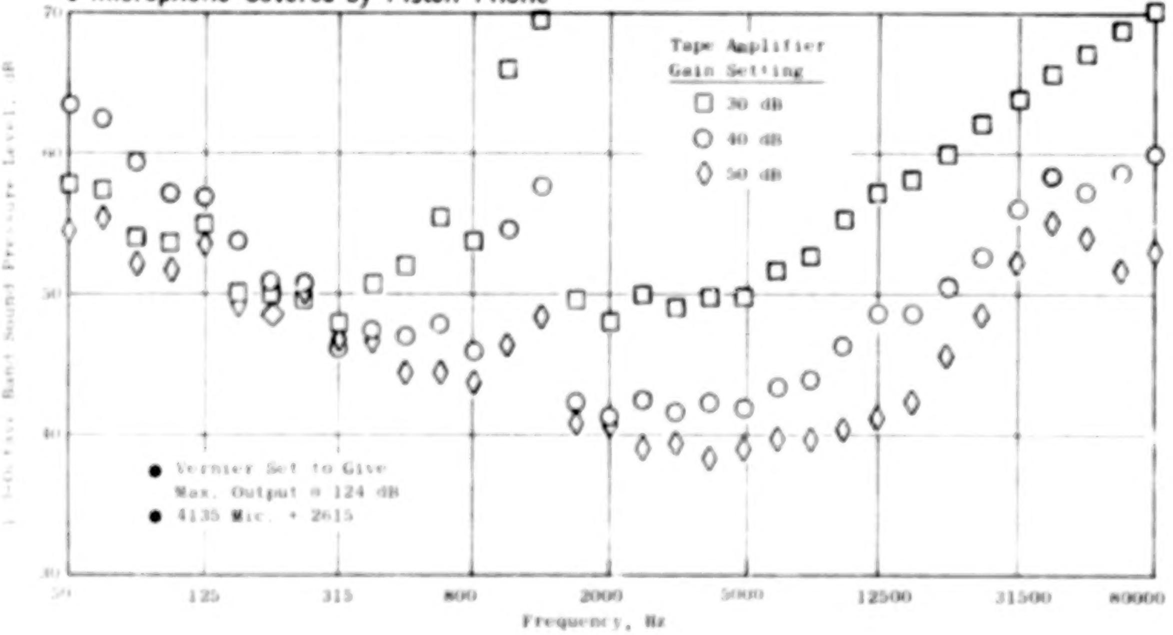

Figure 18. Typical Electronic Noise Floor Spectra for Electronic System at JENOTS.

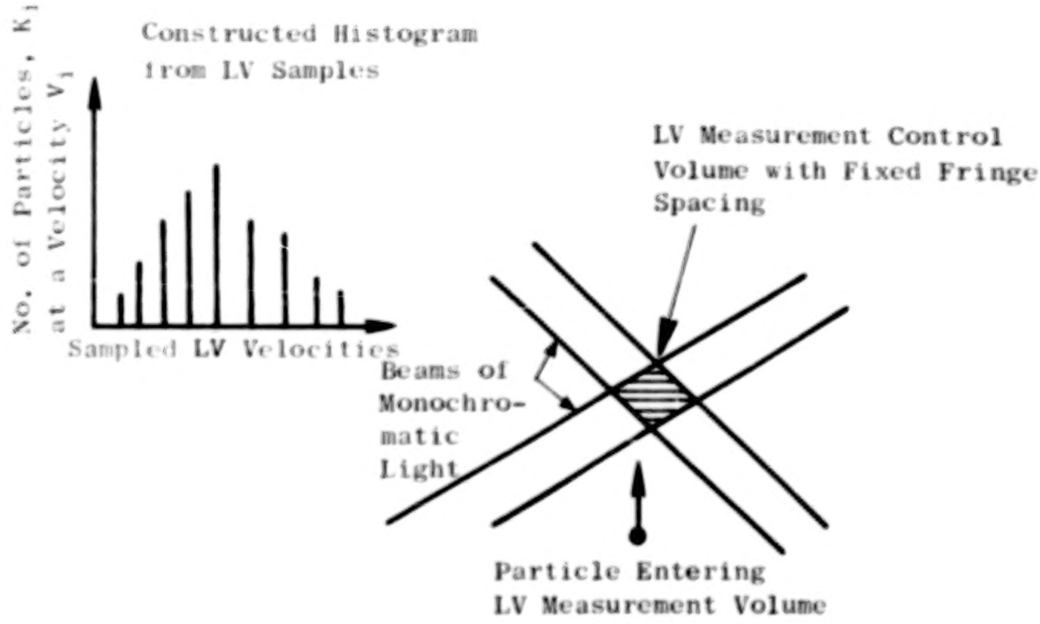
Constructed Histogram
from LV Samples
No. of Particles, K_i
at a Velocity V_i
Sampled LV Velocities
LV Measurement Control
Volume with Fixed Fringe
Spacing
Beams of
Monochro-
matic
Light
Particle Entering
LV Measurement Volume

Figure 19. Schematic of Laser Velocity Measurements.

particle enables the construction of the usual histogram (see insert on Figure 19). Then, by statistical techniques, the mean value (which corresponds to the mean velocity) and standard deviation (which corresponds to the turbulent velocity) are constructed. Although the principle of measurement is easy, the practical aspects of designing an electronic processing unit to monitor valid particles is of no small consequence. Investigators have had great difficulty performing measurements even in low velocity jets, and the extension to heated supersonic jet measurements represents a major achievement. The method of calculation used to obtain the mean velocity and turbulent velocity from laser velocimeter measurements is described below.

3.3.2.2 The Histogram

A histogram is an estimate of the first-order probability density of the amplitude of a given sample. To obtain a velocity histogram, the time-dependent laser velocimeter velocity, V(t), is accumulated and divided into classes bounded by values of velocity increments Vi. For each independent sample of velocity, a class interval is formed such that Vi < V(t) < Vi+1. During a measurement period, Ki number of velocity samples are accumulated in each sample class Vi. From the total sample of measured velocity points the histogram is constructed as shown in Figure 19. The mean velocity and turbulent velocity derived from the histogram are obtained as described below.

3.3.2.3 Mean Velocity

The mean velocity of the jet, V_J, obtained from the discrete velocity samples is calculated by:

$$V_J = \sum_{\substack{\text{class}\\ \text{interval}}} \left(\frac{V_{i+1} + V_i}{2} \right) \frac{K_i}{N}$$

where

$\frac{V_{i+1} + V_i}{2}$ is the value of the sampled axial velocity component at the center of the class interval

K_i is the number of velocity samples in the class interval

N is the total number of velocity samples ($N = \sum K_i$) in the histogram

[illegible] Turbulent Velocity

To obtain the rms turbulent velocity, u', from the sampled data of each of the histograms, the standard square root of the statistical variance is needed. This calculation is performed using the following equation:

$$u' = \left[\sum_{\substack{\text{All Classes} \\ \text{Intervals}}} \left(\frac{V_{i+1} + V_i}{2} - V_B \right)^2 \frac{K_i}{N} \right]^{\frac{1}{2}}$$

[illegible] Statistical Errors for LV Mean and Turbulent Velocity Measurements

With such large data samples, as obtained through the collection of velocity samples in a laser velocimeter histogram, guidelines for estimating the accuracy of each measurement are required. Tables II and III provide estimates of the percent error obtained for a mean velocity or turbulent velocity LV measurement.

Table II lists the percent error for a 95% confidence statement of a mean-velocity measurement as a function of the total number, N, of velocity samples contained in the histogram, and the turbulence level u'/V_B. Table III lists the percent error for a 95% confidence statement of the turbulent-velocity estimate as a function of N, the total velocity sample. As can be seen from Table II, a fairly small sample of velocity measurements are required to obtain a good estimate of the mean velocity. For the turbulent velocity, the number of data samples required for a good estimate increases substantially. The usual number of samples obtained with the General Electric Laser Velocimeter during a routine data-taking measurement performed during this program is between 2000 to 4000 data samples. For simple and steady-state-type information this amount of samples is sufficient. For more advanced measurements, such as turbulence spectra or two-point cross-correlations, many more data samples are required and are currently obtained on a routine basis.

[illegible] Aerodynamic-Performance Test Data Reduction

This section describes the data analysis procedures used in the aerodynamic-performance test program. Station notations are defined in Figure 7 under Aerodynamic-Performance Test Facility Description, Section 3.1.2. Further details of the data reduction methods are given in the Comprehensive Data Report (CDR) under separate cover.

Table II. Estimated Percent Error in the LV Measurement of Mean Velocity with 95% Confidence.

N	$u'/\bar{V}_f$			
	0.2	0.1	0.05	0.025
10	14.1	7	3.5	1.76
20	9.3	4.7	2.3	1.20
30	7.4	3.7	1.9	0.93
40	6.3	3.2	1.6	0.80
60	5.0	2.6	1.3	0.65
120	3.6	1.8	0.9	0.45

Table III. Estimated Percent Error for LV Turbulent Velocity Measurements with 95% Confidence.

N	Percent Error
20	31.5
40	21.8
60	17.8
120	12.6
240	9.12
480	6.45
960	4.56
5000	2.0
25000	0.89

3.3.3.1 Flow Rates

The mass flow rates through the test nozzles were determined using choked ASME long-radius metering nozzles. For the cold flow model tests, and for all ASME tests (Figure 7), the core nozzle flow rate was calculated at Station 1 and the fan nozzle flow rate was calculated at Station 4. For the hot flow tests (see Figure 7) on the multitube suppressor with ejector, the total model flow was supplied by the hot air supply. This total flow was metered with the choked ASME nozzle at Station 1 and then divided into the fan and core ducts. In order to determine the flow in each duct, special hot flow calibration tests were run. These tests consisted of assembling the test model on the stand with the core duct blanked off downstream of the plenum, thus discharging the entire metered flow through the fan nozzle. Flow data was taken with cold flow and with flow heated to each of the two temperatures encountered in model testing. Discharge flow coefficients were then calculated in the normal way, described in Section 3.3.3.2. These coefficients were calculated using the cold physical fan nozzle exit area such that any change in nozzle area due to temperature effects was accounted for in the flow coefficient. For the actual dual hot flow tests of the multitube suppressor with ejector the blank-off plate was removed, the flow coefficients determined by the calibrations were used to calculate the fan nozzle flow from the flow function, and the core flow rate was derived by subtracting the calculated fan nozzle flow from the metered total flow.

3.3.3.2 Discharge Coefficients

The discharge coefficient is defined as the ratio of the actual measured flow rate through the nozzle to the ideal isentropic flow rate at the flow temperature and pressure. The ideal flow rate is calculated from the flow function using the nozzle physical throat area and the flow temperature and pressure measured by the model instrumentation rakes as shown in Figure 7, Section 3.1.2. Discharge coefficients were calculated for both the core nozzle and the fan nozzle for each model.

3.3.3.3 Nozzle Thrust

The static thrust of an exhaust nozzle is defined as the axial exit momentum of the exhaust flow plus the excess of exit pressure over ambient pressure times the exit area:

$$F = \dot{W}V_e + (P_e - P_{am})A_e$$

The static thrust of the models in this test program was determined by applying the momentum equation to the control volume shown in Figure 7, (Section 3.1.2). The analysis of forces applied to the control volume includes entering stream thrusts F_1 and F_4 (stream thrust equals the momentum plus the static pressure times the area of the entering stream), a balance force (Q), various pressure-area terms and seal tare forces, and the exit stream thrust ($H + P_oA_e$). Summing these forces results in the following equation for the nozzle thrust:

$$H = F_1 + F_4 + P_2 (A_2 - A_1) + P_5 (A_5 - A_4) - P_o (A_2 + A_5) - Q$$

The entering stream thrusts, F_1 and F_4, were the exit stream thrusts of the respective choked, long-radius, ASME metering nozzles.

3.3.3.4 Thrust Coefficient

The static thrust coefficient of the exhaust nozzles is defined as the ratio of the measured nozzle thrust to the ideal thrust of the actual measured mass flow when expanded isentropically from P_T to P_o. For the present dual-flow tests, the ideal thrust is the sum of the fan nozzle ideal thrust and the core nozzle ideal thrust. The thrust coefficient is then:

$$C_T = \frac{H}{\dot{W}_f V_f + \dot{W}_c V_c}$$

The ideal thrusts where calculated using fan and core flow properties measured with the model instrumentation rakes.

3.3.3.5 FluiDyne Force Balance Calibration

The force balance calibration determines the output characteristics of both the force balance flexure and the elastic seals which provide pressure-tight expansion joints between the metric model assembly and the nonmetric facility structure. The output of the strain-gage flexure is very linear with applied load, but the seals provide an additional force which is a function of both axial load and seal pressure. Most of the force carryover results from radial seal deflections required to support the static pressure differentials across the seals when the ducts are pressurized. Consequently, the seal and balance assembly is calibrated under simulated operating conditions of axial load (deflection) and seal differential pressures. The calibration for the FluiDyne mixed-flow facility is further complicated by the fact that the vertical location of the applied horizontal load during a test is a function of the hot/cold-flow split and nozzle pressure ratios; the calibration, therefore, must duplicate both the magnitude and location of the net force which was experienced during a test. As a result of these requirements, it has been found expendient to calibrate "on-point," that is, to determine the balance output characteristics while simultaneously reproducing the horizontal force, force vertical location, and seal pressures experienced at a specific test point.

The horizontal force and force locations for each point are not known exactly until the on-point calibration is completed. The initial test data, therefore, are reduced (by computer) using a preliminary calibration. The computer is programmed so that as it reduces the initial test data it also prints out the required calibration information (calibration load and load location) such that an accurate on-point calibration then can be made.

Calibration consists of blanking off both air ducts in the metric part of the system so that the seals can be pressurized internally as they are during a test. The seals can be pressurized to simulate running levels, and a horizontal load is applied (at the proper vertical location) which gives the same balance output as that experienced at the particular test point being simulated. The apparent balance force, Q (which contains the seal force carryover), then is calculated as follows:

$$Q = L + \Delta P_2 A_2 + \Delta P_5 A_5$$

where: L is the applied calibration load

A_2 is the hot-flow seal duct area

A_5 is the cold-flow seal duct area

ΔP_2 is the pressure difference across the hot-duct seal

ΔP_5 is the pressure difference across the cold-duct seal

This balance force is then used in the equation for nozzle thrust prese d in Section 3.3.3.3.

3.3.3.6 Pressure and Temperature Data

Facility and model temperature data are obtained using shielded chromel/alumel thermocouples. Model total and static pressures were measured using multiple-tube mercury manometers and reduced to absolute pressures as well as dimensionless ratios: $(P/P_T)_f$, $(P/P_T)_c$, and P/P_o.

3.3.3.7 Data Quality

In order to demonstrate the FluiDyne facility data accuracy, two standard ASME long-radius nozzles were tested both prior to and at the conclusion of the model tests. Three combinations of the two nozzles were run: the ASME nozzle on the fan stream meter was run by itself with cold flow, the nozzle on the core stream meter was run by itself with hot flow, and the two nozzles were run simultaneously using cold flow. The checkout tests were made at nozzle pressure ratios and balance loads which were similar to those occurring during actual model testing.

The ASME results are shown in Figure 20 together with known or predicted performance for these nozzles. The known performance levels are based on semiempirical equations from Reference 14. Comparisons between known and measured values are made for three parameters: flow coefficient, thrust coefficient, and dimensionless stream thrust. The dimensionless stream thrust is defined by the equation.

$$f = \frac{H + P_o(A_c + A_f)}{(P_T)_c A_c + (P_T)_f A_f}$$

For ASME tests with both nozzles flowing, the predicted stream thrust and thrust coefficient were calculated from a thrust-weighted average of the predicted values for each of the two ASME nozzles.

The results of both series of ASME testing indicate excellent data accuracy and repeatability between the two tests.

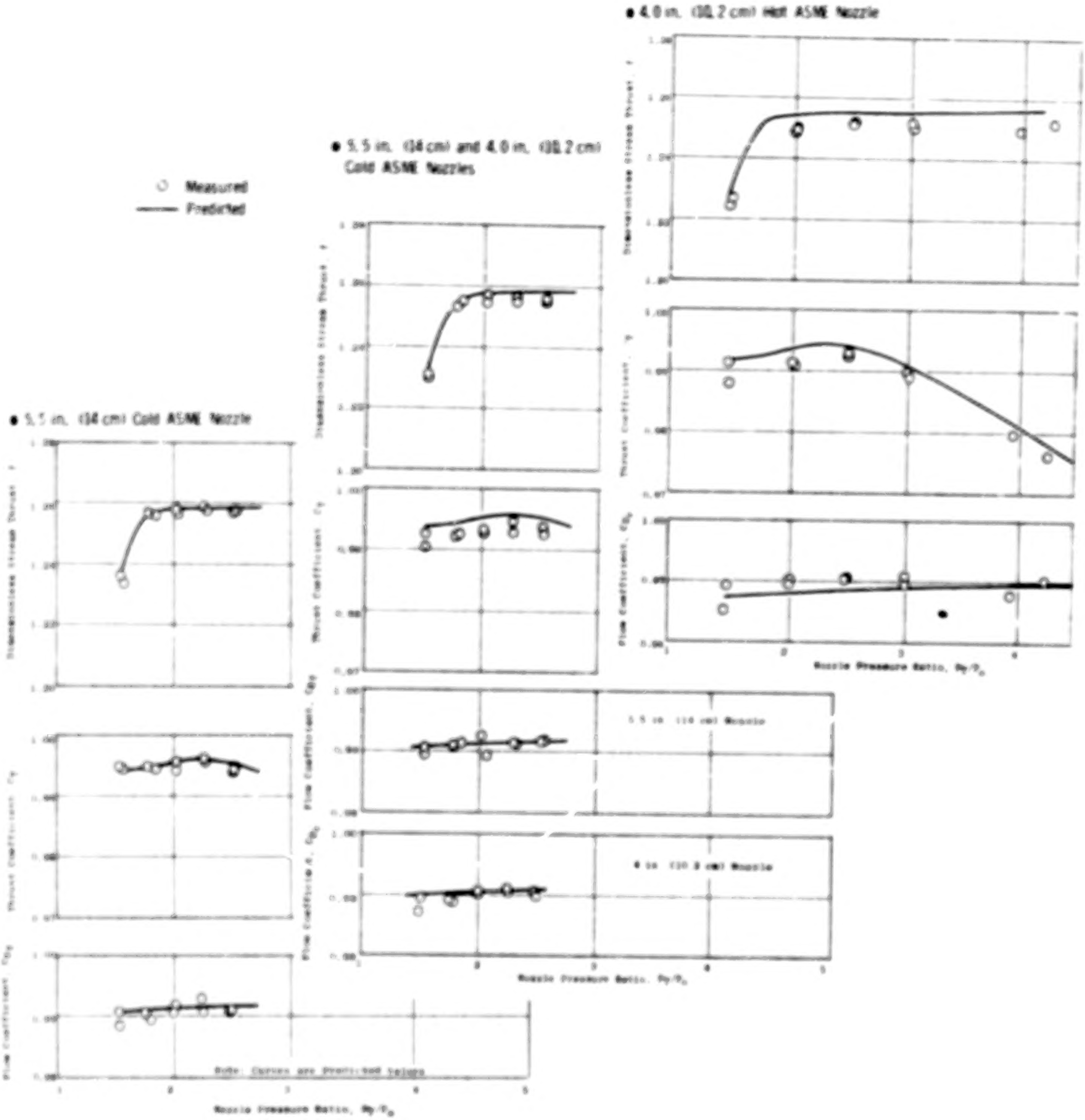

Figure 20. Comparison of Measured and Predicted Thrust and Flow Coefficients for Various ASME Nozzle Setups at FluiDyne Test Facility.

4.0 MODEL DESCRIPTION AND DEFINITION OF TEST MATRICES

This section describes the evolution of the basic DBTF (duct-burning turbofan) model system and the physical characteristics of the test hardware comprising the eleven test configurations. The acoustic cycle test matrix, aerodynamic test plan, and scope of laser velocimeter plume measurements are also detailed.

4.1 MODEL DESIGN - SYSTEM EVOLUTION

Recent studies on advanced cycles applicable to military and commercial high Mach number aircraft have indicated potential system advantages for multiple-flow engines, such as duct-burning turbofans and variable-cycle engines. Dual-flow plug nozzles integrate well with these types of engine systems and possess both thermodynamic performance and mechanical advantages over other types of exhaust systems. Figure 21 is a flowpath schematic representative of an engine exhaust nozzle system utilizing the dual-flow plug design. The main internal performance advantage of this system is that it provides the necessary expansion area for the high Mach flight conditions, with minimum weight and complexity, while maintaining high levels of performance at transonic and subsonic flight conditions. The system also exhibits good installed performance. At high flight Mach numbers, the exhaust gases fill the available expansion area; the associated drag, therefore, is very low. In subsonic flight, the jet plume does not fill the available projected area behind the engine, resulting in effective C/D (convergent/divergent) nozzle boattail and less drag.

In order to apply the dual-flow plug to a duct-burning turbofan, the AST parametric cycle deck (developed under the Advanced Supersonic Technology Propulsion System Study - Contract NAS3-16950 - Reference 15) was used to study duct-burning cycles with high core-energy extraction in order to provide insight into selection of the core/fan area ratio (Ae_c/Ae_f) and the outer annulus radius ratio ($R_{f\text{-inner}}/R_{f\text{-outer}}$). The cycle studies were influenced by the required maximum core total temperature, core jet velocity and duct total temperature [$(T_T)_c$ = 1460° R (811 K); V_c = 1400 ft/sec (426 m/sec); $(T_T)_f$ = 1960° R (1089 K), respectively]. These limits were also included as part of the basic engine cycle design criteria. Additionally, feasibility of mechanically implementing and operating such an engine with a reasonable bypass ratio was considered. After completion of the cycle studies, aerodynamic flowpath lines were developed in engine size and subsequently scaled to fixed-geometry model test nozzles.

Details of the exhaust nozzle system selection are discussed in Volume II of the CDR (under separate cover). System and propulsion nozzle cycle studies with selection of nozzle Ae_c/Ae_f, evolution of the baseline engine nozzle flowpaths in the form of dual-flow plugs, and the rationale of transitioning the baseline engine system nozzle flowpaths into the scale-model

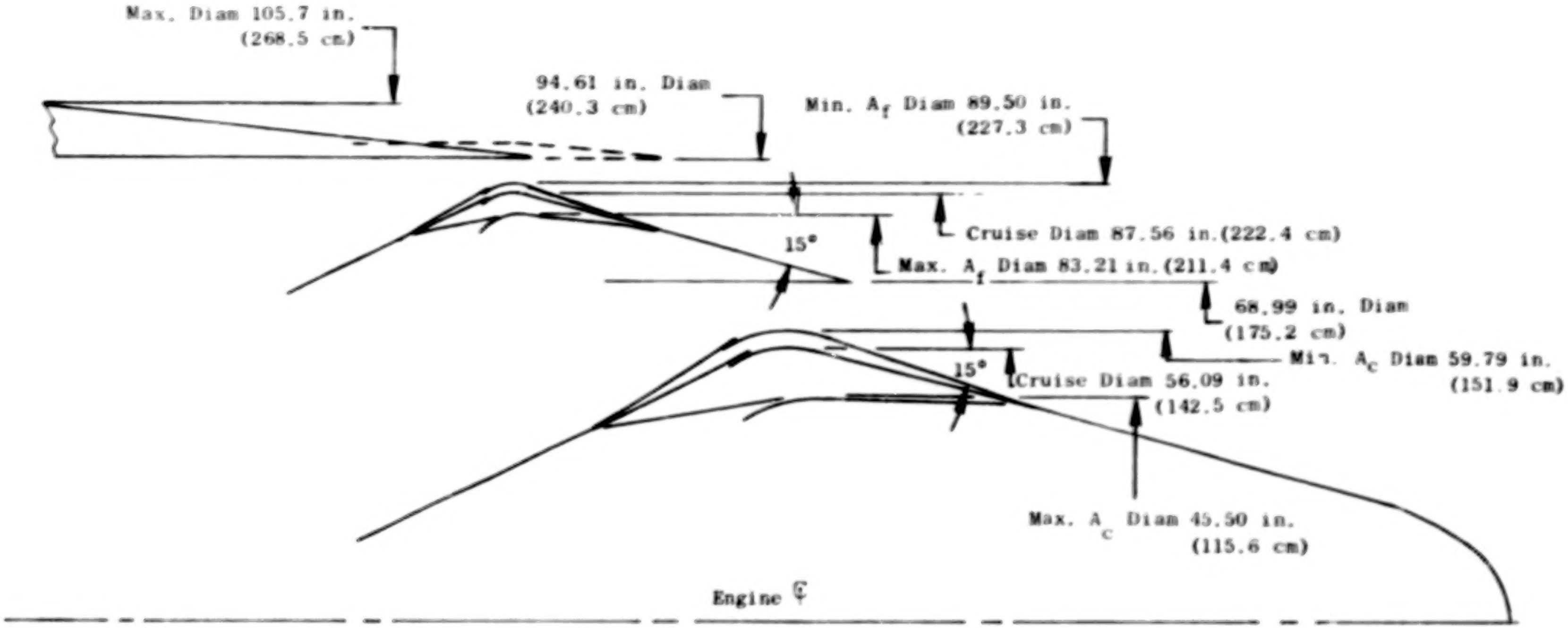
Max. Diam 105.7 in.
(268.5 cm)
94.61 in. Diam
(240.3 cm)
Min. A_f Diam 89.50 in.
(227.3 cm)
Cruise Diam 87.56 in. (222.4 cm)
15°
Max. A_f Diam 83.21 in. (211.4 cm)
68.99 in. Diam
(175.2 cm)
Min. A_c Diam 59.79 in.
(151.9 cm)
15°
Cruise Diam 56.09 in.
(142.5 cm)
Max. A_c Diam 45.50 in.
(115.6 cm)
Engine ℄

Figure 21. Schematic of Engine Propulsion Nozzle System Utilizing Dual-Flow Plug Design.

hardware are also presented in the CDR. Figure 21 depicts the engine-size exhaust nozzle flowpath and Figure 22 transitions this flowpath into the fixed-geometry model system.

Pertinent design-point parameters selected within the study were:

- $Ae_c/Ae_f = 1.55$
- $= 1.0$ (at takeoff $M_{aircraft} = 0.3$)
- $(P_T/P_o)_f = 2.66$
- $(T_T)_f = 1960°$ R (1089 K)
- $V_f = 2415$ ft/sec (736 m/sec)
- $(P_T/P_o)_c = 1.51$
- $(T_T)_c = 1460°$ R (811 K)
- $V_c = 1400$ ft/sec (426 m/sec)

At nondesign-point exhaust nozzle cycle conditions, where core and fan duct throat area variation is required, a mechanical flap and seal arrangement was used in each of the plugs, as seen in Figure 21. This results in a collapsing plug configuration for the engine-size nozzle design. Model hardware, however, was fixed-point design (nonvariable) to meet the takeoff cycle condition.

The scale-model design was based on combined core and fan-duct geometric throat areas equivalent to the throat area of a six-inch diameter (15.24 cm) nozzle. The core and fan-duct nozzles individually were equivalent to 4.63 in. (11.76 cm) and 3.72 in. (9.45 cm) diameter nozzles, respectively. Size selections were influenced by:

a) Requirements to have a common core-to-fan duct area ratio (A_c/A_f), common core flow area, sufficient size for scaling to AST duct-burning turbofan engines, and no less than six-inch (15.24 cm) equivalent diameter.

b) Compatability with aerodynamic-performance test facility where available weight flow at elevated temperature determined maximum model size.

c) Efficient operation of the acoustic-facility burners over a wide range of planned cycle conditions.

d) Allowance for incorporation of multielement suppressor systems where the characteristic frequency range of interest falls within the 80 kHz measuring capability of the facility equipment.

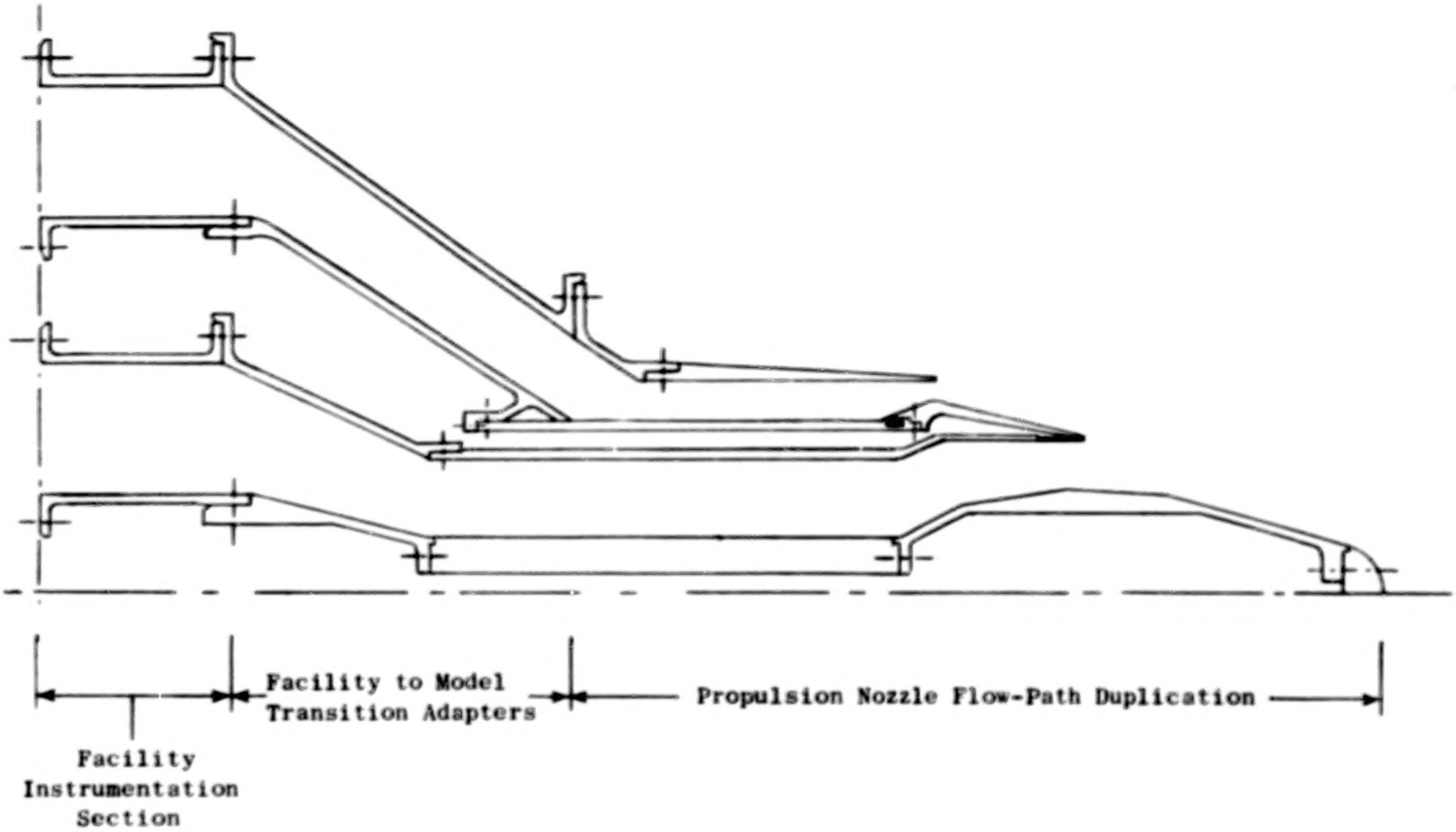
Facility to Model Transition Adapters
Propulsion Nozzle Flow-Path Duplication
Facility Instrumentation Section

Figure 22. Schematic of Model Propulsion Nozzle System Adapted to Test Facility.

4.2 DESCRIPTION OF TEST MODELS

The test hardware consisted of interchangeable model components which were assembled to form eleven test configurations. The components were categorized as follows:

- 1 Multichute fan-duct suppressor
- 1 Multitube fan-duct suppressor
- 1 Hardwall ejector with bellmouth and sharp inlets
- 1 Acoustically treated ejector with bellmouth and sharp inlets
- 1 Partial mechanical shield
- 1 Unsuppressed coannular nozzle with plug
- 1 Unsuppressed coannular nozzle without plug

The eleven test configurations were as follows:

Model 1 Multichute Fan-Suppressor Nozzle

Model 2 Multitube Fan-Suppressor Nozzle

Model 3 Multichute Fan-Suppressor Nozzle with Hardwall Ejector; Bellmouth Inlet

Model 4 Multichute Fan-Suppressor Nozzle with Treated Ejector; Bellmouth Inlet

Model 5 Multitube Fan-Suppressor Nozzle with Hardwall Ejector; Bellmouth Inlet for Acoustic Test; Sharp Inlet for Aerodynamic Test

Model 6 Multitube Fan-Suppressor Nozzle with Treated Ejector; Bellmouth Inlet

Model 7 Unsuppressed Coannular Nozzle with Plug

Model 8 Unsuppressed Coannular Nozzle without Plug

Model 9 Multichute Fan-Suppressor Nozzle with Hardwall Ejector; Sharp Inlet

Model 10 Multichute Fan-Suppressor Nozzle with Partial Mechanical Shield; Sideline Orientation

Model 11 Multichute Fan-Suppressor Nozzle with Partial Mechanical Shield; Flyover Orientation

The eleven test configurations are identified with their proper model number, model title, flowpath schematic, and photograph in Table IV. The model number and title will serve as consistent identification throughout the report.

Table IV. Description of Test Models and Test Types.

Set	Model Number	Title	Flowpath Schematic	Model Photograph	Flow Areas and Discharge Coefficients (1)				Type of Test Performed			Model Details in Figure Numbers
					C_{D_1} Est.	A_1 in.^{2} (cm^2)	C_{D_2} Est.	A_2 in.^{2} (cm^2)	GE REMOTS Farfield Acoustic	GE REMOTS Velocimeter	FluiDyne Aero	
[illegible]	[illegible]	Multichute Fan Suppressor Nozzle			0.975	11.12 (71.74)	0.977	17.21 (111.04)	X	X	X	140
	[illegible]	Multichute Fan Suppressor Nozzle with Hardwall Ejector Bellmouth Inlet			0.975	11.12 (71.74)	0.977	17.21 (111.04)	X			140 144
	[illegible]	Multichute Fan Suppressor Nozzle with Hardwall Ejector Sharp Inlet			0.975	11.12 (71.74)	0.977	17.21 (111.04)	X		X	140, 144
	[illegible]	Multichute Fan Suppressor Nozzle with Treated Ejector Bellmouth Inlet			0.975	11.12 (71.74)	0.977	17.21 (111.04)	X			140, [illegible]
	10	Multichute Fan Suppressor Nozzle with Partial Mechanical Shield-Sideline Orientation	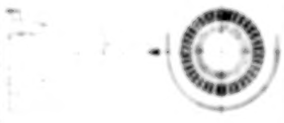		0.975	11.12 (71.74)	0.977	17.21 (111.04)	X			140, 145
	11	Multichute Fan Suppressor Nozzle with Partial Mechanical Shield Flyover Orientation	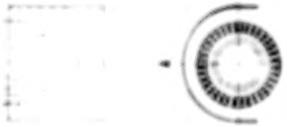		0.975	11.12 (71.74)	0.977	17.21 (111.04)	X			140, 145

Table IV. Description of Test Models and Test Types (Concluded).

Set	Model Number	Title	Flowpath Schematic	Model Photograph	Flow Areas and Discharge Coefficients (1)				Type of Test Performed			Model Details in Figure Numbers
									GE JENOTS			
					C_{D_f} Est.	A_f in.^{2} (cm^2)	C_{D_c} Est.	A_c in.^{2} (cm^2)	Farfield Acoustic	Velocimeter	FluiDyne Aero	
[illegible]	[illegible]	Multitube Fan Suppressor Nozzle			0.948	11.44 (73.81)	0.977	17.21 (111.04)	X	X	X	141
		Multitube Fan Suppressor Nozzle with Hardwall Ejector (Bellmouth Inlet for Acoustic Test Sharp Inlet for Aerodynamic Tests)		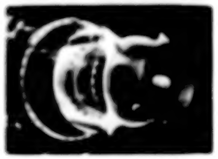	0.948	11.44 (73.81)	0.977	17.21 (111.04)	X		X	141, 144
	[illegible]	Multitube Fan Suppressor Nozzle with Treated Ejector Bellmouth Inlet			0.948	11.44 (73.81)	0.977	17.21 (111.04)	X			141, 144
[illegible]	[illegible]	Unsuppressed Coannular Nozzle with Plug		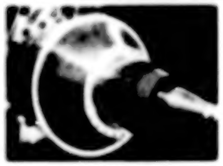	0.980	11.06 (71.38)	0.977	17.21 (111.04)	X	X	X	142
	[illegible]	Unsuppressed Coannular Nozzle without Plug			0.990	10.95 (70.66)	0.994	16.92 (109.14)	X			143

(1) Values Shown Under A_f an A_c are Actual Areas of Test Models

- A_{e_f} (Design) = $C_{D_f} \times A_f$ = 10.84 in.^{2} (69.69 cm^2) } Are Constant for all Models
  A_{e_c} (Design) = $C_{D_c} \times A_c$ = 16.82 in.^{2} (108.48 cm^2)
- C_{D_f} and C_{D_c} are Discharge Coefficients Assigned from Design Study, not from Final Test Data
- $D_e = \sqrt{\frac{4}{\pi}(A_f + A_c)}$

The test models were grouped into three sets as follows:

Set A - Table IV Models 1, 3, 9, 4, 10 and 11 - These models commonly shared the 36-chute fan-duct suppressor and core plug nozzle. Models 3 and 9 added the hardwall ejector with bellmouth and with sharp inlets respectively. The sharp inlet to the ejector was standard for all aerodynamic tests. The bellmouth inlet was normally standard for all acoustic tests except for the Model 3 to 9 direct acoustic comparison of bellmouth to sharp inlets. Model 4 used an acoustically treated ejector with bellmouth inlet of same internal flowlines as the Model 3 hardwall ejector. Models 10 and 11 utilized the partial mechanical shield oriented to evaluate the blockage effect on noise being propagated to a simulated sideline (with respect to the microphone field/observer) for Model 10 and to an observer beneath the flight path for Model 11.

Set B - Table IV Models 2, 5 and 6 - These models commonly shared the 69-tube fan-duct suppressor and core plug nozzle. Models 5 and 6 used respectively the same hardwall and acoustically treated ejectors as used in Set A. The bellmouth inlet to the ejectors was again used for acoustic testing of Models 5 and 6 and the sharp inlet for aerodynamic testing of Model 5. For Model 5 no distinction was made in model number for this inlet variation, as was done for Models 3 and 9 in Set A, as no comparative acoustic test was performed.

Set C - Table IV Models 7 and 8 - These were baseline models, Model 7 being the system unsuppressed baseline in the coannular noncoplanar nozzle form with core and fan-duct plugs and Model 8 being the acoustic unsuppressed baseline in the coannular coplanar nozzle form without core or fan-duct plugs.

As seen in Table IV, each of the eleven test configurations was subjected to far-field acoustic tests at the General Electric, Evendale, JENOTS facility (Section 3.1.1). Laser velocimeter (Section 3.2.2) measurements were made within the jet plume of Models 1, 2, and 7 on the same facility. Internal aerodynamic-performance measurements were made on Models 1, 2, 5, 7, and 9 at the FluiDyne Engineering Corporation's Medicine Lake Aerodynamic Laboratory. The last column of Table IV identifies Figures 140 through 145 (Appendix C) which show in detail the physical dimensions of each model component. Volume II of the CDR describes in detail the model hardware design development including all influencing physical design criteria, materials selection, flow monitoring instrumentation, and test model static pressure instrumentation.

One set of hardware models was manufactured to meet the test requirements of both the GE JENOTS acoustic and the FluiDyne aerodynamic facilities. Static pressure instrumentation was applied to critical drag surfaces including:

- Core-plug flow surfaces
- Fan-plug flow surfaces of the chute and tube suppressors

- Fan-plug flow surfaces of the unsuppressed coannular nozzle with plug
- Base areas of the tube nozzle and chute elements
- Internal flow surfaces of the hardwall ejector

Instrumentation locations are shown schematically in Section 6.0, Aerodynamic Results.

4.3 ACOUSTIC TEST MATRIX

The parametric acoustic test matrix was selected to provide data over a wide range of operating conditions and reflect AST duct-burning turbofan cycles as well as variable-cycle systems. The matrix covered the following ranges:

- Temperature, Core Stream $(T_T)_c$ = ambient to 1460° R (811 K)
- Temperature, Fan Stream $(T_T)_f$ = ambient to 1960° R (1089 K)
- Temperature Differential $(T_T)_f - (T_T)_c = 0°$ to 1000° R
  (0 to 556 K)
- Velocity, Core Stream V_c = 1000 to 2000 ft/sec (305 to 610 m/sec)
- Velocity Ratio V_f/V_c = 0.39 to 2.0

The prime concept under investigation was based on the fan stream having higher velocity and temperature than the core stream, $V_f/V_c > 1.0$ and $T_f - T_c > 0$, with the fan flow in the supersonic range. However, some data were obtained at $V_f/V_c \le 1.0$ and $T_f - T_c \le 0$, with subsonic conditions in the fan stream.

A basic matrix of 60 test points was selected as defined by nominal values in tabular form in Table V and graphically in Figures 23 and 24. Continuity of test point numbers and plot symbols is maintained for cross reference among the table and figures. Table V delineates pertinent core and fan pressure ratios, temperatures, velocities, and core to fan velocity ratios for each of the 60 points. Figure 23 interrelates V_f, V_c and V_f/V_c, showing that fixed nominal values of V_c = 1000, 1100, 1200, 1300, 1400, 1600, 1800, and 2000 ft/sec were set and V_f/V_c ratios over a range of 0.39 to 2.0 were selected to form a systematic matrix, primarily at select values of 0.4, 0.6, 0.8, 1.0, 1.25, 1.5, 1.75, and 2.0. Figure 24 graphically displays the fan and core aerodynamic conditions (i.e., $(P_T/P_O)_{f,c}$; $(T_T)_{f,c}$; $V_{f,c}$ for each of the 60 test points to show specific cycle composition for each point, to allude to the background for data points selection, and to show the interrelationships among test-point sets. Examination of the core conditions

Table V. Acoustic Test Matrix, Aerodynamic Test Conditions (Nominal Values).

Test Point No.	Symbol	Core Cycle					Fan Cycle					
			T_T		V			T_T		V		
		P_T/P_0	°R	K	ft/sec	m/sec	P_T/P_0	°R	K	ft/sec	m/sec	V_F/V_C
1	○	1.29	550	305.6	1000	304.8	1.54	720	400	1000	304.8	1.0
2	↓	↓	↓	↓	↓	↓	1.78	850	472.2	1250	381	1.25
3	↓	↓	↓	↓	↓	↓	2.06	995	552.8	1500	457.2	1.5
4	↓	↓	↓	↓	↓	↓	2.38	1165	647.2	1750	533.4	1.75
5	↓	↓	↓	↓	↓	↓	2.74	1340	744.4	2000	609.6	2.0
6	□	1.63	770	427.8	1100	335.3	1.62	770	427.8	1100	335.3	1.0
7	↓	↓	↓	↓	↓	↓	1.92	925	513.9	1375	419.1	1.25
8	↓	↓	↓	↓	↓	↓	2.26	1095	608.3	1650	502.9	1.5
9	↓	↓	↓	↓	↓	↓	2.60	1280	711.1	1925	586.7	1.75
10	↓	↓	↓	↓	↓	↓	3.00	1485	825	2200	670.6	2.0
11	◇	1.56	1000	555.6	1200	365.8	1.73	825	458.3	1200	365.8	1.0
12	↓	↓	↓	↓	↓	↓	2.06	995	552.8	1500	457.2	1.25
13	↓	↓	↓	↓	↓	↓	2.45	1200	666.7	1800	548.6	1.5
14	↓	↓	↓	↓	↓	↓	2.86	1410	783.3	2100	640.1	1.75
15	↓	↓	↓	↓	↓	↓	3.28	1630	905.6	2400	731.5	2.0
16	△	1.53	1225	680.6	1300	396.2	1.85	885	491.7	1300	396.2	1.0
17	↓	↓	↓	↓	↓	↓	2.22	1075	597.2	1625	495.3	1.25
18	↓	↓	↓	↓	↓	↓	2.64	1300	722.2	1950	594.4	1.5
19	↓	↓	↓	↓	↓	↓	3.11	1540	855.6	2275	693.4	1.75
20	↓	↓	↓	↓	↓	↓	3.57	1790	994.4	2500	762.0	2.0
21	⌂	1.50	1460	811.1	1400	426.7	1.95	960	522.2	1400	426.7	1.0
22	↓	↓	↓	↓	↓	↓	2.38	1165	647.2	1750	533.4	1.25
23	↓	↓	↓	↓	↓	↓	2.86	1410	783.3	2100	640.1	1.5
24	↓	↓	↓	↓	↓	↓	3.35	1670	927.8	2450	746.8	1.75
25	↓	↓	↓	↓	↓	↓	3.90	1960	1088.9	2800	853.4	2.0
26	○	1.45	1000	555.6	1000	304.8	1.54	720	400	1000	304.8	1.0
27	↓	↓	↓	↓	↓	↓	2.06	995	552.8	1500	457.2	1.5
28	↓	↓	↓	↓	↓	↓	2.73	1340	744.4	2000	609.6	2.0
29	⌂	1.86	1000	555.6	1400	426.7	1.95	960	522.2	1400	426.7	1.0
30	↓	↓	↓	↓	↓	↓	2.86	1410	783.3	2100	640.1	1.5
31	↓	↓	↓	↓	↓	↓	3.90	1960	1088.9	2800	853.4	2.0
32	○	1.29	550	305.6	1000	304.8	2.02	720	400	1250	381	1.25
33	↓	↓	↓	↓	↓	↓	2.60	785	436.1	1500	457.2	1.5
34	↓	↓	↓	↓	↓	↓	3.20	1170	650	2000	609.6	2.0
35	□	1.63	770	427.8	1100	335.3	2.60	945	525	1650	502.9	1.5
36	↓	↓	↓	↓	↓	↓	3.05	830	461.1	1650	502.9	1.5
37	↓	↓	↓	↓	↓	↓	2.60	1670	927.8	2200	670.6	2.0
38	◇	1.56	1000	555.6	1200	365.8	2.90	1025	569.4	1800	548.6	1.5
39	↓	↓	↓	↓	↓	↓	2.90	1805	1002.8	2400	731.5	2.0
40	↓	↓	↓	↓	↓	↓	2.65	1960	1088.9	2400	731.5	2.0
41	△	1.53	1225	680.6	1300	396.2	3.20	1940	1077.8	2600	792.5	2.0
42	○	1.29	550	305.6	1000	304.8	1.20	550	305.6	550	167.6	0.55
43	↓	↓	↓	↓	↓	↓	1.36	650	361.1	800	243.8	0.8
44	□	1.63	770	427.8	1100	335.3	1.27	550	305.6	660	201.2	0.6
45	◇	1.56	1000	555.6	1200	365.8	1.20	550	305.6	550	167.6	0.458
46	↓	↓	↓	↓	↓	↓	1.27	650	361.1	720	219.5	0.6
47	↓	↓	↓	↓	↓	↓	1.50	700	388.9	960	292.6	0.8
48	△	1.53	1225	680.6	1300	396.2	1.34	650	361.1	780	237.7	0.6
49	⌂	1.50	1460	811.1	1400	426.7	1.20	550	305.6	550	167.6	0.39
50	↓	↓	↓	↓	↓	↓	1.41	655	363.9	840	256	0.6
51	↓	↓	↓	↓	↓	↓	1.64	775	430.6	1120	341.4	0.8
52	○	1.74	1460	811.1	1600	487.7	3.90	1960	1088.9	2800	853.4	1.75
53	↓	↓	↓	↓	↓	↓	2.19	1060	588.9	1600	487.7	1.0
54	↓	↓	↓	↓	↓	↓	1.50	705	391.7	960	292.6	0.6
55	⌂	2.04	1460	811.1	1800	548.6	3.73	1870	1038.9	2700	823	1.5
56	↓	↓	↓	↓	↓	↓	2.45	1200	666.7	1800	548.6	1.0
57	↓	↓	↓	↓	↓	↓	1.60	760	422.2	1080	329.2	0.6
58	⌂	2.46	1460	811.1	2000	609.6	3.42	1710	950	2500	762	1.25
59	↓	↓	↓	↓	↓	↓	2.73	1340	744.4	2000	609.6	1.0
60	↓	↓	↓	↓	↓	↓	1.73	825	458.3	1200	365.8	0.6

Note: Test Point Numbers are Indicated with the Plot Symbols - Use In Conjunction with Table V and Figure 24.

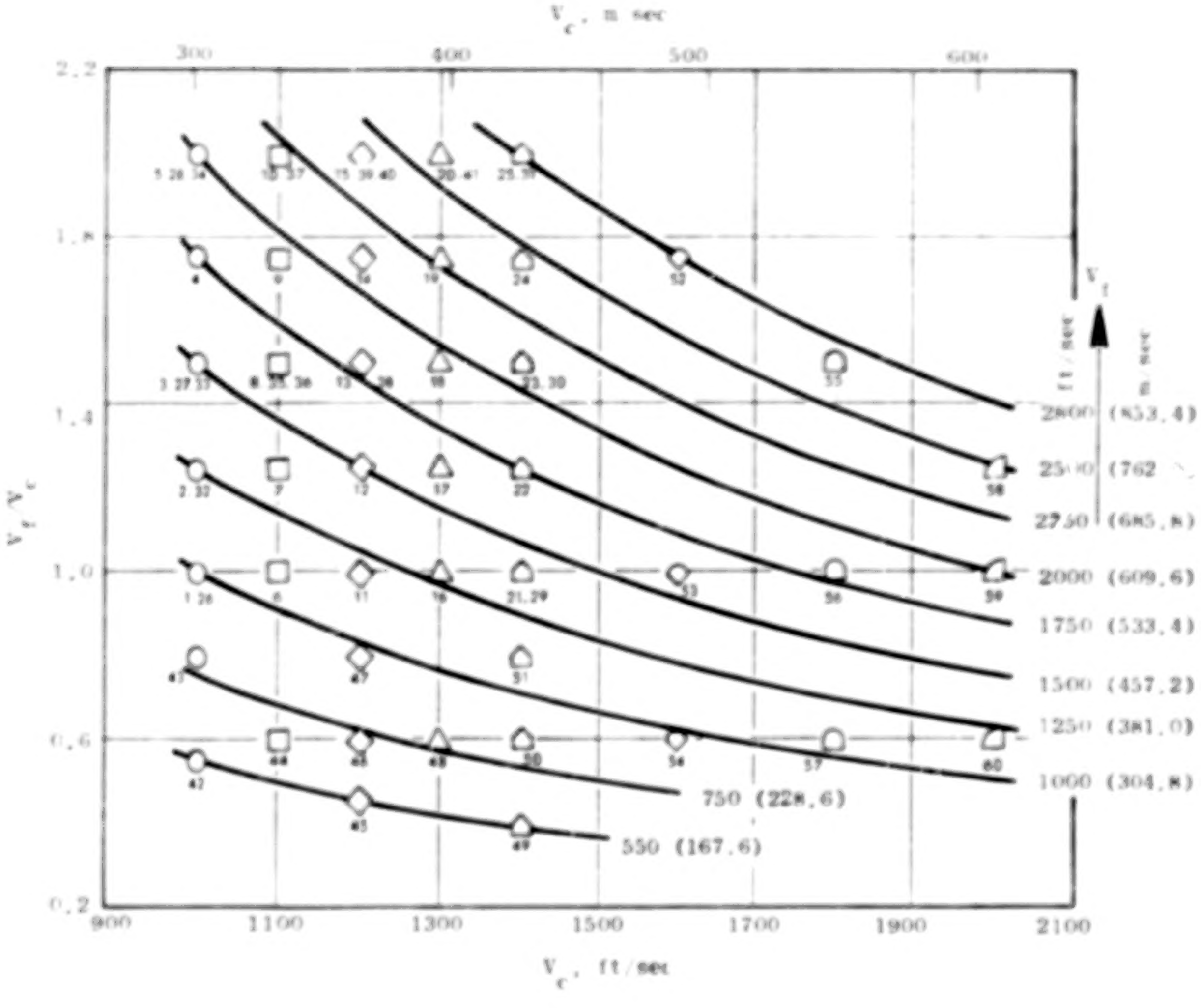

Figure 23. Acoustic Test Matrix, Fan and Core Aerodynamic Test Conditions Interrelating V_f, V_c, and V_f/V_c.

TABLE OF CONTENTS

Section Page

1.0 SUMMARY 1 1/C1

2.0 INTRODUCTION 3 1/C3

3.0 TEST APPARATUS AND PROCEDURES 5 1/C5

3.1 FACILITIES 5 1/C5

3.1.1 General Electric Jet Engine Noise Outdoor Test Stand (JENOTS) Description 6 1/C6
3.1.1.1 Acoustic Arena 6 1/C6
3.1.1.2 Coannular-Flow System 6 1/C6
3.1.1.3 Coannular Frame Section 10 1/C12
3.1.1.4 Plenum Instrumentation Section 10 1/C12
3.1.1.5 Facility Acoustic Validation 12 1/C14
3.1.2 FluiDyne Aerodynamic-Performance Test Facility Description 12 1/C14

3.2 JENOTS INSTRUMENTATION SYSTEMS 16 1/D5

3.2.1 Acoustic Instrumentation Systems 16 1/D5
3.2.2 Laser Velocimeter System 18 1/D8
3.2.2.1 General Arrangement 18 1/D8
3.2.2.2 LV Actuator and Seeding 21 1/D13
3.2.2.3 Signal Processing and Recording 21 1/D13

3.3 DATA REDUCTION METHODS 21 1/D13

3.3.1 Acoustic Data Reduction 22 1/D14
3.3.1.1 JENOTS Data Reduction Systems 22 1/D14
3.3.1.2 Air-Attenuation Corrections 22 1/D14
3.3.1.3 Data-Scaling Procedure 30 1/E12
3.3.1.4 Data Corrections to a Free-Field Environment 30 1/E12
3.3.1.5 Power Level Calculation 30 1/E12
3.3.1.6 Acoustic Measurement Errors, Electronic Noise Floor 30 1/E12
3.3.2 Laser Velocimeter Data Reduction 33 1/F3
3.3.2.1 Basic Idea for LV rms Measurements 33 1/F3
3.3.2.2 The Histogram 36 1/F6
3.3.2.3 Mean Velocity 36 1/F6
3.3.2.4 Turbulent Velocity 37 1/F7
3.3.2.5 Statistical Errors for LV Mean and Turbulent Velocity Measurements 37 1/F7

TABLE OF CONTENTS (continued)

Section Page

3.3.3 Aerodynamic-Performance Test Data Reduction 37 1/F7
3.3.3.1 Flow Rates 39 1/F9
3.3.3.2 Discharge Coefficients 39 1/F9
3.3.3.3 Nozzle Throat 39 1/F9
3.3.3.4 Thrust Coefficient 40 1/F10
3.3.3.5 FluiDyne Force Balance Calibration 40 1/F10
3.3.3.6 Pressure and Temperature Data 41 1/F11
3.3.3.7 Data Quality 41 1/F11

4.0 MODEL DESCRIPTION AND DEFINITION OF TEST MATRICES 44 1/F14

4.1 MODEL DESIGN - SYSTEM EVOLUTION 44 1/F14
4.2 DESCRIPTION OF TEST MODELS 48 1/G6
4.3 ACOUSTIC TEST MATRIX 52 1/G12
4.4 LASER VELOCIMETER TEST MATRIX 56 2/A7
4.5 AERODYNAMIC-PERFORMANCE TEST MATRIX 61 2/B1
4.6 DATA SECTION 61 2/B1

5.0 DISCUSSION OF ACOUSTIC TEST RESULTS 63 2/B3

5.1 ESTABLISHMENT OF GROUND RULES FOR ACOUSTIC COMPARISONS AND DATA ILLUSTRATIONS 63 2/B3

5.1.1 Synthesized Baseline 63 2/B3
5.1.2 Average Conical Nozzle Noise Baseline 64 2/B4
5.1.3 Density Normalization and Presentation of Results 64 2/B4
5.1.3.1 Density Normalization Factors 64 2/B4
5.1.3.2 Presentation of Results 70 2/B13

5.2 UNSUPPRESSED COANNULAR NOZZLES 71 2/B14

5.2.1 High Core-Flow Test Results 71 2/B14
5.2.1.1 Overall Power Level Test Results 71 2/B14
5.2.1.2 Power Spectra Test Results 71 2/B14
5.2.1.3 Perceived Noise Level Test Results 71 2/B14
5.2.1.4 Perceived Noise Level Directivity Test Results 75 2/C6
5.2.1.5 Sound Pressure Level Spectra Test Results 75 2/C6
5.2.2 Low Core-Flow Test Results 75 2/C6
5.2.3 Acoustic Correlations 84 2/D5
5.2.4 Summary Remarks 84 2/D5

5.3 MULTIELEMENT FAN-SUPPRESSOR NOZZLES 88 2/D11

5.3.1 High Core Flow Test Results 88 2/D11
5.3.1.1 Overall Power Level Test Results 88 2/D11
5.3.1.2 Power Spectra Test Results 97 2/E11

TABLE OF CONTENTS (continued)

Section Page

5.3.1.3 Perceived Noise Level Test Results 97 2/E11
5.3.1.4 Sound Pressure Level Spectra Test Results 98 2/E12
5.3.2 Low Core-Flow Test Results 98 2/E12
5.3.3 Comparisons with Unsuppressed Coannular Nozzles 98 2/E12
5.3.4 Summary Remarks 104 2/F9

5.4 MULTIELEMENT FAN-SUPPRESSOR NOZZLES WITH EJECTORS 104 2/F9

5.4.1 Hardwall Ejector Effects 107 2/F12
5.4.1.1 Overall Power Level Test Results 107 2/F12
5.4.1.2 Power Spectra Test Results 107 2/F12
5.4.1.3 Perceived Noise Level Test Results 107 2/F12
5.4.1.4 Sound Pressure Level Test Results 111 2/G2
5.4.2 Treated Ejector Effects 111 2/G2
5.4.2.1 Overall Power Level Test Results 111 2/G2
5.4.2.2 Power Spectra Test Results 115 2/G6
5.4.2.3 Perceived Noise Level Test Results 115 2/G6
5.4.2.4 Sound Pressure Level Test Results 120 2/G11
5.4.3 Inlet Lip Geometry Effects on the Hardwall Ejector 120 2/G11
5.4.3.1 Power Level Test Results 120 2/G11
5.4.3.2 Perceived Noise Level Test Results 124 3/A8
5.4.3.3 Sound Pressure Level Test Results 124 3/A8
5.4.4 Summary Remarks 124 3/A8

5.5 EVALUATION OF A PARTIAL MECHANICAL SHIELD 130 3/B1

5.5.1 Perceived Noise Level Test Results 130 3/B1
5.5.2 Sound Pressure Level Spectra Results 134 3/B6
5.5.3 Summary Remarks 134 3/B6

6.0 DISCUSSION OF AERODYNAMIC-PERFORMANCE TEST RESULTS 140 3/C1

6.1 THRUST COEFFICIENTS 140 3/C1

6.1.1 Unsuppressed Coannular Nozzle with Plug 140 3/C1
6.1.2 Multichute Fan-Suppressor Nozzle 143 3/C5
6.1.3 Multichute Fan-Suppressor Nozzle with Hardwall Ejector with Sharp Lip 143 3/C5
6.1.4 Multitube Fan-Suppressor Nozzle 150 3/C12
6.1.5 Multitube Fan-Suppressor Nozzle with Hardwall Ejector with Sharp Lip 150 3/C12

6.2 EFFECT OF HOT EXHAUST FLOW ON THE THRUST COEFFICIENT OF THE MULTITUBE FAN-SUPPRESSOR NOZZLE WITH HARDWALL EJECTOR WITH SHARP LIP 156 3/D7

TABLE OF CONTENTS (continued)

Section Page

6.3 FLOW COEFFICIENTS 161 3/D14

6.3.1 Unsuppressed Coannular Nozzle with Plug 161 3/D14
6.3.2 Multichute Fan-Suppressor Nozzle 165 3/E6
6.3.3 Multichute Fan-Suppressor Nozzle with Hardwall Ejector with Sharp Lip 165 3/E6
6.3.4 Multitube Fan-Suppressor Nozzle 169 3/E10
6.3.5 Multitube Fan-Suppressor Nozzle with Hardwall Ejector with Sharp Lip 169 3/E10

7.0 DISCUSSION OF LASER VELOCIMETER TEST RESULTS 173 3/E14

7.1 LASER VELOCIMETER PLUME MEASUREMENTS FOR THE UNSUPPRESSED COANNULAR NOZZLE WITH PLUG 173 3/E14

7.1.1 Axial Mean-Velocity Distributions 173 3/E14
7.1.2 Mean-Velocity, Radial-Profile Distributions 176 3/F5
7.1.3 Axial Turbulent-Velocity, Radial-Profile Distributions 176 3/F5

7.2 LASER VELOCIMETER PLUME MEASUREMENTS FOR THE FAN-SUPPRESSED NOZZLES 176 3/F5

7.2.1 Axial Mean-Velocity Distributions 176 3/F5
7.2.2 Mean- and Turbulent-Velocity, Radial-Profile Distributions 180 3/F12
7.2.2.1 Multichute Fan Suppressor 180 3/F12
7.2.2.2 Multitube Fan Suppressor 180 3/F12

7.3 SUMMARY OF OBSERVATIONS 180 3/F12

8.0 DISCUSSION OF ACOUSTIC/AERODYNAMIC-PERFORMANCE CORRELATIONS 186 3/G8

8.1 EVALUATION OF NOISE CANDIDATES FOR DUCT-BURNING TURBOFAN ENGINES 186 3/G8
8.2 LOW CORE-FLOW COMPARISONS 191 4/A6

9.0 CONCLUSIONS AND RECOMMENDATIONS 196 4/A12

9.1 CONCLUSIONS 196 4/A12
9.2 RECOMMENDATIONS 197 4/A13

TABLE OF CONTENTS (concluded)

Section	Page	
APPENDIX A - GENERAL ELECTRIC AIR-ATTENUATION MODEL	199	4/B1
APPENDIX B - POWER LEVEL CALCULATION PROCEDURE	210	4/C1
APPENDIX C - DETAILED DESCRIPTION OF TEST MODELS	214	4/C5
APPENDIX D - ACOUSTIC TEST MATRIX FOR ALL DBTF MODELS AND EXAMPLE DATA PRINT OUT SHEETS	221	4/D3
APPENDIX E - FAN PLUG PRESSURE DISTRIBUTIONS FOR AERODYNAMIC MODEL 5	240	4/F13
APPENDIX F - MODEL 7 AXIAL-VELOCITY PROFILES	249	5/A8
APPENDIX G - MODEL 7 AXIAL-VELOCITY PROFILES WITH NO CORE FLOW	270	5/D7
APPENDIX H - MODEL 7 AXIAL-VELOCITY PROFILES WITH NO FAN FLOW	286	5/F10
APPENDIX I - MODEL 1 AXIAL-VELOCITY PROFILES	295	5/G13
APPENDIX J - MODEL 2 AXIAL-VELOCITY PROFILES	303	6/B6
APPENDIX K - NOMENCLATURE	313	6/C11
REFERENCES	317	6/D1

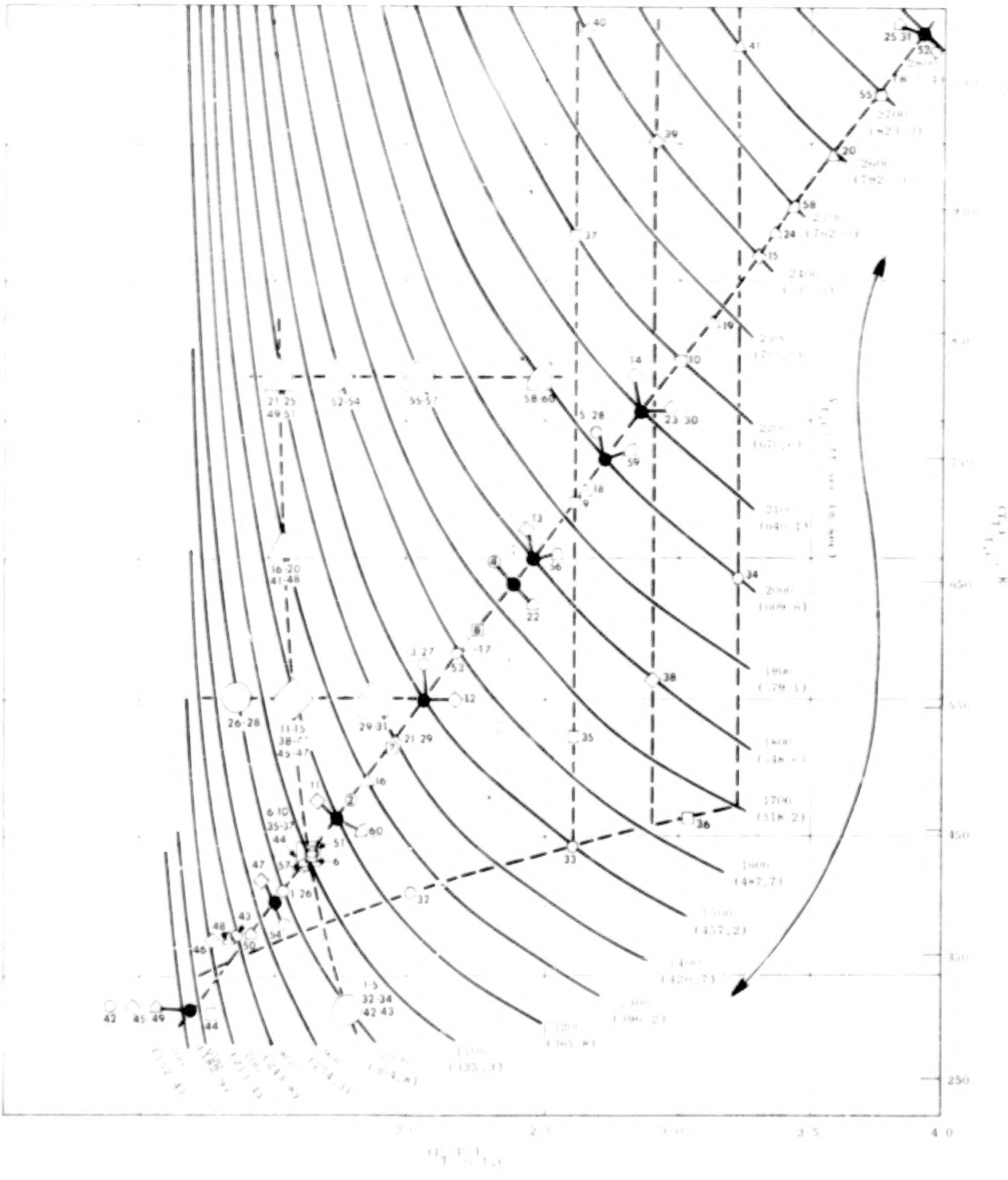

Figure 24. Acoustic Test Matrix, Fan and Core Aerodynamic Test Conditions Interrelating $(T_T)_{f,c}$; $(P_T/P_o)_{f,c}$; and $V_{f,c}$.

shows operation within a DBTF system over-extracted cycle mode with extension to low $(T_T)_c$ and V_c values and with parametric V_c excursions at $(T_T)_c = 1000$ and 1460° R (556 and 811 K). The fan conditions were primarily selected along a straight-line excursion from low pressure ratio and temperature to the maximum values of $(P_T/P_o)_f = 4.0$, $(T_T)_f = 1960°$ R (1089 K), $V_f = 2800$ ft/sec (853 m/sec) principally for best generation of parametric acoustic data applicable to various engine cycles. Of equal significance are the simulations of a conventional DBTF system fan cycles in which low temperature is maintained along a line of increasing $(P_T/P_o)_f$ until simulated duct afterburning is introduced at values of $(P_T/P_o)_f = 2.6$, 2.9 and 3.2. At these $(P_T/P_o)_f$ values, $(T_T)_f$ and V_f excursions are made along vertical lines simulating varying degrees of afterburning.

Table VI is included to relate the specific test points, of the basic 60 total, which were selected for each of the eleven acoustic configurations. Tables XII through XXII in Appendix D tabulate the exact aerodynamic test conditions set for each model acoustic test matrix. The data point numbers used in the tables of Appendix D are formed from three or four digits representing the model number and the nominal test conditions; the last two numbers indicate the test conditions and the first (or first two) indicate the model number.

Within Table VI and Appendix D, it is seen that Models 1, 2, 4, and 7 were tested at points beyond the scope of the basic 60-point matrix. These points were for the purpose of investigating noise generation as a function of core flow alone, fan flow alone, and fan flow with leaky core flow. Specifics of these special test conditions are in the Appendix D tables.

4.4 LASER VELOCIMETER TEST MATRIX

Plume surveys with the laser velocimeter were performed to gain insight into the details of the aerodynamic flow field which generated the noise sources. A total of three test configurations were subjected to LV testing, namely:

- Model 1 Multichute Fan-Suppressor Nozzle
- Model 2 Multitube Fan-Suppressor Nozzle
- Model 7 Unsuppressed Coannular Nozzle With Plug

The aerodynamic test matrix selected was as indicated in Table VII and consisted of test point numbers 23, 25, and 51. Models 1 and 2 were LV tested at all three cycle conditions; Model 7 was LV tested at point 23 only. For each of these test points the core velocity was nominally 1400 ft/sec (427 m/sec), and the fan duct included two supersonic and one subsonic condition. In addition Model 7 was tested with the fan stream and the core stream each flowing alone (test points 73 and 86 respectively).

Table VIII and Figure 25 describe the data planes at which LV measurements were taken. The multichute/tube fan suppressor Models 1 and 2 utilized four basic planes of X/D_{Ref}: 0.03, 1.09, 2.61, and 4.92; X was defined

Table VI. Acoustic Test Schedule.

Model No.	Model Title	Acoustic Test Points
1	Multichute Fan Suppressor Nozzle	1-60 (70,71,72)
2	Multitube Fan Suppressor Nozzle	1-60 (70-76)
3	Multichute Fan Suppressor Nozzle With Hardwall Ejector; Bellmouth Inlet	1,3,5,6,8,10,11,13,15,16,18,20,21,23,25,32,34 36,37,41,42,43,46,49,51
4	Multichute Fan Suppressor Nozzle With Treated Ejector; Bellmouth Inlet	1,3,5,6,8,10,11,13,15,16,18,20,21,23,25,32,34 36,37,41,42,43,46,49,51,52-60 (70-72)
5	Multitube Fan Suppressor Nozzle With Hardwall Ejector; Bellmouth Inlet	1,3,5,6,8,10,11,13,15,16,18,20,21,23,25,32,34, 36,37,41,42,43,46,49,51
6	Multitube Fan Suppressor Nozzle With Treated Ejector; Bellmouth Inlet	1,3,5,6,8,10,11,13,15,16,18,20,21,23,25,32,34, 36,37,41,42,43,46,49,51, 52-60
7	Unsuppressed Coannular Nozzle With Plug	1,3,5,6,8,10,11,13,15,16,18,20,21,23,25-31,33-60 (71-74,80,81,85-87,89,91)
8	Unsuppressed Coannular Nozzle Without Plug	1,3,5,6,8,10,11,13,15,16,18,20,21,23,25-31,33-60
9	Multichute Fan Suppressor Nozzle With Hardwall Ejector; Sharp Inlet	1,3,5,11,13,15,21,23,25,42,43,46,49,51
10	Multichute Fan Suppressor Nozzle With Partial Mechanical Shield; Sideline Orientation	1,3,5,11,13,15,21,23,25,42,43,46,49,51
11	Multichute Fan Suppressor Nozzle With Partial Mechanical Shield; Flyover Orientation	1,3,5,11,13,15,21,23,25,42,43,46,49,51

Table VII. Laser Velocimeter Test Matrix, Aerodynamic Test Conditions (Nominal Values).

Model No.	Test Point No.	Core Cycle					Fan Cycle					V_f/V_c
		P_T/P_o	T_T		V		P_T/P_o	T_T		V		
			° R	K	ft/sec	m/sec		° R	K	ft/sec	m/sec	
1,2&7	23	1.50	1460	811.1	1400	426.7	2.86	1410	783.3	2100	640.1	1.5
1&2	25	↓	↓	↓	↓	↓	3.90	1960	1088.9	2800	853.4	2.0
1&2	51	↓	↓	↓	↓	↓	1.64	775	430.6	1120	341.4	0.8
7	73	↓	↓	↓	↓	↓	~1.00	Amb.	-	~0	-	N/A
7	86	~1.0	~Amb.	-	~0	-	2.86	1410	783.3	2100	640.1	N/A

Table VIII. Laser Velocimeter Data Planes.

Plane Number	Axial Location			Model 1 Pts 23, 25, and 51	Model 2 Pts 23, 25, and 51	Model 7		
	Inches	cm	Normalized*			Dual Flow Pt 23	Fan Only Pt 86	Core Only Pt 73
1 (Fan Exit)	-3.12	-7.92	-0.52			X	X	
2	-0.48	-1.22	-0.08			X	X	
3 (Core Exit)	0.18	0.457	0.03	X	X	X	X	X
4	1.0	2.54	0.17			X	X	
5	2.0	5.08	0.33			X	X	
6	3.0	7.62	0.50			X	X	X
7	4.0	10.16	0.67			X	X	
8	5.0	12.70	0.83			X	X	
9 (Plug Tip Region)	6.54	16.61	1.09	X	X	X	X	X
10	8.1	20.57	1.35			X		
11	12.0	30.48	2.00			X	X	X
12	13.02	33.07	2.17			X		
13	14.0	35.56	2.33			X		
14	15.7	39.88	2.61	X	X	X	X	X
15	20.04	50.90	3.34			X		
16	22.1	56.13	3.68			X	X	
17	25.0	63.50	4.17			X		
18	29.52	74.98	4.92	X	X	X	X	X
19	33.12	84.13	5.52			X		
20	40.0	101.6	6.67			X	X	X

*Axial Distance/Equivalent Diameter = X/D_{Ref} where D_{Ref} = 6 in. (15.24 cm)

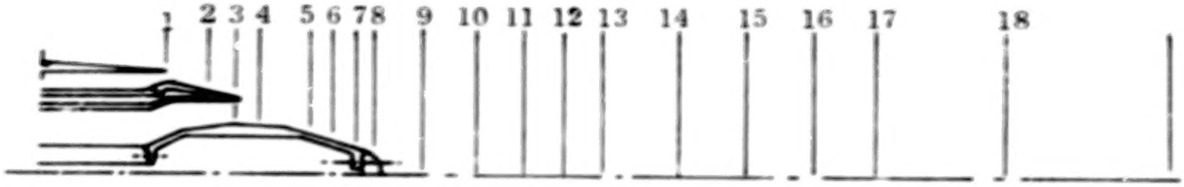
1
2
3
4
5
6
7
8
9
10
11
12
13
14
15
16
17
18

Dual-Flow System Baseline, Model No. 7

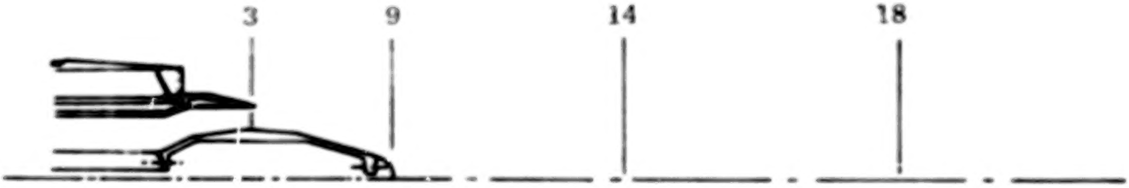

Multichute Suppressor, Model No. 1

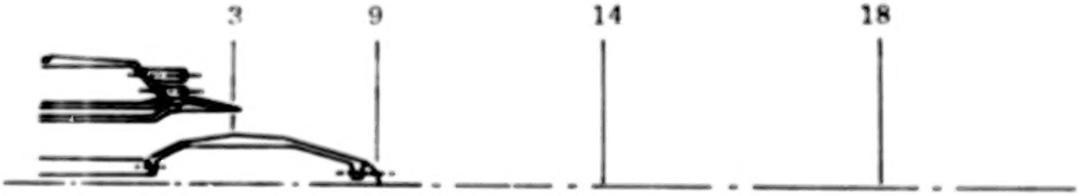

Multitube Suppressor, Model No. 2

Figure 25. Definition of Data Planes for Models 1, 2, and 7.

as zero at the core exit plane and D_{Ref} as the equivalent diameter of the combined dual-flow area, i.e., $D_{Ref} = 6$ in. (15.24 cms). The unsuspressed coannular nozzle, Model 7, used 20 data planes within $X/D_{Ref} = -.52$ to 6.67. The additional planes were utilized so that the complete plume could be mapped. This detail allowed a velocity contour plot to be developed to show the exact nature of the flow.

4.5 AERODYNAMIC-PERFORMANCE TEST MATRIX

Internal aerodynamic-performance measurements were contracted to the FluiDyne Engineering Corporation at their Medicine Lake Aerodynamic Laboratory. Models 1, 2, 5, 7, and 9 were tested in their Channel 11 two-flow static thrust stand. These models consisted of the multichute and multitube fan-suppressor nozzles, with and without the hardwall ejector, plus the unsuppressed coannular nozzle with plug. Each model was subjected to a test matrix using cold (ambient temperature) flow. This normally consisted of holding nominal core pressure ratios, $(P_T/P_o)_c$, at 1.3 and 1.9 while sequentially setting fan pressure ratios, $(P_T/P_o)_f$, at 1.5, 2.25, 3.0, and 4.0.

Hot flow testing was also performed on Model 5, multitube fan suppressor with hardwall ejector, at five cycle points using fan and core exhaust temperatures of 1000 and 1460° R (556 and 811 K).

Table IX displays the actual aerodynamic test matrix as measured during the performance tests of each of the above nozzles.

4.6 DATA SECTION

All the acoustic data described in Section 4.3 are presented in tabular and computer plot form in the companion CDR, CR-135236. The aerodynamic conditions and selected, scale-model, 40-ft arc, corrected-to-free-field, overall sound pressure levels at $\theta_1 = 50°, 70°, 90°, 110°, 130°, 140°$, and 150°, as well as the OAPWL for each of the configurations tested, are included in Appendix D. Also contained in Appendix D are example-data, computer print-out sheets for the model and scaled (full size -8:1) test results contained in the CDR.

Table IX. Aerodynamic Test Matrix.

Model No.	Model Title	$(P_T/P_o)_c$	$(P_T/P_o)_f$	$(T_T)_{c,f}$ °R (°K)
1	Multichute Fan Suppressor Nozzle	1.297	1.548	Ambient ≈ 520 (288.9)
		1.298	2.272	
		1.298	3.064	
		1.298	4.035	
		1.888	1.547	
		1.895	2.270	
		1.897	3.071	
		1.897	4.033	
2	Multitube Fan Suppressor Nozzle	1.302	1.552	
		1.304	2.243	
		1.301	3.048	
		1.301	4.033	
		1.897	1.542	
		1.897	2.250	
		1.895	3.061	
		1.901	4.038	
5	Multitube Fan Suppressor Nozzle With Hardwall Ejector; Sharp Inlet	1.300	1.545	
		1.299	2.255	
		1.299	3.257	
		1.298	4.035	
		1.645	3.258	
		2.001	1.544	
		1.996	2.246	
		1.996	3.254	
		1.997	4.029	
		1.273	2.215	1000 (555.6)
		2.129	4.001	1000 (555.6)
		1.296	2.242	1460 (811.1)
		1.727	3.213	1460 (811.1)
		2.148	4.017	1460 (811.1)
7	Unsuppressed Coannular Nozzle With Plug	1.312	1.490	Ambient ≈ 520 (288.9)
		1.308	3.077	
		1.308	4.034	
		1.886	1.574	
		1.890	3.081	
		1.895	4.033	
9	Multichute Fan Suppressor Nozzle With Hardwall Ejector; Sharp Inlet	1.298	1.541	Ambient ≈ 520 (288.9)
		1.301	2.273	
		1.298	3.061	
		1.301	4.036	
		1.893	1.541	
		1.893	2.247	
		1.893	3.060	
		1.895	4.036	

5.0 DISCUSSION OF ACOUSTIC TEST RESULTS

The acoustic test results for the unsuppressed and the multielement fan-suppressed coannular nozzles are discussed in this section. Most of the test results and nozzle configuration comparisons were performed for test operating conditions applicable to a duct-burning turbofan engine cycle. Such cycles have a high core-energy extraction which results in fan velocity to core velocity ratios greater than or equal to 1.5 ($V_f/V_c \geq 1.5$). In addition to these test conditions, parametric tests were performed at fan to core velocity ratios of less than 1.5 ($V_f/V_c \leq 1.5$). The core stream velocities for all these test conditions were maintained at between 1000 ft/sec (304.8 m/sec) and 2000 ft/sec (609.6 m/sec). The term "high core flow" test results is used herein for all such test points. Other tests were performed such that the core flow was regulated to the test-facility minimum flow, while operating the fan stream at high velocity and temperature; these test points are referred to as "low core flow" test results. The full range of conditions tested for each model and the complete model description are contained in Section 4.0.

Section 5.1 gives a brief description of the baseline system which was used to compare noise levels reduction. The basic density normalization parameter and the "nominal" test conditions for which most of the data comparisons were made are also discussed.

The main acoustic characteristics of the unsuppressed coannular nozzles at high and low core flow settings are reviewed in Section 5.2. This section is significant because the results establish that the basic configurations had substantial noise reduction relative to the baseline of comparison. These results suggest the need for further noise investigations in order to evaluate the impact on future engine cycle applications.

Section 5.3 discusses the two basic multielement fan suppressors designed for the program. Sections 5.4 and 5.5 discuss the tests performed on the multielement suppressors with treated and hardwall ejectors, and on the multichute fan suppressor with a "partial" mechanical shield. These three sections serve to establish guidelines for the future acoustic design of multielement fan-suppressor nozzles. The noise-level reductions obtained are substantial, and designers can look forward to obtaining noise levels lower than FAR 36 (1969) with suppressed multiple-stream engine cycle systems.

5.1 ESTABLISHMENT OF GROUND RULES FOR ACOUSTIC COMPARISONS AND DATA ILLUSTRATIONS

5.1.1 Synthesized Baseline

The baseline chosen for estimating relative levels of noise reduction or suppression is referred to as a "synthesized baseline." This baseline is defined as the noise which would be generated by the fan and core jets operating independently, it is calculated on the basis that the noise of each separate stream is equivalent to the noise of a conical nozzle exhaust operating at the same area, velocity and temperature. Flow interaction and geometry benefits are not included in this definition. The noise for the synthesized baseline is defined by:

$$10 \log_{10} \left[\log^{-1} \left(\frac{\text{Conical Noise}}{10} \right)_f + \log_{10}^{-1} \left(\frac{\text{Conical Noise}}{10} \right)_c \right]$$

Figure 26 pictorially illustrates the baseline definition, while Figure 27 illustrates a sample case from the results of the unsuppressed coannular nozzle with plug (Model 7).

5.1.2 Average Conical Nozzle Noise Baseline

An average conical nozzle baseline was established in order to determine the equivalent conical noise levels for the fan and core streams of the coannular nozzles. Figure 28 summarizes the empirically established normalized maximum Preceived Noise Level (PNL) curve. Data sources used to generate the curve include General Electric model-scale and engine-size tests results as well as other published data. Table X and the legend of Figure 28 summarize the data sources.

The General Electric data were from tests conducted outdoors; data scaling, extrapolation, and ground reflection corrections used to establish the test noise levels are covered in Section 3.4. It should be noted, however, that the normalized maximum PNL characteristic was established only after at least three angles in the aft quadrant were scaled and extrapolated. This conical nozzle data is considered representative and state-of-the-art data for model-scale, outdoor test measurements. A similiar procedure was used to obtain normalized PNL at other angles so that synthesized PNL directivity curves could be generated. The synthesized PNL directivities are used in Section 5.2.1.4.

5.1.3 Density Normalization and Presentation of Results

5.1.3.1 Density Normalization Factor

Many of the test results have been normalized relative to the density power-law factor, $-10 \log (\rho_j/\rho_{ISA})^\omega$, derived for circular nozzles from Reference 1. Figure 29 gives an engineering design curve for this normalization factor. There are no equivalent density power-law expressions for coannular or annular nozzles; the conical nozzle density factors were applied to the unsuppressed and fan suppressed data presented in the text.

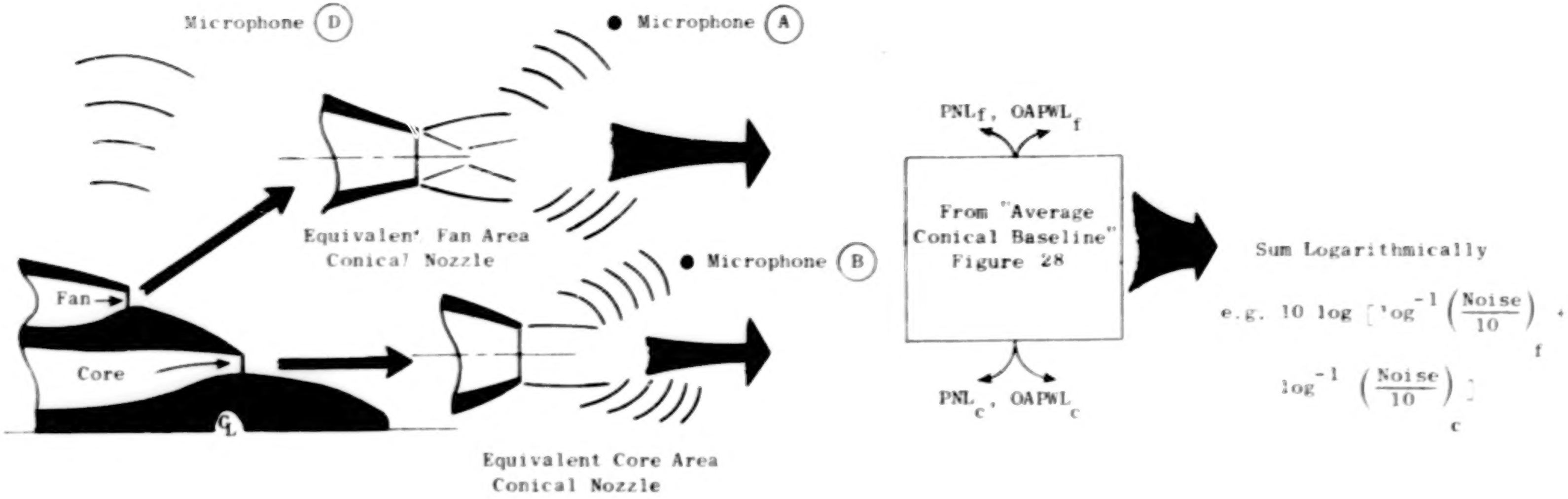
Microphone (D)
Microphone (A)
Microphone (B)
Fan
Core
℄
Equivalent Fan Area Conical Nozzle
Equivalent Core Area Conical Nozzle
PNL_f, OAPWL_f
From "Average Conical Baseline" Figure 28
PNL_c, OAPWL_c
Sum Logarithmically
e.g. 10 log [log⁻¹ (Noise/10)_f + log⁻¹ (Noise/10)_c]

Figure 26. Synthesized Baseline Noise Level Determination.

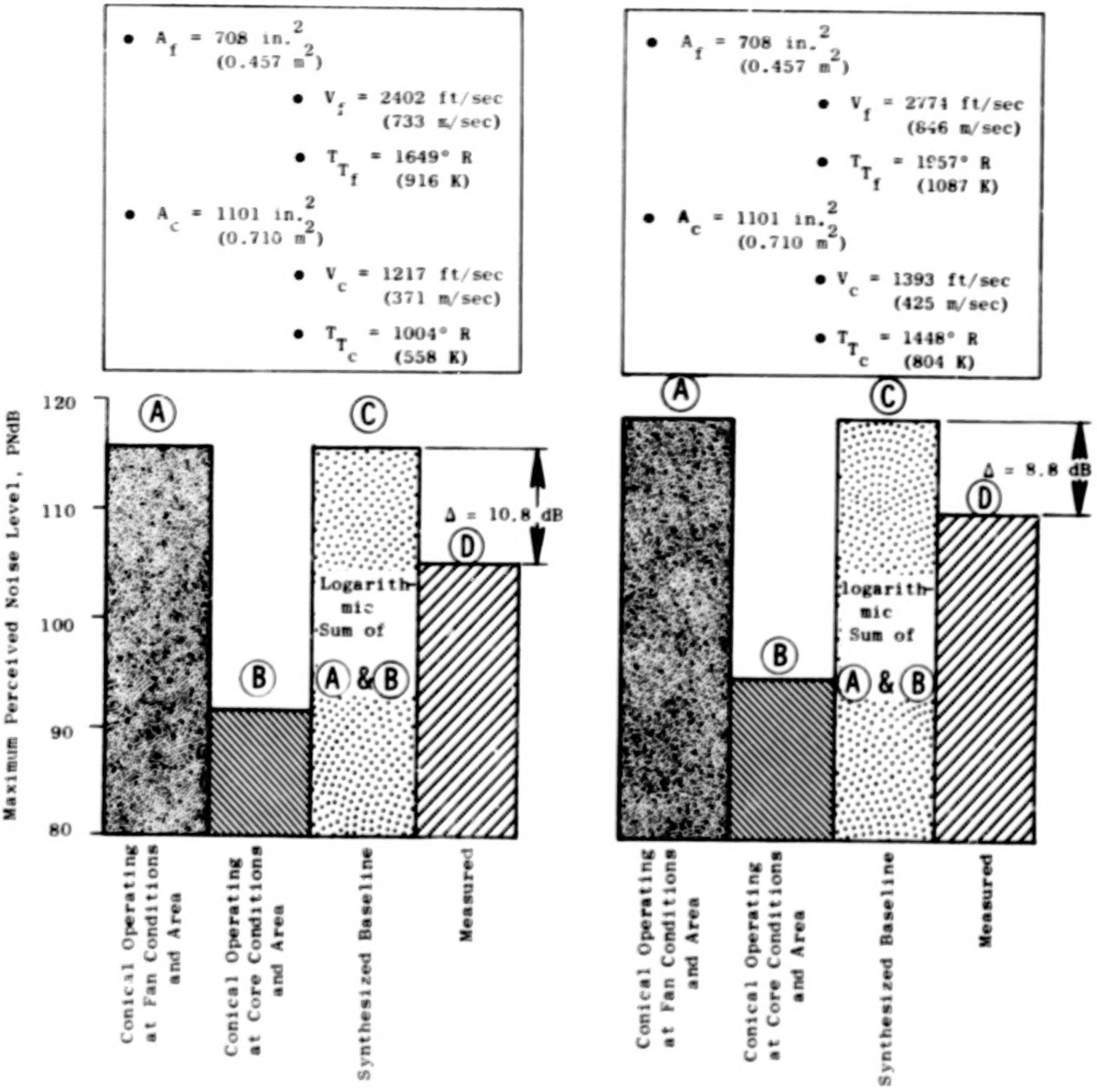

Figure 27. Comparison of Unsuppressed Coannular Nozzle with Plug Noise Levels Vs. Synthesized Baseline Noise Levels.

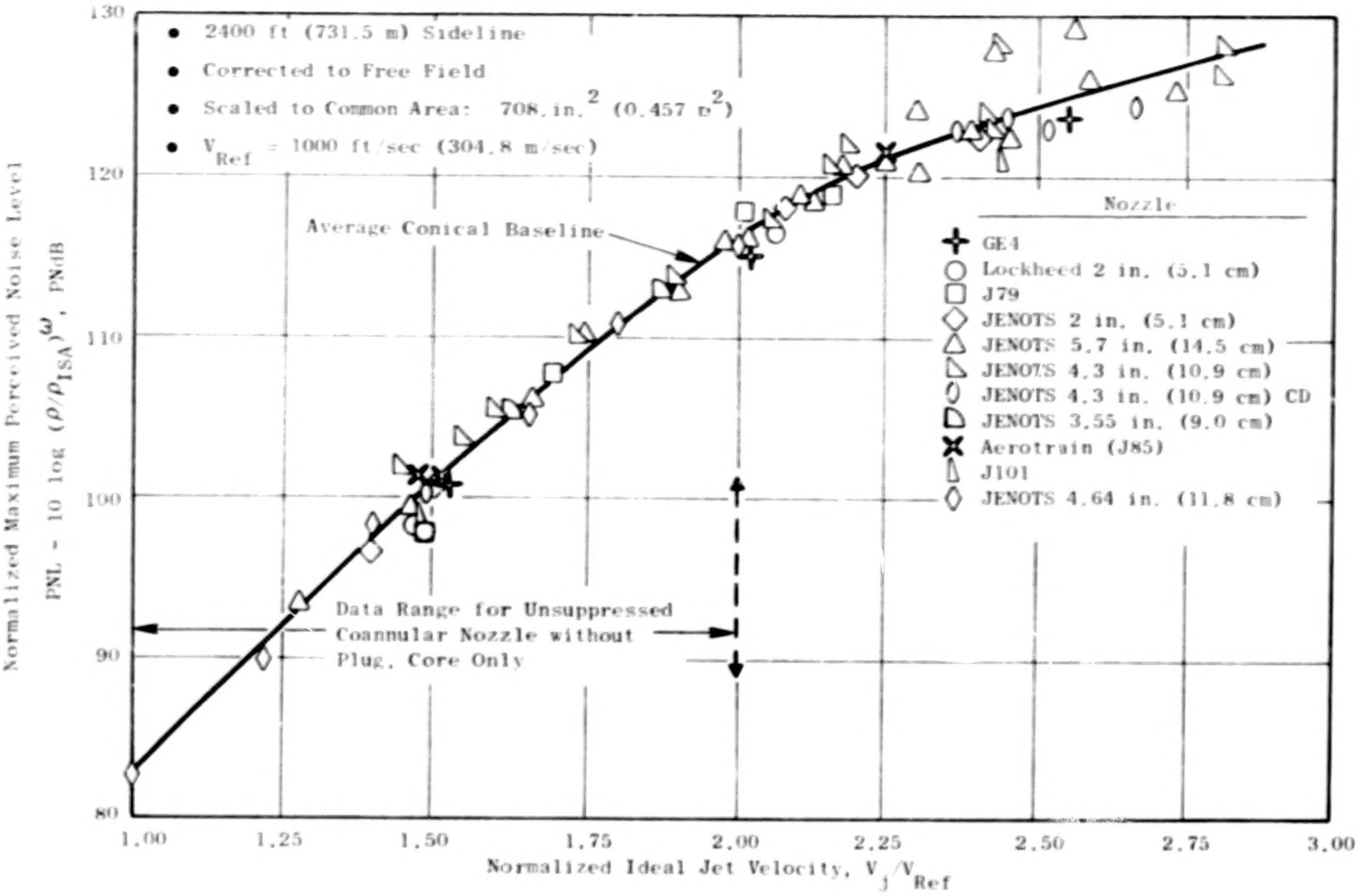

Figure 28. Comparison of Various Scaled-Up or Full-Size Conical Nozzle Maximum Perceived Noise Levels.

Table X. Conical and Convergent-Divergent Nozzle Data Sources

Source	Nozzle Size (Diameter)	Test Site/ Radius	Test Date
GE	5.7 inch (14.5 cm)	JENOTS/40-Foot (12.2 m)	2/16/73
	5.7 inch (14.5 cm)	JENOTS/40-Foot (12.2 m)	2/5/75
	2.0 inch (5.1 cm)	JENOTS/40-Foot (12.2 m)	2/11/75
	4.3 inch (10.9 cm),C/D	JENOTS/40-Foot (12.2 m)	5/6/73
	4.3 inch (10.9 cm)	JENOTS/40-Foot (12.2 m)	5/6/73
	3.55 inch (9.0 cm)	JENOTS/40-Foot (12.2 m)	11/14/73
	11.4 inch (28.9 cm)	Fresno/100 ft (30.5 m)	10/74
	20.8 inch (52.8 cm)	Edwards North Site/160 ft (48.8 m)	10/4/74
	39.4 inch (100.1 cm)	Peebles/250 ft (76.2 m)	6/7/70
	17.0 inch (43.2 cm)	Edwards/150 ft (45.7 m)	9/74
	4.64 inch (11.8 cm)	JENOTS/40 ft (12.2 m)	3/75
Lockheed	2.0 inch (5.1 cm)	Anechoic Room/12 ft (3.7 m)	-
SNECMA	11.4 inch (28.9 cm)	France/164 ft (50 m) Sideline	10/11/74

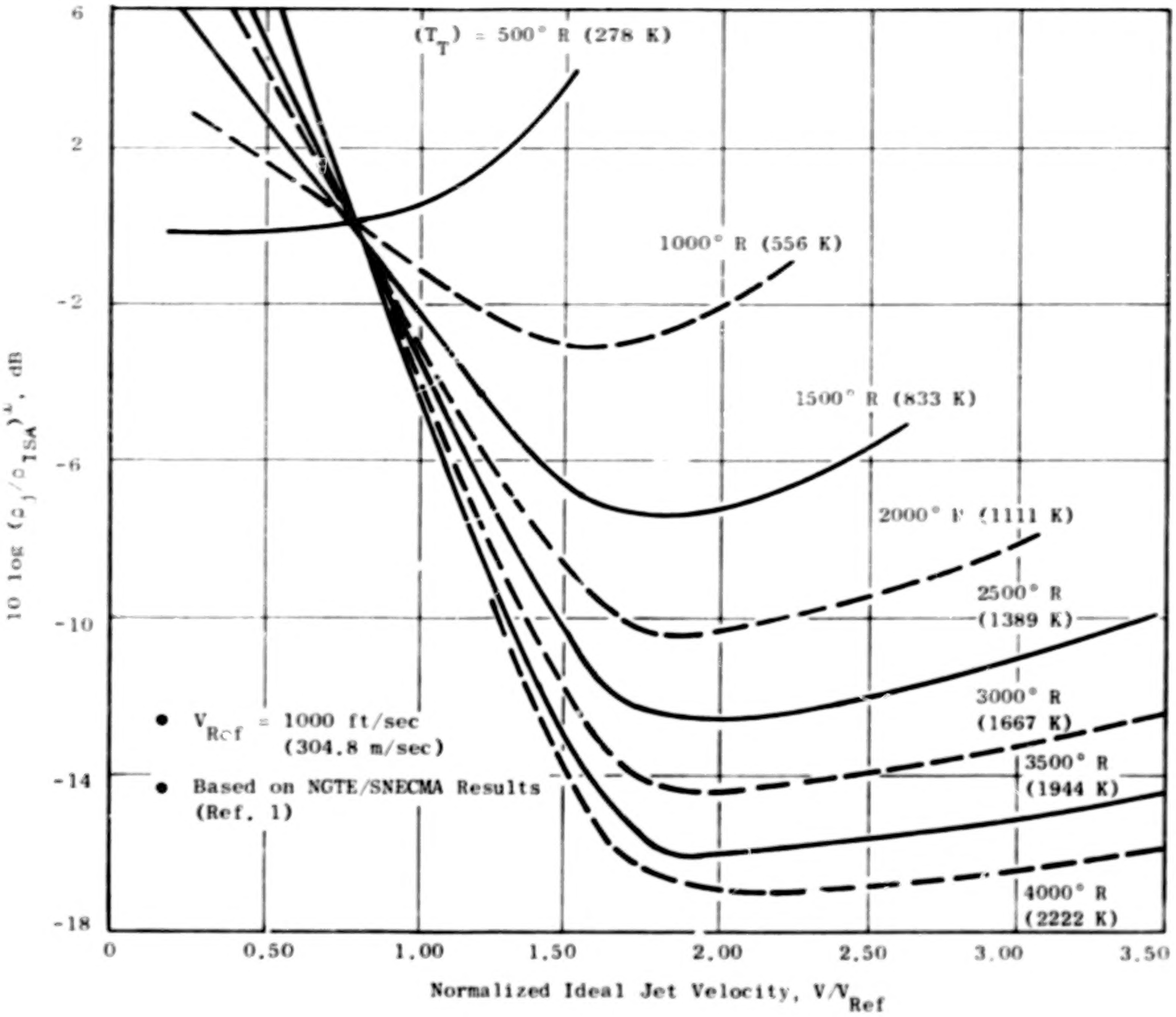

Figure 29. Variation of Density Correction Factor with Ideal Jet Velocity and Temperature.

5.1.3.2 Presentation of Results

Although data comparisons were performed at most of the conditions tested and described in Section 4.3, the test conditions chosen for illustration are the following:

1. V_f = 1800 ft/sec (548.6 m/sec), V_c = 1200 ft/sec (365.8 m/sec) $(P_T/P_o)_f$ = 2.45, $(P_T/P_o)_c$ = 1.56.

   T_{T_F} = 1200° R (667 K), T_{T_C} = 1000° R (556 K)

2. V_f = 2400 ft/sec (731.5 m/sec), V_c = 1200 ft/sec (365.8 m/sec) $(P_T/P_o)_f$ = 3.26, $(P_T/P_o)_c$ = 1.56

   T_{T_f} = 1630° R (906 K), T_{T_c} = 1000° R (556 K)

3. V_f = 2800 ft/sec (853.4 m/sec), V_c = 1400 ft/sec (426.7 m/sec) $(P_T/P_o)_f$ = 3.88, $(P_T/P_o)_c$ = 1.50

   T_{T_f} = 1960° R (1089 K), T_{T_c} = 1460° R (811 K)

Data comparisons at all other conditions are presented in the companion data report CR-135236.

The data presented at the nominal test conditions in this report were all scaled to a full engine size by a factor of 8:1 as described in Section 3.3.1.2. The full-size data were then extrapolated to an effective sideline distance (without extra ground effects, EGA) of 2400 ft (731.5 m). This acoustic range was selected as the test range at which the maximum noise level would be monitored according to the FAR Part 36 sideline monitoring location. This range is equivalent to an aircraft at 2128 ft (646.6 m) sideline distance at an altitude of 1110 ft (338.8 m).

Where appropriate, the acoustic results are presented in the following manner:

- Overall sound power level versus normalized fan jet velocity
- Sound power spectra at three nominal fan/core operating conditions (Section 5.1)
- Maximum perceived noise level versus normalized fan jet velocity.
- Perceived noise level directivity at three nominal fan/core operating conditions
- Sound pressure level spectra at three nominal fan/core operating conditions

5.2 UNSUPPRESSED COANNULAR NOZZLES

This section presents the acoustic characteristics of the unsuppressed coannular nozzles for test conditions representative of the duct-burning turbofan for high core-flow mode ($V_f \geq 1.5\ V_c$). The effect of reducing core flow to about 10% of the fan weight flow is also discussed.

5.2.1 High Core-Flow Test Results

5.2.1.1 Overall Power Level Test Results

Comparisons of normalized overall sound power level (NOAPWL) for all the data taken for $V_f/V_c \geq 1.5$ for the unsuppressed coannular nozzles (with and without a plug) with a synthesized baseline (Σ[Fan + Core]) are shown in Figure 30. The test results show that the unsuppressed coannular nozzles exhibit similar NOAPWL trends. The unsuppressed coannular nozzle with plug (Model 7), however, appears to be about 2 to 3 dB lower in NOAPWL than the unsuppressed coannular nozzle without plug (Model 8); noise reductions relative to the synthesized baseline are seen to be on the order of 6 to 8 dB respectively for the unsuppressed coannular nozzle with plug (Model 7). These levels of noise reduction remain relatively constant throughout the normalized fan jet velocity range of 1.50 to 2.75. These results seem to indicate that the lower noise level of the unsuppressed coannular nozzle with plug (Model 7) may be due to the higher fan radius ratio (R_{rf} =0.902) compared to Model 8 (R_{rf} =0.789).

5.2.1.2 Power Spectra Test Results

Power spectra results for the two unsuppressed coannular nozzles at three nominal operating conditions are shown in Figure 31. The power spectra results reveal the existence of a double-humped characteristic (especially for Model 8, unsuppressed coannular nozzle without plug) usually attributed to the multielement-type suppressor nozzle systems. These results suggest that the high frequency noise is indicative of the high velocity fan jet stream of small annulus height (characteristic dimension); while the low frequency noise is indicative of a downstream or postmerged flow region. The levels of the "humps" of noise also suggest that the initial region and the postmerged region contribute equally to the total noise.

5.2.1.3 Perceived Noise Level Test Results

The normalized maximum perceived noise level versus normalized fan jet velocity for the unsuppressed coannular nozzles is shown in Figure 32. Relative to the synthesized baseline, PNL noise reductions of about 8 to 10 dB are observed for the unsuppressed coannular nozzle with plug (Model 7). The maximum PNL noise reductions are about 2 dB higher in level than their NOAPWL counterparts and they appear to occur at normalized fan velocities between 2.3 and 2.5.

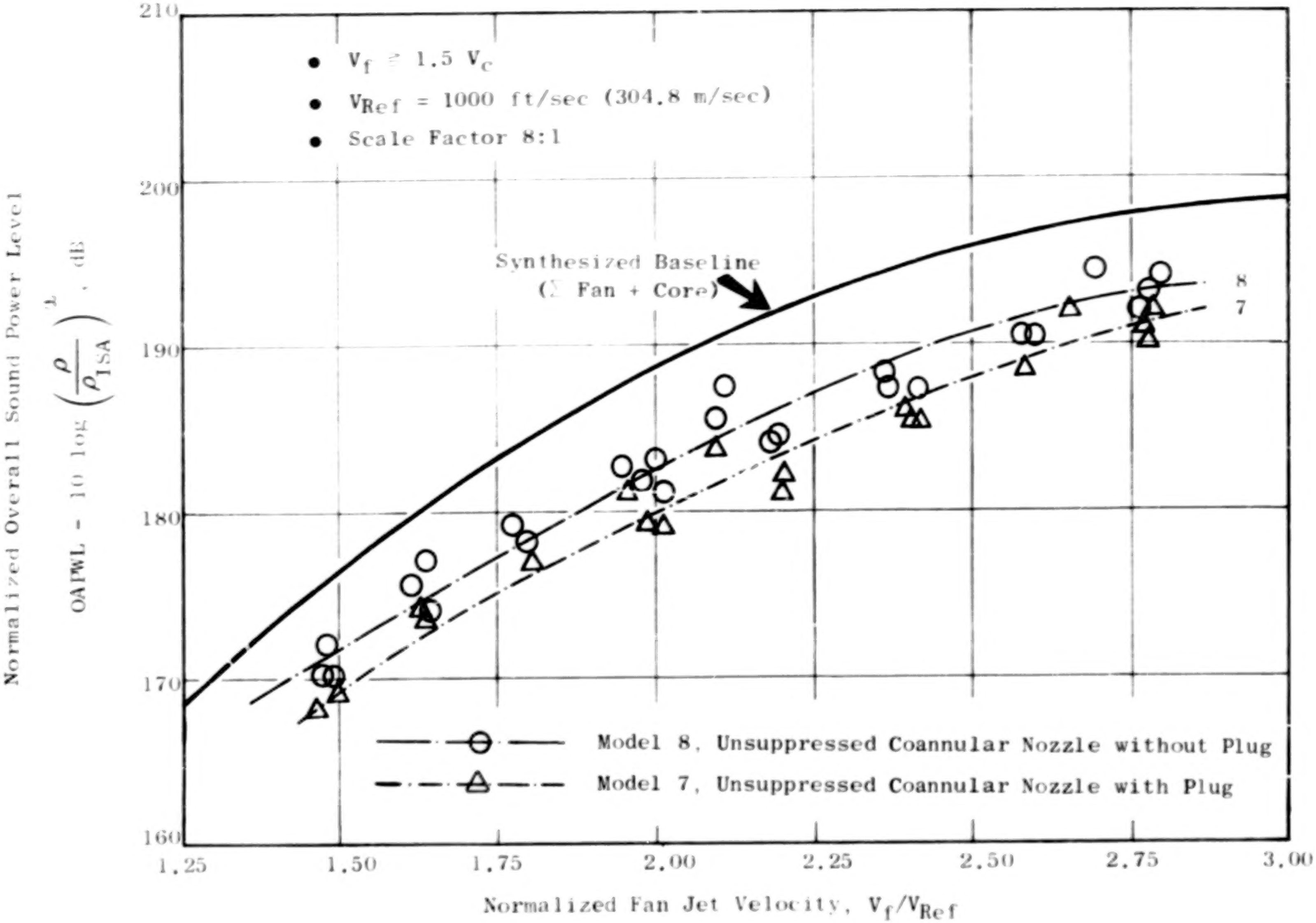

Figure 30. Effect of Fan Jet Velocity on Normalized Overall Sound Power Level of Unsuppressed Coannular Nozzles.

● Scale Factor 8:1

◇ Model 8, Unsuppressed Coannular Nozzle without Plug

△ Model 7, Unsuppressed Coannular Nozzle with Plug

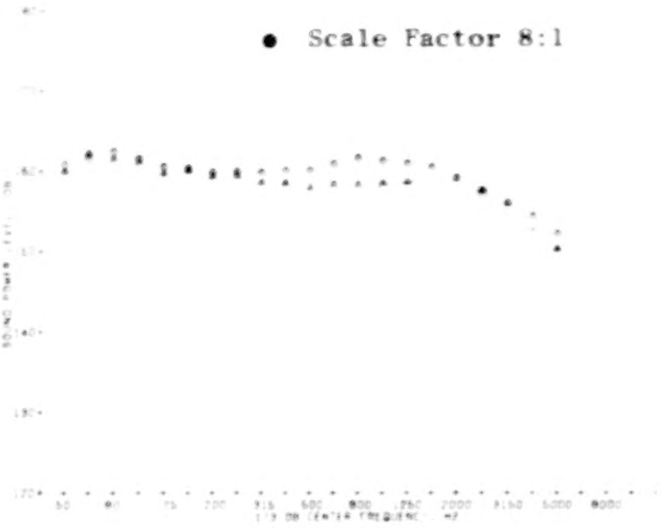

Nominal Conditions

V_f = 1800 ft/sec (548.6 m/sec)

T_{T_f} = 1200° R (667 K)

V_c = 1200 ft/sec (365.8 m/sec)

T_{T_c} = 1000° R (556 K)

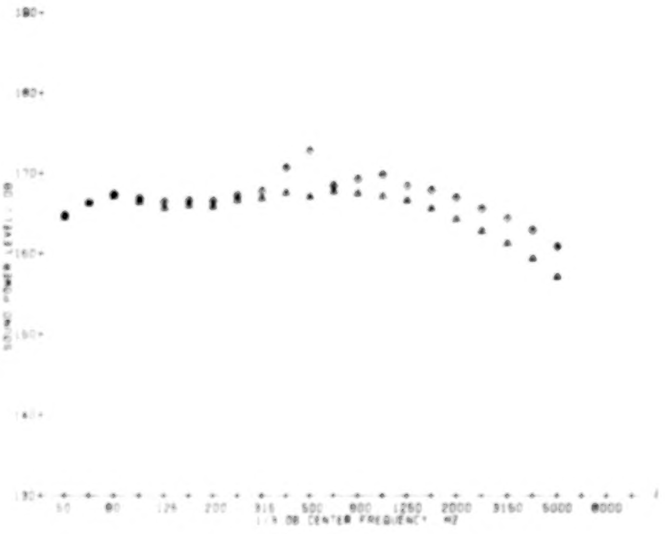

Nominal Conditions

V_f = 2400 ft/sec (731.5 m/sec)

T_{T_f} = 1630° R (906 K)

V_c = 1200 ft/sec (365.8 m/sec)

T_{T_c} = 1000° R (556 K)

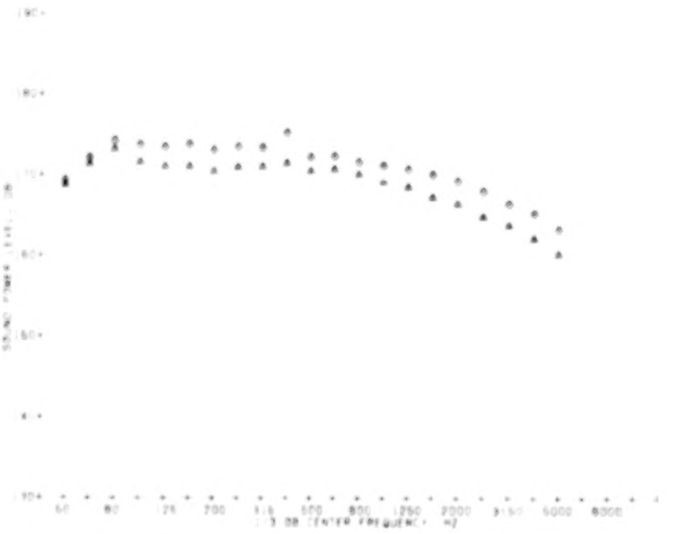

Nominal Conditions

V_f = 2800 ft/sec (853.4 m/sec)

T_{T_f} = 1960° R (1089 K)

V_c = 1400 ft/sec (426.7 m/sec)

T_{T_c} = 1460° R (811 K)

Figure 31. One-Third-Octave Sound Power Spectral Characteristics of Unsuppressed Coannular Nozzles.

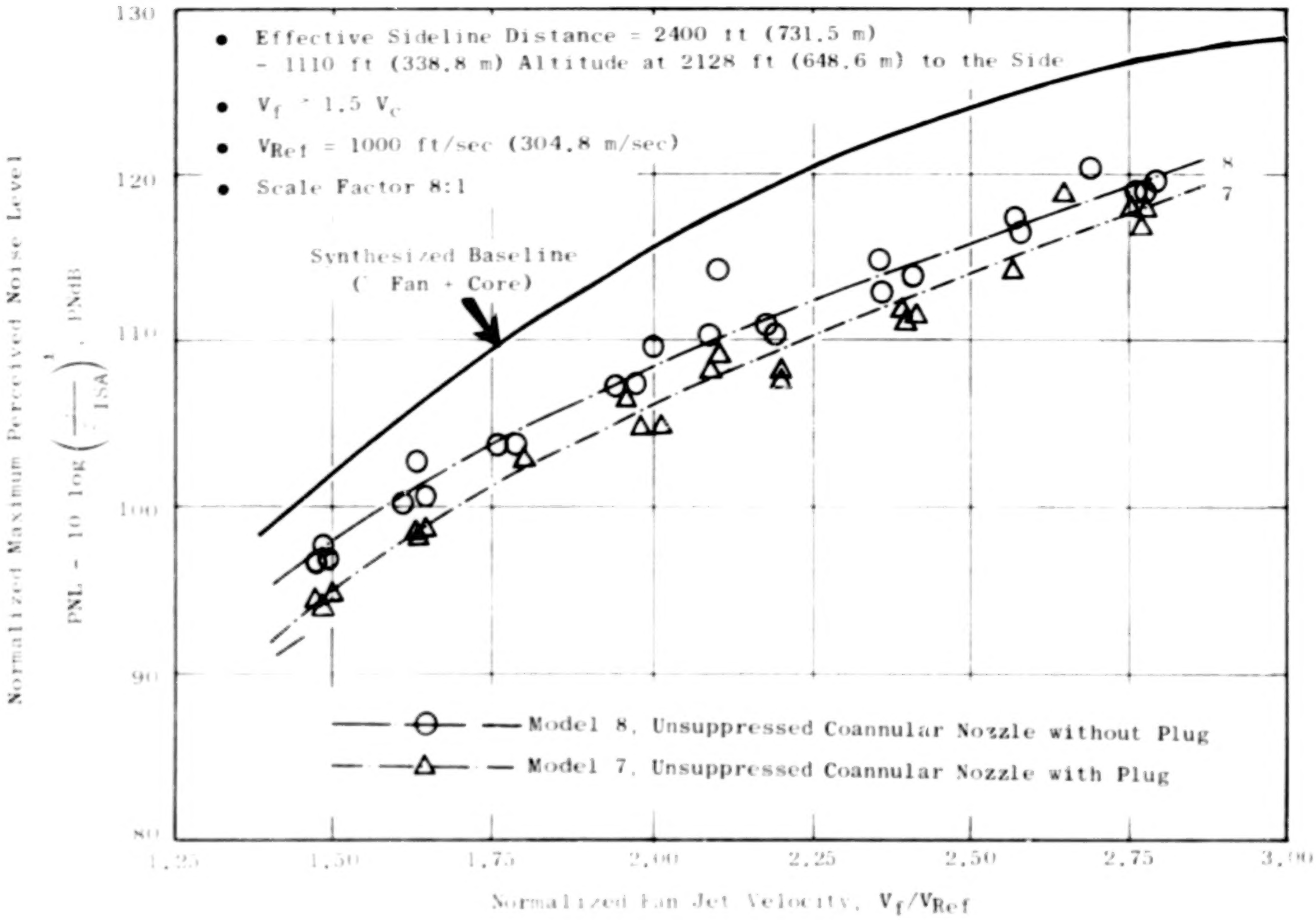

Figure 32. Effect of Fan Jet Velocity on Normalized Maximum Perceived Noise Level of Unsuppressed Coannular Nozzles.

5.2.1.4 Perceived Noise Level Directivity Test Results

The PNL directivity plots on Figure 33 for the unsuppressed coannular nozzles exhibit similar suppression trends to those suppression trends observed in Section 5.2.1.2. The unsuppressed coannular nozzle without plug noise level (Model 8), is consistently higher than the noise level for Model 7, with the difference in noise level increasing from 1 to 3 dB with increasing fan jet velocity.

For both nozzles, noise reduction relative to the synthesized baseline remains fairly constant at the forward angles, then increases from 90° to maximum angle, and finally decreases with increasing angle. At the high velocity conditions and large inlet angles (close to the jet centerline), the noise levels of the synthesized baseline and both coannular nozzles are almost identical. The maximum-angle PNL suppression is observed to increase with increasing velocity, peak at the 2400 ft/sec (731.5 m/sec), and reduce in noise reduction by 1 to 2 dB at the 2800 ft/sec (853.4 m/sec) point.

5.2.1.5 Sound Pressure Level Spectra Test Results

The unsuppressed coannular nozzle SPL spectra comparisons shown in Figures 34 through 36 generally reveal the same characteristics as discussed previously for the power spectra test results in Section 5.2.1.2.

5.2.2 Low Core-Flow Test Results

During the previous discussions dealing with the high core-flow mode of nozzle operation, the effect of curtailing the core flow (e.g. $\dot{\omega}_c/\dot{\omega}_f \leq 10\%$) and the subsequent impact on noise level was briefly touched upon. In reality these "low core flow" studies provided acoustic results which have potential application for a variety of AST acoustic nozzle design concepts.

Most of the low core-flow experiments were carried out on the unsuppressed coannular nozzle with plug (Model 7), and the multitube fan-suppressor nozzle (Model 2), to be discussed later in Section 5.3.2. Several data points were also documented for the unsuppressed coannular nozzle without plug (Model 8). As was discussed in Section 5.2.1, Model 7 noise levels were 2 to 3 dB lower in magnitude than those of Model 8. Comparison of Figure 37 and 32 shows that, at high fan velocities (and supercritical pressure ratios), inhibiting the amount of core flow is less detrimental for the higher radius-ratio configuration (Model 7). Figure 38 illustrates that, at these low amounts of core flow, suppression is maintained within 1-2 dB as compared to the test measurements for high amounts of core flow.

Figure 38 shows a comparison of low core tests with high core tests for the unsuppressed coannular nozzle with plug (Model 7) over a wide range of fan velocities. Relative to the synthesized baseline, both the low core and high core tests show similar noise reduction levels; in the higher fan jet

- Effective Sideline Distance = 2400 ft (731.5 m) - 1110 ft (338.8 m) Altitude at 2128 ft (648.6 m) to the Side
- Scale Factor 8:1

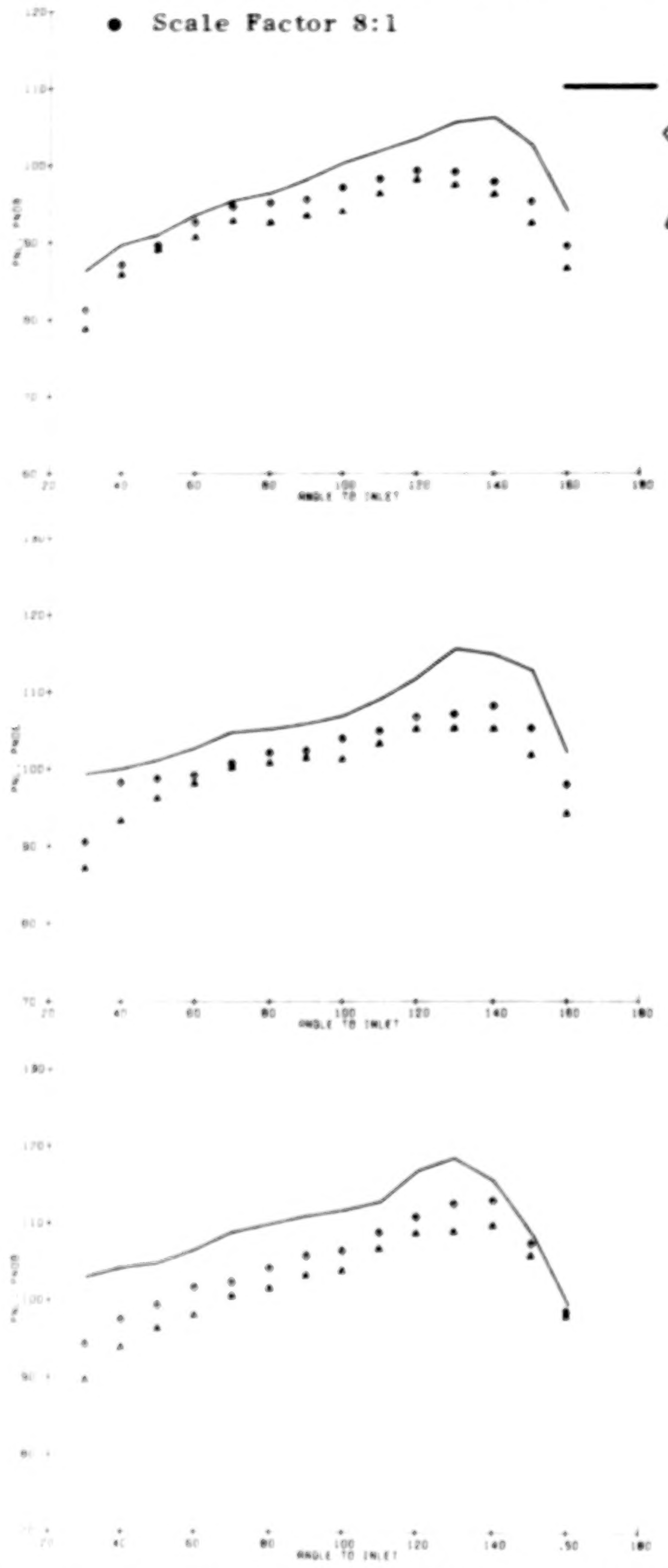

——— Synthesized Baseline (Σ Fan + Core)

◇ Model 8, Unsuppressed Coannular Nozzle without Plug

△ Model 7, Unsuppressed Coannular Nozzle with Plug

Nominal Conditions

V_f = 1800 ft/sec (548.6 m/sec)

T_{T_f} = 1200° R (667 K)

V_c = 1200 ft/sec (365.8 m/sec)

T_{T_c} = 1000° R (556 K)

Nominal Conditions

V_f = 2400 ft/sec (731.5 m/sec)

T_{T_f} = 1630° R (906 K)

V_c = 1200 ft/sec (365.8 m/sec)

T_{T_c} = 1000° R (556 K)

Nominal Conditions

V_f = 2800 ft/sec (853.4 m/sec)

T_{T_f} = 1960° R (1089 K)

V_c = 1400 ft/sec (426.7 m/sec)

T_{T_c} = 1460° R (811 K)

Figure 33. PNL Directivity Characteristics of Unsuppressed Coannular Nozzles.

- Effective Sideline Distance = 2400 ft (731.5 m)
  - 1110 ft (338.8 m) Altitude at 2128 ft (648.6 m) to the Side
- Scale Factor 8:1

◇ Model 8, Unsuppressed Coannular Nozzle without Plug

△ Model 7, Unsuppressed Coannular Nozzle with Plug

Nominal Conditions

V_f = 1800 ft/sec (548.6 m/sec)

T_{T_f} = 1200° R (667 K)

V_c = 1200 ft/sec (365.8 m/sec)

T_{T_c} = 1000° R (556 K)

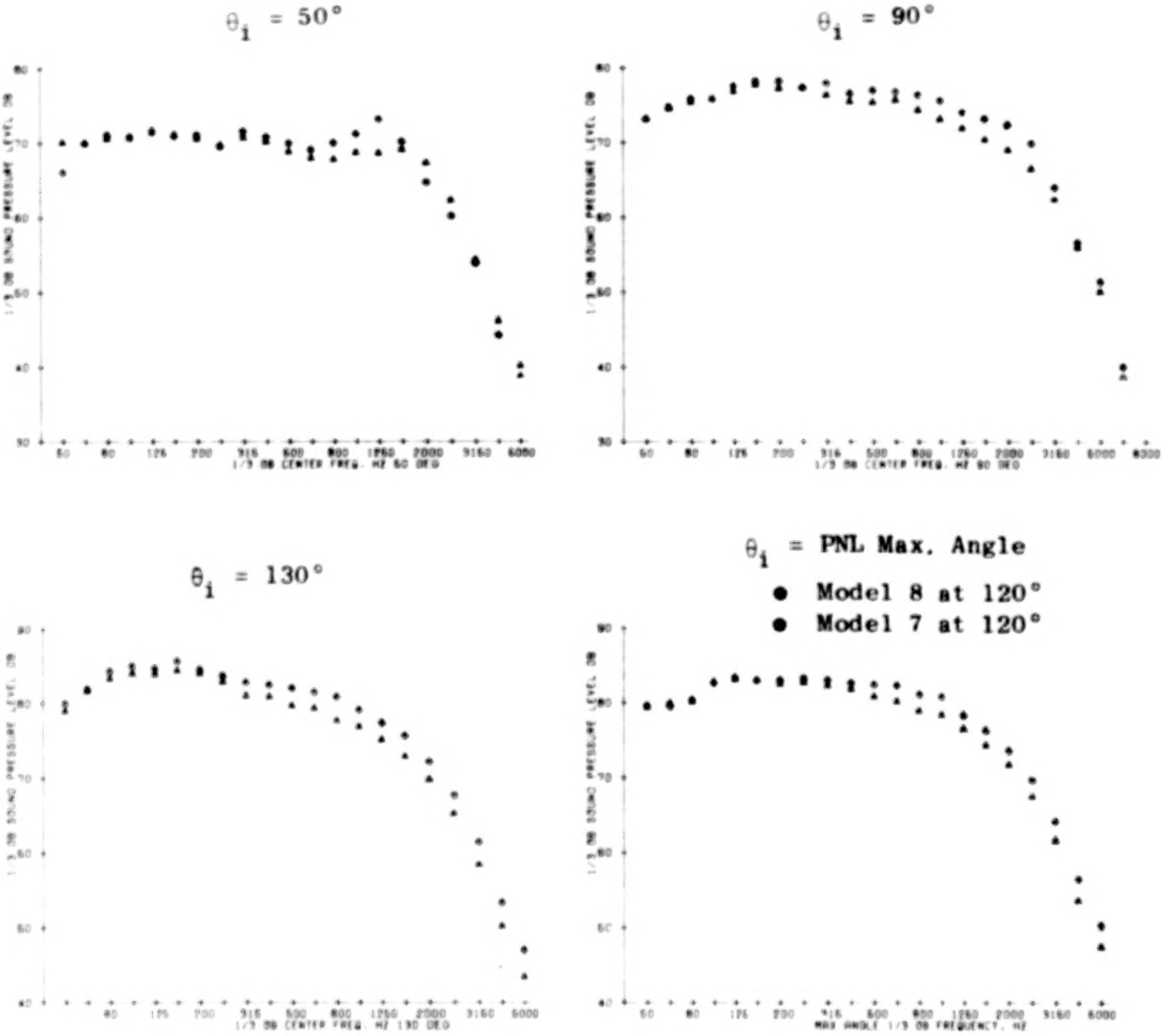

θ_i = 50°

θ_i = 90°

θ_i = 130°

θ_i = PNL Max. Angle

● Model 8 at 120°

● Model 7 at 120°

Figure 34. Unsuppressed Coannular Nozzle SPL Spectra Comparisons at V_f = 1800 ft/sec (548.6 m/sec) and V_c = 1200 ft/sec (365.8 m/sec).

- Effective Sideline Distance = 2400 ft (731.5 m) - 1110 ft (338.8 m) Altitude at 2128 ft (648.6 m) to the Side
- Scale Factor 8:1

Nominal Conditions

◇ Model 8, Unsuppressed Coannular Nozzle without Plug

△ Model 7, Unsuppressed Coannular Nozzle with Plug

V_f = 2400 ft/sec (731.5 m/sec)
T_{T_f} = 1630° R (906 K)
V_c = 1200 ft/sec (365.8 m/sec)
T_{T_c} = 1000° R (556 K)

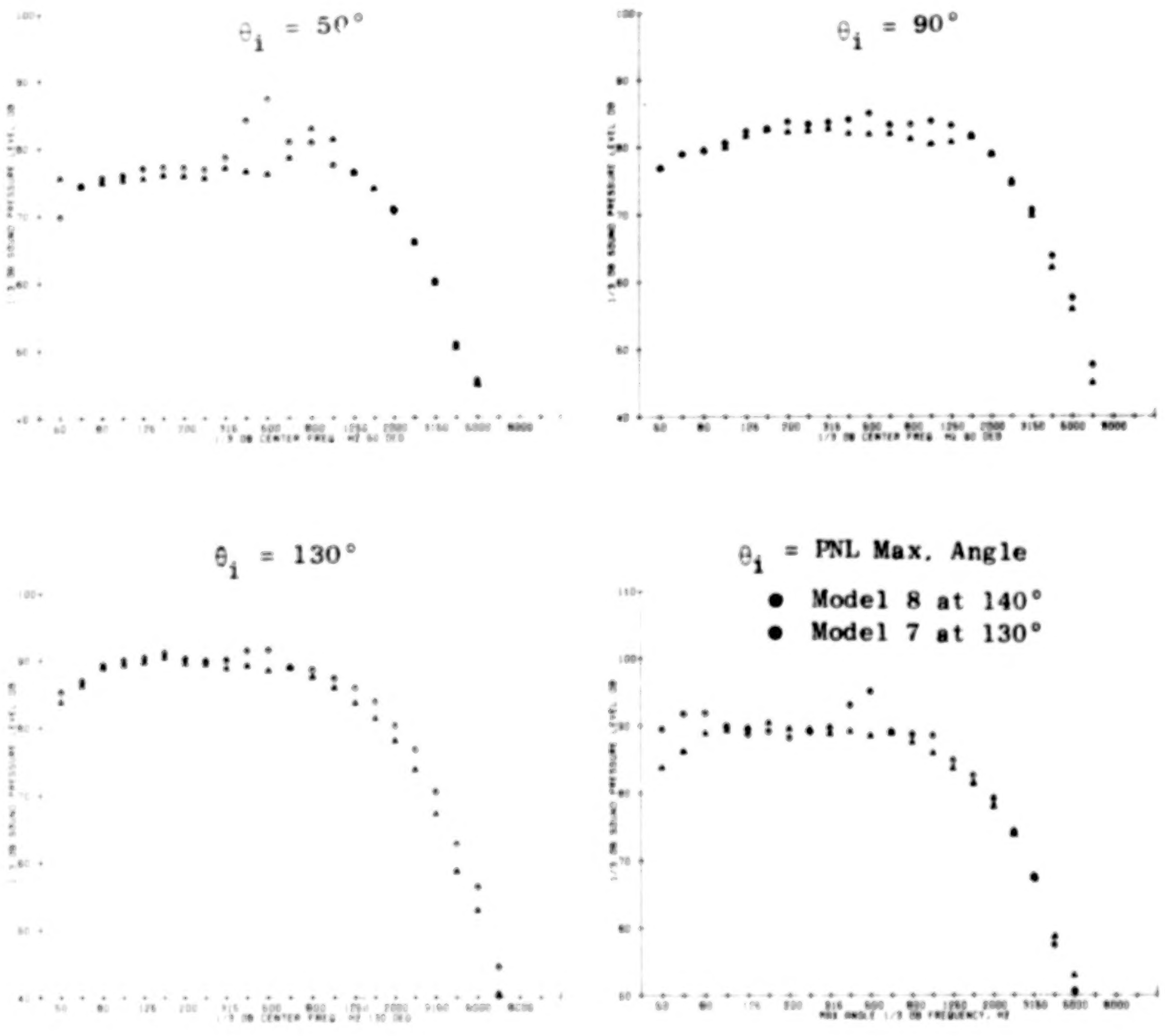
θ_i = 50°

θ_i = 90°

θ_i = 130°

θ_i = PNL Max. Angle
- ● Model 8 at 140°
- ● Model 7 at 130°

Figure 35. Unsuppressed Coannular Nozzle SPL Spectra Comparisons at V_f = 2400 ft/sec (731.5 m/sec) and V_c = 1200 ft/sec (365.8 m/sec).

- Effective Sideline Distance = 2400 ft (731.5 m)
  - 1110 ft (338.8 m) Altitude at 2128 ft (648.6 m) to the Side
- Scale Factor 8:1

Nominal Conditions

V_f = 2800 ft/sec (853.4 m/sec)
T_{T_f} = 1960° R (1089 K)
V_c = 1400 ft/sec (426.7 m/sec)
T_{T_c} = 1460° R (811 K)

◇ Model 8, Unsuppressed Coannular Nozzle without Plug

△ Model 7, Unsuppressed Coannular Nozzle with Plug

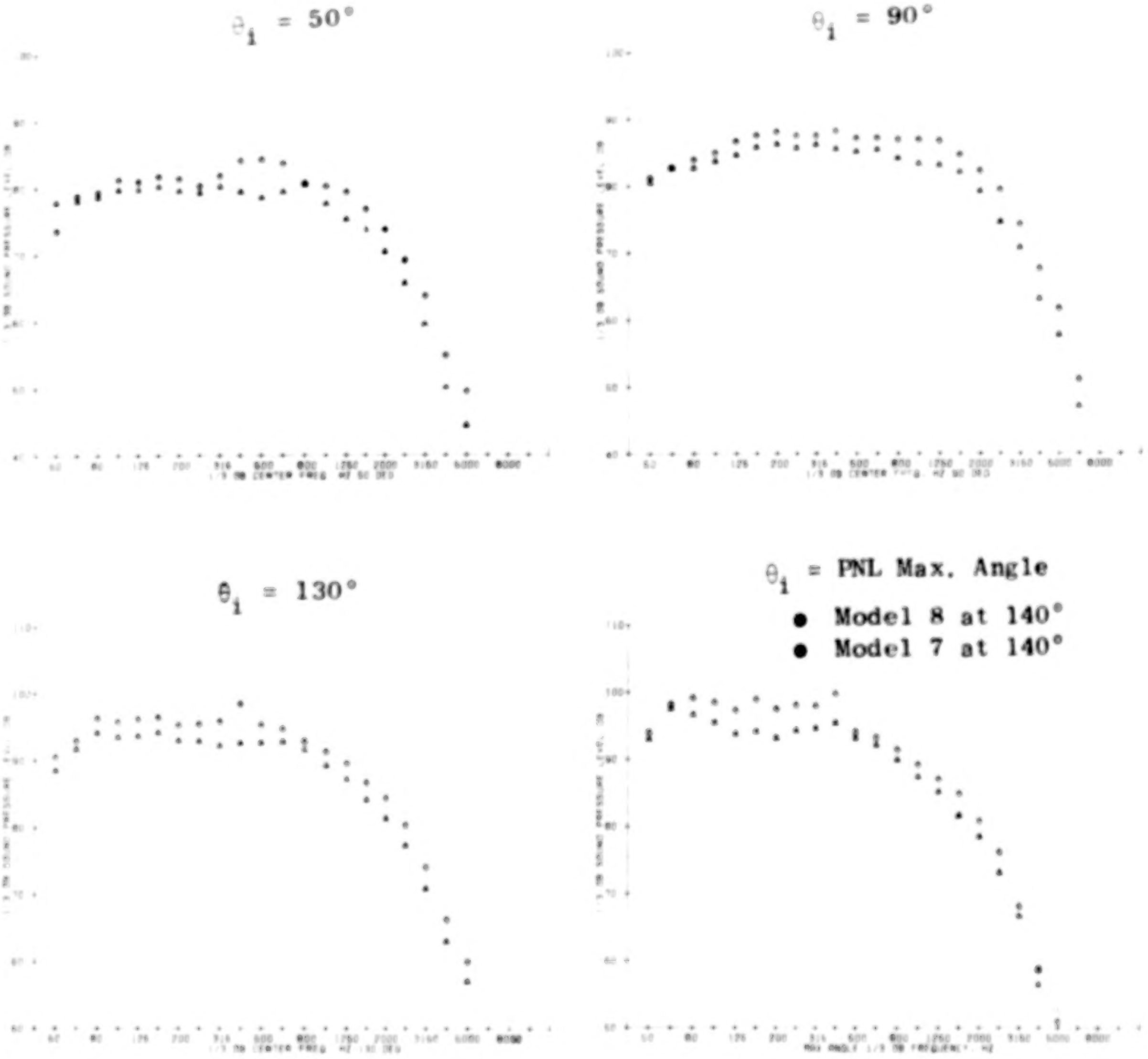

Figure 36. Unsuppressed Coannular Nozzle SPL Spectra Comparisons at V_f = 2800 ft/sec (853.4 m/sec) and V_c = 1400 ft/sec (426.7 m/sec).

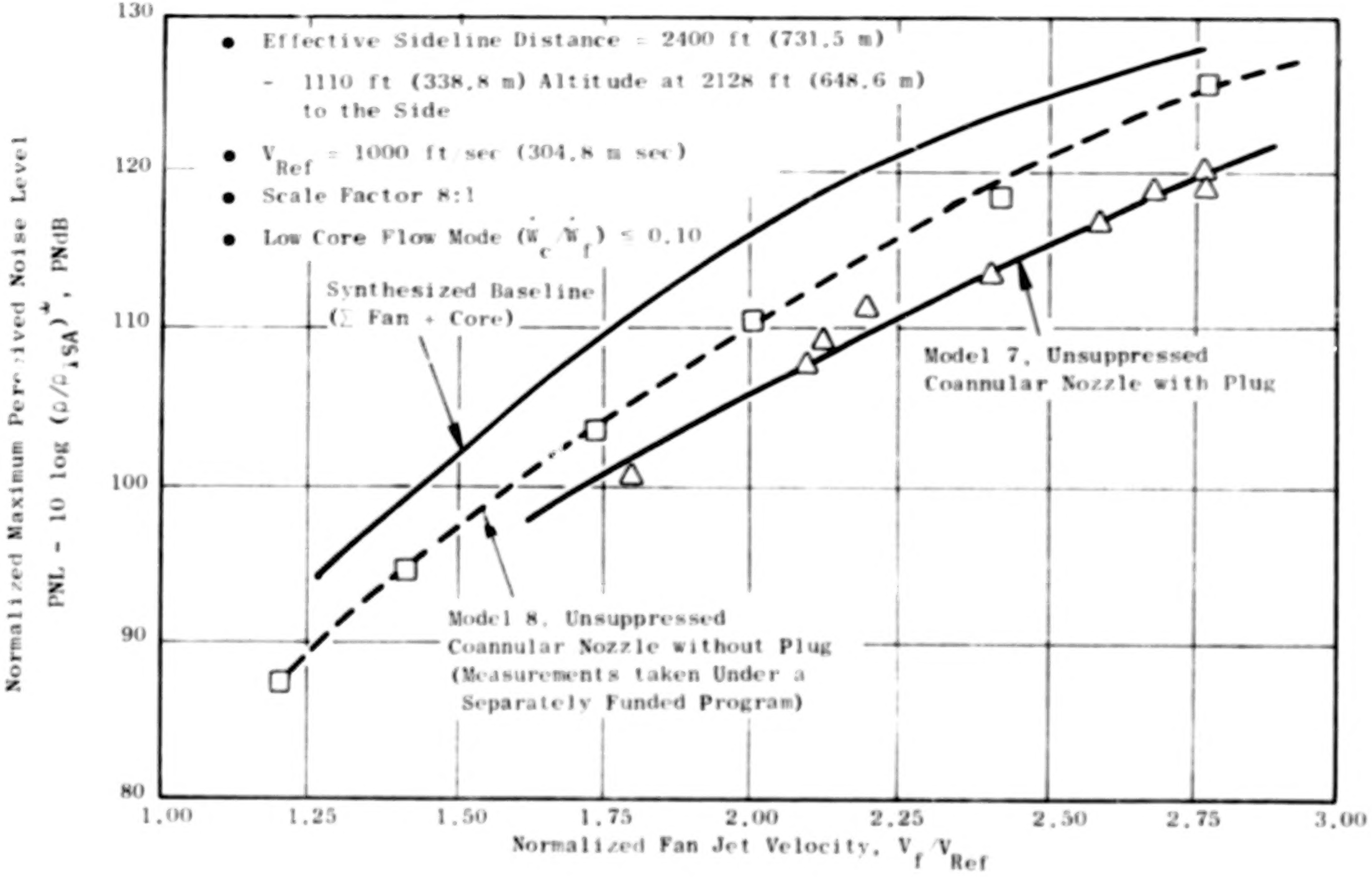

Figure 37. Effect of Fan Jet Velocity on Unsuppressed Coannular Nozzles During Low Core-Flow Operation.

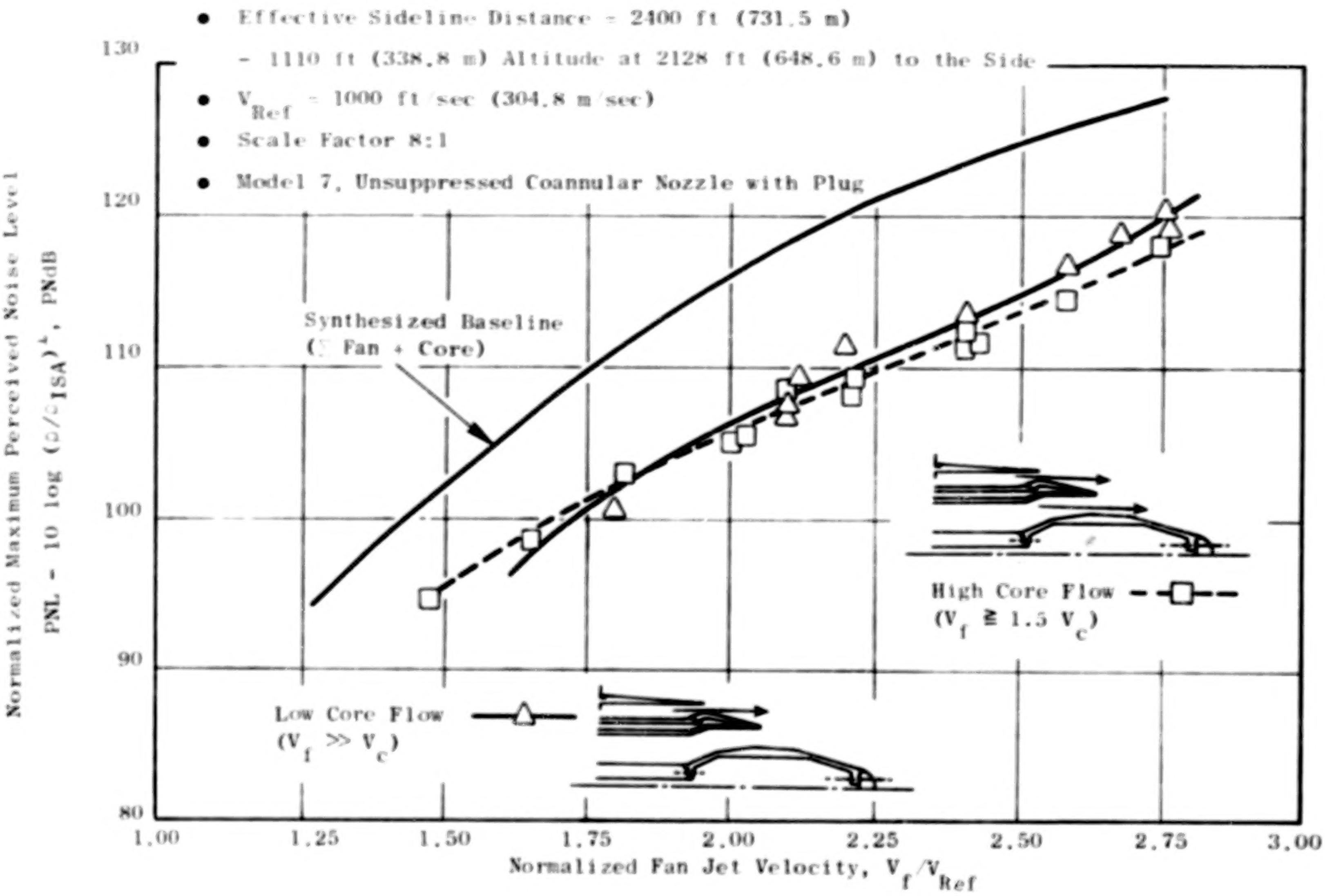

Figure 38. Effect of Core Flow and Fan Velocity on Normalized Perceived Noise Level on the Unsuppressed Coannular Nozzle with Plug (Model 7).

- Effective Sideline Distance = 2400 ft (731.5 m)

  - 1110 ft (338.8 m) Altitude at 2128 ft (648.6 m) to the Side

- Scale Factor 8:1

- Model 7, Unsuppressed Coannular Nozzle with Plug

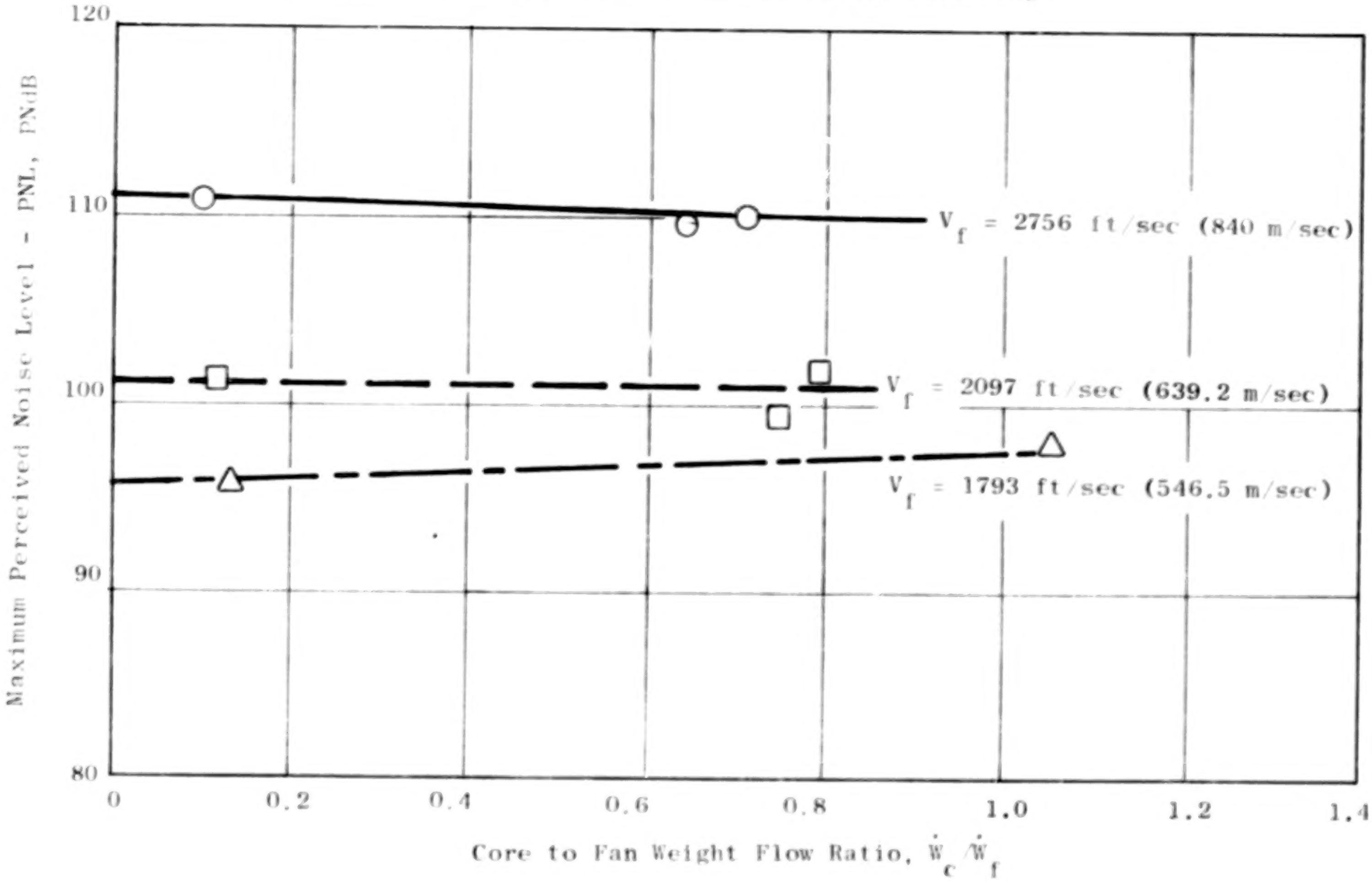

Figure 39. Core/Fan Weight-Flow Ratio Effect on Maximum Perceived Noise Level on the Unsuppressed Coannular Nozzle with Plug (Model 7).

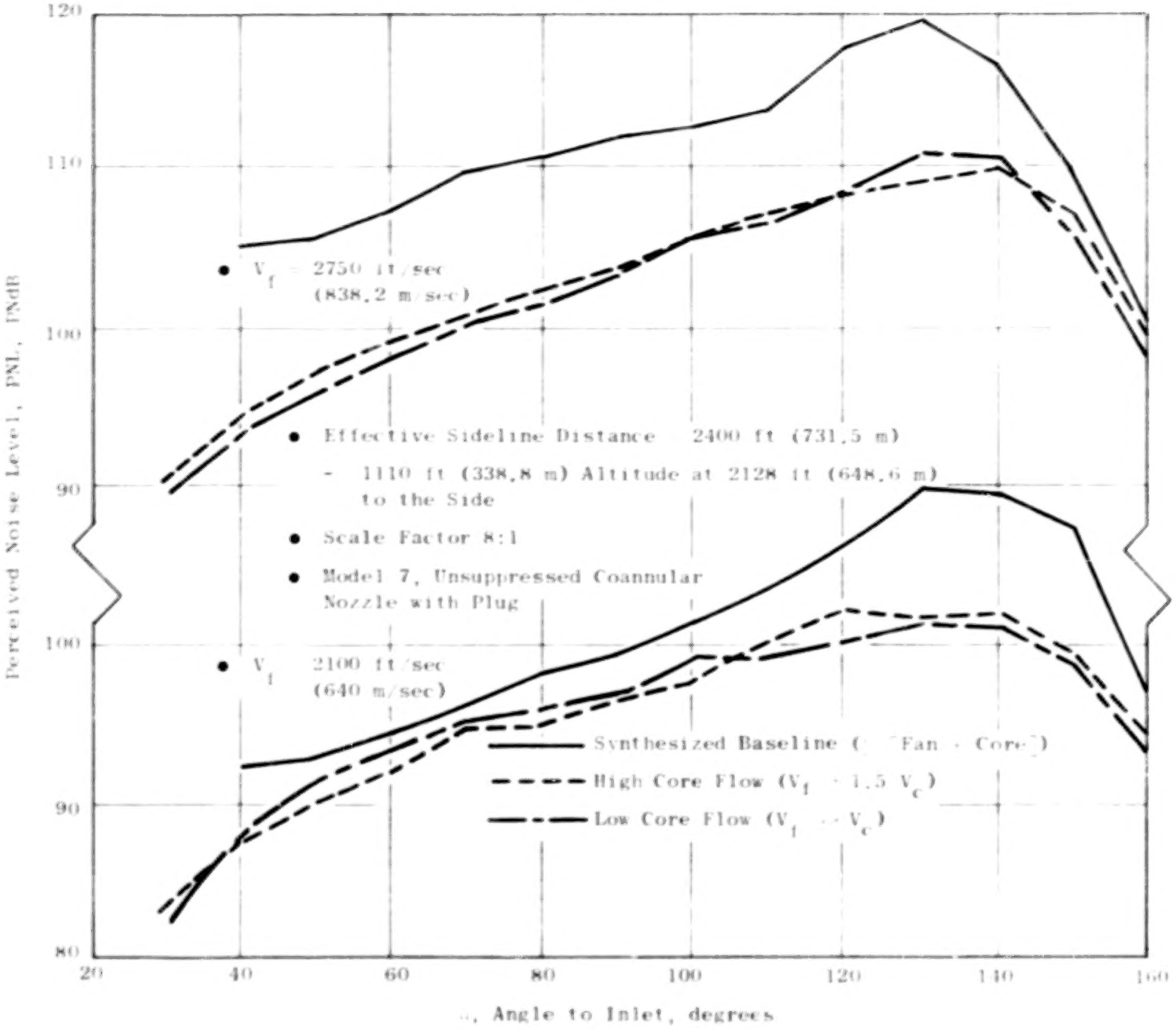

Figure 40. Effect of Core Flow on PNL Directivity on the Unsuppressed Coannular Nozzle with Plug (Model 7).

velocity regions the high core-flow results are the more favorable while at lower fan jet velocities the low core-flow results show a slight advantage.

Figure 39 illustrates the sensitivity of maximum perceived noise level with core to fan weight-flow ratio for the unsuppressed coannular nozzle with plug for fan velocities of 2756 ft/sec (840 m/sec), 2097 ft/sec (639.2 m/sec), and 1793 ft/sec (546.5 m/sec). One observation is that the $PNL_{max.}$ is relatively insensitive at the weight-flow ratios shown (ω_c/ω_f = 0.1 to 0.8); the impact of this result is that, if the noise benefits observed above are maintained for weight-flow ratios of 5% or less, a high radius-ratio annular nozzle with a low amount of inner core flow has a greater range of applicability for advanced-concept engine cycles than just a duct-burning turbofan cycle.

The effect of core flow on PNL directivity and SPL spectra are illustrated for completeness in Figures 40 and 41. The test results are for fan velocities of 2750 ft/sec (838.2 m/sec) and 2100 ft/sec (640 m/sec). These results illustrate the similarity of acoustic trends between low core and high core-flow test conditions, as well as indicate that directivity and spectral shaping can be accomplished by management of the core stream flow.

5.2.3 Acoustic Correlations

All the results presented above were for fan to core velocity ratios greater than 1.5. Figures 42 and 43 show normalized OAPWL test results for all the fan to core velocity ratios tested, less than one as well as greater than one. In obtaining the normalized density corrections for these results, the $(P_T/P_o)_c$ and T_{T_c} were used to calculate the density correction $\omega \times 10 \log (\rho/\rho_{ISA})$, when $V_f/V_c \leq 1$. When $V_f/V_c > 1$ the fan stream parameters were used to calculate the density correction terms.

Figures 42 and 43 show that the overall power level distributions with fan jet velocity are rather systematic for values of increasing velocity ratio of V_f/V_c = 0.6 to 2.0; this observation is true for the unsuppressed coannular nozzles with and without a plug (Models 7 and 8). As shown, the fan velocity power-law dependencies can be as high as 11 and as low as 5 depending upon the velocity ratio selected. The systematic trends exhibited, and the rather minimal data scatter observed in Figures 42 and 43 suggest that a better collapsing or similarity velocity parameter exists which may depend on core stream as well as fan stream velocity.

5.2.4 Summary Remarks*

In general, the results presented in this section have shown that unsuppressed coannular nozzles can provide PNL suppressions of 8 to 10 PNdB

---

* See Author's note at the end of Section 9 for comments on new measurements and findings regarding unsuppressed, high-radius-ratio, coannular plug nozzles.

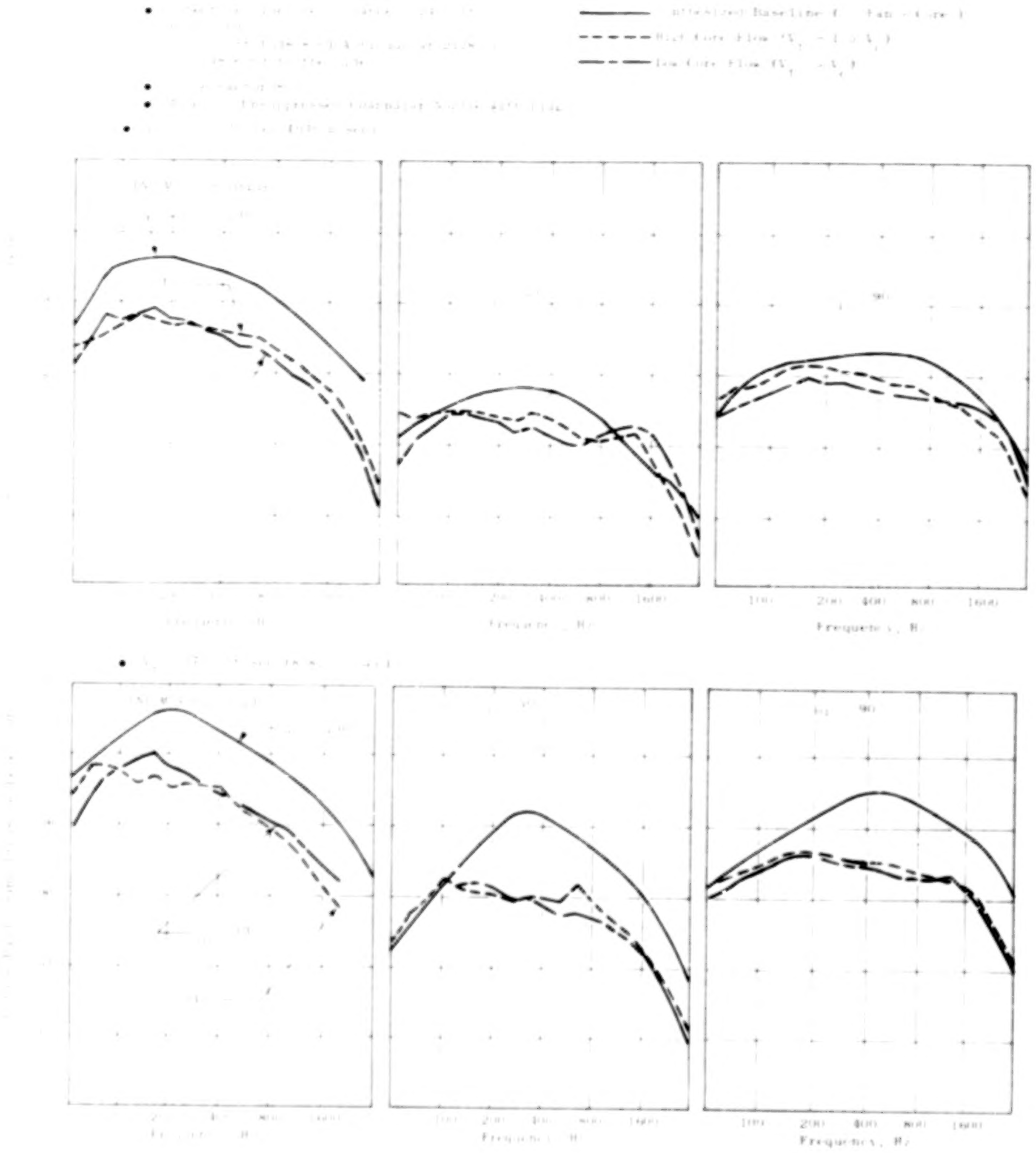

Figure 41. Effect of Core Flow on Unsuppressed Coannular Nozzle with Plug (Model 7) SPL Spectra.

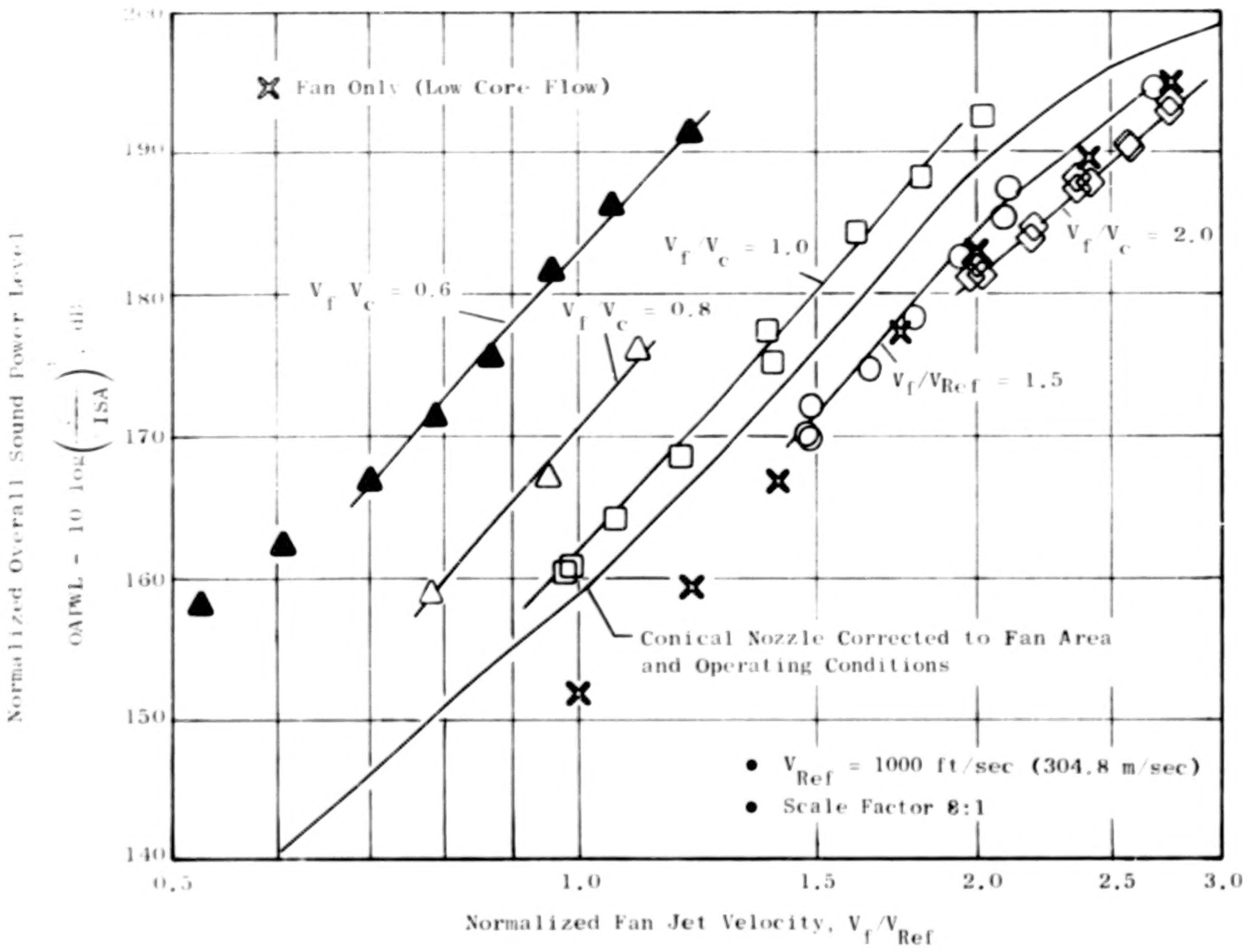

Figure 42. Effect of Fan to Core Velocity Ratio on Normalized Overall Sound Power Level of Unsuppressed Coannular Nozzle without Plug (Model 8).

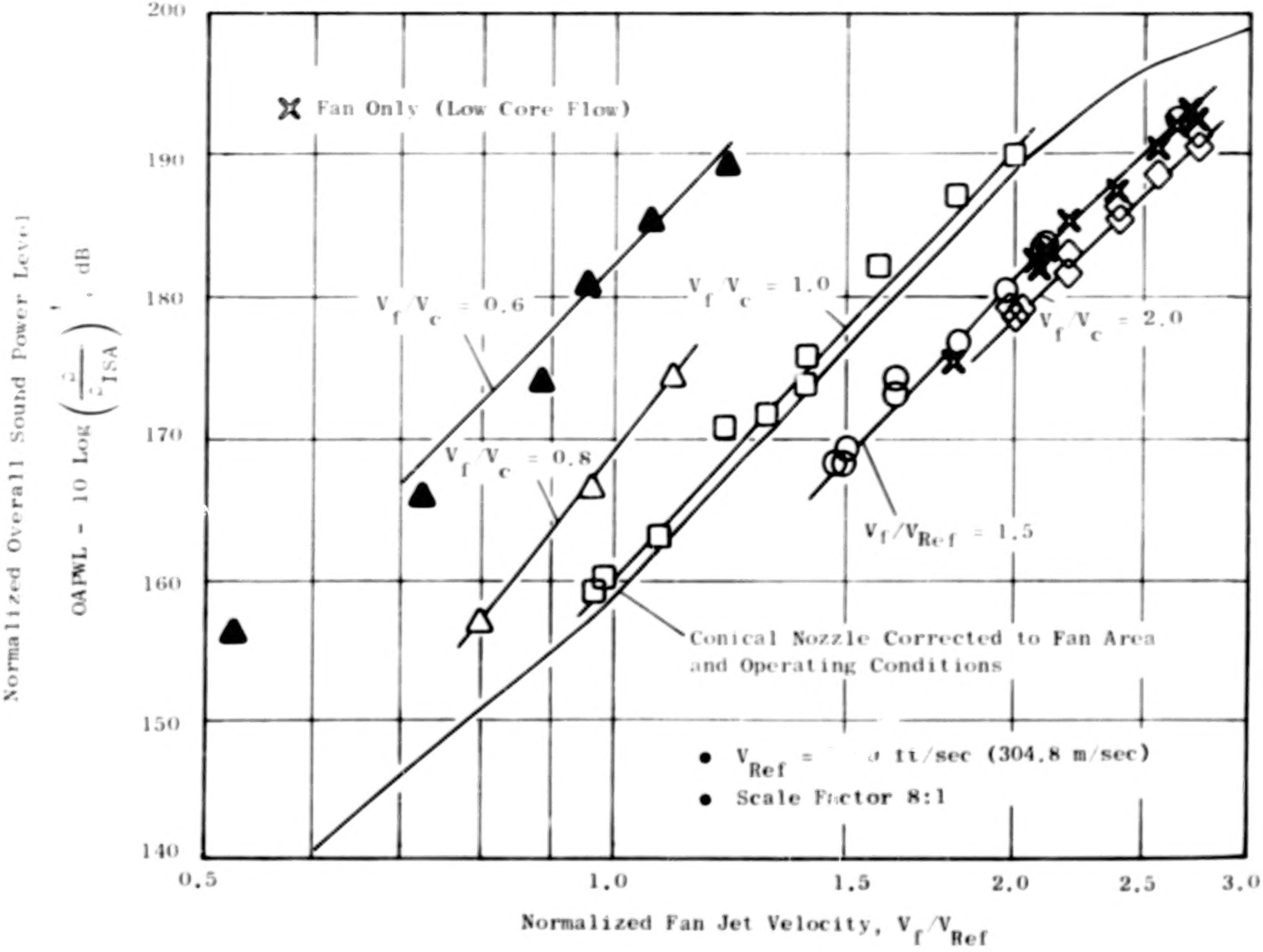

Figure 43. Effect of Fan to Core Velocity Ratio on Normalized Overall Sound Power Level of Unsuppressed Coannular Nozzle with Plug (Model 7).

relative to a synthesized baseline. The unsuppressed coannular nozzle with plug suppression levels (10 PNdB) are comparable to what has been previously attained by mechanical-type suppressors; furthermore, curtailing the core flow of the unsuppressed coannular nozzle with plug to values under 10% of the fan flow only reduces the suppression by 2 PNdB.

5.3 MULTIELEMENT FAN-SUPPRESSOR NOZZLES

The noise reduction characteristics of two multielement fan suppressors are discussed below. Only the suppressor systems with no ejectors are discussed in this section since they represent a system which possesses both performance and mechanical advantages over conventional-type C/D exhaust nozzles. When integrated with high Mach number military or commercial aircraft and future advanced-technology engines (such as duct-burning turbofans, variable-cycle engines, etc), the dual-flow plug nozzle which is especially amenable to mechanical implementation of jet noise suppressers offers very attractive system advantages. As with the unsuppressed coannular nozzles (Section 5.2), most of the acoustic results for the multielement fan-suppressor nozzles are presented for the high core flow mode. Very preliminary results obtained during low core-flow operation for one of the suppressor nozzles, the multitube fan-suppressor nozzle (Model 2), are also shown. Comparisons with the unsuppressed coannular nozzle results (from Section 5.2) are included; the data presentation and format is similar to that presented in Section 5.2.

5.3.1 High Core-Flow Test Results

5.3.1.1 Overall Power Level Test Results

The multichute (Model 1) and multitube (Model 2) fan-suppressor nozzle acoustic results are shown in Figures 44 through 51. Figures 44 and 45 present normalized overall sound power level versus normalized fan jet velocity plots for all the data taken on the multielement fan-suppressor nozzles (Model 1 and Model 2). The noise levels and trends are very similar between the two nozzles and, as will be discussed in Section 5.3.3, both fan-suppressor nozzles provide substantial power level reduction ranging from 2 dB at $V_f/V_c \simeq 1.0$ up to 5 dB at $V_f/V_c \simeq 1.5$, relative to the unsuppressed coannular nozzle with plug (Model 7), as can be seen by comparing Figure 44 and 45 to 43.

The high core-flow NOAPWL data corresponding to $V_f/V_c \simeq 1.5$ are compared with a synthesized baseline ([Fan + Core]) in Figure 46. The differences between the multichute (Model 1) and the multitube (Model 2) fan-suppressor nozzles are within 1 dB throughout the entire normalized fan jet velocity range (V_f/V_c = 1.5 to 2.75); however, the multitube data are consistently below those of the multichute suppressor nozzle. Noise reductions relative to the synthesized baseline nozzle remain essentially constant (12 to 13 dB) for normalized fan jet velocities above 2.0. It is interesting to note that even at a normalized fan jet velocity of 1.5 the noise reduction is 8 dB.

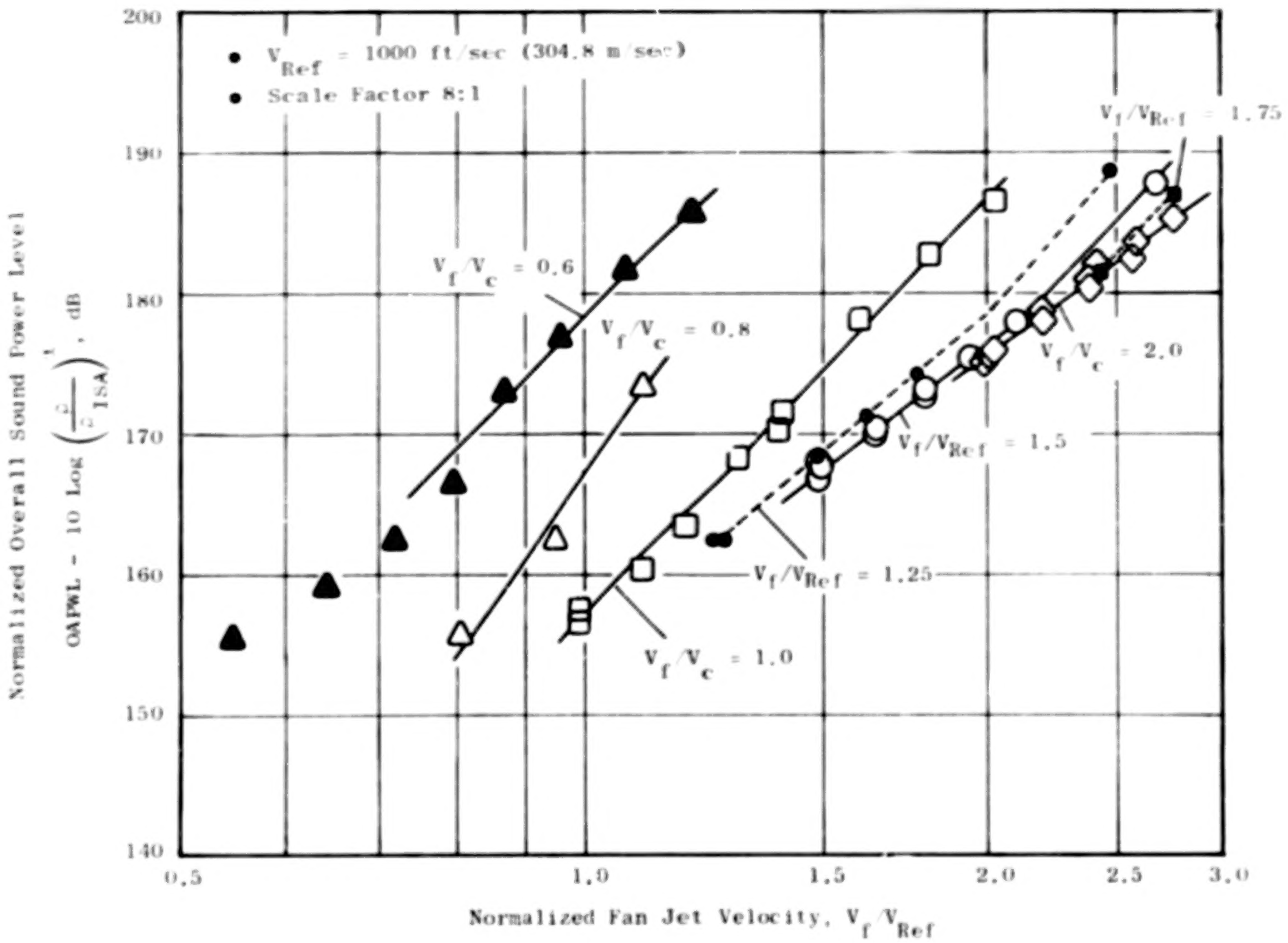

Figure 44. Effect of Fan to Core Velocity Ratio on Normalized Overall Sound Power Level of Multichute Fan Suppressor Nozzle (Model 1).

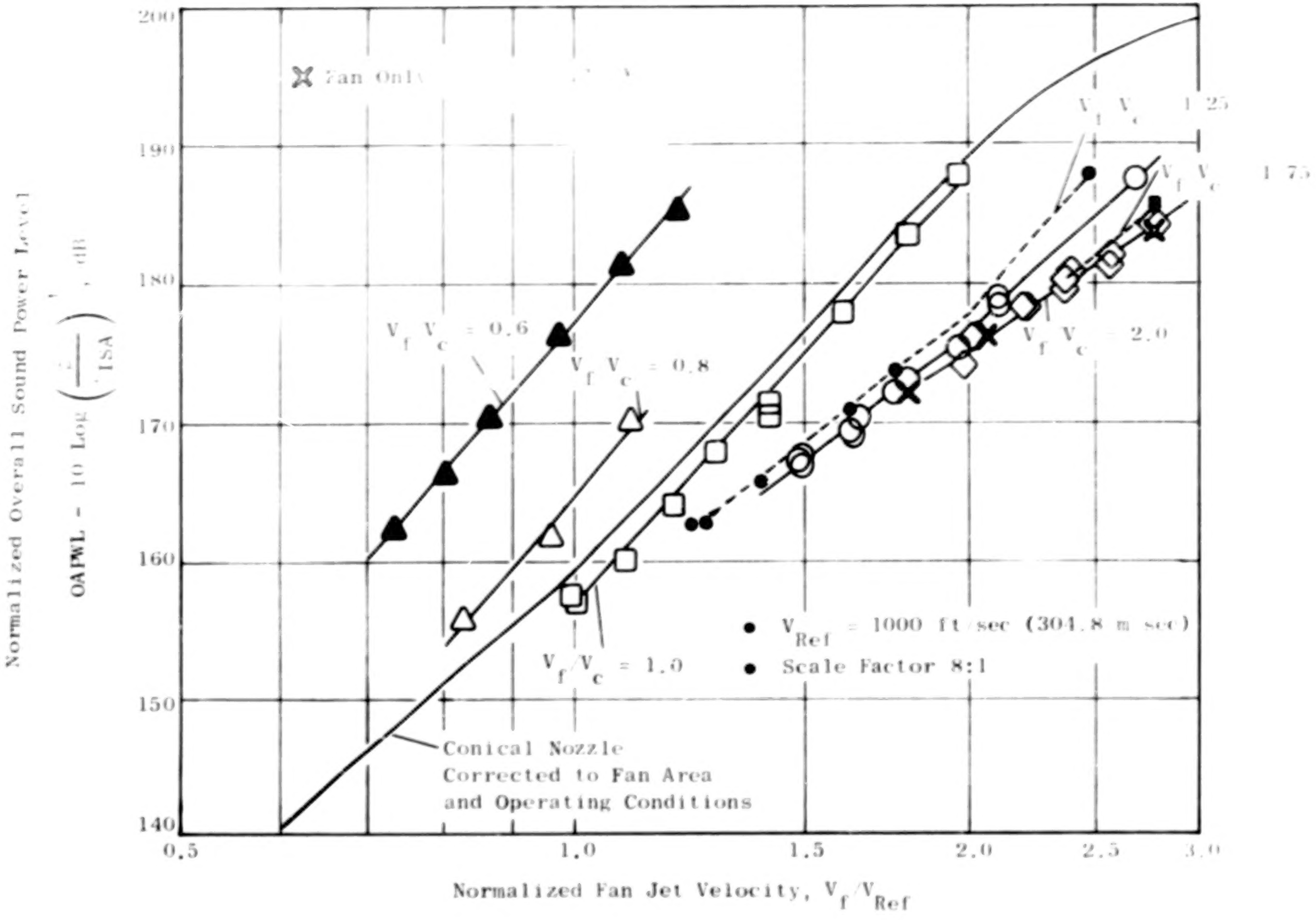

Figure 45. Effect of Fan to Core Velocity Ratio on Normalized Overall Sound Power Level of Multitube Fan Suppressor Nozzle (Model 2).

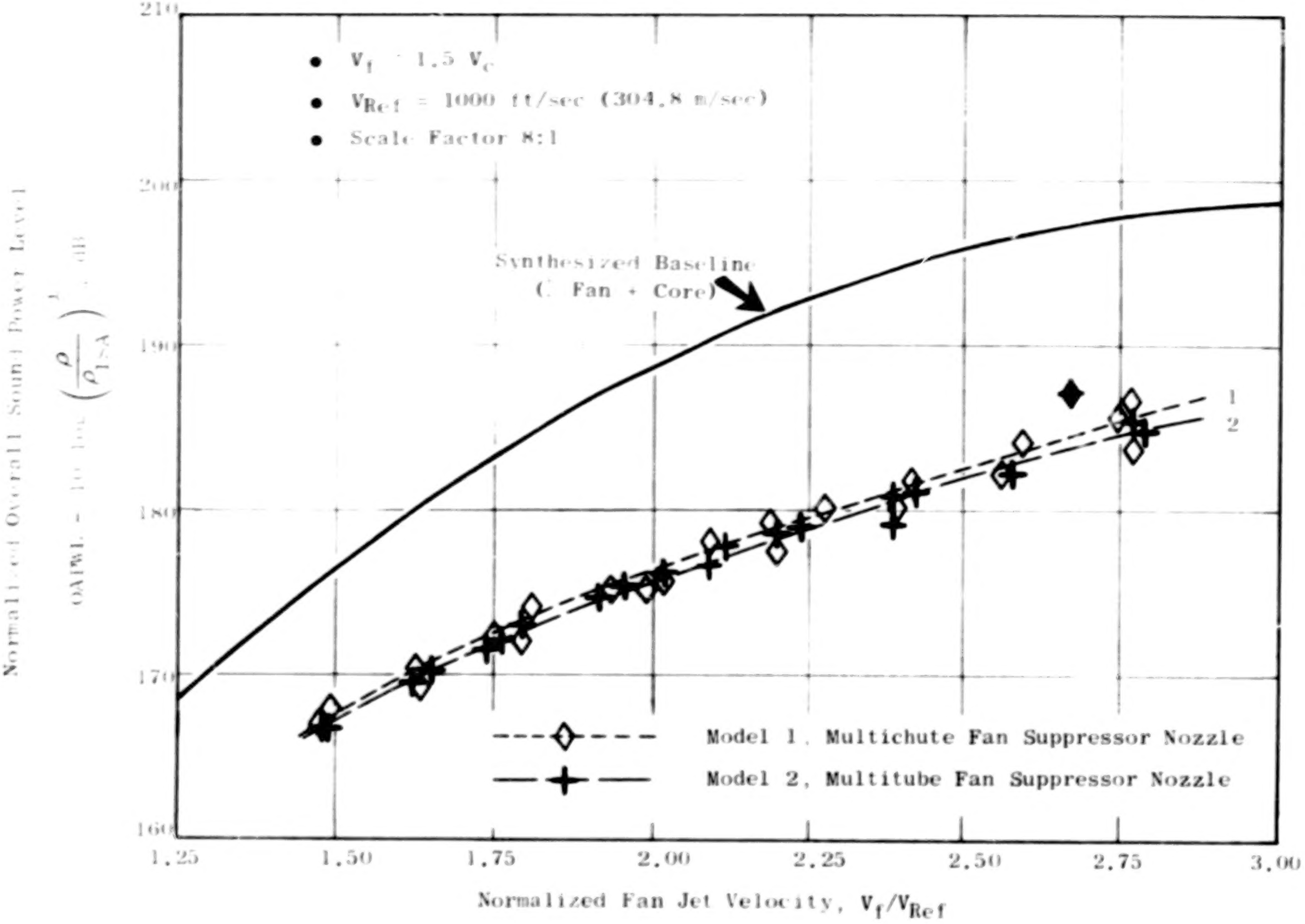

Figure 46. Effect of Fan Jet Velocity on Normalized Overall Sound Power Level of Multi-element Fan Suppressor Nozzles.

● Scale Factor 8:1

□ Model 1, Multichute Fan Suppressor Nozzle

○ Model 2, Multitube Fan Suppressor Nozzle

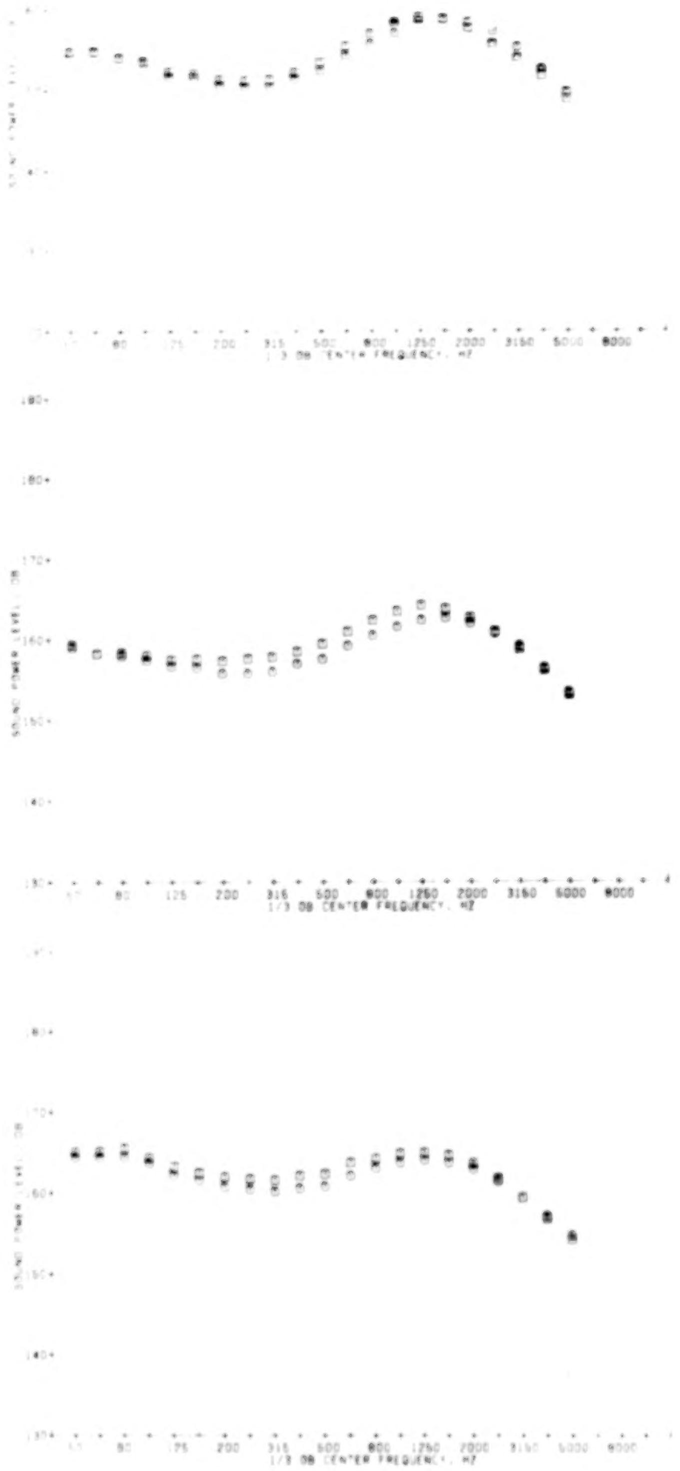

Nominal Conditions

V_f = 1800 ft/sec (548.6 m/sec)

T_{T_f} = 1200° R (667 K)

V_c = 1200 ft/sec (365.8 m/sec)

T_{T_c} = 1000° R (556 K)

Nominal Conditions

V_f = 2400 ft/sec (731.5 m/sec)

T_{T_f} = 1630° R (906 K)

V_c = 1200 ft/sec (365.8 m/sec)

T_{T_c} = 1000° R (556 K)

Nominal Conditions

V_f = 2800 ft/sec (853.4 m/sec)

T_{T_f} = 1960° R (1089 K)

V_c = 1400 ft/sec (426.7 m/sec)

T_{T_c} = 1460° R (811 K)

Figure 47. One-Third-Octave Sound Power Spectral Characteristics of Multi-element Fan Suppressor Nozzles.

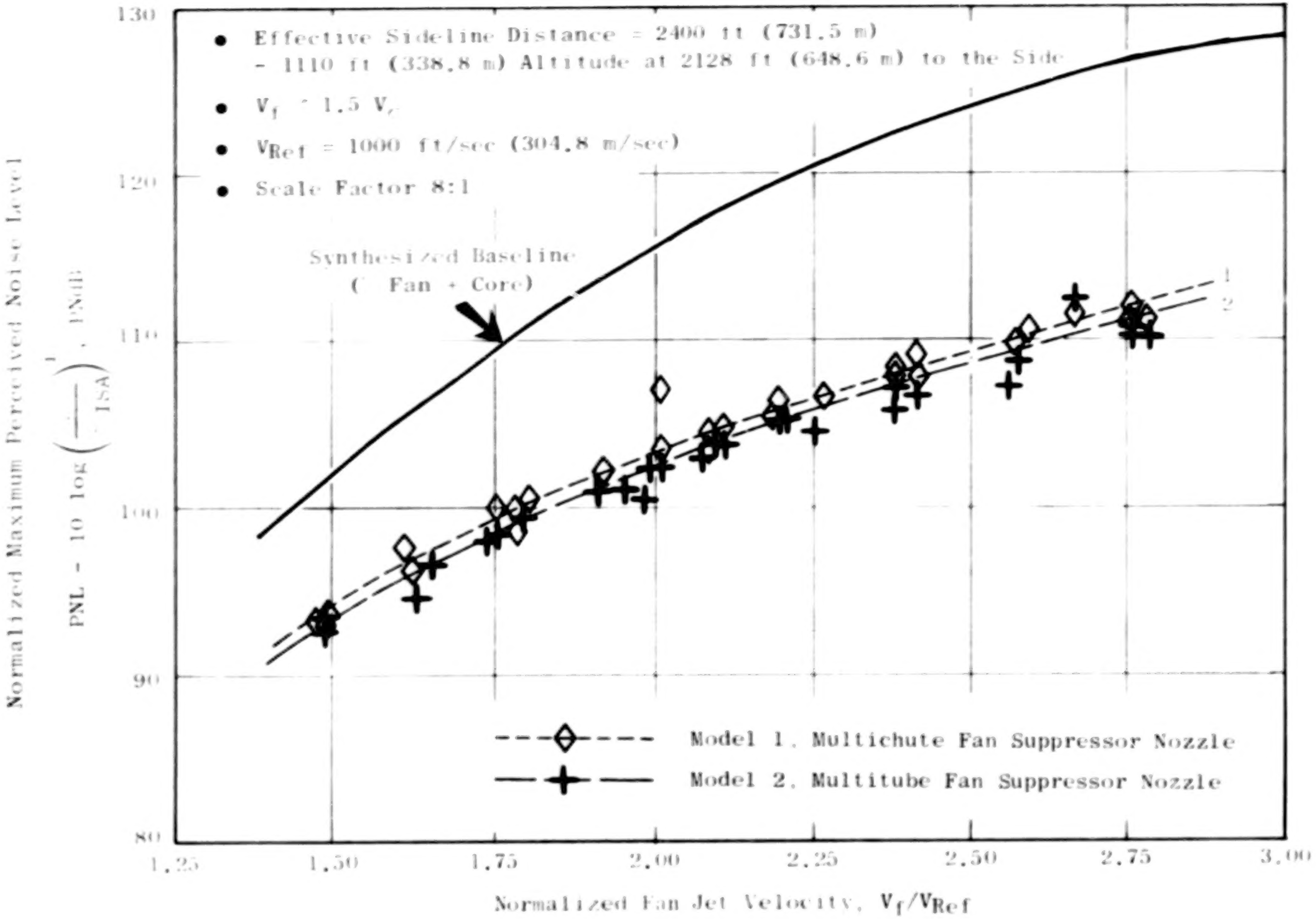

Figure 48. Effect of Fan Jet Velocity on Normalized Maximum Perceived Noise Level of Multielement Fan Suppressor Nozzles.

- Effective Sideline Distance = 2400 ft (731.5 m)
  - 1110 ft (338.8 m) Altitude at 2128 ft (648.6 m) to the Side
- Scale Factor 8:1

—— Synthesized Baseline (Σ Fan + Core)

☐ Model 1, Multichute Fan Suppressor Nozzle

○ Model 2, Multitube Fan Suppressor Nozzle

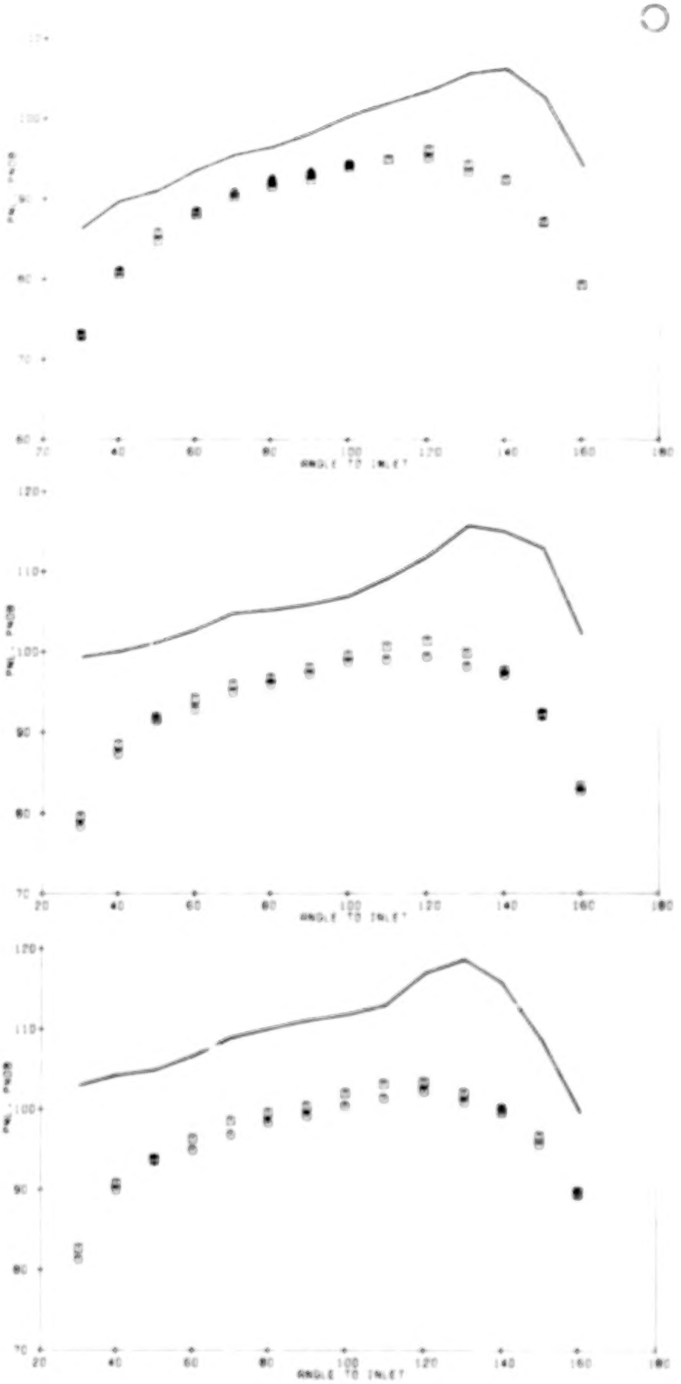

Nominal Conditions

V_f = 1800 ft/sec (548.6 m/sec)

T_{T_f} = 1200° R (667 K)

V_c = 1200 ft/sec (365.8 m/sec)

T_{T_c} = 1000° R (556 K)

Nominal Conditions

V_f = 2400 ft/sec (731.5 m/sec)

T_{T_f} = 1630° R (906 K)

V_c = 1200 ft/sec (365.8 m/sec)

T_{T_c} = 1000° R (556 K)

Nominal Conditions

V_f = 2800 ft/sec (853.4 m/sec)

T_{T_f} = 1960° R (1089 K)

V_c = 1400 ft/sec (426.7 m/sec)

T_{T_c} = 1460° R (811 K)

Figure 49. PNL Directivity Characteristics of Multielement Fan Suppressor Nozzles.

- Effective Sideline Distance = 2400 ft (731.5 m)
  - 1110 ft (338.8 m) Altitude at 2128 ft (648.6 m) to the Side
- Scale Factor 8:1

Nominal Conditions

☐ Model 1, Multichute Fan Suppressor Nozzle

○ Model 2, Multitube Fan Suppressor Nozzle

V_f = 1800 ft/sec (548.6 m/sec)

T_{T_f} = 1200° R (667 K)

V_c = 1200 ft/sec (365.8 m/sec)

T_{T_c} = 1000° R (556 K)

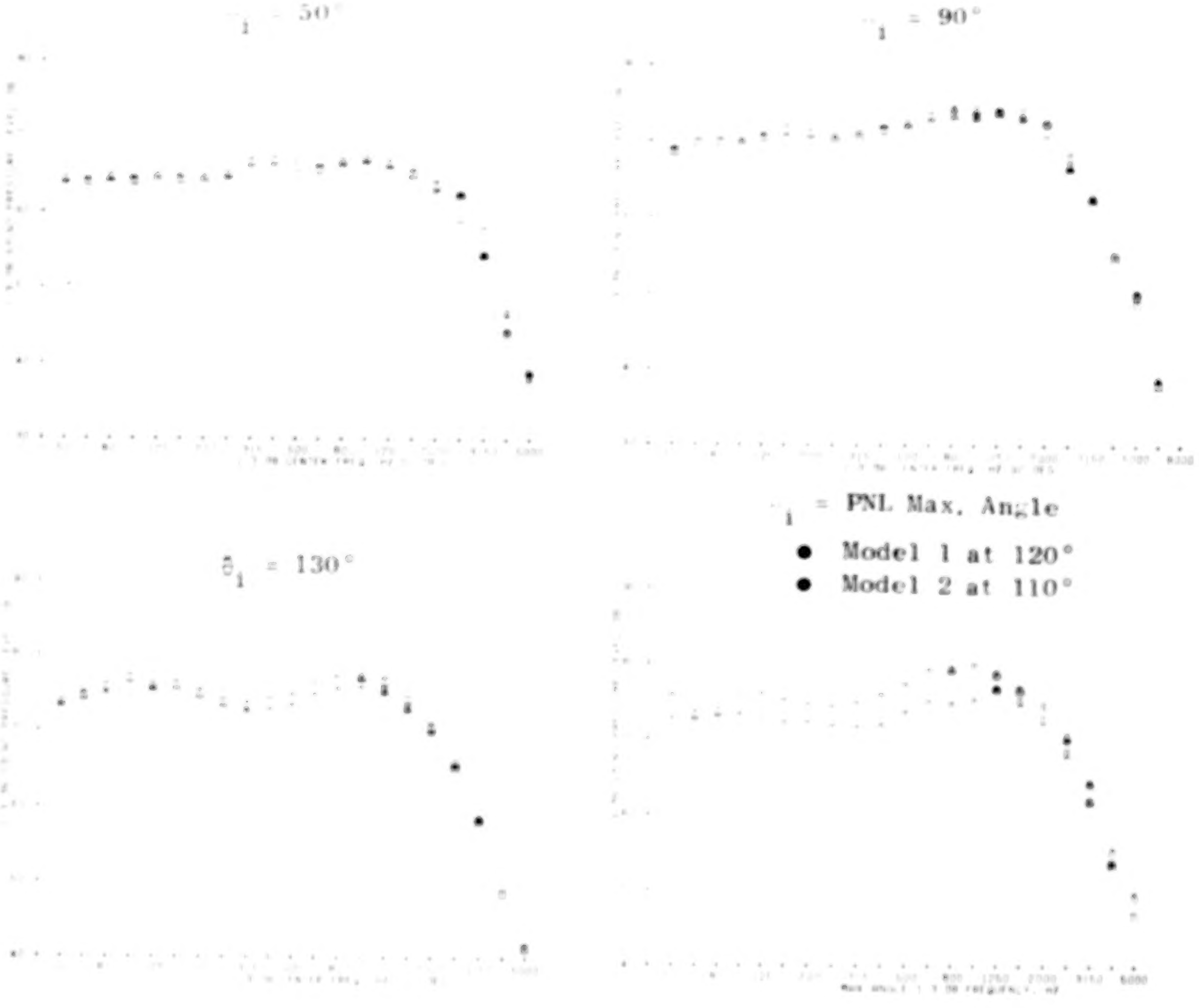

Figure 50. Multielement Fan Suppressor Nozzle SPL Spectra Comparisons at V_f = 1800 ft/sec (548.6 m/sec) and V_c = 1200 ft/sec (365.8 m/sec).

- Effective Sideline Distance = 2400 ft (731.5 m)
  - 1110 ft (338.8 m) Altitude at 2128 ft (648.6 m) to the Side
- Scale Factor 8:1

Nominal Conditions

☐ Model 1, Multichute Fan Suppressor Nozzle

○ Model 2, Multitube Fan Suppressor Nozzle

V_f = 2400 ft/sec (731.5 m/sec)

T_{T_f} = 1630° R (906 K)

V_c = 1200 ft/sec (365.8 m/sec)

T_{T_c} = 1000° R (556 K)

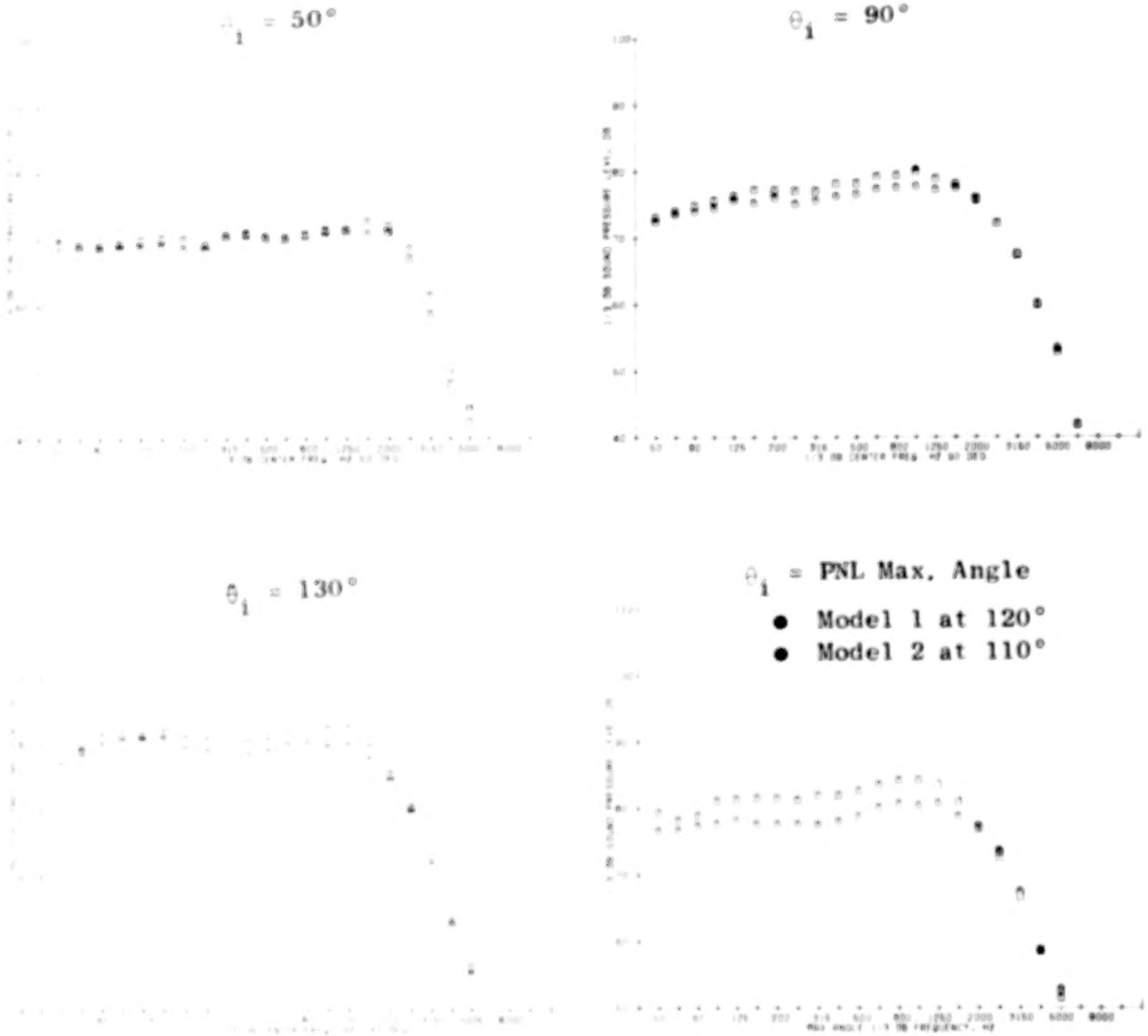

Figure 51. Multielement Fan Suppressor Nozzle SPL Spectra Comparisons at V_f = 2400 ft/sec (731.5 m/sec) and V_c = 1200 ft/sec (365.8 m/sec).

5.3.1.2 Power Spectra Test Results

The power spectra results shown in Figure 47 for the multichute (Model 1) and multitube (Model 2) fan-suppressor nozzles basically substantiate the normalized sound power level results shown in Figure 46. Figure 47 shows the power spectra results for the three illustrative test conditions. These results show that the multitube fan-suppressor nozzle is consistently ~1 dB lower over the entire spectrum range than the multichute fan-suppressor nozzle. Both suppressors exhibit the double-humped frequency characteristic. For these results, however, the noise field appears to be dominated by the premerged or high frequency noise region. The low frequency noise content, as well as the high frequency noise levels, remains essentially the same for both suppressors with increasing velocity. As expected, the low frequency noise portion of the spectrum tends to contribute more to the total noise with increasing velocity. This result implies greater importance of the merged-flow region in ultimately defining the velocity range of noise suppression. A closer look at the spectra also reveals that the lower noise levels of the multitube fan suppressor (Model 2) can be traced to its better midfrequency suppression characteristics. Comparison of Model 1 and Model 2 spectra, Figure 47, also shows that maximum midfrequency suppression occurs in the 2400 ft/sec (731.5 m/sec) region for the multitube fan-suppressor nozzle (Model 2). This verifies the normalized overall power level results of Figure 45 which also show that Model 2 maximum NOAPWL reduction (relative to the synthesized baseline) was obtained at 2400 ft/sec (731.5 m/sec).

5.3.1.3 Perceived Noise Level Test Results

The normalized maximum perceived noise level results for the multi-element fan-suppressor nozzles are shown in Figure 48; the test results are seen to be similar in trend to the normalized overall sound power level plots shown in Figure 46. $PNL_{max.}$ noise reductions relative to the synthesized baseline (Σ[Fan + Core]) are observed to range from 13 to 15 PNdB for the normalized fan jet velocity range of 2.0 to 2.75. Although PNL differences between the two fan-suppressor nozzles are within 1 PNdB, the multitube fan-suppressor nozzle (Model 2) is consistently lower throughout the entire normalized fan jet velocity range (i.e., $V_f/V_c = 1.5$ to 2.75).

The noise reduction capabilities of the two suppressor nozzles are further illustrated in the perceived noise level directivity plots on Figure 49. The PNL directivities also show that the multitube fan suppressor nozzle (Model 2) maintains its advantage over the multichute fan-suppressor nozzle (e.g., ~1 PNdB lower) over the entire inlet angle range of interest ($\theta_i = 40°$ to 160°). The PNL angular variation of Models 1 and 2 show the classical migration of maximum noise angle to lower inlet angles. Maximum-angle suppression of both Models 1 and 2 increases with velocity (relative to the synthesized baseline), and at 2800 ft/sec (853.4 m/sec) it appears to be still increasing. It is also evident from Figure 49 that noise reduction potential for both fan-suppressor nozzles tends to decrease with lower inlet angles (e.g., in the forward quadrant).

5.3.1.4 Sound Pressure Level Spectra Test Results

The SPL spectra for the multichute and multitube fan-suppressor nozzles (Models 1 and 2) are shown in Figures 50 through 52 at the illustrative test conditions for θ_i = 50°, 90°, 130°, and maximum PNL. These test results show trends similar to the power spectra counterparts shown in Figure 47. The multitube suppressor (Model 2) is still observed to be more effective than the multichute suppressor (Model 1) at the maximum angle, particularly at the 2400 ft/sec (731.5 m/sec) point. As observed in the power spectra, the multitube (Model 2) reduction (relative to Model 1) occurs primarily in the 0.100 to 1.25 kHz range. The premerged/coalesced jet noise frequency humps also are evident. These noise humps tend to "wash out" (e.g., merged region tends to dominate and spread out) as inlet angle is decreased.

5.3.2 Low Core-Flow Test Results

Several data points were also documented for the multitube fan-suppressor nozzle (Model 2) in the low core-flow mode. The insensitivity to core/fan weight flow ($\dot{W}_c/\dot{W}_f$) is illustrated in Figures 53 and 54. The plots of maximum perceived noise levels of Figures 53 and 54 show that erosion in noise suppression potential relative to the synthesized baseline is less than 1 PNdB during the low core-flow mode.

The PNL directivity at a fan jet velocity of 2750 ft/sec (838.2 m/sec) (Figure 55) exhibits the same characteristics observed during the unsuppressed coannular nozzle with plug (Model 7) low core-flow tests. Little or no effect on perceived noise level is observed in the inlet angle, (θ_i), range of 40° to 160°. It is interesting to note that, at angles close to the jet (i.e., large inlet angles), the "low core flow" perceived noise levels are 2 to 3 PNdB lower than the conventional or high core-flow results. This same trend was observed during tests on Model 7, the unsuppressed coannular nozzle with plug.

5.3.3 Comparisons with Unsuppressed Coannular Nozzles

Noise reduction potential of the multielement fan-suppressor nozzles relative to the synthesized baseline (Section 5.1) was noted throughout Section 5.3. However, comparison against actual unsuppressed coannular nozzles (Models 7 and 8) may provide a better yardstick of noise suppression capability for the fan-suppressor nozzles (Models 1 and 2).

Figure 56 compares the unsuppressed coannular and fan-suppressor nozzles on the basis of normalized maximum perceived noise level versus normalized fan jet velocity. Multielement fan-suppressor nozzle noise reductions tend to increase in the 2.5 to 2.75 normalized fan jet velocity range, exhibiting ΔPNL's between 5 to 7 PNdB and 6.5 to 8.0 PNdB relative to Model 7 (unsuppressed coannular nozzle with plug) and Model 8 (unsuppressed coannular nozzle without plug), respectively. In addition, noise suppression is still observed at the lower normalized fan jet velocities (between 1.5 to 2.5).

- Effective Sideline Distance = 2400 ft (731.5 m) - 1110 ft (338.8 m) Altitude at 2128 ft (648.6 m) to the Side
- Scale Factor 8:1

Nominal Conditions

☐ **Model 1, Multichute Fan Suppressor Nozzle**

○ **Model 2, Multitube Fan Suppressor Nozzle**

V_f = 2800 ft/sec (853.4 m/sec)
T_{T_f} = 1960° R (1089 K)
V_c = 1400 ft/sec (426.7 m/sec)
T_{T_c} = 1460° R (811 K)

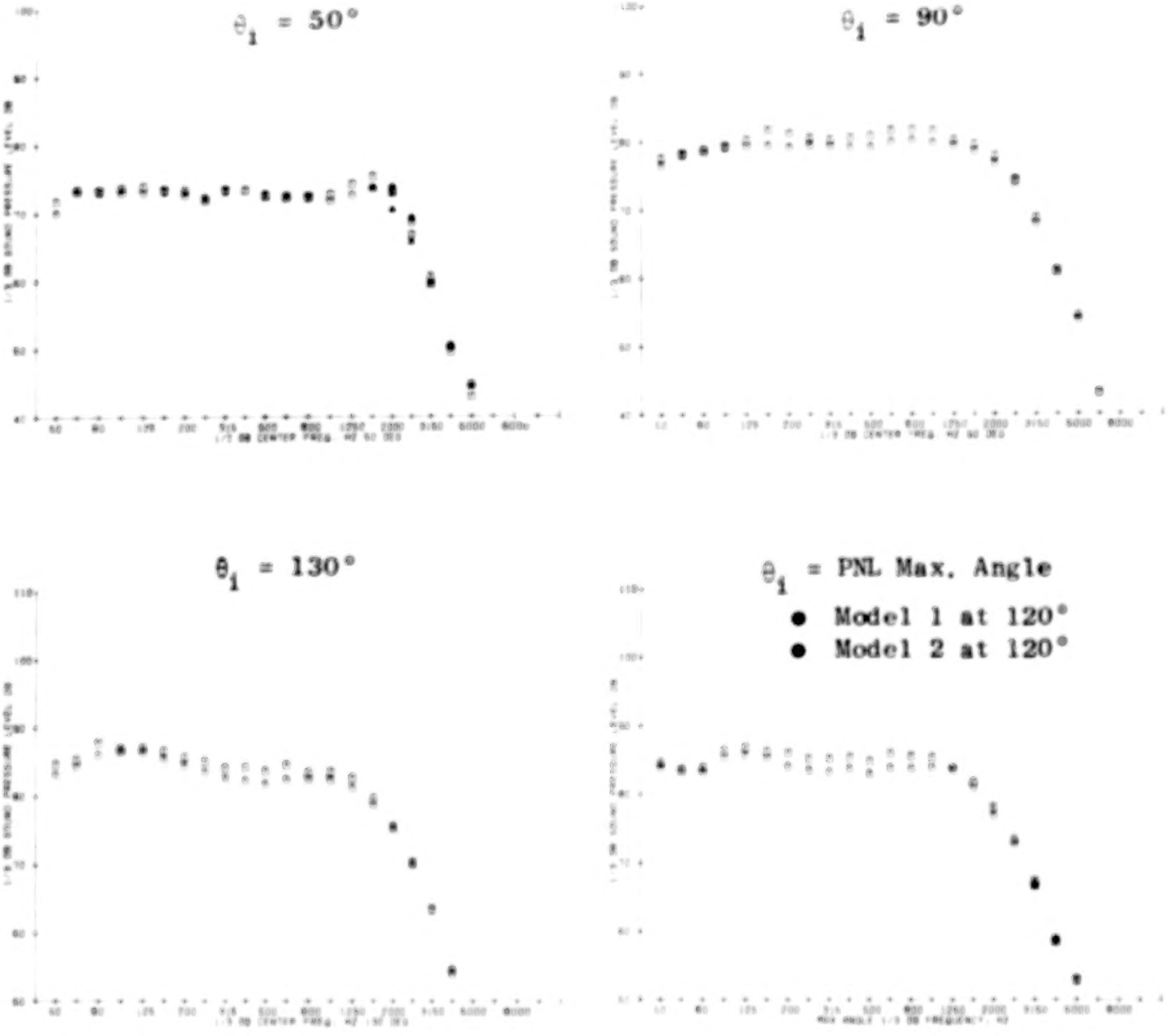

Figure 52. Multielement Fan Suppressor Nozzle SPL Spectra Comparisons at V_f = 2800 ft/sec (853.4 m/sec) and V_c = 1400 ft/sec (426.7 m/sec).

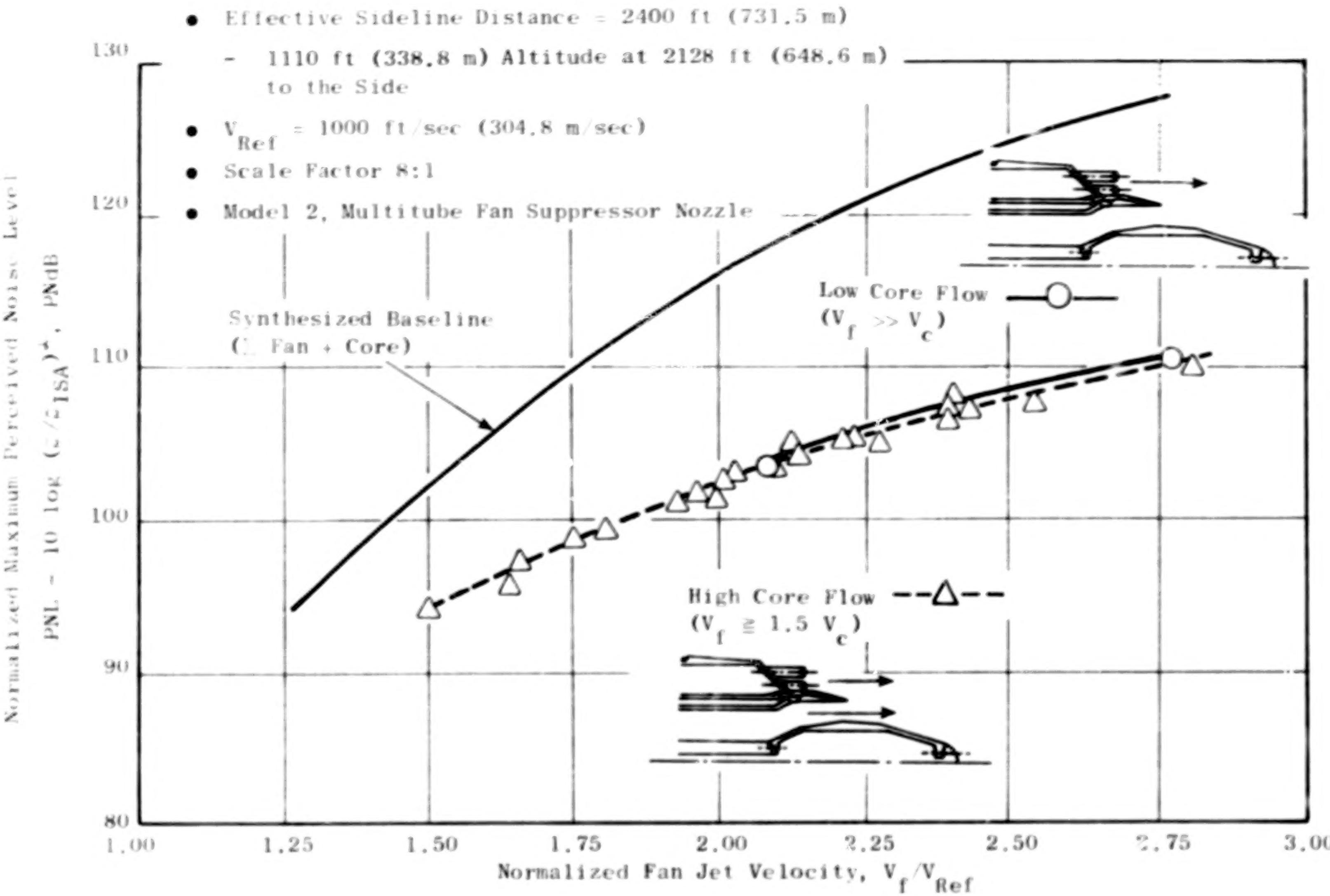

Figure 53. Effect of Core Flow and Fan Velocity on Normalized Maximum Perceived Noise Level of the Multitube Fan Suppressor Nozzle (Model 2).

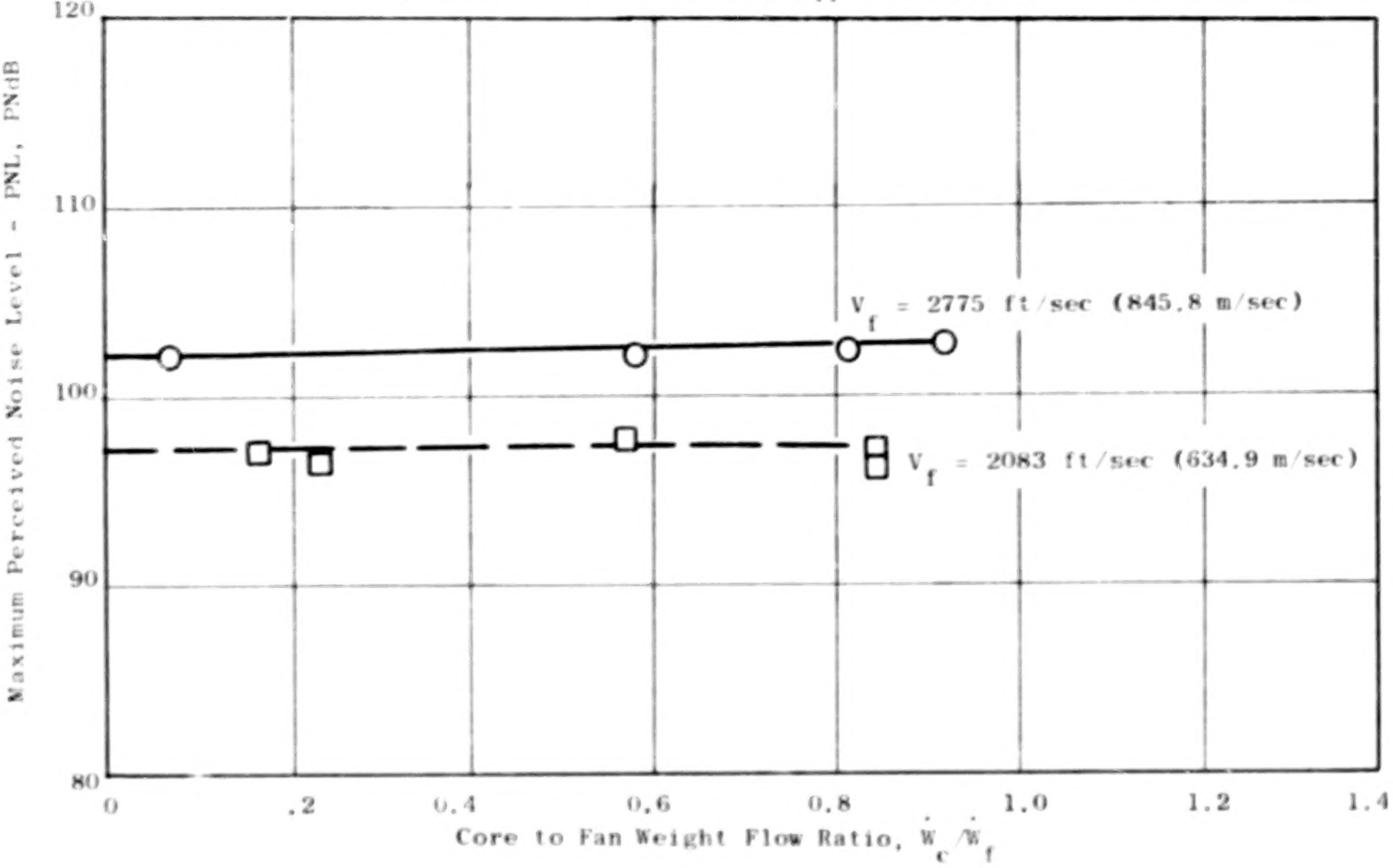

- Effective Sideline Distance = 2400 ft (731.5 m)
  - 1110 ft (338.8 m) Altitude at 2128 ft (648.6 m) to the Side
- Scale Factor 8:1
- Model 2 Multitube Fan Suppressor **Nozzle**

Figure 54. Core/Fan Weight-Flow Ratio Effect on Maximum Perceived Noise Level of the Multitube Fan Suppressor Nozzle (Model 2).

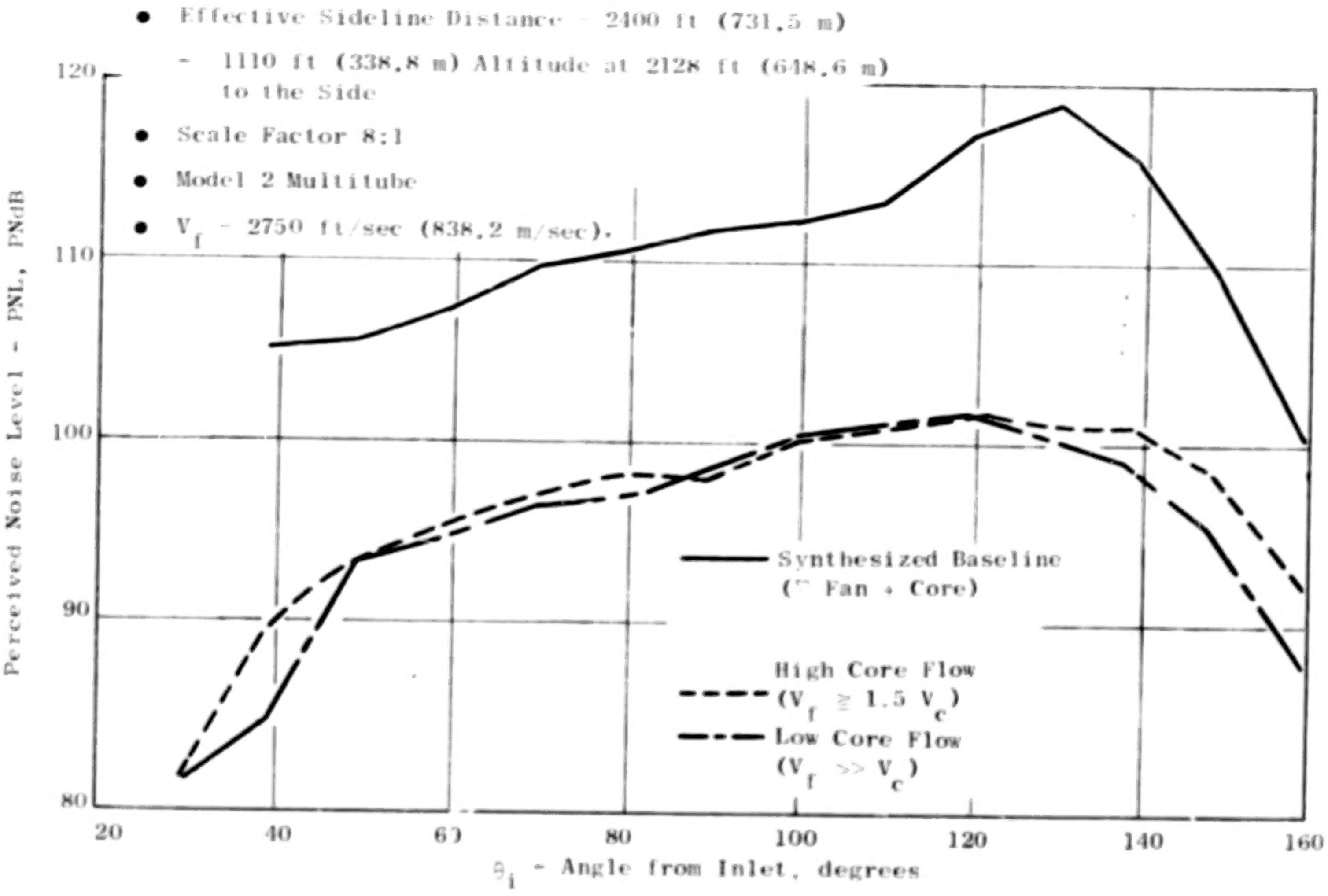

Figure 55. Effect of Core Flow on PNL Directivity of the Multitube Fan Suppressor Nozzle (Model 2).

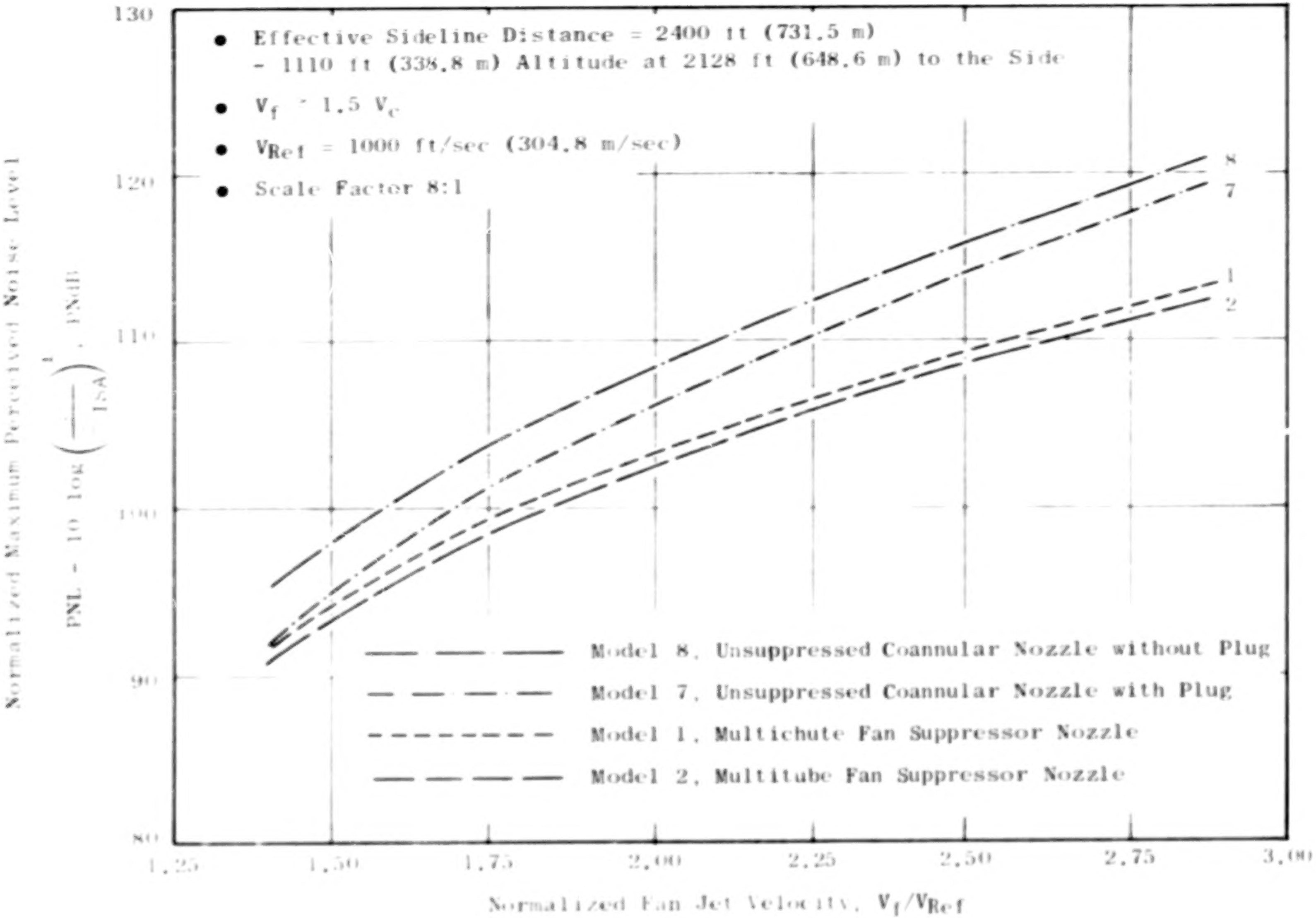

Figure 56. Comparison of Normalized Maximum Perceived Noise Levels Vs. Fan Jet Velocity for Unsuppressed Coannular Nozzles and Multielement Fan Suppressor Nozzles.

The perceived noise level angular variations for the unsuppressed coannular and fan-suppressor nozzles are summarized in Figure 57. Noise reduction potential is maintained for both fan-suppressor nozzles (Models 1 and 2) over the entire inlet angle range; furthermore, forward angle (e.g., $\theta_i \leq 90°$) fan-suppressor nozzle noise reduction capability appears to reach its maximum level at the 2400 ft/sec (731.5 m/sec) fan jet velocity condition and then decreases with either increasing or decreasing fan jet velocity.

The SPL spectra comparisons at $\theta_i = 130°$ shown in Figure 58 provide some insight into how the noise reduction of the fan-suppressor nozzles comes about. Examination of Figure 58 shows that both fan-suppressor nozzle sound pressure levels are substantially lower than their unsuppressed coannular nozzle counterparts in the low and midfrequency range for all velocities. At high frequencies (i.e. > 1250 Hz) the suppression is seen to be small (particularly relative to Model 7, unsuppressed coannular nozzle with plug) until the 2800 ft/sec (853.4 m/sec) fan jet velocity point.

5.3.4 Summary Remarks

Overall, both fan-suppressor nozzles proved to be extremely efficient acoustically relative to the unsuppressed coannular nozzles (e.g., ΔPNL ≈ 5 to 6 PNdB). In terms of suppression relative to a synthesized baseline, a suppression of 15 PNdB was obtained.

Implementation of these configurations in a multiple-stream exhaust nozzle will depend on the structural/mechanical ingenuity of the design, the aerodynamic penalties incurred, and the stringency of noise pollution regulatory standards to be imposed on future advanced, supersonic-cruise vehicles.

5.4 MULTIELEMENT FAN-SUPPRESSOR NOZZLES WITH EJECTORS

The multitube and multichute fan-suppressor nozzles (Models 2 and 1 respectively) discussed in Section 5.3 were subsequently evaluated acoustically using a common conical ejector with a bellmouth inlet. Acoustically treated liners and hardwall liners were included in this series of acoustic tests (see Section 4.0 for test matrix). In addition, the sharp-lip inlet utilized during the aerodynamic-performance tests (see Section 6.0) was installed on the hardwall ejector with the multichute fan-suppressor nozzle and evaluated to assess the impact on noise level of flow separating from the ejector inlet inner lip surface under static operating conditions, ($M_{external} = 0$).

The data presentation generally follows the format outlined in Sections 5.1 and 5.2, with emphasis on the 2400 ft/sec (731.5 m/sec) fan jet velocity 1200 ft/sec (365.8 m/sec) core jet velocity operating condition. The discussion is divided into three parts:

- Effective Sideline Distance = 2400 ft (731.5 m)
  - 1110 ft (338.8 m) Altitude at 2128 ft (648.6 m) to the Side
- Scale Factor 8:1

◇ Model 8, Unsuppressed Coannular Nozzle without Plug

□ Model 1, Multichute Fan Suppressor Nozzle

△ Model 7, Unsuppressed Coannular Nozzle with Plug

○ Model 2, Multitube Fan Suppressor Nozzle

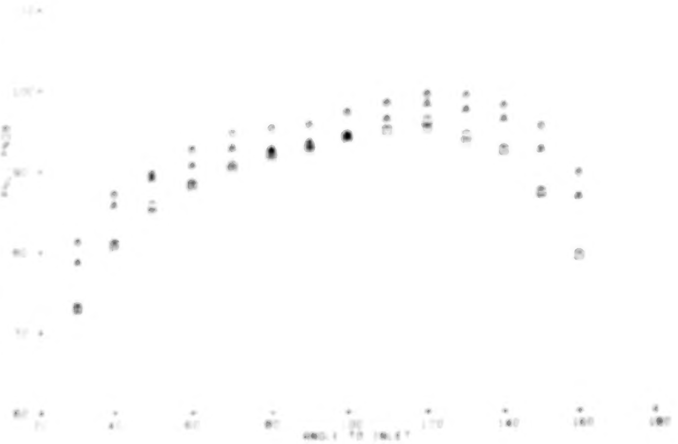

Nominal Conditions

V_f = 1800 ft/sec (548.6 m/sec)

T_{T_f} = 1200° R (667 K)

V_c = 1200 ft/sec (365.8 m/sec)

T_{T_c} = 1000° R (556 K)

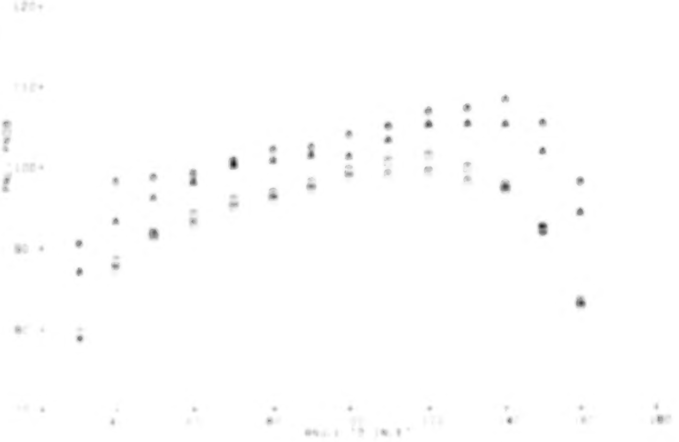

Nominal Conditions

V_f = 2400 ft/sec (731.5 m/sec)

T_{T_f} = 1630° R (906 K)

V_c = 1200 ft/sec (365.8 m/sec)

T_{T_c} = 1000° R (556 K)

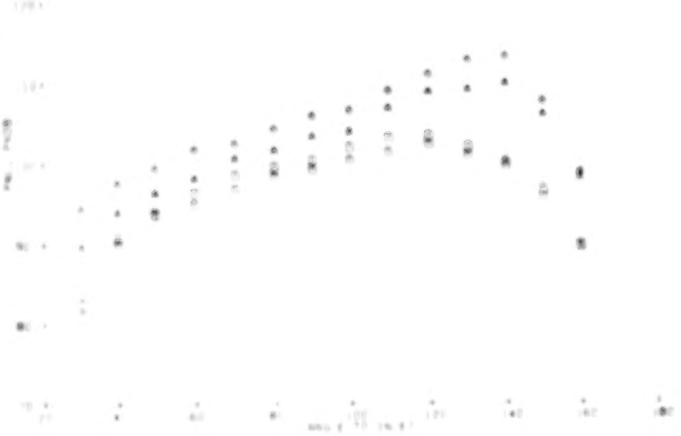

Nominal Conditions

V_f = 2800 ft/sec (853.4 m/sec)

T_{T_f} = 1960° R (1089 K)

V_c = 1400 ft/sec (426.7 m/sec)

T_{T_c} = 1460° R (811 K)

Figure 57. PNL Directivity Comparisons Between Unsuppressed Coannular Nozzles and Multielement Fan Suppressor Nozzles.

- Effective Sideline Distance = 2400 ft (731.5 m)
  - 1110 ft (338.8 m) Altitude at 2128 ft (648.6 m) to the Side
- Scale Factor 8:1
- θ_i = 130°

◇ Model 8, Unsuppressed Coannular Nozzle without Plug

△ Model 7, Unsuppressed Coannular Nozzle with Plug

□ Model 1, Multichute Fan Suppressor Nozzle

○ Model 2, Multitube Fan Suppressor Nozzle

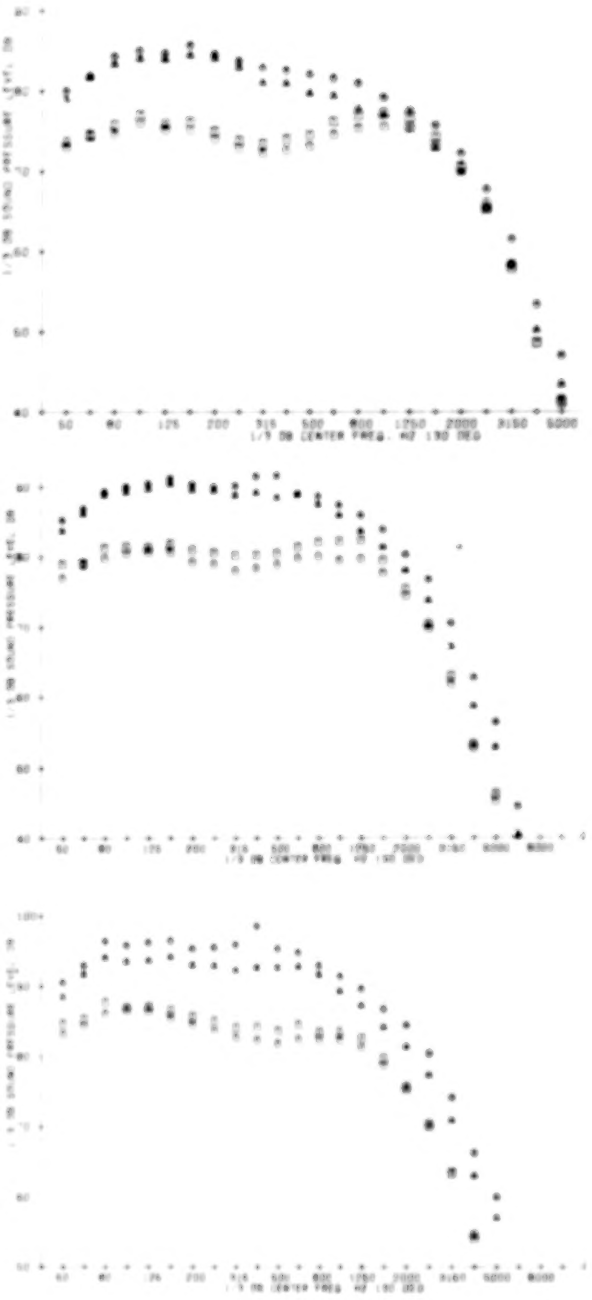

Nominal Conditions

V_f = 1800 ft/sec (548.6 m/sec)

T_{T_f} = 1200° R (667 K)

V_c = 1200 ft/sec (365.8 m/sec)

T_{T_c} = 1000° R (556 K)

Nominal Conditions

V_f = 2400 ft/sec (731.5 m/sec)

T_{T_f} = 1630° R (906 K)

V_c = 1200 ft/sec (365.8 m/sec)

T_{T_c} = 1000° R (556 K)

Nominal Conditions

V_f = 2800 ft/sec (853.4 m/sec)

T_{T_f} = 1960° R (1089 K)

V_c = 1400 ft/sec (426.7 m/sec)

T_{T_c} = 1460° R (811 K)

Figure 58. SPL Spectra Comparisons Between Unsuppressed Coannular Nozzles and Multielement Fan Suppressor Nozzles.

- Hardwall Ejector Effects
- Treated Ejector Effects
- Ejector Lip Geometry Effects

5.4.1 Hardwall Ejector Effects

5.4.1.1 Overall Power Level Test Results

The conical hardwall ejector described in Section 4.0 was tested on the multitube suppressor (Model 2) and multichute fan suppressor (Model 1). These hardwall ejector nozzles are designated as Model 5 and Model 3 for the multitube and multichute fan-suppressor nozzles respectively. Figure 59 summarizes the effect of the hardwall ejector on normalized overall sound power level (NOAPWL). In general, the hardwall ejector is observed to be acoustically more effective (e.g. more noise reduction) with the multichute fan-suppressor nozzle (Model 3) than with the multitube suppressor (Model 5). The test results show Model 3 NOAPWL noise reductions of 3.5 to 2 dB, in contrast to the 1.5 to 1 dB of Model 5, over the entire normalized fan jet velocity range when compared to the respective suppressed nozzles without ejector.

5.4.1.2 Power Spectra Test Results

The use of a hardwall ejector, from an acoustical point of view, should provide the induced flow necessary to affect the turbulent structure of the postmerged region of the jet, hence reducing the midfrequencies and low frequencies below those of the basic multielement fan-suppressor nozzle. Figure 60 shows typical power spectra at a fan jet velocity of 2400 ft/sec (731.5 m/sec) for each of the hardwall ejector nozzles (Models 5 and 3). The NOAPWL noise reduction relative to the basic suppressor nozzles comes about through a reduction in midfrequency noise; furthermore, the Model 3 sound power levels are consistently below the basic suppressor (Model 1) for the entire frequency range. This is not the case, however, for the multitube nozzle counterparts (Models 2 and 5) and, as a result, the multitube nozzle did not provide the level of noise suppression observed for the multichute nozzles (Models 1 and 3). Examination of Figure 60 shows that the ejector was ineffective at the low frequencies, both for the multichute and the multitube configurations, suggesting that the ejector affected the merging jet but not the merged jet.

5.4.1.3 Perceived Noise Level Test Results

Contrary to the normalized overall sound power level trends shown in Figure 59, the normalized maximum perceived noise level ($NPNL_{max.}$) results of Figure 61 show that essentially no benefit was derived from the hardwall ejector when combined with either fan-suppressor nozzle. As will be shown

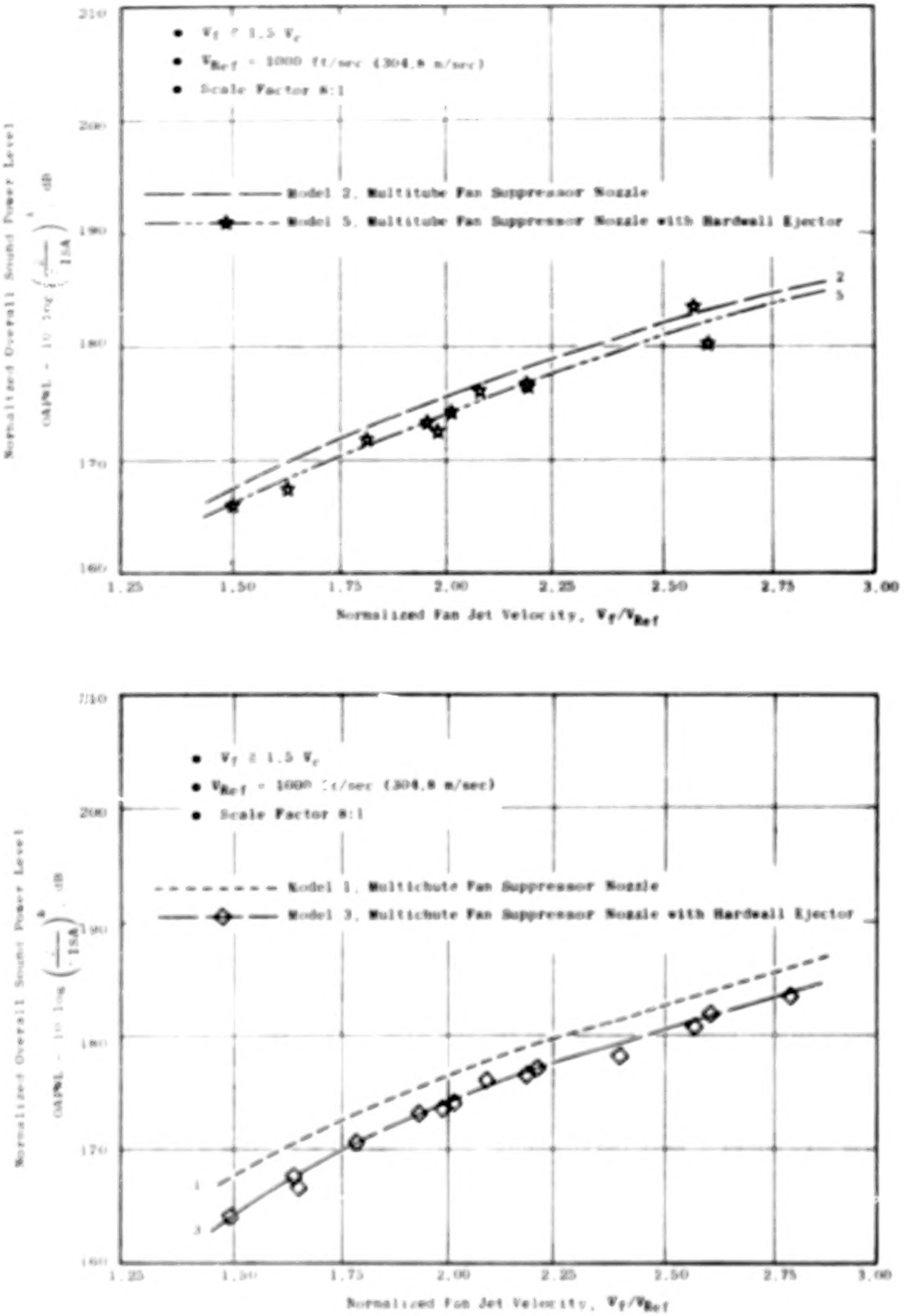

Figure 59. Effect of Hardwall Ejectors on Multielement Fan Suppressor Nozzle Normalized Overall Sound Power Level.

- Scale Factor 8:1

Nominal Conditions

V_f = 2400 ft/sec (731.5 m/sec)
T_{T_f} = 1630° R (906 K)
V_c = 1200 ft/sec (365.8 m/sec)
T_{T_c} = 1000° R (556 K)

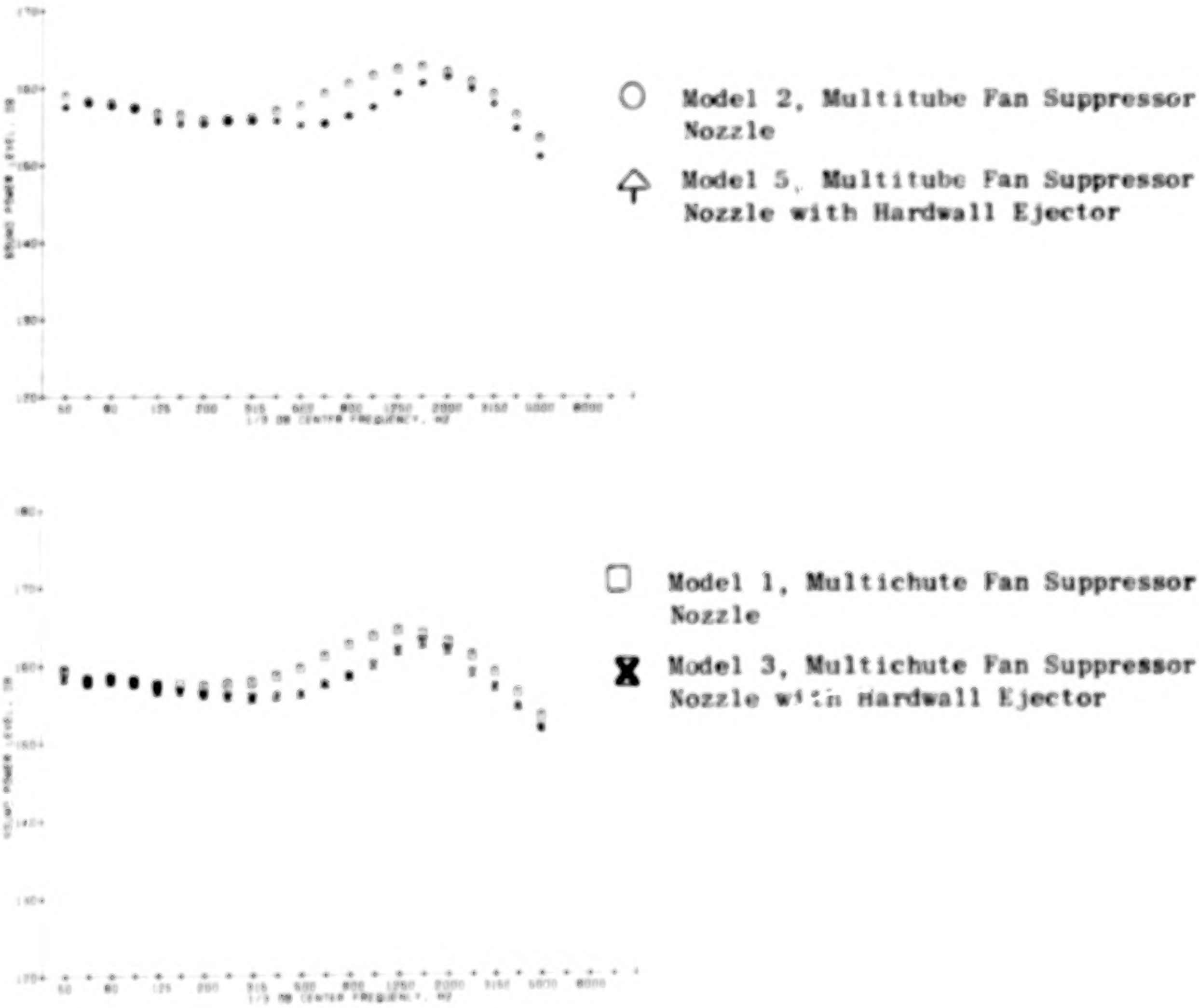

Figure 60. Effect of Hardwall Ejectors on Multielement Fan Suppressor Nozzle One-Third-Octave Sound Power Spectra.

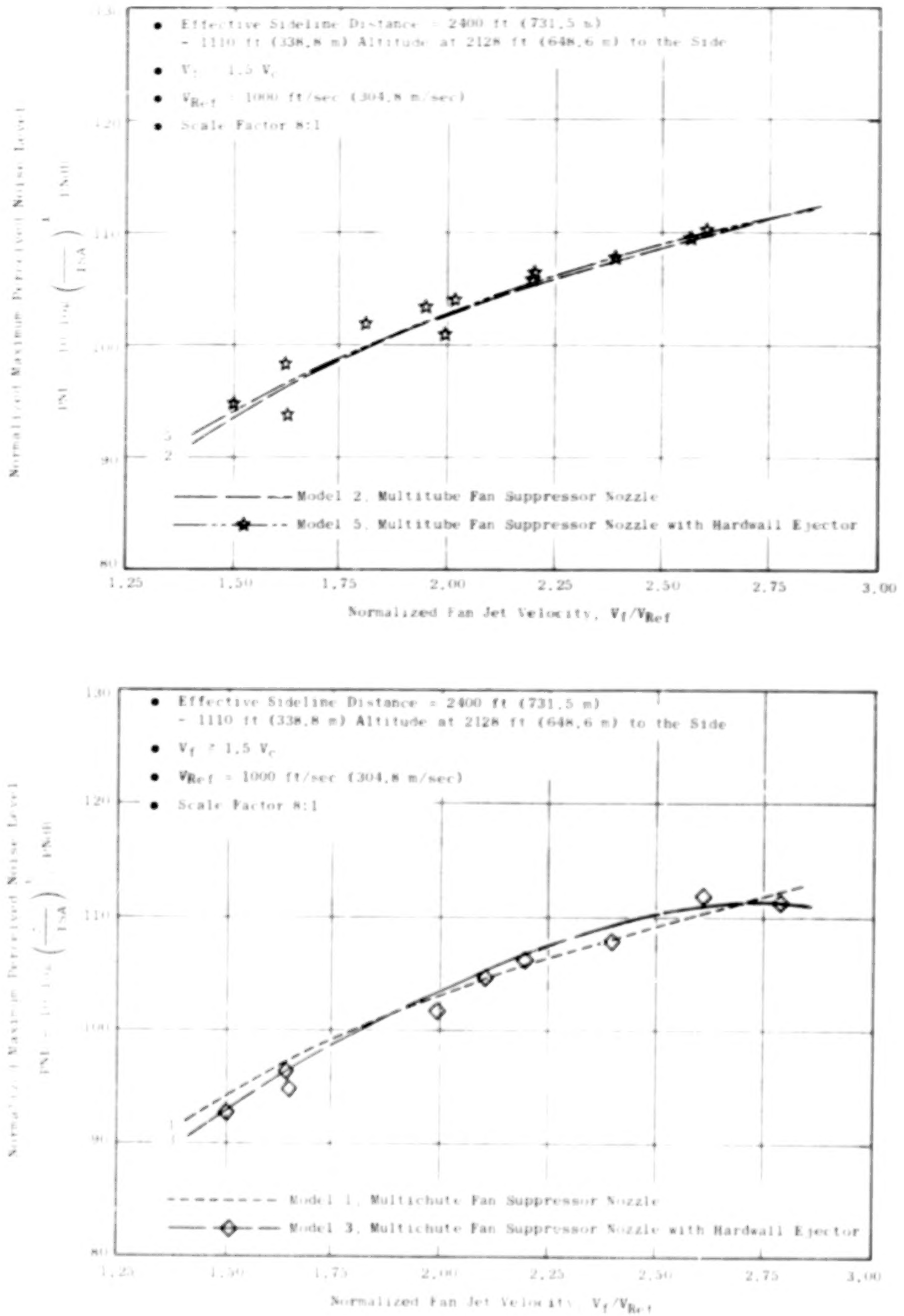

Figure 61. Effect of Hardwall Ejectors on Multielement Fan Suppressor Nozzle Normalized Maximum Perceived Noise Level.

later, this is due to the high sound pressure levels exhibited by the hardwall ejector at the critical Noy-weighting frequencies.

Examination of the PNL directivity characteristics over the entire fan jet velocity range show them to be quite consistent for both multielement fan-suppressor nozzles with hardwall ejector.

On a maximum PNL basis (e.g., suppressor versus suppressor with hardwall ejector maximum noise level), the maximum noise angle is not appreciably affected. In those cases where migration of the peak-noise angle of the hardwall ejector nozzle to lower inlet angles was observed, the change was no more than 10°. This very systematic angular variation is illustrated in Figure 62. The directivity plots show that, for aft-quadrant inlet angles greater than 130°, the hardwall ejector provides from 2 to 4 PNdB noise reduction over the basic suppressor nozzle counterparts. The noise reduction characteristics of the hardwall ejector nozzles at these aft angles are indicative of the midfrequency-dominated portion of the jet spectrum which is primarily influenced by changes in the merging regions brought about by the introduction of the ejector-induced flow. In the 80° to 110° inlet angle region, the hardwall ejector PNL's show either no benefit or higher noise levels than their basic suppressor nozzle counterparts. Alternately, for inlet angles less than 60° (forward quadrant) a consistent noise reduction benefit is observed for both hardwall ejector nozzles.

5.4.1.4 Sound Pressure Level Test Results

The one-third-octave SPL spectra shown in Figures 63 and 64 for the 2400 ft/sec (731.5 m/sec) test point basically substantiate the PNL directivity trends described above. Examination of the 90° and PNL maximum angle spectra show that the higher frequency portion of the hardwall ejector nozzles (Models 5 and 3) is equal to or slightly higher than the basic suppressor nozzles (Models 2 and 1). The spectra for the 130° inlet angle illustrate the good noise-reduction characteristics observed in the PNL directivity plots (Figure 62) for both hardwall ejector nozzles (Models 5 and 3). Similar characteristics are observed for the 50° inlet angle spectra.

5.4.2 Treated Ejector Effects

The two multielement fan-suppressor nozzles tested with an acoustically treated ejector are described in Section 4.0. The internal flowpath of the treated ejector as well as the bellmouth inlet are identical to that of the hardwall ejector, while the outer dimensions were increased slightly to accommodate the acoustic treatment and faceplate.

5.4.2.1 Overall Power Level Test Results

Comparison of Untreated and Treated Ejector Test Results - The noise suppression benefit associated with the introduction of an acoustically lined

- Effective Sideline Distance = 2400 ft (731.5 m)
  - 1110 ft (338.8 m) Altitude at 2128 ft (648.6 m) to the Side
- Scale Factor 8:1

Nominal Conditions

V_f = 2400 ft/sec (731.5 m/sec)
T_{T_f} = 1630° R (906 K)
V_c = 1200 ft/sec (365.8 m/sec)
T_{T_c} = 1000° R (556 K)

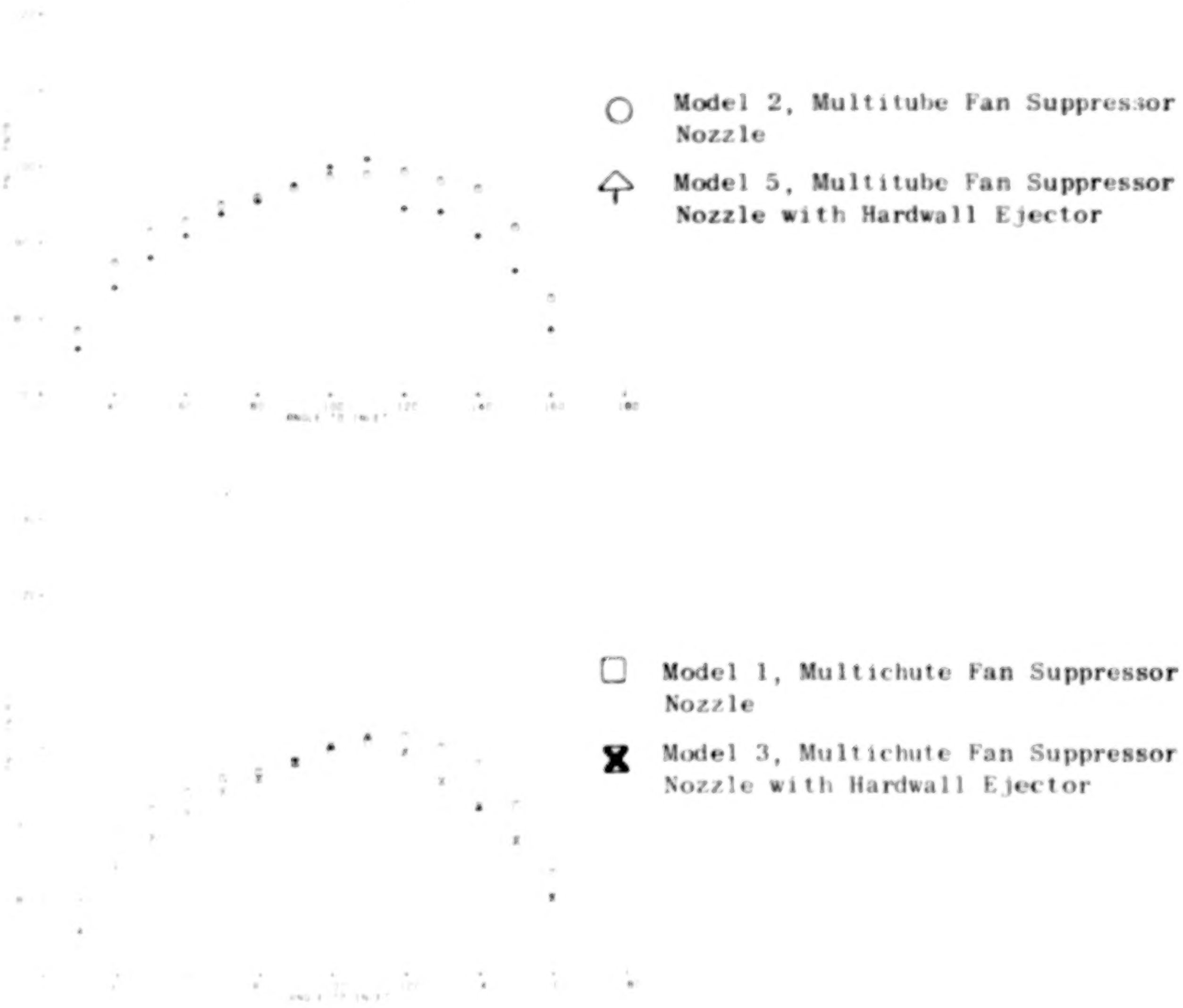

Figure 62. Effect of Hardwall Ejectors on Multielement Fan Suppressor Nozzle PNL Directivity.

- Effective Sideline Distance = 2400 ft (731.5 m)
  - 1110 ft (338.8 m) Altitude at 2128 ft (648.6 m) to the Side
- Scale Factor 8:1

Nominal Conditions

V_f = 2400 ft/sec (731.5 m/sec)

T_{T_f} = 1630° R (906 K)

V_c = 1200 ft/sec (365.8 m/sec)

TT_c = 1000° R (556 K)

○ Model 2, Multitube Fan Suppressor Nozzle

⇧ Model 5, Multitube Fan Suppressor Nozzle with Hardwall Ejector

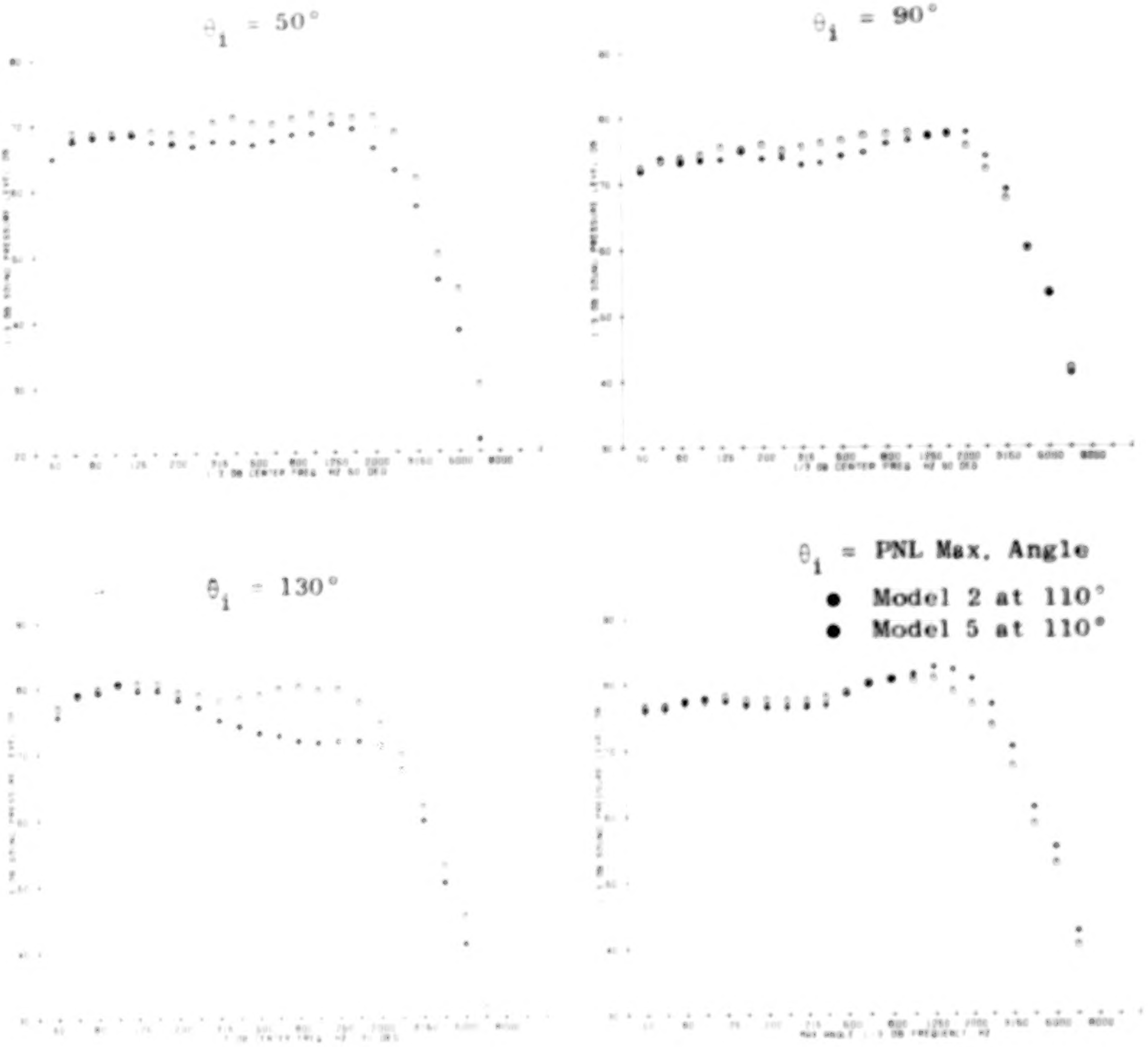

Figure 63. Effect of Hardwall Ejector on Multitube Fan Suppressor Nozzle SPL Spectra.

- Effective Sideline Distance = 2400 ft (731.5 m)
  - 1110 ft (338.8 m) Altitude at 2128 ft (648.6 m) to the Side
- Scale Factor 8:1

Nominal Conditions

☐ Model 1, Multichute Fan Suppressor Nozzle

☒ Model 3, Multichute Fan Suppressor Nozzle with Hardwall Ejector

V_f = 2400 ft/sec (731.5 m/sec)
T_{T_f} = 1630° R (906 K)
V_c = 1200 ft/sec (365.8 m/sec)
T_{T_c} = 1000° R (556 K)

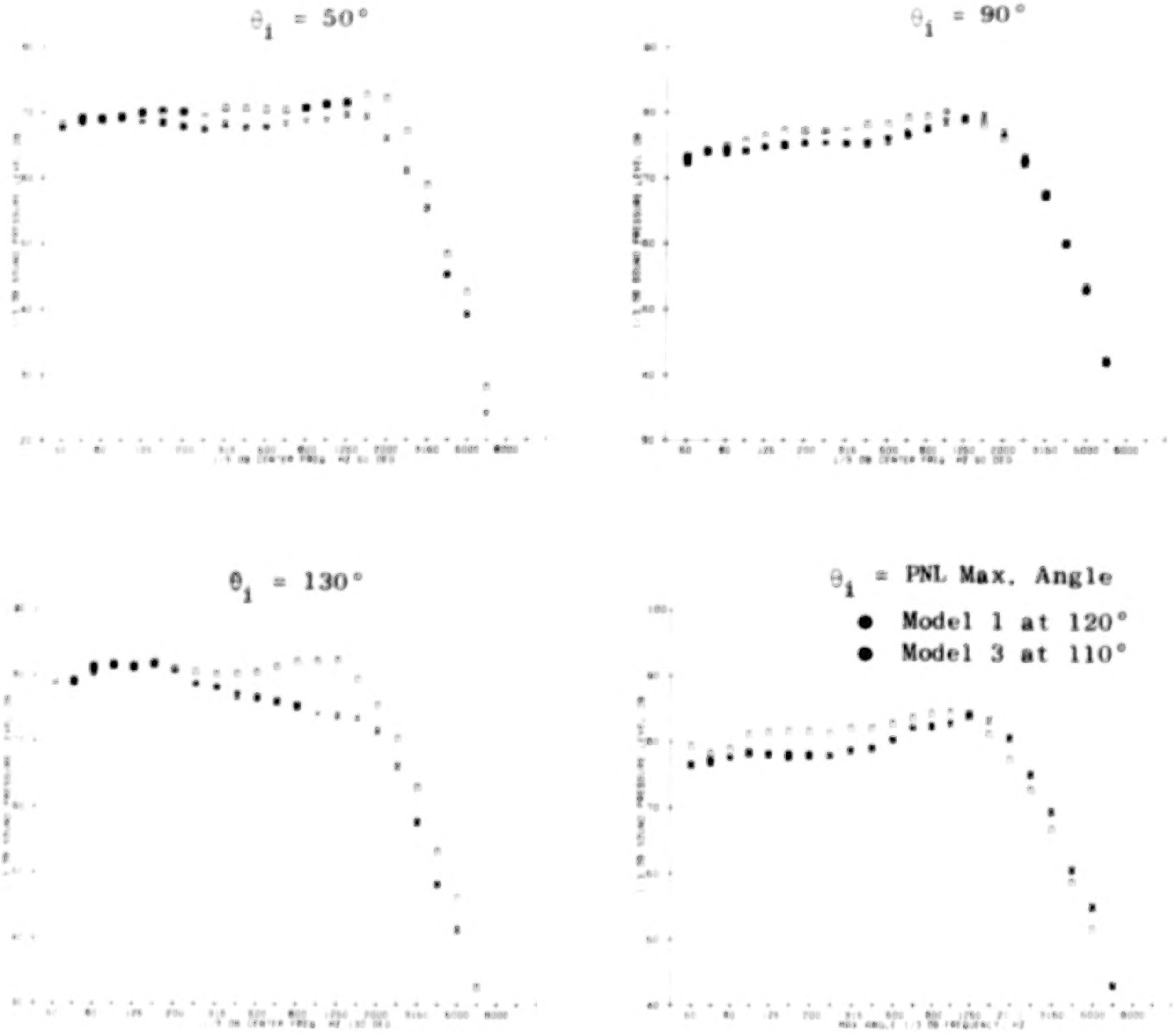

Figure 64. Effect of Hardwall Ejector on Multichute Fan Suppressor Nozzle SPL Spectra.

ejector in place of a hardwall ejector is summarized in terms of normalized overall sound power level in Figure 65. The treated ejector results show that noise reductions relative to the hardwall ejector nozzle occur over the entire normalized fan jet velocity range tested. The treated ejector was found to be more effective when applied to the multitube fan-suppressor nozzle (Model 6) than when used with the multichute suppressor (Model 4). NOAPWL noise reductions are found to be 2.5 to 2.0 dB for the Model 6 relative to the hardwall ejector nozzle (Model 5) and to be 1 dB for the companion multichute nozzle (Model 4 versus Model 3).

Comparison of Treated Ejector and Basic Fan Suppressor Test Results - The treated ejector results relative to the basic suppressor test data (Models 1 and 2) are illustrated by comparing Figure 65 with Figure 59. The noise reduction attributable to the treated ejector is found to be 4 to 3 dB for both the multitube (Model 6 vs 2) and multichute (Model 4 vs 1) nozzles. Additional comparisons of these data for the multitube suppressor with treated ejector (Model 6) with the data for the multichute suppressor with treated ejector (Model 4) as shown in Figure 65 indicate that the normalized overall sound power levels obtained are the same for both configurations at any given fan jet velocity.

5.4.2.2 Power Spectra Test Results

Power spectra comparisons for the fan jet velocity condition of 2400 ft/sec (731.5 m/sec) is shown in Figure 66. Since the NOAPWL noise reductions noted in Figure 65 remained essentially constant with increasing normalized fan jet velocity for both multielement nozzles, the power spectra shown in Figure 66 adequately describe the effectiveness of the ejector acoustic treatment over the hardwall ejector case. The reduced midfrequency to high frequency content for both treated ejector nozzles (Models 6 and 4) clearly illustrates the benefits of adding an acoustic liner to the hardwall ejector.

5.4.2.3 Perceived Noise Level Test Results

The normalized fan jet velocity dependency on normalized maximum perceived noise level, NPNL, is shown on Figure 67 for both treated ejector nozzle systems (Models 4 and 6) and their hardwall ejector companion nozzles (Models 3 and 5). The multitube fan-suppressor nozzle with treated ejector is approximately 3 PNdB lower than its hardwall nozzle counterpart for the entire normalized fan jet velocity range. The addition of the acoustic liner in the multichute fan-suppressor nozzle with hardwall ejector system proved, at least from a NPNL basis, to be acoustically more effective than the multitube nozzle system (e.g. noise reductions ranging from 3 PNdB at low fan jet velocity increasing to about 4 PNdB in the midvelocity range and decreasing to 2 to 2.5 PNdB at high velocities). Overall, the installation of an ejector with an acoustically treated liner on either multielement fan-suppressor nozzle can provide NPNL reductions of 4 to 3 PNdB over the entire normalized fan jet velocity region (compare Figures 67 and 61).

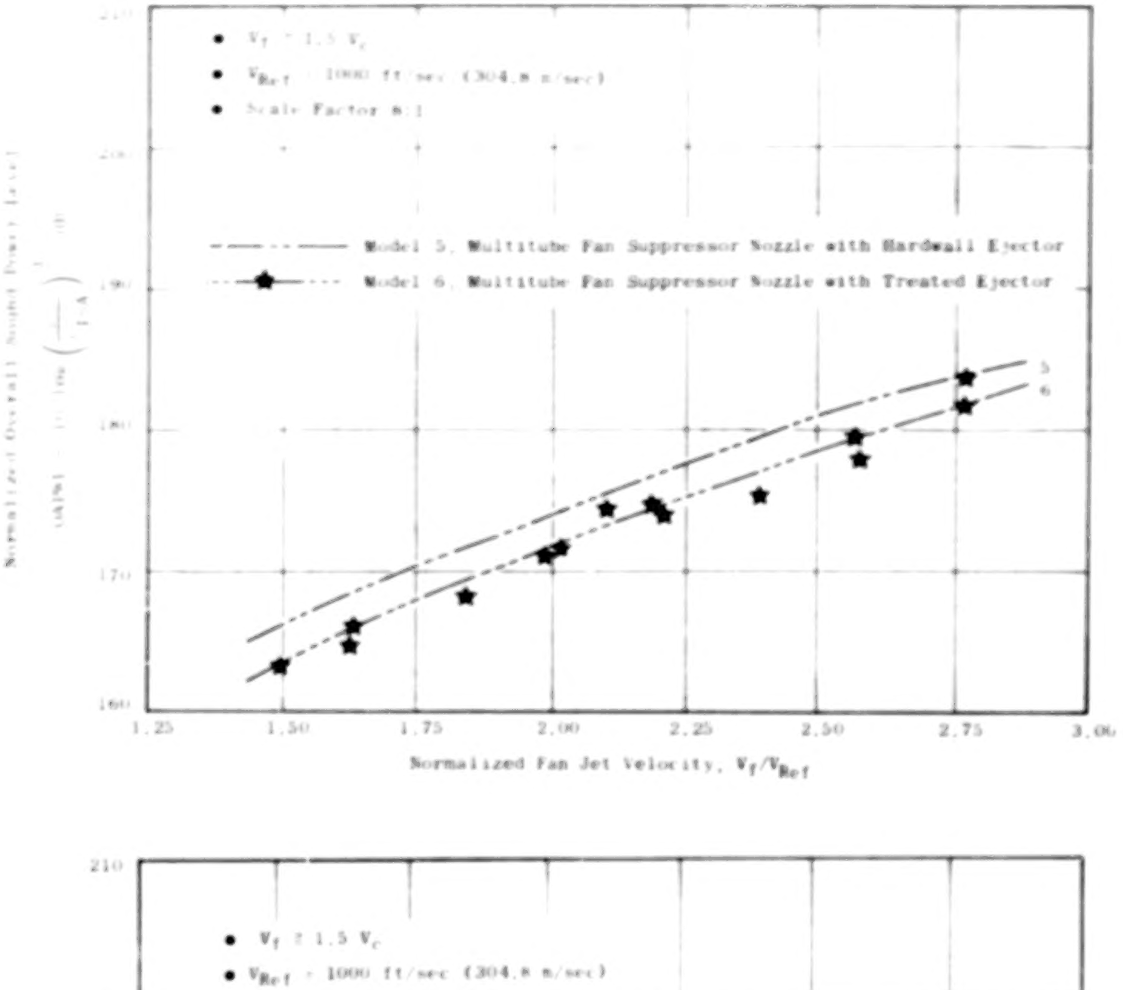

Figure 65. Comparison of Normalized Overall Sound Power Level from Multielement Fan Suppressor Nozzles with Hardwall and Treated Ejectors.

- Scale Factor 8:1

Nominal Conditions

V_f = 2400 ft/sec (731.5 m/sec)
T_{T_f} = 1630° R (906 K)
V_c = 1200 ft/sec (365.8 m/sec)
T_{T_c} = 1000° R (556 K)

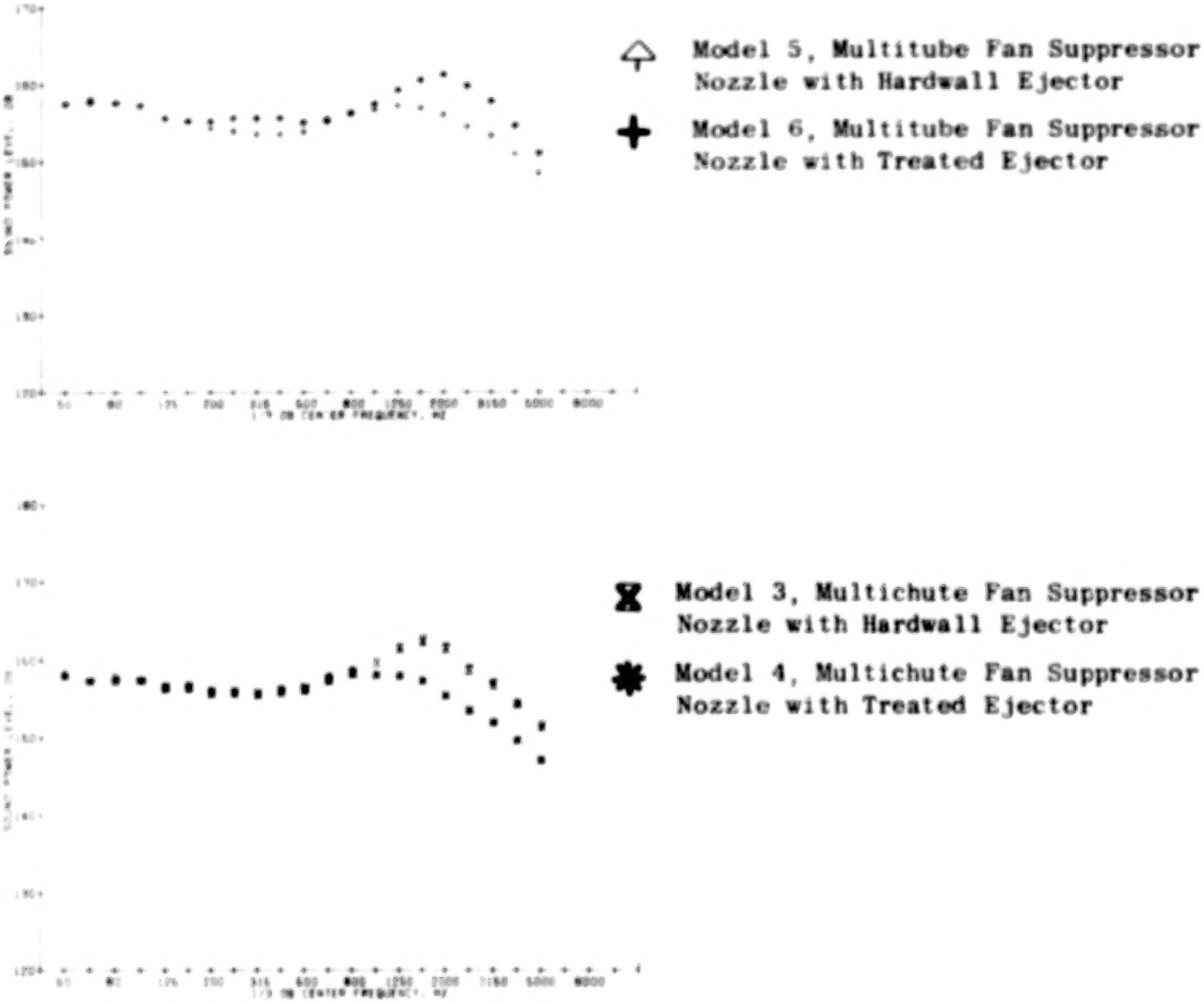

Figure 66. Comparison of One-Third Sourd Power Spectra from Multielement Fan Suppressor Nozzles with Hardwall and Treated Ejectors.

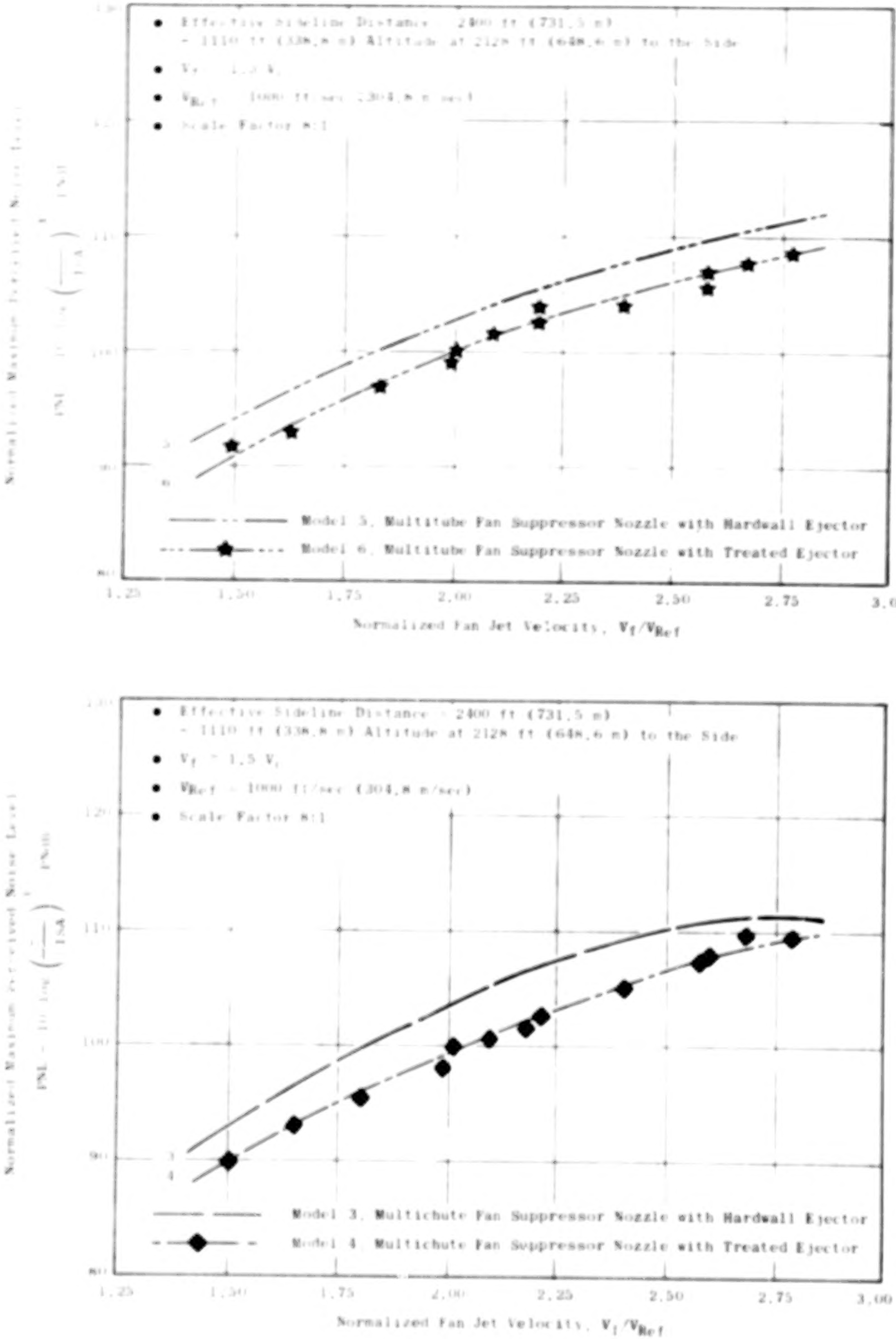

Figure 67. Comparison of Normalized Maximum Perceived Noise Level from Multielement Fan Suppressor Nozzles with Hardwall and Treated Ejectors.

- Effective Sideline Distance = 2400 ft (731.5 m)
  - 1110 ft (338.8 m) Altitude at 2128 ft (648.6 m) to the Side
- Scale Factor 8:1

Nominal Conditions

V_f = 2400 ft/sec (731.5 m/sec)
T_{T_f} = 1630° R (906 K)
V_c = 1200 ft/sec (365.8 m/sec)
T_{T_c} = 1000° R (556 K)

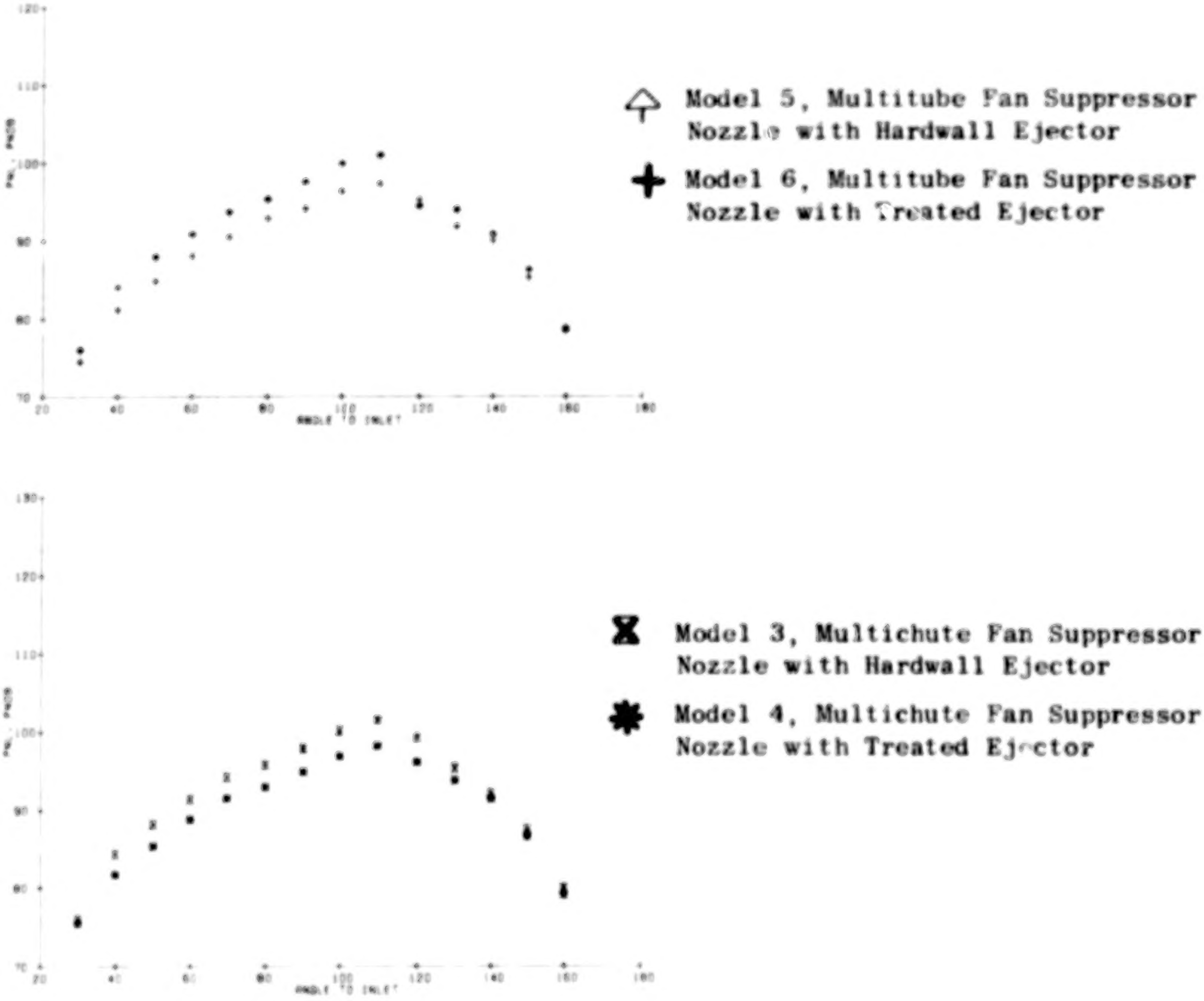

Figure 68. Comparison of PNL Directivity from Multielement Fan Suppressor Nozzles with Hardwall and Treated Ejectors.

The PNL directivity plots shown in Figure 68 are an example comparison of the acoustically treated ejector test results with the hardwall ejector test results for the suppressed coannular fan nozzle configurations. The aft inlet angle (e.g. $_i$ = 120° to 160°) PNL's of both the hardwall and treated ejectors on the multitube and multichute fan-suppressor nozzles are similar; this is because the low and midfrequency portions of the spectrum, as discussed previously in Section 5.4.1, are primarily influenced by changes in the merging region which are brought about by the ejector-induced flow. Alternately, ejector nozzle PNL reductions directly attributable to the acoustic liner are observed at all inlet angles below 120° for both multi-element systems (Model 4 versus Model 3 and Model 6 versus Model 5).

5.4.2.4 Sound Pressure Level Spectrum Test Results

Sample sound pressure level comparisons of the treated ejector and hardwall ejector test results are shown in Figures 69 and 70. The results exhibit the same trends observed in the power spectrum results of Figure 66. The effect of adding acoustic treatment to the hardwall ejector for both multielement nozzles introduces SPL noise reductions in the midfrequency to high frequency range at all observed angles. The SPL characteristics shown in these two figures explain more clearly the PNL results discussed previously. The aft angles (such as 130°) are dominated by low frequency noise which is not affected by the liner. At other angles (50° to 110°) the spectra is flat over a large frequency range, including those frequencies absorbed by the liner. The result is a significant reduction on the noise level at angles forward of 120°.

5.4.3 Inlet Lip Geometry Effects on the Hardwall Ejector

A series of tests was formulated to evaluate the impact on jet noise due to incorporating a realistic, flight-type inlet (hereafter referred to as a "sharp lip") compared to idealized bellmouth-type inlet results discussed in Section 5.4.2. Static acoustic testing of ejectors is usually conducted with an ideal bellmouth inlet, but such results could yield misleading conclusions regarding the actual ejector noise reduction capabilities. For this test series the coannular multichute fan suppressor was used. The maximum conical ejector diameter and its respective axial location relative to the multichute fan-suppressor nozzle were maintained for both series of lip-geometry tests. The contoured bellmouth inlet, however, extended 1.88 in. (4.78 cm) upstream of the leading edge of the sharp-lip inlet (see Section 4.0 for more details). The hardwall ejector was used as the test configuration for this evaluation.

5.4.3.1 Power Level Test Results

The normalized overall sound power plot on Figure 71 indicates that substitution of the sharp inlet (Model 9) for the bellmouth inlet (Model 3) on the hardwall ejector increases the noise levels 1 to 2 dB over the entire velocity range. Examination of the sharp-lip ejector nozzle (Model 9) power

- Effective Sideline Distance = 2400 ft (731.5 m)
  - 1110 ft (338.8 m) Altitude at 2128 ft (648.6 m) to the Side
- Scale Factor 8:1

Nominal Conditions

V_f = 2400 ft/sec (731.5 m/sec)

T_{T_f} = 1630° R (906 K)

V_c = 1200 ft/sec (365.8 m/sec)

T_{T_c} = 1000° R (556 K)

♀ Model 5, Multitube Fan Suppressor Nozzle with Hardwall Ejector

✚ Model 6, Multitube Fan Suppressor Nozzle with Treated Ejector

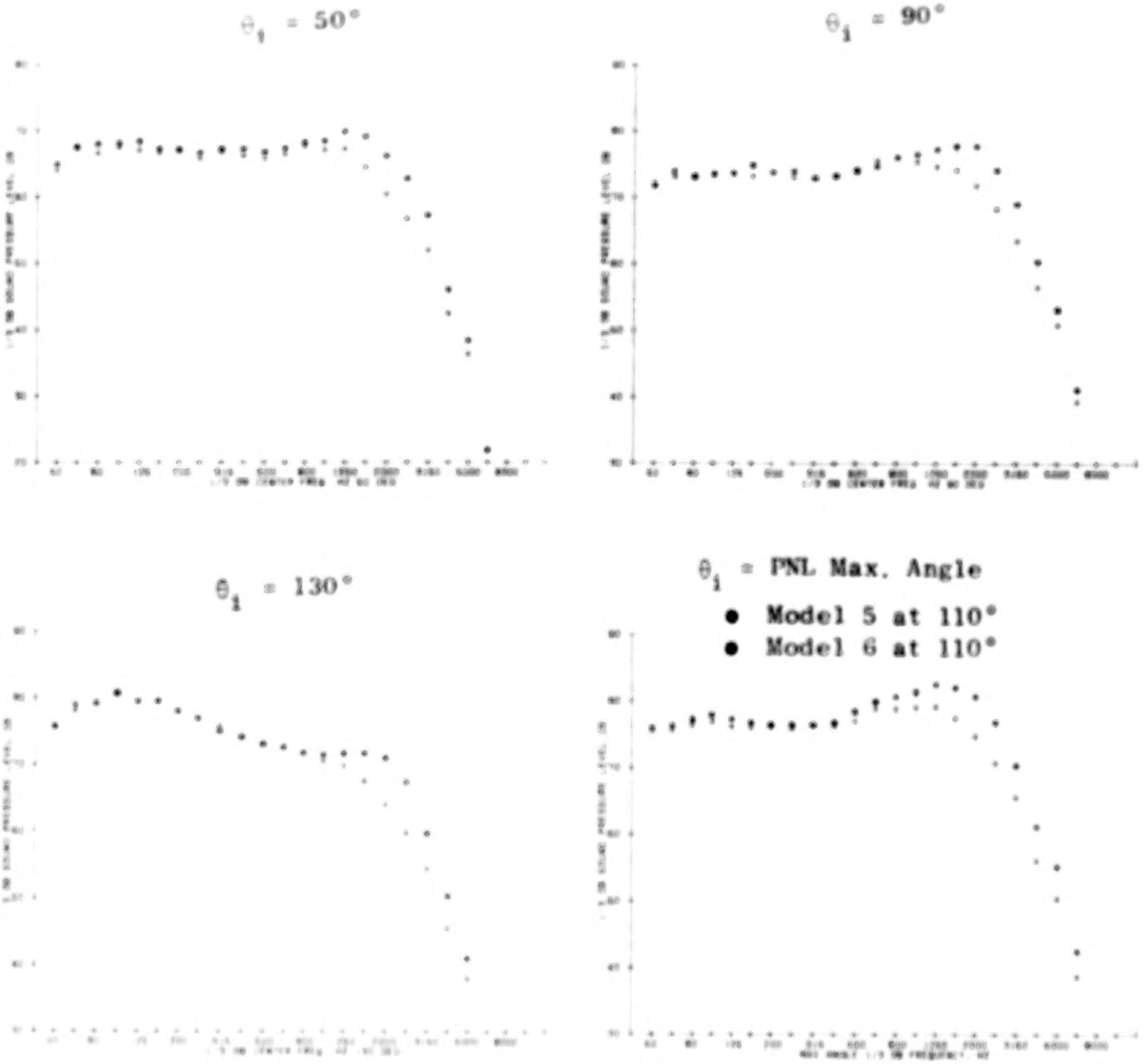

θ_i = 50°

θ_i = 90°

θ_i = 130°

θ_i = PNL Max. Angle

- Model 5 at 110°
- Model 6 at 110°

Figure 69. Comparison of SPL Spectra from Multitube Fan Suppressor Nozzle with Hardwall and Treated Ejectors.

- Effective Sideline Distance = 2400 ft (731.5 m)
  - 1110 ft (338.8 m) Altitude at 2128 ft (648.6 m) to the Side
- Scale Factor 8:1

Nominal Conditions

✖ Model 3, Multichute Fan Suppressor Nozzle with Hardwall Ejector

✱ Model 4, Multichute Fan Suppressor Nozzle with Treated Ejector

V_f = 2400 ft/sec (731.5 m/sec)
T_{T_f} = 1630° R (906 K)
V_c = 1200 ft/sec (365.8 m/sec)
T_{T_c} = 1000° R (556 K)

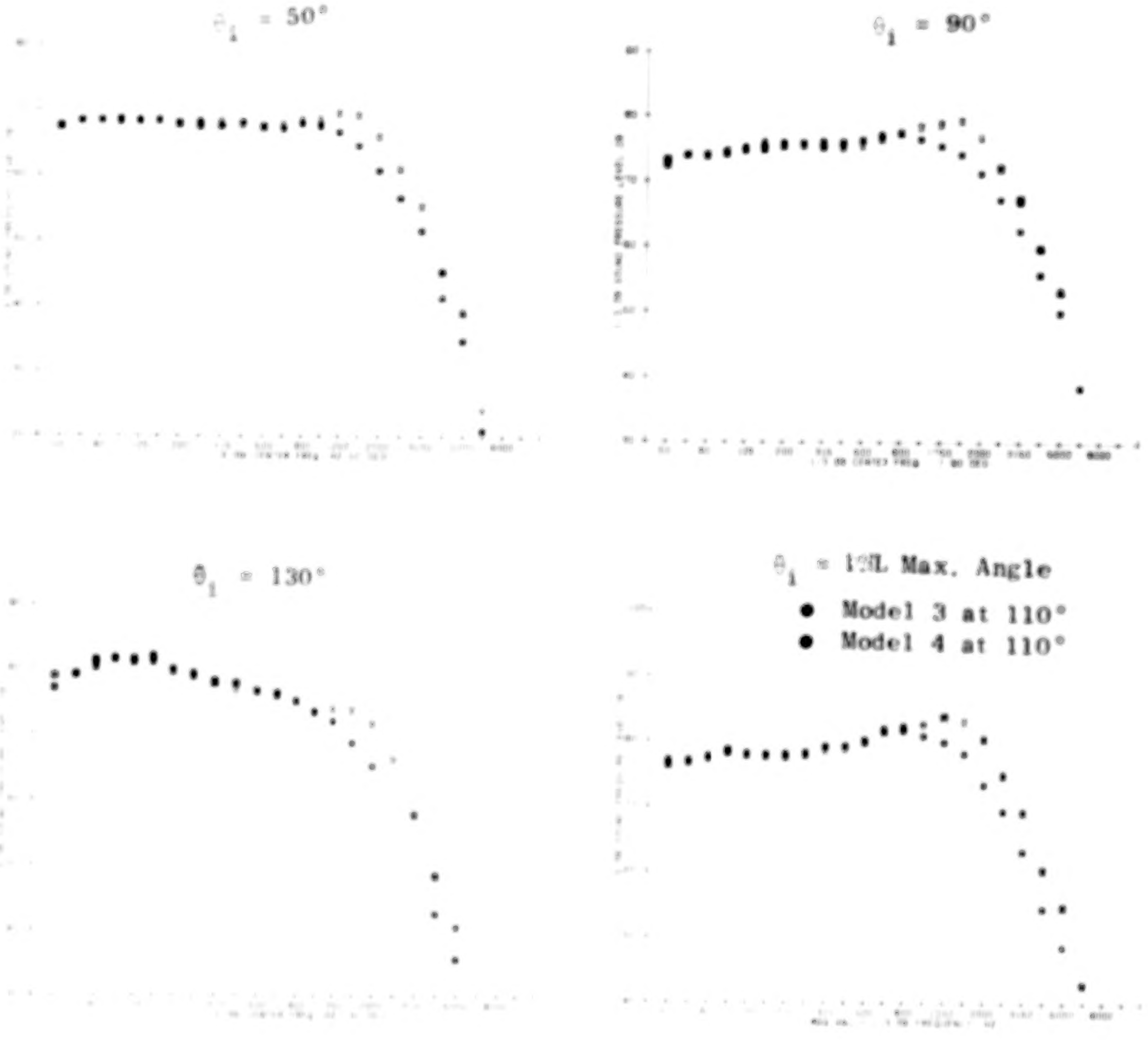

Figure 70. Comparison of SPL Spectra from Multichute Fan Suppressor Nozzle with Hardwall and Treated Ejector.

TABLE OF CONTENTS

Section — Page

1.0 SUMMARY 1 1/C1

2.0 INTRODUCTION 3 1/C3

3.0 TEST APPARATUS AND PROCEDURES 5 1/C5

3.1 FACILITIES 5 1/C5

3.1.1 General Electric Jet Engine Noise Outdoor Test Stand (JENOTS) Description 6 1/C6
3.1.1.1 Acoustic Arena 6 1/C6
3.1.1.2 Coannular-Flow System 6 1/C6
3.1.1.3 Coannular Frame Section 10 1/C12
3.1.1.4 Plenum Instrumentation Section 10 1/C12
3.1.1.5 Facility Acoustic Validation 12 1/C14
3.1.2 FluiDyne Aerodynamic-Performance Test Facility Description 12 1/C14

3.2 JENOTS INSTRUMENTATION SYSTEMS 16 1/D5

3.2.1 Acoustic Instrumentation Systems 16 1/D5
3.2.2 Laser Velocimeter System 18 1/D8
3.2.2.1 General Arrangement 18 1/D8
3.2.2.2 LV Actuator and Seeding 21 1/D13
3.2.2.3 Signal Processing and Recording 21 1/D13

3.3 DATA REDUCTION METHODS 21 1/D13

3.3.1 Acoustic Data Reduction 22 1/D14
3.3.1.1 JENOTS Data Reduction Systems 22 1/D14
3.3.1.2 Air-Attenuation Corrections 22 1/D14
3.3.1.3 Data-Scaling Procedure 30 1/E12
3.3.1.4 Data Corrections to a Free-Field Environment 30 1/E12
3.3.1.5 Power Level Calculation 30 1/E12
3.3.1.6 Acoustic Measurement Errors, Electronic Noise Floor 30 1/E12
3.3.2 Laser Velocimeter Data Reduction 33 1/F3
3.3.2.1 Basic Idea for LV rms Measurements 33 1/F3
3.3.2.2 The Histogram 36 1/F6
3.3.2.3 Mean Velocity 36 1/F6
3.3.2.4 Turbulent Velocity 37 1/F7
3.3.2.5 Statistical Errors for LV Mean and Turbulent Velocity Measurements 37 1/F7

TABLE OF CONTENTS (continued)

Section Page

3.3.3 Aerodynamic-Performance Test Data Reduction 37 1/F7
3.3.3.1 Flow Rates 39 1/F9
3.3.3.2 Discharge Coefficients 39 1/F9
3.3.3.3 Nozzle Throat 39 1/F9
3.3.3.4 Thrust Coefficient 40 1/F10
3.3.3.5 FluiDyne Force Balance Calibration 40 1/F10
3.3.3.6 Pressure and Temperature Data 41 1/F11
3.3.3.7 Data Quality 41 1/F11

4.0 MODEL DESCRIPTION AND DEFINITION OF TEST MATRICES 44 1/F14

4.1 MODEL DESIGN - SYSTEM EVOLUTION 44 1/F14
4.2 DESCRIPTION OF TEST MODELS 48 1/G6
4.3 ACOUSTIC TEST MATRIX 52 1/G12
4.4 LASER VELOCIMETER TEST MATRIX 56 2/A7
4.5 AERODYNAMIC-PERFORMANCE TEST MATRIX 61 2/B1
4.6 DATA SECTION 61 2/B1

5.0 DISCUSSION OF ACOUSTIC TEST RESULTS 63 2/B3

5.1 ESTABLISHMENT OF GROUND RULES FOR ACOUSTIC COMPARISONS AND DATA ILLUSTRATIONS 63 2/B3

5.1.1 Synthesized Baseline 63 2/B3
5.1.2 Average Conical Nozzle Noise Baseline 64 2/B4
5.1.3 Density Normalization and Presentation of Results 64 2/B4
5.1.3.1 Density Normalization Factors 64 2/B4
5.1.3.2 Presentation of Results 70 2/B13

5.2 UNSUPPRESSED COANNULAR NOZZLES 71 2/B14

5.2.1 High Core-Flow Test Results 71 2/B14
5.2.1.1 Overall Power Level Test Results 71 2/B14
5.2.1.2 Power Spectra Test Results 71 2/B14
5.2.1.3 Perceived Noise Level Test Results 71 2/B14
5.2.1.4 Perceived Noise Level Directivity Test Results 75 2/C6
5.2.1.5 Sound Pressure Level Spectra Test Results 75 2/C6
5.2.2 Low Core-Flow Test Results 75 2/C6
5.2.3 Acoustic Correlations 84 2/D5
5.2.4 Summary Remarks 84 2/D5

5.3 MULTIELEMENT FAN-SUPPRESSOR NOZZLES 88 2/D11

5.3.1 High Core Flow Test Results 88 2/D11
5.3.1.1 Overall Power Level Test Results 88 2/D11
5.3.1.2 Power Spectra Test Results 97 2/E11

TABLE OF CONTENTS (continued)

Section	Page	
5.3.1.3 Perceived Noise Level Test Results	97	2/E11
5.3.1.4 Sound Pressure Level Spectra Test Results	98	2/E12
5.3.2 Low Core-Flow Test Results	98	2/E12
5.3.3 Comparisons with Unsuppressed Coannular Nozzles	98	2/E12
5.3.4 Summary Remarks	104	2/F9
5.4 MULTIELEMENT FAN-SUPPRESSOR NOZZLES WITH EJECTORS	104	2/F9
5.4.1 Hardwall Ejector Effects	107	2/F12
5.4.1.1 Overall Power Level Test Results	107	2/F12
5.4.1.2 Power Spectra Test Results	107	2/F12
5.4.1.3 Perceived Noise Level Test Results	107	2/F12
5.4.1.4 Sound Pressure Level Test Results	111	2/G2
5.4.2 Treated Ejector Effects	111	2/G2
5.4.2.1 Overall Power Level Test Results	111	2/G2
5.4.2.2 Power Spectra Test Results	115	2/G6
5.4.2.3 Perceived Noise Level Test Results	115	2/G6
5.4.2.4 Sound Pressure Level Test Results	120	2/G11
5.4.3 Inlet Lip Geometry Effects on the Hardwall Ejector	120	2/G11
5.4.3.1 Power Level Test Results	120	2/G11
5.4.3.2 Perceived Noise Level Test Results	124	3/A8
5.4.3.3 Sound Pressure Level Test Results	124	3/A8
5.4.4 Summary Remarks	124	3/A8
5.5 EVALUATION OF A PARTIAL MECHANICAL SHIELD	130	3/B1
5.5.1 Perceived Noise Level Test Results	130	3/B1
5.5.2 Sound Pressure Level Spectra Results	134	3/B6
5.5.3 Summary Remarks	134	3/B6
6.0 DISCUSSION OF AERODYNAMIC-PERFORMANCE TEST RESULTS	140	3/C1
6.1 THRUST COEFFICIENTS	140	3/C1
6.1.1 Unsuppressed Coannular Nozzle with Plug	140	3/C1
6.1.2 Multichute Fan-Suppressor Nozzle	143	3/C5
6.1.3 Multichute Fan-Suppressor Nozzle with Hardwall Ejector with Sharp Lip	143	3/C5
6.1.4 Multitube Fan-Suppressor Nozzle	150	3/C12
6.1.5 Multitube Fan-Suppressor Nozzle with Hardwall Ejector with Sharp Lip	150	3/C12
6.2 EFFECT OF HOT EXHAUST FLOW ON THE THRUST COEFFICIENT OF THE MULTITUBE FAN-SUPPRESSOR NOZZLE WITH HARDWALL EJECTOR WITH SHARP LIP	156	3/D7

TABLE OF CONTENTS (continued)

Section Page

6.3 FLOW COEFFICIENTS 161 3/D14

6.3.1 Unsuppressed Coannular Nozzle with Plug 161 3/D14
6.3.2 Multichute Fan-Suppressor Nozzle 165 3/E6
6.3.3 Multichute Fan-Suppressor Nozzle with Hardwall Ejector with Sharp Lip 165 3/E6
6.3.4 Multitube Fan-Suppressor Nozzle 169 3/E10
6.3.5 Multitube Fan-Suppressor Nozzle with Hardwall Ejector with Sharp Lip 169 3/E10

7.0 DISCUSSION OF LASER VELOCIMETER TEST RESULTS 173 3/E14

7.1 LASER VELOCIMETER PLUME MEASUREMENTS FOR THE UNSUPPRESSED COANNULAR NOZZLE WITH PLUG 173 3/E14

7.1.1 Axial Mean-Velocity Distributions 173 3/E14
7.1.2 Mean-Velocity, Radial-Profile Distributions 176 3/F5
7.1.3 Axial Turbulent-Velocity, Radial-Profile Distributions 176 3/F5

7.2 LASER VELOCIMETER PLUME MEASUREMENTS FOR THE FAN-SUPPRESSED NOZZLES 176 3/F5

7.2.1 Axial Mean-Velocity Distributions 176 3/F5
7.2.2 Mean- and Turbulent-Velocity, Radial-Profile Distributions 180 3/F12
7.2.2.1 Multichute Fan Suppressor 180 3/F12
7.2.2.2 Multitube Fan Suppressor 180 3/F12

7.3 SUMMARY OF OBSERVATIONS 180 3/F12

8.0 DISCUSSION OF ACOUSTIC/AERODYNAMIC-PERFORMANCE CORRELATIONS 186 3/G8

8.1 EVALUATION OF NOISE CANDIDATES FOR DUCT-BURNING TURBOFAN ENGINES 186 3/G8
8.2 LOW CORE-FLOW COMPARISONS 191 4/A6

9.0 CONCLUSIONS AND RECOMMENDATIONS 196 4/A12

9.1 CONCLUSIONS 196 4/A12
9.2 RECOMMENDATIONS 197 4/A13

TABLE OF CONTENTS (concluded)

Section	Page	
APPENDIX A - GENERAL ELECTRIC AIR-ATTENUATION MODEL	199	4/B1
APPENDIX B - POWER LEVEL CALCULATION PROCEDURE	210	4/C1
APPENDIX C - DETAILED DESCRIPTION OF TEST MODELS	214	4/C5
APPENDIX D - ACOUSTIC TEST MATRIX FOR ALL DBTF MODELS AND EXAMPLE DATA PRINT OUT SHEETS	221	4/D3
APPENDIX E - FAN PLUG PRESSURE DISTRIBUTIONS FOR AERODYNAMIC MODEL 5	240	4/F13
APPENDIX F - MODEL 7 AXIAL-VELOCITY PROFILES	249	5/A8
APPENDIX G - MODEL 7 AXIAL-VELOCITY PROFILES WITH NO CORE FLOW	270	5/D7
APPENDIX H - MODEL 7 AXIAL-VELOCITY PROFILES WITH NO FAN FLOW	286	5/F10
APPENDIX I - MODEL 1 AXIAL-VELOCITY PROFILES	295	5/G13
APPENDIX J - MODEL 2 AXIAL-VELOCITY PROFILES	303	6/B6
APPENDIX K - NOMENCLATURE	313	6/C11
REFERENCES	317	6/D1

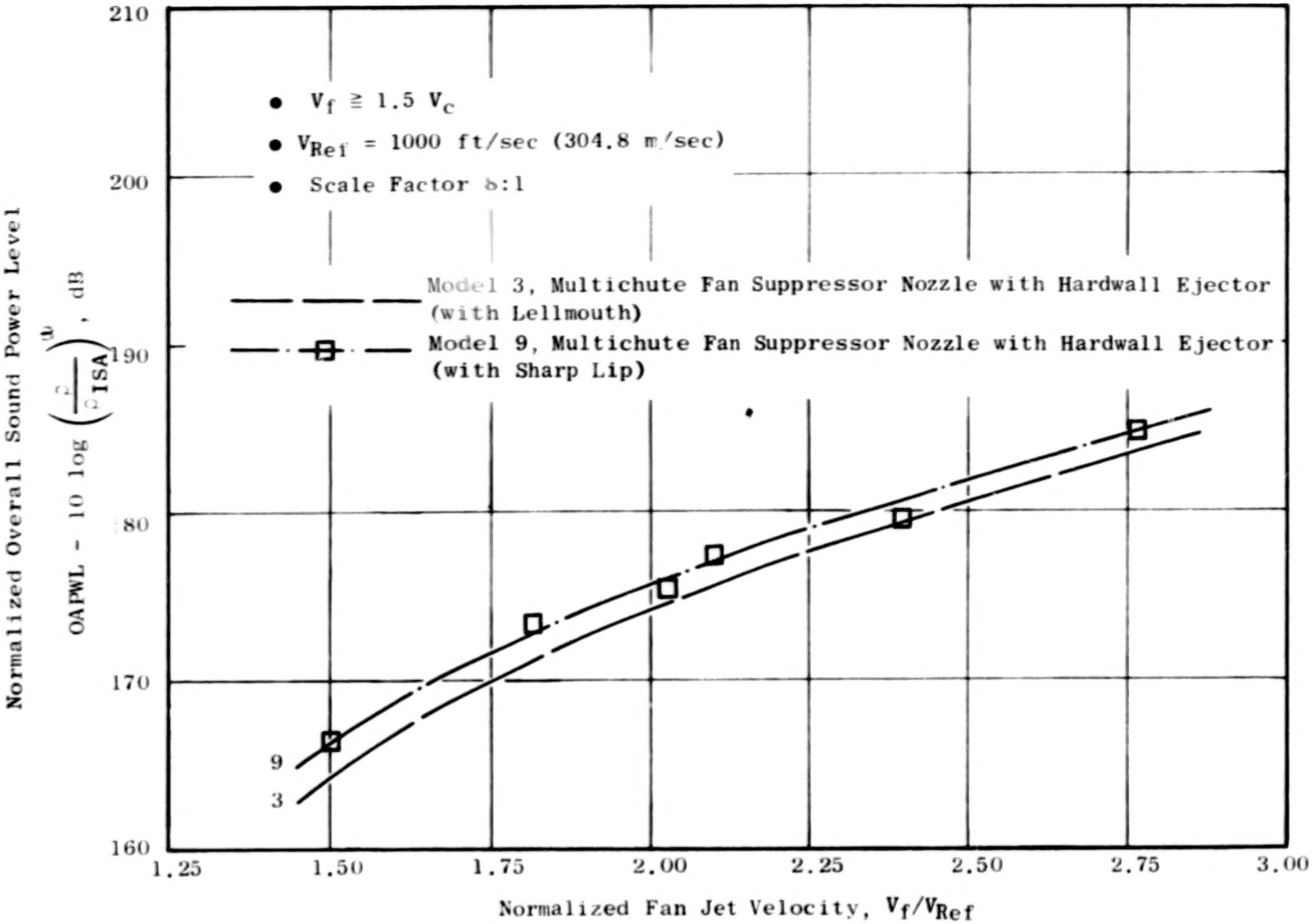

Figure 71. Effect of Ejector Lip Geometry on Multichute Fan Suppressor Nozzles with Hardwall Ejector Normalized Overall Power Level.

spectra (Figure 72) shows that the increase in overall sound power level shown in Figure 71 can be traced to an enhancement in sound power level in the midfrequency to high frequency hump centered around 1630 Hz. The difference between the sharp lip (Model 9) and bellmouth inlet (Model 3) ejector nozzle power spectra in the hump region is also seen to diminish with increasing fan jet velocity.

5.4.3.2 Perceived Noise Level Test Results

Figure 73 shows about the same normalized perceived noise level (NPNL), at normalized fan jet velocity greater than 2.0, for the hardwall ejectors with either a sharp lip or bellmouth inlet. Alternately, at normalized velocities below 2.0, the sharp-lip ejector nozzle (Model 9) is noisier than its bellmouth inlet (Model 3) counterpart. The PNL directivity plots presented on Figure 74 show that the NPNL trends just discussed (see Figure 73) are also applicable to most of the sideline inlet angles, with the forward sideline angle generally exhibiting more pronounced differences.

5.4.3.3 Sound Pressure Level Test Results

The one-third-octave SPL's in Figure 75 and 76 basically reflect the power spectra discussed above. The SPL spectra corresponding to the maximum perceived noise levels (Figure 75) tend to substantiate the NPNL differences noted on Figure 73 between the sharp lip (Model 9) and bellmouth inlet (Model 3) ejector nozzles; Model 9 is noisier than Model 3 up to 2000 ft/sec (609.6 m/sec), about the same thereafter. Moreover, the SPL spectra at a fan jet velocity of 2400 ft/sec (731.5 m/sec), shown in Figure 76, substantiate the observations made in the PNL directivity discussion; the detrimental effects of the sharp-lip ejector nozzle (Model 9) are more apparent at the forward inlet angles.

5.4.4 Summary Results

In summary, this section has shown that the addition of an acoustically treated ejector on the multielement fan-suppressor nozzles increased the suppression levels by 3 PNdB (e.g., ΔPNdB 17 to 17.5 PNdB relative to a synthesized baseline). Both hardwall ejectors (with bellmouth or with sharp-lip inlets) proved to be acoustically ineffective. At velocities below 2000 ft/sec (609.6 m/sec), the sharp-lip inlet hardwall ejector was found to be noisier than its bellmouth counterpart. The results suggest that lip geometry is not a factor when operating at velocities above 2000 ft/sec (609.6 m/sec); however, the utilization of a bellmouth inlet below this velocity range will tend to overestimate the noise reduction capabilities of the ejector.

● Scale Factor 8:1

⧗ Model 3, Multichute Fan Suppressor Nozzle with Hardwall Ejector (Bellmouth)

✖ Model 9, Multichute Fan Suppressor with Hardwall Ejector (Sharp Lip)

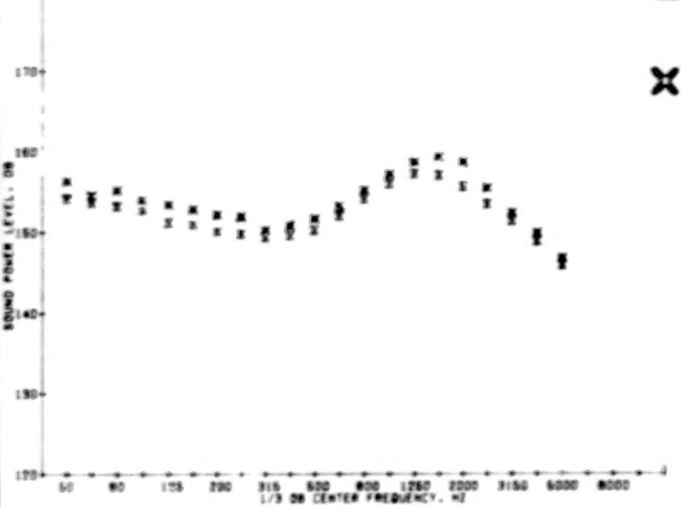

Nominal Conditions

V_f = 1800 ft/sec (548.6 m/sec)

T_{T_f} = 1200° R (667 K)

V_c = 1200 ft/sec (365.8 m/sec)

T_{T_c} = 1000° R (556 K)

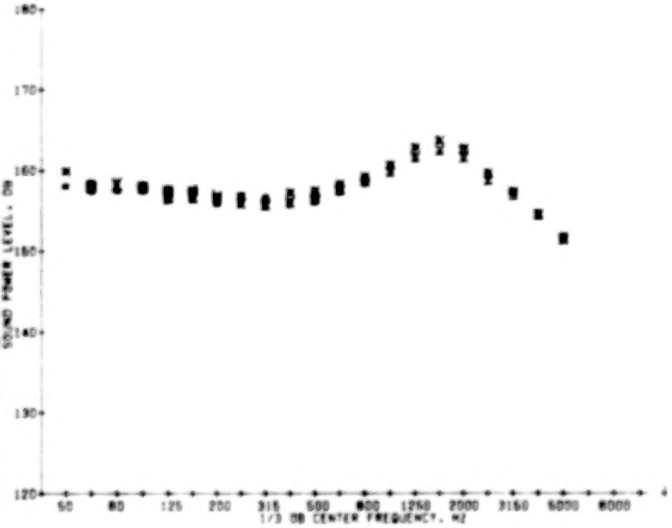

Nominal Conditions

V_f = 2400 ft/sec (731.5 m/sec)

T_{T_f} = 1630° R (906 K)

V_c = 1200 ft/sec (365.8 m/sec)

T_{T_c} = 1000° R (556 K)

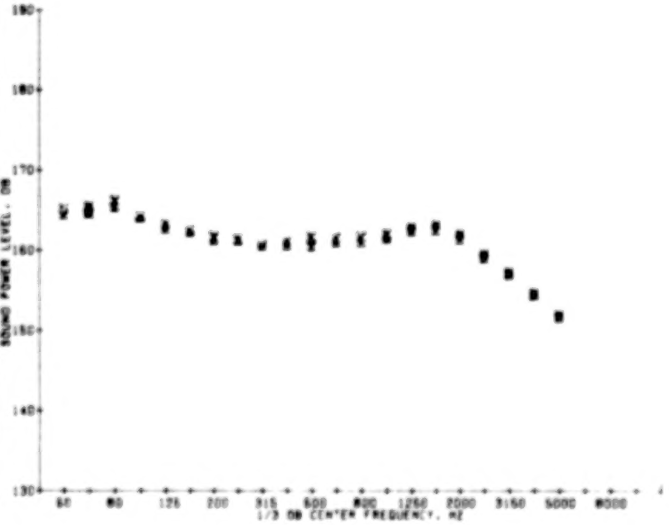

Nominal Conditions

V_f = 2800 ft/sec (853.4 m/sec)

T_{T_f} = 1960° R (1089 K)

V_c = 1400 ft/sec (426.7 m/sec)

T_{T_c} = 1460° R (811 K)

Figure 72. Effect of Ejector Lip Geometry on Multichute Fan Suppressor Nozzles with Hardwall Ejector One-Third-Octave Sound Power Spectra.

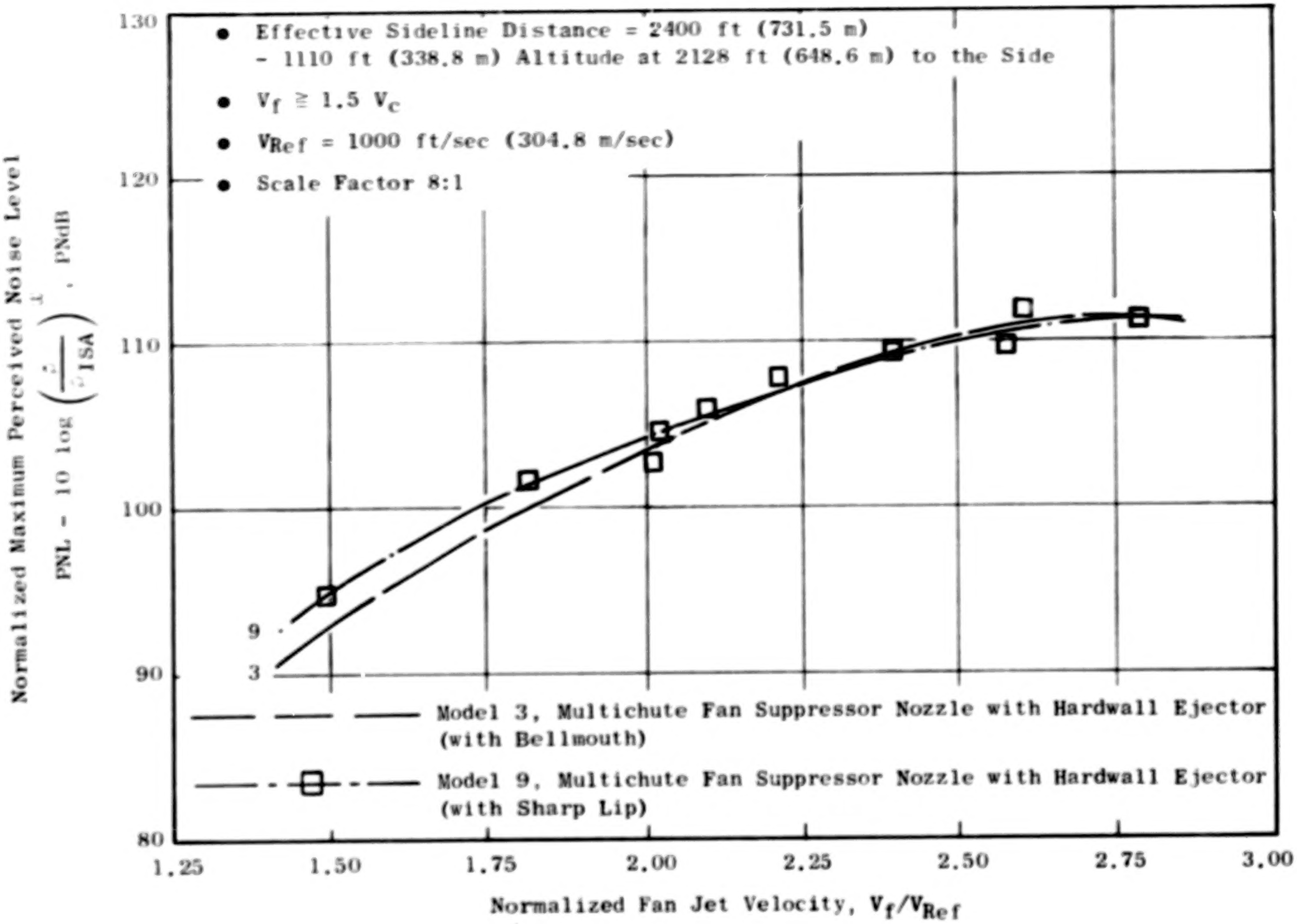

Figure 73. Effect of Ejector Lip Geometry on Multichute Fan Suppressor Nozzles with Hardwall Ejector Normalized Maximum Perceived Noise Level.

- Effective Sideline Distance = 2400 ft (731.5 m)
  - 1110 ft (338.8 m) Altitude at 2128 ft (648.6 m) to the Side
- Scale Factor 8:1

X Model 3, Multichute Fan Suppressor Nozzle with Hardwall Ejector (Bellmouth)

X Model 9, Multichute Fan Suppressor with Hardwall Ejector (Sharp Lip)

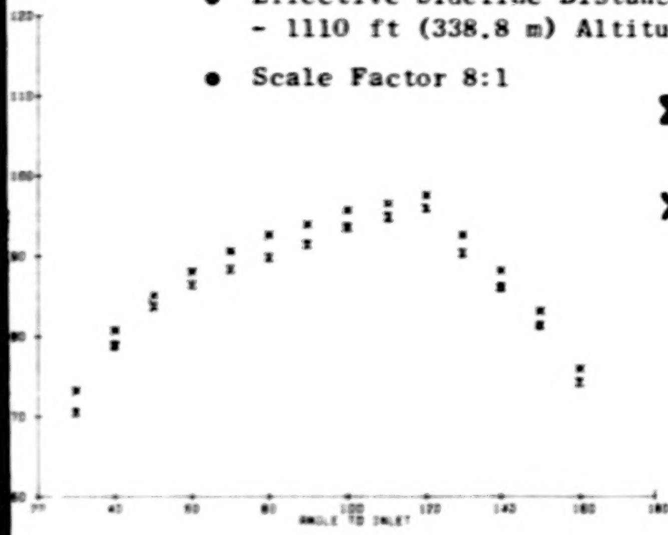

Nominal Conditions

V_f = 1800 ft/sec (548.6 m/sec)
T_{T_f} = 1200° R (667 K)
V_c = 1200 ft/sec (365.8 m/sec)
T_{T_c} = 1000° R (556 K)

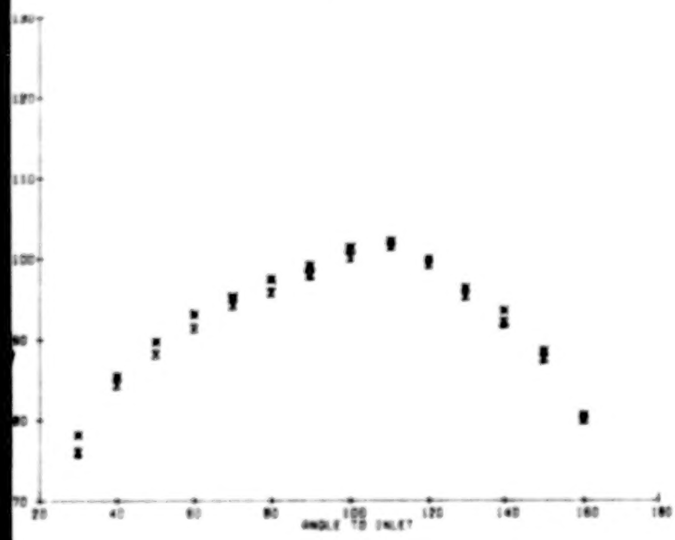

Nominal Conditions

V_f = 2400 ft/sec (731.5 m/sec)
T_{T_f} = 1630° R (906 K)
V_c = 1200 ft/sec (365.8 m/sec)
T_{T_c} = 1000° R (556 K)

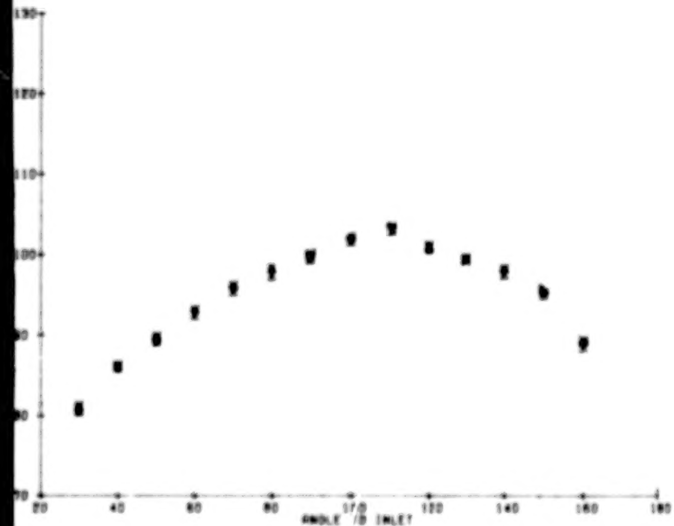

Nominal Conditions

V_f = 2800 ft/sec (853.4 m/sec)
T_{T_f} = 1960° R (1089 K)
V_c = 1400 ft/sec (426.7 m/sec)
T_{T_c} = 1460° R (811 K)

Figure 74. Effect of Ejector Lip Geometry on Multichute Fan Suppressor Nozzles with Hardwall Ejector PNL Directivity.

- Effective Sideline Distance = 2400 ft (731.5 m)
  - 1110 ft (338.8 m) Altitude at 2128 ft (648.6 m) to the Side
- Scale Factor 8:1
- Maximum PNL Noise Angle

⧗ **Model 3, Multichute Fan Suppressor Nozzle with Hardwall Ejector (Bellmout**

✖ **Model 9, Multichute Fan Suppressor with Hardwall Ejector (Sharp Lip)**

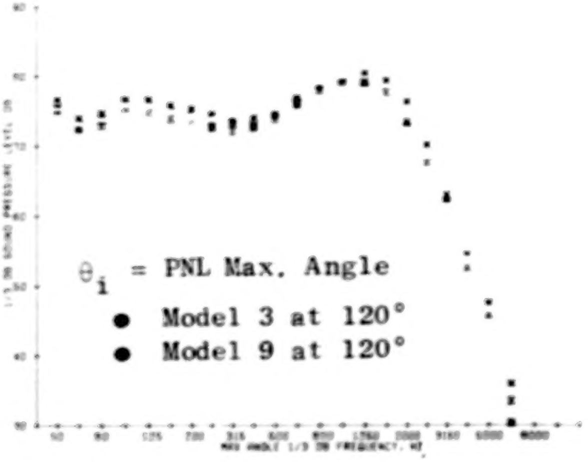

Nominal Conditions

V_f = 1800 ft/sec (548.6 m/sec)

T_{T_f} = 1200° R (667 K)

V_c = 1200 ft/sec (365.8 m/sec)

T_{T_c} = 1000° R (556 K)

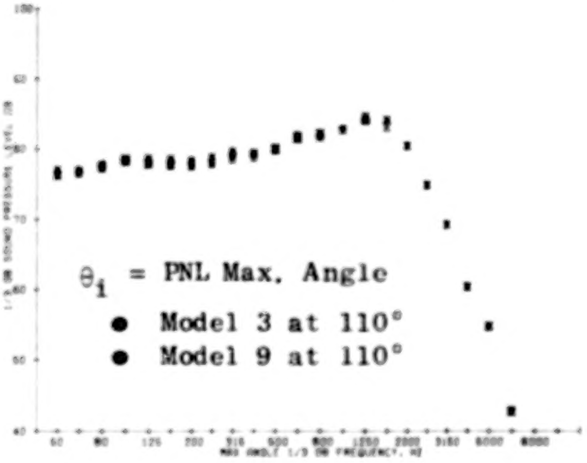

Nominal Conditions

V_f = 2400 ft/sec (731.5 m/sec)

T_{T_f} = 1630° R (906 K)

V_c = 1200 ft/sec (365.8 m/sec)

T_{T_c} = 1000° R (556 K)

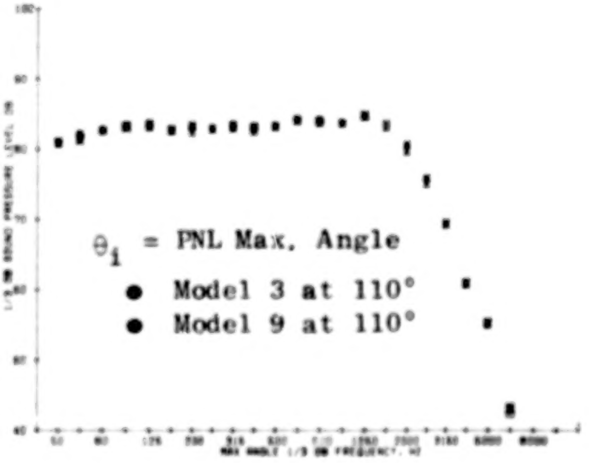

Nominal Conditions

V_f = 2800 ft/sec (853.4 m/sec)

T_{T_f} = 1960° R (1089 K)

V_c = 1400 ft/sec (426.7 m/sec)

T_{T_c} = 1460° R (811 K)

Figure 75. Effect of Ejector Lip Geometry on Multichute Fan Suppressor with Hardwall Ejector SPL Spectra at Maximum PNL Noise Angle.

- Effective Sideline Distance = 2400 ft (731.5 m)
  - 1110 ft (338.8 m) Altitude at 2128 ft (648.6 m) to the Side
- Scale Factor 8:1

Nominal Conditions

⧗ **Model 3, Multichute Fan Suppressor Nozzle with Hardwall Ejector (Bellmouth)**	V_f = 2400 ft/sec (731.5 m/sec)
	T_{T_f} = 1630° R (906 K)
⌧ **Model 9, Multichute Fan Suppressor with Hardwall Ejector (Sharp Lip)**	V_c = 1200 ft/sec (365.8 m/sec)
	T_{T_c} = 1000° R (556 K)

θ_i = 50° θ_i = 90°

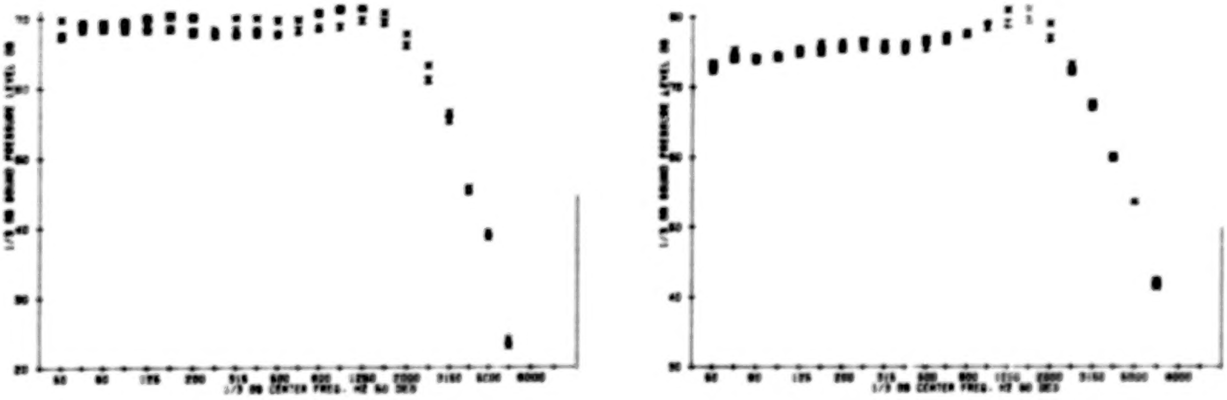

θ_i = 130° θ_i = PNL Max. Angle

- Model 3 at 110°
- Model 9 at 110°

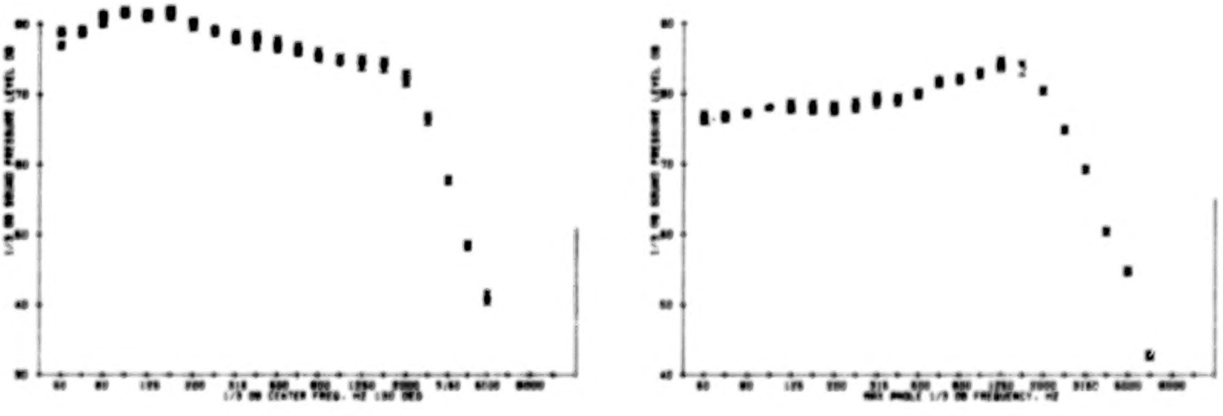

Figure 76. Effect of Ejector Lip Geometry on Multichute Fan Suppressor with Hardwall Ejector SPL Spectra.

5.5 EVALUATION OF A PARTIAL MECHANICAL SHIELD

The acoustic evaluation of a partial mechanical shield in place of an ejector was included as part of the test program with the view that the partial shield may have the same potential acoustic advantages as a hardwall ejector (i.e., block the high frequency noise generated near the nozzle exit and refocus it away from the ground during aircraft flyover) for the same overall weight. The partial mechanical shield offers an advantage over the ejector in that it can have greater length than an ejector of equivalent weight; also, it has the possible mechanical advantage that it may be easier to stow.

The partial mechanical shield was tested with the multichute fan-suppressor nozzle in both the flyover and sideline orientation because this is an asymmetric configuration. Because of this asymmetry the microphones were moved and placed at the 55-inch (1.4 m) rather than at the 16-foot (4.88 m) height in order to orient the test models in a suitable plane relative to the acoustic arena.

In order to evaluate the effect on ground reflections of this lower microphone height, the multichute fan suppressor with the treated ejector was tested at both microphone heights. Comparisons of the measured spectra at the 50°, 90°, and 130° microphone locations for two test points are shown in Figures 77 and 78. For the 90° and 130° positions there is fair agreement between the measured data at the two microphone heights for frequencies above 1600 Hz. When the data is scaled 8:1 for full-size comparisons, the data shifts nine bands; therefore, the data above 200 Hz at full size is relatively free of ground reflection differences between the two microphone heights. The only exception is a ground reflection reinforcement which is sometimes seen between 2000 and 3150 Hz (315 to 400 Hz full size). At the 50° angle, the influence of ground reflections is much more pronounced, particularly at the high velocity test point. The lower microphone height has a higher ground reflection contribution at high frequency than does the 16-ft (4.88 m) height. Overall, the change in microphone heights for this evaluation was considered adequate. The reader is cautioned that the acoustic results in this section are in absolute levels and care must be exercised when comparing with other data in this report.

5.5.1 Perceived Noise Level Test Results

In Figure 79, the maximum PNL values at the 2400-foot (731.5 m) sideline location are compared for the multichute fan-suppressor nozzle (Model 1), and for the multichute fan-suppressor nozzle with a partial mechanical shield in both the sideline orientation (Model 10) and the flyover orientation (Model 11). The comparison is made as a function of the fan velocity and includes only test points having $V_f/V_c \geq 1.5$. On this maximum PNL basis, the partial shield is not effective in reducing the noise relative to the measured multichute fan-suppressor noise levels. The results with the partial shield are consistent with those shown for the multichute fan-

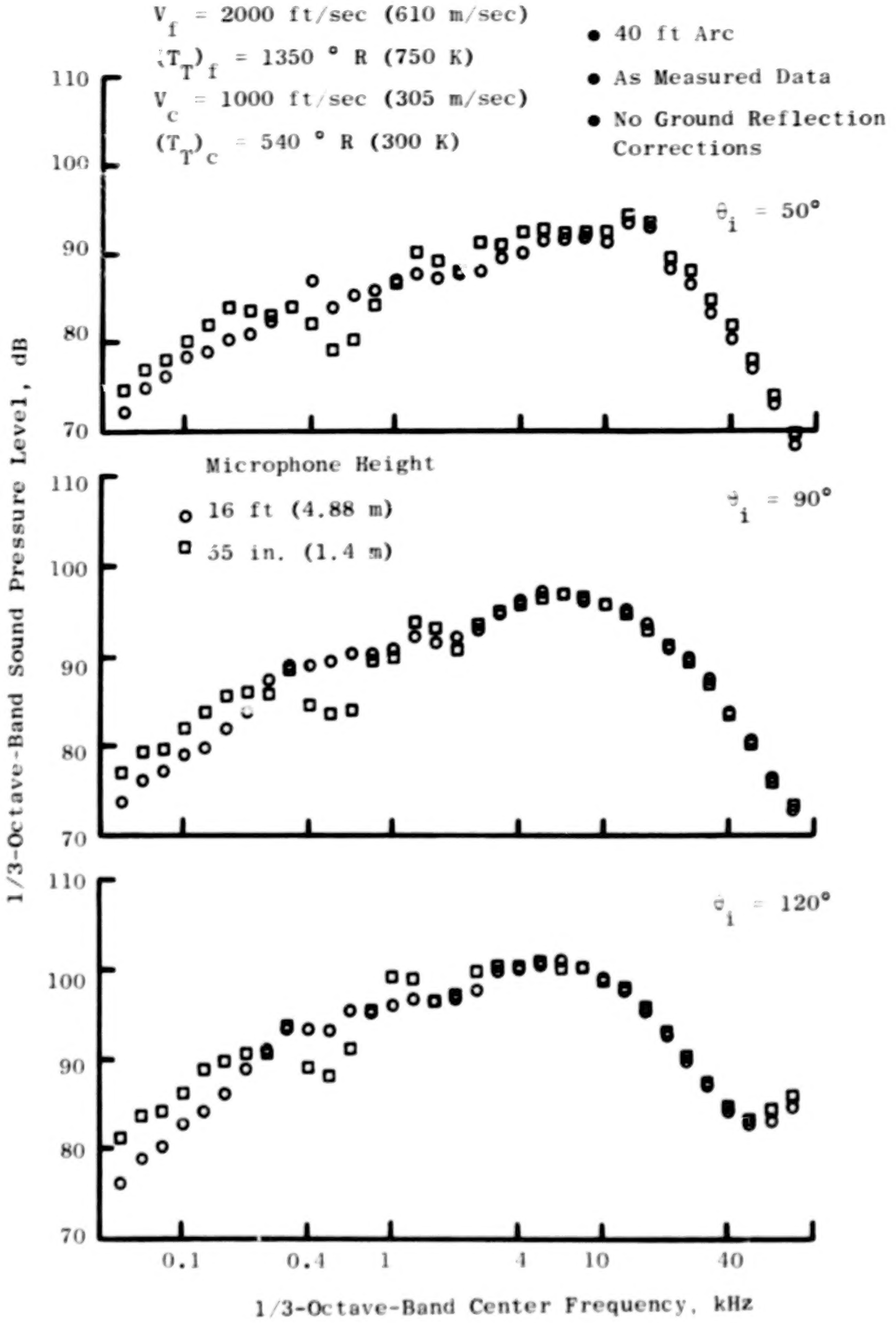

Figure 77. Model Scale Spectral Comparisons of Measured Data at Two Microphone Heights for the Multichute Fan Suppressor with a Treated Ejector.

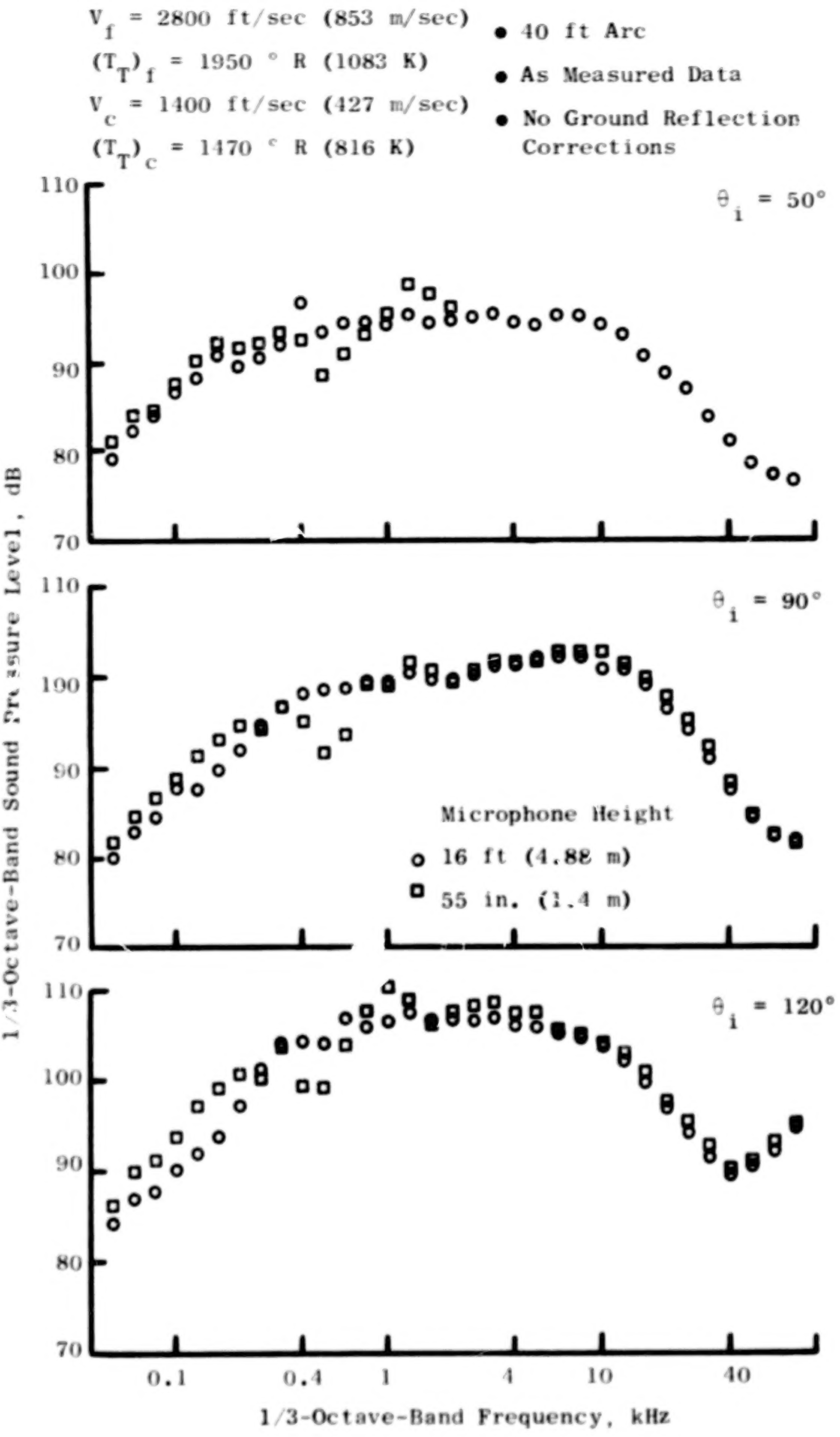

Figure 78. Model Scale Spectral Comparisons of Measured Data at Two Microphone Heights for the Multichute Fan Suppressor with a Treated Ejector.

- Effective Sideline Distance = 2400 ft (731.5 m)
  1100 ft (338.8 m) Altitude at 2128 ft (648.6 m) to the Side
- Scaled 8:1
- $V_f/V_c = 1.5$

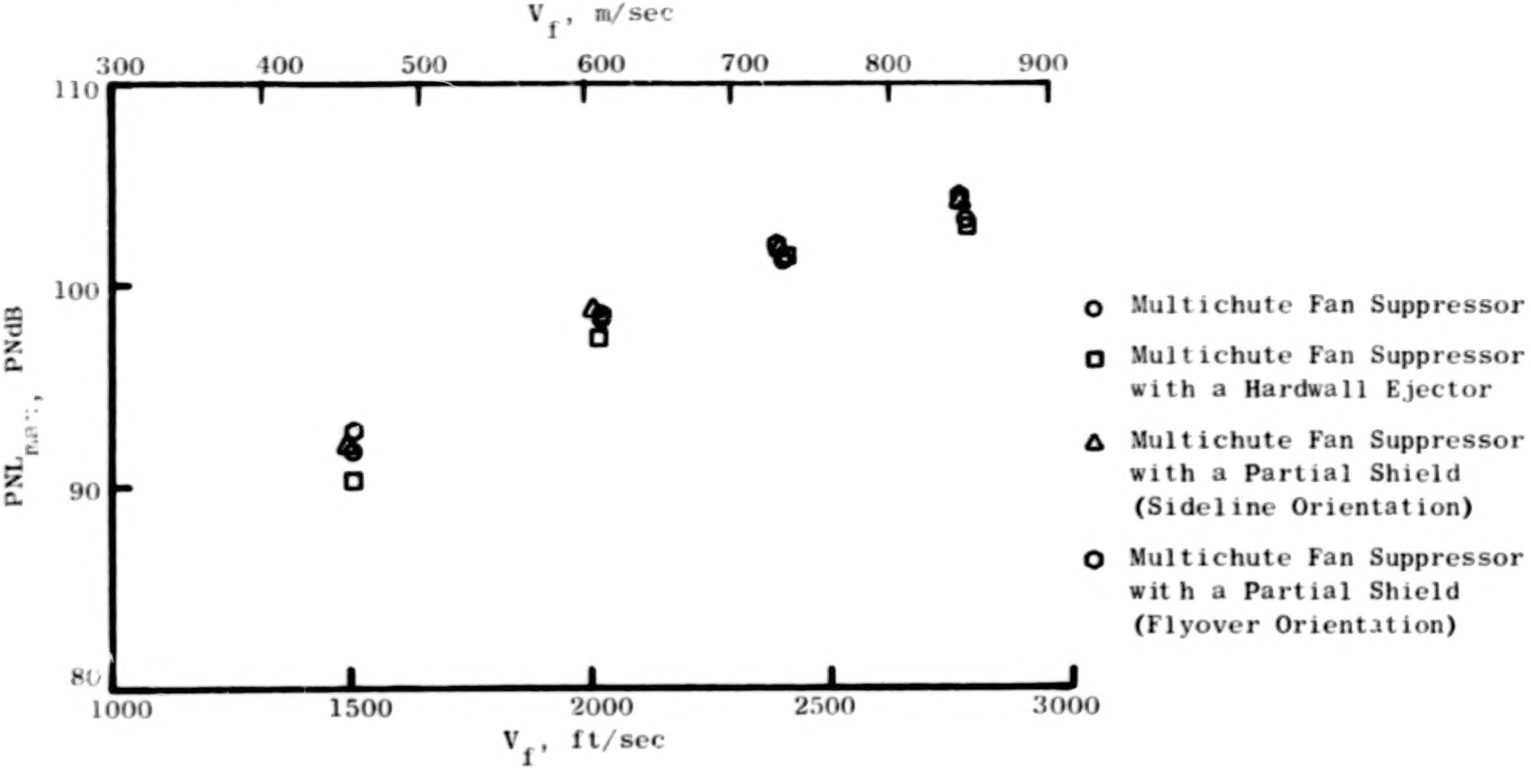

Figure 79. Maximum PNL for the Multichute Fan Suppressor with a Partial Shield Compared to the Multichute Fan Suppressor Alone and with Hardwall Ejector.

suppressor nozzle with the hardwall ejector (Model 3); they show little effectiveness at the maximum angle. Also, it is noted that there is no significant difference between the results for sideline and flyover orientations of the partial shield.

In Figures 80 and 81, the PNL directivity is compared for these same configurations at the 2400-foot sideline (731.5 m) for four test points. On this basis the multichute fan-suppressor nozzle with the hardwall ejector is more effective than the partial shield. At the maximum angle, the PNL levels are nearly the same; however, at other angles the hardwall ejector does reduce the PNL relative to that of the multichute fan-suppressor nozzle while the results with the partial shield generally show no suppression. The noise increases of the partial mechanical shield configuration relative to the multichute fan-suppressor nozzle at forward angles are probably due to increased ground reflections at the low microphone height.

5.5.2 Sound Pressure Level Spectra Results

Sound pressure level spectra test results shown in Figure 82 illustrate that the partial shield has little advantage at either the sideline or flyover orientations. Spectra comparisons at the 90° and 120° inlet angles (Figures 83 and 84) also show that the partial shield is generally ineffective. The only significant deviation from the noise spectra of the multichute fan-suppressor nozzle is at frequencies near 400 Hz, where there is a noise increase. This noise increase is attributed to a ground reflection reinforcement at the 55-inch (1.4 m) microphone height. This was seen previously in the comparison of measured data at the two different microphone heights (Figures 77 and 78).

5.5.3 Summary Remarks

From these results it can be concluded that for the multichute fan-suppressor nozzle the partial mechanical shield is not an effective noise suppressor. It is significant to note that the multichute fan-suppressor nozzle with the partial mechanical shield does not achieve noise reductions similar to the multichute fan-suppressor nozzle with the hardwall ejector (Model 3) even though the partial mechanical shield had a greater length than the hardwall ejector. A possible explanation is that the ejector does not really act as a shield but instead mixes low velocity air with the jet and thereby reduces the jet noise. It is also possible that the jet noise leaks around the edges of the partial shield and negates the shielding effect.

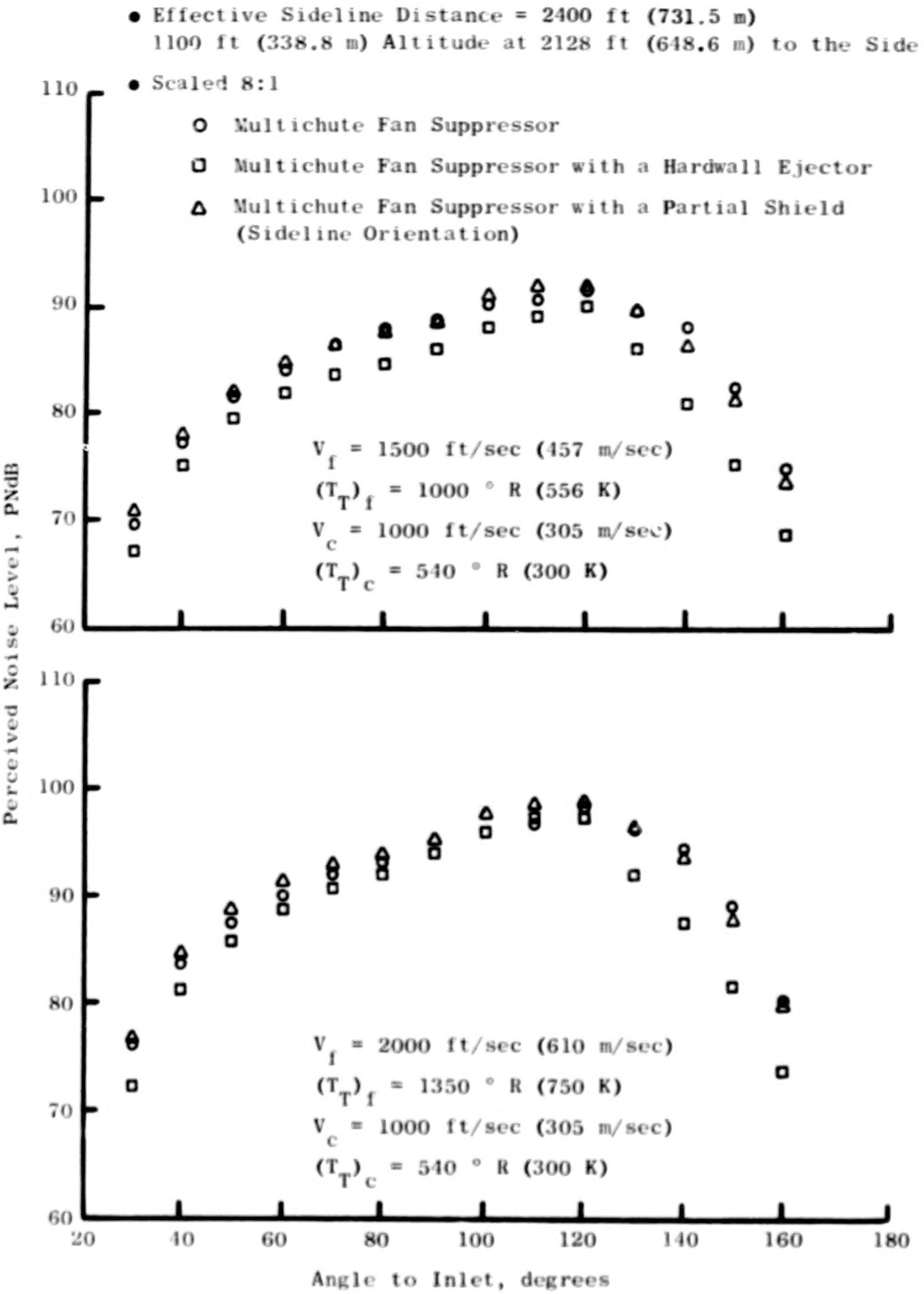

Figure 80. PNL Directivity for the Multichute Fan Suppressor with a Partial Shield Compared to a Hardwall Ejector and the Multichute Fan Suppressor Alone.

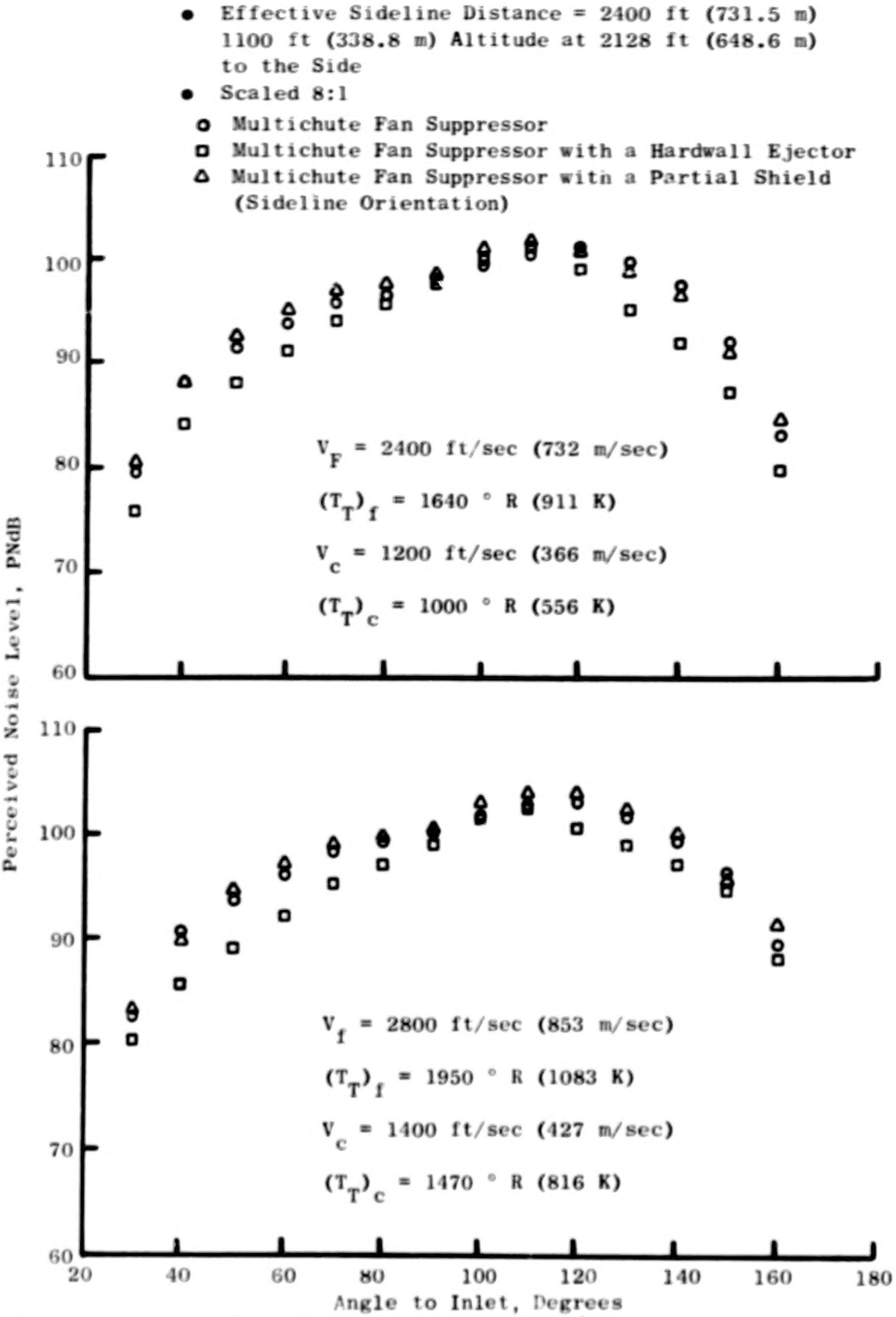

Figure 81. PNL Directivity for the Multichute Fan Suppressor with a Partial Shield Compared to a Hardwall Ejector and the Multichute Fan Suppressor Alone.

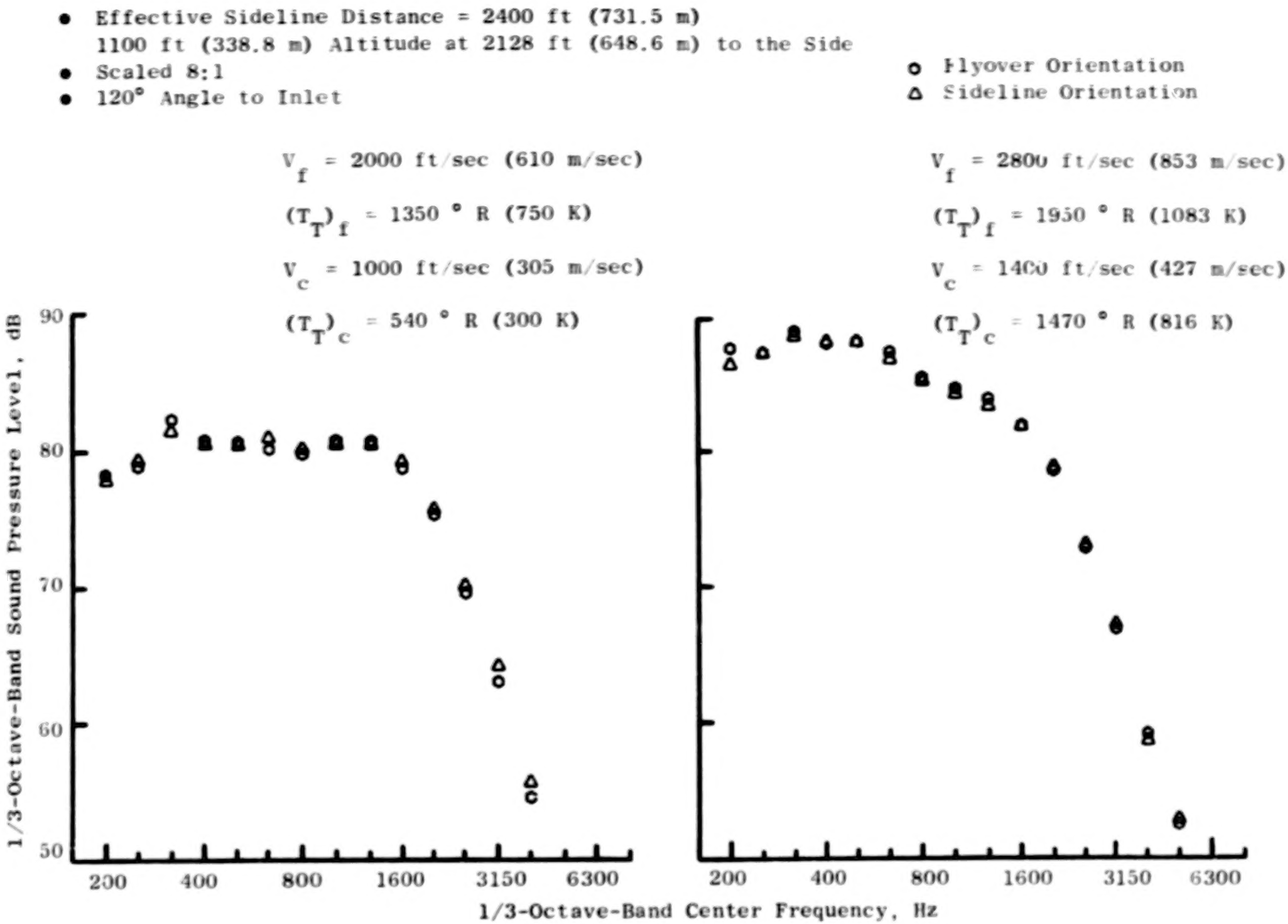

Figure 82. Spectral Comparisons of Multichute Fan Suppressor with a Partial Shield in the Sideline and Overhead Positions.

- Effective Sideline Distance = 2400 ft (731.5 m)
  1100 ft (338.8 m) Altitude at 2128 ft (648.6 m) to the Side
- Scaled 8:1

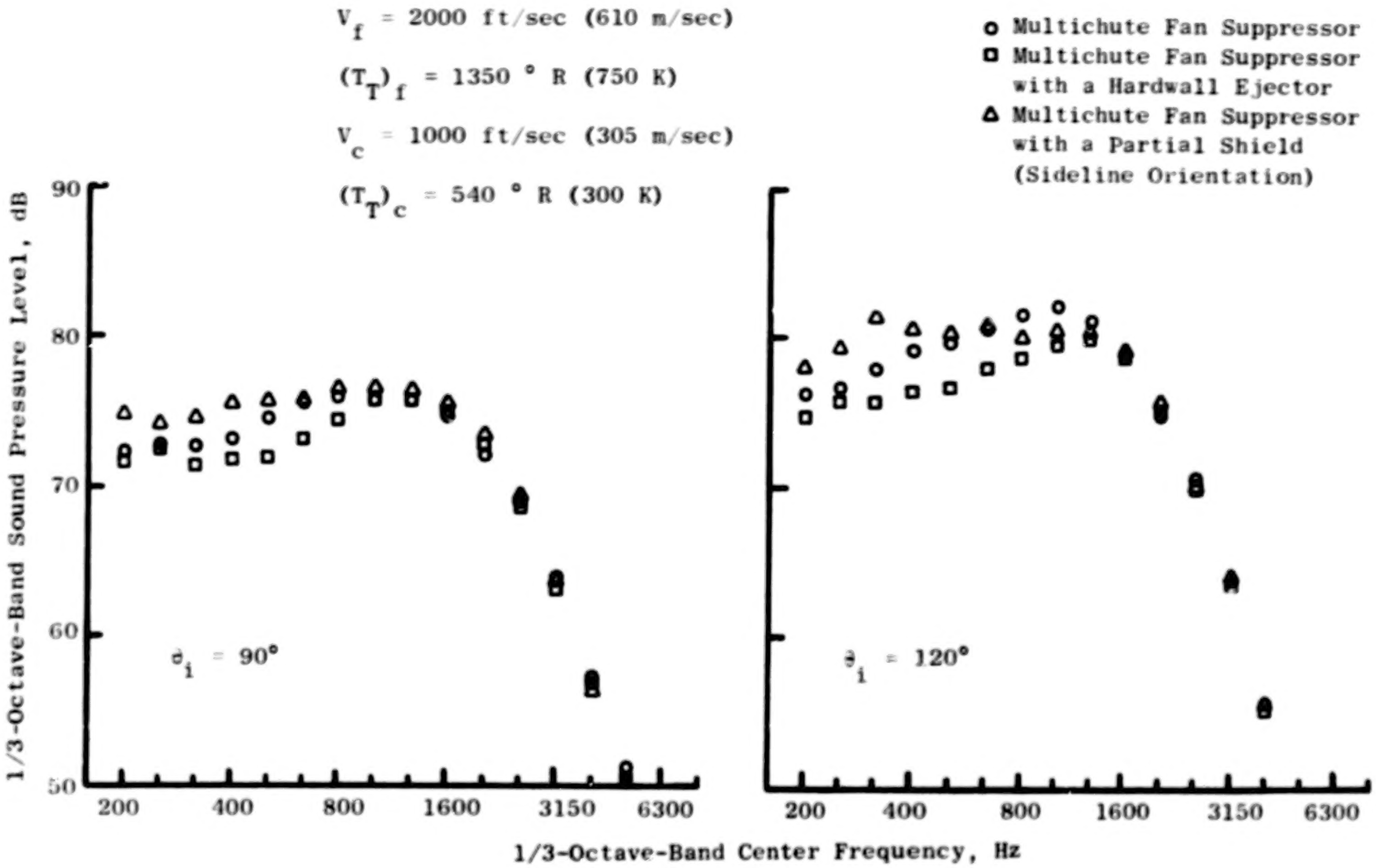

Figure 83. Spectral Characteristics of the Multichute Fan Suppressor with a Partial Shield Compared to a Hardwall Ejector and the Multichute Fan Suppressor Alone.

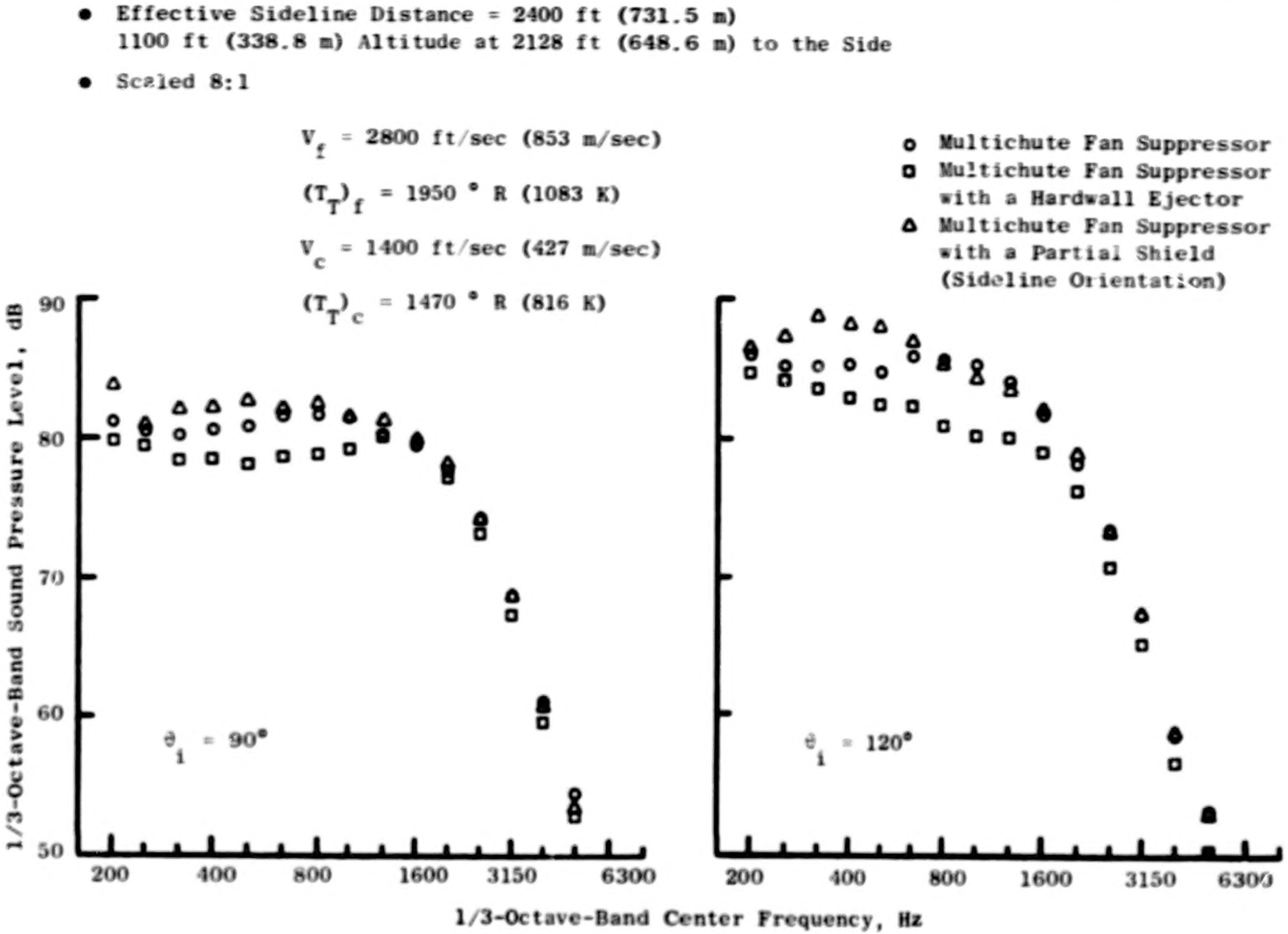

Figure 84. Spectral Characteristics of the Multichute Fan Suppressor with a Partial Shield Compared to a Hardwall Ejector and the Multichute Fan Suppressor Alone.

6.0 DISCUSSION OF AERODYNAMIC-PERFORMANCE TEST RESULTS

The aerodynamic-performance tests were run independent of the acoustic tests and were conducted in the FluiDyne static thrust stand described in Section 3.1.2. Five of the nine acoustic models were selected for performance testing; the same model hardware was used for both performance and acoustic testing. These five configurations were the unsuppressed coannular nozzle with plug (Model 7), the multichute fan-suppressor nozzle (Model 1), multitube fan-suppressor nozzle (Model 2), and the multichute and multitube fan-suppressor nozzles with the sharp-lip hardwall ejector (Models 9 and aerodynamic 5 respectively). The unsuppressed coannular nozzle without plug model, the acoustically treated ejector, the partial shield, and the bellmouth ejector were not tested for performance.

The aerodynamic test matrix was selected to cover the same range of fan and core pressure ratios as in the acoustic tests, and it was run parametrically: a core nozzle pressure ratio was set and data taken at several fan pressure ratios; the core pressure ratio was then reset at a second condition and data taken at the same fan pressure ratios. The basic matrix consisted of fan pressure ratios of 1.5, 2.25, 3.0, and 4.0 at core pressure ratios of 1.3 and 1.9. The majority of testing was conducted with cold exhaust flow (approximately ambient temperature). The multitube fan-suppressor nozzle with hardwall ejector with sharp lip (aerodynamic Model 5) was run with hot flow, in addition to the cold flow tests, in order to investigate any differences in performance level. The following results and discussion apply only to the cold flow tests unless otherwise stated.

The principal parameters measured by the test were nozzle thrust coefficient, flow coefficients of both the core duct and the fan duct, and static pressures on the nozzle plugs, suppressor base areas, and ejector inner surface. The test results and discussion are presented in the following subsections.

6.1 THRUST COEFFICIENTS

6.1.1 Unsuppressed Coannular Nozzle with Plug

The thrust coefficients for the unsuppressed coannular nozzle with plug (Model 7) are shown in Figure 85 as a function of fan duct pressure ratio. The thrust coefficient at a fan pressure ratio of 3.0 (representative of takeoff operation) is 0.972 for a core pressure ratio of 1.3 and 0.964 for a core pressure ratio of 1.9. The static pressures, nondimensionalized by the ambient pressure, are shown in Figures 86 and 87 for the core and fan plugs respectively. The core flow exhibits a rapid expansion in the region of the abrupt angular change in the plug contour aft of the nozzle throat. This area of subambient pressure is more severe at the 1.9 core pressure ratio than at the 1.3 core pressure ratio, resulting in lower pressure recovery on the plug

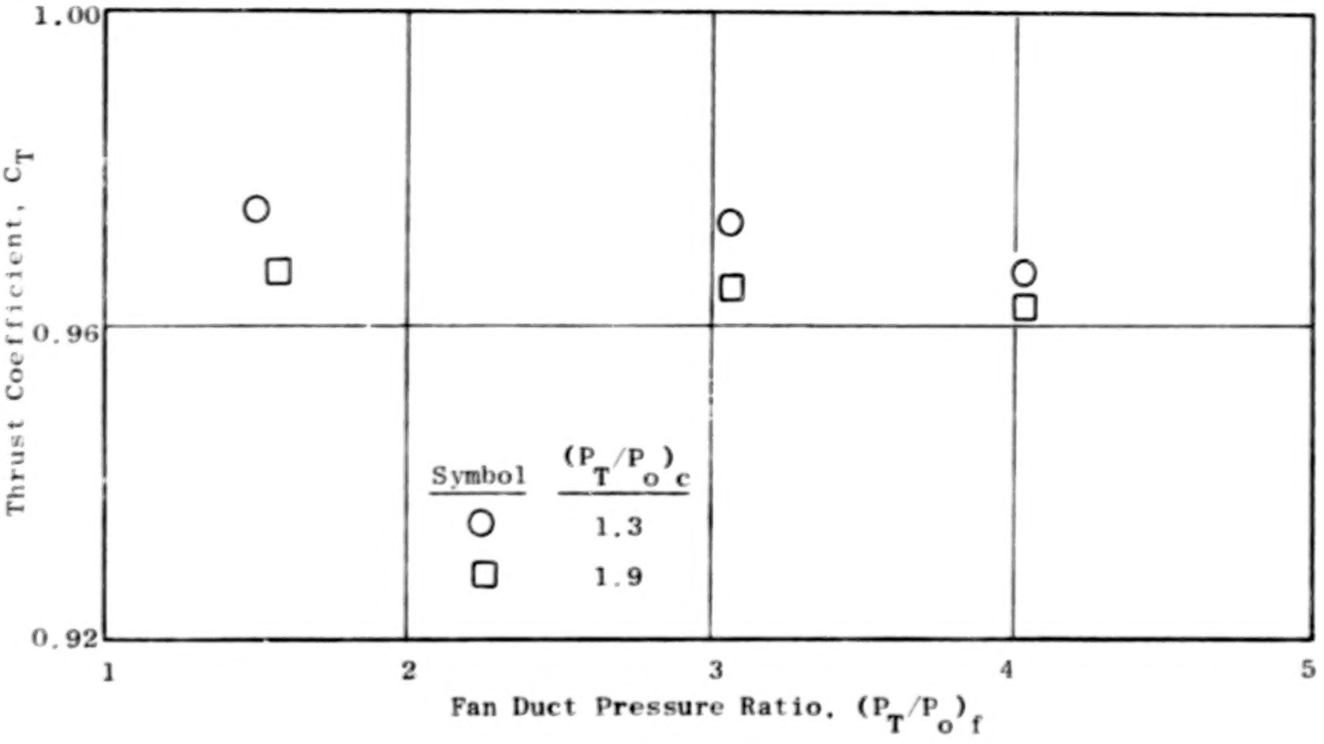

Figure 85. Thrust Coefficients for the Unsuppressed Coannular Nozzle with Plug (Model 7).

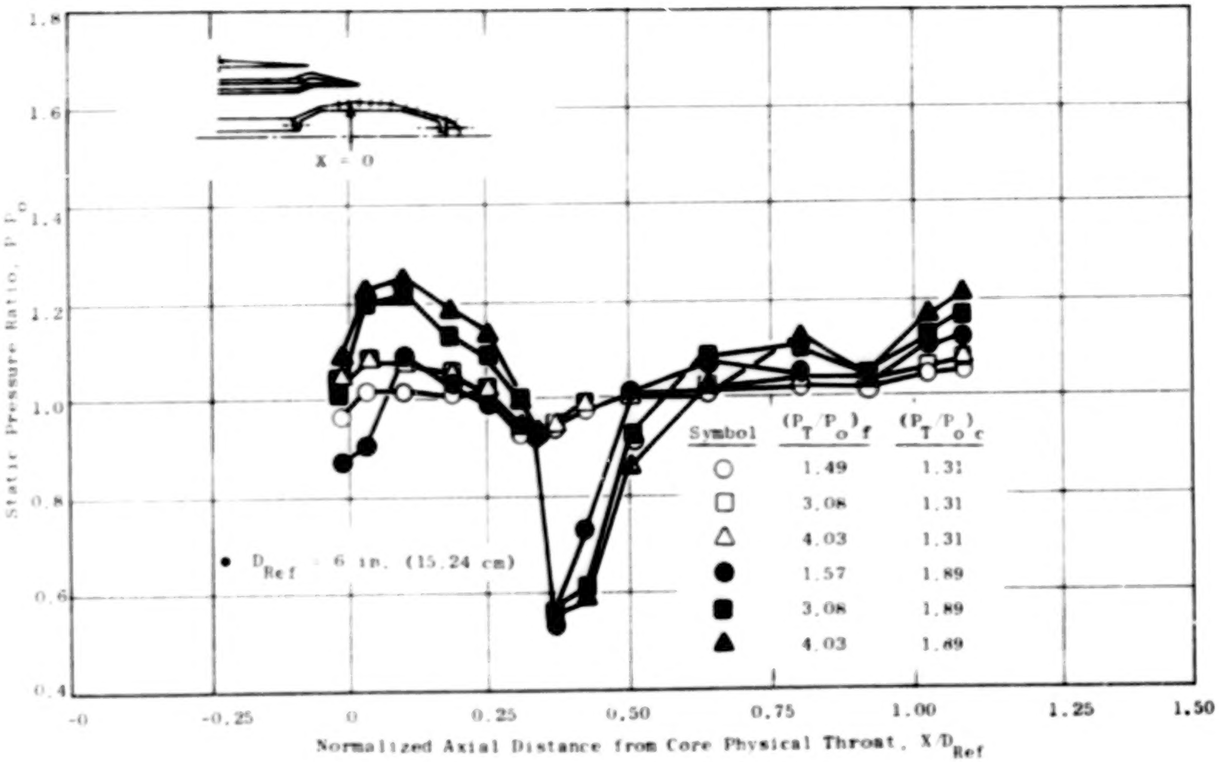

Figure 86. Core Plug Pressure Distributions, Unsuppressed Coannular Nozzle with Plug (Model 7).

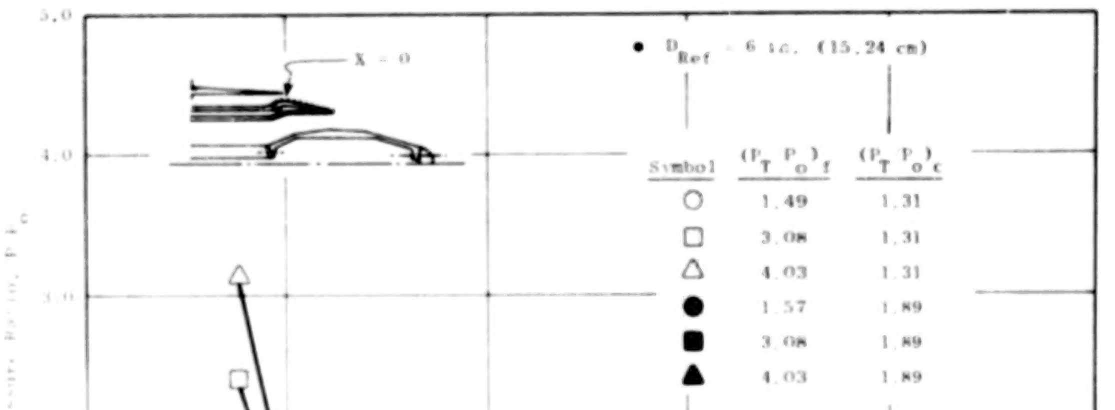

Figure 87. Fan Plug Pressure Distributions, Unsuppressed Coannular Nozzle with Plug (Model 7).

and decreasing performance relative to the 1.3 pressure ratio. This decreased pressure recovery is illustrated further in Figure 88 which presents the core and fan plug pressure forces, derived by a pressure-area integration of the static pressures, for a fan pressure ratio of 3.0 at core pressures of 1.3 and 1.9. These pressure forces are divided by the nozzle ideal thrust to demonstrate their relative importance to the thrust coefficient. At a core pressure ratio of 1.3, Figure 88 shows that the core plug contributes approximately 0.8% thrust and the fan plug -0.8% thrust, resulting in a zero net force on the two plugs. At a core pressure ratio of 1.9 the core plug has 0.2% drag force and, when added to the 0.9% loss in thrust of the fan plug, results in a -1.1% total plug pressure force.

6.1.2 Multichute Fan-Suppressor Nozzle

Thrust coefficients for the multichute fan suppressor nozzle (Model 1) are presented in Figure 89. The peak thrust coefficient is 0.96, with little or no difference between the two core pressure ratios tested. Suppressors generally incur a large performance loss due to low pressure in the suppressor base area. On the annular-chute suppressor, however, the short height and significant depth of the chutes (see Section 3.3.3) combine to provide adequate ventilation by ambient air, resulting in nearly ambient base pressures. Figure 90 shows the chute base pressure measurements normalized by the ambient pressure. An area-weighted average chute base pressure derived from the static pressures in Figure 90 is shown in Figure 91 for varying fan duct pressure ratio. The average base pressure is consistently near 99.5% of ambient; this results in very little base drag (as is demonstrated by the pressure force drag which is also shown in Figure 91). The integrated base pressure force on the chutes is shown in Figure 91 to vary from 0.1% to 0.3% of the nozzle ideal thrust.

6.1.3 Multichute Fan-Suppressor Nozzle with Hardwall Ejector with Sharp Lip

Model 9 was generated by adding the sharp-lipped, hardwall ejector to the multichute fan-suppressor nozzle (Model 1). Thrust coefficients for the multichute fan-suppressor nozzle with hardwall ejector with sharp lip (Model 9) are presented in Figure 92. The ejector increased the nozzle static performance significantly: from 0.957 to 0.995 at a core pressure ratio of 1.3 and a fan pressure ratio of 3.0, and from 0.958 to 0.983 at a core pressure ratio of 1.9 and a fan pressure ratio of 3.0. The effect of the ejector was to aspirate the suppressor base area as well as the fan and core plugs, causing lower pressures. These lower pressures were accompanied by subambient pressures on the ejector inner surface. The effect on the chute base pressures can be seen by comparing the static pressures for Model 9, shown in Figure 93, to those of the multichute fan-suppressor nozzle (Model 1) in Figure 90. Similarly, comparison of Figure 94 with Figure 95 and Figure 96 with Figure 97 illustrates the effect of the ejector on the fan and core plug static pressures. These low pressures tend to lower the nozzle performance; however, this loss in performance is more than offset

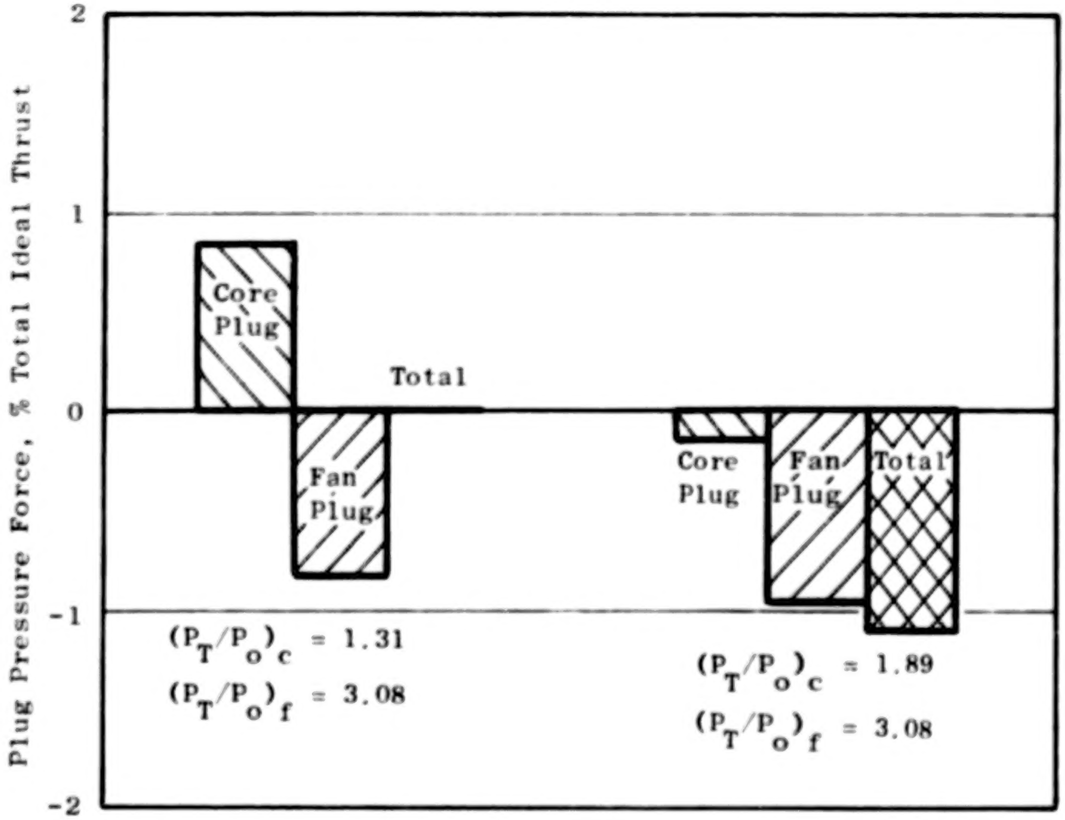

Figure 88. Integrated Plug Pressure Forces, Unsuppressed Coannular Nozzle with Plug (Model 7).

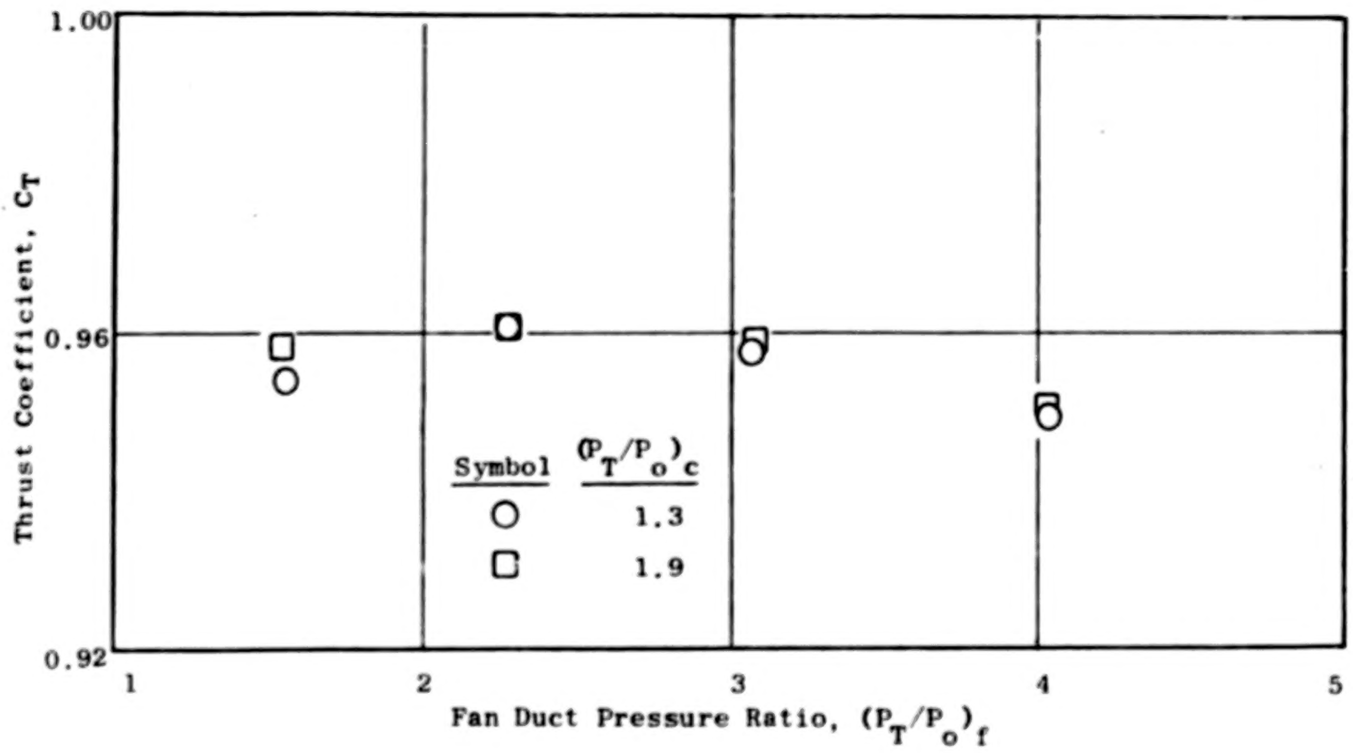

Figure 89. Thrust Coefficients for the Multichute Fan Suppressor Nozzle (Model 1).

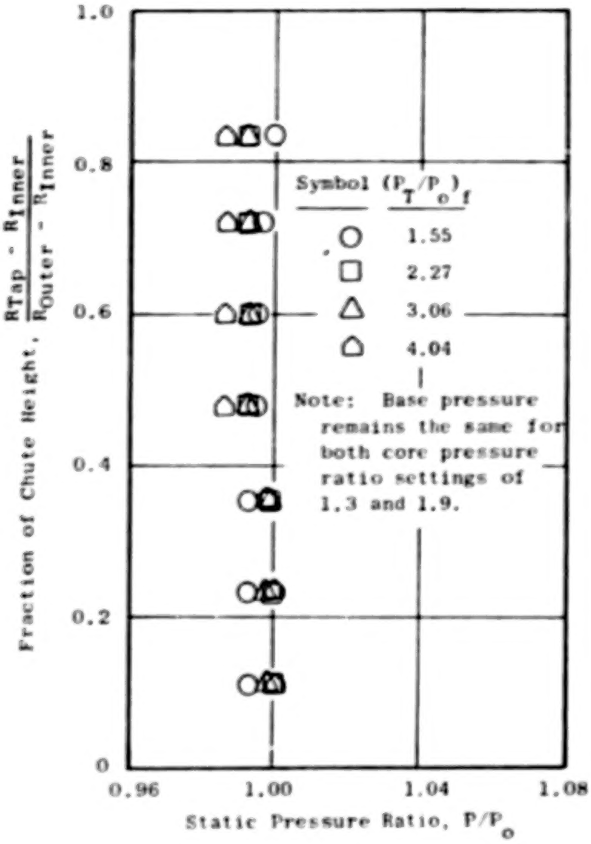

Figure 90. Chute Base Pressure Distributions, Multichute Fan Suppressor (Model 1).

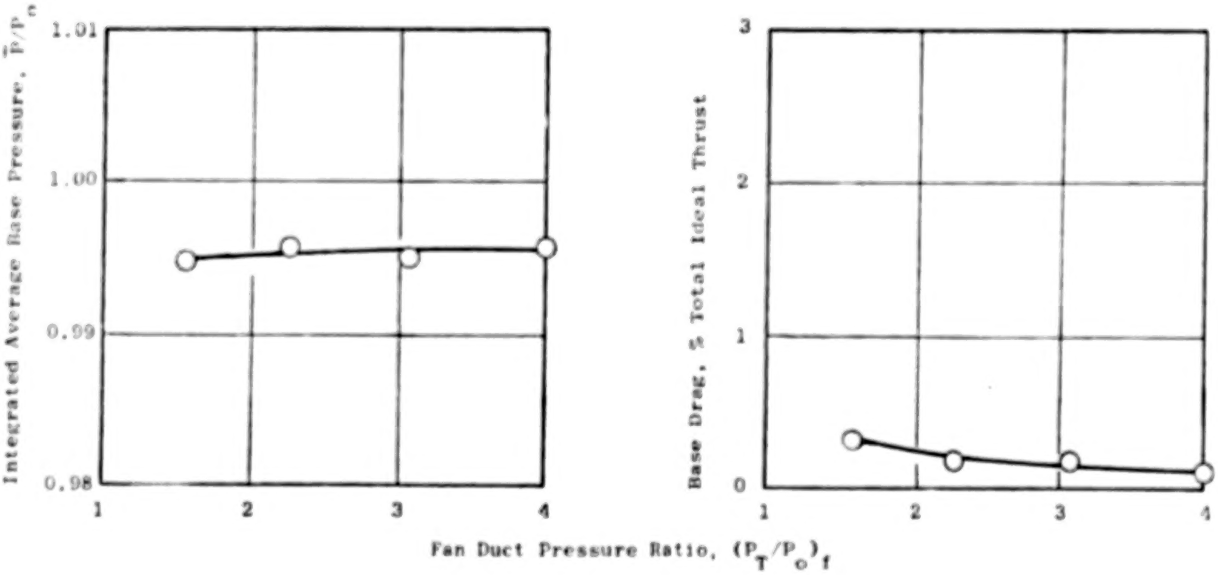

Figure 91. Chute Average Base Pressure and Base Drag, Multichute Fan Suppressor (Model 1).

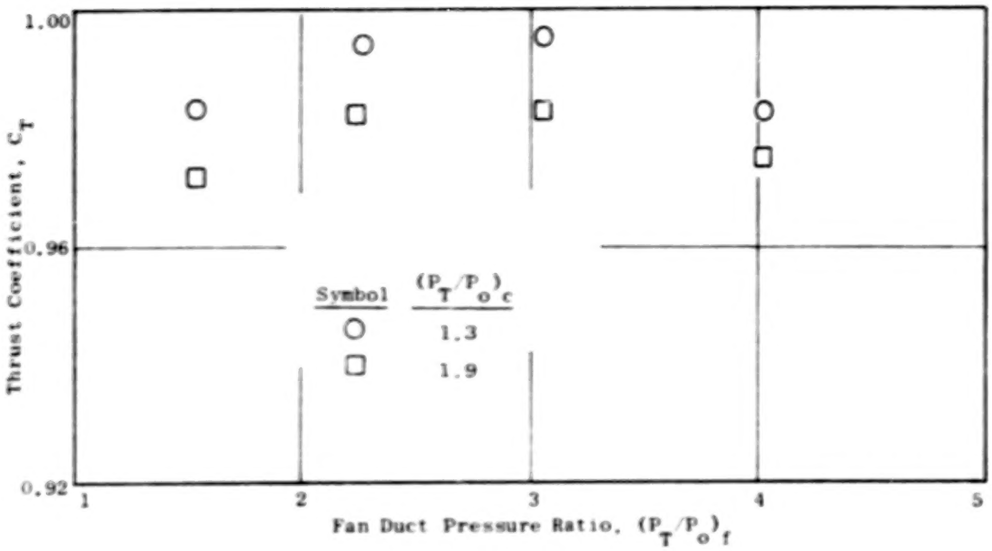

Figure 92. Thrust Coefficients for the Multichute Fan Suppressor with Hardwall Ejector with Sharp Lip (Model 9).

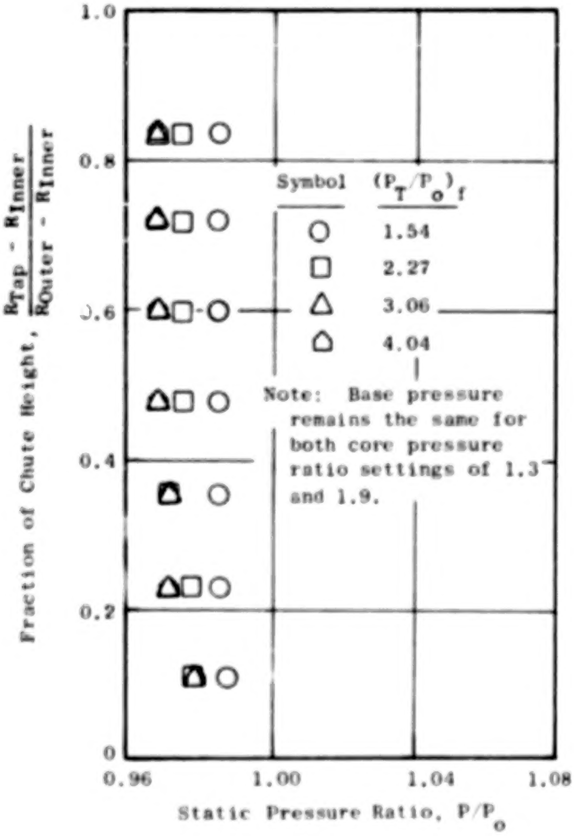

Figure 93. Chute Base Pressure Distributions, Multichute Fan Suppressor Nozzle with Hardwall Ejector with Sharp Lip (Model 9).

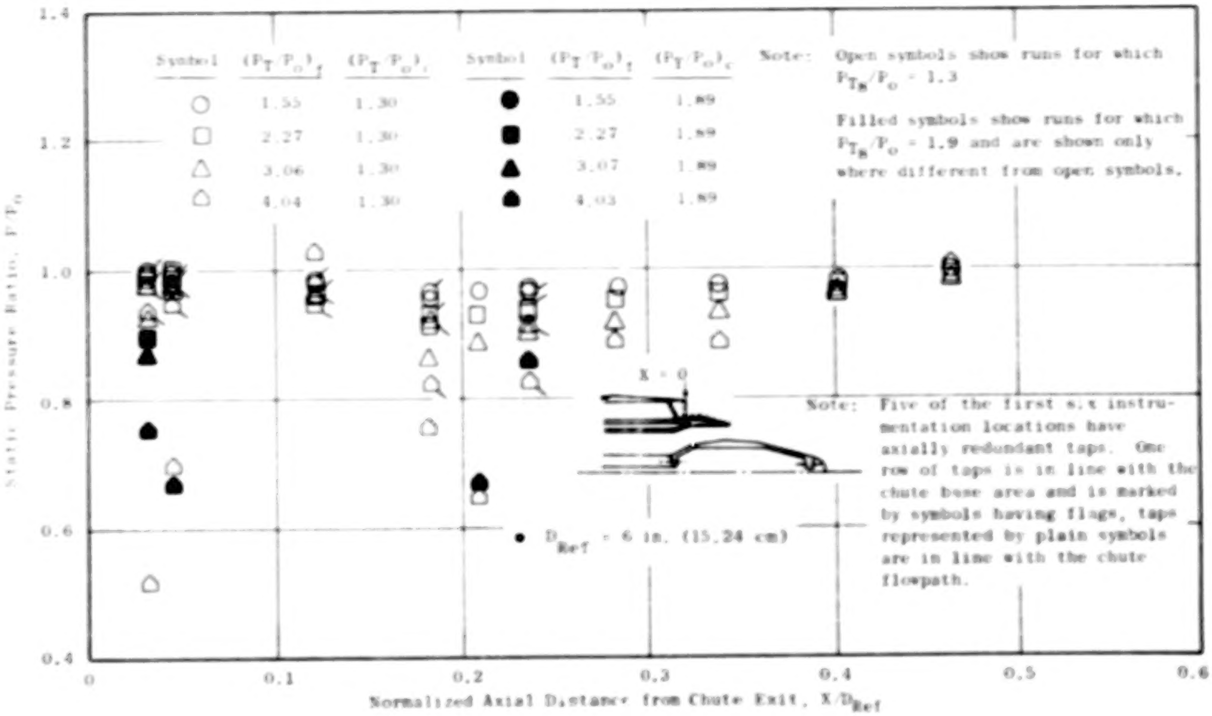

Figure 94. Fan Plug Pressure Distributions, Multichute Fan Suppressor Nozzle (Model 1).

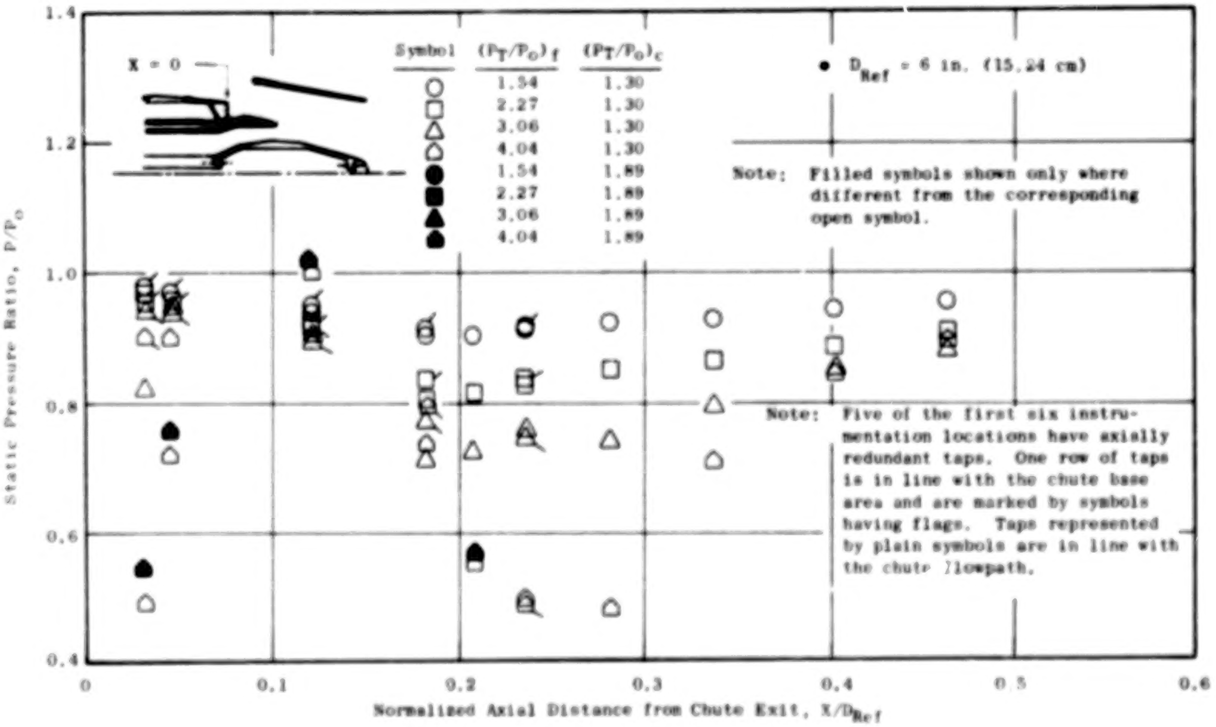

Figure 95. Fan Plug Pressure Distributions, Multichute Fan Suppressor Nozzle with Hardwall Ejector with Sharp Lip (Model 9).

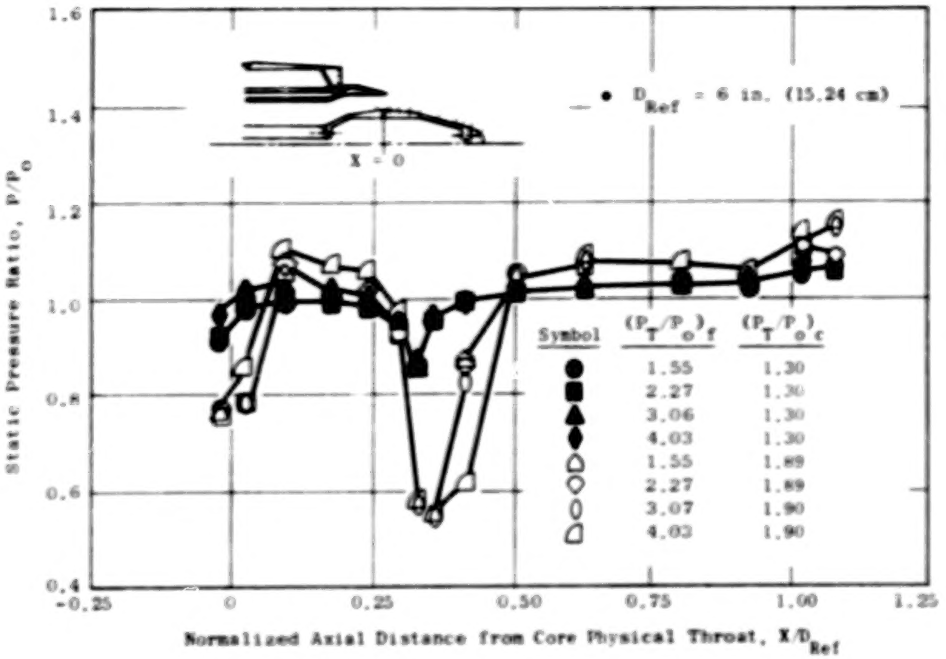

Figure 96. Core Plug Pressure Distributions, Multichute Fan Suppressor Nozzle (Model 1).

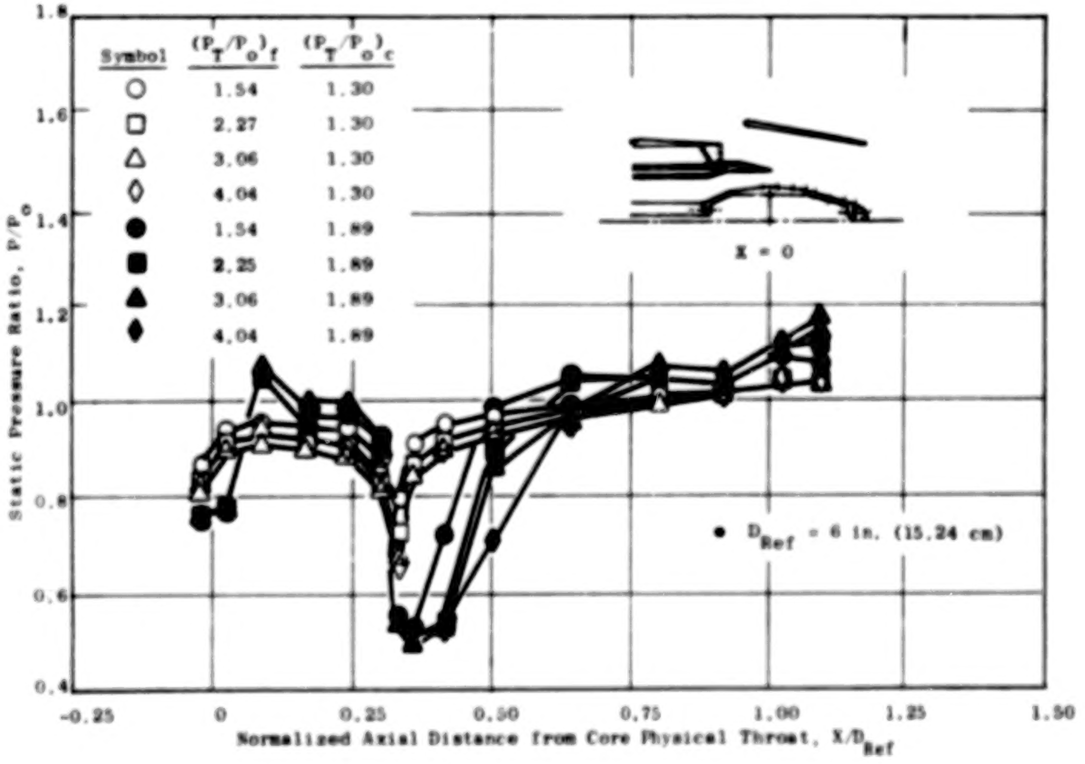

Figure 97. Core Plug Pressure Distributions, Multichute Fan Suppressor with Hardwall Ejector with Sharp Lip (Model 9).

by increased thrust due to subambient pressures on the forward-facing ejector flow surface. These static pressures, shown in Figures 98 and 99, are well below ambient pressure and contribute a large thrust component.

The effect of the ejector on nozzle performance is more explicitly demonstrated in Figure 100 which shows the plug, suppressor, and ejector pressure forces, as well as the total of these forces, as a percentage of nozzle ideal thrust for the chute suppressor with and without the ejector. The ejector thrust is the dominant force, contributing 10.7% to the nozzle thrust coefficient. The difference in the totals of these forces on the nozzle surfaces shows that the multichute fan-suppressor nozzle with hardwall ejector with sharp lip (Model 9) total force is 3.7% higher than multichute fan-suppressor nozzle (Model 1); this corresponds well with the 3.8% difference in measured thrust coefficient.

6.1.4 Multitube Fan-Suppressor Nozzle

Thrust coefficient levels for the multitube fan-suppressor nozzle (Model 2) are presented in Figure 101. The peak thrust coefficients, occuring at a fan pressure ratio of 3.0 for this model, were 0.951 for a core pressure ratio of 1.3 and 0.953 for a core pressure ratio of 1.9. The suppressor base area, in this case consisting of the baseplate in which the tubes were mounted, contributed only a small thrust loss. The static pressures on the baseplate, shown in Figure 102, remain near ambient over the outer half of the annulus. The area-weighted average base pressure and the resultant base drag, in terms of percent of nozzle ideal thrust, are shown in Figure 103. The average base pressure ranges from 98.5% to 99.5% of the ambient pressure, representing a 0.6% to 0.3% thrust decrement.

6.1.5 Multitube Fan-Suppressor Nozzle with Hardwall Ejector with Sharp Lip

Aerodynamic Model 5 consisted of adding the sharp-lipped, hardwall ejector to the multitube fan-suppressor nozzle (Model 2). Thrust coefficients for aerodynamic Model 5 are shown in Figure 104. At a fan duct pressure ratio of 1.5 the ejector provided little or no thrust augmentation compared to the multitube fan-suppressor nozzle. The augmentation increased steadily as the fan duct pressure ratio increased, reaching approximately 3.5% and a thrust coefficient of 0.983 at a pressure ratio of 4.0. Model 5 exhibits different thrust coefficient characteristics than the multichute counterpart (Model 9), compare Figures 92 and 104. This is partly attributed to the larger physical dimensions of the multitube fan-suppressor configuration; when a common ejector is utilized, the multitube fan-suppressor/ejector combination is tighter than the multichute fan-suppressor/ejector configuration. The effect of the ejector on the multitube fan suppressor nozzle was similar to that on the multichute fan-suppressor nozzle in that pressures on the plug surfaces and suppressor base area were lowered, and the thrust augmentation was provided by low pressures on the forward-facing ejector surface. Figure 105 shows that the tube baseplate static pressure distributions

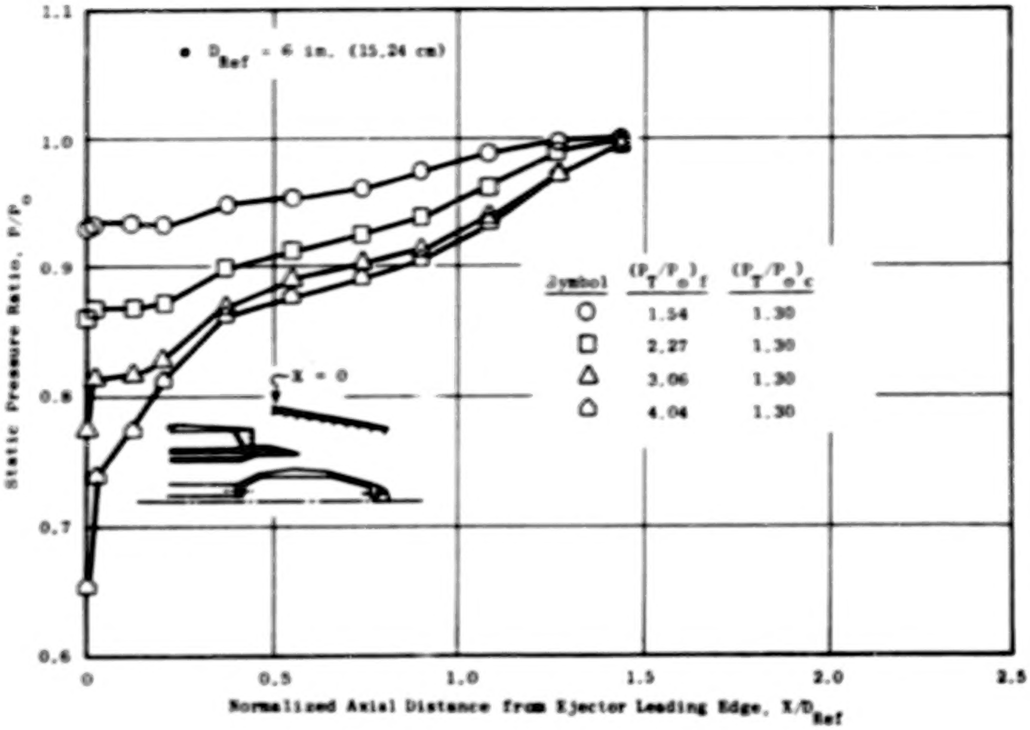

Figure 98. Ejector Pressure Distributions, Multichute Fan Suppressor Nozzle with Hardwall Ejector with Sharp Lip (Model 9), $(P_T/P_o)_c = 1.3$.

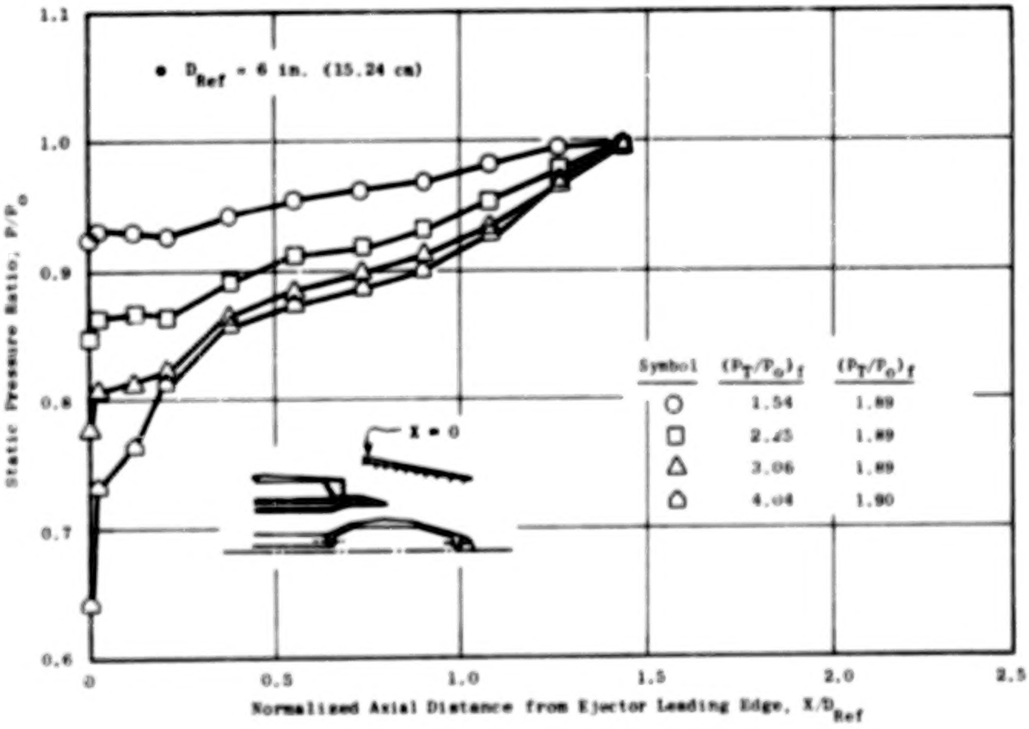

Figure 99. Ejector Pressure Distributions, Multichute Fan Suppressor Nozzle with Hardwall Ejector with Sharp Lip (Model 9), $(P_T/P_o)_c = 1.9$.

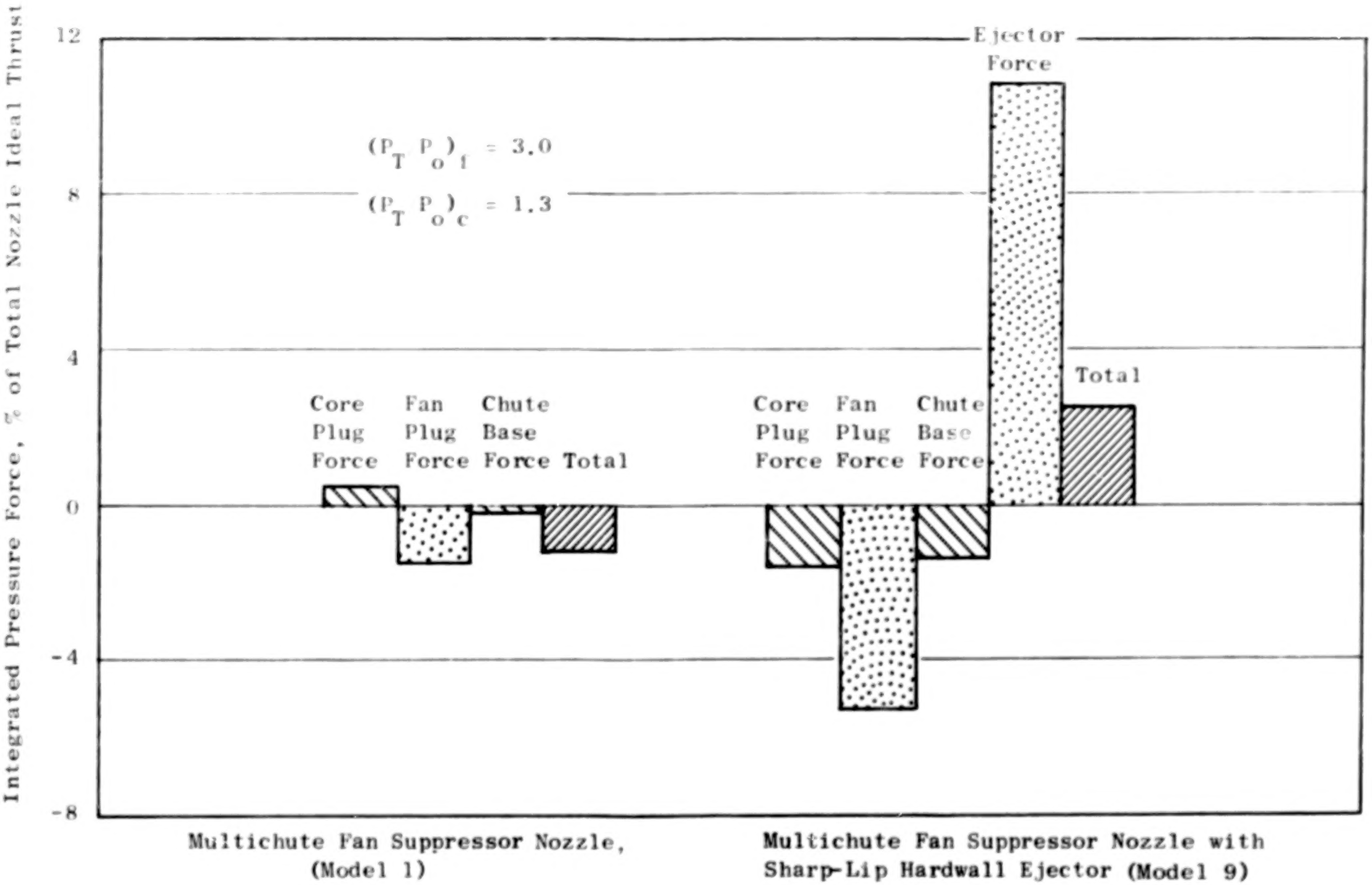

Figure 100. Integrated Model Surface Pressure Forces, Multichute Fan Suppressor Nozzle (Model 1) and Multichute Fan Suppressor Nozzle with Hardwall Ejector with Sharp Lip (Model 9).

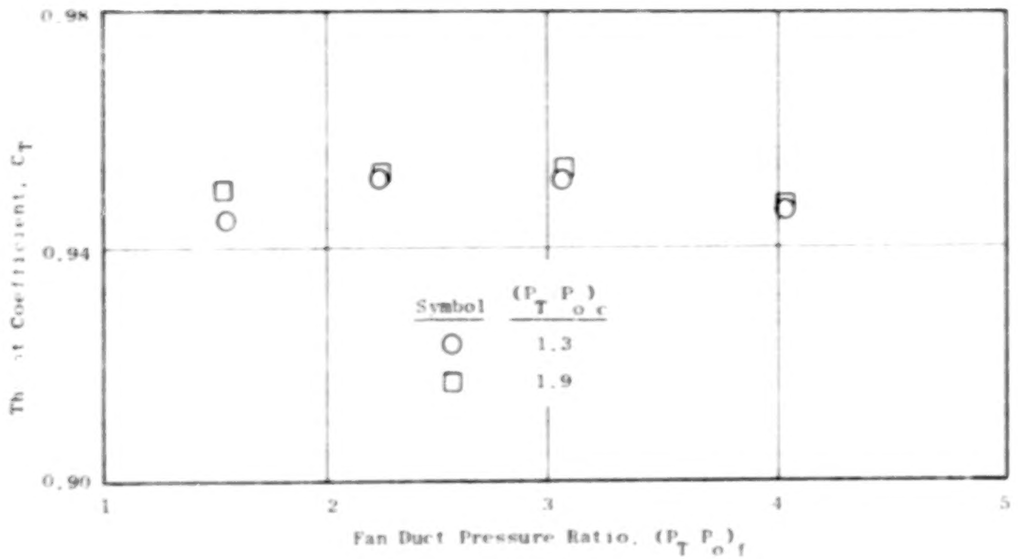

Figure 101. **Thrust Coefficients for the Multitube Fan Suppressor Nozzle (Model 2).**

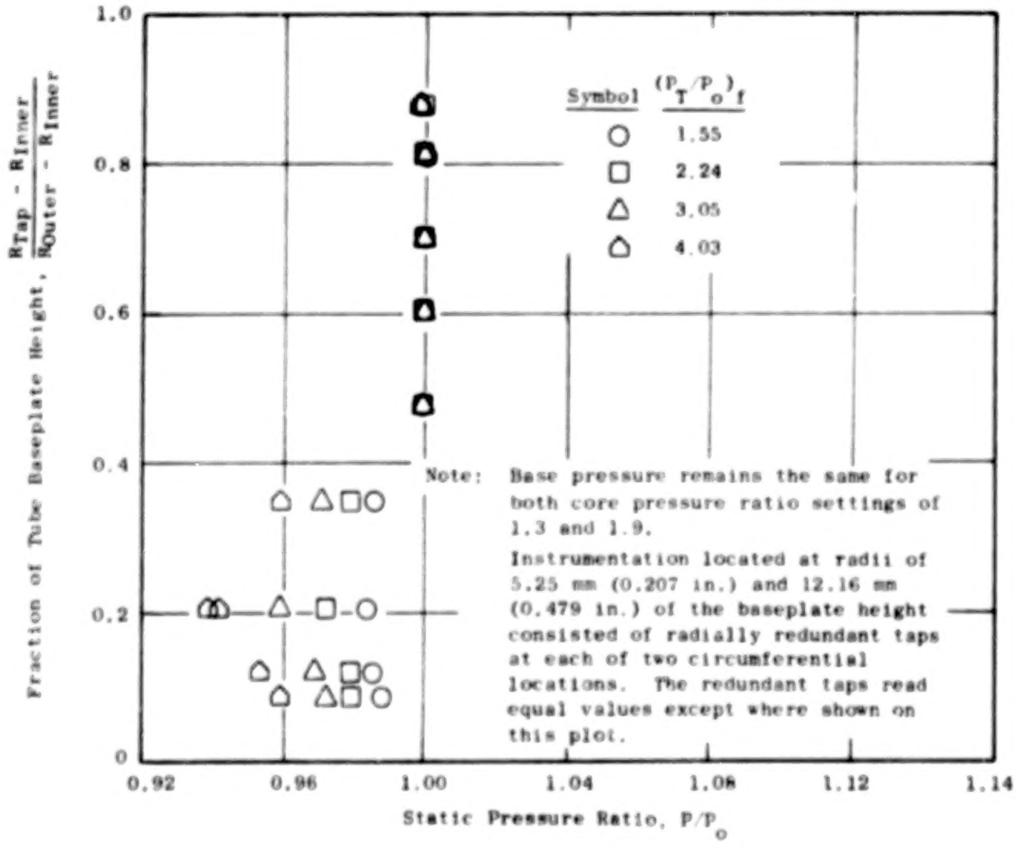

Note: Base pressure remains the same for both core pressure ratio settings of 1.3 and 1.9.

Instrumentation located at radii of 5.25 mm (0.207 in.) and 12.16 mm (0.479 in.) of the baseplate height consisted of radially redundant taps at each of two circumferential locations. The redundant taps read equal values except where shown on this plot.

Figure 102. **Tube Baseplate Pressure Distributions, Multitube Fan Suppressor Nozzle (Model 2).**

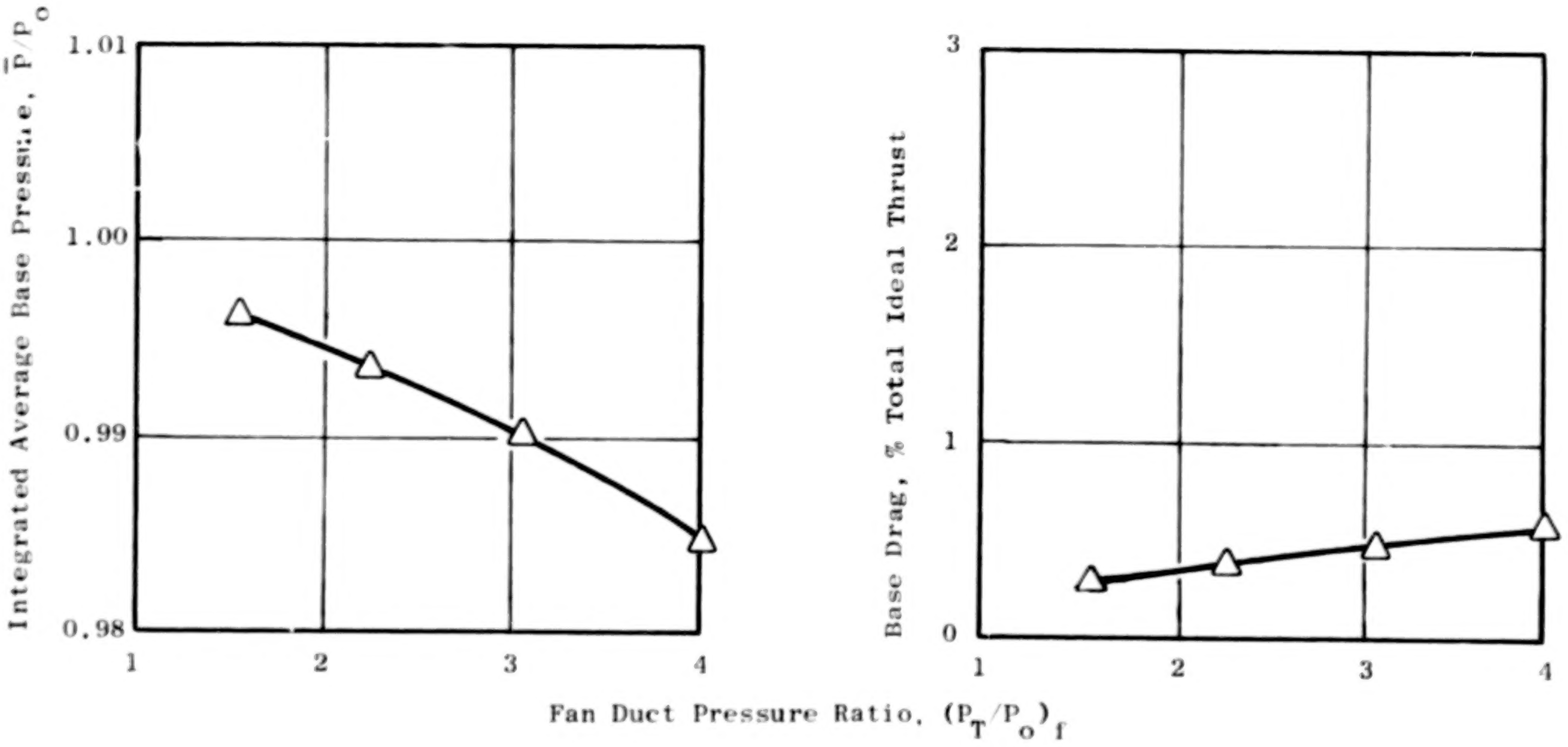

Figure 103. Tube Baseplate Average Base Pressure and Base Drag, Multitube Fan Suppressor Nozzle (Model 2).

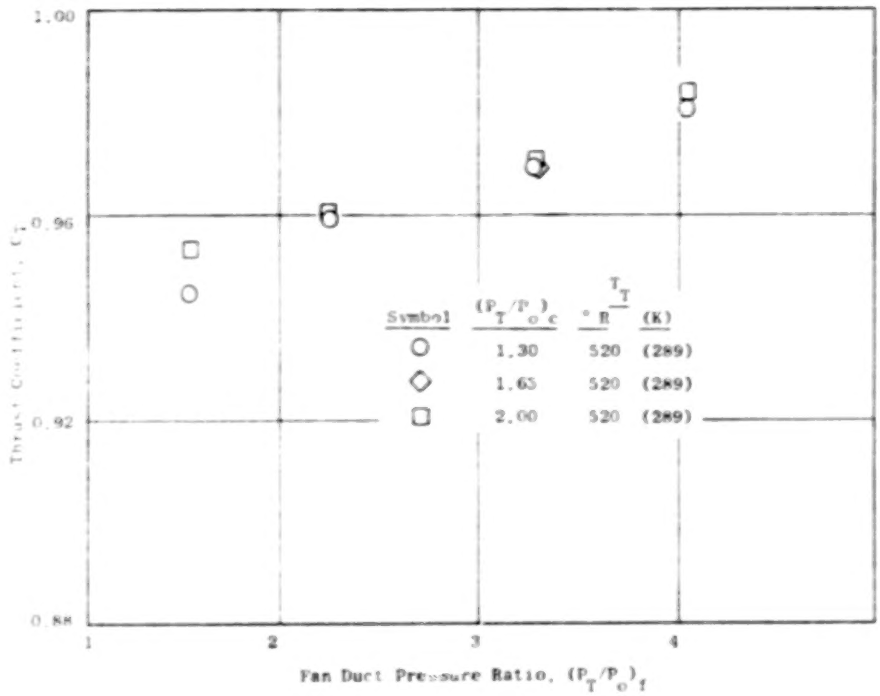

Figure 104. Thrust Coefficients for the Multitube Fan Suppressor Nozzle with Hardwall Ejector with Sharp Lip (Aerodynamic Model 5).

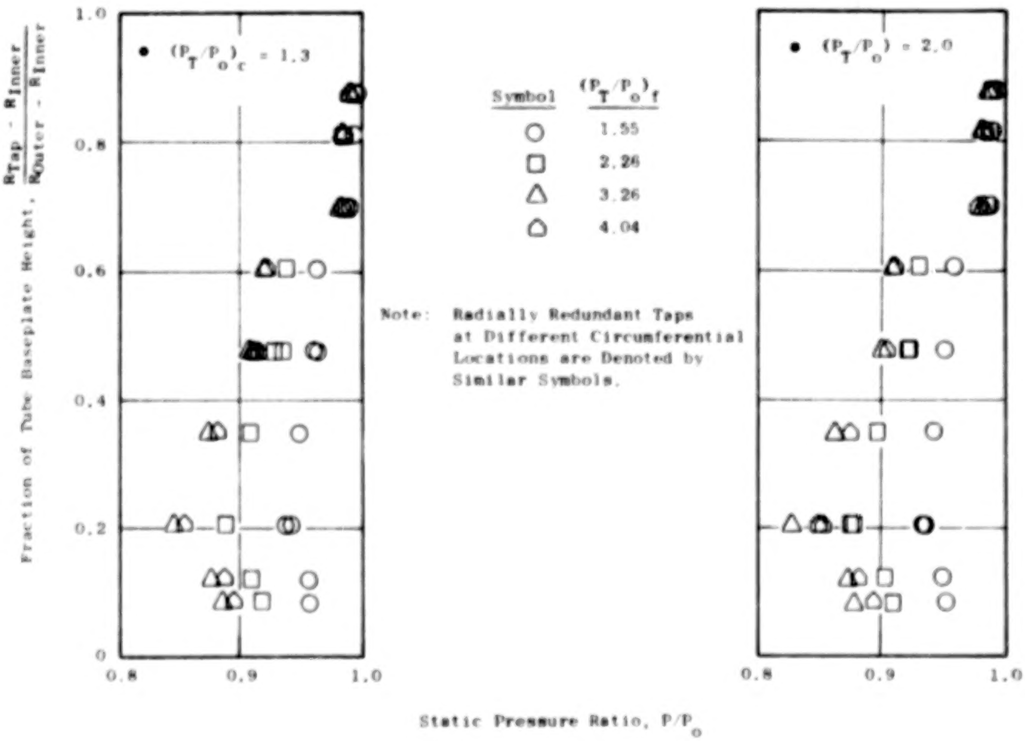

Figure 105. Tube Baseplate Pressure Distributions, Multitube Fan Suppressor Nozzle with Hardwall Ejector with Sharp Lip (Aerodynamic Model 5).

for aerodynamic Model 5 are significantly lower than those of the tubes without ejector shown in Figure 102. Static pressure distributions on the ejector inner surface are subambient, as shown on Figure 106. The integrated pressure forces on the nozzle surfaces are shown in Figure 107 as a percent of nozzle thrust for the multitube fan-suppressor nozzle (Model 2) and the multitube fan-suppressor nozzle with hardwall ejector with sharp lip (aerodynamic Model 5). The effect of the ejector is to increase the drag on all nozzle surfaces, but the thrust force on the ejector (equal to 13.5% for the case shown in Figure 107) offsets this drag. Figure 107 shows the total pressure force on the plug and suppressor base surfaces to equal -1.2% for Model 2 and +3.5% for aerodynamic Model 5. This does not compare well with the difference of +1.9% in measured thrust coefficient for the two nozzles at the operating condition represented; the difference is attributed to the fact that other thrust loss items which are not reflected in the pressure integrations are introduced by the ejector. The dominant additional loss is the increase in pressure drag on the tube ends near their exit. The ends of the tubes are near the ejector inlet plane where the pressure is very low (as illustrated by the ejector pressure distributions of Figure 106) and where the base area is significant due to tube convergence near the exit.

6.2 EFFECT OF HOT EXHAUST FLOW ON THE THRUST COEFFICIENT OF THE MULTITUBE FAN-SUPPRESSOR NOZZLE WITH HARDWALL EJECTOR WITH SHARP LIP

The multitube fan-suppressor nozzle with hardwall ejector with sharp lip (aerodynamic Model 5) was used to evaluate differences in ejector nozzle performance between cold exhaust flow and hot exhaust flow. The test facility could supply hot air through the core air supply only. Hot testing was therefore conducted by blanking off the fan supply duct and splitting the fan and core flows from a common plenum fed by the core air supply; this procedure dictated that only one fan-to-core flow ratio could be run during the hot tests. The flow split was controlled by the open area in the core choke plate, which was designed to give pressure ratios similar to the range of cold flow test points. For core pressure ratios of 1.3, 1.7, and 2.1 the corresponding fan pressure ratios were 2.2, 3.2, and 4.0. All three of these points were run at fan and core exhaust temperatures of approximately 1386° R (770 K); the first and last points were also run at approximately 990° R (550 K). Cold flow tests were run at the same three pressure ratio combinations to provide a side-by-side comparison of results. The cold flow temperatures was approximately 520° R (289 K).

The thrust coefficients for these tests are compared in Figure 108. The thrust coefficients for the hot flow tests fall below the cold flow results by 0.7% to 0.9% at the two lower pressure ratio points. At the highest pressure ratio, thrust levels for all three temperatures are close together with the intermediate temperature case only 0[illegible] higher than cold data and 0.5% higher than the high temperature condition. Static pressure distributions on the model surfaces indicate generally higher static pressures with hot exhaust flow. Pressures on the ejector are compared in Figure 109.

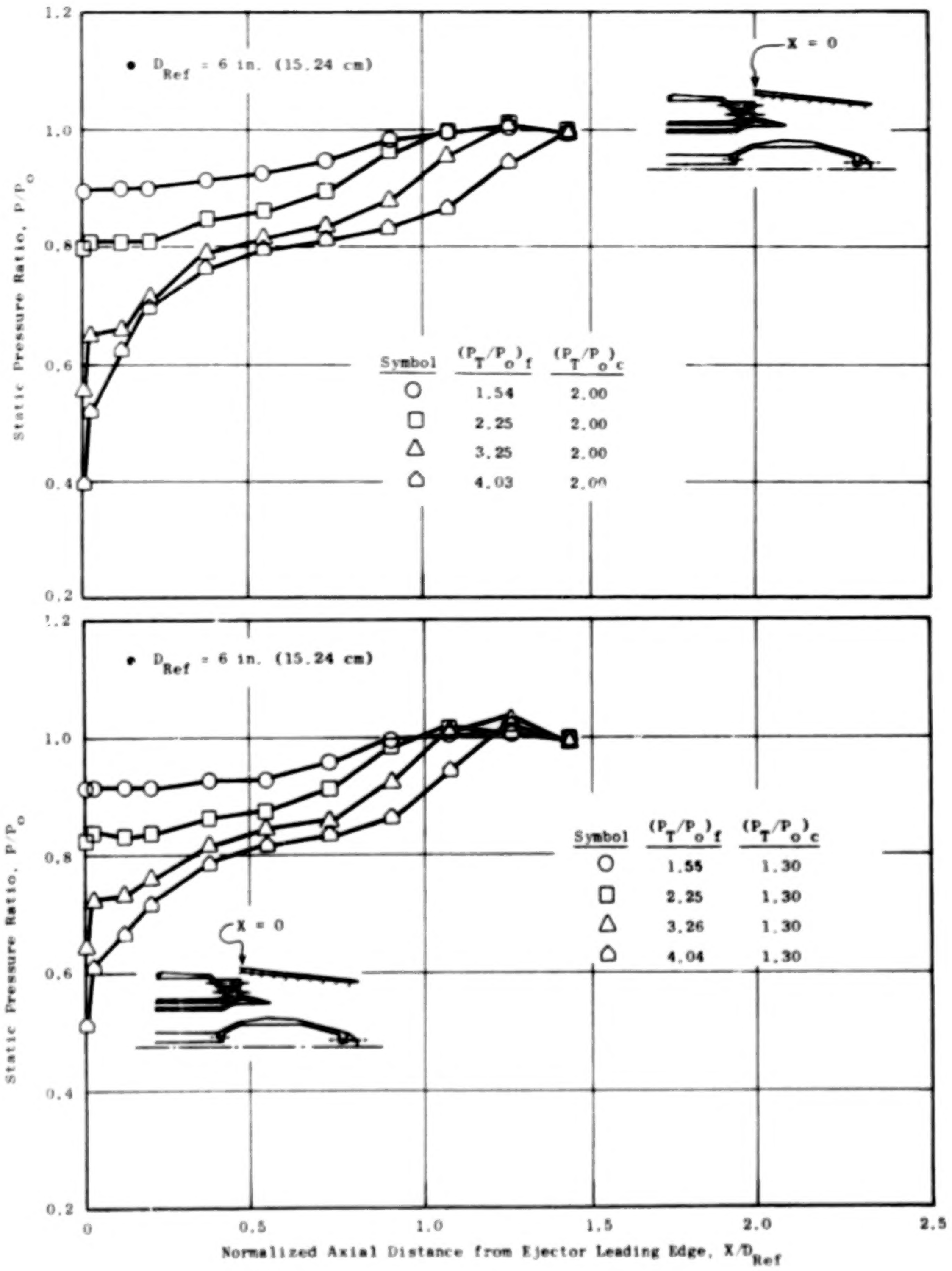

Figure 106. Ejector Pressure Distributions, Multitube Fan Suppressor Nozzle with Hardwall Ejector with Sharp Lip (Aerodynamic Model 5).

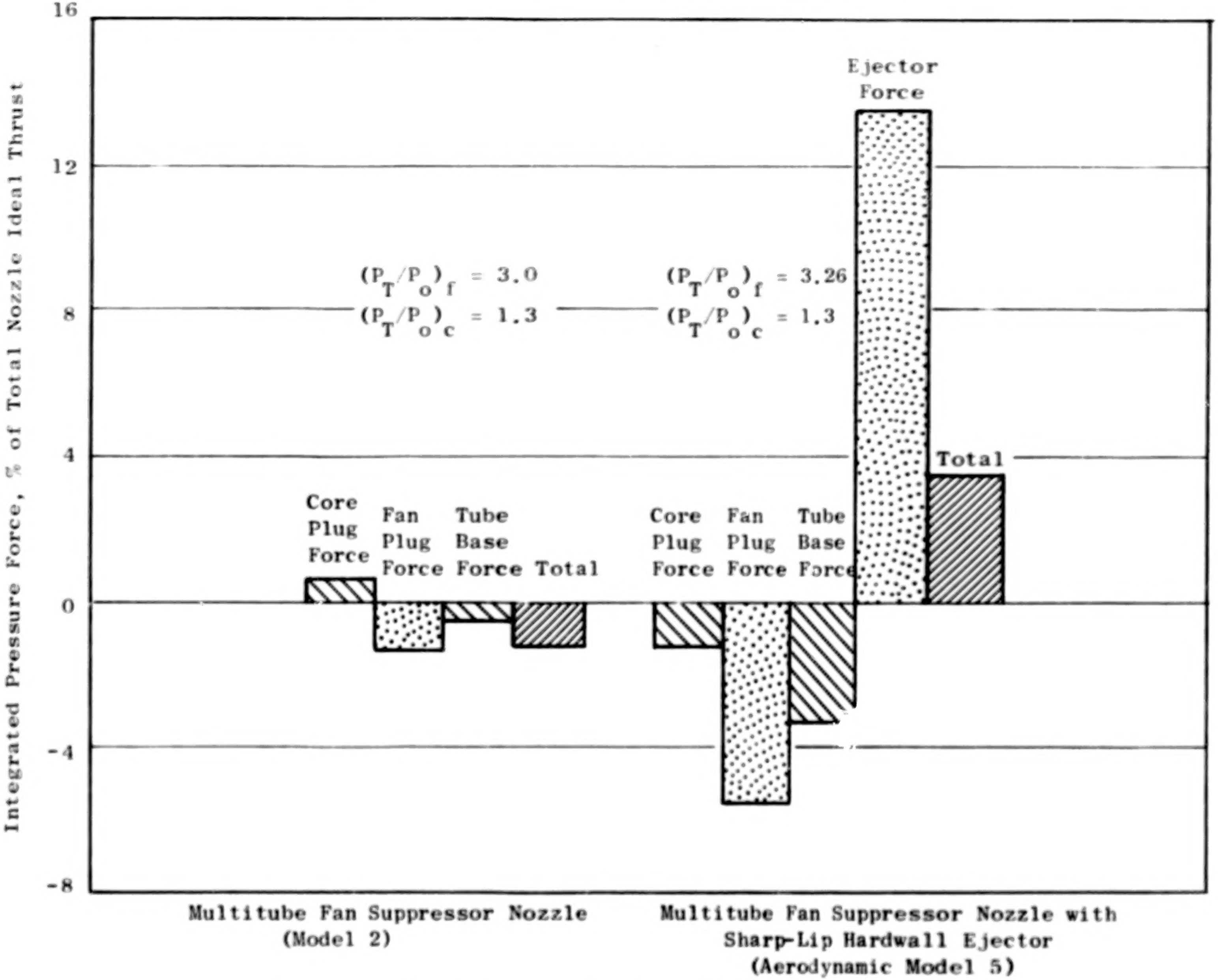

Figure 107. Integrated Model Surface Pressure Forces, Multitube Fan Suppressor Nozzle (Model 2) and Multitube Fan Suppressor Nozzle with Hardwall Ejector with Sharp Lip (Aerodynamic Model 5).

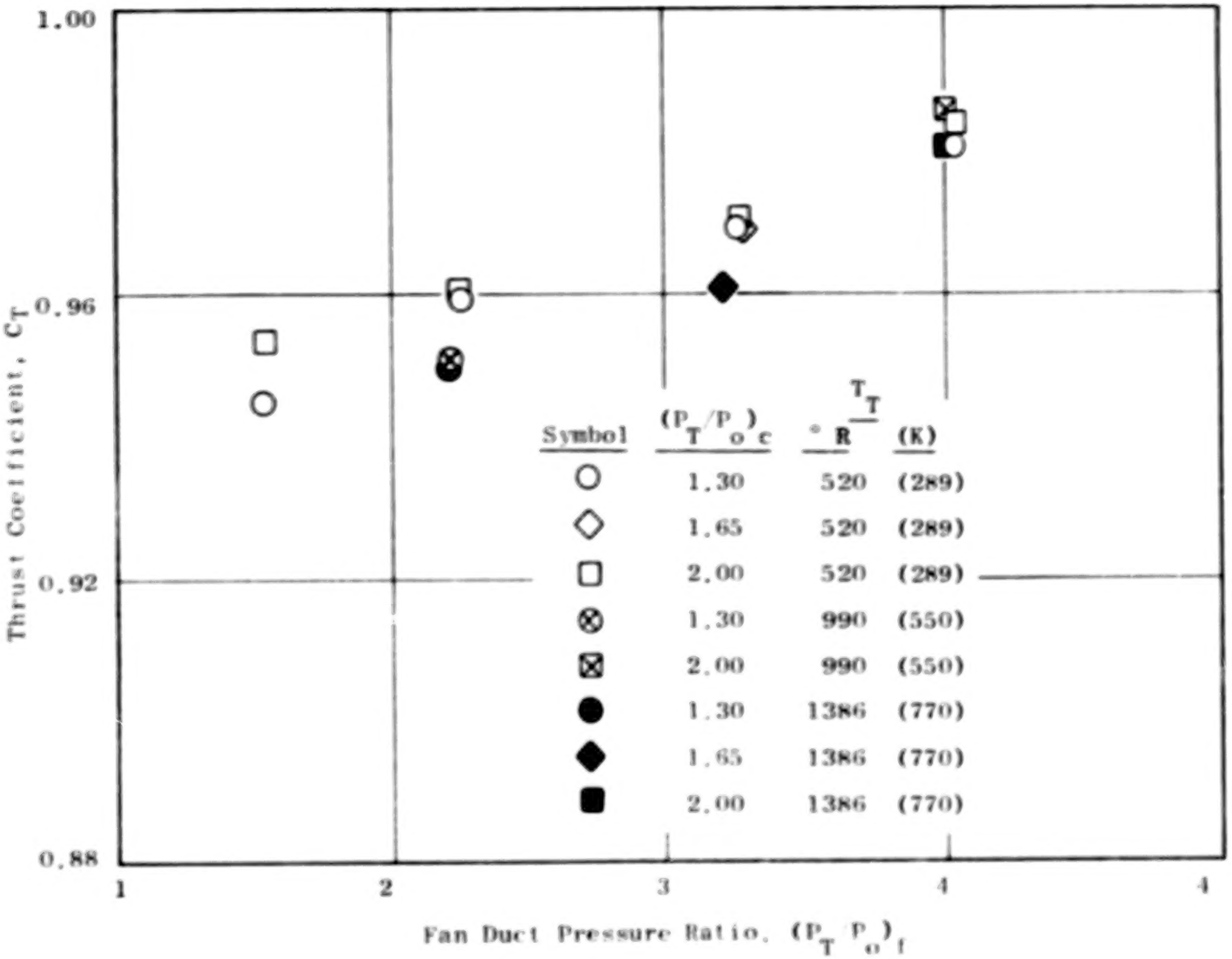

Figure 108. Thrust Coefficients for Hot and Cold Flow Tests on the Multitube Fan Suppressor Nozzle with Hardwall Ejector with Sharp Lip (Aerodynamic Model 5).

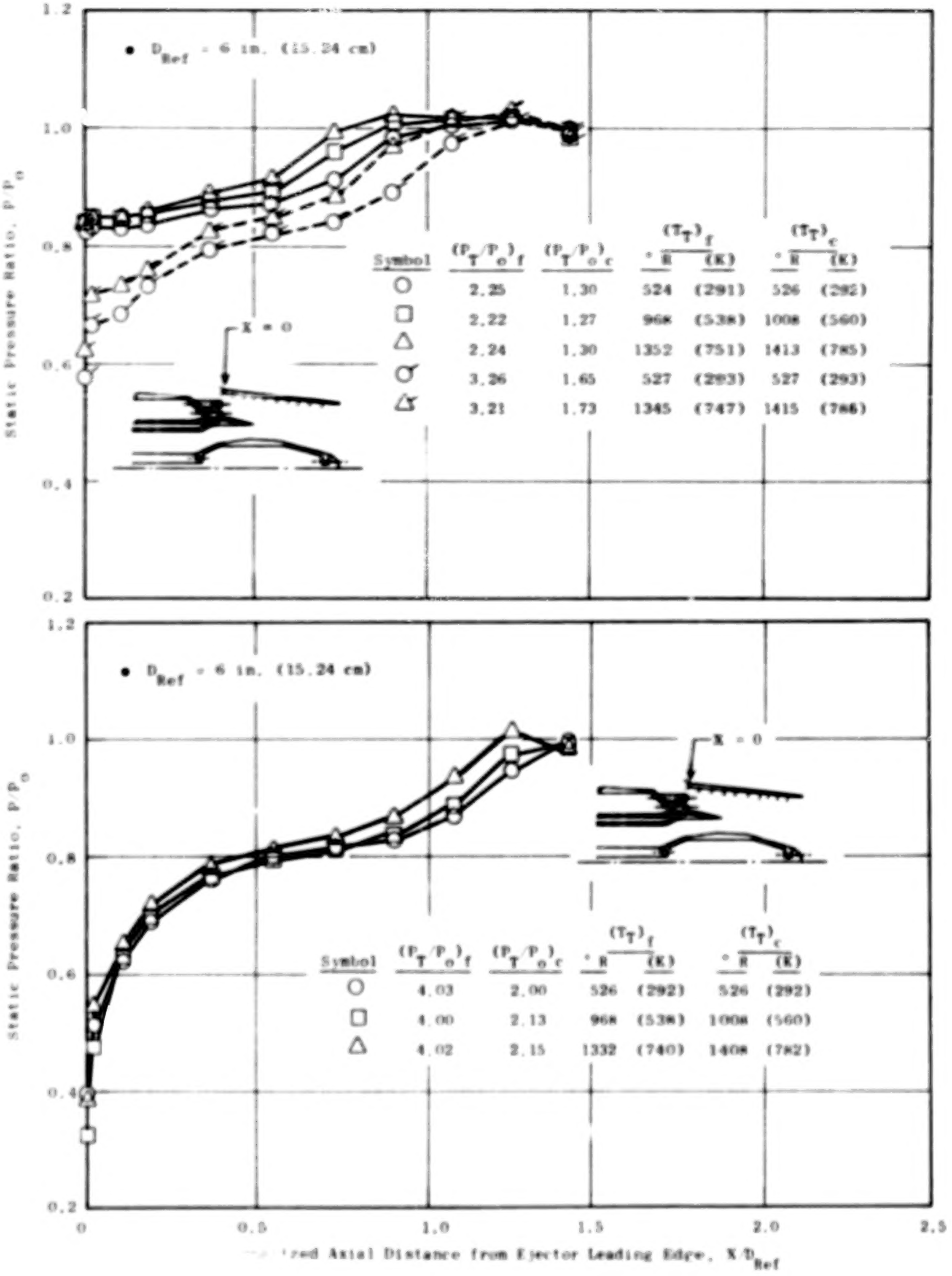

Figure 109. Comparison of Hot and Cold Flow Ejector Pressure Distributions, Multitube Fan Suppressor Nozzle with Hardwall Ejector with Sharp Lip (Aerodynamic Model 5).

Figure 109 shows higher static pressures at the ejector wall, at the higher temperatures, for all fan pressure ratios; however, the difference becomes smaller as the fan pressure ratio increases. These characteristics are also exhibited both by the fan plug and by the core plug static pressures. Comparison of these pressure distributions at different temperatures are contained in Appendix E. The suppressor base area static pressures show no definitive trend with temperature, as shown by the base pressure plots also included in Appendix E. In order to evaluate the effect of the pressure changes in terms of thrust, the pressure forces on these surfaces were calculated by pressure-area integrations. Figure 110 shows the resultant forces for each model surface nondimensionalized by the nozzle total ideal thrust and plotted as a function of fan pressure ratio. The higher pressures at the hot temperatures produce slightly lower drag on the core and fan plugs and somewhat lower thrust on the ejector shroud. These separate forces are summed in Figure 111. The total pressure force is calculated to represent 0.7% to 1.2% lower thrust for hot tests at the lower two pressure ratio points. At the high pressure ratio point, the cold flow and highest temperature flow pressure forces are 0.6% and 1% in thrust, respectively, below the intermediate temperature point. The trend and magnitude of these pressure integrations are very close to those differences observed in the thrust measurements. The small differences experienced in thrust coefficient levels between hot and cold testing at the lower pressure ratios are attributed to slightly higher static pressures on the ejector with the hot exhaust flow. This effect is diminished at the high pressure ratio point. These preliminary tests suggest that low pressure ratio ejector nozzle testing at ambient (cold) conditions will tend to overestimate the thrust coefficient by as much as 1%. This should be acceptable for comparison and screening studies; however, when certification type of information is required, it is recommended that hot-flow tests be conducted.

6.3 FLOW COEFFICIENTS

6.3.1 Unsuppressed Coannular Nozzle with Plug

Flow coefficient characteristics for the fan duct of the unsuppressed coannular nozzle with plug (Model 7) are shown in Figure 112. At choked flow conditions the coefficients are between 0.986 and 0.989; at an unchoked pressure ratio of 1.5 the flow coefficients increase to between 1.01 and 1.024. The increase is due to a small internal expansion (the exit area at the tip of the outer shroud is slightly larger than the throat, or minimum, area) and the local curvature of the inner flow surface in the region of the throat. The area expansion downstream of the throat acts as a diffuser when the flow is subsonic. Since the static pressure of the stream at the exit must equal ambient pressure, the pressure at the smaller area of the throat is less than ambient. The curvature of the plug crown locally accelerates the flow to even lower pressures than indicated by the exit-to-throat area ratio. These subambient pressures on the fan plug in the region of the throat can be seen in the static pressure distributions for the fan duct pressure ratio of 1.5 as shown in Figure 87. The Mach number through the throat is, therefore, higher than the ideal Mach number indicated by the nozzle total-to-ambient pressure ratio and results in higher than ideal flow rates.

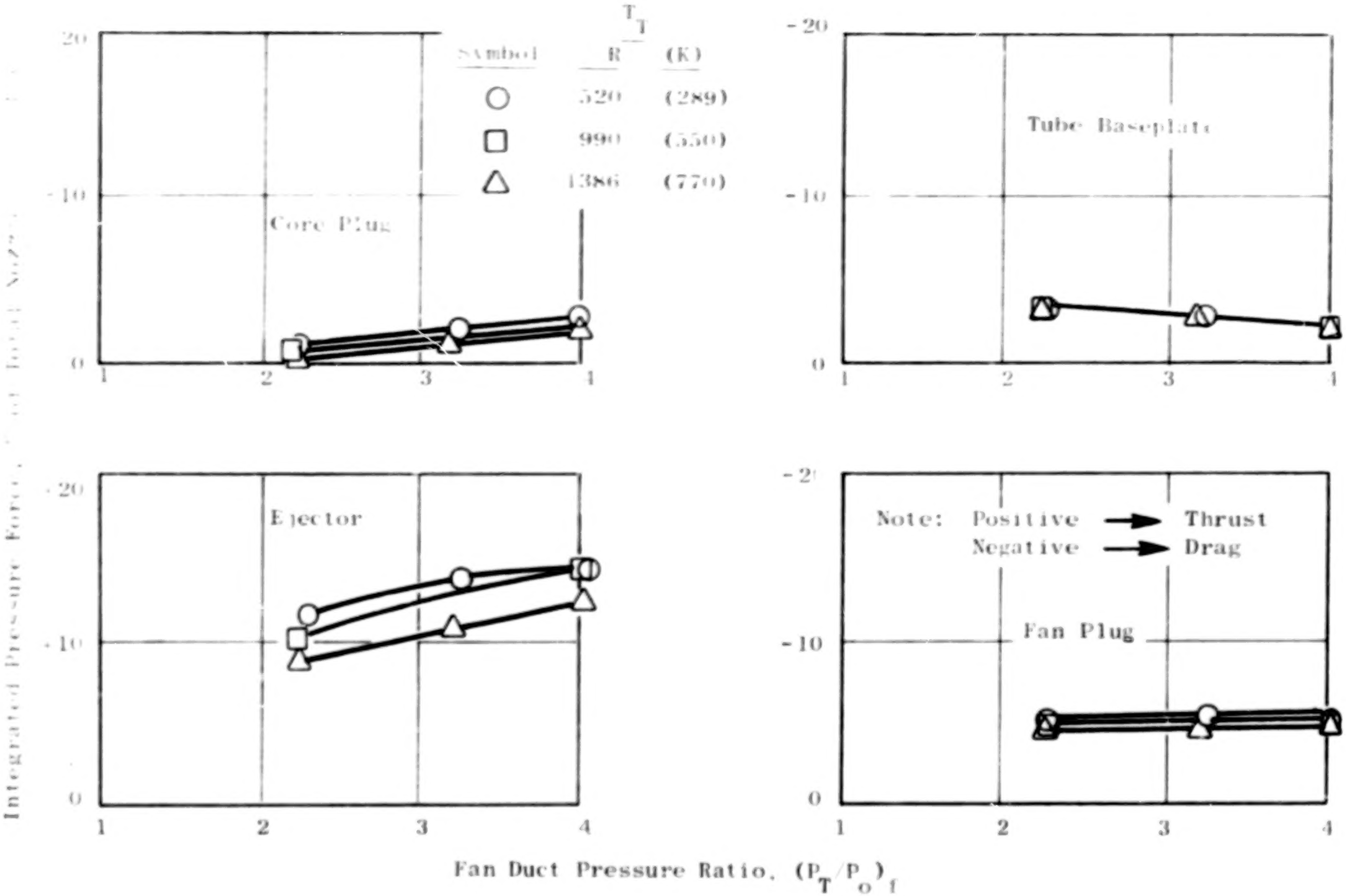

Figure 110. Comparison of Hot and Cold Flow Integrated Pressure Forces, Multitube Fan Suppressor Nozzle with Hardwall Ejector with Sharp Lip (Aerodynamic Model 5).

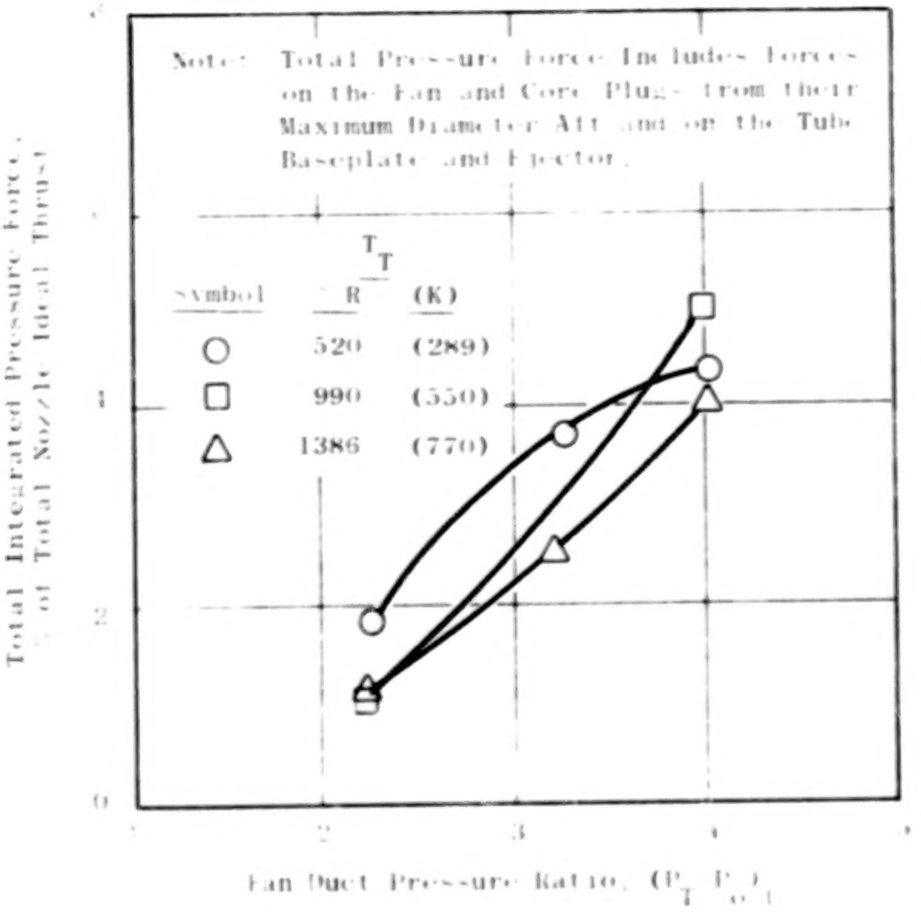

Figure 111. Comparison of Hot and Cold Flow Total Integrated Pressure Forces, Multitube Fan Suppressor Nozzle with Hardwall Ejector with Sharp Lip (Aerodynamic Model 5)

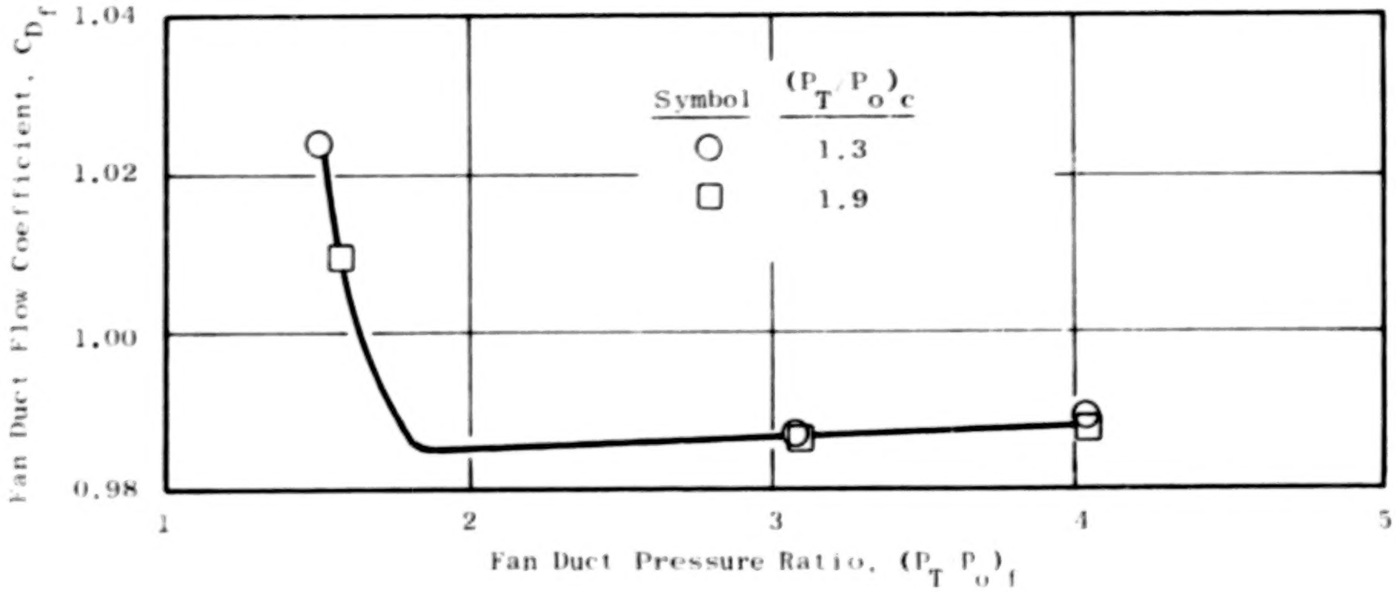

Figure 112. Fan Duct Flow Coefficients for the Unsuppressed Coannular Nozzle with Plug (Model 7).

The core duct flow coefficients for the unsuppressed coannular nozzle with plug (Model 7) are shown in Figure 113. These coefficients were strongly influenced by the fan exhaust stream. The interaction of the fan and core streams at the tip of the fan plug, combined with the flat shape of the core plug at that region, results in a deflection of the outer boundary of the core flow by the fan stream. This forms an aerodynamic boundary restricting the core flow to an area smaller than the physical throat. As the fan pressure ratio and jet velocity increase, the restriction increases, lowering the core flow coefficient. Also, the core flow coefficient increases as the core pressure ratio increases. To verify that the interference from the fan stream is depressing the core flow coefficient, the core was run at a pressure ratio of 1.9 with the fan stream shut off. The resultant flow coefficient of 0.984 equals the value measured with the core stream at a pressure ratio of 1.9 and the fan at 1.5 (the point of minimum interference by the fan flow).

6.3.2 Multichute Fan-Suppressor Nozzle

Figure 114 shows fan and core duct flow coefficients for the multichute fan-suppressor nozzle (Model 1). The fan nozzle flow coefficient increases from approximately 0.969 to 0.977 as the fan pressure ratio increases from 2.2 to 4.0. This increase is larger than normal; the flow coefficient is generally relatively constant once a nozzle is choked. The increase is attributed to a slight opening up of the chute suppressor exit area as the chutes deflect under increasing pressure load. At the unchoked pressure ratio of 1.5, the fan duct flow coefficient decreases to 0.947. This decrease at unchoked pressure ratio is typical of a convergent nozzle and would be expected of the chute suppressor (the minimum nozzle area is the exit of the suppressor). The core duct flow coefficient of Model 1, shown in Figure 114, is unaffected by the fan stream for fan pressure ratios of 1.5, 2.2, and 3.0 at core pressure ratios of both 1.3 and 1.9 (unlike the unsuppressed coannular nozzle with plug). The flow coefficient is approximately 0.985 at a core pressure ratio of 1.9, for all fan pressure ratios. At a core pressure ratio of 1.3, the coefficient increases to 0.992 at all fan duct pressure ratios except 4.0. This increase is due to the internal expansion area and plug curvature in the throat region, as previously described for the unsuppressed coannular nozzle with plug (Model 7) fan duct. At a core pressure ratio of 1.3 and a fan pressure ratio of 4.0, the core flow coefficient decreases to 0.946 because of interference by the fan stream.

6.3.3 Multichute Fan Suppressor Nozzle with Hardwall Ejector with Sharp Lip

The fan and core nozzle flow coefficients for the multichute fan-suppressor with hardwall ejector with sharp lip (Model 9) are shown in Figure 115. Addition of the ejector does not affect the flow coefficient of the chutes for choked flow. At a pressure ratio of 1.5 the coefficient is

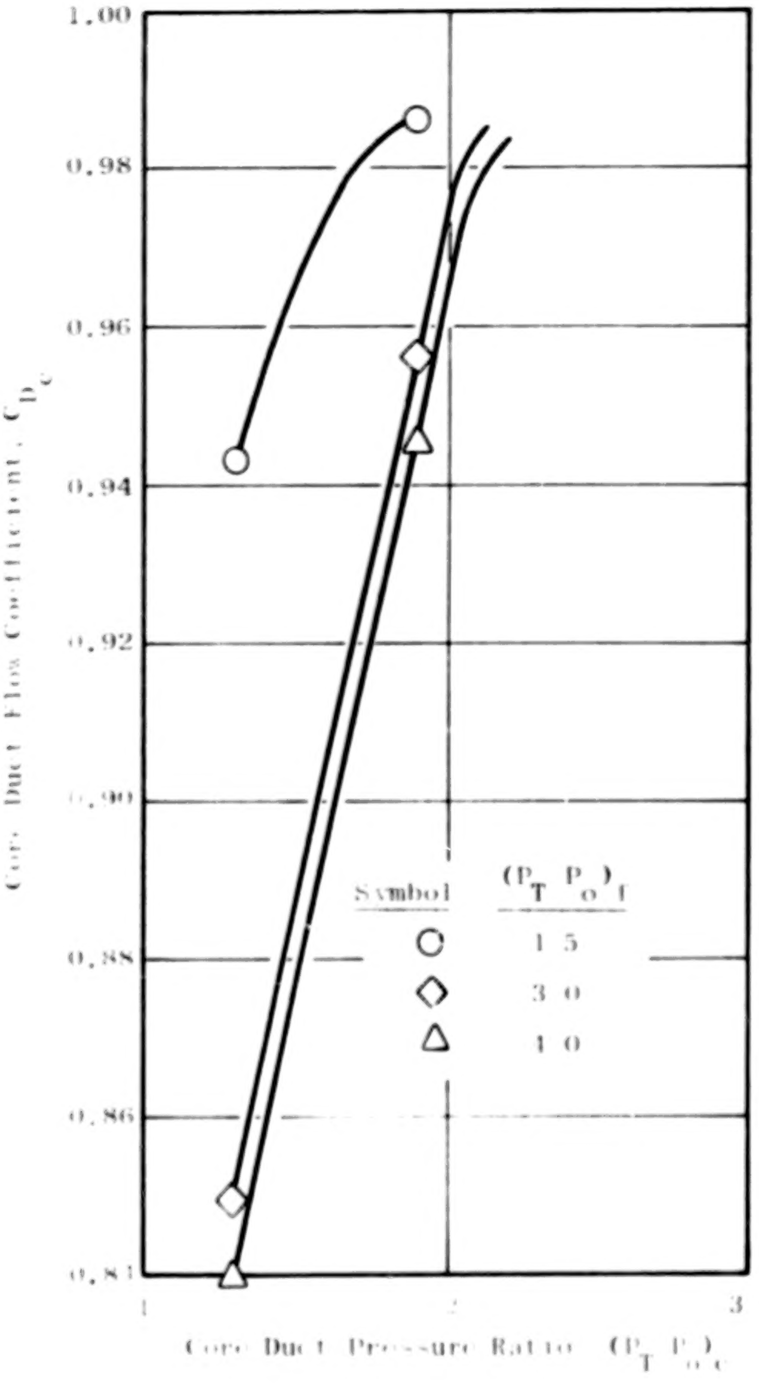

Figure 113. Core Duct Flow Coefficients for the Unsuppressed Coannular Nozzle with Plug (Model 7).

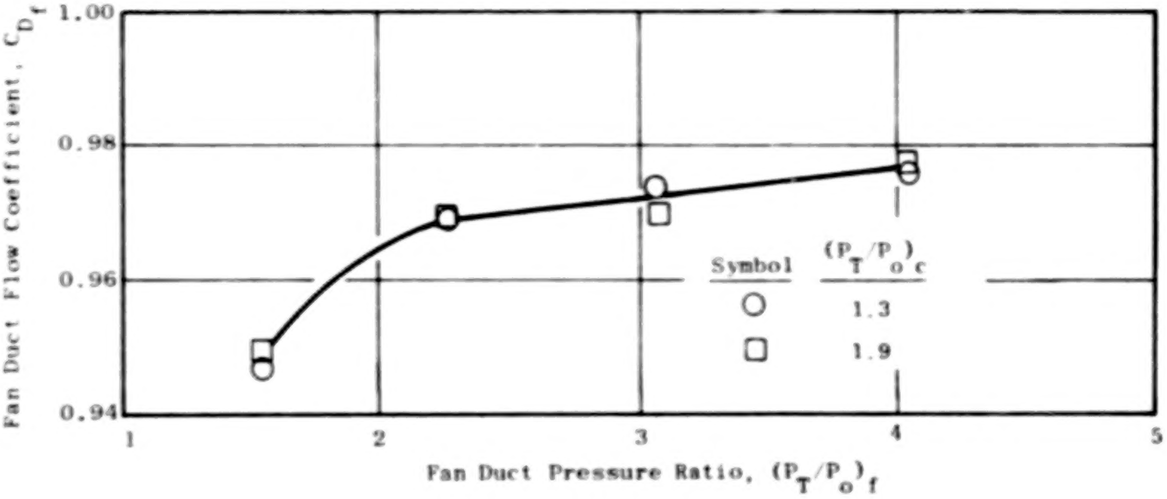

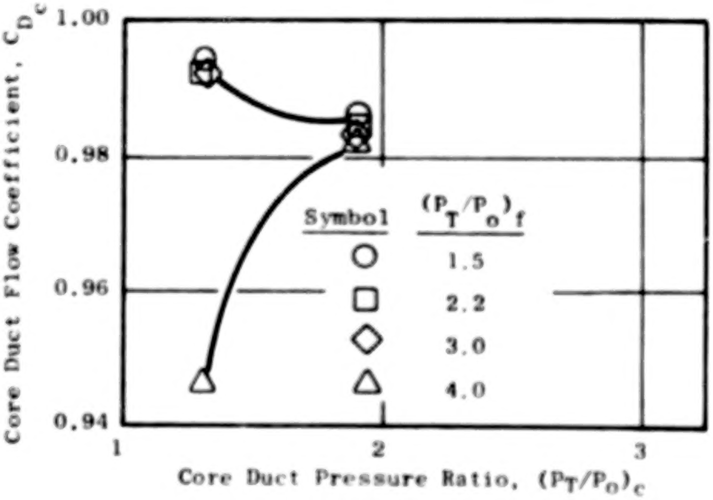

Figure 114. Fan and Core Duct Flow Coefficients for the Multichute Fan Suppressor Nozzle (Model 1).

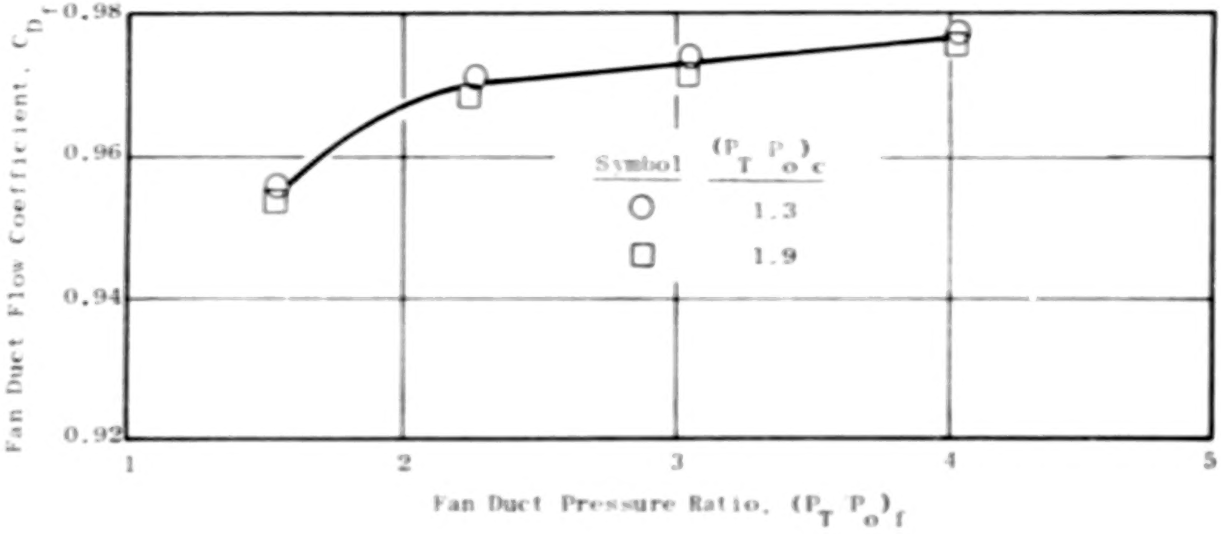

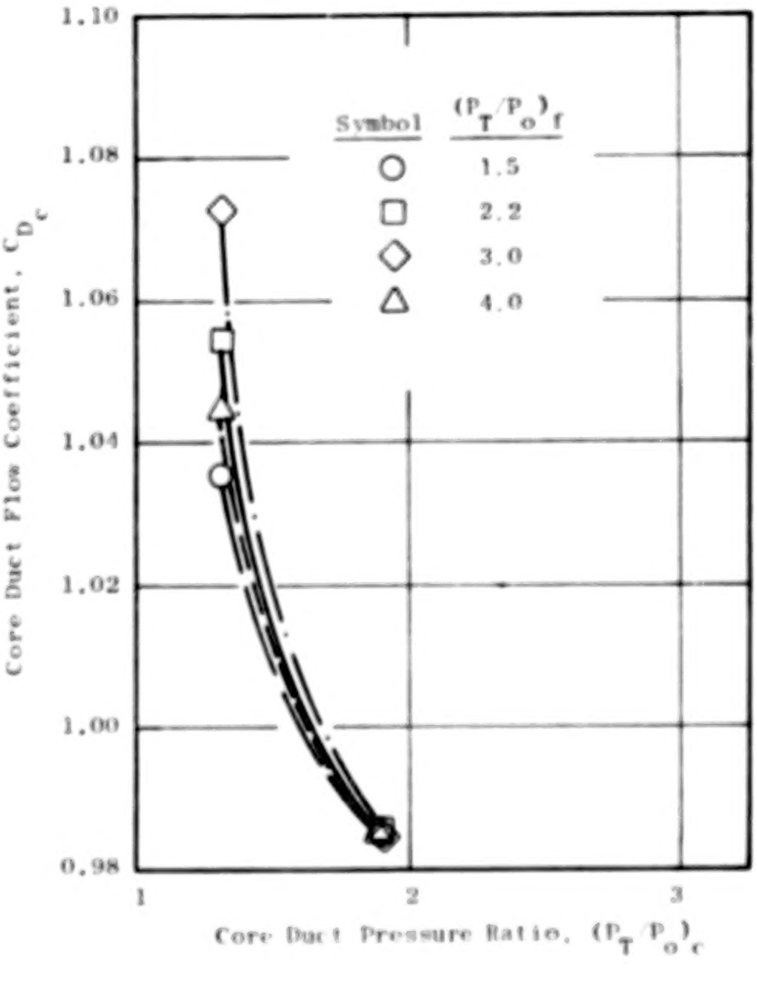

Figure 115. Fan and Core Duct Flow Coefficients for the Multichute Fan Suppressor Nozzle with Hardwall Ejector with Sharp Lip (Model 9).

0.955, slightly higher than the 0.947 measured on the chute suppressor without the ejector. The ejector had the effect of lowering the static pressures in the region of the chute exits (see Section 6.1.3 for discussion), thereby increasing the exit Mach number and the nozzle flow rate. Similarily, the ejector does not effect the core flow coefficient at a core pressure ratio of 1.9 but increases the coefficients at the core pressure ratio of 1.3. This increase in core duct flow coefficient with decreasing core pressure is similar to that observed, and previously described, for the multichute fan suppressor nozzle without ejector in Section 6.3.2.

6.3.4 Multitube Fan-Suppressor Nozzle

Flow coefficient characteristics for the multitube fan-suppressor nozzle (Model 2) are presented in Figure 116. The fan duct coefficient is approximately 0.944 for fan pressure ratios of 2.2 or greater. The decrease in flow coefficient as the pressure is decreased into the subsonic flow regime is as expected for a convergent nozzle. The core nozzle flow coefficient of Model 2 was measured to be 0.985 at a core pressure ratio of 1.9 and 1.0 at a core pressure ratio of 1.3. The core flow coefficient is not dependent on the fan duct operating conditions.

6.3.5 Multitube Fan-Suppressor Nozzle with Hardwall Ejector with Sharp Lip

The fan and core flow coefficient characteristics for the multitube fan-suppressor nozzle with hardwall ejector with sharp lip (aerodynamic Model 5) are shown in Figure 117. The ejector does not change either the core or fan flow coefficient from the values measured on the multitube fan-suppressor nozzle (Model 2) for choked flow pressure ratios. For unchoked flow, the ejector has the effect of increasing the core and fan flow coefficients by lowering the local ambient pressure.

As described in Section 3.3.3.1, fan and core flow rates were measured during hot flow testing on aerodynamic Model 5 by utilizing a special calibration of the fan duct flow coefficient. The fan duct coefficient characteristics determined in this calibration, and used for the calculation of fan duct flow rate in the hot flow tests, are shown in Figure 118. These flow coefficients were calculated using the cold nozzle throat area (see Section 3.3.3.1) such that the increase in flow coefficient at the high temperature is indicative of the increase in physical throat area due to thermal expansion. The resultant core duct flow coefficients, calculated using the calibrated fan duct flow coefficients as described in Section 3.3.3.1, are also shown in Figure 118.

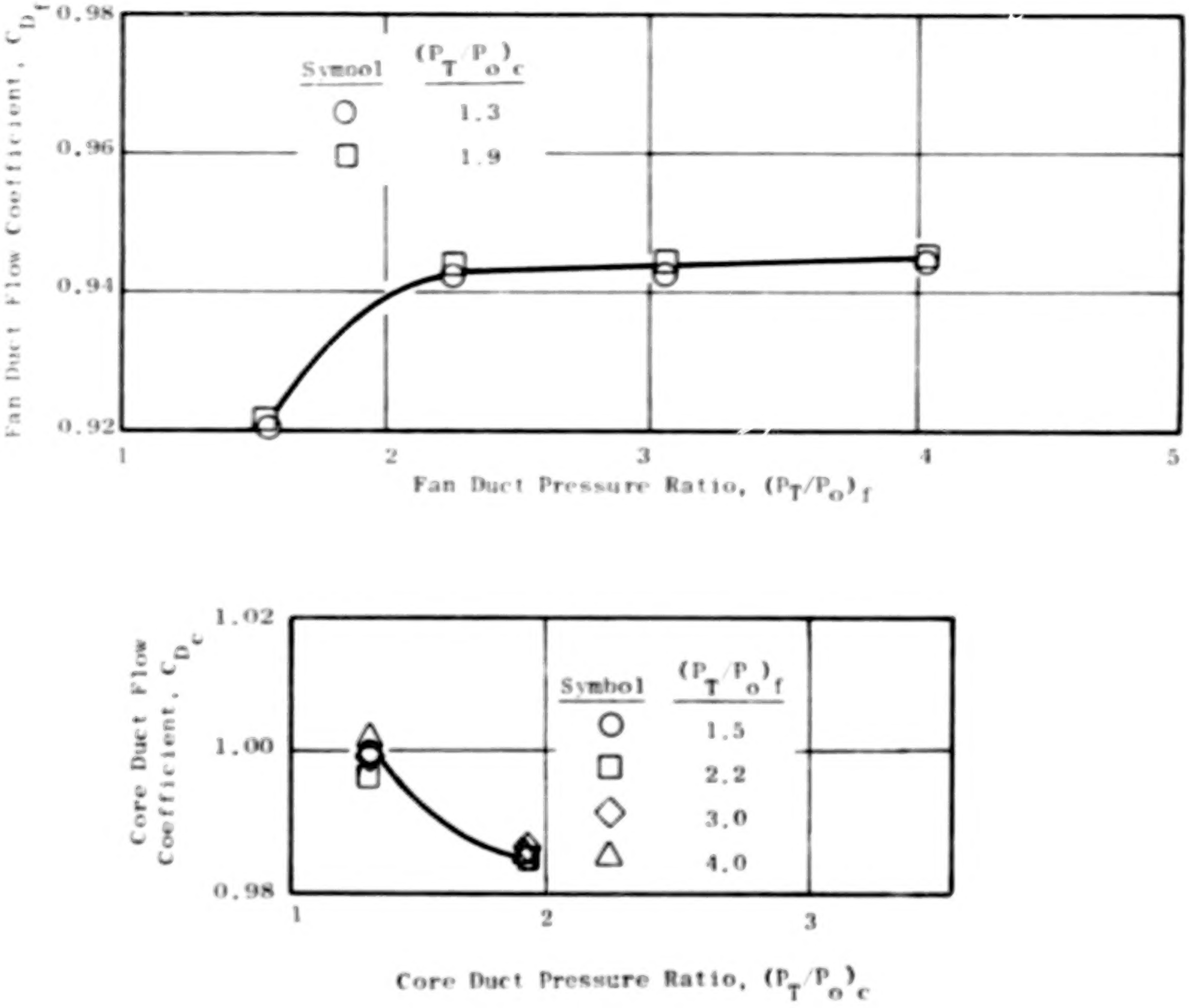

Figure 116. Fan and Core Duct Flow Coefficients for the Multitube Fan Suppressor Nozzle (Model 2).

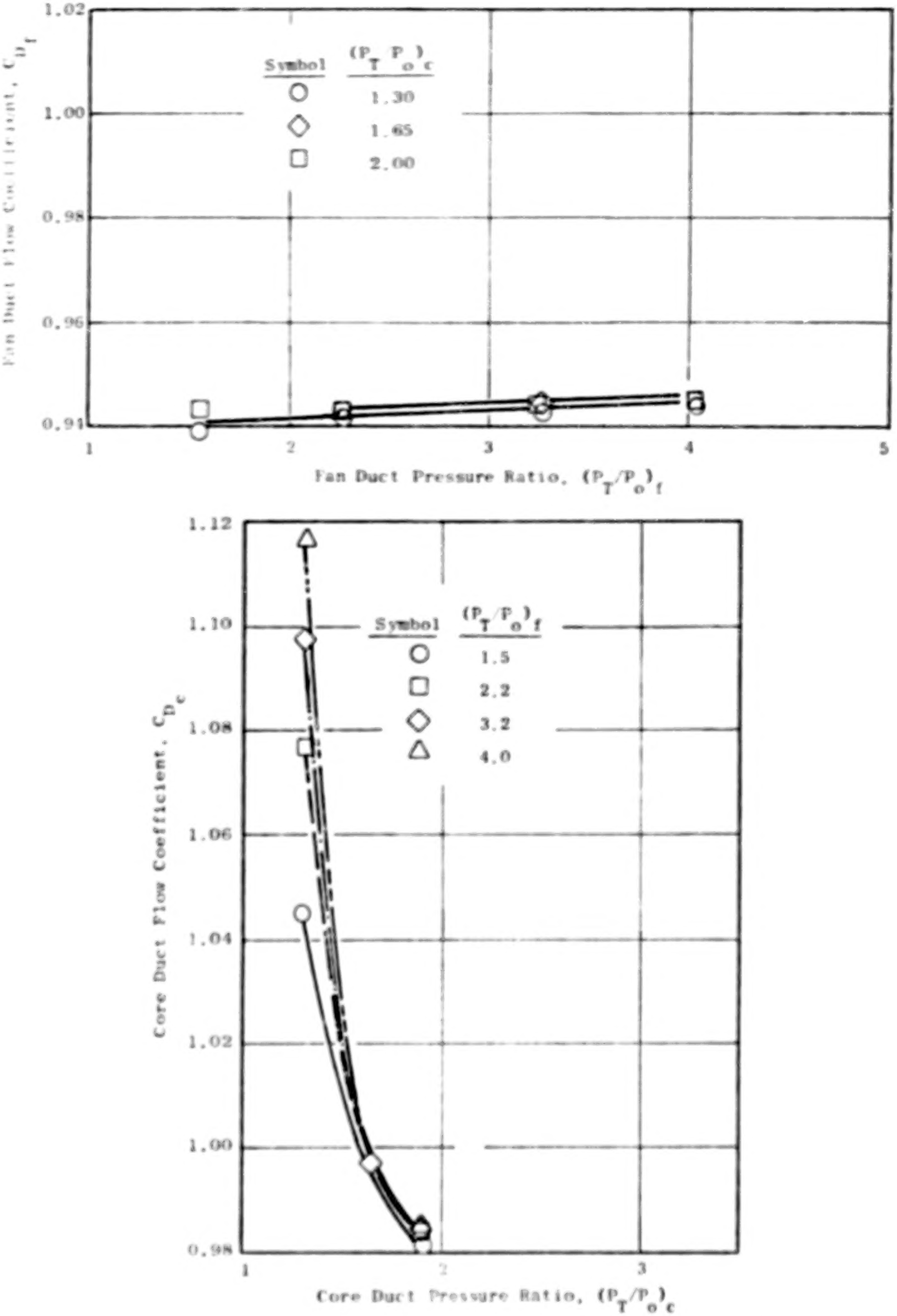

Figure 117. Fan and Core Duct Flow Coefficients for the Multitube Fan Suppressor Nozzle with Hardwall Ejector with Sharp Lip (Aerodynamic Model 5).

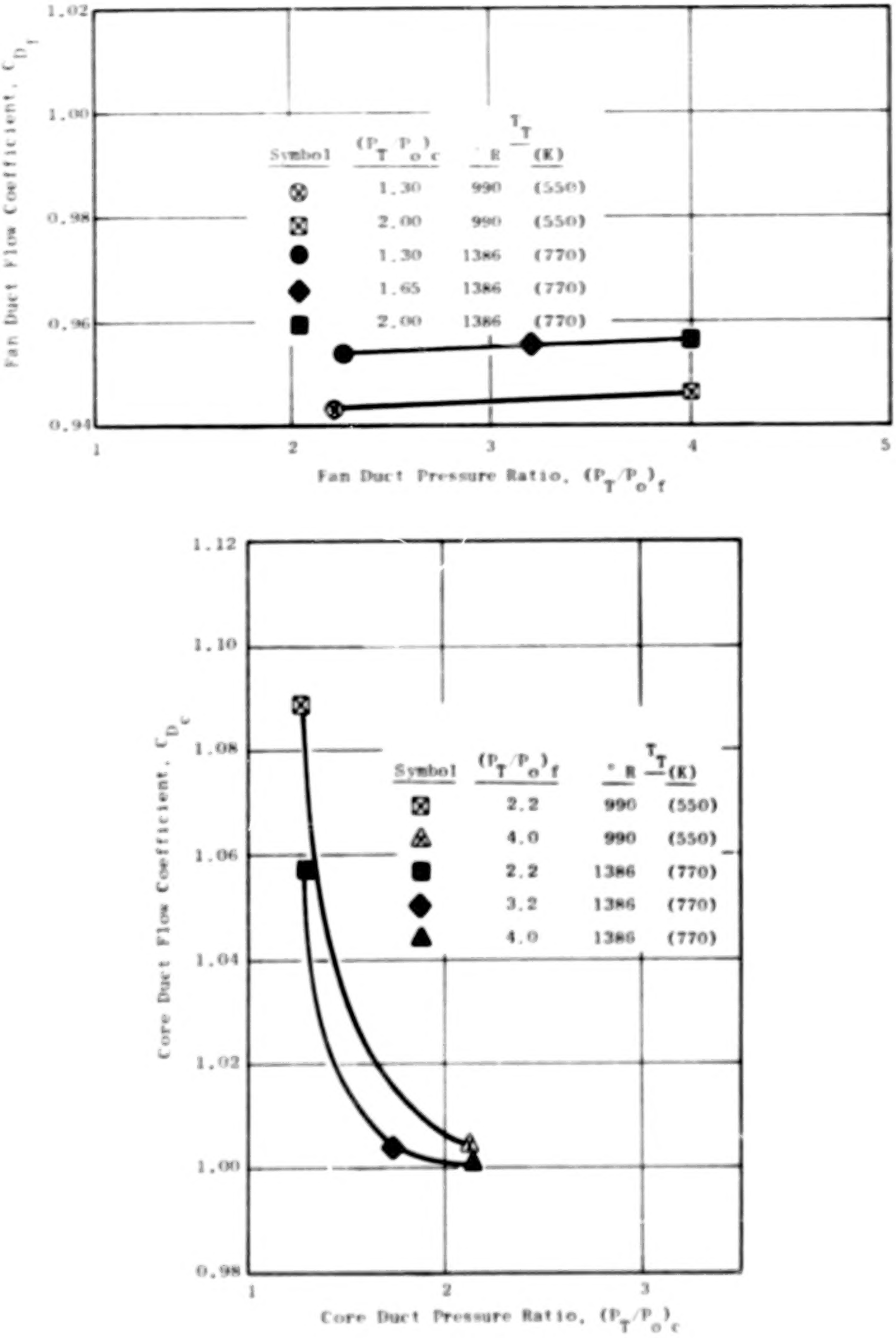

Figure 118. Hot Flow Fan and Core Duct Flow Coefficients for the Multitube Fan Suppressor Nozzle with Hardwall Ejector with Sharp Lip (Aerodynamic Model 5).

7.0 DISCUSSION OF LASER VELOCIMETER TEST RESULTS

A series of laser velocimeter measurements were performed on the unsuppressed and the fan-suppressed configurations in an attempt to gain a better insight into the aerodynamic and acoustic turbulent-mixing characteristics of coannular acoustic nozzles. Sections 3.2.2 and 3.3.2 describe General Electric's laser velocimeter system and data reduction procedures, and Section 4 describes the test matrix for which laser velocimeter measurements were performed. The results obtained from these laser velocimeter measurements are discussed below.

7.1 LASER VELOCIMETER PLUME MEASUREMENTS FOR THE UNSUPPRESSED COANNULAR NOZZLE WITH PLUG

7.1.1 Axial Mean-Velocity Distributions

One of the first questions that arise when an exhaust nozzle reduces the radiated noise is how quickly the exhaust nozzle flow mixes with the ambient air. In a qualitative manner, the amount that an exhaust nozzle can reduce the mean velocity relative to a baseline, such as a conical nozzle, reflects a corresponding amount of acoustic radiation reduction.

As a first illustration, Figure 119 shows the axial distribution of the peak mean velocity for the unsuppressed coannular nozzle with plug. The operating conditions for these test results are V_f = 2100 ft/sec (640.5 m/sec), $(P_T/P_o)_f = 2.86$, $(T_T)_f = 1411°$ R (784 K); V_c = 1400 ft/sec (427 m/sec), $(P_T/P_o)_c = 1.5$, $(T_T)_c = 1461°$ R (812 K). These measurements indicate that the unsuppressed coannular nozzle with plug rapidly reduces the mean velocity with axial distance downstream; within three equivalent diameters the mean velocity has decayed considerably. Compared to typical conical nozzle data the axial peak mean velocity for the unsuppressed coannular nozzle with plug is seen to be considerably reduced. This reduction in mean velocity is a positive corroboration of the acoustic reduction results shown in Section 5.

As a second illustration of the velocity mixing characteristics of the unsuppressed coannular nozzle with plug, Figure 120 compares axial mean-velocity decay characteristics of the coannular flow (taken from Figure 119) with annular flow (flow in fan stream annulus only).* Also shown for illustration is the core-stream-alone, axial-velocity decay for the core stream conditions of the coannular flow test results. The velocity decay results for the annular flow show a sizeable mean-velocity decay similar to, although less than, the coannular flow results. These results suggest that a high radius ratio in the fan stream is helpful in establishing lower noise levels for a coannular nozzle.

---

*Although the core stream controls were set for no core flow, there was some leakage in the core region due to an imperfect shutoff valve arrangement.

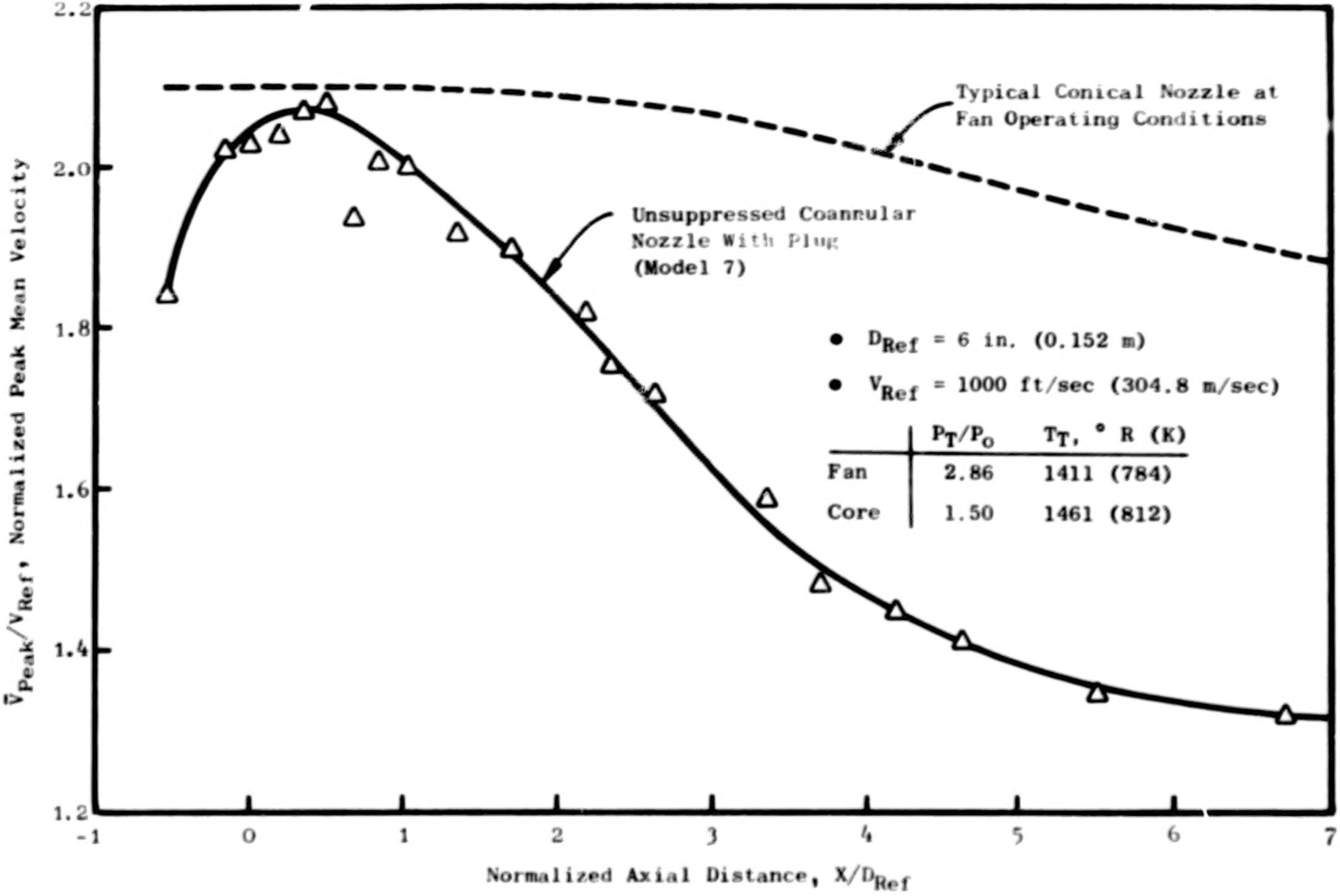

Figure 119. Comparison of Laser Velocimeter Measured Axial Peak Mean Velocity Distributions Between an Unsuppressed Coannular Nozzle with Plug and a Typical Conical Nozzle.

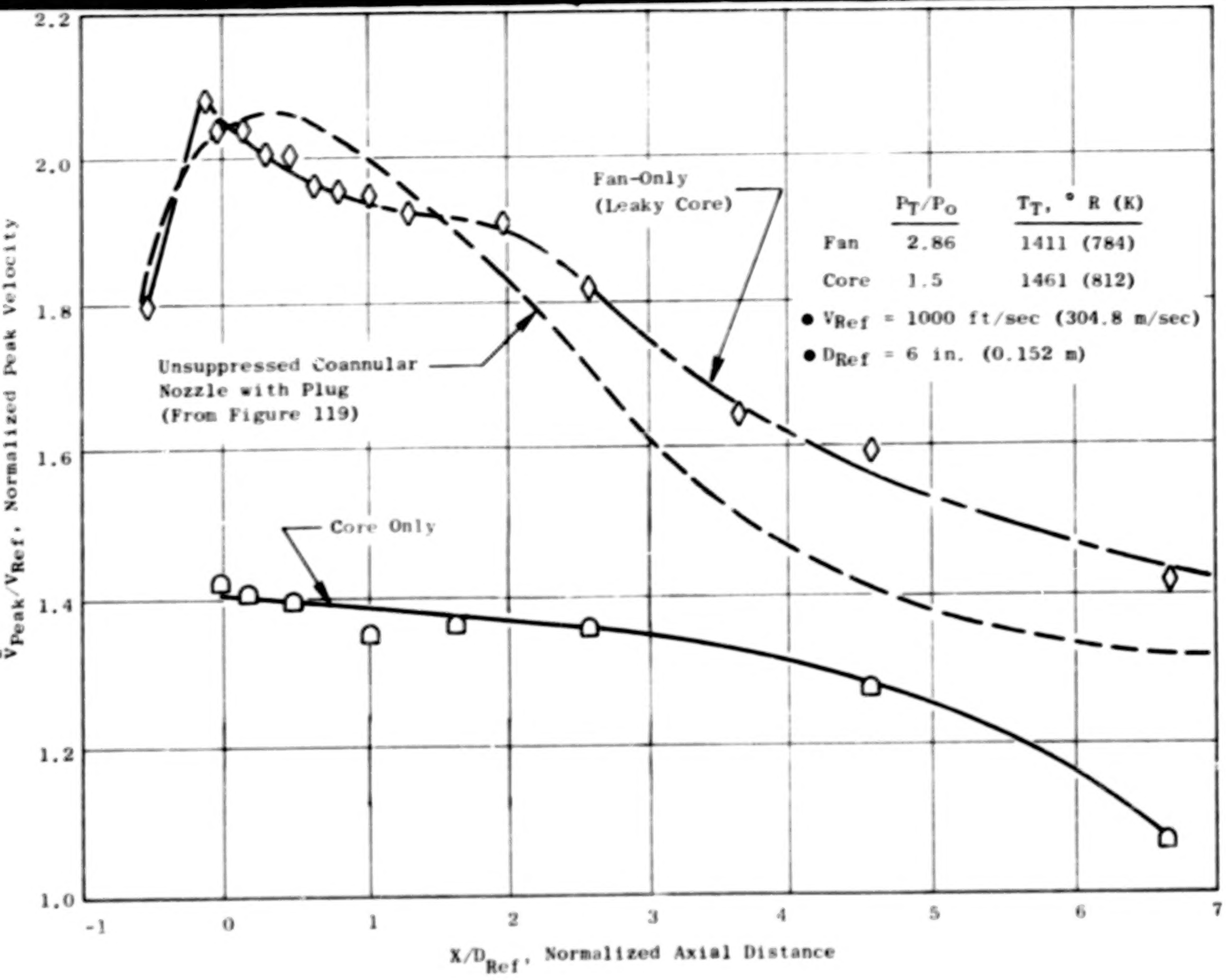

Figure 120. Comparison of Laser Velocimeter Measured Axial Peak Mean Velocity Distributions for an Unsuppressed Coannular Nozzle with Plug; Fan-Alone Flow and Core-Alone Flow.

7.1.2 Mean-Velocity, Radial-Profile Distributions

Illustration of radial distributions of mean velocity at several axial plume stations for the unsuppressed coannular nozzle with plug is shown in Figure 121. The cycle operating conditions for these results are the same as those results shown in Figure 119. The axial stations illustrated are X/D_{ref} = 0, 1.025, 2.61, 4.61, and 6.67. It is observed that at $X/D_{ref} = 0$ (the axial station located slightly aft of the outer fan plug), a highly peaked mean-velocity profile of the core stream exists. As the axial station is increased from 0 to 6.67 the two streams merge and the mean-velocity profile smooths out. The final radial profile ($X/D_{Ref} = 6.67$) shows that the outer stream has steadily decayed to the core stream velocity and the th it core stream velocity has begun to decay. These results, as well as the results from Figure 119 and 120, indicate that the high radius ratio (or small annulus gap) of the outer fan stream enhances ambient air entrainment and results in a substantial mean-velocity reduction and, therefore, a lower noise-signature nozzle. Appendices F,G, and H are provided for completeness. Appendix F contains a comprehensive series of the radial mean-velocity profiles between X/D_{ref} of - 0.52 and 6.67 for the test conditions shown on Figure 121. Appendix G contains radial mean-velocity profiles for a case with the fan stream flowing at $P_T/P_o = 2.86$, T_T = 1411° R (784 K) and the core stream not flowing [$(P_T/P_o)_c \approx 1.0$]. Appendix H contains measurements of mean radial-velocity profiles with no fan flow and the core operating at $P_T = 1.5$, T_T = 1461° R (812 K).

7.1.3 Axial Turbulent-Velocity, Radial-Profile Distributions

Examples of the local turbulence level radial-profile distributions for the unsuppressed coannular nozzle with plug are shown in Figure 122. These turbulence measurements are companion measurements to the mean-velocity measurements shown on Figure 121. Of particular notice is the high local turbulence level at the periphery of the fan exhaust nozzle as compared to the inner core mixing region. These turbulence measurements support the conclusions from the mean-velocity measurements: that the rapid decay of mean velocity must be associated with high levels of turbulence generation in the outer stream mixing regions.

7.2 LASER VELOCIMETER PLUME MEASUREMENTS FOR THE FAN-SUPPRESSED NOZZLES

7.2.1 Axial Mean-Velocity Distributions

The mean-velocity decay exhibited by the fan-suppressed coannular nozzles with plug indicates a noise reduction similar to that discussed in Section 7.1.1. To illustrate this, Figure 123 shows a comparison of axial distributions of the peak mean velocity for the multichute and multitube fan suppressors of a typical conical nozzle versus the unsuppressed coannular nozzle with plug. For the operating condition shown, the peak mean-velocity decay for both of the fan-suppressed nozzles is greater than

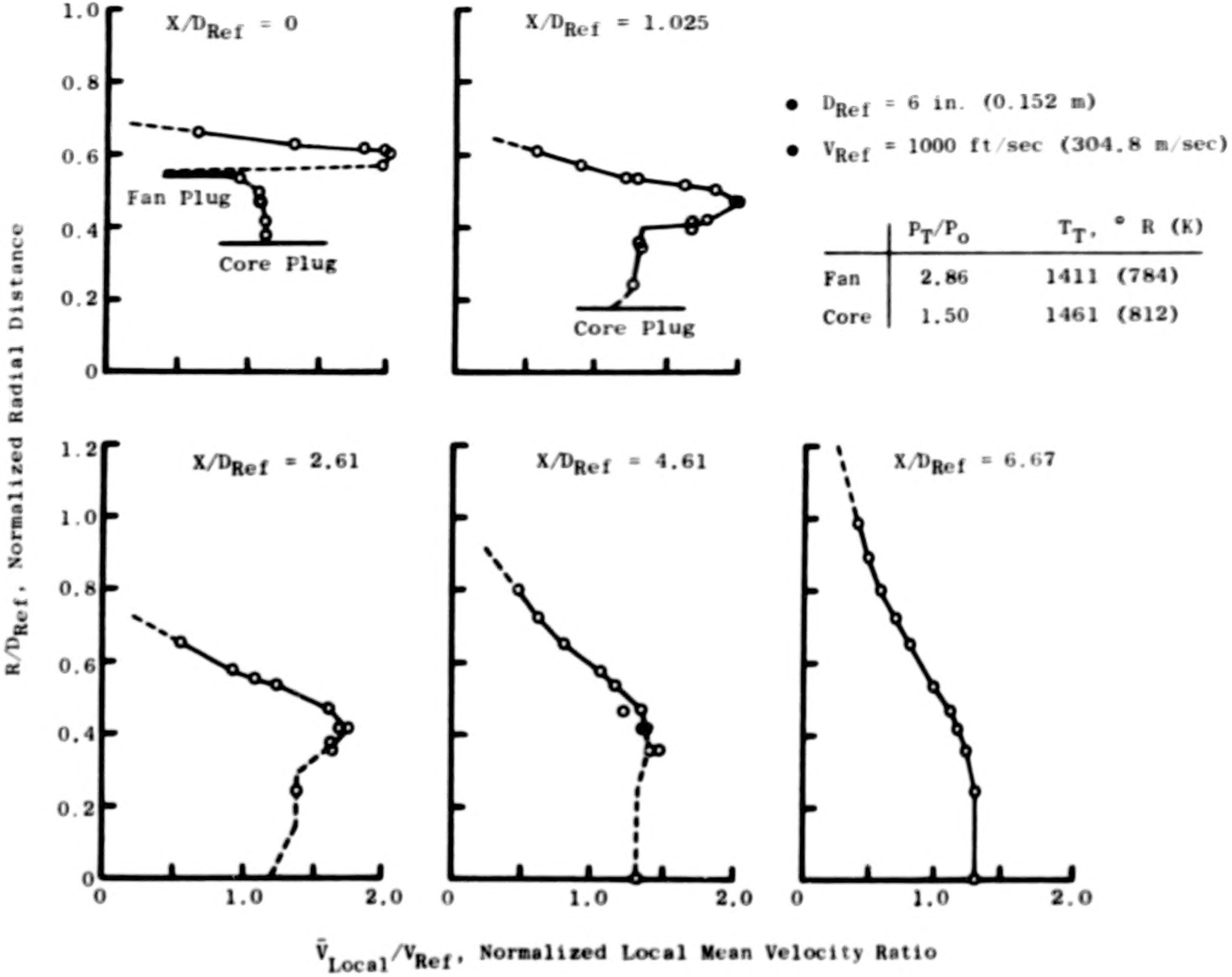

Figure 121. Laser Velocimeter Measured Mean Velocity Radial Profiles at Several Axial Stations for the Unsuppressed Coannular Nozzle with Plug (Model 7).

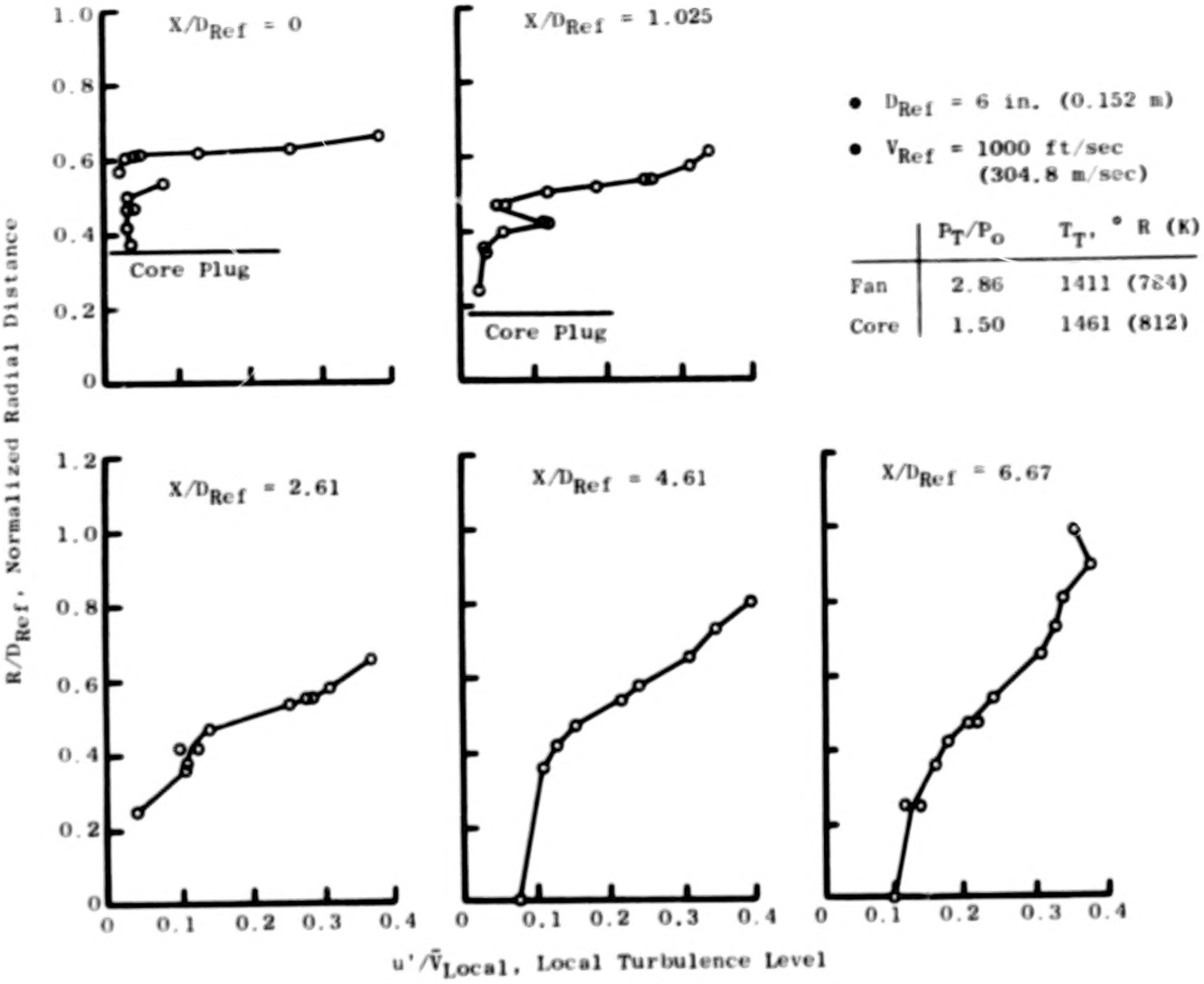

Figure 122. Laser Velocimeter Measured Local Turbulence Velocity Radial Profiles at Several Axial Stations for the Unsuppressed Coannular Nozzle with Plug (Model 7).

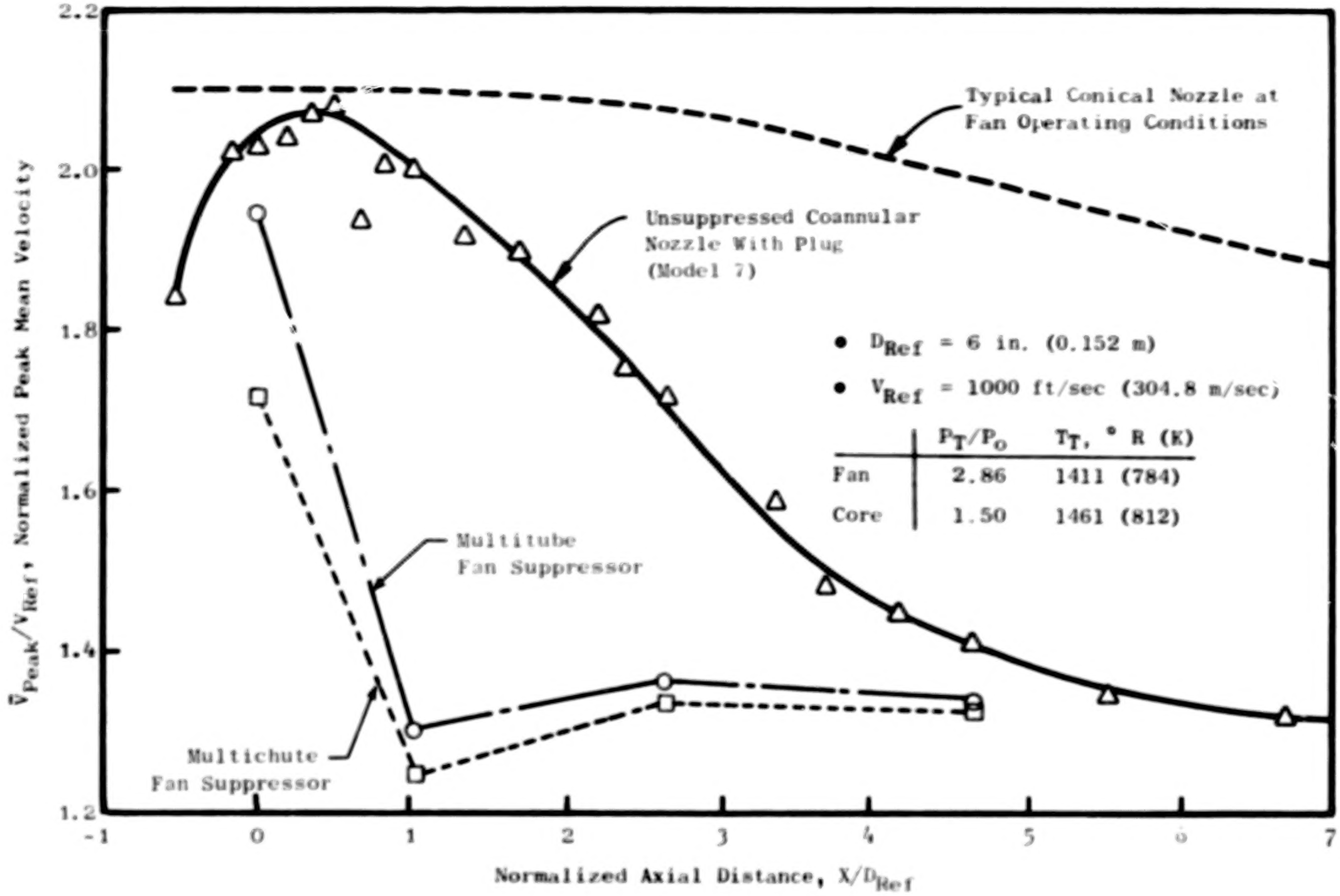

Figure 123. Comparison of Laser Velocimeter Measured Axial Peak Mean Velocity Distributions for the Multichute and Tube Fan Suppressor, the Unsuppressed Coannular Nozzle with Plug, and a Typical Conical Nozzle.

179

either the conical nozzle or the unsuppressed coannular nozzle with plug. These results indicate that the characteristic dimensions of the individual chutes and tubes are governing the mixing and therefore the reduction in radiated noise.

7.2.2 Mean- and Turbulent-Velocity, Radial-Profile Distributions

7.2.2.1 Multichute Fan Suppressor

Figures 124 and 125 show mean- and turbulent-velocity radial-profile distributions for the multichute fan suppressor at V_f = 2100 ft/sec (640.5 m/sec), $(P_T/P_o)_f$ = 2.86, T_{T_f} = 1411° R (784 K); V_c = 1400 ft/sec (427 m/sec), $(P_T/P_o)_c$ = 1.5, and T_{T_c} = 1461° R (812 K). These measured velocity profiles can be compared directly with those shown on Figures 121 and 122. Figure 124 shows that, in addition to the greater decay in axial mean velocity, the multichute fan suppressor also exhibits a broader radial mean-velocity distribution than the unsuppressed coannular nozzle with plug. The broader radial velocity distribution is indicative of the chute directing the flow more outward from the nozzle axis and therefore enhancing the velocity decay. The results also show that by the time the flow has reached one reference diameter downstream, or by the end of the core plug, the fan flow has nearly decayed to the core velocity condition. Somewhat past this axial location the flow field is probably behaving similar to that of an equivalent conical nozzle.

7.2.2.2 Multitube Fan Suppressor

The mean-velocity and turbulent-velocity radial distributions for the multitube fan suppressor are shown in Figure 126 and 127. These profiles may be compared with the velocity profiles of the unsuppressed coannular nozzle with plug and the multichute fan suppressor in Figures 121, 122, 124 and 125. The measurements in Figures 126 and 127 show that at X/D_{Ref} = 0 the individual tube velocity profiles are discernible, but at X/D_{Ref} = 1.0 (tip of the core plug) the individuality of the tube velocity profiles is washed out and the fan velocity has nearly decayed to the core stream velocity. As was discussed for the multichute fan suppressor, the velocity profile past the core plug should approach that of an equivalent conical nozzle.

For completeness, laser velocimeter measurements of radial velocity profiles at two test conditions other than those presented above are given in Appendices I and J for the multichute and multitube fan-suppressor nozzles respectively.

7.3 SUMMARY OF OBSERVATIONS

The primary observation made in this section is that a substantial decay in the mean-velocity axial distribution is obtained for the coannular-flow nozzles with plug, suppressed or unsuppressed, relative to a conical nozzle.

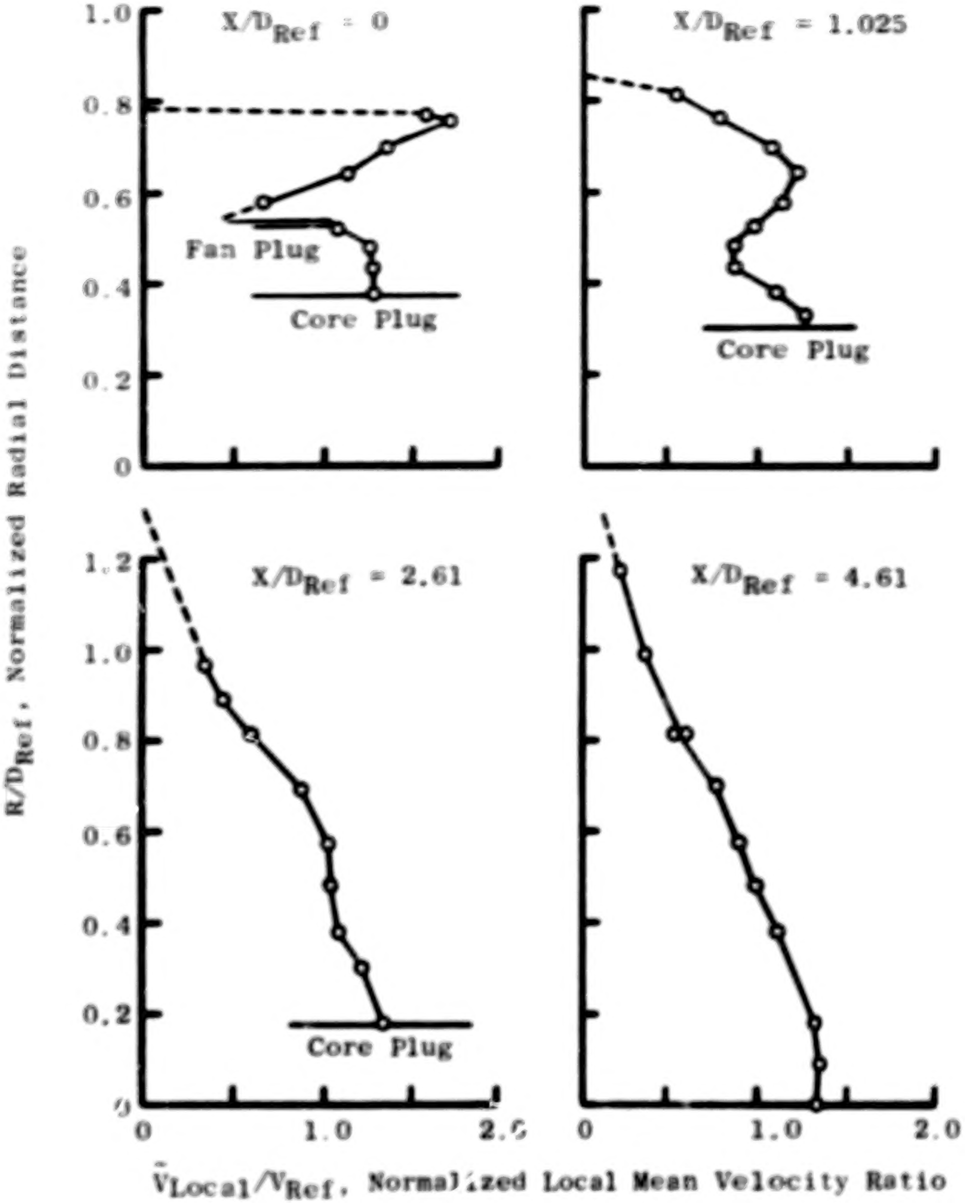

- D_{Ref} = 6 in. (0.152 m)
- V_{Ref} = 1000 ft/sec (304.8 m/sec)

	P_T/P_o	T_T, ° R (K)
Fan	2.86	1411 (784)
Core	1.50	1461 (812)

Figure 124. Laser Velocimeter Measured Mean Velocity Radial Profiles at Several Axial Stations for the Multichute Fan Suppressor Nozzle (Model 1).

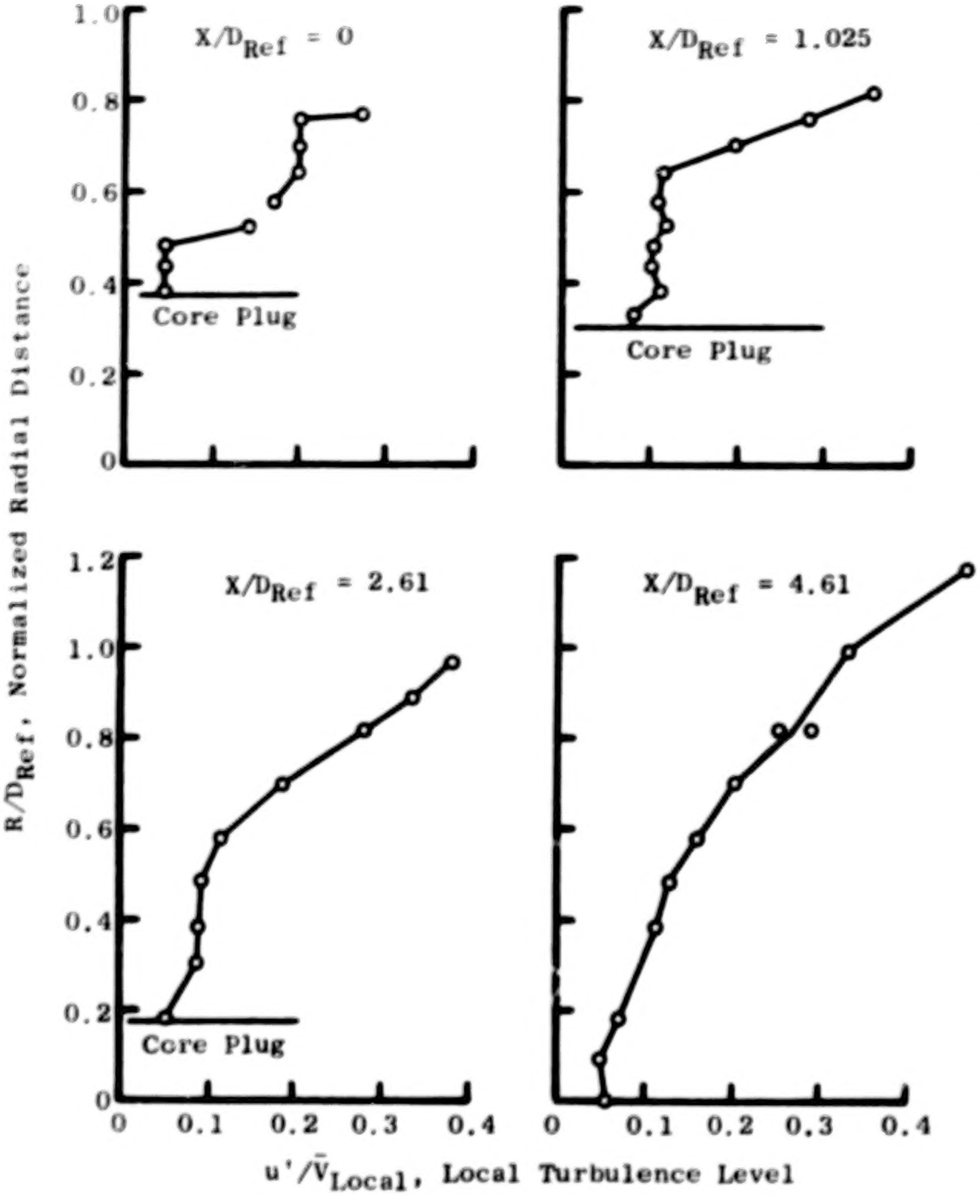

- D_{Ref} = 6 in. (0.152 m)
- V_{Ref} = 1000 ft/sec (304.8 m/sec)

	P_T/P_o	T_T, ° R (K)
Fan	2.86	1411 (784)
Core	1.50	1461 (812)

Figure 125. Laser Velocimeter Measured Local Turbulence Velocity Radial Profiles at Several Axial Stations for the Multichute Fan Suppressor Nozzle (Model 1).

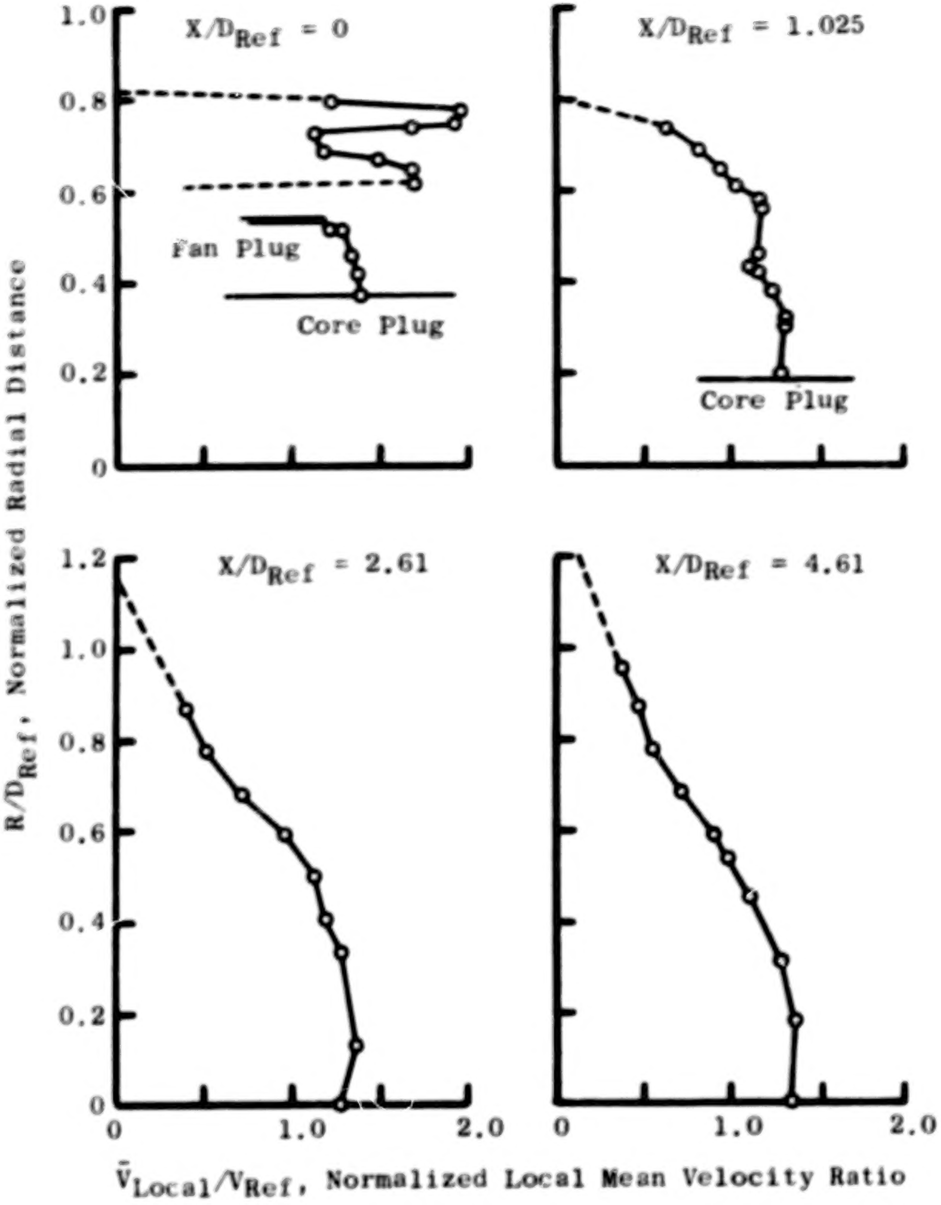

- D_{Ref} = 6 in. (0.152 m)
- V_{Ref} = 1000 ft/sec (304.8 m/sec)

	P_T/P_o	T_T, ° R (K)
Fan	2.86	1411 (784)
Core	1.50	1461 (812)

Figure 126. Laser Velocimeter Measured Mean Velocity Radial Profiles at Several Axial Stations for the Multitube Fan Suppressor Nozzle (Model 2).

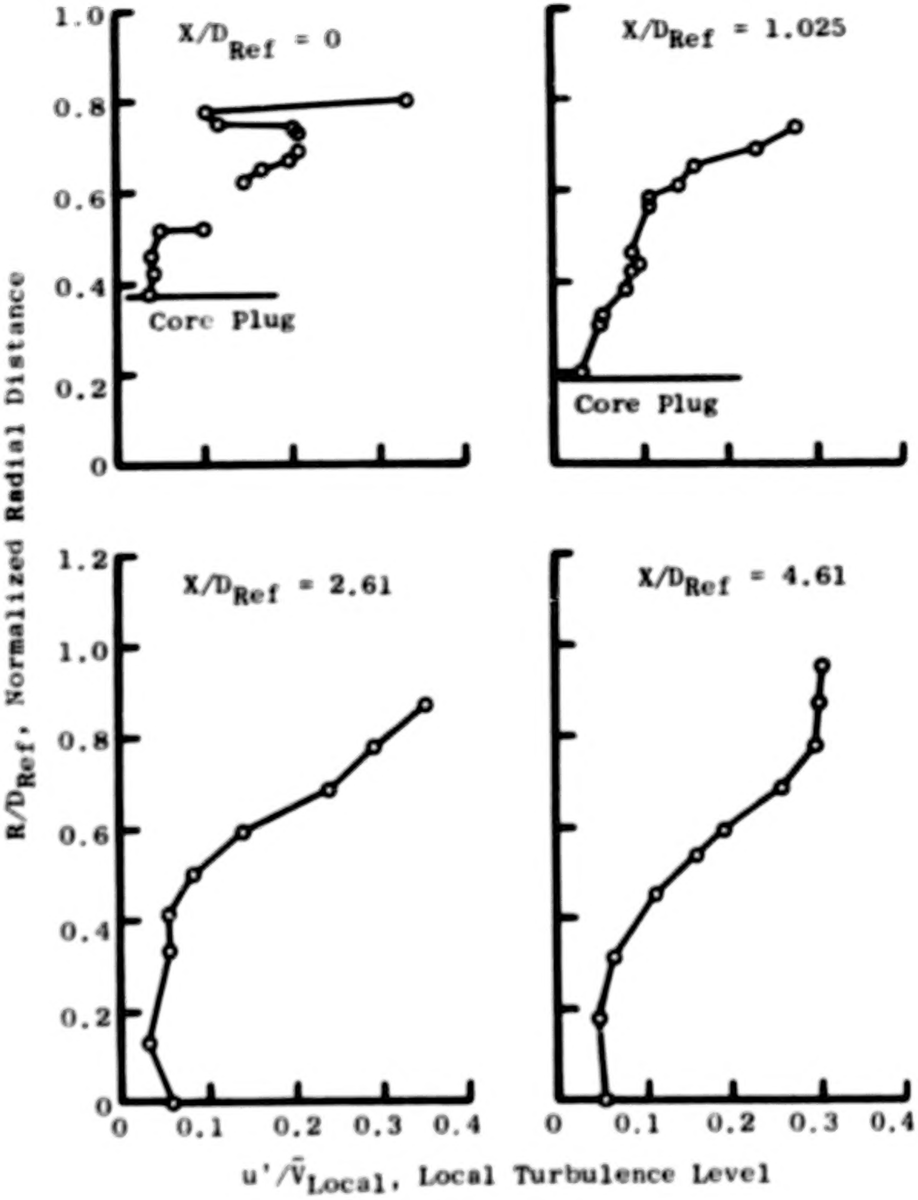

- D_{Ref} = 6 in. (0.152 m)
- V_{Ref} = 1000 ft/sec (304.8 m/sec)

	P_T/P_o	T_T, ° R (K)
Fan	2.86	1411 (784)
Core	1.50	1461 (812)

Figure 127. Laser Velocimeter Measured Local Turbulence Velocity Radial Profiles at Several Axial Stations for the Multitube Fan Suppressor Nozzle (Model 2).

This reduction in mean velocity can be phenomenologically associated with a reduction in the noise. The velocity decay occurs for the annular flow (fan operating only) as well as for the coannular flow test cases. These results are not suprising for the coannular flow nozzles having a fan suppressor since it is known for turbojet suppressors that this mean-velocity decay phenomenon occurs and is a basis for multitube and multichute suppressor designs. The amount of velocity decay and the resultant noise reduction obtained with the unsuppressed coannular and annular nozzles with plug was not anticipated beforehand.

The results also show that geometry and flow management between the core and fan can regulate the amount of velocity decay, and the amount of noise reduction. Qualifying the precise trade between the velocity profile management and noise management was beyond the scope of this program; however, results from other studies at the General Electric Company indicate that, in addition to the turbulent mixing noise reduction benefits observed for the coannular nozzles, other flow interaction and noise reduction mechanisms are at work.

8.0 DISCUSSION OF ACOUSTIC/AERODYNAMIC-PERFORMANCE CORRELATIONS

The acoustic suppression and aerodynamic-performance characteristics of the unsuppressed coannular and multielement fan-suppressor nozzles are summarized in Sections 5.0 and 6.0 respectively. The following paragraphs attempt to correlate the salient noise-suppression capabilities with the demonstrated static-performance trends for each nozzle system for duct-burning turbofan engine cycles. The section concludes with a preliminary geometry-related correlation scheme for collapsing "low core flow" coannular nozzle noise levels.

8.1 EVALUATION OF NOISE CANDIDATES FOR DUCT-BURNING TURBOFAN ENGINES

In order to bring the results of the acoustic and aerodynamic-performance tests into focus, this section develops an overall assessment of the relative merits of the various test model configurations. A typical engine cycle condition that is representative of the duct-burning turbofan engine cycle is a fan pressure ratio of 3.24 (fan jet ideal velocity of 2400 ft/sec or 732 m/sec) and a $(P_T^{\bullet}/P_O)_C = 1.56$ (core jet ideal velocity of 1200 ft/sec or 366 m/sec). The various test model configurations are compared at this condition, and the acoustic and aerodynamic-performance tests are summarized.

The noise suppression capability of all the exhaust systems evaluated are summarized in bar graph form on Figure 128 in terms of normalized perceived noise level. As noted earlier, the unsuppressed coannular nozzle with plug (Model 7) demonstrated significant suppression (∿ 10 PNdB relative to a synthesized baseline) with none of the aerodynamic-performance penalties usually associated with a mechanical suppressor. In addition, studies on advanced cycles applicable to military and commercial high Mach number aircraft have shown that dual-flow plug nozzles similar to the unsuppressed coannular nozzle with plug integrate well with these types of engine systems and possess performance, mechanical, and weight advantages over other types of exhaust systems.

The addition of a multielement (either multichute or multitube) fan suppressor to the basic unsuppressed coannular nozzle with plug adds another 4.5 to 5.0 PNdB suppression. The multichute fan-suppressor nozzle is more practical from a mechanical design point of view. Mechanical design studies have shown that deployment and stowage mechanisms for the chute-type fan suppressors appear feasible within a practical engine nacelle envelope.

The test results show that hardwall ejectors designed to be mechanically practical offer no apparent acoustic benefit. Acoustically treated ejectors, however, will add another 2.0 to 3.0 PNdB of suppression. The weight penalties incurred by the addition of the treated ejector may be a limiting feature for such an acoustic nozzle system; however, the overall level of noise reduction obtained for the multielement fan suppressors with treated

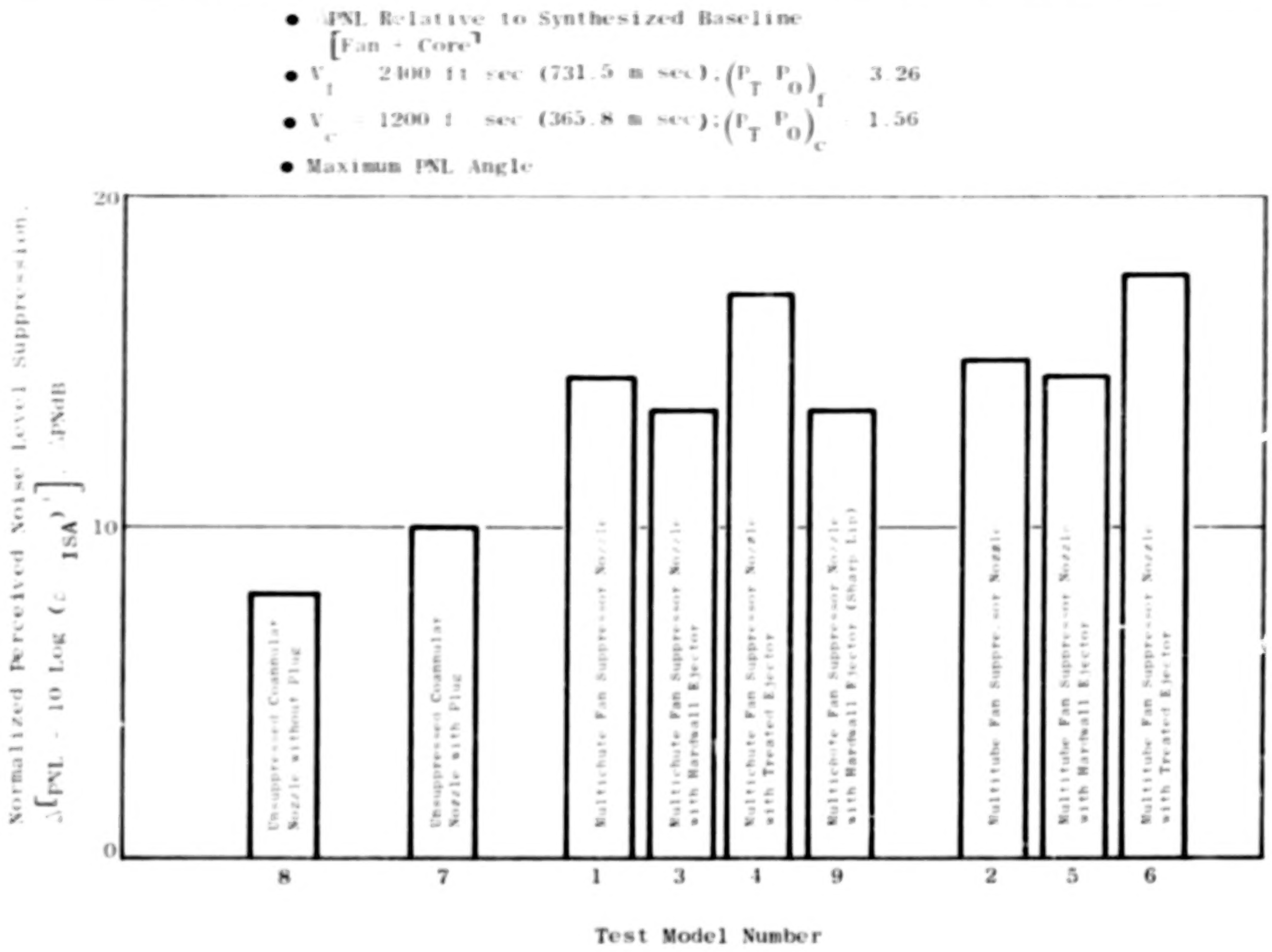

Figure 128. Acoustic Suppression Relative to Synthesized Baseline for Conditions Typical of DBTF Engines at Takeoff.

]

ejectors was 17 to 17.5 PNdB. These high levels of noise reduction are a positive step toward developing practical acoustic nozzle suppressor system designs for future high performance, separate-flow engine applications.

The static aerodynamic-performance levels of the tested models are shown in Figure 129; the performance characteristics are shown in terms of thrust coefficient change relative to the unsuppressed coannular nozzle with plug (Model 7). The thrust loss shown for the multielement fan suppressors is relatively low at the selected engine cycle condition. Both multielement fan suppressors are operating near their aerodynamic design conditions. The thrust loss of the multichute fan-suppressor nozzle is found to be approximately 75% of that with the multitube fan-suppressor nozzle.

Statically, the hardwall ejectors are observed to provide thrust augmentation. For an acoustically treated ejector at takeoff conditions ($M = 0.3$ to 0.36), two performance penalties can be shown to degrade the ejector performance. First of all, the effect of acoustic treatment in an ejector can represent 2 to 5% loss in thrust coefficient relative to a hardwall ejector (SST Phase II Program Contract DOT-FA72-2814). The apparent reason for this thrust loss is the large viscous effect over the perforated faceplate in the ejector and, hence, impairment of the flow entrainment. Secondly, the thrust loss due to adverse, wind-on, ejector performance of external flow over the ejector surfaces can represent a 2 to 4% decrease in thrust coefficient. The net result is that installed ejector performance at takeoff conditions does not appear beneficial; also, ejector weight and stowage problems make the mechanical feasibility very dubious. Thus, the acoustic benefit of 2.5 PNdB for a treated ejector is negated by performance penalties and mechanical design problems at takeoff conditions when used strictly for acoustic purposes.

The static acoustic and aerodynamic-performance tradeoff for the multielement fan-suppressor nozzles is shown in Figure 130. The unsuppressed coannular nozzle with plug (Model 7) is the reference and the acoustic levels of the two multielement fan-suppressor nozzles are comparable; however, the thrust loss of the multichute fan suppressor is 75% of that of the multitube. On the basis of the trade parameter, $\Delta PNL/\Delta C_T$, the multichute is a better fan-suppressor nozzle (3.75 $\Delta PNL/\Delta C_T$ versus 3.03 $\Delta PNL/\Delta C_T$). In general both multielement fan-suppressor nozzle systems show excellent results on a traded basis. In fact, if the noise/performance trade were to be referenced to a simple conical nozzle (i.e. $C_T = 0.985$), the $\Delta PNL/\Delta C_T$ would be about 5.0. Furthermore, if this noise/performance trade relative to a conical nozzle was extended to the unsuppressed coannular nozzle with plug (Model 7), the resulting $\Delta PNL/\Delta C_T$ would be in excess of 6.0, a very viable low noise nozzle candidate.

Overall, the multichute fan-suppressor nozzle has demonstrated good jet noise suppression, a relatively small thrust loss, and good mechanical feasibility. For an engine system requiring a total suppression of 14 to 15 PNdB, the multichute fan-suppressor nozzle system offers a viable solution.

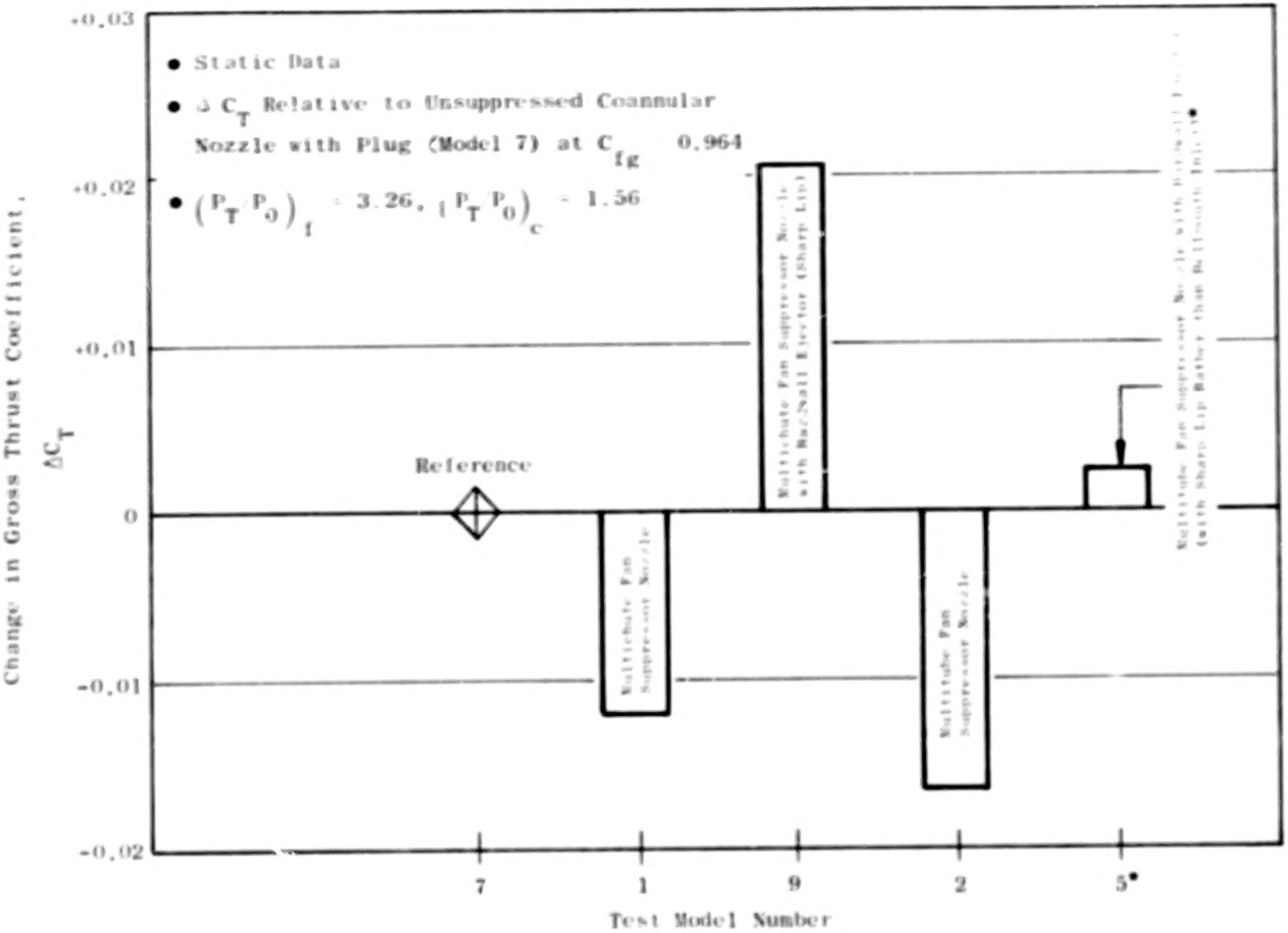

Figure 129. Aerodynamic Performance Summary Relative to Unsuppressed Coannular Nozzle with Plug for Conditions Typical of DBTF Engines at Takeoff.

- Static Data
- ΔPNL and ΔC_T Relative to Unsuppressed Coannular Nozzle with Plug (Model 7)
- V_f = 2400 ft/sec (731.5 m/sec); (P_T/P_o) = 3.26
- V_c = 1200 ft/sec (365.8 m/sec); (P_T/P_o) = 1.56

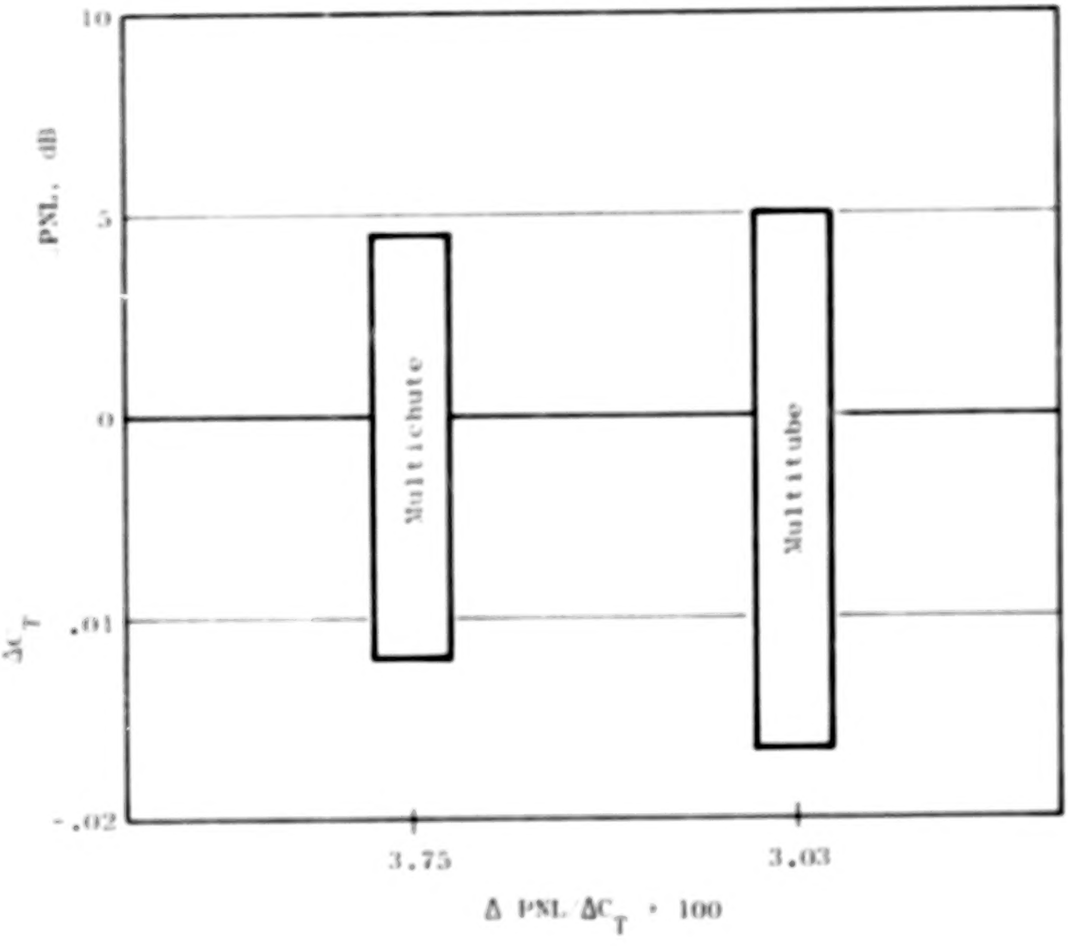

Figure 130. Acoustic/Aerodynamic Performance Relative to Unsuppressed Coannular Nozzle with Plug for Conditions Typical of DBTF Engines at Takeoff.

TABLE OF CONTENTS

Section	Page	
1.0 SUMMARY	1	1/C1
2.0 INTRODUCTION	3	1/C3
3.0 TEST APPARATUS AND PROCEDURES	5	1/C5
3.1 FACILITIES	5	1/C5
3.1.1 General Electric Jet Engine Noise Outdoor Test Stand (JENOTS) Description	6	1/C6
3.1.1.1 Acoustic Arena	6	1/C6
3.1.1.2 Coannular-Flow System	6	1/C6
3.1.1.3 Coannular Frame Section	10	1/C12
3.1.1.4 Plenum Instrumentation Section	10	1/C12
3.1.1.5 Facility Acoustic Validation	12	1/C14
3.1.2 FluiDyne Aerodynamic-Performance Test Facility Description	12	1/C14
3.2 JENOTS INSTRUMENTATION SYSTEMS	16	1/D5
3.2.1 Acoustic Instrumentation Systems	16	1/D5
3.2.2 Laser Velocimeter System	18	1/D8
3.2.2.1 General Arrangement	18	1/D8
3.2.2.2 LV Actuator and Seeding	21	1/D13
3.2.2.3 Signal Processing and Recording	21	1/D13
3.3 DATA REDUCTION METHODS	21	1/D13
3.3.1 Acoustic Data Reduction	22	1/D14
3.3.1.1 JENOTS Data Reduction Systems	22	1/D14
3.3.1.2 Air-Attenuation Corrections	22	1/D14
3.3.1.3 Data-Scaling Procedure	30	1/E12
3.3.1.4 Data Corrections to a Free-Field Environment	30	1/E12
3.3.1.5 Power Level Calculation	30	1/E12
3.3.1.6 Acoustic Measurement Errors, Electronic Noise Floor	30	1/E12
3.3.2 Laser Velocimeter Data Reduction	33	1/F3
3.3.2.1 Basic Idea for LV rms Measurements	33	1/F3
3.3.2.2 The Histogram	36	1/F6
3.3.2.3 Mean Velocity	36	1/F6
3.3.2.4 Turbulent Velocity	37	1/F7
3.3.2.5 Statistical Errors for LV Mean and Turbulent Velocity Measurements	37	1/F7

TABLE OF CONTENTS (continued)

Section Page

3.3.3 Aerodynamic-Performance Test Data Reduction 37 1/F7
3.3.3.1 Flow Rates 39 1/F9
3.3.3.2 Discharge Coefficients 39 1/F9
3.3.3.3 Nozzle Throat 39 1/F9
3.3.3.4 Thrust Coefficient 40 1/F10
3.3.3.5 FluiDyne Force Balance Calibration 40 1/F10
3.3.3.6 Pressure and Temperature Data 41 1/F11
3.3.3.7 Data Quality 41 1/F11

4.0 MODEL DESCRIPTION AND DEFINITION OF TEST MATRICES 44 1/F14

4.1 MODEL DESIGN - SYSTEM EVOLUTION 44 1/F14
4.2 DESCRIPTION OF TEST MODELS 48 1/G6
4.3 ACOUSTIC TEST MATRIX 52 1/G12
4.4 LASER VELOCIMETER TEST MATRIX 56 2/A7
4.5 AERODYNAMIC-PERFORMANCE TEST MATRIX 61 2/B1
4.6 DATA SECTION 61 2/B1

5.0 DISCUSSION OF ACOUSTIC TEST RESULTS 63 2/B3

5.1 ESTABLISHMENT OF GROUND RULES FOR ACOUSTIC COMPARISONS AND DATA ILLUSTRATIONS 63 2/B3

5.1.1 Synthesized Baseline 63 2/B3
5.1.2 Average Conical Nozzle Noise Baseline 64 2/B4
5.1.3 Density Normalization and Presentation of Results 64 2/B4
5.1.3.1 Density Normalization Factors 64 2/B4
5.1.3.2 Presentation of Results 70 2/B13

5.2 UNSUPPRESSED COANNULAR NOZZLES 71 2/B14

5.2.1 High Core-Flow Test Results 71 2/B14
5.2.1.1 Overall Power Level Test Results 71 2/B14
5.2.1.2 Power Spectra Test Results 71 2/B14
5.2.1.3 Perceived Noise Level Test Results 71 2/B14
5.2.1.4 Perceived Noise Level Directivity Test Results 75 2/C6
5.2.1.5 Sound Pressure Level Spectra Test Results 75 2/C6
5.2.2 Low Core-Flow Test Results 75 2/C6
5.2.3 Acoustic Correlations 84 2/D5
5.2.4 Summary Remarks 84 2/D5

5.3 MULTIELEMENT FAN-SUPPRESSOR NOZZLES 88 2/D11

5.3.1 High Core Flow Test Results 88 2/D11
5.3.1.1 Overall Power Level Test Results 88 2/D11
5.3.1.2 Power Spectra Test Results 97 2/E11

TABLE OF CONTENTS (continued)

Section | Page

5.3.1.3 Perceived Noise Level Test Results . 97 2/E11
5.3.1.4 Sound Pressure Level Spectra Test Results 98 2/E12
5.3.2 Low Core-Flow Test Results 98 2/E12
5.3.3 Comparisons with Unsuppressed Coannular Nozzles 98 2/E12
5.3.4 Summary Remarks 104 2/F9

5.4 MULTIELEMENT FAN-SUPPRESSOR NOZZLES WITH EJECTORS 104 2/F9

5.4.1 Hardwall Ejector Effects 107 2/F12
5.4.1.1 Overall Power Level Test Results 107 2/F12
5.4.1.2 Power Spectra Test Results 107 2/F12
5.4.1.3 Perceived Noise Level Test Results 107 2/F12
5.4.1.4 Sound Pressure Level Test Results 111 2/G2
5.4.2 Treated Ejector Effects 111 2/G2
5.4.2.1 Overall Power Level Test Results 111 2/G2
5.4.2.2 Power Spectra Test Results 115 2/G6
5.4.2.3 Perceived Noise Level Test Results 115 2/G6
5.4.2.4 Sound Pressure Level Test Results 120 2/G11
5.4.3 Inlet Lip Geometry Effects on the Hardwall Ejector 120 2/G11
5.4.3.1 Power Level Test Results 120 2/G11
5.4.3.2 Perceived Noise Level Test Results 124 3/A8
5.4.3.3 Sound Pressure Level Test Results 124 3/A8
5.4.4 Summary Remarks 124 3/A8

5.5 EVALUATION OF A PARTIAL MECHANICAL SHIELD 130 3/B1

5.5.1 Perceived Noise Level Test Results 130 3/B1
5.5.2 Sound Pressure Level Spectra Results 134 3/B6
5.5.3 Summary Remarks 134 3/B6

6.0 DISCUSSION OF AERODYNAMIC-PERFORMANCE TEST RESULTS 140 3/C1

6.1 THRUST COEFFICIENTS 140 3/C1

6.1.1 Unsuppressed Coannular Nozzle with Plug 140 3/C1
6.1.2 Multichute Fan-Suppressor Nozzle 143 3/C5
6.1.3 Multichute Fan-Suppressor Nozzle with Hardwall Ejector with Sharp Lip 143 3/C5
6.1.4 Multitube Fan-Suppressor Nozzle 150 3/C12
6.1.5 Multitube Fan-Suppressor Nozzle with Hardwall Ejector with Sharp Lip 150 3/C12

6.2 EFFECT OF HOT EXHAUST FLOW ON THE THRUST COEFFICIENT OF THE MULTITUBE FAN-SUPPRESSOR NOZZLE WITH HARDWALL EJECTOR WITH SHARP LIP 156 3/D7

TABLE OF CONTENTS (continued)

Section	Page	
6.3 FLOW COEFFICIENTS	161	3/D14
6.3.1 Unsuppressed Coannular Nozzle with Plug	161	3/D14
6.3.2 Multichute Fan-Suppressor Nozzle	165	3/E6
6.3.3 Multichute Fan-Suppressor Nozzle with Hardwall Ejector with Sharp Lip	165	3/E6
6.3.4 Multitube Fan-Suppressor Nozzle	169	3/E10
6.3.5 Multitube Fan-Suppressor Nozzle with Hardwall Ejector with Sharp Lip	169	3/E10
7.0 DISCUSSION OF LASER VELOCIMETER TEST RESULTS	173	3/E14
7.1 LASER VELOCIMETER PLUME MEASUREMENTS FOR THE UNSUPPRESSED COANNULAR NOZZLE WITH PLUG	173	3/E14
7.1.1 Axial Mean-Velocity Distributions	173	3/E14
7.1.2 Mean-Velocity, Radial-Profile Distributions	176	3/F5
7.1.3 Axial Turbulent-Velocity, Radial-Profile Distributions	176	3/F5
7.2 LASER VELOCIMETER PLUME MEASUREMENTS FOR THE FAN-SUPPRESSED NOZZLES	176	3/F5
7.2.1 Axial Mean-Velocity Distributions	176	3/F5
7.2.2 Mean- and Turbulent-Velocity, Radial-Profile Distributions	180	3/F12
7.2.2.1 Multichute Fan Suppressor	180	3/F12
7.2.2.2 Multitube Fan Suppressor	180	3/F12
7.3 SUMMARY OF OBSERVATIONS	180	3/F12
8.0 DISCUSSION OF ACOUSTIC/AERODYNAMIC-PERFORMANCE CORRELATIONS	186	3/G8
8.1 EVALUATION OF NOISE CANDIDATES FOR DUCT-BURNING TURBOFAN ENGINES	186	3/G8
8.2 LOW CORE-FLOW COMPARISONS	191	4/A6
9.0 CONCLUSIONS AND RECOMMENDATIONS	196	4/A12
9.1 CONCLUSIONS	196	4/A12
9.2 RECOMMENDATIONS	197	4/A13

TABLE OF CONTENTS (concluded)

Section	Page	
APPENDIX A - GENERAL ELECTRIC AIR-ATTENUATION MODEL	199	4/B1
APPENDIX B - POWER LEVEL CALCULATION PROCEDURE	210	4/C1
APPENDIX C - DETAILED DESCRIPTION OF TEST MODELS	214	4/C5
APPENDIX D - ACOUSTIC TEST MATRIX FOR ALL DBTF MODELS AND EXAMPLE DATA PRINT OUT SHEETS	221	4/D3
APPENDIX E - FAN PLUG PRESSURE DISTRIBUTIONS FOR AERODYNAMIC MODEL 5	240	4/F13
APPENDIX F - MODEL 7 AXIAL-VELOCITY PROFILES	249	5/A8
APPENDIX G - MODEL 7 AXIAL-VELOCITY PROFILES WITH NO CORE FLOW	270	5/D7
APPENDIX H - MODEL 7 AXIAL-VELOCITY PROFILES WITH NO FAN FLOW	286	5/F10
APPENDIX I - MODEL 1 AXIAL-VELOCITY PROFILES	295	5/G13
APPENDIX J - MODEL 2 AXIAL-VELOCITY PROFILES	303	6/B6
APPENDIX K - NOMENCLATURE	313	6/C11
REFERENCES	317	6/D1

One of the most important results of the acoustic tests performed on this program was the demonstrated suppression inherent in the unsuppressed coannular nozzle arrangements. High levels of suppression were obtained without mechanical suppressor elements and their associated thrust losses; thus, the unsuppressed coannular nozzle with plug (Model 7) is an attractive exhaust system which should be considered in future advanced, supersonic-cruise vehicle/multiple-engine cycle studies.

8.2 LOW CORE-FLOW COMPARISONS

The previous sections present the aerodynamic and acoustic trends associated with duct-burning turbofan/high core-extraction engine cycles as well as some insight on the impact of reducing the fan/core velocity ratios below 1.0. As discussed in Sections 5.3 and 5.4, when the core flow is inhibited ($V_f >> V_c$), acoustic effectiveness is essentially retained. This characteristic obviously makes the high radius-ratio annular nozzle/"low core flow" concept very amenable to other advanced engine cycles.

Annular nozzles with and without low amounts of center flow have often been considered as potential suppression concepts. As early as 1957, acoustic tests were conducted on small, subsonic, coannular/coplanar nozzles of various diameters and velocity ratios (Reference 16): annulus radius ratios ranged from 0.65 to 0.85. In general, it was found that these coannular/coplanar jets have substantial noise reduction. Some of the high fan/core velocity ratio (> 3.0) data in Reference 16 were utilized in a portion of the correlations to follow.

In 1969, the Naval Air Propulsion Test Center published a report (Reference 17) summarizing all of the studies and model exhaust-suppressor experiments, noise and performance, conducted at the center from 1963 to 1969. Most of the testing was carried out at a pressure ratio of 2.0 and 1368° R (760 K), using 2.6-inch (6.6 cm) equivalent diameter nozzles. In the course of those experiments, it was found that high radius annular nozzles with so-called center-aspiration (e.g., vented to ambient) exhibited substantial sound power level reductions ranging from 6.5 dB to 11.0 dB for annulus radius ratios of 0.82 to 0.96, respectively. One of the suppressor nozzles evaluated was an eight-lobe, ventilated-to-ambient, annular nozzle; however, the results were somewhat less attractive ($\sim$ 2 to 3 dB noise reduction) than the results of the program documented in this report. Performance (C_T) was less than desirable due to the large inner flow area which was vented to ambient. Reductions of ΔC_T relative to a circular nozzle ranged anywhere from 5 to 10%. Pressurization (flowing) of the inner flow area probably could have improved this somewhat.

In the American SST program, Boeing and General Electric conducted extensive tests on various high suppression (12-20 ΔPNdB) exhaust systems. These were probably some of the first exhaust systems where consideration was given to installation complexity on aircraft/engine systems. In the Boeing Summary report (Reference 18) all the activity on the SST program from 1966 to 1971, is summarized; Reference 18 also includes a "pure" annulus nozzle with the center ventilated to ambient and a suppressed version with 60 well-ventilated lobes. Peak PNL suppressions at a 1500-ft (457.2 m) sideline were found to range from 6.3 to 13.5 PNdB, at a velocity of 2400 ft/sec (731.5 m/sec), for the unsuppressed and suppressed annulus nozzle concepts, respectively. Static aerodynamic-performance losses were on the high side; thrust losses (ΔC_T referenced to conical nozzle) were found to range from 8 to 9.3% for both annular nozzles.

As seen from the above discussion, high radius-ratio annular nozzles with low amounts of center or core flow have previously been studied, but they have not been pursued for a variety of reasons.

The tests conducted by General Electric on this program have prompted a second look at some of these early experimental results in the hope of establishing some correlating parameter(s) as well as establishing some evaluation of their noise/performance trades. The study conducted and summarized below considered only low core flow, low core velocity, or center-hole-ventilated-to-ambient configurations.

A correlating parameter that was found useful was the mean-circumference/annulus-height ratio, first used at the Naval Air Propulsion Test Center (NAPTC). This correlation factor was useful in that it combined two key parameters: effective peripheral shear area and characteristic height, both of which can be related to some measure of the noise reduction measured in the far field. The mean circumference can be envisioned as indicative of the low frequency noise generation region, i.e. the merged and postmerged portion of the jet, while the annulus height could be the characteristic dimension controlling the high frequency portion of the jet noise spectrum.

Figure 131 summarizes overall power level reductions for some of the early low jet velocity coannular (at high V_f/V_c's) and annular flow (with small amounts of center flow) test results along with results of unsuppressed coannular nozzles from this program. Considering that the suppression levels shown were obtained from various testing approaches, (e.g., reverberant rooms, outdoor test stands, etc.), the data collapse is seen to be quite good. Only one piece of data is suspect and that was obtained during the 1957 period with a rather high core velocity, even though the fan velocity was a factor 3 greater. In spite of this, the trend is clear; it suggests that unsuppressed annular nozzles with low core flows are most effective (ΔOAPWL ≈ 8.9 dB) around 60 to 80 mean-circumference/annulus-height range (radius ratio ≈ 0.85 to 0.90). Above 60 to 80 mean-circumference/annulus-heights the acoustic/performance payoff appears insignificant. The lower half of Figure 131 presents some aerodynamic-performance results obtained by NAPTC in terms of thrust loss relative to a conical nozzle at a pressure ratio of 2.0; however, aerodynamic-performance data recorded by Boeing during the SST high suppression program phase (Reference 18) suggest these NAPTC thrust decrements are too low by at least a factor of two.

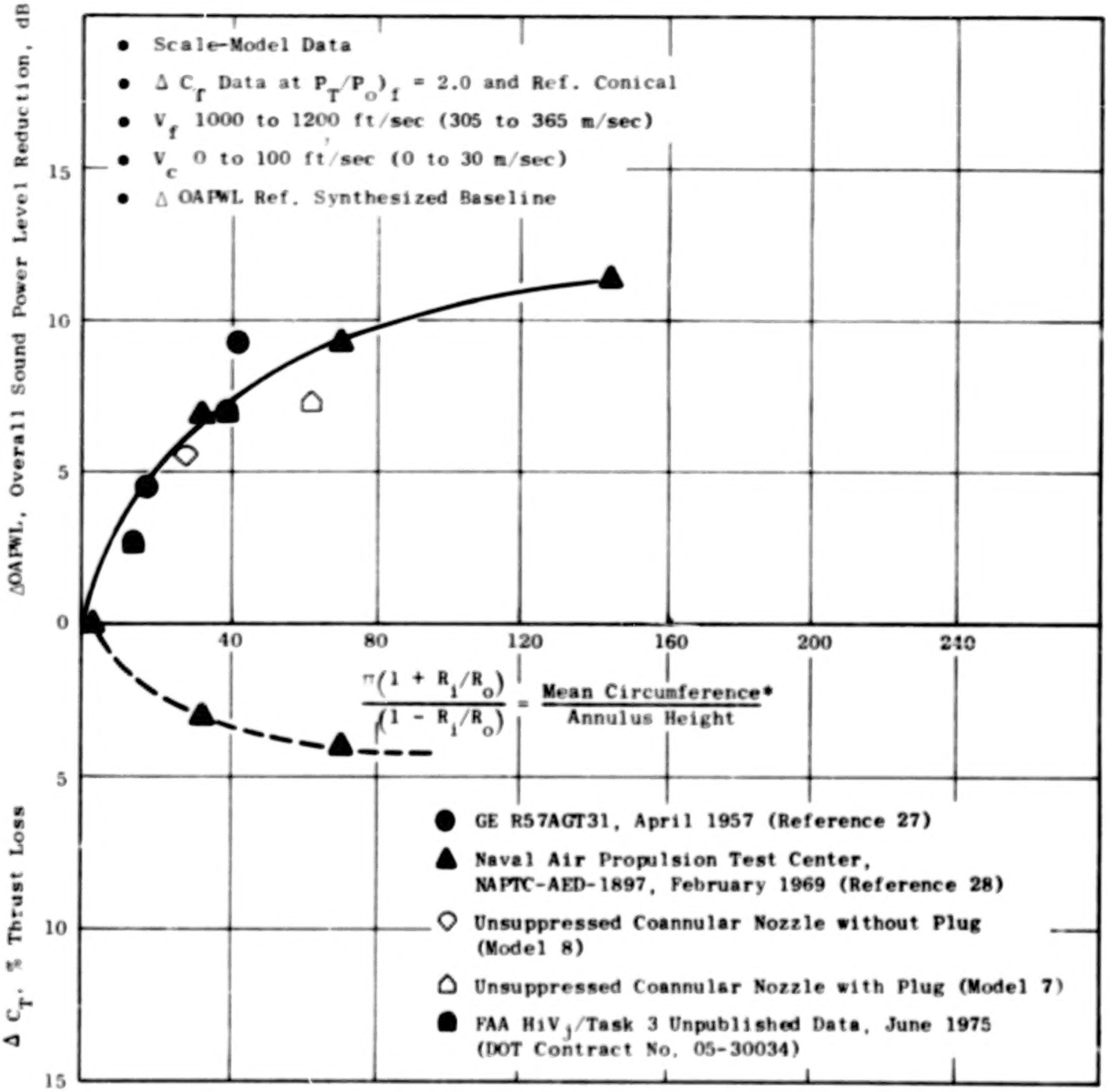

*

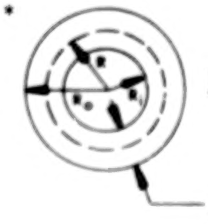
R
R$_o$
R$_i$
Fan Annulus: h = R$_o$ - R$_i$

$$\frac{\text{Mean Circumference}}{\text{Annulus Height}} = \frac{2\pi R}{h} = \frac{2\pi\left(\frac{R_o + R_i}{2}\right)}{R_o - R_i} = \frac{\pi(1 + R_i/R_o)}{(1 - R_i/R_o)}$$

Figure 131. Single-Stream Annular Nozzle Inherent Suppression Correlation.

The above evaluation was further substantiated by reviewing test results of fan-suppressed and unsuppressed coannular nozzles in terms of peak PNL, as shown in Figure 132. Considering the diversity of designs and sources of data, definite trends are apparent. Suppressed fan nozzle noise reductions up to 15 PNdB are possible in the 20 to 30 mean-circumference/annular-height ratio range (radius ratio ≈ 0.75), while unsuppressed noise reductions up to 10 PNdB, corresponding to radius ratios of 0.90, are indicated.

In summary, the aerodynamic and acoustic data suggest that further development work in optimizing the various critical aerodynamic and geometric nozzle parameters could conceivably yield high acoustic/aerodynamic-performance payoffs. This is particularly true if the unsuppressed "inherent suppression" levels can be maximized and maintained during flight conditions.

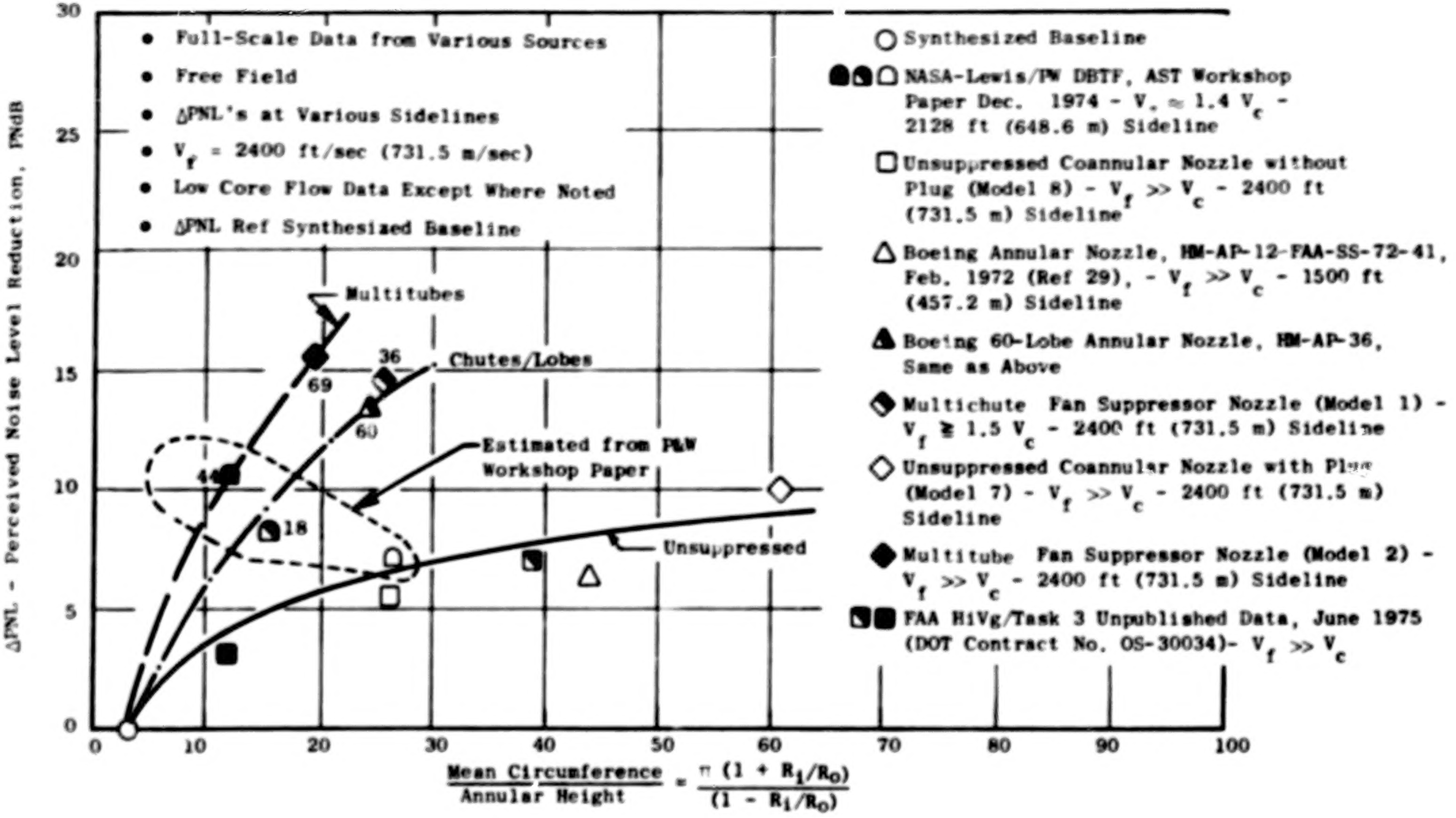

Figure 132. Correlations of PNL Suppression for Potential Unsuppressed/Suppressed Annular Nozzles with Low Core Flow Relative to Synthesized Baseline Data.

9.0 CONCLUSIONS AND RECOMMENDATIONS

9.1 CONCLUSIONS*

A total of 11 coannular nozzle configurations with fan velocities suitable for duct-burning turbofan and other multiple-flow, advanced, supersonic transport (AST) engine applications were tested in model scale. Configurations were selected and designed to represent practical separate-flow exhaust systems.

When compared to jet noise levels predicted by summing the noise of two independent and equivalent jet streams without any interaction benefits, all the configurations tested exhibited very significant noise reductions. The static aerodynamic-performance degradation was relatively small.

A large bank of acoustic and aerodynamic data for these configurations was obtained; over 600 acoustic data points covering fan to core velocity ranges of 0.4 to 2.0, temperatures from ambient to 1960° R (1089 K), and nozzle total pressure ratios from 1.16 to 3.9 were taken. The following are the most significant results:

- The unsuppressed, coannular nozzle with plug exhibited up to 10 PNdB noise reduction (ΔPNdB) when compared to predicted noise levels of the sum of two independent but equivalent jet streams. Good static aerodynamic-performance (gross thrust coefficient, C_T, = 0.97) was also obtained.

- When the unsuppressed, coannular, plug nozzles were tested with small amounts of core-stream flow, substantial noise reduction was maintained (8 PNdB noise reduction levels).

- The multielement fan-suppressor nozzle systems demonstrated noise reduction levels of 15 PNdB.

- From comparisons of noise levels of the unsuppressed coannular-flow nozzles with and without a plug, and from laser velocimeter velocity-decay measurements, the importance of a high radius ratio design for high suppression may be inferred.

- Aerodynamic-performance penalties were relatively small; static noise/performance ($\Delta PNL/\Delta C_T$) trades of greater than 3.0 resulted when referenced to the unsuppressed, coannular nozzle with plug.

- The addition of an acoustically treated ejector on the multielement fan-suppressor nozzles increased the suppression levels to 17 to 18 PNdB.

- Hardwall ejectors essentially offered no acoustic benefit on a PNdB basis.

- A partial mechanical shield showed no measureable noise reduction capability when tested with the multichute fan-suppressor nozzle.

- Laser velocimeter plume surveys provided useful information of velocity gradients, shear boundaries, and turbulence levels in the jet flow. Suppression levels were seen to be qualitatively in agreement with the velocity-profile decay characteristics documented.

9.2 RECOMMENDATIONS

Based on the studies conducted during the contract effort, the following items warrant future investigation:

- A systematic investigation of the aerodynamic-performance and noise-reduction features of the unsuppressed, coannular, acoustic nozzle with plug should be undertaken. This investigation should include parametric studies of the key geometric variables (area ratio, radius ratio, core plug shape, etc.) and flow-management effects (low core flows, high core flows, velocity and temperature profile influences, etc.).

- The flight effect on the noise characteristics and the aerodynamic performance of the unsuppressed, coannular-flow nozzles with plug should be undertaken.

- Detailed acoustic prediction schemes for the unsuppressed, coannular-flow plug nozzles should be formulated from the existing data sources as well as from any results which become available from future test programs.

---

*Author's note: Since the completion of the work for this contract, a considerable amount of new testing has been performed on high-radius-ratio, coannular, plug nozzles under contract NAS3-19777. The results of these tests will be published at a later date; however, it is worthwhile to indicate, to the interested reader, some of the newer findings.

1. When referencing suppression levels to a conical nozzle, analysis of test measurements indicates comparison should be made at equivalent specific thrust (ideal total thrust/ideal total weight flow). This is particularly true for the overall acoustic properties such as $\text{OASPL}_{\text{max}}$, OHPWL, and PNL_{max}; for these overall acoustic parameters, the specific thrust is the recommended correlating parameter rather than, say, the outer-stream velocity. However, when correlation of SPL spectra is approached, it is fully expected that the outer-stream velocity will play a role in the proper selection of characteristic velocity (particularly for high-frequency, coannular-plug-nozzle noise).

2. The unsuppressed, coannular, plug nozzles enjoy two types of jet-noise reduction. The first is turbulent-mixing-noise reduction observed in the aft quadrant. (Turbulent-mixing noise is here meant to include all the usual jet-noise generation mechanisms such as turbulent mixing, convection amplification, fluid shielding, etc.) The second type of noise reduction is associated with shock-generated noise observed in the forward quadrant.

3. In selecting an "optimum" coannular-plug-nozzle arrangement the choice of the outer-stream radius ratio, the inner-to-outer-stream velocity ratio, and the inner-to-outer-stream area ratio need to be considered.

4. Wind tunnel aerodynamic measurements indicate that aircraft simulated-flight thrust coefficients are quite good for the unsuppressed, coannular, plug nozzles: $C_T \approx 0.97$ at $M_o = 0.36$.

APPENDIX A

GENERAL ELECTRIC AIR-ATTENUATION MODEL

The air attenuation used for JENOTS data was developed in 1973 by R.G. Fogg of General Electric (Reference 8). Mr. Fogg noticed that a linear extrapolation of the SAE/ARP 866 curves (Reference 4) or the prediction of Harris (Reference 6) tended to distort the spectral shape for frequencies above 20 kHz when the data was scaled or PWL was calculated as seen in Figures 133 and 134. He hypothesized that this distortion was the result of applying excessive air attenuation at the high frequencies. From Harris' data, it was clear that the molecular absorption diminished in percent of the total absorption as the frequency increased leaving the classical absorption as the dominant attenuator. By curve fitting the trends of the classical and molecular absorption with frequency at various humidities and a temperature such as in Figure 135, a family of prediction curves as shown in Figure 136 was developed. For comparison, a similar presentation from Harris (Reference 6) and Evans (Reference 9) is given in Figures 137 and 138 respectively.

Table XI is a listing of the computer program used to generate the correction factors. With the wet and dry bulb temperatures given in the "Acoustic Test Matrix for all DBTF Models" - Appendix D, Tables XII through XXII, one can calculate the value of the air-attenuation corrections applied to the data presented in this report.

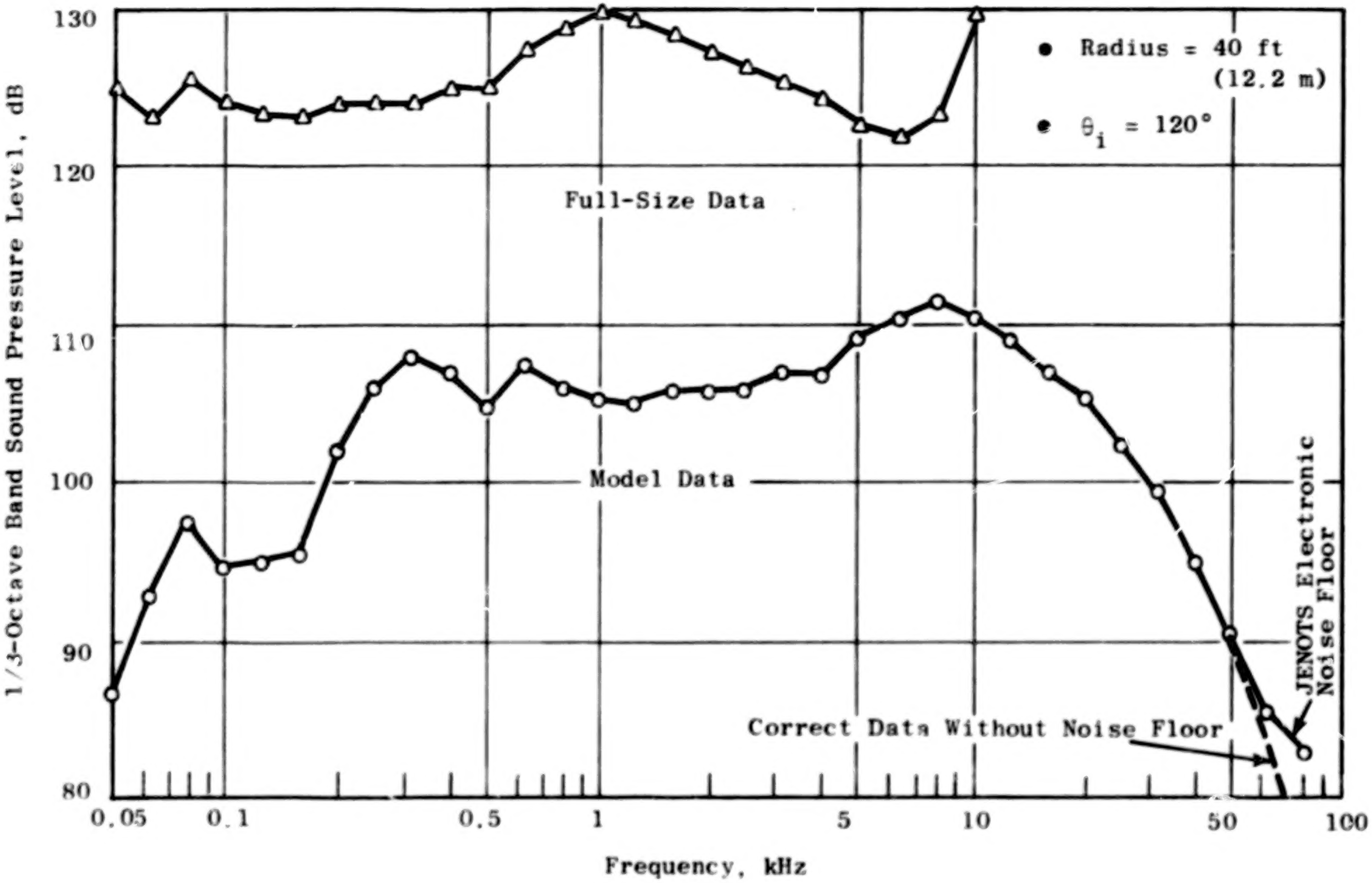

Figure 133. JENOTS Data: SPL Spectra, FSDR Program Calculation.

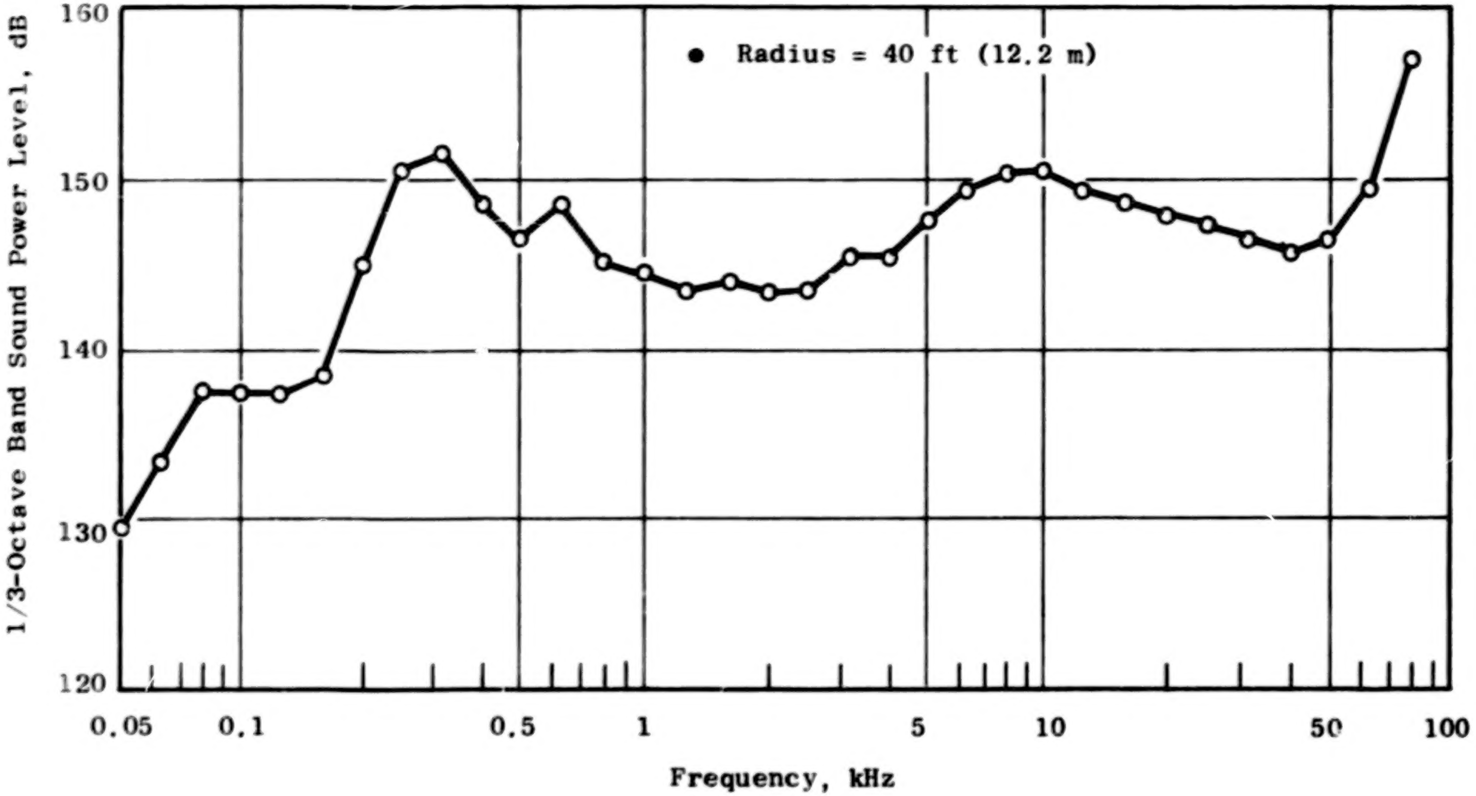

Figure 134. JENOTS Data: SPL Spectra, FSDR Program Calculation.

201

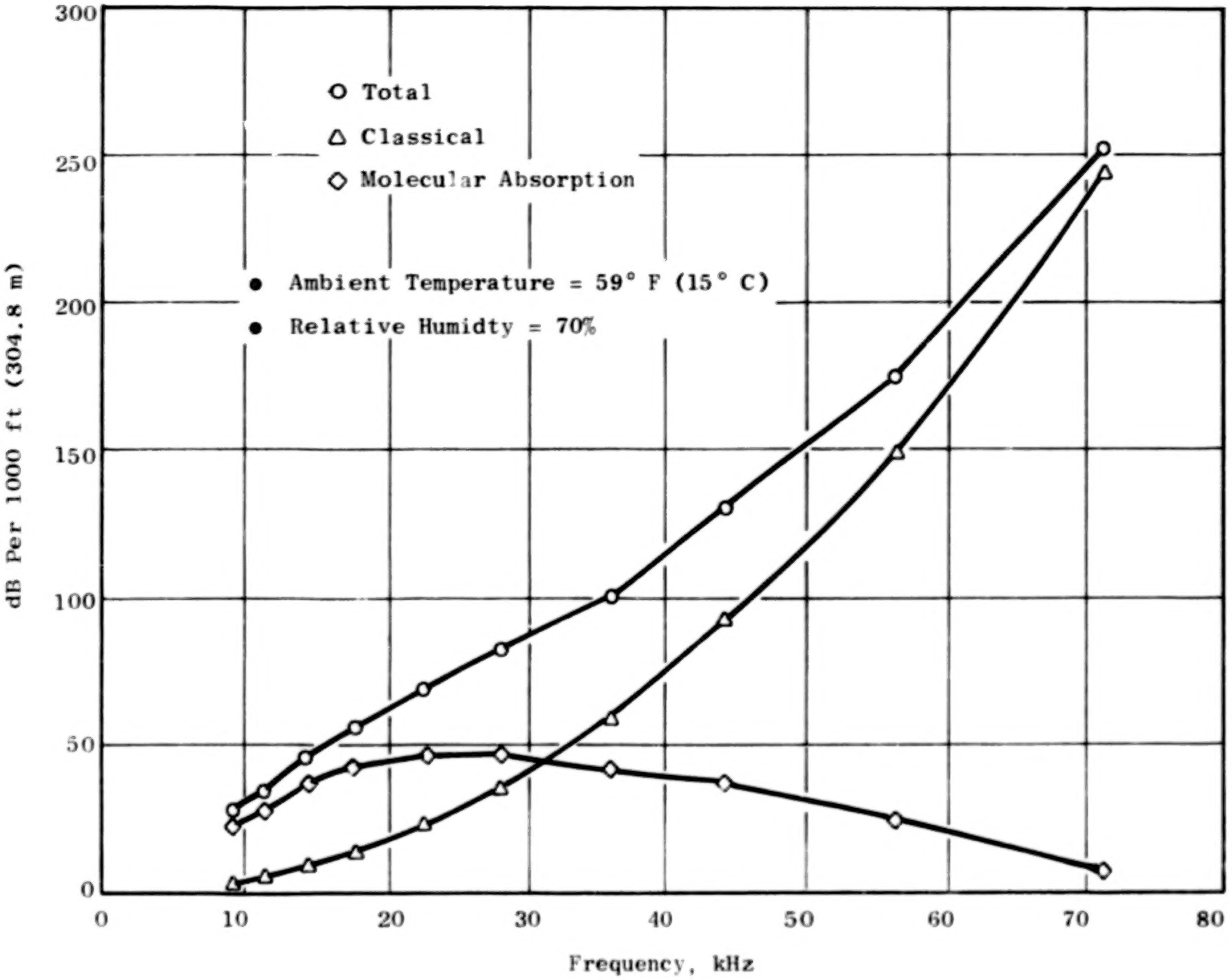

Figure 135. Revised Atmospheric Correction Factors.

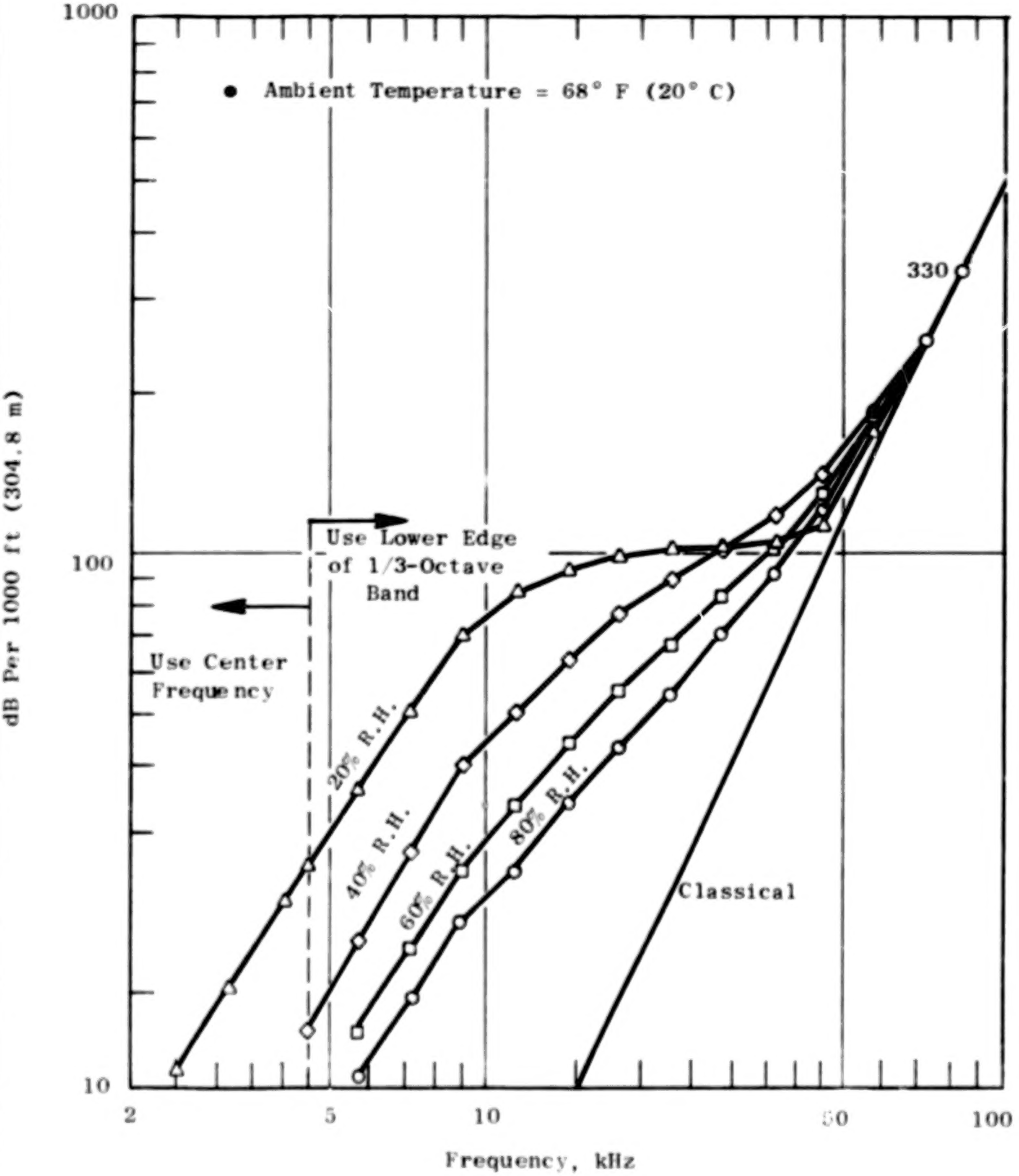

Figure 136. Revised Atmospheric Absorption.

(Reference Figure 3.2, Page 3-3, "Harris Handbook of Noise"

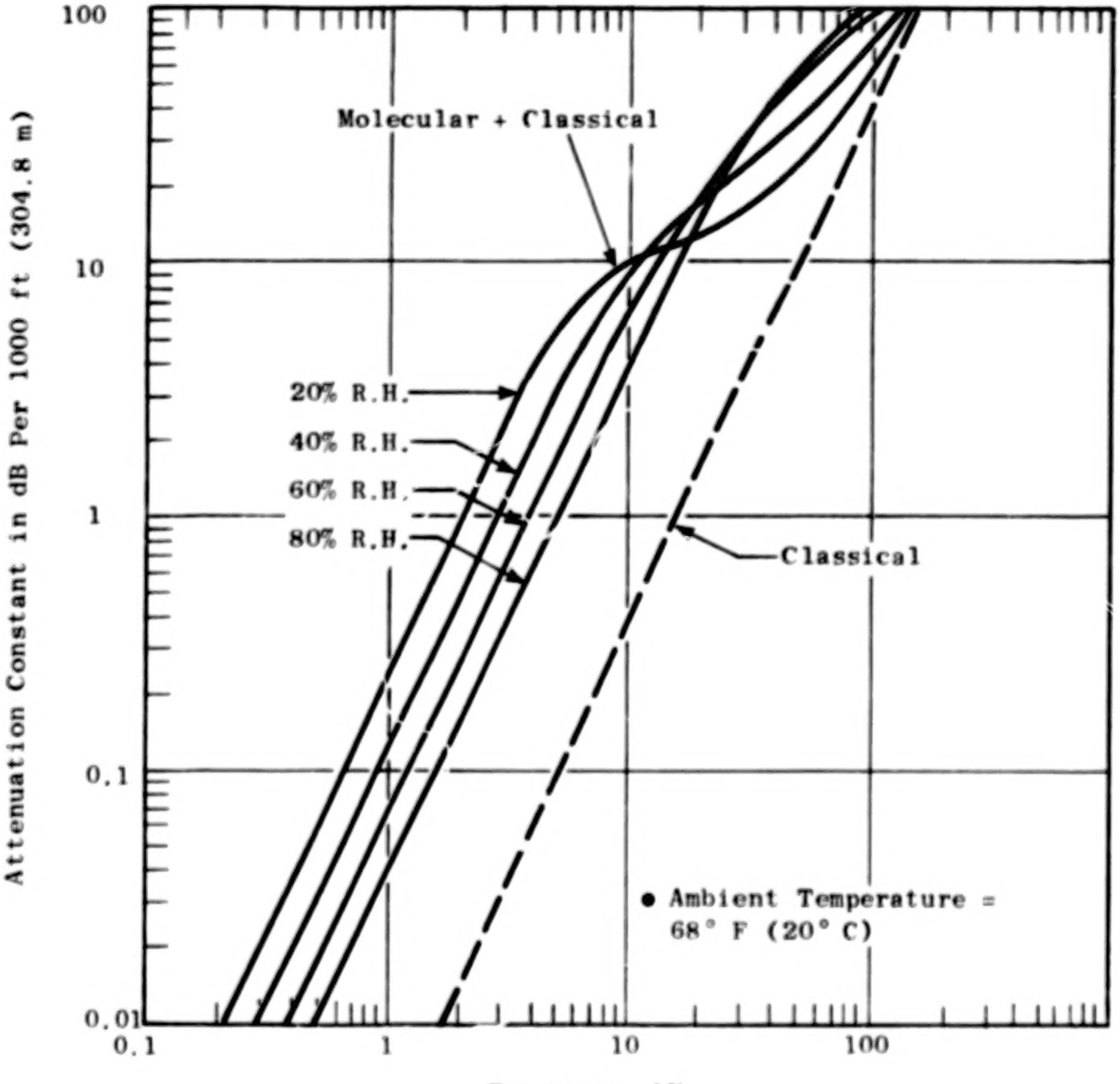

Figure 137. Atmospheric Attenuation Factors.

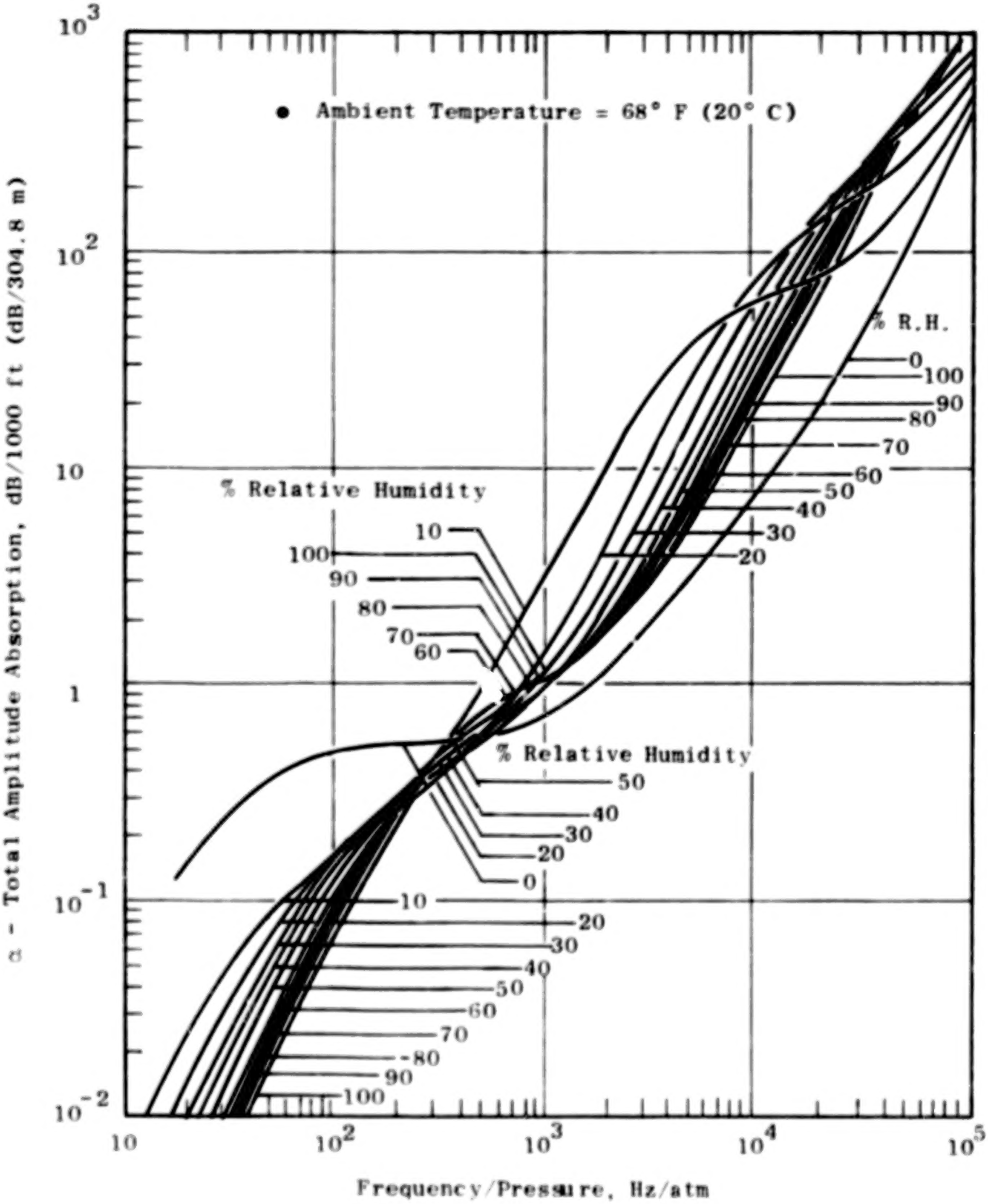

Figure 138. Total Absorption of Sound in Air as a Function of Frequency.

Table XI. Listing of the GE Air-Attenuation Correction Computer Program.

```
10 REM THIS PROGRAM PROVIDES CORRECTION FACTORS AND INCREMENTAL
11 REM SPHERICAL AREAS FOR THE FAR FIELD CALCULATIONS. SEE TIME
12 REM SHARE PROGRAM "FARFLD". INPUT AMBIENT ATMOSPHERIC
13 REM CONDITIONS AND ARC RADIUS AT LINE 90. INPUT MICROPHONE
14 REM ANGLE LOCATIONS AT LINE 840.
30 DIM C(24),E(24),F(24),G(24),H(24),K(24),M(20),N(20)
31 DIM P(20),S(20),Z(20)
40 FOR I = 1 TO 24
50 READ F(I)
60 DATA 500,630,800,1000,1250,1600,2000,2500,3150,4000,
70 DATA 5000,6300,8000,10000,12500,16000,20000,25000,
71 DATA 31500,40000,50000,63000,80000,100000
72 NEXT I
75 REM "T1" IS WET BULB TEMPERATURE IN DEGREES F. "T3" IS
76 REM ATMOSPHERIC TEMPEATURE IN DEGREES F. "P1" IS ATMOSPHERIC
77 REM PRESSURE IN INCHES OF HG. "R2" IS SPHERICAL RADIUS IN FT.
80 READ T1,T3,P1,R2
90 DATA 33,40,29.921,1000
95 REM THE FOLLOWING CALCULATIONS ARE FOR ABSOLUTE HUMIDITY.
100 LET T2 = ((5/9)*(T1 - 32)) + 273.16
110 LET X1 = 647.27 - T2
111 READ B6,B7,B8,B9
112 DATA 3.2437814,5.86826E-3,1.1702379E-8
113 DATA 0.89
120 LET A5 = B6 + B7*X1 + B8*X1↑3
130 LET A1 = 1 + 2.187846E-3*X1
140 LET A2 = (X1/T2)*(A5/A1)
141 READ C6,C7
142 DATA 218.167,14.6959
150 LET P = (C6/10↑A2)*C7
160 LET A3 = ((P1*0.49115)-P)*(T3 - T1)
170 LET P2 = P - ((A3)/(2755 - 1.28*T1))
171 READ C8,C9,D5,D6
172 DATA 144,460,85.7,16.02E3
180 LET A4 = ((P2*C8)/((T3 + C9)*D5))*D6
181 PRINT "AMBIENT TEMPERATURE =";T3;"DEGREES F"
182 PRINT "WET BULB TEMPERATURE =";T1;"DEGREES F"
183 PRINT "BAROMETRIC PRESSURE =";P1;"INCHES OF HG"
184 PRINT
185 PRINT "ABSOLUTE HUMIDITY (HA) =";A4;"GRAMS PER CUBIC METER"
187 LET D1 = P1/29.921
188 LET D2 = (T3 + 460)/519
```

Table XI. Listing of the GE Air-Attenuation Correction Computer Program (Continued).

```
189 LET D3 = (SQR(D2))/D1
190 PRINT " IMPEDENCE CORRECTED TO STD. DAY =";D3*2.227525E-6
191 PRINT
192 PRINT
193 REM THE FOLLOWING CALCULATIONS ARE FOR ALPHA MOL MAX
200 REM H MOL MAX
205 READ F1,F2,F3,F4,F5,F6
210 FOR I = 1 TO 24
220 IF F(I) > 4000 THEN 227
225 LET A6 = F(I)
226 GO TO 230
227 LET A6 = B9*F(I)
230 LET LET H(I) = 0.028961*A6↑0.51093
235 IF F(I) > 4000 THEN 250
240 LET A6 = F(I)
245 GO TO 260
250 LET A6 = B9*F(I)
260 LET C(I) = A6*0.00357451*EXP(0.0117537*T3)
261 IF A6 < 8900 THEN 266
263 DATA .15023777E02,.83707731E-02,.36541712E-06,.56857640E-11
264 DATA -0.31243498E-16,.0117537
265 LET C(I) = (F1+F2*A6+F3*A6↑2+F4*A6↑3+F5*A6↑4)*EXP(F6*(T3-59))
266 IF F(I) > 4000 THEN 269
267 LET A6 = F(I)
268 GO TO 270
269 LET A6 = B9*F(I)
270 LET Y4 = 0.279129E-7*A6↑2.05403
280 LET Y5 = 0.261933E-7*A6↑2.05081
290 LET K(I) = Y5 + (Y4 - Y5)*(T3 -32)/68
300 REM THE FOLLOWING CALCULATIONS ARE FOR ALPHA MOL OVER
301 REM ALPHA MOL MAX
305 LET A7 = A4/H(I)
310 IF A7 > 6.5 THEN 440
320 IF A7 < 1.0 THEN 380
330 LET Y1 = (0.13955546E-2*A7) - 0.35055924E-1
340 LET Y2 = (Y1*A7) + 0.28072773
350 LET Y3 = (Y2*A7) - 0.10581673E1
360 LET Z(I) = (Y3*A7) + 0.18209020E1
370 GO TO 450
380 LET Y1 = (0.74335316E1*A7) - 0.171860E2
390 LET Y2 = (Y1*A7) + 0.11814166E2
400 LET Y3 = (Y2*A7) - 0.23792759E1
```

Table XI. Listing of the GE Air-Attenuation Correction Computer Program (Continued).

```
410 LET Y4 = (Y3*A7) + 0.13220157E1
420 LET Z(I) = (Y4*A7) + 0.5230581E-3
430 GP TO 450
440 LET Z(I) = 0.2
450 LET Z(I) = 0.001*INT(1000*Z(I) + 0.5)
460 LET E(I) = Z(I)*C(I)
470 REM THE FOLLOWING CALCULATIONS ARE FOR THE EGA CORRECTION
480 LET R1 = R2
510 LET C1 = (0.20411435E-20*R1) - 0.66703093E-16
520 LET C2 = (C1*R1) + 0.72854603E-12
530 LET C3 = (C2*R1) - 0.32650913E-8
540 LET C4 = (C3*R1) + 0.49614255E-5
550 LET C5 = (C4*R1) + 0.44663072E-2
560 LET G1 = (C5*R1) + 0.59387702
570 LET E1 = (0.16573369E-24*R1) - 0.46152934E-20
580 LET E2 = (E1*R1) + 0.32361609E-16
590 LET E3 = (E2*R1) + 0.39118972E-13
600 LET E4 = (E3*R1) - 0.10464995E-8
610 LET E5 = (E4*R1) + 0.29126338E-5
620 LET E6 = (E5*R1) - 0.54370996E-3
630 LET G2 = (E6*R1) + 0.59506112
650 IF R1 <= 4000 THEN 680
660 LET G1 = 5.010264
670 LET G2 = 15.44041 + 0.0001*(R1 - 4000)
680 IF F(I) = 63 THEN 720
690 IF F(I) >= 2000 THEN 740
700 LET Z1 = 0.2*((LOG(F(I)/62.5))/LOG(2))
710 GO TO 750
720 LET Z1 = 0
730 GO TO 750
740 LET Z1 = 1.0
750 LET G(I) = (Z1*(G1 - G2)) + G2
760 NEXT I
765 PRINT "CORRECTION FACTORS IN DB AT ARC RADIUS =";B2;
766 PRINT "FEET"
770 PRINT "FREQUENCY";TAB(11);"CLASSICAL";TAB(22);
771 PRINT "MOL.ABSORB.";TAB(36);"TOTAL ABSORB";TAB(51);
772 PRINT "EGA";TAB(63);"TOTAL CORR"
790 FOR I = 1 TO 24
800 PRINT F(I);TAB(8);K(I)*R2/1000;TAB(22);E(I)*R2/1000;
801 PRINT TAB (36);(K(I)+E(I))*R2/1000;TAB(51);G(I);TAB(63);
802 PRINT ((K(I)+E(I))*R2/1000)+G(I)
```

Table XI. Listing of the GE Air-Attenuation Correction Computer Program (Concluded).

```
810 NEXT I
820 REM THE FOLLOWING CALCULATIONS ARE FOR STRIP AREA
821 PRINT
822 PRINT
825 PRINT "ANGLE LOCATION","STRIP AREA FOR";R2;
826 PRINT "FOOT SPHERICAL RADIUS"
827 PRINT "(DEGREES)","SQ. FT.)"
830 REM "M(I)" AND "N(I)" ARE ANGLES WHICH DEFINE THE ARC
831 REM ASSIGNED TO EACH MICROPHONE. "P(I)" IS THE
840 REM MICROPHONE LOCATION ANGLE.
845 READ F1,F2,F3,F4
846 DATA 1.5,3.1416,2,0.0174533
850 READ N
855 DATA 17
860 FOR I = 1 TO N
870 READ P(I)
875 NEXT I
880 DATA 0,10,20,30,40,50,60,70,80,90,100,110
881 DATA 120,130,140,150,160
895 FOR I = 1 TO N
900 LET M(I) = P(I) - (P(I) - P(I-1))/F3
910 LET N(I) = (P(I+1) - P(I))/F3 +P(I)
915 IF I = 1 THEN 917
916 GO TO 920
917 LET M(I) = P(I) - (P(I+1)-P(I))/F3
920 IF M(I) < 0 THEN 940
930 GO TO 950
940 LET M(I) = 0
950 IF N(I) > 180 THEN 970
954 IF I = N THEN 962
958 GO TO 980
960 GO TO 980
962 LET N(I) = P(I) + (P(I) - P(I-1))/F3
966 GO TO 980
970 LET N(I) = 180
980 LET S(I) = F1*F2*R2↑F3*(COS(M(I)*F4) - COS(N(I)*F4))
990 PRINT P(I),S(I)
995 NEXT I
1000 END
```

APPENDIX B

POWER LEVEL CALCULATION PROCEDURE

This appendix presents the procedure utilized in the General Electric data reduction computer program to calculate acoustic power level. This existing program did not utilize ground reflection corrections; hence, all the DBTF computer printouts reflect levels on the basis of a three-quarter sphere. A short paragraph describing the correction procedure for full-spherical radiation utilized for all the acoustic data presented in the final report concludes this appendix.

In its basic form the sound power can be handled as the energy density or energy flowing through a unit area in a unit time and expressed in watts as:

$$W = (\text{Intensity}) \times (\text{Area})$$

The acoustic power level by definition is expressed as the logarithm of a ratio as:

$$PWL = 10 \log (W/W_{Ref})$$

where the reference power is chosen as 10^{-13} watts. Now intensity can be expressed as:

$$I = P^2/\rho c$$

For a unit pressure of one dyne on a standard day we find that:

$$P^2/\rho c = 2.2275248 \times 10^{-6}$$

In practice, the impedance (ρc) is corrected from actual conditions by multiplying by $\delta\sqrt{\theta}$, where **theta is T_o/T_{Std} and delta is P_o/P_{Std}.**

The pressure term comes from the measured SPL values which are defined as:

$$SPL = 10 \log (P^2/P^2_{Ref})$$

In our work by definition, P_{Ref} = 0.0002 microbar and we can write $P^2 = 4 \times 10^{-8} \times 10^{SPL/10}$.

The sound pressure is assumed to propagate with a spherical wave front. The area of the truncated spherical surface to be used in calculation depends upon the reflection coefficient as well as the source height.

Thus, $A = 2\pi R^2 [(1 + q) + H/R\ (1 - q)]$

where:

R = distance from source to microphone

H = source height above flat ground

q = reflection coefficient of the ground surface
q = 1 for a perfect reflector and q = 0 for a perfect absorber

Assume that the source height is small compared to the measuring distance so that H/R can be set to zero. Assume that q = 0.5.

Then, $A = 2\pi R^2 \times 1.5$

which reduces to the area of a three-quarter sphere. The surface area is portioned into strips and assigned to microphone positions as follows:

Deriviation of the Spherical Strip Area Relationship

a) Let:

A = Spherical area segment assigned to point "p"

S = Circumference

R = Spherical radius

θ = Angle in horizontal plane

γ = Angle in vertical plane
(See Figure 139 for definition of geometric relationship.)

b) Next:
For a given intersecting plane and defining angle, γ, the circumference is computed as $S = \int_0^{2\pi} R \times \Delta\gamma$ so that the increment is $Rd\gamma$.

c) Now:
For a particular strip area, the radius used to calculate the circumference is related to the spherical radius by $R' = R \times \sin\theta$.

d) Also:
The strip width is given by $R \times d\theta$.

e) Thus:
The incremental stip area is $(R \times d\theta)(R \times \sin\theta)(d\gamma)$.

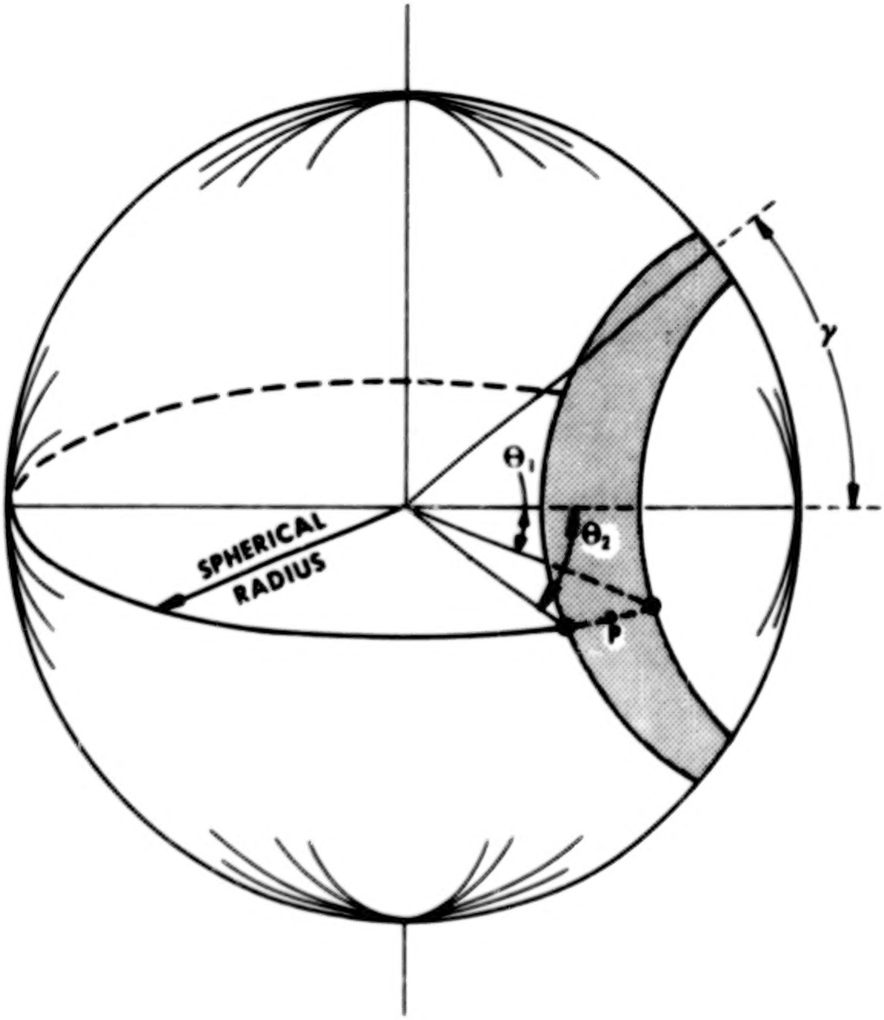
γ
Θ₁
Θ₂
SPHERICAL
RADIUS
φ

Figure 139. Spherical Strip Area Calculation, Definition of Geometry.

f) Therefore:

Considering limits we have

$$A = R^2 \int_0^{\frac{3}{2}\pi} d\gamma \times \int_{\theta_1}^{\theta_2} \sin \theta \times d \theta$$

$$A = \frac{3}{2} \pi R^2 \left[- \cos \theta_2 - (- \cos \theta_1)\right]$$

$$A = \frac{3}{2} \pi R^2 (\cos \theta_2)$$

Returning to the original power definition, we can now write the incremetnal power as:

$$\Delta W = 1/\rho c \times \Delta A \times P^2$$

or:

$$\Delta W = (2.2275248 \times 10^{-6}) \times \sqrt{\theta/\delta}\ 8\ [3/2\pi R^2(\cos \theta_1 - \cos \theta_2)] \times (4 \times 10^{-8}) \times 10^{SPL/10}$$

Thus, the power level is:

$$PWL = 10 \log \frac{\Sigma \Delta W}{10^{-13}}$$

Correction to Free Field

All the acoustic power print-out data, from the procedure just described, presented in this final report were adjusted to reflect full-spherical radiation.

When the data have been corrected for ground reflections, influence of the ground plane has been essentially eliminated and the sound power radiates over the total spherical area. The adjustment to levels calculated on the basis of a three-quarter pressure sphere (as was the case in the DBTF computer printouts) is as follows:

Note: surface area of sphere is $4\pi R^2$

surface area of 3/4 sphere is $3\pi R^2$

Thus, adjustment to Power Level is $10 \log_{10} 4\pi R^2 - 10 \log_{10} 3\pi R^2$
$\Delta = 10 \log_{10} 4\pi - 10 \log_{10} 3\pi = 10.99-9.74 = 1.25$; e.g. 1.3 dB was added to the computer printout PWL to account for true free-field conditions.

APPENDIX C

DETAILED DESCRIPTION OF TEST MODELS

Figures 140 through 145 are dimensioned schematic illustrations of the test models discussed in this report.

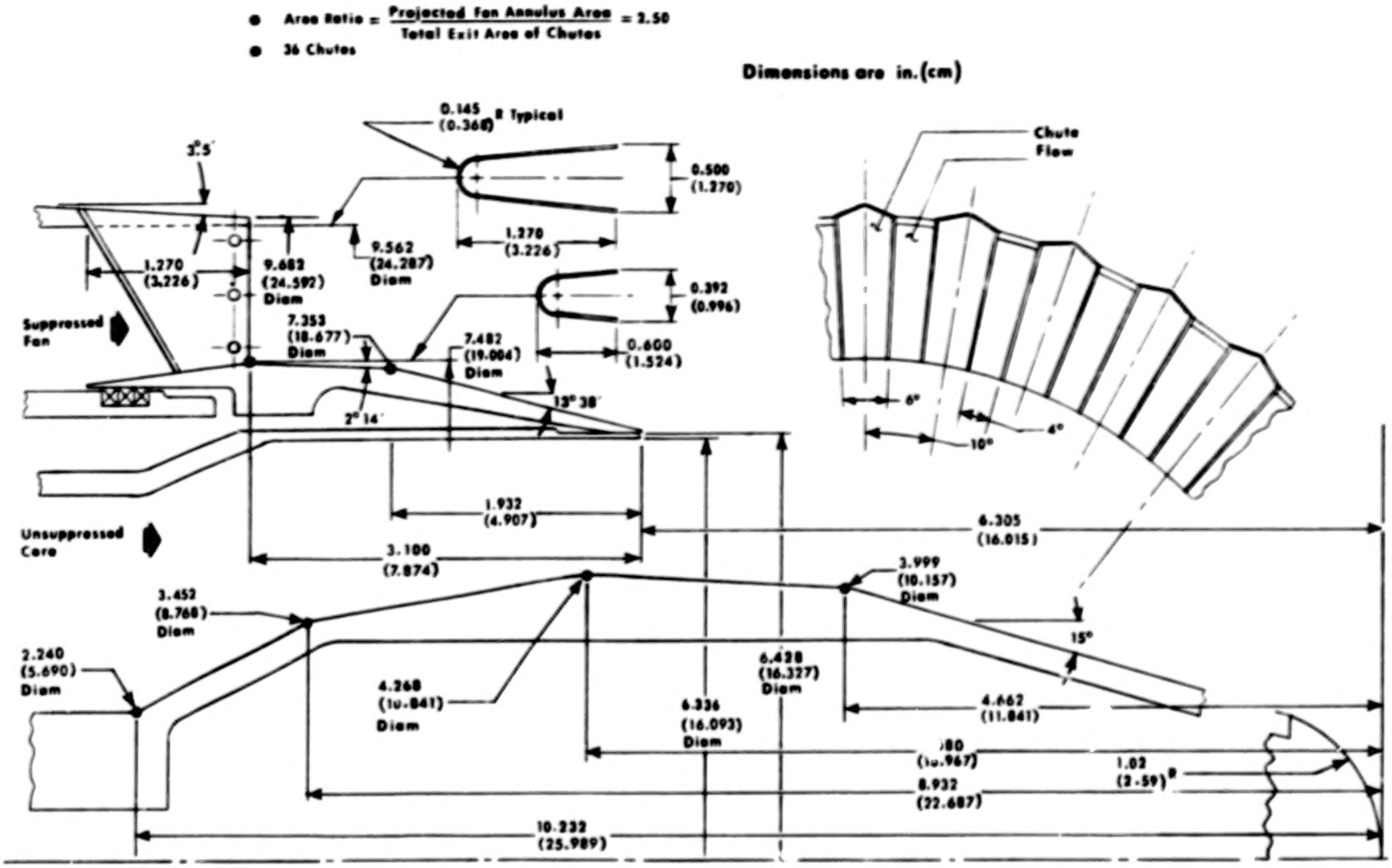
Area Ratio = Projected Fan Annulus Area / Total Exit Area of Chutes = 2.50
36 Chutes
Dimensions are in. (cm)
0.145 (0.368) R Typical
3.5°
0.500 (1.270)
1.270 (3.226)
1.270 (3.226)
9.682 (24.592) Diam
9.562 (24.287) Diam
0.392 (0.996)
Suppressed Fan
7.353 (18.677) Diam
7.482 (19.004) Diam
0.600 (1.524)
13° 38′
2° 14′
Chute
Flow
6°
10°
4°
1.932 (4.907)
Unsuppressed Core
3.100 (7.874)
6.305 (16.015)
3.999 (10.157) Diam
3.452 (8.768) Diam
15°
2.240 (5.690) Diam
4.268 (10.841) Diam
6.428 (16.327) Diam
6.336 (16.093) Diam
4.662 (11.841)
(16.967)
1.02 (2.59) R
8.932 (22.687)
10.232 (25.989)

Figure 140. Multichute Fan Suppressor Nozzle Schematic (for Models 1, 3, 4, 9, 10, and 11).

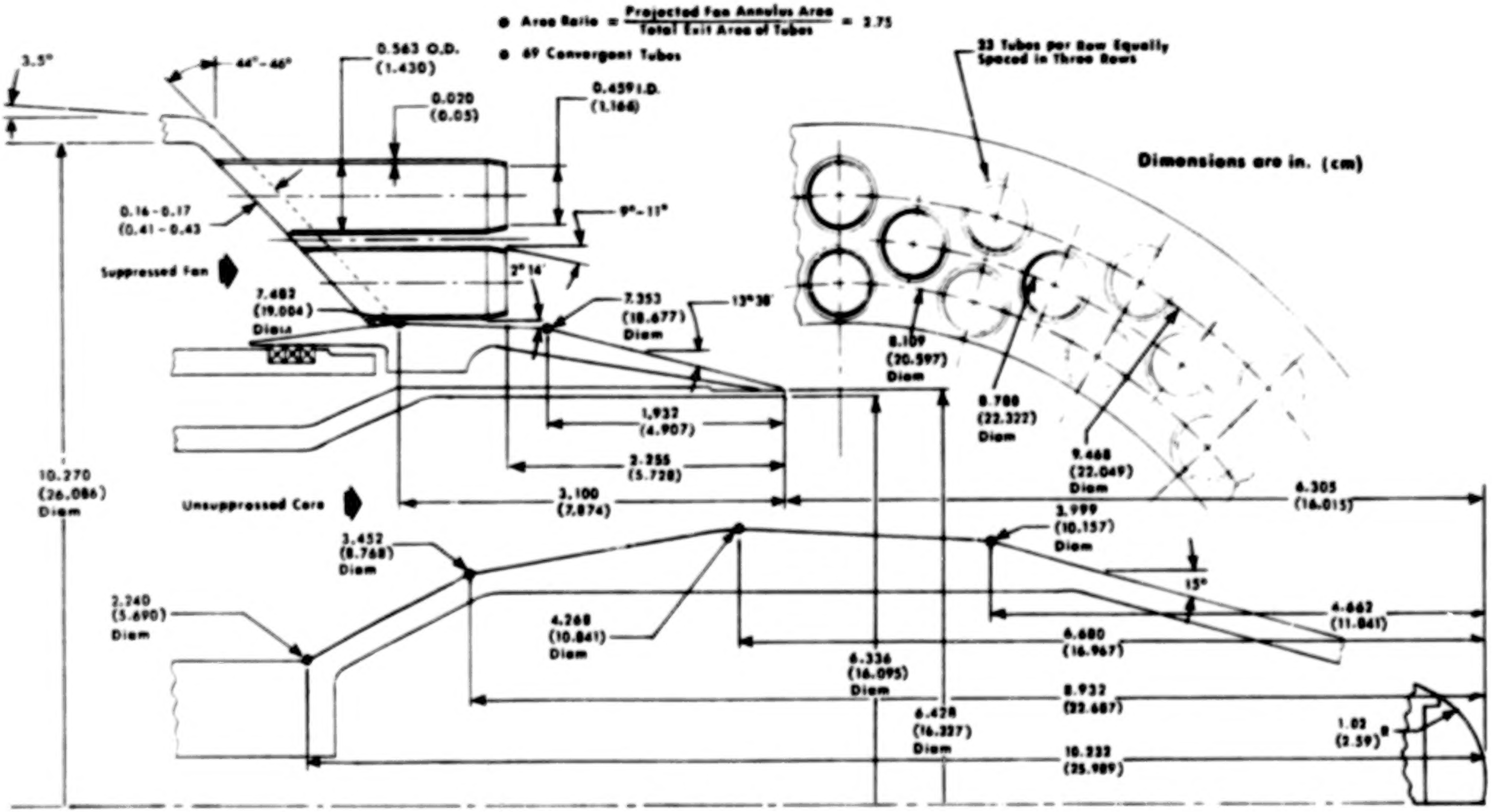
● Area Ratio = Projected Fan Annulus Area / Total Exit Area of Tubes = 2.75
● 69 Convergent Tubes
23 Tubes per Row Equally Spaced in Three Rows
Dimensions are in. (cm)
3.5°
44°-46°
0.563 O.D. (1.430)
0.020 (0.05)
0.459 I.D. (1.166)
0.16 - 0.17 (0.41 - 0.43)
9°-11°
Suppressed Fan
2° 14'
7.482 (19.004) Diam
7.353 (18.677) Diam
13°30'
8.109 (20.597) Diam
8.788 (22.322) Diam
9.468 (22.049) Diam
1,932 (4.907)
2.255 (5.728)
3,100 (7.874)
6.305 (16.015)
10.270 (26.086) Diam
Unsuppressed Core
3.452 (8.768) Diam
2.240 (5.690) Diam
4.268 (10.841) Diam
3.999 (10.157) Diam
15°
4.662 (11.841)
6.680 (16.967)
6.336 (16.095) Diam
6.428 (16.327) Diam
8.932 (22.687)
10.232 (25.989)
1.02 (2.59) R

Figure 141. Multitube Fan Suppressor Nozzle Schematic (For Models 2, 5, and 6).

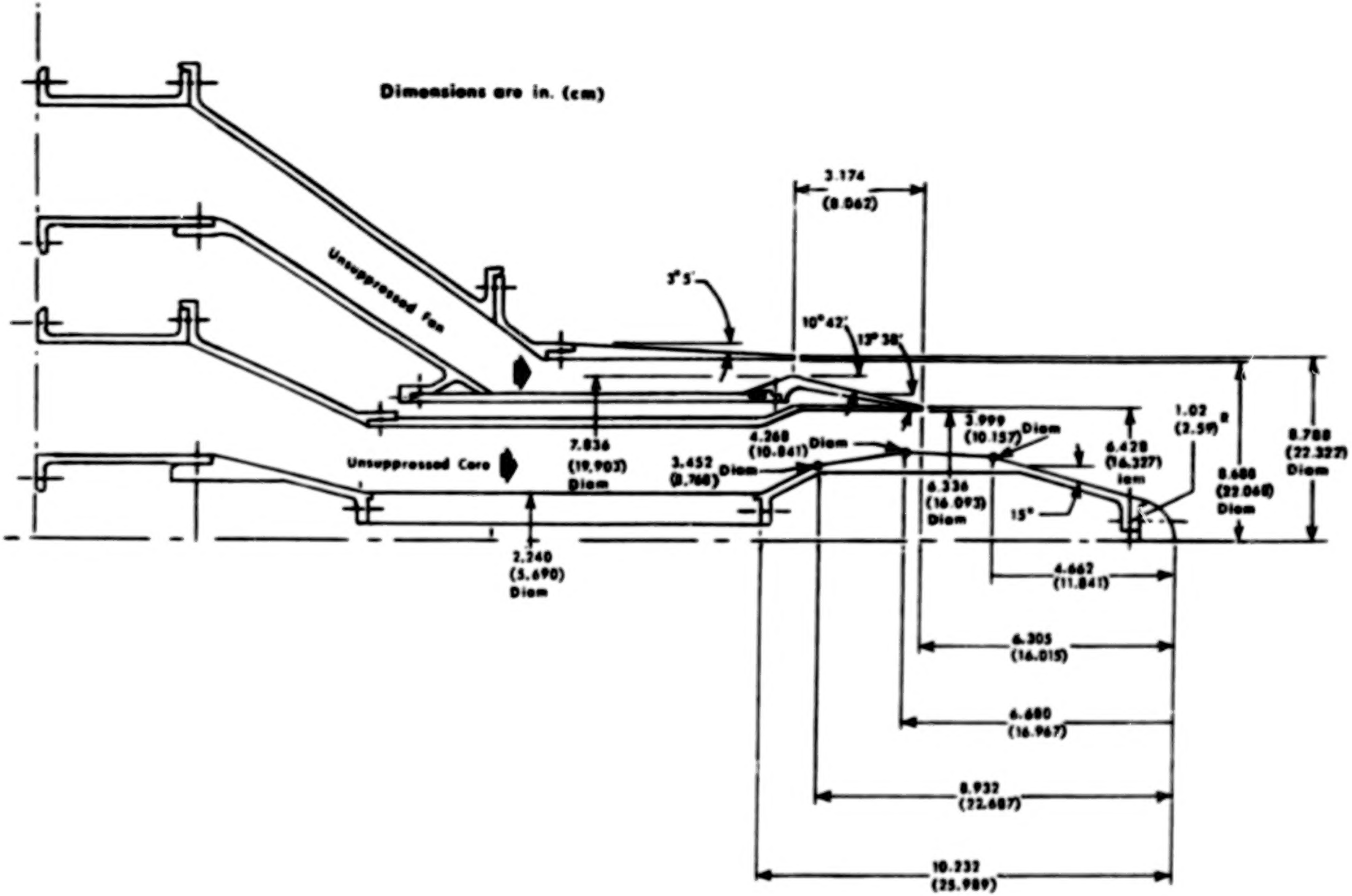
Dimensions are in. (cm)
Unsuppressed Fan
Unsuppressed Core
3.174
(8.062)
3°5'
10°42'
13°38'
7.836
(19.903)
Diam
4.268
(10.841)
Diam
3.452
(8.768)
Diam
3.999
(10.157)
Diam
6.336
(16.093)
Diam
6.428
(16.327)
iam
1.02
(2.59) R
15°
8.688
(22.068)
Diam
8.788
(22.327)
Diam
2.240
(5.690)
Diam
4.662
(11.841)
6.305
(16.015)
6.680
(16.967)
8.932
(22.687)
10.232
(25.989)

Figure 142. Unsuppressed Coannular Nozzle with Plug Schematic (Model 7).

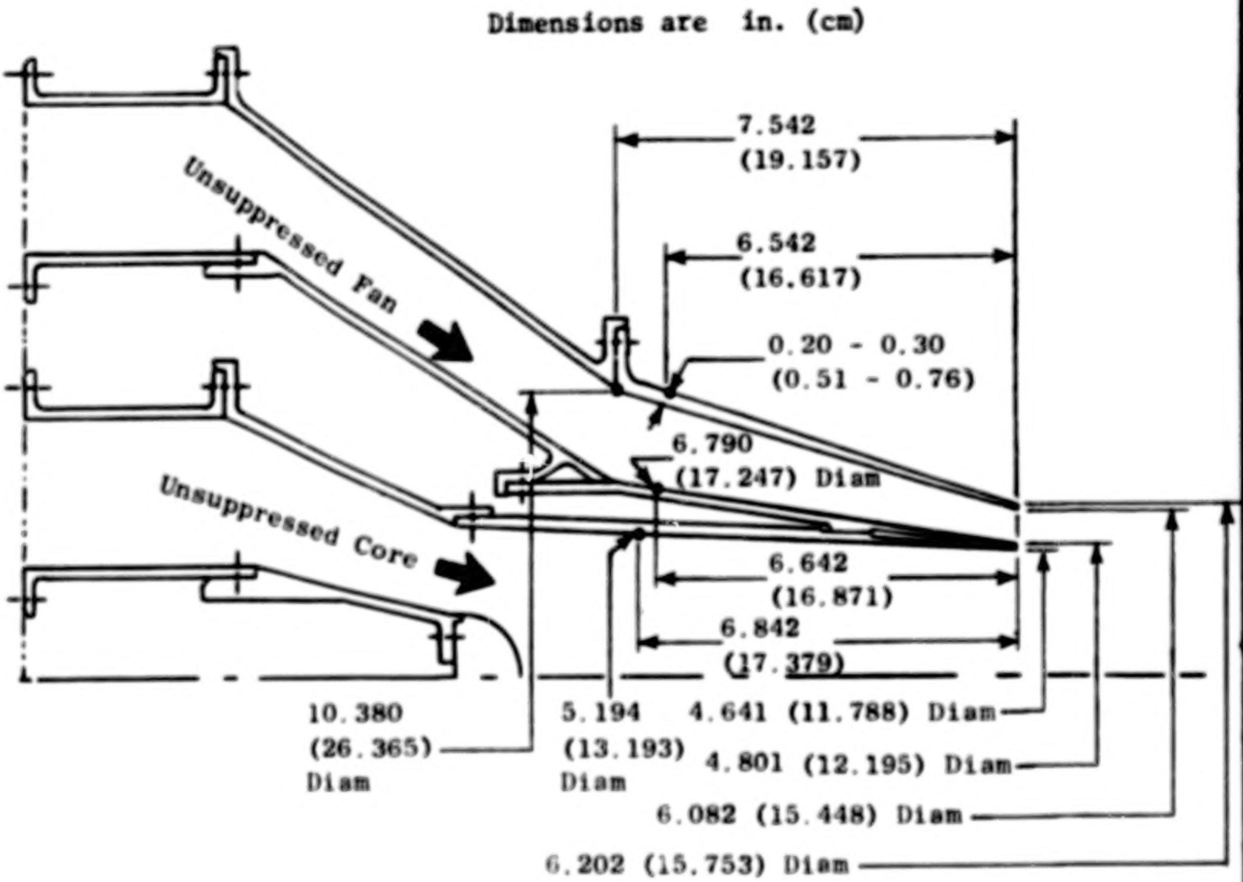
Dimensions are in. (cm)
Unsuppressed Fan
Unsuppressed Core
7.542
(19.157)
6.542
(16.617)
0.20 - 0.30
(0.51 - 0.76)
6.790
(17.247) Diam
6.642
(16.871)
6.842
(17.379)
10.380
(26.365)
Diam
5.194
(13.193)
Diam
4.641 (11.788) Diam
4.801 (12.195) Diam
6.082 (15.448) Diam
6.202 (15.753) Diam

Figure 143. Unsuppressed Coannular Nozzle without Plug Schematic (Model 8).

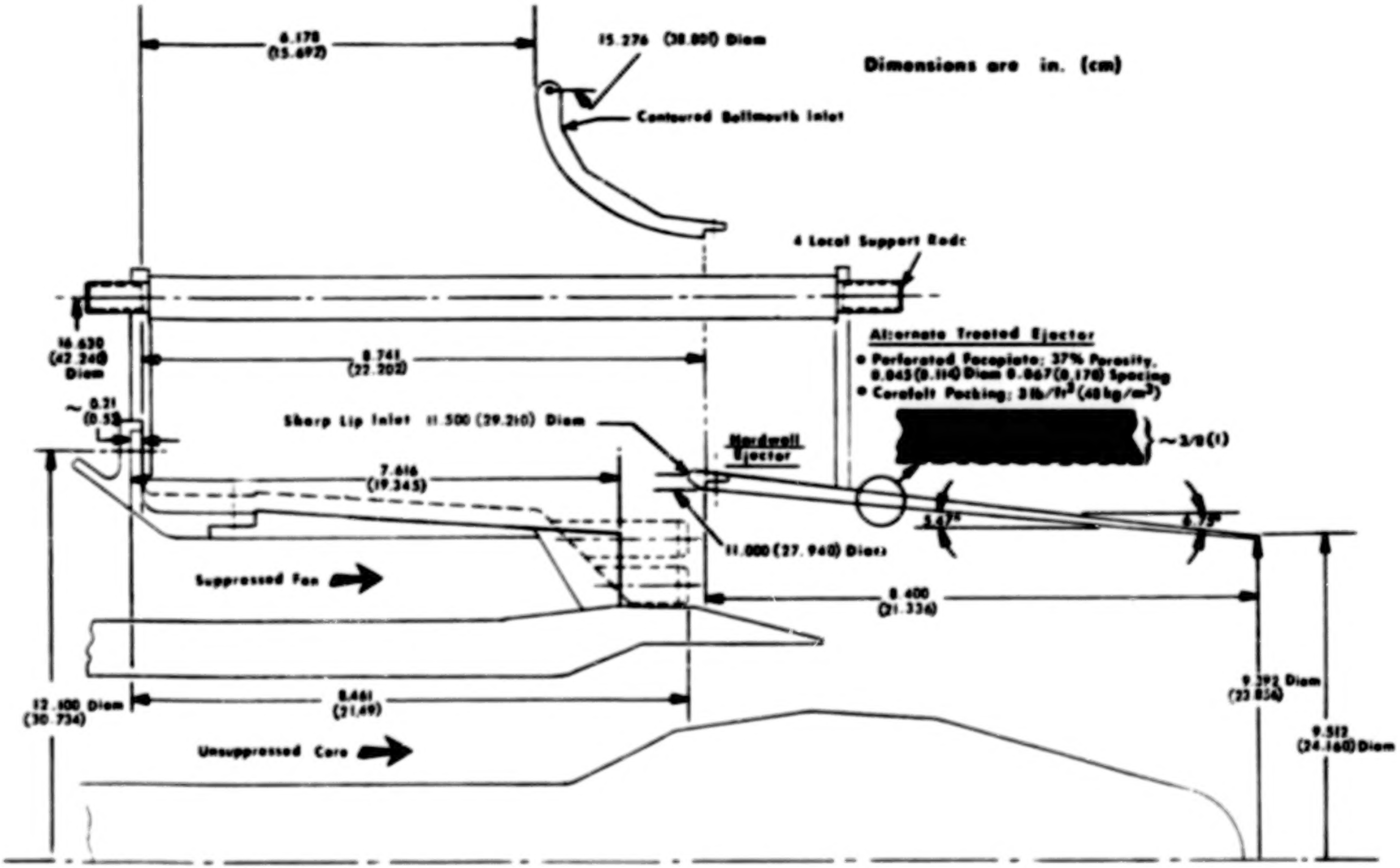
Dimensions are in. (cm)
6.178 (15.692)
15.276 (38.801) Diam
Contoured Bellmouth Inlet
4 Local Support Rods
16.630 (42.240) Diam
8.741 (22.202)
Alternate Treated Ejector
• Perforated Faceplate; 37% Porosity, 0.045 (0.114) Diam 0.067 (0.170) Spacing
• Coralfoil Packing; 3 lb/ft³ (48 kg/m³)
~3/8 (1)
~ 0.21 (0.53)
Sharp Lip Inlet 11.500 (29.210) Diam
Hardwall Ejector
7.616 (19.345)
5.47°
6.75°
11.000 (27.940) Diam
Suppressed Fan
8.400 (21.336)
12.100 Diam (30.734)
8.461 (21.49)
9.392 Diam (23.856)
9.512 (24.160) Diam
Unsuppressed Core

Figure 144. Multielement Fan Suppressor Nozzle with Hardwall/Treated Ejector Schematic (Models 4 and 6, Treated Ejectors; Models 3, 5, and 9, Hardwall Ejectors).

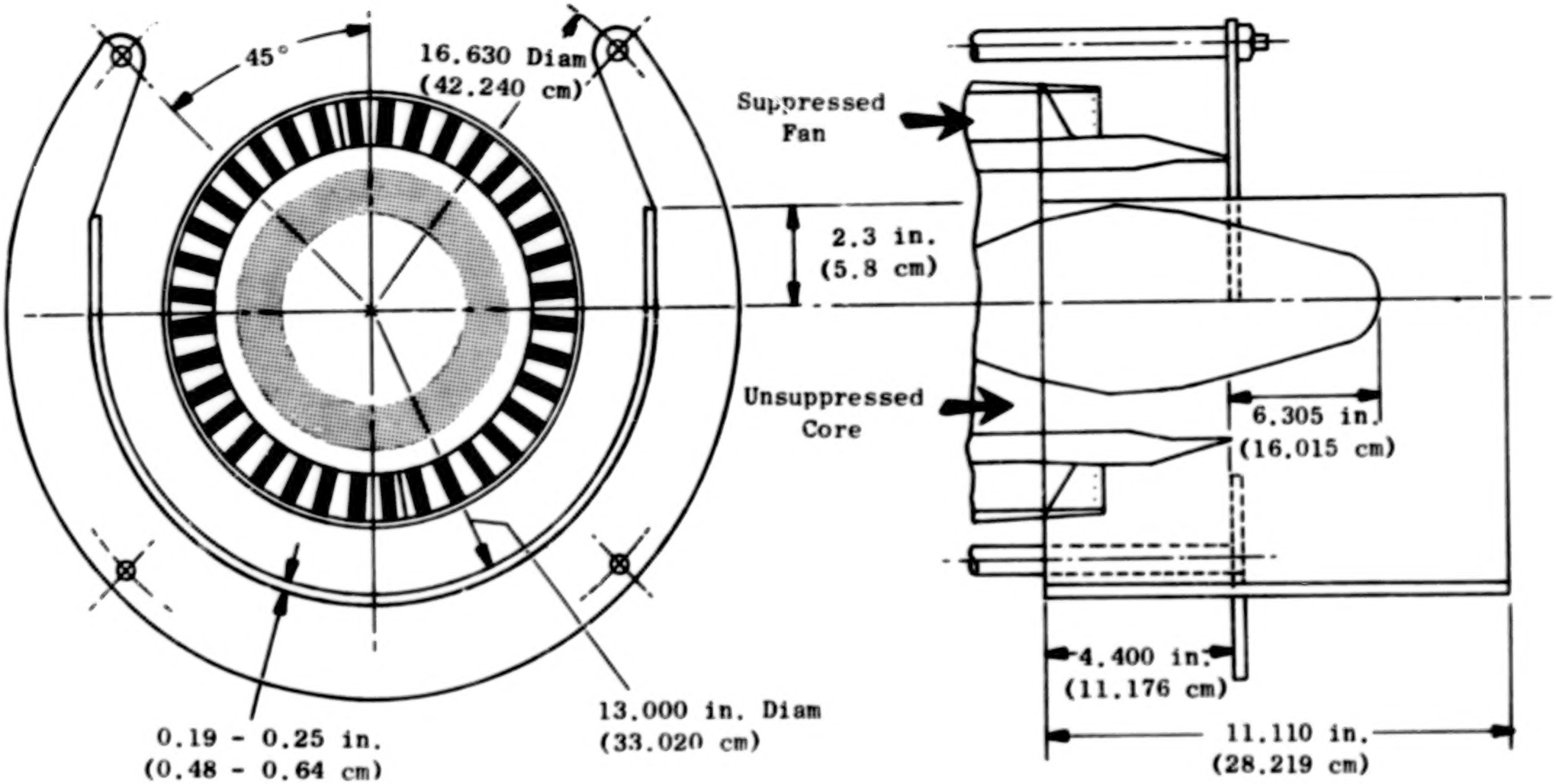
45°
16.630 Diam
(42.240 cm)
Suppressed
Fan
2.3 in.
(5.8 cm)
Unsuppressed
Core
6.305 in.
(16.015 cm)
4.400 in.
(11.176 cm)
11.110 in.
(28.219 cm)
13.000 in. Diam
(33.020 cm)
0.19 - 0.25 in.
(0.48 - 0.64 cm)

Figure 145. Multichute Fan Suppressor Nozzle with Partial Mechanical Shield Schematic (Models 10 and 11).

APPENDIX D

ACOUSTIC TEST MATRIX FOR ALL DBTF MODELS AND EXAMPLE DATA PRINT OUT SHEETS

This Appendix contains listings of all the aerodynamic conditions tested for each of the configurations and selected OASPL and OAPWL for each condition. Figure 146 defines the parameters listed in the acoustic test matrix presented in Tables XII through XXII.

Also contained in this Appendix are examples of the data computer print-out sheets contained in the CDR, Report CR-135236. This information is contained in Tables XXII through XXVI. Table XXIII illustrates and defines the computer sheet print-out format. Table XXIV is an example data sheet print out for model-scale 40-ft arc test results. Table XXV shows an example data sheet print out for scaled (full size) acoustic data at a 320-ft arc, and Table XXVI illustrates extrapolated, scaled-to-full-size, acoustic measurements to the 1969 FAR Part 36 monitoring location of 2128-ft sideline with an aircraft at an altitude of 1110 ft (designated as 2400-ft sideline in Table XXVI).

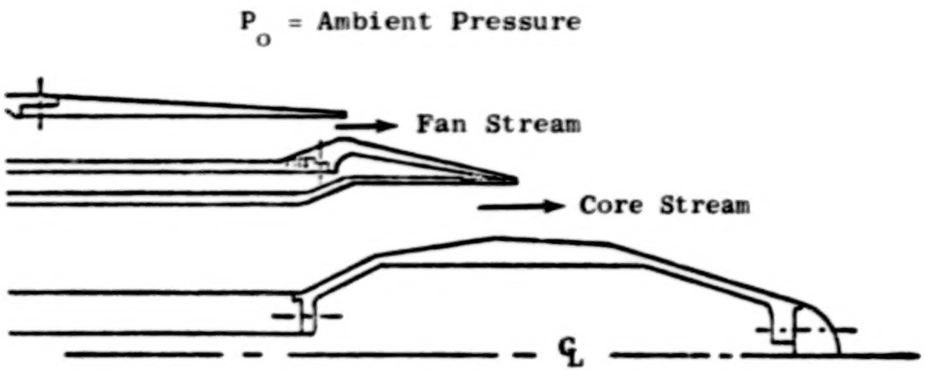
P_o = Ambient Pressure
Fan Stream
Core Stream
$\mathrm{C_L}$

Fan Stream

$(P_T/P_o)_f$ = Fan Nozzle Total Pressure Ratio

T_{T_f} = Fan Nozzle Total Temperature

V_f = Fan Nozzle Fully Expanded Velocity

A_f = Fan Nozzle Geometric Throat Area

Core Stream

$(P_T/P_o)_c$ = Core Nozzle Total Pressure Ratio

T_{T_c} = Core Nozzle Total Temperature

V_c = Core Nozzle Fully Expanded Velocity

A_c = Core Nozzle Geometric Throat Area

Figure 146. Definition of Parameters Utilized in Tables XII through XXII.

Table XII. Acoustic Test Matrix, Aerodynamic Test Conditions, DBTF Model 1.

A_c = 17.21 in.^{2} = 0.0111 m^2
A_f = 11.12 in.^{2} = 0.00717 m^2

Data Pt.	$(P_T/P_0)_c$	$(P_T/P_0)_f$	A_f/A_c	V_f/V_c	V_c (ft/sec)	V_f (ft/sec)	T_{T_c} (° R)	T_{T_f} (° R)	T_{Dry} (° F)	T_{Wet} (° F)	Barom (in. Hg)	OASPL, dB (Model Scale, 40-ft Arc, Standard Day Data) θ, Angle to Inlet 50°	70°	90°	110°	130°	140°	150°	OAPWL* dB
101	1.775	1.531	0.646	1.01	986	995	535	718	64	53	29.26	91.8	92.9	94.6	97.0	99.4	101.0	101.7	138.6
102	1.797	1.779	0.646	1.25	994	1246	533	852	64	53	29.26	94.9	96.2	97.8	100.5	102.8	103.8	103.7	141.8
103	1.804	2.057	0.646	1.50	999	1500	535	1004	64	53	29.26	97.9	99.6	101.2	104.2	106.5	107.5	107.1	145.6
104	1.789	2.376	0.646	1.77	996	1759	539	1171	64	53	29.26	101.7	104.0	104.3	107.8	109.8	110.7	110.4	149.3
105	1.786	2.726	0.646	2.03	997	2021	541	1353	64	53	29.26	103.4	104.9	106.4	110.1	112.2	113.3	112.6	151.3
106	1.629	1.631	0.646	1.00	1163	1106	777	780	66	53	29.30	93.0	94.3	96.0	99.1	112.5	104.3	105.8	141.5
107	1.626	1.916	0.646	1.24	1100	1366	775	915	66	53	29.30	95.9	97.5	99.4	102.5	105.2	106.6	107.3	
108	1.624	2.260	0.646	1.49	1103	1647	782	1084	70	57	29.32	99.6	101.8	103.1	106.3	108.3	109.5	109.5	147.6
109	1.626	2.608	0.646	1.75	1101	1932	777	1289	70	[illegible]	29.325	102.6	103.9	105.6	109.0	111.2	112.3	112.2	150.4
110	1.632	3.003	0.646	2.00	1105	2209	778	1491	70	57	29.325	105.1	106.2	107.9	111.3	113.6	114.5	114.5	
111	1.565	1.724	0.646	0.99	1200	1186	996	811	69	55	29.325	94.2	95.6	97.7	101.0	104.7	106.8	108.0	143.5
112	1.558	2.053	0.646	1.25	1196	1490	998	993	69	55	29.323	97.2	99.4	101.2	104.5	107.5	109.4	110.1	146.5
113	1.556	2 454	0.646	1.50	1197	1801	1002	1188	70	57	29.325	100.8	103.0	104.5	108.0	110.6	112.1	112.7	149.8
114	1.569	2.865	0.646	1.74	1215	2113	1015	1418	69	55	29.332	96.1	106.1	107.6	111.1	113.4	114.8	115.2	
115	1.570	3.274	0.646	1.98	1209	2396	1006	1642	69	55	29.33	96.9	108.1	110.0	113.7	116.0	116.8	117.2	
116	1.536	1.892	0.646	0.99	1302	1291	1218	875	69	55	29.325	96.0	97.6	99.8	103.3	107.3	109.6	110.8	145.9
117	1.535	2.226	0.646	1.24	1299	1615	1214	1060	67	54	29.30	99.5	101.7	103.4	106.8	109.9	112.0	113.1	149.0
118	1.525	2.644	0.646	1.51	1292	1947	1217	1292	70	57	29.325	102.5	104.5	106.0	109.6	112.4	114.2	115.0	151.5
119	1.530	3.112	0.646	1.75	1301	2278	1226	1542	70	56	29.35	105.3	107.6	109.1	112.7	115.0	116.7	117.3	154.2
120	1.531	3.495	0.646	1.98	1302	2578	1226	1810	70	56	29.35	107.9	108.9	110.7	114.6	117.0	118.4	119.2	155.9
121	1.508	1.946	0.646	1.01	1390	1400	1443	941	69	55	29.327	97.5	99.2	101.5	104.9	109.2	111.6	112.7	147.8
122	1.516	2.385	0.646	1.26	1400	1759	1447	1166	67	54	29.328	101.4	103.3	104.9	108.7	112.3	114.5	115.6	151.1
123	1.498	2.864	0.646	1.52	1386	2103	1457	1405	70	56	29.35	103.7	105.9	107.8	111.3	114.3	116.1	117.1	153.3
124	1.498	3.365	0.646	1.76	1384	2433	1453	1667	67	56	29.35	106.5	108.3	110.2	113.8	116.5	118.3	119.2	155.4
125	1.507	3.888	0.646	1.99	1402	2784	1471	1968	67	56	29.35	109.2	110.7	112.6	116.6	119.4	121.0	122.6	158.1
126	1.360	1.530	0.646	0.99	1008	998	1004	724	64	53	29.26	90.1	91.9	93.4	96.5	99.6	101.1	101.9	138.2
127	1.351	2.053	0.646	1.49	997	1487	1003	990	69	[illegible]	29.327	96.5	98.7	100.5	103.5	106.0	106.8	106.5	144.8
128	1.344	2.725	0.646	2.04	990	2018	1004	1351	67	54	29.30	102.8	104.6	106.2	109.7	111.9	112.5	112.0	150.9
129	1.868	1.947	0.646	0.99	1402	1388	998	924	69	55	29.323	98.4	99.9	101.9	105.5	109.9	112.9	114.4	148.9
130	1.860	2.866	0.646	1.50	1400	2098	1002	[illegible]	[illegible]	55	29.332	94.7	106.0	108.0	111.6	114.7	117.0	118.3	153.8
131	1.851	3.886	0.646	1.99	1404	2790	1015	1977	67	56	29.355	109.0	110.7	112.6	116.4	119.0	120.8	122.4	158.0
132	1.793	2.016	0.646	1.26	997	1252	538	718	61	52	29.389	96.2	97.4	98.6	101.4	104.1	104.7	104.6	142.9
133	1.798	2.596	0.646	1.69	1002	1694	541	778	61	52	29.389	102.9	103.5	103.4	106.0	108.3	108.9	108.6	147.8
134	1.783	3.197	0.646	2.01	994	1997	539	1171	64	53	29.26	105.9	106.7	107.4	110.3	112.9	113.9	113.3	152.2
135	1.630	2.613	0.646	1.49	1103	1647	777	940	66	53	29.30	101.9	102.8	103.7	106.9	109.4	110.6	111.0	148.7
136	1.625	3.045	0.646	1.50	1093	1642	768	823	66	53	29.30	105.1	105.9	105.3	107.1	110.1	111.5	111.5	150.0
137	1.625	2.618	0.646	[illegible]	1108	2204	788	1660	70	56	29.335	103.1	105.3	107.6	111.3	112.8	113.9	113.4	152.0
138	1.561	2.899	0.646	[illegible]	1200	1798	1001	1026	67	54	29.328	104.0	104.9	105.4	108.3	111.5	113.0	113.9	150.8
139	1.563	2.895	0.646	[illegible]	1203	2395	1002	1796	67	56	29.36	105.2	106.7	108.9	113.0	114.7	115.8	116.0	153.7
140	1.564	2.664	0.646	2.01	1207	2426	1010	1970	67	56	29.36	104.1	106.7	109.3	113.2	114.3	115.4	115.5	153.5

*OAPWL's are shown for a 3/4 sphere; to correct the levels to full sphere, add 1.3 dB.
Tabulated OAPWL's are correct; where blanks are found, the OAPWL was found to be erroneous.

Table XII. Acoustic Test Matrix, Aerodynamic Test Conditions, DBTF Model 1 (Concluded).

A_c = 17.21 in.^{2} = 0.0111 m^2
A_f = 11.12 in.^{2} = 0.00717 m^2

												OASPL, dB (Model Scale, 40-ft Arc, Standard Day Data)							
												θ, Angle to Inlet							
Data Pt.	$(P_T/P_O)_c$	$(P_T/P_O)_f$	A_f/A_c	V_f/V_c	V_c (ft/sec)	V_f (ft/sec)	T_{T_c} (° R)	T_{T_f} (° R)	T_{Dry} (° F)	T_{Wet} (° F)	Barom (in. Hg)	50°	70°	90°	110°	130°	140°	150°	OAPWL* dB
141	1.525	3.206	0.646	2.01	1295	2601	1224	1954	67	56	29.363	106.9	108.9	111.3	115.3	116.9	118.2	118.7	155.9
142	1.794	1.19	0.646	0.56	975	548	515	513	59	51	29.382	90.8	91.7	93.1	95.7	98.5	100.7	101.6	137.8
143	1.788	1.354	0.646	0.81	997	806	540	648	61	52	29.389	91.1	92.0	93.5	94.1	99.0	100.8	102.0	138.1
144	1.634	1.266	0.646	0.58	1097	639	764	522	59	51	29.395	90.4	91.7	93.6	97.4	101.4	104.3	105.5	140.5
145	1.568	1.195	0.646	0.47	1201	560	993	526	59	51	29.393	92.3	93.5	95.8	100.3	104.9	107.5	109.2	143.5
146	1.557	1.268	0.646	0.61	1186	719	984	656	61	52	29.391	91.4	92.8	94.9	99.2	103.6	106.4	107.6	142.3
147	1.562	1.492	0.646	0.79	1195	950	992	696	61	52	29.391	92.5	94.0	95.7	99.8	103.9	106.3	107.6	142.4
148	1.533	1.336	0.646	0.61	1296	793	1211	662	59	51	29.391	93.4	94.7	99.1	101.2	106.1	108.7	110.0	144.6
149	1.510	1.194	0.646	0.40	1393	561	1665	528	59	51	29.391	95.6	96.8	99.2	103.5	108.8	111.6	112.8	149.7
150	1.512	1.419	0.646	0.62	1391	868	1636	659	59	51	29.391	95.1	96.3	98.7	103.0	108.1	111.0	111.9	
151	1.510	1.643	0.646	0.80	1394	1109	1668	773	59	51	29.391	96.0	97.3	99.5	103.7	108.5	110.9	112.0	
152	1.744	3.871	0.646	1.72	1611	2770	1660	1956	67	56	29.365	109.3	111.4	113.3	117.2	120.8	123.3	125.2	159.7
153	1.745	2.198	0.646	1.00	1610	1607	1657	1064	63	53	29.37	102.0	113.4	105.3	109.5	114.5	117.2	118.3	152.8
154	1.751	1.504	0.646	0.60	1610	959	1669	695	63	53	29.375	99.0	100.2	102.3	106.9	113.2	116.6	117.5	151.5
155	2.044	3.712	0.646	..48	1808	2680	1661	1880	67	56	29.362	109.5	111.3	113.4	117.4	122.2	125.6	126.8	160.9
156	2.048	2.446	0.646	1.01	1807	1817	1655	1212	65	54	29.37	105.0	106.6	108.3	112.6	118.9	122.5	122.4	157.0
157	2.041	1.600	0.646	0.60	1801	1076	1652	766	63	53	29.375	102.8	103.7	105.9	110.7	118.2	121.7	121.9	155.9
158	2.483	3.402	0.646	1.24	2013	2499	1659	1735	65	54	29.363	110.2	111.8	113.8	117.6	125.0	128.1	127.6	162.3
159	2.478	2.726	0.646	1.01	2008	2029	1655	1364	65	54	29.37	108.7	110.1	111.5	116.0	124.1	126.9	126.1	161.0
160	2.472	1.730	0.646	0.60	1999	1199	1666	825	63	53	29.37	107.3	108.3	109.5	114.3	123.2	126.5	124.9	160.0
170	1.02	3.889	0.646	11.67	238	2778	830	1960	78	59	29.382	107.9	110.0	111.5	115.6	118.4	119.6	119.9	
171	1.011	2.855	0.646	13.57	155	2103	659	1609	78	59	29.39	103.9	106.3	106.6	110.3	112.8	113.6	112.7	
172	1.012	2.451	0.646	11.56	157	1815	627	1208	78	59	29.39	100.6	102.5	104.0	107.2	110.2	110.7	109.7	168.8

*The OAPWL's are shown for a 3/4 sphere; to correct the levels to full sphere, add 1.3 dB.
Tabulated OAPWL's are correct; where blanks are found, the OAPWL was found to be erroneous.

Table XIII. Acoustic Test Matrix, Aerodynamic Test Conditions, DBTF Model 2.

A_c = 17.21 in.^{2} = 0.0111 m^2
A_f = 11.43 in.^{2} = 0.00737 m^2

Data Pt.	$(P_T/P_0)_c$	$(P_T/P_0)_f$	A_f/A_c	V_f/V_c	V_c (ft/sec)	V_f (ft/sec)	T_{T_c} (° R)	T_{T_f} (° R)	T_{Dry} (° F)	T_{Wet} (° F)	Barom (in Hg)	OASPL, dB (Model Scale, 40-ft Arc, Standard Day Data) θ, Angle to Inlet 50°	70°	90°	110°	130°	140°	150°	OAPWL* dB
201	1.793	1.532	0.664	0.986	1009	995	552	718	64	50	29.660	93.1	96.3	95.4	97.5	99.5	101.6	102.5	139.2
202	1.793	1.779	0.664	1.225	1010	1237	552	839	64	50	29.662	96.2	97.6	98.8	101.0	102.7	104.1	104.1	142.3
203	1.796	2.058	0.664	1.468	1012	1486	553	984	63	49	29.665	99.4	101.0	102.1	104.0	105.7	107.2	107.3	145.7
204	1.796	2.381	0.064	1.728	1012	1749	554	1155	63	49	29.668	102.3	103.5	104.8	107.1	108.5	110.0	109.4	148.6
205	1.795	2.721	0.064	1.990	1010	2010	552	1362	61	48	29.670	105.2	105.8	107.0	109.2	110.9	112.4	112.1	151.0
206	1.635	1.622	0.664	0.997	1099	1096	767	775	69	56	29.628	93.9	95.0	96.6	99.2	101.8	104.1	105.3	141.2
207	1.632	1.921	0.664	1.260	1098	1384	767	936	69	56	29.623	97.5	98.8	100.3	102.8	104.9	106.7	107.5	144.8
208	1.632	1.256	0.664	1.514	1098	1663	767	1106	70	55	29.620	100.7	102.0	103.6	105.9	107.7	109.5	110.0	147.5
209	1.631	2.607	0.664	1.757	1097	1927	766	1282	70	55	29.613	103.5	104.5	105.7	108.2	110.1	111.6	111.8	149.9
210	1.632	3.012	0.664	2.018	1097	2214	766	1495	70	55	29.610	105.4	[illegible]	107.9	110.5	112.4	118.4	114.3	153.0
211	1.567	1.734	0.664	0.995	1199	1193	992	813	73	56	29.595	95.8	96.8	98.7	101.3	104.5	107.1	108.5	143.8
212	1.569	2.084	0.664	1.237	1201	1486	992	982	73	56	29.595	98.6	100.1	101.8	104.2	107.0	109.3	110.6	146.5
213	1.567	2.456	0.664	1.497	1204	1803	1000	1190	72	55	29.600	101.9	103.6	104.7	107.6	109.7	111.9	112.8	149.5
214	1.569	2.862	0.664	1.733	1208	2094	1005	1393	72	55	29.602	104.7	105.6	107.1	109.7	112.0	114.1	126.9	151.7
215	1.567	3.278	0.664	1.976	1211	2390	1010	1632	72	55	29.608	107.0	107.6	108.8	111.9	114.3	116.3	117.0	153.7
216	1.523	1.826	0.664	1.998	1294	1292	1226	878	73	59	29.520	97.1	98.6	99.9	102.7	106.6	109.4	110.9	145.8
217	1.525	2.224	0.664	1.253	1295	1623	1226	1071	73	59	29.525	100.5	101.8	103.3	106.1	109.3	111.8	113.0	148.7
218	1.526	2.658	0.664	1.518	1295	1966	1223	1311	73	59	29.525	103.6	106.7	106.0	109.0	111.5	114.0	115.1	151.2
219	1.535	3.096	0.664	1.738	1307	2272	1227	1540	75	58	29.578	105.3	106.3	107.7	110.9	113.8	116.4	117.4	153.3
220	1.541	3.555	0.664	1.955	1315	2571	1233	1782	75	58	29.560	107.2	108.5	109.7	113.2	116.2	118.8	119.5	155.5
221	1.498	1.966	0.664	1.025	1380	1416	1665	960	74	58	29.530	98.6	100.3	101.7	104.9	108.7	111.6	113.0	147.8
222	1.503	2.383	0.664	1.272	1390	1768	1656	1179	74	58	29.530	102.0	103.3	104.7	107.8	111.1	114.2	115.2	150.6
223	1.503	2.865	0.664	1.528	1395	2132	1665	1642	74	58	29.530	105.1	106.0	107.3	110.5	113.5	116.4	117.5	153.0
224	1.501	3.349	0.664	1.747	1392	2432	1665	1664	76	58	29.550	106.9	107.7	109.2	112.8	115.8	119.8	119.8	155.4
225	1.495	3.895	0.664	2.028	1380	2799	1652	1986	76	58	29.540	108.8	109.6	111.4	114.9	118.2	120.8	121.6	157.2
226	1.368	1.535	0.664	1.013	990	1003	995	726	69	54	29.632	91.0	92.6	93.9	96.4	98.7	100.7	101.2	137.9
227	1.351	2.057	0.664	1.509	993	1499	995	1002	75	58	29.590	97.6	99.4	100.9	103.3	105.4	107.1	106.7	145.0
228	1.368	2.736	0.664	2.045	990	2025	997	1356	75	58	29.582	103.5	104.1	105.7	108.3	110.5	117.1	112.0	151.3
229	1.861	1.963	0.664	1.016	1392	1415	989	951	62	53	29.420	100.1	101.2	102.7	106.0	110.1	113.4	115.3	
230	1.863	2.866	0.664	1.515	1399	2119	998	1425	62	52	29.415	105.6	106.2	107.6	111.1	114.2	117.1	118.8	
231	1.856	3.856	0.664	1.988	1395	2773	998	1962	62	52	29.410	109.6	110.0	111.5	115.6	118.8	120.9	122.6	
232	1.791	2.019	0.664	1.261	997	1257	538	723	61	48	29.677	97.6	99.0	100.2	102.1	107.5	104.6	104.9	143.4
233	1.793	2.600	0.664	1.500	999	1499	560	782	61	48	29.675	103.0	103.5	103.8	105.1	106.7	108.4	108.7	147.6
234	1.796	3.182	0.664	1.981	1005	1991	566	1167	61	48	29.673	106.4	107.0	107.3	109.5	111.7	113.5	113.5	151.8
235	1.620	2.597	0.664	1.501	1090	1636	768	933	62	52	29.410	102.9	102.8	103.3	106.0	108.4	110.2	110.8	

*The OAPWL's are shown for a 3/4 sphere; to correct the levels to full sphere, add 1.3 dB.
Tabulated OAPWL's are correct; where blanks are found, the OAPWL was found to be erroneous.

Table XIII. Acoustic Test Matrix, Aerodynamic Test Conditions, DBTF Model 2 (Concluded).

A_c = 17.21 in.² = 0.0111 m²
A_f = 11.43 in.² = 0.00737 m²

												OASPL, dB (Model Scale, 40-ft Arc, Standard Day Data) θ, Angle to Inlet							
Data Pt.	$(P_T/P_0)_c$	$(P_T/P_0)_f$	A_f/A_c	V_f/V_c	V_c (ft/sec)	V_f (ft/sec)	T_{T_c} (° R)	T_{T_f} (° R)	T_{Dry} (° F)	T_{Wet} (° F)	Barom (in. Hg)	50°	70°	90°	110°	130°	140°	150°	OAPWL,* dB
236	1.630	3.043	0.664	1.504	1092	1642	762	823	65	52	29.410	105.4	105.2	104.5	106.8	109.3	111.2	111.9	
237	1.627	2.996	0.664	2.020	1102	2226	778	1706	65	52	29.410	106.8	105.6	106.9	110.4	112.1	113.4	113.6	
238	1.559	2.856	0.664	1.477	1196	1766	997	1101	62	52	29.410	106.3	106.8	106.9	108.0	110.9	112.7	113.7	
239	1.557	2.889	0.664	2.000	1198	2396	1003	1800	62	52	29.413	106.3	106.8	108.4	111.9	114.0	115.3	116.1	
240	1.556	2.669	0.664	2.006	1201	2409	1010	1954	62	52	29.413	105.7	108.4	108.3	111.8	113.7	114.9	115.5	
241	1.531	3.192	0.664	1.978	1308	2587	1236	1938	62	53	29.413	105.3	107.3	109.1	112.6	115.6	116.7	118.6	156.5
242	1.799	1.202	0.664	0.573	996	571	536	531	57	47	29.688	91.1	92.3	93.8	95.7	98.3	100.9	102.3	137.9
243	1.790	1.361	0.664	0.831	996	828	539	675	57	47	29.678	91.7	92.8	94.1	96.2	98.3	100.6	101.7	138.0
244	1.640	1.262	0.664	0.577	1109	640	775	529	56	44	29.688	91.3	92.4	94.4	97.7	101.4	104.4	106.2	140.6
245	1.564	1.203	0.664	0.477	1201	573	998	530	57	47	29.682								
246	1.562	1.272	0.664	0.611	1196	730	991	667	64	50	29.652	91.9	93.0	95.3	98.6	102.8	106.1	107.9	142.0
247	1.552	1.499	0.664	0.815	1182	963	983	707	66	50	29.648	93.0	93.9	95.9	99.0	102.5	105.5	107.2	141.8
248	1.534	1.364	0.664	0.616	1301	801	1219	659	64	50	29.648	93.9	94.9	97.1	100.7	105.1	108.7	110.4	144.3
249	1.516	1.206	0.664	0.410	1399	574	1665	532	57	47	29.680	96.1	97.3	99.7	103.3	108.4	111.8	113.3	147.1
250	1.514	1.413	0.664	0.616	1405	865	1660	662	62	53	29.620	95.2	96.1	98.4	102.9	108.0	111.1	112.6	146.8
251	1.508	1.463	0.664	0.798	1392	1111	1668	776	69	56	29.640	96.4	97.6	99.7	103.1	107.6	110.9	112.5	146.4
252	1.762	3.867	0.664	1.715	1616	2772	1671	1958	76	58	29.560	109.1	110.1	111.7	115.2	119.6	123.1	126.7	158.8
253	1.760	2.189	0.664	0.986	1612	1590	1667	1047	75	58	29.530	101.9	103.1	104.9	108.3	113.2	117.5	118.2	152.5
254	1.739	1.695	0.664	0.606	1608	974	1660	727	75	58	29.530	97.9	98.9	101.0	106.9	110.7	116.1	117.1	150.8
255	2.067	3.715	0.664	1.476	1816	2680	1671	1878	76	58	29.560	109.7	110.5	111.9	115.5	120.9	126.9	126.1	160.6
256	2.066	2.458	0.664	1.003	1806	1810	1653	1197	75	58	29.530	105.3	106.5	108.2	112.1	117.9	124.1	122.7	157.6
257	2.065	1.591	0.664	0.601	1807	1086	1659	787	75	58	29.590	103.0	104.1	105.8	110.5	116.9	121.1	121.4	155.5
258	2.458	3.430	0.664	1.229	2006	2466	1664	1681	76	58	29.535	110.6	111.1	112.5	116.0	123.3	128.2	128.0	161.9
259	2.456	2.720	0.664	0.984	2003	1970	1661	1290	75	58	29.530	108.9	109.7	111.2	114.9	122.8	130.2	126.2	162.0
260	2.664	1.725	0.664	0.600	2002	1202	165[illegible]	833	75	58	29.535	107.6	108.4	109.7	113.8	121.7	126.3	126.9	159.6
270	---	3.850	0.664	---	---	2775	---	1967	62	53	29.413	109.0	109.2	110.7	114.7	117.8	119.7	120.6	
271	---	2.826	0.664	---	---	2081	---	1396	62	53	29.413	106.5	105.2	105.7	109.1	111.4	117.1	112.1	
272	---	2.667	0.664	---	---	1817	---	1216	68	56	29.683	100.9	102.1	103.9	106.4	108.7	108.7	108.9	148.1
273	1.718	---	0.664	---	1586	---	1656	---	---	---	---	110.5	111.7	114.2	118.1	124.3	117.1	118.2	158.9
274	2.058	---	0.664	---	1816	---	1660	---	---	---	---	104.9	105.9	108.1	112.3	119.8	123.0	123.5	157.5
275	2.436	---	0.664	---	1993	---	1650	---	60	63	29.495	108.9	109.5	111.0	115.5	126.3	127.2	126.5	161.3
276	3.106	---	0.664	---	2202	---	1667	---	60	63	29.500	115.4	115.5	115.8	119.5	129.3	131.4	129.4	165.3

*The OAPWL's are shown for a 1/4 sphere; to correct the levels to full sphere, add 1.3 dB. Tabulated OAPWL's are correct; where blanks are found the OAPWL was found to be erroneous.

Table XIV. Acoustic Test Matrix, Aerodynamic Test Conditions, DBTF Model 3.

A_c = 17.21 in.^{2} = 0.0111 m^2
A_f = 11.12 in.^{2} = 0.00717 m^2

												OASPL, dB (Model Scale, 40-ft Arc, Standard Day Data)							
												θ, Angle to Inlet							
Data Pt.	$(P_T/P_o)_c$	$(P_T/P_o)_f$	A_f/A_c	V_f/V_c	V_c (ft/sec)	V_f (ft/sec)	TT_c (° R)	TT_f (° R)	T_{Dry} (° F)	T_{Wet} (° F)	Barom (in. Hg)	50°	70°	90°	110°	130°	140°	150°	OAPWL* dB
301	1.787	1.531	0.646	0.980	1008	988	553	708	69	56	29.415	91.1	91.9	93.3	96.1	98.4	99.8	101.2	137.6
303	1.789	2.060	0.646	1.485	1013	1504	557	1007	69	56	29.418	96.3	97.4	99.1	103.0	103.2	103.1	104.0	142.9
305	1.791	2.722	0.646	1.969	1024	2016	568	1349	70	54	29.415	101.6	103.5	105.8	110.2	108.3	108.2	108.5	149.2
306	1.620	1.620	0.646	0.999	1088	1087	765	763	72	55	29.40	92.1	93.0	94.4	97.6	100.4	102.3	103.9	139.6
308	1.626	2.256	0.646	1.497	1096	1641	770	1077	71	54	29.41	98.1	99.7	101.4	105.7	105.4	105.8	107.2	105.6
310	1.639	2.993	0.646	1.971	1113	2194	783	1474	71	55	29.375	103.2	105.7	107.9	112.6	110.6	111.1	112.0	151.4
311	1.561	1.721	0.646	0.992	1198	1188	998	816	72	55	29.405	93.7	94.7	96.3	100.0	103.4	105.6	107.3	142.2
313	1.554	2.443	0.646	1.505	1191	1793	995	1182	71	54	29.41	99.9	101.4	103.5	107.9	107.6	108.7	110.6	148.0
315	1.577	3.265	0.646	1.974	1217	2402	1008	1652	72	55	29.39	104.0	106.6	109.3	113.9	112.7	113.9	115.5	153.0
316	1.524	1.830	0.646	1.005	1287	1293	1210	877	72	55	29.405	95.4	96.4	98.4	102.3	105.9	108.1	109.9	144.6
318	1.526	2.638	0.646	1.497	1299	1945	1229	1292	71	54	29.41	100.9	102.9	105.2	109.7	109.9	111.6	13.8	150.0
320	1.531	3.549	0.646	1.979	1301	2575	1225	1789	72	56	29.365	104.6	107.3	110.3	115.0	115.1	116.6	118.5	154.6
321	1.505	1.948	0.646	1.002	1384	1387	1438	922	72	55	29.405	96.5	97.9	100.1	104.2	107.8	110.1	112.0	146.6
323	1.494	2.862	0.646	1.526	1378	2103	1450	1405	71	55	29.37	102.5	104.8	107.3	112.0	112.0	114.0	115.9	152.0
325	1.501	3.873	0.646	1.999	1395	2788	1470	1978	71	55	29.35	106.3	108.6	111.4	116.0	117.8	119.8	121.9	156.8
332	1.793	2.014	0.646	1.243	1013	1259	556	728	69	56	29.418	94.5	95.4	96.5	99.3	101.3	101.7	102.9	140.4
334	1.795	3.190	0.646	1.937	1027	1989	570	1163	70	54	29.415	103.0	104.7	105.9	110.1	109.5	109.8	110.1	149.9
336	1.628	3.042	0.646	1.518	1088	1652	758	834	72	55	29.39	102.7	103.8	104.3	106.6	107.5	108.4	109.6	148.0
337	1.641	2.607	0.646	1.990	1113	2215	781	1682	71	55	29.385	102.0	104.7	107.7	112.5	109.3	109.8	110.7	150.8
341	1.529	3.189	0.646	1.990	1309	2605	1243	1966	72	56	29.356	104.5	107.4	110.5	115.1	114.0	115.4	117.3	154.2
342	1.790	1.190	0.646	0.564	992	559	534	536	65	53	29.40	90.2	91.3	92.9	95.8	98.1	100.2	101.6	137.5
343	1.788	1.351	0.646	0.793	1021	810	567	663	69	56	29.415	90.5	91.4	92.8	95.6	97.9	99.0	101.5	137.3
346	1.562	1.266	0.646	0.612	1195	731	991	683	69	56	29.413	91.8	93.2	95.2	98.9	102.9	105.5	107.4	141.8
349	1.501	1.193	0.646	0.407	1384	563	1446	537	65	53	29.40	95.4	96.6	99.2	103.2	107.9	110.6	112.2	146.5
351	1.508	1.641	0.646	0.798	1393	1111	1450	778	69	56	29.40	93.1	96.2	98.4	102.6	107.0	109.6	111.2	145.6

*The OAPWL's are shown for a 3/4 sphere; to correct the levels to full sphere, add 1.3 dB.
Tabulated OAPWL's are correct; where blanks are found the OAPWL was found to be erroneous.

Table XV. Acoustic Test Matrix, Aerodynamic Test Conditions, DBTF Model 4.

A_c = 17.[illegible] in.^{2} = 0.0111 m^2
A_f = 11.1[illegible] in.^{2} = 0.00717 m^2

												OASPL, dB (Model Scale, 40-ft Arc, Standard Day Data)							
												θ, Angle to Inlet							
Data Pt.	$(P_T/P_O)_c$	$(P_T/P_O)_f$	A_f/A_c	V_f/V_c	V_c (ft/sec)	V_f (ft/sec)	T_{T_c} (° R)	T_{T_f} (° R)	T_{Dry} (° F)	T_{Wet} (° F)	Barom (in. Hg)	50°	70°	90°	110°	130°	140°	150°	OAPWL* dB
401	1.797	1.560	0.646	1.011	989	1000	528	716	61	52	29.45	92.2	92.6	94.0	96.3	98.4	100.1	101.5	137.8
403	1.781	2.068	0.646	1.491	1010	1506	557	1006	65	54	29.45	96.3	97.3	98.8	101.4	102.0	103.5	104.4	142.0
405	1.778	2.722	0.646	2.000	1011	2022	561	1356	65	54	29.455	100.4	102.4	104.4	107.6	107.3	108.3	108.7	147.3
406	1.629	1.631	0.646	1.004	1098	1102	771	774	64	55	29.365	92.5	93.2	94.9	98.0	100.7	103.2	104.8	140.4
408	1.634	2.266	0.646	1.499	1103	1653	774	1088	69	55	29.35	97.4	98.7	100.5	103.5	104.1	105.8	107.6	144.3
410	1.626	2.992	0.646	1.988	1102	2191	779	1471	69	55	29.33	101.3	103.5	105.4	109.2	109.2	110.2	111.5	149.0
411	1.565	1.736	0.646	0.999	1201	1200	997	820	63	54	29.45	93.8	95.0	97.0	100.3	103.9	106.7	108.3	142.9
413	1.559	2.449	0.646	1.508	1196	1803	997	1192	65	54	29.455	98.7	100.3	102.2	105.5	106.9	108.9	110.9	146.6
415	1.563	3.311	0.646	2.027	1184	2400	973	1634	72	56	29.33	99.4	100.6	102.8	106.0	107.2	109.5	111.3	146.9
416	1.529	1.847	0.646	1.006	1298	1306	1222	882	66	54	29.36	95.0	96.2	99.3	102.1	105.7	108.2	110.1	144.5
418	1.528	2.631	0.646	1.490	1301	1939	1228	1288	69	55	29.35	99.7	101.8	103.7	111.8	109.1	111.3	113.5	149.6
420	1.535	3.568	0.646	1.969	1310	2580	1234	1789	72	56	29.33	103.8	106.4	109.0	113.5	115.0	116.7	118.7	
421	1.507	1.952	0.646	1.006	1389	1397	1465	933	66	54	29.35	96.1	97.3	99.7	103.6	107.6	110.3	112.3	145.3
423	1.514	2.862	0.646	1.505	1401	2109	1453	1413	69	56	29.45	101.1	103.1	105.4	108.3	111.6	114.1	116.2	146.8
425	1.509	3.898	0.646	1.984	1404	2786	1469	1948	69	56	29.45	105.4	107.8	110.8	115.1	118.1	120.1	122.3	156.7
432	1.776	2.022	0.646	1.275	987	1258	535	742	61	52	29.45	95.1	95.8	97.1	99.1	100.2	101.4	102.6	140.1
434	1.778	3.170	0.646	1.949	1020	1988	566	1167	65	54	29.455	101.6	104.0	105.5	108.0	108.8	109.8	110.2	148.5
436	1.633	3.047	0.646	1.499	1100	1649	770	830	66	54	29.36	101.5	103.6	104.1	105.8	106.9	108.6	109.8	147.3
437	1.641	2.617	0.646	1.999	1111	2221	777	1686	72	56	29.33	100.5	102.8	105.0	108.7	108.8	109.1	110.3	148.3
441	1.534	3.193	0.646	1.971	1315	2592	1244	1946	72	56	29.33	103.1	105.1	108.0	112.6	113.6	115.2	117.4	152.7
442	1.791	1.187	0.646	0.570	1002	571	544	567	73	58	29.365	89.9	91.2	92.7	95.4	98.0	100.0	101.5	137.1
443	1.794	1.359	0.646	0.818	986	807	526	645	61	52	29.445	90.6	91.4	92.9	95.3	97.9	99.7	101.1	137.1
446	1.559	1.258	0.646	0.601	1196	719	998	677	63	54	29.45	92.1	93.3	95.3	99.0	103.3	106.0	107.8	147.1
449	1.497	1.187	0.646	0.411	1384	569	1456	563	73	58	29.365	94.8	96.1	98.6	102.7	107.6	110.1	111.8	146.0
451	1.507	1.642	0.646	0.797	1394	1111	1454	777	73	58	29.365	94.8	95.9	98.4	107.6	107.1	109.6	111.5	145.5
452	1.746	3.894	0.646	1.723	1617	2786	1468	1968	72	56	29.33	106.8	108.7	111.4	115.8	119.8	122.8	125.4	158.9
453	1.750	2.194	0.646	0.996	1614	1608	1456	1068	73	56	29.33	100.0	101.1	103.5	107.4	112.8	116.2	118.0	151.6
454	1.750	1.695	0.646	0.592	1617	957	1463	703	73	58	29.34	98.4	99.2	101.7	106.1	112.1	115.1	117.2	150.8
455	2.040	3.710	0.646	1.482	1810	2683	1468	1884	72	56	29.33	107.2	108.7	111.4	115.8	121.1	125.1	127.0	160.2
456	2.046	2.448	0.646	1.006	1809	1819	1461	1214	73	58	29.33	103.4	106.5	106.6	111.0	117.7	121.8	122.5	156.1
457	1.981	1.591	0.646	0.608	1771	1076	1460	775	73	58	29.335	100.9	101.7	106.2	108.6	115.6	119.7	120.8	
458	2.478	3.418	0.646	1.237	2013	2490	1463	1718	72	56	29.33	108.6	109.9	112.0	116.6	123.7	127.5	128.0	161.7
459	2.478	2.736	0.646	1.003	2011	2018	1459	1366	72	56	29.33	107.1	108.2	110.1	114.6	122.8	126.4	126.0	160.2
460	2.468	1.733	0.646	0.609	2001	1219	1451	850	73	58	29.33	106.2	106.9	108.6	113.4	122.4	126.4	124.9	159.6
470	---	3.884	0.646	---	---	2778	---	1961	69	56	29.45	104.9	107.0	109.9	113.8	116.5	118.2	119.5	154.8
471	---	2.859	0.646	---	---	2102	---	1605	69	56	29.45	100.5	101.8	104.3	108.0	107.2	108.0	108.0	147.4
472	---	2.452	0.646	---	---	1796	---	1183	69	56	29.448								

*The OAPWL's are shown for a 1/4 sphere; to correct the levels to full sphere, add 1.3 dB. Tabulated OAPWL's are correct; where blanks are found the OAPWL was found to be erroneous.

Table XVI. Acoustic Test Matrix, Aerodynamic Test Conditions, DBTF Model 5.

A_c = 17.21 $in.^2$ = 0.0111 m^2
A_f = 11.43 $in.^2$ = 0.00737 m^2

											OASPL, dB (Model Scale, 40-ft Arc, Standard Day Data)							
											θ, Angle to Inlet							
Data Pt.	$(P_T/P_o)_c$	$(P_T/P_o)_f$	A_f/A_c	V_f/V_c	V_c (ft/sec)	V_f (ft/sec)	T_{T_c} (° R)	T_{T_f} (° R)	T_{Dry} (° F)	T_{Wet} (° F)	Barom (in. Hg)	50°	70°	90°	110°	130°	140°	150°	OAPWL* dB
501	1.789	1.536	0.664	1.007	989	996	532	716	65	60	29.271	92.0	92.9	94.3	97.3	58.9	99.7	101.0	138.2
503	1.802	2.062	0.664	1.501	1000	1501	537	1002	65	60	29.271	97.9	98.6	100.6	104.5	104.1	103.4	104.1	144.2
505	1.800	2.730	0.664	2.002	1006	2014	545	1343	66	60	29.271	102.0	103.5	105.9	110.3	107.5	107.6	108.1	149.4
506	1.626	1.624	0.664	0.992	1090	1081	763	751	66	60	29.280	92.9	93.8	95.2	98.8	100.8	102.7	104.2	140.2
508	1.630	2.259	0.664	1.484	1095	1625	766	1056	66	60	29.273	100.0	100.8	102.5	106.6	105.6	106.1	107.2	146.6
510	1.640	2.991	0.664	1.991	1104	2199	768	1481	66	60	29.270	103.7	105.1	107.6	112.1	109.4	110.5	111.5	151.1
511	1.569	1.735	0.664	0.976	1217	1188	1019	805	68	61	29.280	94.7	95.7	97.5	101.7	103.9	106.1	107.7	143.2
513	1.569	2.452	0.664	1.514	1199	1815	988	1207	68	61	29.280	100.7	102.1	104.2	109.2	107.7	109.0	110.8	149.0
515	1.570	3.262	0.664	1.992	1199	2388	988	163°	68	61	29.280	103.7	106.0	108.5	113.1	111.3	113.2	114.8	
516	1.545	1.846	0.664	0.992	1312	1301	1222	877	69	53	29.485	96.3	97.0	98.9	102.9	106.0	107.6	110.0	145.0
518	1.536	2.636	0.664	1.504	1298	1952	1211	1302	69	53	29.500	101.8	103.2	105.1	109.8	109.4	110.8	113.5	150.1
520	1.544	3.543	0.664	1.964	1310	2573	1219	1788	68	61	29.280	104.3	107.0	109.8	114.3	113.5	115.9	117.9	
521	1.515	1.946	0.664	0.989	1396	1381	1660	916	69	53	29.490	97.2	98.1	100.2	104.3	107.8	109.6	111.9	146.6
523	1.504	2.847	0.664	1.505	1389	2091	1650	1397	69	53	29.500	102.5	104.3	106.2	110.9	111.1	113.6	115.7	151.7
525	1.501	3.867	0.664	1.997	1390	2776	1660	1963	68	61	29.280	105.3	107.8	110.9	115.4	116.1	118.7	121.0	
532	1.824	2.027	0.664	1.233	1015	1252	563	713	68	54	29.552	96.3	96.7	97.2	100.2	102.0	101.3	103.1	141.3
534	1.814	3.174	0.664	1.957	1018	1992	551	1170	68	54	29.550	102.9	104.1	105.2	109.1	108.1	107.9	109.4	149.1
536	1.630	3.053	0.664	1.491	1092	1628	761	806	69	54	29.510	102.9	103.6	103.6	105.7	106.4	106.7	108.6	147.4
537	1.646	2.597	0.664	1.983	1108	2197	770	1661	69	54	29.505	101.6	103.7	106.2	110.9	108.1	108.2	109.9	149.9
541	1.543	3.198	0.664	1.973	1320	2605	1239	1963	69	54	29.520	104.2	106.3	108.8	133.3	112.9	114.6	117.3	153.1
542	1.790	1.207	0.664	0.589	975	517	517	525	65	60	29.255	90.2	91.5	92.9	95.7	97.7	99.7	101.2	137.2
543	1.789	1.355	0.664	0.800	996	797	539	635	65	60	29.270	90.5	91.7	93.3	96.1	98.1	99.7	101.1	137.5
546	1.560	1.274	0.664	0.606	1192	722	990	647	65	60	29.270	91.9	93.5	95.7	99.4	102.3	105.6	107.5	141.9
549	1.520	1.204	0.664	0.411	1404	577	1446	537	65	60	29.265	95.7	97.0	99.4	103.6	108.2	111.3	112.9	146.9
551	1.515	1.636	0.664	0.790	1395	1102	1439	769	65	60	29.273	95.6	96.7	99.1	103.3	106.8	109.6	111.5	145.8

*The OAPWL's are shown for a 3/4 sphere; to correct the levels to full sphere, add 1.3 dB.
Tabulated OAPWL's are correct; where blanks are found the OAPWL was found to be erroneous.

Table XVII. Acoustic Test Matrix, Aerodynamic Test Conditions, DBTF Model 6.

A_c = 17.21 in.^{2} = 0.0111 m^2
A_f = 11.43 in.^{2} = 0.00737 m^2

Data Pt.	$(P_T/P_0)_c$	$(P_T/P_0)_f$	A_f/A_c	V_f/V_c	V_c (ft/sec)	V_f (ft/sec)	T_{T_c} (°R)	T_{T_f} (°R)	T_{Dry} (°F)	T_{Wet} (°F)	Barom (in. Hg)	OASPL, dB (Model Scale, 40-ft Arc, Standard Day Data) θ, Angle to Inlet							OAPWL* dB
												50°	70°	90°	110°	130°	140°	150°	
601	1.791	1.535	0.664	0.981	1002	983	544	698	73	58	29.165	91.2	92.2	93.6	96.2	98.6	100.0	100.9	137.7
603	1.791	2.056	0.664	1.484	1005	1491	548	993	73	58	29.170	96.0	97.0	98.7	101.8	101.5	102.5	103.6	142.0
605	1.790	2.724	0.664	1.987	1011	2009	555	1340	73	58	29.170	100.8	101.9	103.9	107.0	105.8	106.9	107.5	146.8
606	1.620	1.615	0.664	1.987	1081	1067	755	739	73	58	29.165	91.3	92.6	94.3	97.2	99.7	102.3	103.5	
608	1.624	2.254	0.664	1.494	1088	1625	761	1057	73	58	29.170	97.6	98.6	100.2	103.9	103.5	105.6	106.5	
610	1.629	2.989	0.664	2.007	1094	2196	765	1479	73	58	29.170	100.9	103.0	105.1	108.9	107.7	109.4	110.6	148.4
611	1.564	1.735	0.664	0.987	1209	1193	1011	812	73	58	29.165	93.4	94.5	96.5	99.8	101.0	106.0	107.4	
613	1.563	2.455	0.664	1.529	1196	1829	992	1223	73	58	29.165	98.3	99.7	101.9	105.4	106.0	108.5	110.1	
615	1.567	3.266	0.664	1.983	1203	2385	997	1630	75	57	29.160	101.6	104.1	106.4	110.4	110.7	112.9	114.4	
616	1.530	1.832	0.664	1.990	1296	1283	1217	863	73	60	29.177	95.0	95.9	97.7	101.3	105.0	107.7	109.4	144.3
618	1.535	2.647	0.664	1.484	1307	1939	1228	1280	75	61	29.170	100.5	101.7	103.3	107.3	108.5	111.0	113.1	
620	1.531	3.550	0.664	1.983	1299	2576	1220	1790	77	60	29.170	102.9	105.6	107.8	112.9	113.5	116.0	117.5	
621	1.504	1.968	0.664	0.995	1386	1379	1445	912	73	60	29.177	96.4	97.4	99.6	103.1	107.0	109.9	111.5	146.1
623	1.517	2.856	0.664	1.494	1400	2092	1444	1394	75	61	29.170	101.6	103.0	104.8	108.9	110.7	113.5	115.9	150.7
625	1.508	3.876	0.664	1.977	1397	2762	1453	1962	77	60	29.170	104.6	106.7	109.1	113.3	115.8	118.1	120.2	154.9
632	1.784	2.019	0.664	1.261	986	1243	531	706	73	60	29.175	95.1	95.6	96.7	99.0	100.4	101.0	101.9	140.3
634	1.788	3.193	0.664	1.991	1000	1991	543	1164	73	60	29.175	103.4	103.8	104.8	107.3	107.3	108.2	108.7	148.2
636	1.616	3.039	0.664	1.503	1088	1635	768	817	73	60	29.175	102.6	102.9	103.0	106.6	105.5	107.1	108.0	146.7
637	1.625	2.603	0.664	2.017	1088	2196	759	1654	75	61	29.170	100.6	102.4	104.5	108.4	106.4	107.8	109.0	147.9
641	1.520	3.201	0.664	1.995	1292	2577	1228	1920	77	60	29.170	102.6	104.8	107.2	111.4	112.0	116.0	116.1	151.8
642	1.789	1.195	0.664	0.566	985	558	527	521	66	60	29.140	90.0	91.3	92.8	95.3	97.9	99.8	101.0	137.2
643	1.788	1.354	0.664	0.799	1006	804	551	648	68	62	29.160	90.0	91.2	92.7	95.1	97.9	99.8	100.8	137.1
646	1.551	1.261	0.664	0.607	1182	718	985	688	68	62	29.160	91.6	93.2	94.8	98.3	102.3	104.9	106.7	141.4
649	1.518	1.207	0.664	0.411	1400	575	1444	526	66	60	29.160	95.4	96.8	99.1	102.8	108.1	110.9	112.2	146.6
651	1.515	1.637	0.664	0.791	1395	1103	1438	770	68	62	29.160	94.9	96.1	98.3	102.3	106.6	109.3	111.1	146.2
652	1.739	3.893	0.664	1.730	1599	2767	1444	1944	77	60	29.170	105.8	107.5	109.6	113.8	117.5	120.8	123.2	156.9
653	1.741	2.175	0.664	0.999	1601	1600	1445	1068	78	60	29.160	99.6	100.6	102.7	106.5	111.5	115.2	117.1	151.1
654	1.742	1.503	0.664	0.601	1604	964	1449	703	78	60	29.160	98.0	99.1	100.9	105.1	111.5	115.0	116.5	150.4
655	2.052	3.708	0.664	1.476	1807	2668	1452	1864	78	60	29.170	106.7	108.2	110.3	114.2	119.8	123.6	125.6	159.3
656	2.038	2.455	0.664	1.001	1799	1813	1451	1203	78	60	29.160	103.5	104.2	106.3	110.5	116.2	120.5	121.4	155.6
657	2.043	1.602	0.644	0.591	1804	1066	1456	750	78	60	29.160	101.8	102.8	104.6	109.2	116.3	120.7	120.8	154.8
658	2.470	3.426	0.644	1.236	2006	2479	1458	1701	77	60	29.170	109.0	110.1	111.5	115.0	122.3	126.5	127.2	160.7
659	2.465	2.724	0.644	1.001	2005	2007	1459	1336	78	60	29.160	107.6	108.7	109.9	113.4	121.1	125.4	125.1	159.2
660	2.470	1.724	0.644	0.598	2000	1195	1448	822	78	60	29.160	106.6	107.6	108.9	113.0	121.6	125.3	124.3	158.9

*The OAPWL's are shown for a 3/4 sphere; to correct the levels to full sphere, add 1.3 dB.
Tabulated OAPWL's are correct; where blanks are found the OAPWL was found to be erroneous.

Table XVIII. Acoustic Test Matrix, Aerodynamic Test Conditions, DBTF Model 7.

A_c = 17.21 in.^{2} = 0.0111 m^2
A_f = 11.06 in.^{2} = 0.00714 m^2

Data Pt.	$(P_T/P_0)_c$	$(P_T/P_0)_f$	A_f/A_c	V_f/V_c	V_c (ft/sec)	V_f (ft/sec)	TT_c (° R)	TT_f (° R)	T_{Dry} (° F)	T_{Wet} (° F)	Barom (in. Hg)	OASPL, dB (Model Scale, 40-ft Arc, Standard Day Data) θ, Angle to Inlet 50°	70°	90°	110°	130°	140°	150°	OAPWL* dB
701	1.277	1.508	0.643	1.00	968	969	514	705	69	40	29.503	94.6	95.[illegible]	96.9	99.2	101.8	104.7	104.7	141.6
703	1.782	2.043	0.643	1.53	964	1474	508	978	69	40	29.605	98.9	100.0	102.4	105.3	108.5	109.9	109.5	146.8
705	1.779	2.712	0.643	2.09	965	2018	511	1356	69	40	29.512	106.6	107.1	108.6	111.8	115.7	117.0	116.5	153.8
706	1.632	1.612	0.643	0.99	1094	1083	762	765	63	39	29.670	96.0	96.3	98.2	101.9	104.6	108.5	110.1	144.6
708	1.634	2.254	0.643	1.50	1102	1654	772	1095	65	40	29.690	102.3	103.3	104.8	108.5	111.0	114.3	114.9	
710	1.642	2.980	0.643	1.99	1110	2209	775	1499	69	40	29.520	110.1	110.6	111.3	114.7	118.9	120.8	121.3	
711	1.583	1.738	0.643	0.99	1218	1210	1002	834	67	41	29.531	97.8	98.5	100.6	104.8	109.0	112.1	113.8	151.1
713	1.597	2.456	0.6[illegible]	1.47	1228	1811	1000	1200	56	65	29.522	105.0	105.8	106.9	110.8	115.1	117.4	118.2	153.3
715	1.590	3.275	0.643	1.97	1217	2402	1004	1649	56	65	29.510	112.3	113.2	113.2	117.2	122.0	124.6	124.8	160.1
716	1.532	1.849	0.643	1.01	1298	1304	1218	878	59	67	29.483	99.2	99.9	102.2	106.2	111.1	114.5	115.6	149.6
718	1.525	2.460	0.643	1.52	1294	1963	1222	1316	56	65	29.515	106.5	107.7	109.0	113.2	117.6	120.0	121.1	156.0
720	1.536	3.552	0.643	1.98	1303	2584	1219	1800	58	67	29.505	112.3	113.8	116.5	118.7	123.9	126.4	127.6	161.9
721	1.518	1.951	0.643	1.00	1407	1404	1436	942	55	66	29.552	101.5	102.3	104.6	108.9	114.1	117.0	118.7	
723	1.513	2.873	0.643	1.50	1403	2100	1439	1997	58	67	29.485	107.3	108.6	110.6	115.0	119.7	122.8	124.1	158.2
725	1.509	3.877	0.643	1.99	1393	2774	1448	1957	58	67	29.500	113.0	116.3	115.9	120.6	126.0	128.9	129.7	164.1
726	1.369	1.526	0.643	0.97	1018	989	1004	717	52	66	29.531	92.7	93.7	95.7	99.5	103.0	105.5	106.7	
727	1.377	2.076	0.643	1.46	1027	1499	1003	993	52	66	29.525	98.7	100.0	102.1	105.7	109.2	111.0	111.7	
728	1.389	2.734	0.643	1.96	1035	2024	992	1354	55	66	29.518	106.0	107.0	108.1	112.5	116.7	118.5	119.1	154.6
729	1.873	1.967	0.643	1.00	1399	1397	992	936	59	67	29.475	102.0	102.8	104.6	108.2	113.8	117.6	119.0	152.6
730	1.869	2.861	0.643	1.50	1406	2110	1003	1415	59	67	29.472	109.2	110.1	110.9	115.0	119.6	122.7	124.3	158.5
731	1.860	3.864	0.643	1.98	1400	2777	1002	1965	50	62	29.818	113.7	116.6	116.0	120.8	125.5	127.6	129.2	163.5
733	1.790	2.601	0.643	1.55	971	1504	512	787	60	37	29.662	105.0	105.9	105.0	107.3	109.6	112.6	112.3	149.7
734	1.794	3.179	0.643	2.03	981	1991	520	1168	63	39	29.670	110.4	111.6	110.9	113.7	116.4	119.5	119.5	156.1
735	1.661	2.577	0.643	1.48	1105	1639	769	943	65	60	29.672	106.4	106.9	106.4	109.4	112.1	115.5	116.2	152.1
736	1.651	3.025	0.643	1.47	1113	1636	772	822	65	60	29.685	111.0	111.5	109.6	111.2	113.8	117.1	117.8	154.6
737	1.619	2.604	0.643	2.03	1090	2208	768	1676	50	62	29.825	106.2	106.9	108.9	113.2	117.2	118.0	118.9	154.9
738	1.552	2.897	0.643	1.52	1189	1804	995	1033	68	59	28.990	107.2	107.6	107.6	110.9	115.8	117.8	118.5	154.3
739	1.566	2.902	0.643	2.00	1205	2408	1003	1811	50	62	29.830	107.5	108.7	111.2	115.9	120.4	121.7	122.9	158.0
740	1.552	2.657	0.643	2.03	1193	2426	1002	1975	50	62	29.830	106.3	107.6	110.5	115.3	119.2	120.4	121.6	156.9
741	1.528	3.188	0.643	1.98	1307	2585	1261	1937	51	61	29.830	110.8	111.8	113.6	118.2	123.2	126.9	126.5	161.1
742	1.768	1.176	0.643	0.55	950	525	699	506	60	37	29.655	93.0	92.7	94.3	97.2	98.4	102.0	103.1	138.8
743	1.764	1.335	0.643	0.84	954	798	505	669	60	37	29.660	93.5	93.1	95.0	97.8	98.9	102.7	103.9	139.0
744	1.61	1.266	0.643	0.59	1097	648	768	536	68	59	28.995	93.3	93.1	95.1	98.3	112.6	115.6	117.0	149.1
745	1.555	1.176	0.643	0.44	1191	525	994	507	60	37	29.535	94.1	94.9	97.6	101.2	106.5	109.7	110.8	145.1
746	1.576	1.276	0.643	0.60	1218	725	1013	655	67	41	29.533	94.6	95.5	98.1	101.8	107.1	110.4	111.6	145.6
747	1.581	1.506	0.643	0.79	1218	967	1006	708	67	41	29.532	95.8	96.5	99.1	102.8	107.9	110.9	112.4	146.3
748	1.539	1.341	0.643	0.61	1308	804	1224	668	68	59	28.980	97.5	96.8	98.9	103.1	108.6	111.8	113.3	147.4
749	1.513	1.206	0.643	0.40	1403	562	1460	508	68	60	29.488	97.8	98.6	101.2	105.0	111.0	114.6	115.5	149.4
750	1.506	1.617	0.643	0.63	1392	881	1652	680	68	60	29.485	99.0	98.9	101.8	105.6	110.1	114.9	116.1	149.9
751	1.509	1.631	0.643	0.80	1397	1111	1656	787	68	60	29.485	100.7	101.0	103.2	106.8	111.1	115.3	116.9	150.5
752	1.736	3.073	0.643	1.73	1603	2778	1656	1464	51	61	29.833	113.9	114.7	116.5	121.1	126.8	129.8	131.1	164.9
753	1.757	2.171	0.643	0.98	1616	1585	1651	1090	68	60	29.480	105.6	105.9	108.4	112.5	117.6	122.6	124.1	157.4
754	1.755	1.696	0.643	0.59	1623	959	1666	706	50	62	29.485	102.9	103.2	105.5	109.7	115.5	120.5	121.6	155.0
755	2.063	3.096	0.643	1.67	1808	2663	1661	1861	51	61	29.832	113.7	114.2	116.3	121.0	127.5	131.2	131.7	165.5
756	2.056	2.426	0.643	0.99	1421	1803	1670	1203	68	60	29.480	109.2	109.5	111.7	116.1	122.4	127.4	128.0	161.4

*The OAPWL's shown are for a 3/4 sphere; to correct the levels to full sphere, add 1.3 dB. Tabulated OAPWL's are correct; where blanks are found, the OAPWL was found to be erroneous.

Table XVIII. Acoustic Test Matrix, Aerodynamic Test Conditions, DBTF Model 7 (Concluded).

A_c = 17.21 in.^{2} = 0.0111 m^2
A_f = 11.06 in.^{2} = 0.00714 m^2

Data Pt.	$(P_T/P_0)_c$	$(P_T/P_0)_f$	A_f/A_c	V_f/V_c	V_c (ft/sec)	V_f (ft/sec)	T_{T_c} (° R)	T_{T_f} (° R)	T_{Dry} (° F)	T_{Wet} (° F)	Barom (in. Hg)	OASPL, dB (Model Scale, 40-ft Arc, Standard Day Data) θ, Angle to Inlet 50°	70°	90°	110°	130°	140°	150°	OAPWL* dB
757	2.066	1.589	0.643	0.59	1819	1069	1459	768	48	40	29.480	106.5	106.7	109.1	113.3	120.3	125.6	125.6	159.2
758	2.461	3.401	0.643	1.24	1999	2485	1452	1717	53	42	29.828	116.0	114.3	116.4	121.1	129.2	132.4	131.9	166.2
759	2.460	2.725	0.643	1.01	1993	2007	1445	1336	53	42	29.825	112.0	112.1	114.0	118.6	121.9	130.6	130.0	164.3
760	2.560	1.750	0.643	0.60	2039	1222	1456	841	48	40	29.480	110.6	110.6	112.8	117.3	125.7	130.3	128.6	163.3
770	---	3.842	0.643	---	---	2756	---	1966	53	42	29.818	113.1	114.0	116.2	120.7	128.7	130.9	129.9	165.1
771	---	2.832	0.643	---	---	2097	---	1410	53	42	29.825	107.2	107.7	109.6	113.2	119.0	121.7	123.1	157.2
772	---	2.410	0.643	---	---	1793	---	1198	53	42	29.823	102.7	103.5	105.4	109.1	113.3	115.2	116.5	151.9
773	1.510	---	0.643	---	1398	---	1455	---	53	42	29.812	98.2	99.7	101.6	105.3	110.6	112.9	113.8	148.5
776	1.364	---	0.643	---	1195	---	989	---	53	42	29.812	94.7	96.0	98.3	102.1	106.6	109.0	110.1	145.0
780	---	3.721	0.643	---	---	2672	---	1866	---	---	---	112.3	112.9	115.6	118.7	128.9	130.3	130.3	165.0
781	---	3.565	0.643	---	---	2578	---	1788	---	---	---	112.0	112.6	116.7	118.1	127.4	128.9	129.6	164.0
785	---	3.012	0.643	---	---	2210	---	1490	---	---	---	108.7	108.8	110.6	113.5	122.6	125.1	125.4	159.7
786	---	2.866	0.643	---	---	2111	---	1415	---	---	---	107.0	107.2	109.2	112.1	120.8	122.9	124.0	158.0
787	---	3.819	0.643	---	---	2767	---	1938	---	---	---	112.9	113.7	116.0	119.5	130.2	130.4	130.1	165.6
789	---	2.907	0.643	---	---	2403	---	1801	---	---	---	107.7	108.5	110.8	114.1	123.7	125.3	125.6	160.1
791	---	2.091	0.643	---	---	2098	---	1901	---	---	---	102.3	104.0	106.6	109.6	115.4	116.9	119.4	153.4

*The OAPWL's shown are for a 3/4 sphere; to correct the levels to full sphere, add 1.3 dB.
Tabulated OAPWL's are correct; where blanks are found, the OAPWL was found to be erroneous.

Table XIX. Acoustic Test Matrix, Aerodynamic Test Conditions, DBTF Model 8.

$A_c = 17.21\ \text{in.}^2 = 0.0111\ \text{m}^2$
$A_f = 11.12\ \text{in.}^2 = 0.00717\ \text{m}^2$

												OASPL, dB (Model Scale, 40-ft Arc, Standard Day Data)							
												θ, Angle to Inlet							
Data Pt.	$(P_T/P_o)_c$	$(P_T/P_o)_f$	A_f/A_c	V_f/V_c	V_c (ft/sec)	V_f (ft/sec)	TT_c (° R)	TT_f (° R)	T_{Dry} (° F)	T_{Wet} (° F)	Barom (in. Hg)	50°	70°	90°	110°	130°	140°	150°	OAPWL* dB
801	1.771	1.503	0.647	1.02	955	978	503	723	41	34	29.615	95.9	96.4	98.3	100.6	102.7	104.8	104.7	142.3
803	1.767	2.024	0.647	1.53	968	1481	520	998	42	34	29.615	100.7	101.7	103.6	106.7	109.9	111.1	110.2	148.1
805	1.769	2.699	0.647	2.08	969	2016	519	1357	41	34	29.615	108.2	109.2	110.2	113.8	117.9	118.8	119.0	156.0
806	1.59	1.589	0.647	1.00	1068	1067	765	763	44	34.5	29.617	97.0	97.4	99.2	102.3	106.1	108.9	109.2	145.1
808	1.621	2.252	0.647	1.52	1089	1651	765	1092	44	34.5	29.620	103.3	104.3	106.1	109.7	113.6	115.2	115.3	151.8
810	1.637	2.983	0.647	2.01	1095	2200	759	1487	45	35	29.610	110.7	112.0	112.6	116.5	121.0	122.2	122.6	158.9
811	1.56	1.728	0.647	1.00	1195	1191	994	815	52	41	29.525	98.4	99.5	101.6	105.2	110.0	112.5	113.3	148.1
813	1.568	2.424	0.647	1.49	1203	1797	996	1196	52	41	29.510	105.6	107.1	108.1	112.1	116.5	118.3	119.3	156.6
815	1.59	3.269	0.647	1.94	1219	2366	994	1603	53	42	29.550	114.1	114.3	114.6	118.6	123.4	126.1	126.8	162.1
816	1.566	1.835	0.647	1.00	1310	1306	1216	888	51	41	29.500	---	---	---	---	---	---	---	---
818	1.569	2.654	0.647	1.49	1310	1950	1209	1292	51	41	29.550	108.9	109.9	110.7	114.4	119.1	121.5	122.9	158.0
820	1.537	3.565	0.647	1.97	1309	2580	1229	1791	43	35	29.595	114.6	114.3	116.1	120.4	126.0	128.5	128.7	163.8
821	1.523	1.965	0.647	0.99	1397	1386	1425	923	51	41	29.500	101.7	103.0	105.4	109.3	115.3	117.9	118.6	153.1
823	1.518	2.859	0.647	1.50	1405	2112	1453	1420	44	38	29.590	112.2	[illegible]	114.0	117.7	122.6	126.5	127.4	161.9
825	1.497	3.888	0.647	2.01	1388	2784	1463	1968	44	36	29.590	115.6	115.6	118.2	122.6	128.6	131.6	131.1	166.2
826	1.352	1.533	0.647	1.02	972	990	950	709	52	41	29.530	93.4	94.6	[illegible]	99.7	103.0	104.9	105.3	141.6
827	1.363	2.058	0.647	1.49	1002	1493	985	994	52	41	29.510	99.6	101.3	103.3	106.8	110.8	111.7	111.4	148.1
828	1.365	2.732	0.647	1.99	1007	2004	992	1330	52	41	29.512	110.1	111.2	110.8	114.8	118.9	121.6	122.1	157.7
829	1.862	1.950	0.647	1.00	1395	1395	994	932	52	41	29.520	102.7	103.9	105.9	109.8	115.6	118.8	120.0	
830	1.878	2.853	0.647	1.49	1405	2096	996	1400	53	42	29.510	108.5	110.2	111.9	116.6	121.5	124.1	125.5	159.9
831	1.852	3.884	0.647	[illegible]	1612	2771	1026	1951	44	35	29.595	116.1	116.3	117.4	122.2	127.7	130.3	131.0	165.4
833	1.702	2.586	0.647	1.5[illegible]	971	1487	511	773	41	34	29.615	107.1	108.2	108.0	109.4	112.0	113.8	113.0	152.1
834	1.772	3.153	0.647	2.03	974	1980	523	1163	40	33	29.615	110.5	111.2	111.5	114.7	119.2	120.6	120.7	157.6
835	1.626	2.584	0.647	1.49	1089	1620	761	918	44	34.5	29.620	108.5	109.1	108.4	110.9	114.8	116.5	117.5	154.2
836	1.638	3.013	0.647	1.49	1101	1637	766	925	44	34.5	29.620	113.0	113.5	113.6	114.1	117.5	118.6	119.8	157.5
837	1.627	2.591	0.647	2.00	1095	2185	768	1647	53	42	29.550	106.9	108.7	110.7	115.1	119.3	120.1	120.5	157.0
838	1.576	2.858	0.647	1.48	1203	1777	986	1013	52	41	29.510	110.9	112.5	111.2	113.6	117.8	119.4	121.3	
839	1.566	2.886	0.647	1.98	1199	2371	993	1765	43	35	29.595	110.3	110.5	113.0	117.5	122.5	124.1	124.3	160.0
840	1.566	2.658	0.647	2.00	1208	2421	1007	1968	43	35	29.595	109.0	109.2	112.9	117.7	121.7	123.3	124.2	159.9
841	1.526	3.199	0.647	2.01	1295	2597	1227	1951	44	35	29.593	112.6	112.6	115.5	119.9	125.0	127.0	127.7	162.7
842	1.770	1.160	0.647	0.54	976	527	527	555	51	40	29.552	92.6	93.8	95.1	97.8	101.0	103.2	104.1	140.0
843	1.763	1.337	0.647	0.81	963	781	515	638	42	34	29.615	94.4	94.9	96.6	98.8	101.1	103.7	103.9	140.9
844	1.612	1.223	0.647	0.56	1080	606	761	545	51	40	29.532	92.6	93.9	96.1	99.9	104.6	106.8	108.0	143.3
845	1.538	1.174	0.647	0.46	1172	541	989	543	51	40	29.550	94.2	95.4	97.6	101.6	107.0	110.0	111.0	145.4
846	1.567	1.252	0.647	0.58	1201	700	995	655	52	41	29.550	94.9	96.2	98.5	102.3	107.7	110.7	111.8	146.2
847	1.558	1.498	0.647	0.80	1191	956	990	699	52	41	29.535	96.0	97.0	99.0	102.7	108.0	111.0	112.0	146.4
848	1.535	1.337	0.647	0.61	1298	787	1212	667	51	41	29.510	96.6	97.6	100.0	104.0	110.1	113.3	114.3	148.6
849	1.481	1.159	0.647	0.38	1364	520	1451	563	52	41	29.550	97.6	98.9	101.3	105.7	111.5	114.6	115.3	149.6
850	1.504	1.433	0.647	0.62	1399	869	1469	642	51	41	29.500	98.9	99.8	102.3	106.3	112.8	115.9	116.6	151.1
851	1.513	1.646	0.647	0.79	1396	1109	1445	771	51	41	29.500	99.9	101.2	103.4	107.5	113.8	116.6	117.2	151.7
852	1.742	3.883	0.647	1.74	1606	2801	1453	1992	43	36	29.590	114.5	114.7	118.0	122.5	129.1	132.1	131.7	166.5
853	1.748	2.191	0.647	1.00	1616	1608	1462	1069	43	35	29.580	106.6	106.2	109.2	113.5	120.9	123.7	124.7	158.5
854	1.777	1.508	0.647	0.59	1631	960	1451	694	43	35	29.583	103.9	103.3	106.4	111.0	119.1	122.2	122.6	156.6
855	2.032	3.720	0.647	1.51	1786	2698	1436	1901	44	36	29.590	114.6	114.8	118.1	122.6	129.9	133.1	132.0	167.0
856	2.035	2.467	0.647	1.01	1803	1816	1460	1201	43	35	29.580	109.9	109.2	112.5	116.9	125.1	128.2	128.3	162.5
857	2.051	1.595	0.647	0.59	1807	1067	1453	758	43	35	29.583	107.1	106.2	109.4	114.0	123.2	126.3	125.4	160.0
858	2.458	3.418	0.647	1.25	1998	2489	1453	1717	44	36	29.590	116.8	116.3	118.6	122.8	131.3	133.7	131.9	167.5
859	2.469	2.733	0.647	1.01	2000	2023	1499	1353	43	35	29.580	116.6	115.5	117.4	121.2	130.1	132.4	131.0	166.4
860	2.460	1.725	0.647	0.60	2005	1201	1461	832	43	35	29.580	114.5	113.5	114.8	119.0	129.6	131.9	129.9	165.4

*The OAPWL's shown are for a 3/4 sphere; to correct the levels to full sphere, add 1.3 dB. Tabulated OAPWL's are correct; where blanks are found, the OAPWL was found to be erroneous.

Table XX. Acoustic Test Matrix, Aerodynamic Test Conditions, DBTF Model 9.

A_c = 17.21 in.^{2} = 0.0111 m^2
A_f = 11.12 in.^{2} = 0.00717 m^2

												OASPL, dB (Model Scale, 40-ft Arc, Standard Day Data) θ, Angle to Inlet							
Data Pt.	$(P_T/P_o)_c$	$(P_T/P_o)_f$	A_f/A_c	V_f/V_c	V_c (ft/sec)	V_f (ft/sec)	T_{T_c} (° R)	T_{T_f} (° R)	T_{Dry} (° F)	T_{Wet} (° F)	Barom (in. Hg)	50°	70°	90°	110°	130°	140°	150°	OAPWL* dB
901	1.792	1.529	0.646	0.980	1011	991	554	715	74	58	29.439	95.0	95.6	95.9	98.0	100.1	101.8	102.9	139.8
903	1.794	2.049	0.646	1.472	1016	1496	559	1003	74	58	29.432	97.9	99.4	101.0	104.4	105.1	105.2	105.5	144.7
905	1.791	2.729	0.646	1.986	1019	2024	563	1357	74	58	29.432	102.4	105.0	107.0	110.8	109.5	109.5	109.5	150.2
911	1.559	1.727	0.646	0.996	1192	1187	990	811	74	58	29.425	96.0	96.8	98.4	101.6	105.0	107.3	108.7	144.0
913	1.564	2.452	0.646	1.508	1205	1817	1005	1209	74	58	29.422	101.2	103.3	105.5	109.3	109.4	110.5	112.1	149.7
915	1.564	3.239	0.646	1.980	1209	2394	1013	1643	74	58	29.42	105.5	107.7	110.5	114.4	113.6	114.9	116.0	153.9
921	1.513	1.951	0.646	0.996	1397	1391	1449	926	75	60	29.41	98.1	99.5	101.5	105.4	109.3	112.3	113.5	148.1
923	1.496	2.862	0.646	1.523	1380	2102	1451	1404	75	60	29.415	103.9	106.1	108.5	112.6	113.3	115.6	117.1	153.2
925	1.495	3.876	0.646	2.002	1385	2773	1463	1957	74	58	29.415	106.6	109.1	111.7	116.4	118.2	120.3	122.3	157.3
962	1.784	1.182	0.646	0.557	1015	565	562	570	79	61	29.39	94.1	96.8	97.3	98.7	99.1	101.6	103.6	140.0
963	1.785	1.354	0.646	0.791	1020	807	567	654	79	61	29.39	95.2	93.5	94.2	97.8	100.2	102.3	103.0	
946	1.562	1.270	0.646	0.595	1201	714	1001	643	79	61	29.41	93.7	94.6	101.3	99.7	104.1	107.4	108.7	143.7
949	1.516	1.180	0.646	0.403	1403	566	1453	576	79	61	29.39	96.7	97.4	99.7	103.9	109.0	112.2	113.5	147.7
951	1.515	1.644	0.646	0.787	1402	1103	1454	765	75	60	29.41	97.2	97.4	99.3	103.0	107.7	110.6	112.0	146.4

*The OAPWL's shown are for a 3/4 sphere; to correct the levels to full sphere, add 1.3 dB.
Tabulated OAPWL's are correct; where blanks are found, the OAPWL was found to be erroneous.

Table XXI. Acoustic Test Matrix, Aerodynamic Test Conditions, DBTF Model 10.

A_c = 17.21 in.^{2} = 0.0111 m^2
A_f = 11.12 in.^{2} = 0.00717 m^2

Data Pt.	$(P_T/P_O)_c$	$(P_T/P_O)_f$	A_f/A_c	V_f/V_c	V_c (ft/sec)	V_f (ft/sec)	T_{T_c} (° R)	T_{T_f} (° R)	T_{Dry} (° F)	T_{Wet} (° F)	Barom (in. Hg)	OASPL, dB (Model Scale, 40-ft Arc, Standard Day Data) θ, Angle to Inlet 50°	70°	90°	110°	130°	140°	150°	OAPWL* dB
1001	1.792	1.522	0.646	0.598	989	987	530	717	59	55	29.472	93.1	94.5	96.7	99.1	101.1	103.6	104.7	143.6
1003	1.795	2.061	0.646	1.496	997	1492	537	991	59	55	29.478	98.6	100.2	102.5	105.5	106.4	107.3	108.1	148.0
1005	1.798	2.721	0.646	1.977	1013	2003	553	1333	59	55	29.488	104.5	105.8	108.5	111.9	112.5	113.2	113.4	153.9
1011	1.570	1.733	0.646	0.995	1197	1191	984	811	62	56	29.490	96.1	97.2	99.6	103.2	106.6	109.4	109.6	148.0
1013	1.563	2.448	0.646	1.509	1195	1803	990	1193	61	55	29.485	103.1	104.2	106.8	110.0	111.5	113.5	114.1	153.5
1015	1.565	3.266	0.646	1.982	1206	2391	1005	1638	61	55	29.485	108.2	109.4	112.3	115.9	116.0	117.7	118.3	157.6
1021	1.511	1.968	0.646	1.001	1399	1400	1458	927	62	56	29.490	99.5	100.8	103.5	107.4	110.9	113.5	113.0	151.5
1023	1.495	2.844	0.646	1.526	1380	2106	1453	1417	62	56	29.483	105.6	106.9	109.4	112.8	115.0	117.0	117.3	156.1
1025	1.506	3.855	0.646	1.976	1401	2768	1470	1956	62	56	29.485	110.4	112.0	114.4	118.2	120.1	122.2	122.8	160.8
1042	1.788	1.199	0.646	0.576	972	560	513	516	56	53	29.463	90.7	92.2	94.6	97.1	99.2	102.4	103.1	141.2
1043	1.786	1.366	0.646	0.819	989	810	534	640	59	55	29.460	91.4	93.0	95.2	97.5	99.7	102.4	103.2	142.0
1046	1.558	1.251	0.646	0.596	1186	707	981	671	56	53	29.459	92.8	94.6	97.5	101.3	105.2	108.5	108.6	146.2
1049	1.518	1.184	0.646	0.392	1396	547	1433	527	56	53	29.461	96.5	98.5	101.7	105.8	110.1	113.5	112.8	150.2
1051	1.510	1.634	0.646	0.784	1392	1092	1444	758	62	56	29.490	97.4	99.1	101.9	106.0	109.6	112.4	111.9	150.1

*The OAPWL's shown are for a 3/4 sphere; to correct the levels to full sphere, add 1.3 dB.
Tabulated OAPWL's are correct; where blanks are found, the OAPWL was found to be erroneous.

Table XXII. Acoustic Test Matrix, Aerodynamic Test Conditions, DBTF Model 11.

A_c = 17.21 in.^{2} = 0.0111 m^2
A_f = 11.12 in.^{2} = 0.00717 m^2

Data Pt.	$(P_T/P_O)_c$	$(P_T/P_O)_f$	A_f/A_c	V_f/V_c	V_c (ft/sec)	V_f (ft/sec)	T_{T_c} (° R)	T_{T_f} (° R)	T_{Dry} (° F)	T_{Wet} (° F)	Barom (in. Hg)	OASPL, dB (Model Scale, 40-ft Arc, Standard Day Data) θ, Angle to Inlet 50°	70°	90°	110°	130°	140°	150°	OAPWL* dB
1101	1.790	1.533	0.646	0.991	1006	997	549	720	68	59	29.675	93.6	96.6	96.6	98.7	101.2	103.3	104.6	142.9
1103	1.787	2.059	0.646	1.492	1006	1501	551	1004	68	59	29.675	98.0	99.1	101.1	105.0	107.0	116.6	107.5	150.1
1105	1.791	2.725	0.646	1.985	1016	2017	560	1349	68	59	29.679	103.26	106.9	107.6	111.5	112.0	111.9	112.6	117.5
1111	1.566	1.725	0.646	0.968	1208	1169	1010	788	68	57	29.665	95.9	97.0	99.5	103.2	106.9	108.8	109.8	148.1
1113	1.560	2.448	0.646	1.509	1193	1800	991	1190	68	57	29.675	101.8	102.9	105.7	109.6	111.6	112.5	113.2	152.6
1115	1.563	3.255	0.646	1.976	1206	2383	1008	1631	68	59	29.675	106.6	108.2	110.9	115.5	115.9	116.8	117.7	157.2
1121	1.497	1.963	0.646	1.018	1378	1403	1643	936	70	57	29.665	98.8	100.0	102.7	107.2	110.9	112.7	112.7	151.3
1123	1.499	2.861	0.646	1.519	1388	2109	1658	1416	70	57	29.665	104.8	106.1	109.0	113.6	115.3	116.6	117.3	156.6
1125	1.502	3.882	0.646	1.997	1390	2776	1657	1959	70	57	29.502	109.6	111.2	116.1	118.8	119.7	121.2	122.2	160.7
1142	1.788	1.107	0.646	0.565	1002	566	546	556	66	57	29.690	91.1	92.8	95.0	97.5	99.9	102.6	103.8	142.1
1143	1.791	1.357	0.646	0.802	1013	812	557	656	68	59	29.680	92.3	93.5	96.0	98.1	100.2	102.6	104.2	142.2
1146	[illegible]	[illegible]	0.646	[illegible]	[illegible]	716	987	660	68	59	29.685	93.2	94.8	97.8	101.3	105.2	108.0	108.5	144.6
1149	1.506	1.185	0.646	0.419	1392	582	1652	596	66	57	29.690	92.5	94.3	97.2	101.1	104.7	106.9	106.8	144.8
1151	1.502	1.625	0.646	0.795	1388	1103	1653	782	68	57	29.665								

*The OAPWL's shown are for a 3/4 sphere; to correct the levels to full sphere, add 1.3 dB.
Tabulated OAPWL's are correct; where blanks are found, the OAPWL was found to be erroneous.

Table XXIII. Full-Scale Data-Reduction Program Format.

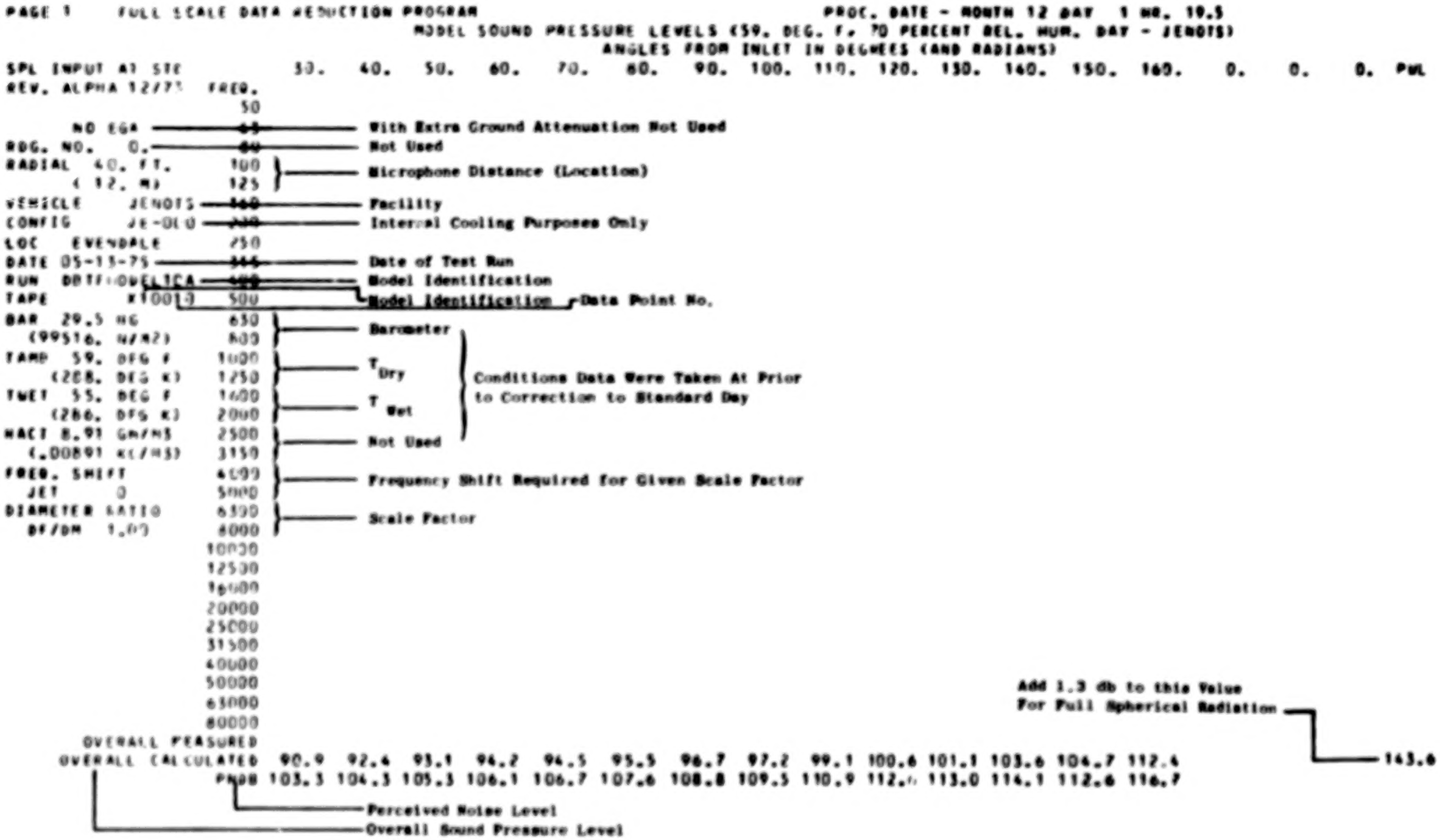

```
PAGE 1    FULL SCALE DATA REDUCTION PROGRAM                                  PROC. DATE - MONTH 12 DAY  1 HR. 19.5
                                   MODEL SOUND PRESSURE LEVELS (59. DEG. F, 70 PERCENT REL. HUM. DAY - JENOTS)
                                                         ANGLES FROM INLET IN DEGREES (AND RADIANS)
SPL INPUT AT STE          30.   40.   50.   60.   70.   80.   90.  100.  110.  120.  130.  140.  150.  160.    0.    0.    0.  PWL
REV. ALPHA 12/75  FREQ.
                     50
      NO EGA ------- 63 -------- With Extra Ground Attenuation Not Used
RDG. NO.   0. ------ 80 -------- Not Used
RADIAL  40. FT.     100 }
      ( 12. M)      125 }------- Microphone Distance (Location)
VEHICLE    JENOTS - 160 -------- Facility
CONFIG     JE-OLO - 200 -------- Internal Cooling Purposes Only
LOC   EVENDALE      250
DATE 05-13-75 ----- 315 -------- Date of Test Run
RUN  DBTF/OVELICA - 400 -------- Model Identification
TAPE       KT0013   500 -------- Model Identification  -Data Point No.
BAR  29.5 HG        630 }
  (99516. N/M2)     800 }------- Barometer       }
TAMP  59. DEG F    1000 }                        }
    (288. DEG K)   1250 }------- T Dry           } Conditions Data Were Taken At Prior
TWET  55. DEG F    1600 }                        } to Correction to Standard Day
    (286. DEG K)   2000 }------- T Wet           }
HACT 8.91 GM/M3    2500 }
  (.00891 KG/M3)   3150 }------- Not Used
FREQ. SHIFT        4000 }
  JET      0       5000 }------- Frequency Shift Required for Given Scale Factor
DIAMETER RATIO     6300 }
  DF/DM  1.00      8000 }------- Scale Factor
                  10000
                  12500
                  16000
                  20000
                  25000
                  31500
                  40000
                  50000                                                                  Add 1.3 db to this Value
                  63000                                                                  For Full Spherical Radiation --
                  80000                                                                                                 |
   OVERALL MEASURED                                                                                                     |
   OVERALL CALCULATED  90.9  92.4  93.1  94.2  94.5  95.5  96.7  97.2  99.1 100.6 101.1 103.6 104.7 112.4                 ---- 143.6
      |           PNDB 103.3 104.3 105.3 106.1 106.7 107.6 108.8 109.5 110.9 112.0 113.0 114.1 112.6 116.7
      |             |
      |             |-------- Perceived Noise Level
      |---------------------- Overall Sound Pressure Level
```

Table XXIV. Scale-Model Acoustic Data.

```
PAGE 1     FULL SCALE DATA REDUCTION PROGRAM                              PROC. DATE - MONTH 00 DAY  0 HR.  0.0
                                   MODEL SOUND PRESSURE LEVELS (59. DEG. F, 70 PERCENT REL. HUM. DAY - JENOTS)
                                                          ANGLES FROM INLET IN DEGREES (AND RADIANS)
SPL INPUT AT STD            30.    40.    50.    60.    70.    80.    90.   100.   110.   120.   130.   140.   150.   160.     0.     0.     0.   PWL
REV. ALPHA 12/73  FREQ. (0.52)(0.70)(0.87)(1.05)(1.22)(1.40)(1.57)(1.75)(1.92)(2.09)(2.27)(2.44)(2.62)(2.79)(0.   )(0.   )(0.   )
                     50   70.3   70.1   70.9   69.9   70.7   71.3   71.4   72.5   73.4   75.1   78.3   81.0   85.3   87.7                      118.9
        NO EGA       63   73.1   73.3   73.6   73.5   73.8   75.6   75.0   75.4   76.6   78.6   81.8   84.6   89.0   90.6                      122.2
RDG. NO.   9x        80   75.1   75.7   76.5   75.4   75.0   75.4   77.6   77.0   79.3   81.9   85.5   88.4   91.5   93.4                      125.1
RADIAL  40. FT.     100   78.1   78.1   78.9   77.6   77.9   79.6   81.9   82.8   84.0   85.9   88.4   93.0   97.3   98.2                      129.0
       ( 12. M)     125   81.4   79.7   79.9   80.2   79.9   82.4   84.6   85.4   86.7   89.2   91.7   95.3   99.0   99.8                      131.9
VEHICLE    JENOTS   160   85.9   82.9   83.4   82.6   83.1   84.9   87.6   87.9   90.4   91.9   93.6   97.1  100.1  100.9                      133.6
CONFIG     JE-060   200   86.0   85.0   83.0   83.5   84.0   85.8   87.0   88.3   90.5   93.9   97.1  100.9  103.0  103.5                      136.2
LOC   EVENDALE      250   87.0   87.5   86.5   86.0   86.3   87.3   88.0   89.5   95.3   98.0  100.0  102.8  106.2  105.1                      138.7
DATE 05-08-75       315   89.3   87.3   86.8   87.8   89.5   89.4   88.8   93.3   94.0   97.0  101.0  103.6  108.7  110.5                      140.7
RUN  COTF-MODEL 4   400   86.1   83.9   87.8   86.5   88.1   88.4   90.3   92.6   95.0   98.1   98.0  105.0  108.7  105.3                      140.4
TAPE        x40230  500   87.8   87.8   88.3   86.8   87.9   88.9   91.4   92.9   94.7   96.7   99.4  105.9  108.1  105.3                      140.3
BAR  29.3 HG        630   88.1   87.9   87.9   86.4   88.2   87.8   91.1   93.4   95.9   97.4  100.7  105.3  107.6  104.6                      140.1
  (99111. N/M2)     800   86.9   87.9   87.6   88.0   89.8   89.3   90.9   93.9   95.8   99.3  101.4  104.0  104.2  103.4                      139.0
TAMB  69. DEG F    1000   87.6   85.9   87.8   87.4   88.5   89.9   91.7   93.3   96.1   99.1  101.2  100.9  100.6   97.9                      137.2
     (294. DEG K)  1250   85.7   86.4   87.4   87.8   88.5   89.2   91.4   93.4   94.9   98.4  101.3  102.2   97.7   94.9                      137.0
TWET  55. DEG F    1600   85.0   87.0   87.1   87.7   88.8   90.0   91.8   93.5   95.1   97.8   99.8   99.2   95.1   92.2                      135.7
     (286. DEG K)  2000   86.1   85.8   86.3   88.2   89.7   90.4   91.8   93.3   95.0   96.9   98.7   98.0   94.8   91.8                      135.1
HACT 0.    GM/M3   2500   84.8   87.1   87.0   87.0   88.6   89.7   91.9   93.1   95.0   96.3   96.7   96.7   93.4   90.0                      134.2
  (0.      KG/M3)  3150   84.6   85.9   87.3   88.2   89.1   90.3   92.0   93.9   95.3   96.6   96.9   95.1   93.1   90.6                      134.4
FREQ. SHIFT        4000   83.2   86.9   87.0   88.3   89.9   91.6   93.9   94.7   96.8   96.6   95.0   93.8   91.8   89.3                      134.6
  JET     0        5000   83.0   87.0   87.1   88.8   91.3   93.3   95.0   94.3   98.1   97.7   95.2   94.1   91.5   89.6                      135.7
DIAMETER RATIO     6300   82.7   87.9   88.5   90.3   92.6   93.7   94.7   96.1   98.0   97.7   94.6   93.7   91.6   89.6                      135.9
  DF/DM  1.00      8000   82.5   87.5   88.3   90.3   92.5   93.8   94.0   96.4   98.0   97.2   93.4   92.5   90.4   88.7                      135.9
                  10000   81.8   88.5   89.3   90.6   92.0   92.4   93.0   96.3   97.9   96.4   92.9   90.8   90.2   88.9                      135.7
                  12500   81.6   89.4   90.5   91.5   91.9   91.4   92.7   95.0   96.5   95.1   91.7   89.7   90.4   89.3                      135.2
                  16000   78.8   86.3   86.8   89.4   90.1   89.8   90.9   93.4   95.0   93.1   89.3   87.3   87.1   85.2                      133.8
                  20000   75.8   83.6   84.6   85.6   86.6   86.8   88.4   93.2   92.8   90.6   86.5   83.8   83.8   82.4                      131.4
                  25000   73.3   81.8   83.3   84.4   84.6   85.1   86.8   88.5   89.5   87.6   83.8   81.0   82.6   81.0                      129.6
                  31500   70.2   78.0   79.3   81.2   81.5   83.6   84.9   86.3   86.5   85.2   81.1   78.7   81.0   79.2                      127.7
                  40000   67.9   75.1   76.8   78.4   78.4   80.2   81.9   82.8   83.2   82.0   77.7   76.1   81.3   77.0                      125.4
                  50000   66.9   71.6   72.8   74.4   74.5   77.1   79.8   79.8   80.3   80.9   75.9   76.9   83.8   80.9                      124.7
                  63000   67.0   68.2   69.4   70.6   71.4   75.9   77.9   77.9   77.6   81.8   75.1   78.6   85.8   83.3                      126.4
                  80000   67.7   65.6   66.1   68.6   69.6   76.7   78.0   77.4   75.6   82.8   79.9   79.4   87.9   84.8                      130.3
       OVERALL MEASURED
     OVERALL CALCULATED   99.1  100.5  101.1  101.8  103.1  104.0  105.4  107.4  109.3  110.3  111.6  114.1  116.2  114.9                      150.8
                   PNDB  110.3  112.2  112.5  113.3  115.0  116.3  117.9  119.5  121.4  122.1  122.7  123.2  123.9  122.4
```

237

Table XXV. Scaled (Full Size) Acoustic Data.

```
PAGE 1    FULL SCALE DATA REDUCTION PROGRAM                                       PROC. DATE - MONTH 32 DAY  0 HR.  0.0
                              FULL SIZE SOUND PRESSURE LEVELS SCALED FROM MODEL DATA (59. DEG. F. 70 PERCENT REL. HUM. DAY - JENOTS)
                                                             ANGLES FROM INLET IN DEGREES (AND RADIANS)
SPL INPUT AT STD          30.    40.    50.    60.    70.    80.    90.   100.   110.   120.   130.   140.   150.   160.      0.     0.     0.  PWL
REV. ALPHA 12/73  FREQ. (0.52)(0.70)(0.87)(1.05)(1.22)(1.40)(1.57)(1.75)(1.92)(2.09)(2.27)(2.44)(2.62)(2.79)(0.    )(0.    )(0.    )
                     50   86.4   84.2   92.3   86.9   88.7   89.5   90.8   93.1   95.6   99.3   99.5  106.5  110.5  107.6                     160.0
      NO EGA         63   87.3   87.6   89.3   87.3   88.2   89.9   92.5   93.7   95.4   97.4   99.5  106.4  108.1  105.8                     158.7
REG. NO.   0.        80   86.6   88.2   88.2   87.2   86.4   88.7   91.6   94.4   96.7   98.7  102.2  106.3  108.4  106.8                     159.3
RADIAL 323. FT.     100   86.5   87.9   88.1   88.8   89.9   89.8   91.9   94.6   96.3  100.3  102.5  105.0  104.0  104.5                     157.8
       ( 98. 4)     125   87.3   86.4   88.5   88.2   89.3   90.7   92.2   94.3   96.4   99.8  101.7  103.4  101.1   98.9                     156.3
VEHICLE    JENOTS   160   86.5   86.9   88.1   88.5   89.2   90.4   92.7   94.2   95.9   99.4  101.8  102.5   98.9   95.7                     155.7
CONFIG     JET200   200   85.8   87.7   87.7   88.2   89.8   91.0   92.5   94.5   95.8   98.2  100.1   99.5   96.6   93.0                     154.2
L.C  EVENDALE       250   86.6   86.8   86.8   88.9   90.2   90.6   92.3   93.8   95.5   97.6   98.9   98.5   95.8   91.5                     153.6
DATE 05-08-75       315   85.5   87.5   86.0   87.9   89.1   90.7   92.4   93.9   95.5   97.6   98.0   97.7   93.7   90.0                     153.2
RUN  CBTF-MODEL 4   400   85.3   87.9   88.3   89.2   90.1   91.6   92.8   94.1   95.3   97.4   96.4   96.4   93.6   89.9                     152.9
TAPE       X40230   500   84.4   87.2   88.3   89.3   90.9   93.1   94.1   96.0   96.8   97.2   95.8   95.1   91.8   89.5                     153.3
BAR  29.5 HG        630   85.0   87.8   89.6   90.6   92.3   94.1   96.1   97.3   98.8   97.5   95.5   94.0   92.0   89.9                     154.6
  (99448. N/M2)     800   85.1   88.6   90.1   91.7   93.2   94.8   95.2   97.7   98.6   98.0   94.7   94.3   92.2   88.7                     154.6
TAMB  69. DEG F    1000   84.7   88.2   90.5   91.9   93.2   94.0   94.7   97.4   99.0   97.1   94.1   93.2   90.8   89.1                     154.1
     (294. DEG K)  1250   84.9   89.6   91.1   91.9   92.9   93.5   93.9   97.4   98.8   96.8   93.0   92.1   91.3   90.3                     154.2
THET  56. DEG F    1600   85.4   90.4   92.3   92.5   92.9   92.9   93.9   96.8   98.2   96.0   92.2   91.6   92.1   90.7                     154.0
     (286. DEG K)  2000   83.2   88.7   90.5   91.1   91.7   91.0   92.4   95.1   96.4   94.0   90.2   89.0   89.0   87.1                     152.4
HACT 0.   GM/M3    2500   84.6   85.9   87.4   88.4   88.5   88.1   90.3   92.5   93.9   91.9   87.8   86.1   85.9   83.7                     150.2
  (.      KG/M3)   3150   78.1   83.6   85.3   86.7   86.2   86.7   88.6   90.1   90.9   88.7   84.9   82.8   83.1   81.3                     148.2
FREQ. SHIFT        4000   74.4   79.9   82.0   83.4   83.2   84.8   86.1   87.1   87.4   85.9   81.5   79.9   80.0   77.9                     146.0
   JET      0      5000   71.7   76.9   78.9   80.4   81.5   80.8   82.7   83.8   84.2   82.9   78.0   77.4   76.9   75.6                     143.0
DIAMETER RATIO     6300   66.6   72.5   75.0   76.1   75.2   76.0   79.8   80.5   80.5   81.6   75.6   76.6   75.2   73.0                     141.2
   DF/DP  0.00     8000   67.6   69.0   70.9   71.4   71.9   71.7   77.9   78.7   77.7   81.9   75.4   70.6   76.1   79.1                     141.7
                  10000   68.1   66.0   67.3   67.0   70.0   68.9   78.9   79.1   75.5   84.5   76.6   80.1   77.6   77.3                     149.4
     OVERALL CALCULATED   98.3  100.6  102.2  102.4  103.5  104.9  105.9  108.0  109.8  110.5  111.1  113.9  115.0  112.9                     160.4
                   PNDB  106.9  110.8  112.4  113.0  113.7  114.1  115.7  117.9  119.1  118.5  116.3  116.7  118.2  115.2
```

Table XXVI. Extrapolated, Scaled (Full Size) Acoustic Data.

```
PAGE 4    FULL SCALE DATA REDUCTION PROGRAM                            PROC. DATE - MONTH 32 DAY  0 HR.  0.0

                          FULL SIZE SOUND PRESSURE LEVELS SCALED FROM MODEL DATA (59. DEG. F, 70 PERCENT REL. HUM, DAY)
                                                 ANGLES FROM INLET IN DEGREES (AND RADIANS)
SPL INPUT AT STD          30.   40.   50.   60.   70.   80.   90.  100.  110.  120.  130.  140.  150.  160.     0.     0.     0.
REV. ALPHA 12/73  FREQ. (0.52)(0.70)(0.87)(1.05)(1.22)(1.40)(1.57)(1.75)(1.92)(2.09)(2.27)(2.44)(2.62)(2.79)(0.  )(0.  )(0.  )
                     50   62.6  62.6  72.3  68.0  70.4  71.7  73.2  75.3  77.3  80.4  79.5  84.9  88.6  80.3
      NO EGA         63   63.4  65.9  69.2  68.2  70.9  72.0  74.0  75.9  77.2  78.5  79.4  84.7  84.1  78.4
SIDELINE 2400. FT.   80   62.5  66.5  68.1  68.2  70.2  70.9  73.9  76.5  78.4  79.7  82.1  84.6  84.4  79.2
      (731.52 M)    100   62.3  66.1  67.9  69.6  71.1  71.0  74.1  76.7  77.9  81.1  82.2  83.2  79.0  76.7
RFA     0. RPM      125   63.0  64.4  68.2  69.0  70.8  72.7  74.3  76.3  77.9  80.7  81.4  81.4  76.0  70.9
  (    0. RAD/SEC)  160   61.9  64.8  67.8  69.2  70.7  72.3  74.7  76.1  77.4  80.1  81.4  80.4  74.4  67.3
RFK     0. RPM      200   61.0  65.4  67.0  68.0  70.9  72.7  74.4  79.7  77.1  78.8  79.5  77.1  71.0  64.2
  (    0. RAD/SEC)  250   61.5  64.3  65.9  69.3  71.4  72.2  74.0  75.4  76.5  78.0  78.1  75.9  70.7  62.3
RFD     0. RPM      315   60.0  64.7  66.9  67.6  70.8  72.1  74.0  79.2  76.9  77.7  76.8  74.0  68.1  60.1
  (    0. RAD/SEC)  400   59.2  64.6  66.0  69.1  70.8  72.7  74.1  75.3  76.0  77.2  75.0  73.1  67.5  59.3
AIRFLOW RATIO       500   57.7  63.4  66.4  68.8  71.3  73.9  75.1  76.8  77.0  76.7  74.8  71.3  69.1  57.9
  WF/WH  0.00       630   57.4  63.3  67.2  69.6  72.2  74.5  76.7  77.7  78.8  76.5  73.1  70.4  64.4  56.9
                    800   56.3  63.3  67.0  70.1  72.6  74.7  75.3  77.6  78.0  76.4  71.6  68.9  63.4  54.0
VEHICLE    JENOTS  1000   54.6  61.9  66.5  69.1  71.9  73.3  74.1  76.6  77.6  75.0  70.2  66.0  60.7  52.7
CONFIG     JE-080  1250   53.1  61.9  66.1  68.6  70.7  72.0  72.5  75.9  76.6  73.5  68.0  64.5  59.5  51.0
LOC   EVENDALE     1600   51.1  60.9  65.7  67.9  69.5  70.2  71.4  74.1  74.8  71.4  65.7  62.2  57.9  47.9
DATE 09-08-75      2000   48.1  57.0  62.1  64.9  66.9  66.9  68.5  71.0  71.6  67.0  61.0  57.3  51.9  39.9
RUN  CBTF-MODEL 4  2500   39.3  51.0  56.4  60.0  61.5  62.1  64.5  66.5  67.0  63.4  56.0  51.2  44.6  30.2
TAPE       X40230  3150   30.1  43.6  50.1  54.5  55.9  57.5  59.7  60.9  60.6  56.5  49.7  42.8  35.1  17.9
FAN TIP SPEED      4000   16.2  32.2  40.4  45.7  47.9  50.8  52.5  53.3  52.1  48.2  40.0  32.2  21.8
         FT/SEC    5000    7.7  24.7  33.6  39.5  41.8  44.0  46.4  46.9  46.0  41.6  32.0  25.2  12.9
                   6300          7.2  19.0  25.7  28.4  31.1  35.5  35.6  33.7  31.2  19.6  11.3
                   8000                       6.6  12.6  14.3  21.4  21.4  17.7  17.1   2.8
                  10000                                         5.3   4.4
    OVERALL CALCULATED    72.5  76.4  79.9  81.1  83.2  84.8  86.5  88.3  89.4  90.3  90.4  91.9  90.8  85.2
                   PNDB   74.3  81.2  85.5  87.6  89.8  91.8  92.7  94.8  95.6  94.2  92.3  91.4  87.9  80.7
```

APPENDIX E

FAN PLUG PRESSURE DISTRIBUTIONS FOR AERODYNAMIC MODEL 5

The fan plug pressure distributions recorded during testing of the multitube fan-suppressor nozzle with hardwall ejector with the sharp-lip inlet (aerodynamic Model 5) are presented in Figures 147 through 154.

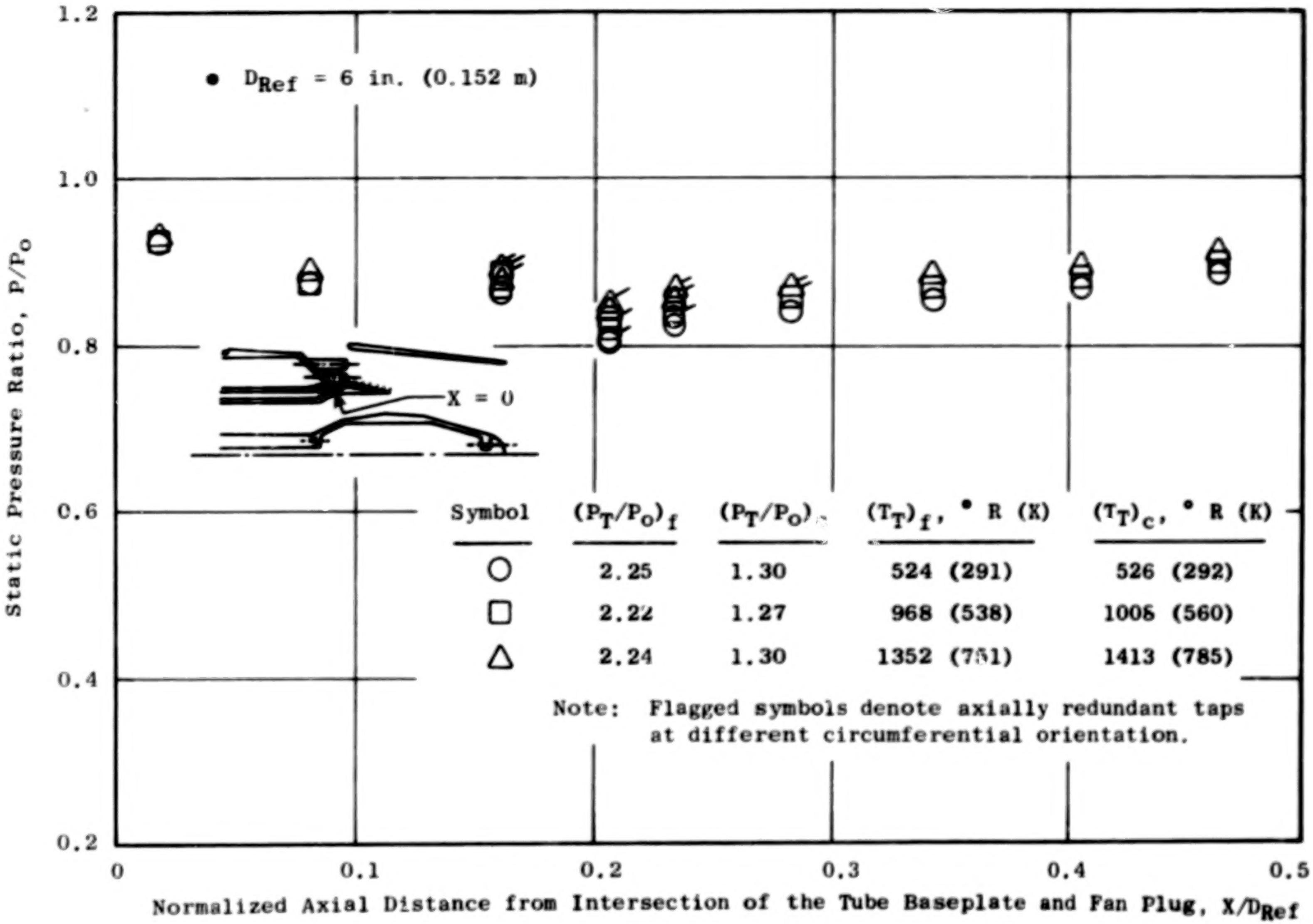

Figure 147. Comparison of Hot and Cold Flow Fan Plug Pressure Distributions, Multitube Fan Suppressor Nozzle with Hardwall Ejector (Sharp Lip); Aerodynamic Model 5, $(P_T/P_o)_f$ = 2.25.

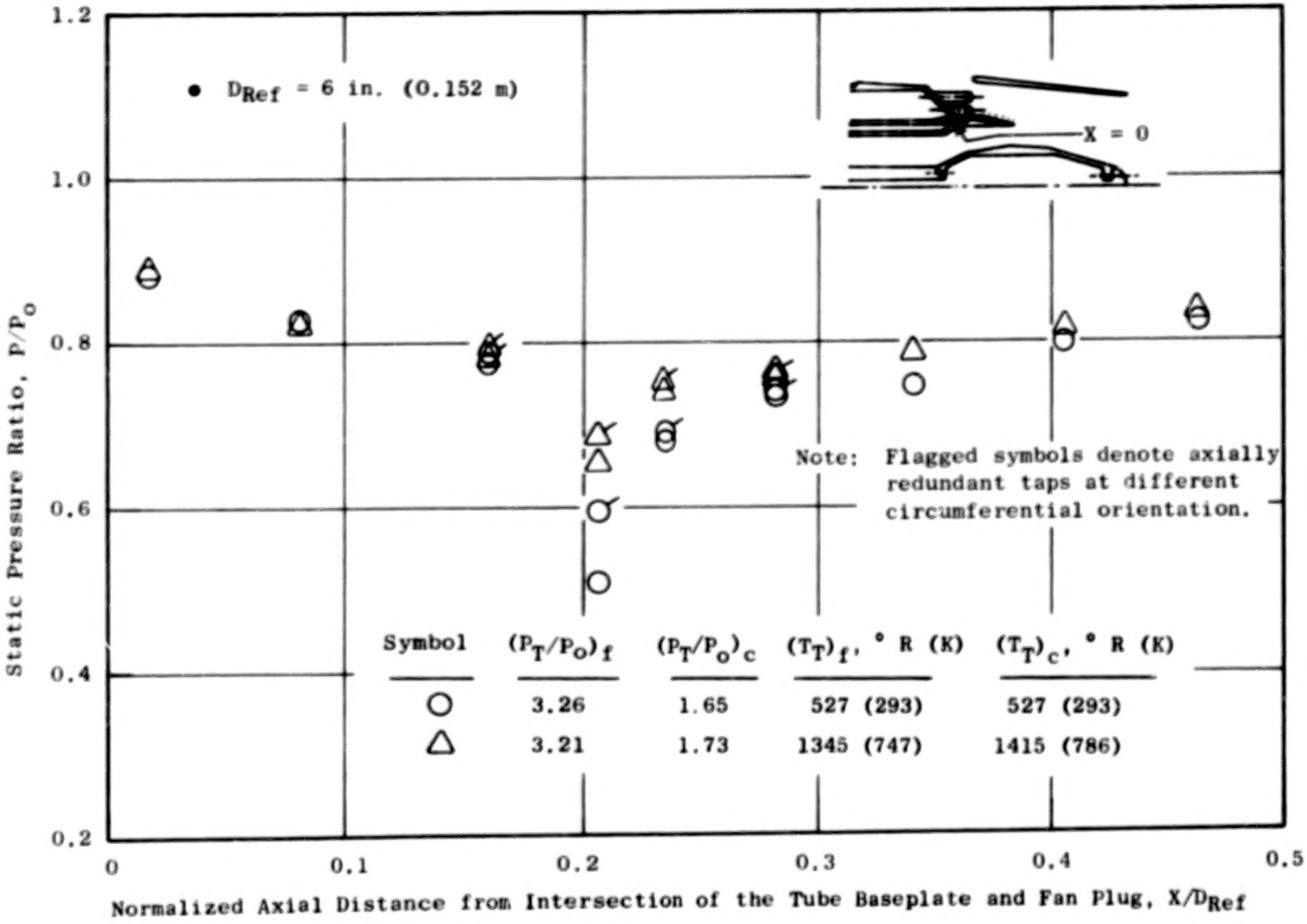

Figure 148. Comparison of Hot and Cold Flow Fan Plug Pressure Distributions, Multitube Fan Suppressor Nozzle with Hardwall Ejector (Sharp Lip); Aerodynamic Model 5, $(P_T/P_o)_f$ = 3.2.

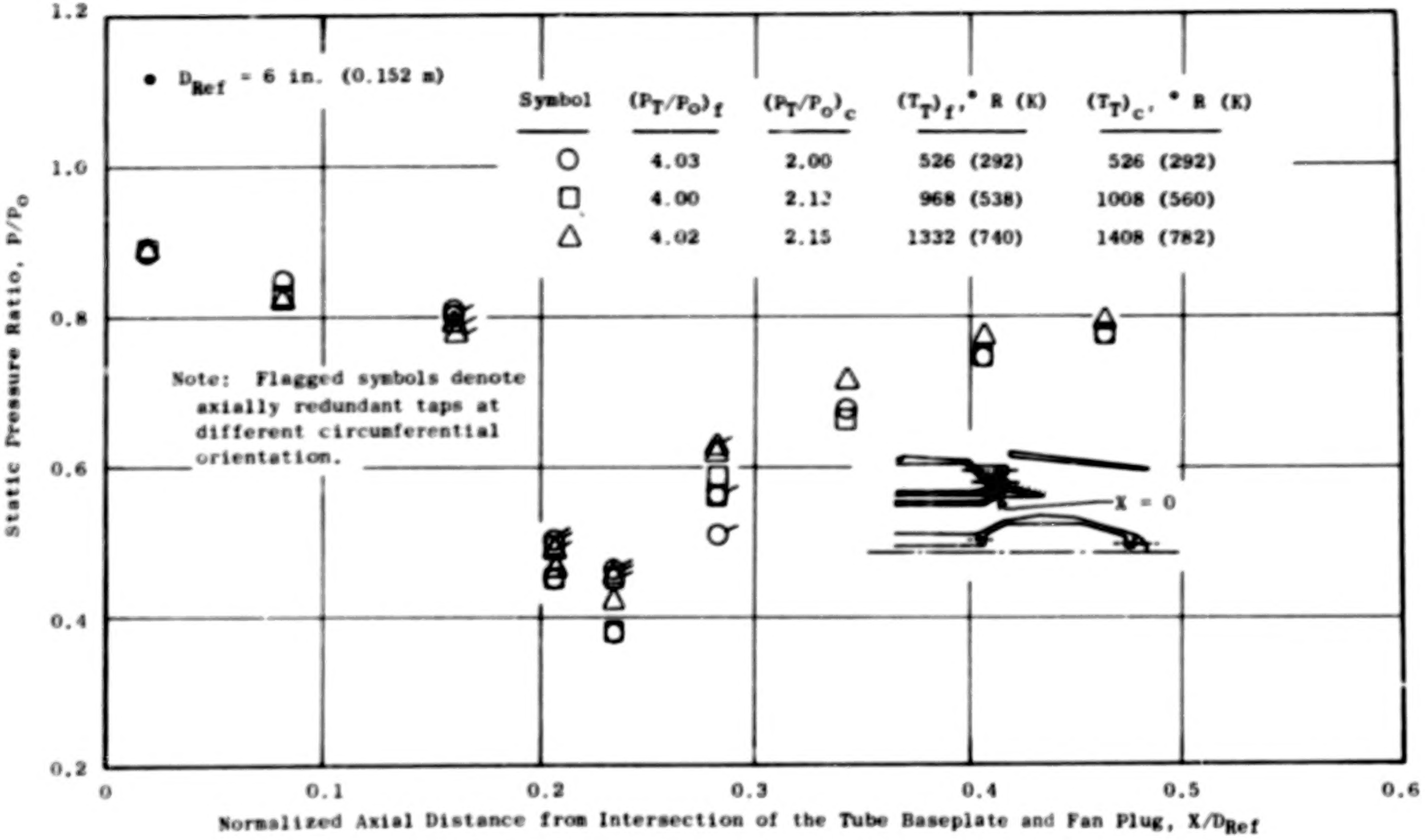

Figure 149. Comparison of Hot and Cold Flow Fan Plug Pressure Distributions, Multitube Fan Suppressor Nozzle with Hardwall Ejector (Sharp Lip); Aerodynamic Model 5, $(P_T/P_o)_f = 4.0$.

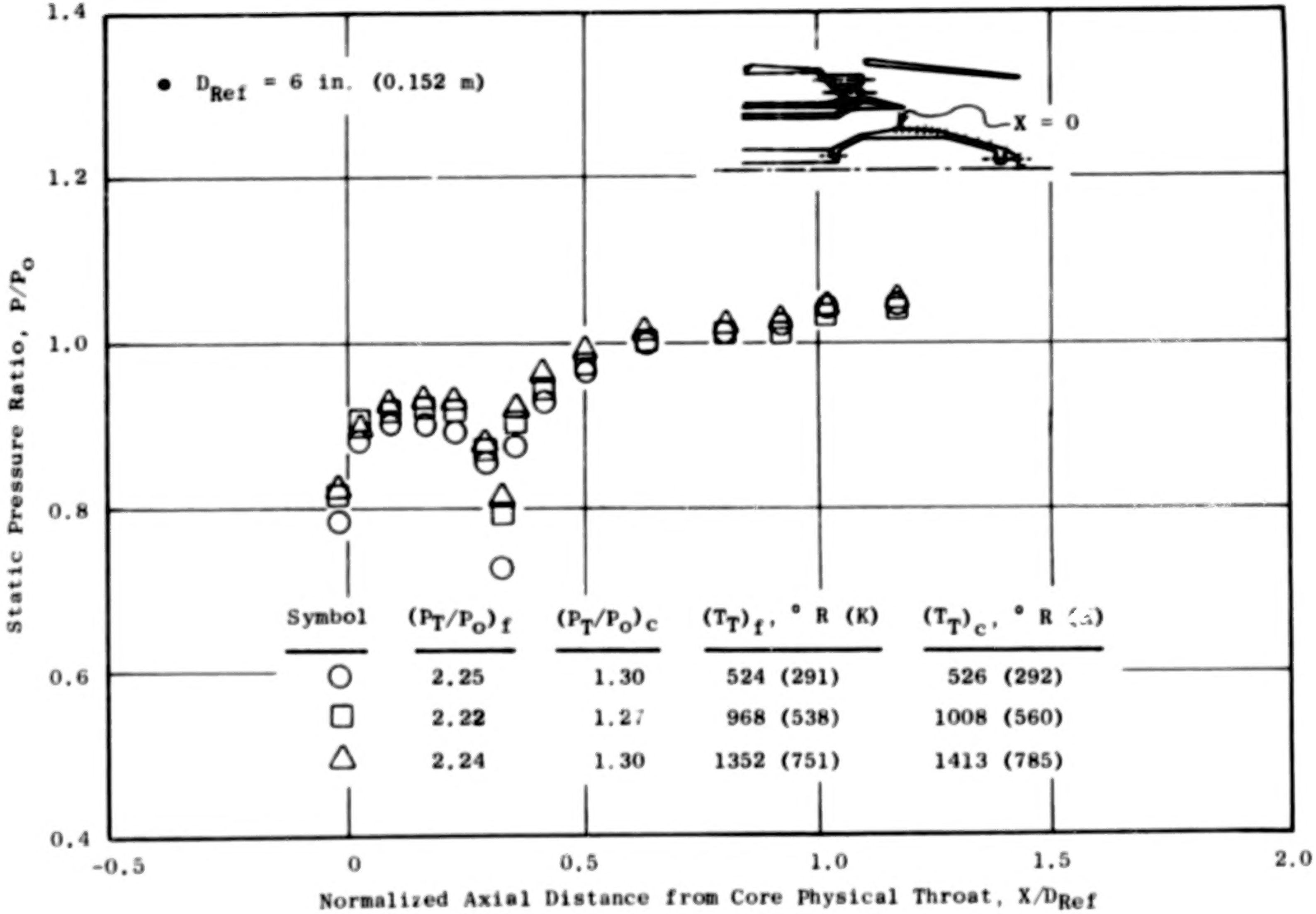

Symbol	$(P_T/P_o)_f$	$(P_T/P_o)_c$	$(T_T)_f$, ° R (K)	$(T_T)_c$, ° R (K)
○	2.25	1.30	524 (291)	526 (292)
□	2.22	1.27	968 (538)	1008 (560)
△	2.24	1.30	1352 (751)	1413 (785)

Figure 150. Comparison of Hot and Cold Flow Core Plug Pressure Distributions, Multitube Fan Suppressor Nozzle with Hardwall Ejector (Sharp Lip); Aerodynamic Model 5, $(P_T/P_o)_f$ = 2.25.

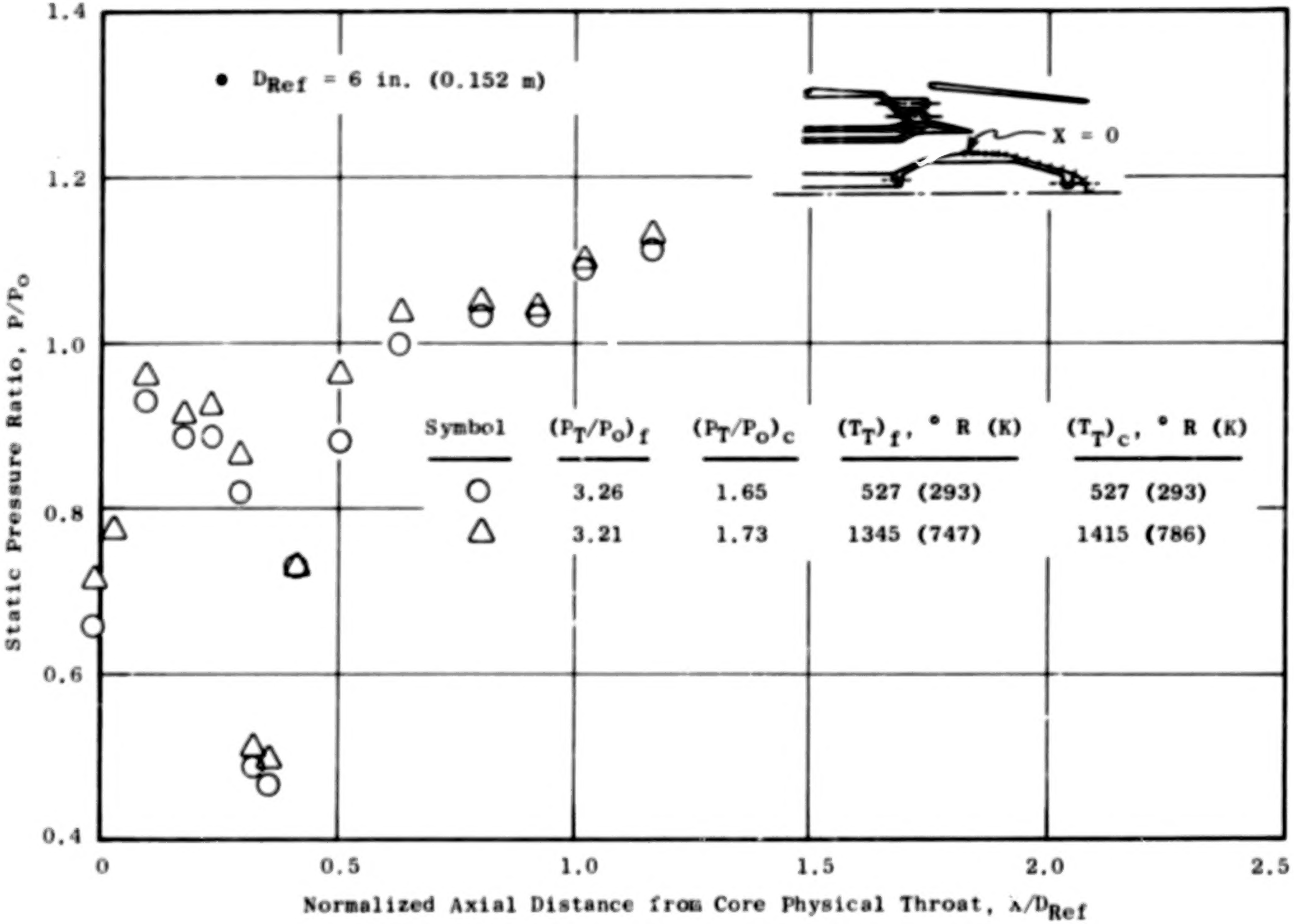

Figure 151. Comparison of Hot and Cold Flow Core Plug Pressure Distributions, Multitube Fan Suppressor Nozzle with Hardwall Ejector (Sharp Lip); Aerodynamic Model 5, $(P_T/P_o)_f = 3.25$.

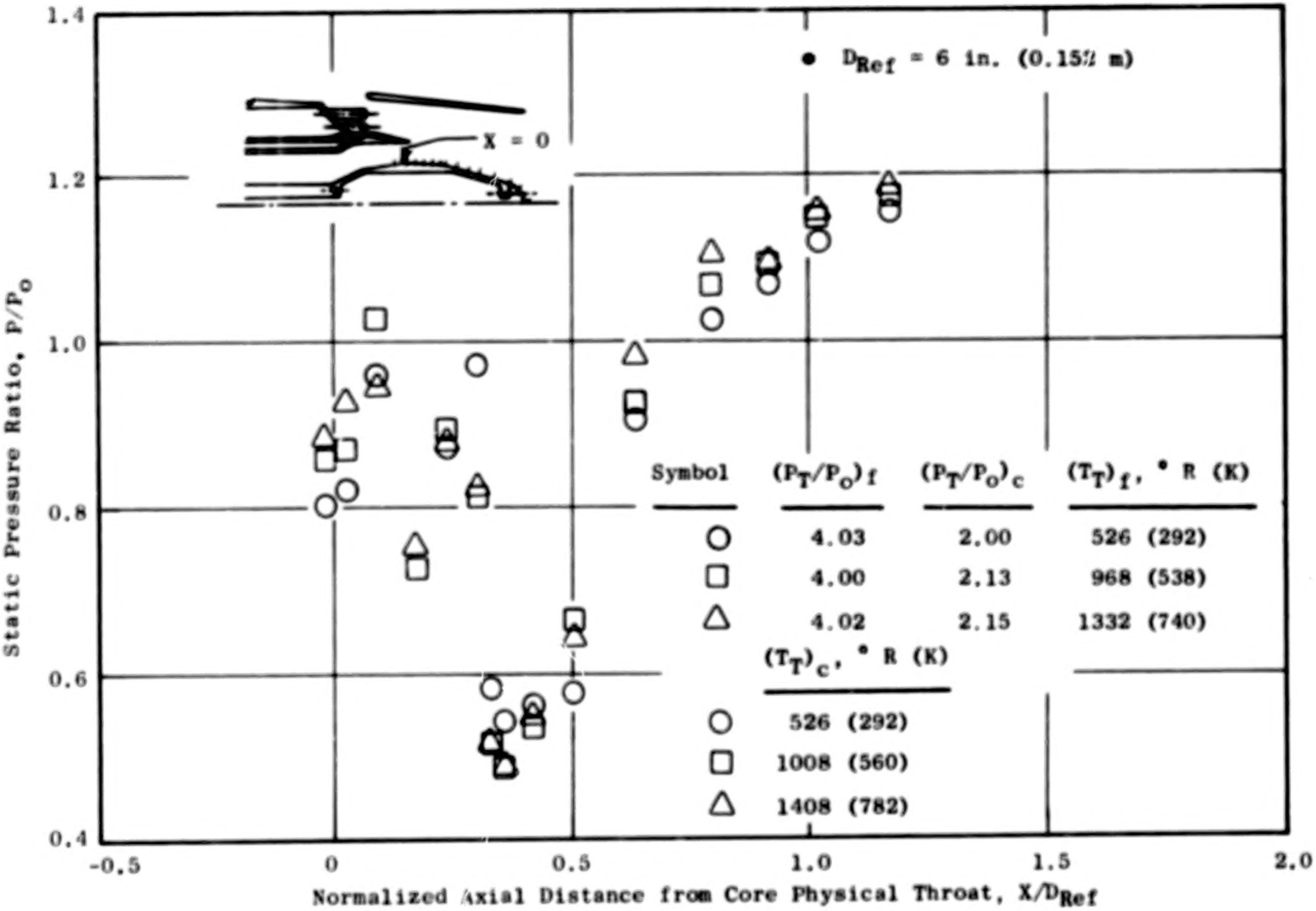

Figure 152. Comparison of Hot and Cold Flow Core Plug Pressure Distributions, Multitube Fan Suppressor Nozzle with Hardwall Ejector (Sharp Lip); Aerodynamic Model 5, $(P_T/P_o)_f$ = 4.00.

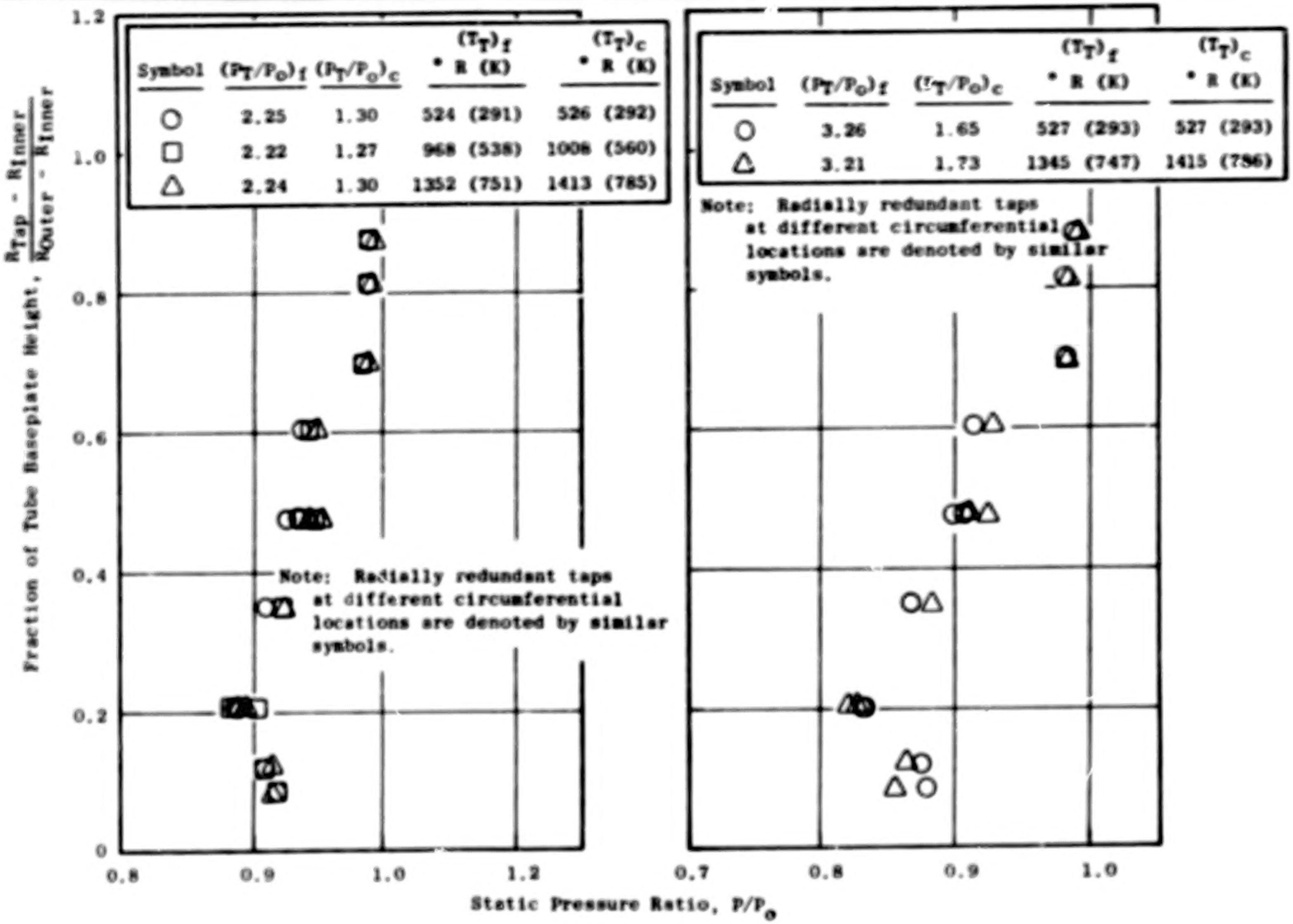

Note: Radially redundant taps at different circumferential locations are denoted by similar symbols.

Note: Radially redundant taps at different circumferential locations are denoted by similar symbols.

Figure 153. Comparison of Hot and Cold Flow Tube Baseplate Pressure Distributions, Multitube Fan Suppressor Nozzle with Hardwall Ejector (Sharp Lip); Aerodynamic Model 5, $(P_T/P_o)_f$ = 2.25 and 3.25.

TABLE OF CONTENTS

Section	Page	
1.0 SUMMARY	1	1/C1
2.0 INTRODUCTION	3	1/C3
3.0 TEST APPARATUS AND PROCEDURES	5	1/C5
3.1 FACILITIES	5	1/C5
3.1.1 General Electric Jet Engine Noise Outdoor Test Stand (JENOTS) Description	6	1/C6
3.1.1.1 **Acoustic Arena**	6	1/C6
3.1.1.2 Coannular-Flow System	6	1/C6
3.1.1.3 Coannular Frame Section	10	1/C12
3.1.1.4 Plenum Instrumentation Section	10	1/C12
3.1.1.5 Facility Acoustic Validation	12	1/C14
3.1.2 FluiDyne Aerodynamic-Performance Test Facility Description	12	1/C14
3.2 JENOTS INSTRUMENTATION SYSTEMS	16	1/D5
3.2.1 Acoustic Instrumentation Systems	16	1/D5
3.2.2 Laser Velocimeter System	18	1/D8
3.2.2.1 General Arrangement	18	1/D8
3.2.2.2 LV Actuator and Seeding	21	1/D13
3.2.2.3 Signal Processing and Recording	21	1/D13
3.3 DATA REDUCTION METHODS	21	1/D13
3.3.1 Acoustic Data Reduction	22	1/D14
3.3.1.1 JENOTS Data Reduction Systems	22	1/D14
3.3.1.2 Air-Attenuation Corrections	22	1/D14
3.3.1.3 Data-Scaling Procedure	30	1/E12
3.3.1.4 Data Corrections to a Free-Field Environment	30	1/E12
3.3.1.5 Power Level Calculation	30	1/E12
3.3.1.6 Acoustic Measurement Errors, Electronic Noise Floor	30	1/E12
3.3.2 Laser Velocimeter Data Reduction	33	1/F3
3.3.2.1 Basic Idea for LV rms Measurements	33	1/F3
3.3.2.2 The Histogram	36	1/F6
3.3.2.3 Mean Velocity	36	1/F6
3.3.2.4 Turbulent Velocity	37	1/F7
3.3.2.5 Statistical Errors for LV Mean and Turbulent Velocity Measurements	37	1/F7

TABLE OF CONTENTS (continued)

Section Page

3.3.3 Aerodynamic-Performance Test Data Reduction 37 1/F7
3.3.3.1 Flow Rates 39 1/F9
3.3.3.2 Discharge Coefficients 39 1/F9
3.3.3.3 Nozzle Throat 39 1/F9
3.3.3.4 Thrust Coefficient 40 1/F10
3.3.3.5 FluiDyne Force Balance Calibration 40 1/F10
3.3.3.6 Pressure and Temperature Data 41 1/F11
3.3.3.7 Data Quality 41 1/F11

4.0 MODEL DESCRIPTION AND DEFINITION OF TEST MATRICES 44 1/F14

4.1 MODEL DESIGN - SYSTEM EVOLUTION 44 1/F14
4.2 DESCRIPTION OF TEST MODELS 48 1/G6
4.3 ACOUSTIC TEST MATRIX 52 1/G12
4.4 LASER VELOCIMETER TEST MATRIX 56 2/A7
4.5 AERODYNAMIC-PERFORMANCE TEST MATRIX 61 2/B1
4.6 DATA SECTION 61 2/B1

5.0 DISCUSSION OF ACOUSTIC TEST RESULTS 63 2/B3

5.1 ESTABLISHMENT OF GROUND RULES FOR ACOUSTIC COMPARISONS AND DATA ILLUSTRATIONS 63 2/B3

5.1.1 Synthesized Baseline 63 2/B3
5.1.2 Average Conical Nozzle Noise Baseline 64 2/B4
5.1.3 Density Normalization and Presentation of Results 64 2/B4
5.1.3.1 Density Normalization Factors 64 2/B4
5.1.3.2 Presentation of Results 70 2/B13

5.2 UNSUPPRESSED COANNULAR NOZZLES 71 2/B14

5.2.1 High Core-Flow Test Results 71 2/B14
5.2.1.1 Overall Power Level Test Results 71 2/B14
5.2.1.2 Power Spectra Test Results 71 2/B14
5.2.1.3 Perceived Noise Level Test Results 71 2/B14
5.2.1.4 Perceived Noise Level Directivity Test Results 75 2/C6
5.2.1.5 Sound Pressure Level Spectra Test Results 75 2/C6
5.2.2 Low Core-Flow Test Results 75 2/C6
5.2.3 Acoustic Correlations 84 2/D5
5.2.4 Summary Remarks 84 2/D5

5.3 MULTIELEMENT FAN-SUPPRESSOR NOZZLES 88 2/D11

5.3.1 High Core Flow Test Results 88 2/D11
5.3.1.1 Overall Power Level Test Results 88 2/D11
5.3.1.2 Power Spectra Test Results 97 2/E11

TABLE OF CONTENTS (continued)

Section Page

5.3.1.3 Perceived Noise Level Test Results 97 2/E11
5.3.1.4 Sound Pressure Level Spectra Test Results 98 2/E12
5.3.2 Low Core-Flow Test Results 98 2/E12
5.3.3 Comparisons with Unsuppressed Coannular Nozzles 98 2/E12
5.3.4 Summary Remarks 104 2/F9

5.4 MULTIELEMENT FAN-SUPPRESSOR NOZZLES WITH EJECTORS 104 2/F9

5.4.1 Hardwall Ejector Effects 107 2/F12
5.4.1.1 Overall Power Level Test Results 107 2/F12
5.4.1.2 Power Spectra Test Results 107 2/F12
5.4.1.3 Perceived Noise Level Test Results 107 2/F12
5.4.1.4 Sound Pressure Level Test Results 111 2/G2
5.4.2 Treated Ejector Effects 111 2/G2
5.4.2.1 Overall Power Level Test Results 111 2/G2
5.4.2.2 Power Spectra Test Results 115 2/G6
5.4.2.3 Perceived Noise Level Test Results 115 2/G6
5.4.2.4 Sound Pressure Level Test Results 120 2/G11
5.4.3 Inlet Lip Geometry Effects on the Hardwall Ejector 120 2/G11
5.4.3.1 Power Level Test Results 120 2/G11
5.4.3.2 Perceived Noise Level Test Results 124 3/A8
5.4.3.3 Sound Pressure Level Test Results 124 3/A8
5.4.4 Summary Remarks 124 3/A8

5.5 EVALUATION OF A PARTIAL MECHANICAL SHIELD 130 3/B1

5.5.1 Perceived Noise Level Test Results 130 3/B1
5.5.2 Sound Pressure Level Spectra Results 134 3/B6
5.5.3 Summary Remarks 134 3/B6

6.0 DISCUSSION OF AERODYNAMIC-PERFORMANCE TEST RESULTS 140 3/C1

6.1 THRUST COEFFICIENTS 140 3/C1

6.1.1 Unsuppressed Coannular Nozzle with Plug 140 3/C1
6.1.2 Multichute Fan-Suppressor Nozzle 143 3/C5
6.1.3 Multichute Fan-Suppressor Nozzle with Hardwall Ejector with Sharp Lip 143 3/C5
6.1.4 Multitube Fan-Suppressor Nozzle 150 3/C12
6.1.5 Multitube Fan-Suppressor Nozzle with Hardwall Ejector with Sharp Lip 150 3/C12

6.2 EFFECT OF HOT EXHAUST FLOW ON THE THRUST COEFFICIENT OF THE MULTITUBE FAN-SUPPRESSOR NOZZLE WITH HARDWALL EJECTOR WITH SHARP LIP 156 3/D7

TABLE OF CONTENTS (continued)

Section		Page	
6.3	FLOW COEFFICIENTS	161	3/D14
6.3.1	Unsuppressed Coannular Nozzle with Plug	161	3/D14
6.3.2	Multichute Fan-Suppressor Nozzle	165	3/E6
6.3.3	Multichute Fan-Suppressor Nozzle with Hardwall Ejector with Sharp Lip	165	3/E6
6.3.4	Multitube Fan-Suppressor Nozzle	169	3/E10
6.3.5	Multitube Fan-Suppressor Nozzle with Hardwall Ejector with Sharp Lip	169	3/E10
7.0	DISCUSSION OF LASER VELOCIMETER TEST RESULTS	173	3/E14
7.1	LASER VELOCIMETER PLUME MEASUREMENTS FOR THE UNSUPPRESSED COANNULAR NOZZLE WITH PLUG	173	3/E14
7.1.1	Axial Mean-Velocity Distributions	173	3/E14
7.1.2	Mean-Velocity, Radial-Profile Distributions	176	3/F5
7.1.3	Axial Turbulent-Velocity, Radial-Profile Distributions	176	3/F5
7.2	LASER VELOCIMETER PLUME MEASUREMENTS FOR THE FAN-SUPPRESSED NOZZLES	176	3/F5
7.2.1	Axial Mean-Velocity Distributions	176	3/F5
7.2.2	Mean- and Turbulent-Velocity, Radial-Profile Distributions	180	3/F12
7.2.2.1	Multichute Fan Suppressor	180	3/F12
7.2.2.2	Multitube Fan Suppressor	180	3/F12
7.3	SUMMARY OF OBSERVATIONS	180	3/F12
8.0	DISCUSSION OF ACOUSTIC/AERODYNAMIC-PERFORMANCE CORRELATIONS	186	3/G8
8.1	EVALUATION OF NOISE CANDIDATES FOR DUCT-BURNING TURBOFAN ENGINES	186	3/G8
8.2	LOW CORE-FLOW COMPARISONS	191	4/A6
9.0	CONCLUSIONS AND RECOMMENDATIONS	196	4/A12
9.1	CONCLUSIONS	196	4/A12
9.2	RECOMMENDATIONS	197	4/A13

TABLE OF CONTENTS (concluded)

Section | Page

APPENDIX A - GENERAL ELECTRIC AIR-ATTENUATION MODEL 199 4/B1
APPENDIX B - POWER LEVEL CALCULATION PROCEDURE 210 4/C1
APPENDIX C - DETAILED DESCRIPTION OF TEST MODELS 214 4/C5
APPENDIX D - ACOUSTIC TEST MATRIX FOR ALL DBTF MODELS AND EXAMPLE DATA PRINT OUT SHEETS 221 4/D3
APPENDIX E - FAN PLUG PRESSURE DISTRIBUTIONS FOR AERODYNAMIC MODEL 5 240 4/F13
APPENDIX F - MODEL 7 AXIAL-VELOCITY PROFILES 249 5/A8
APPENDIX G - MODEL 7 AXIAL-VELOCITY PROFILES WITH NO CORE FLOW 270 5/D7
APPENDIX H - MODEL 7 AXIAL-VELOCITY PROFILES WITH NO FAN FLOW 286 5/F10
APPENDIX I - MODEL 1 AXIAL-VELOCITY PROFILES 295 5/G13
APPENDIX J - MODEL 2 AXIAL-VELOCITY PROFILES 303 6/B6
APPENDIX K - NOMENCLATURE 313 6/C11
REFERENCES 317 6/D1

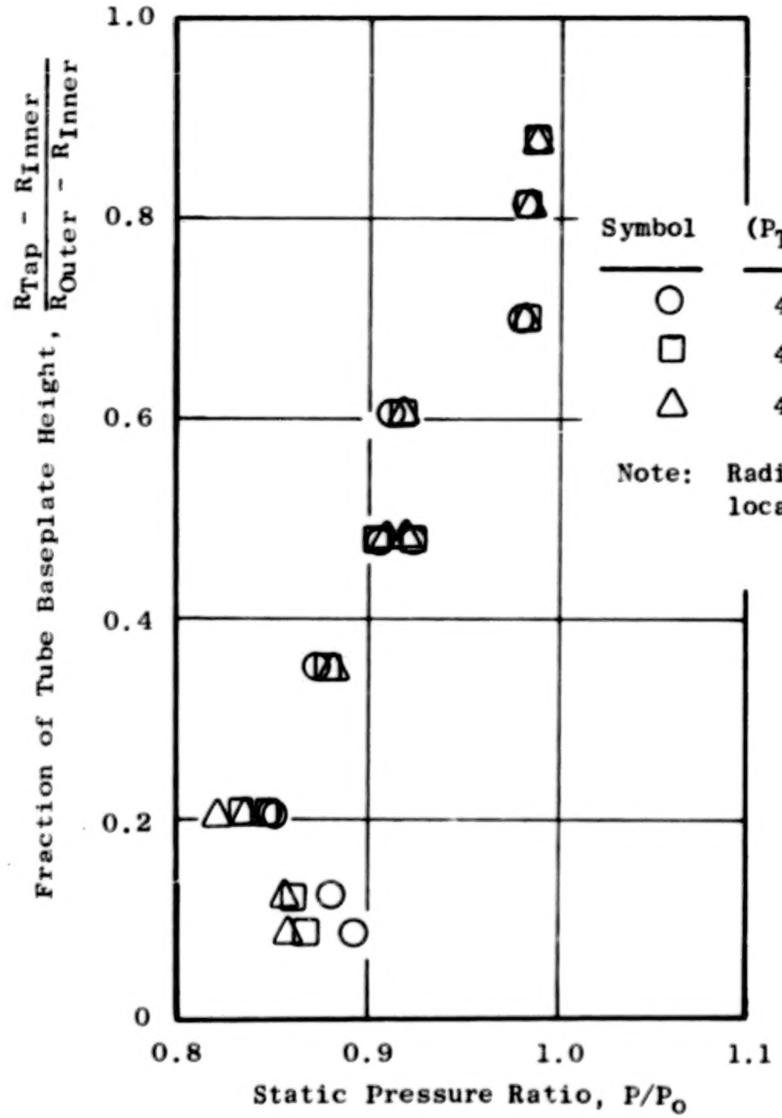

Symbol	$(P_T/P_o)_f$	$(P_T/P_o)_c$	$(T_T)_f$, ° R (K)	$(T_T)_c$, ° R (K)
○	4.03	2.00	526 (292)	526 (292)
□	4.00	2.13	968 (538)	1008 (560)
△	4.02	2.15	1332 (740)	1408 (782)

Note: Radially redundant taps at different circumferential locations are denoted by similar symbols.

Figure 154. Comparison of Hot and Cold Flow Tube Baseplate Pressure Distributions, Multitube Fan Suppressor Nozzle with Hardwall Ejector (Sharp Lip); Aerodynamic Model 5, $(P_T/P_o)_f = 4.0$.

APPENDIX F

MODEL 7 AXIAL-VELOCITY PROFILES

Laser velocimeter measurements of axial-velocity profiles for the unsuppressed coannular nozzle with plug (Model 7) are presented in Figures 155 through 174 for the following conditions:

	P_T/P_o	T_T, ° R (K)	V_J, ft/sec	(m/sec)
Fan	2.86	1411 (784)	2100	(640.5)
Core	1.50	1461 (812)	1400	(427.0)

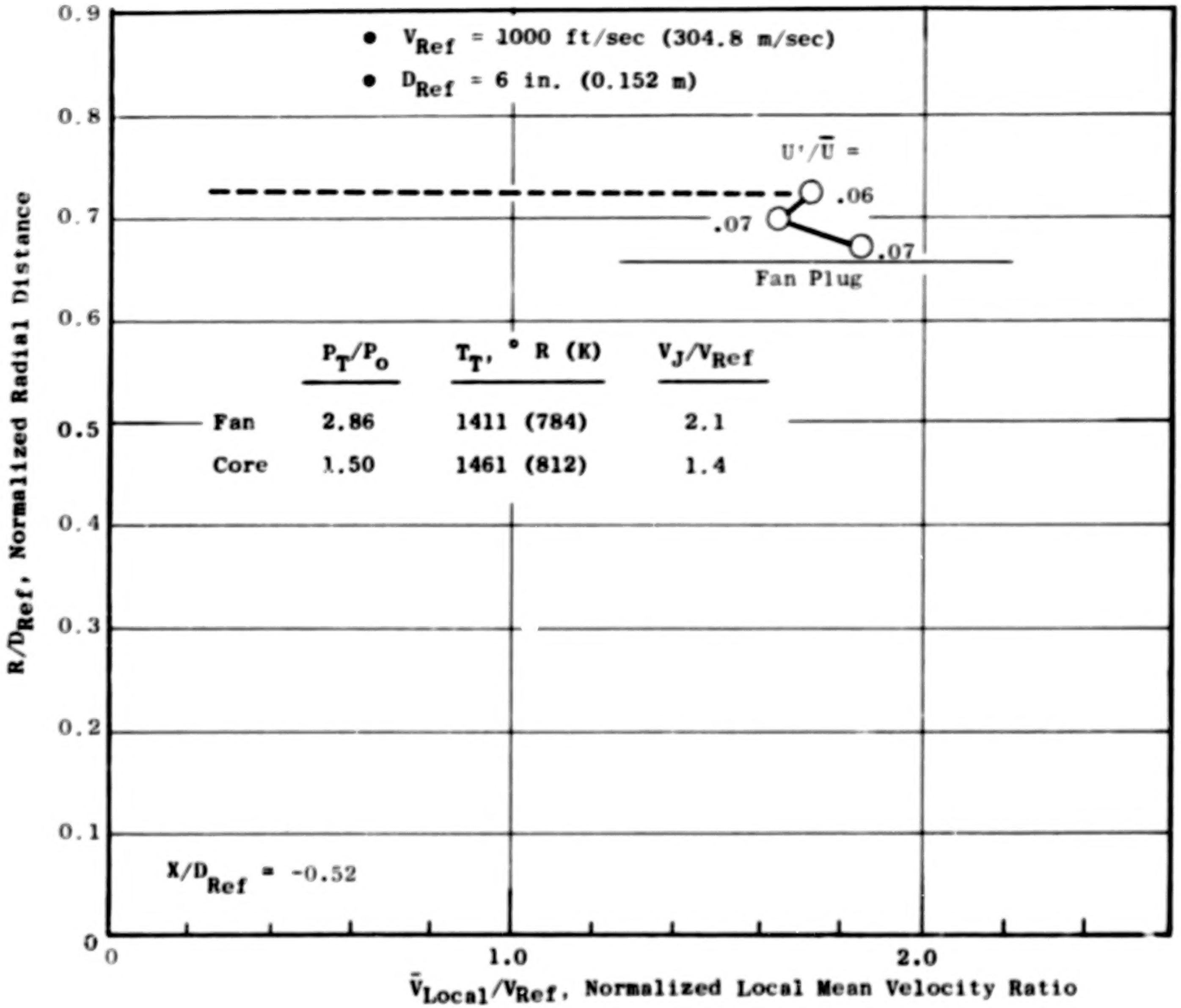

Figure 155. Laser Velocimeter Velocity Profile and Turbulence Measurement; Unsuppressed Coannular Nozzle with Plug (Model 7) at X/D_{Ref} = -0.52.

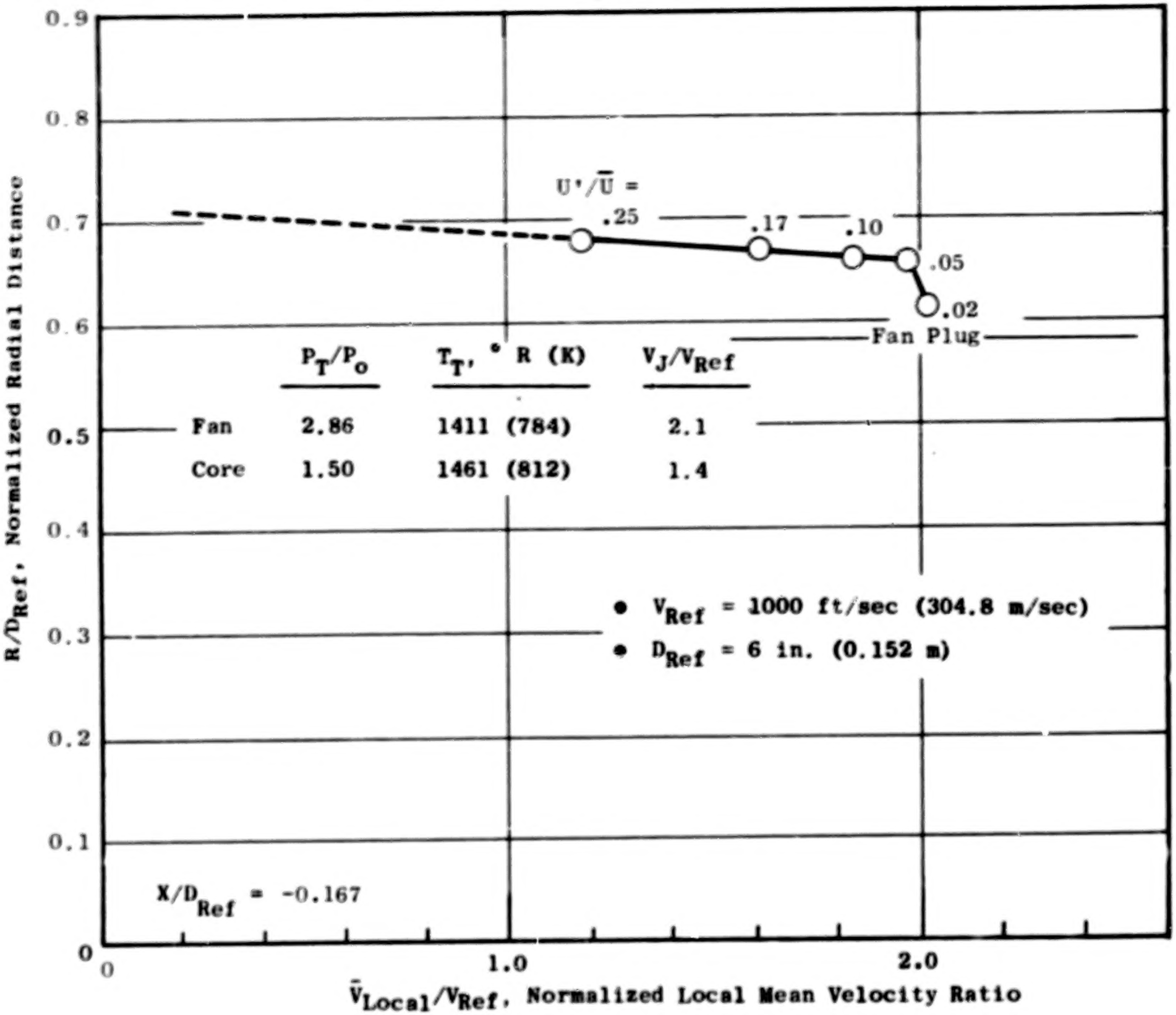

Figure 156. Laser Velocimeter Velocity Profile and Turbulence Measurement; Unsuppressed Coannular Nozzle with Plug (Model 7) at X/D_{Ref} = -0.167.

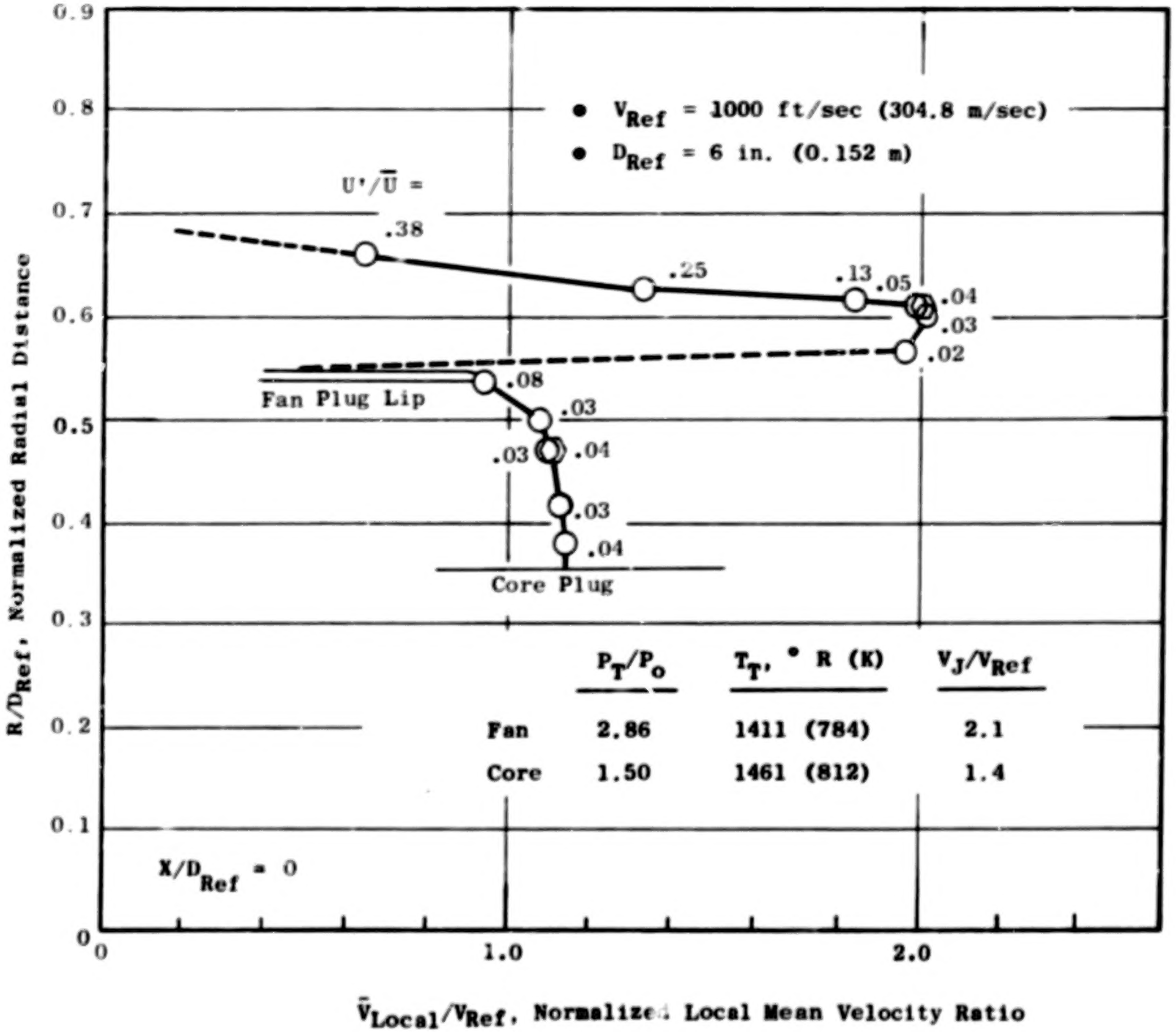

	P_T/P_o	T_T, ° R (K)	V_J/V_{Ref}
Fan	2.86	1411 (784)	2.1
Core	1.50	1461 (812)	1.4

Figure 157. Laser Velocimeter Velocity Profile and Turbulence Measurement; Unsuppressed Coannular Nozzle with Plug (Model 7) at X/D_{Ref} = 0.

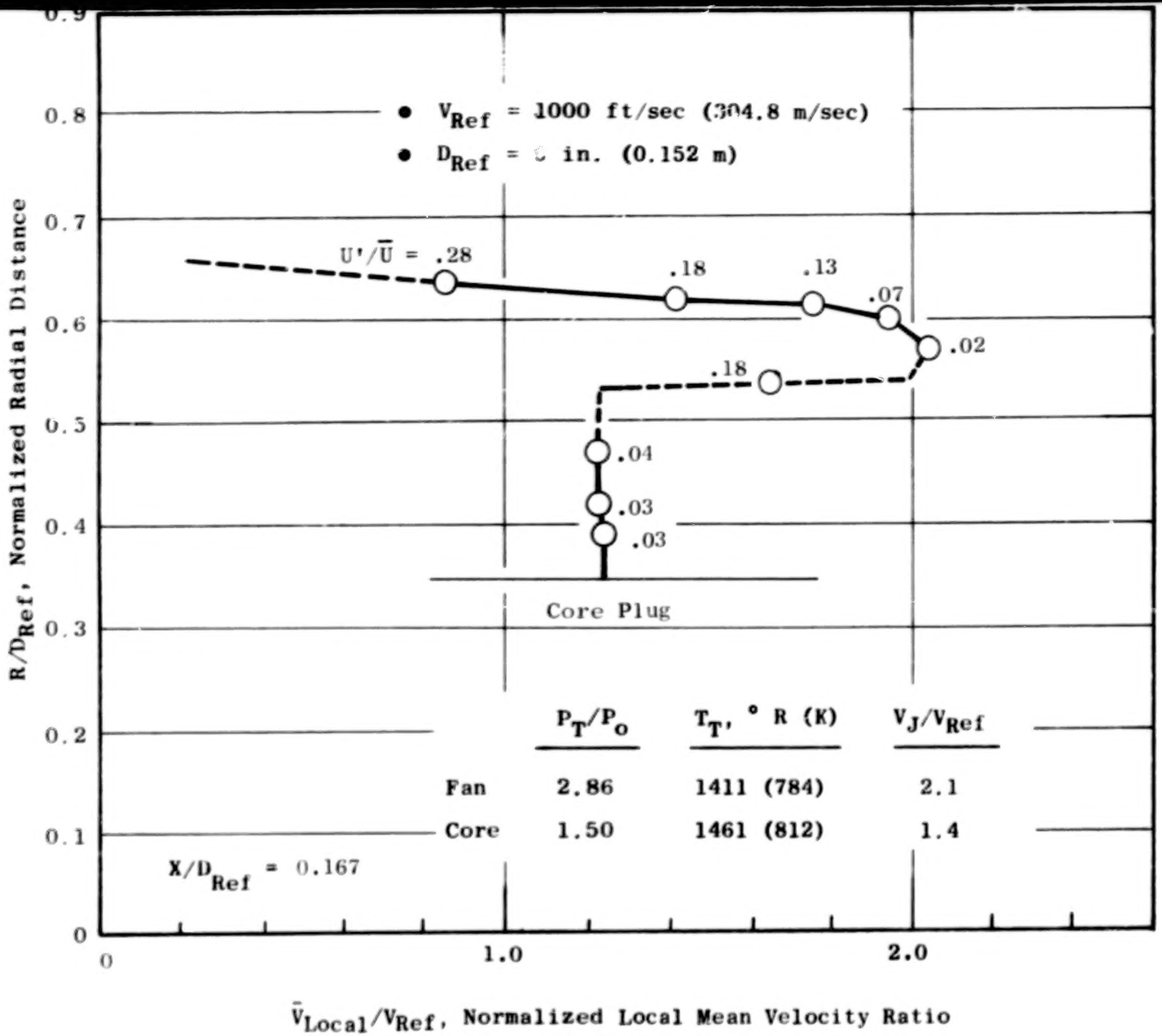

	P_T/P_o	T_T, ° R (K)	V_J/V_{Ref}
Fan	2.86	1411 (784)	2.1
Core	1.50	1461 (812)	1.4

Figure 158. Laser Velocimeter Velocity Profile and Turbulence Measurement; Unsuppressed Coannular Nozzle with Plug (Model 7) at X/D_{Ref} = 0.167.

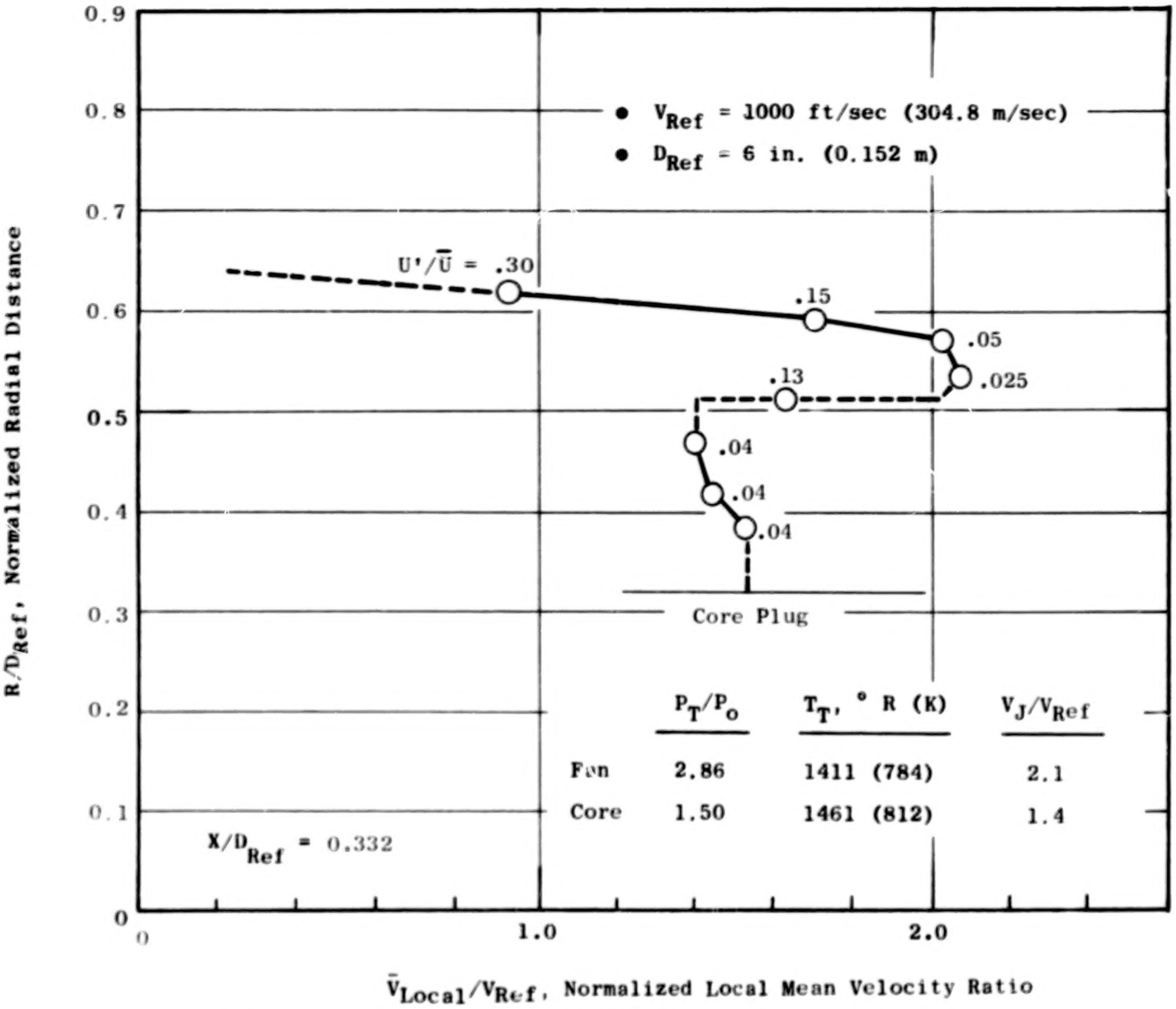

Figure 159. Laser Velocimeter Velocity Profile and Turbulence Measurement; Unsuppressed Coannular Nozzle with Plug (Model 7) at X/D_{Ref} = 0.332.

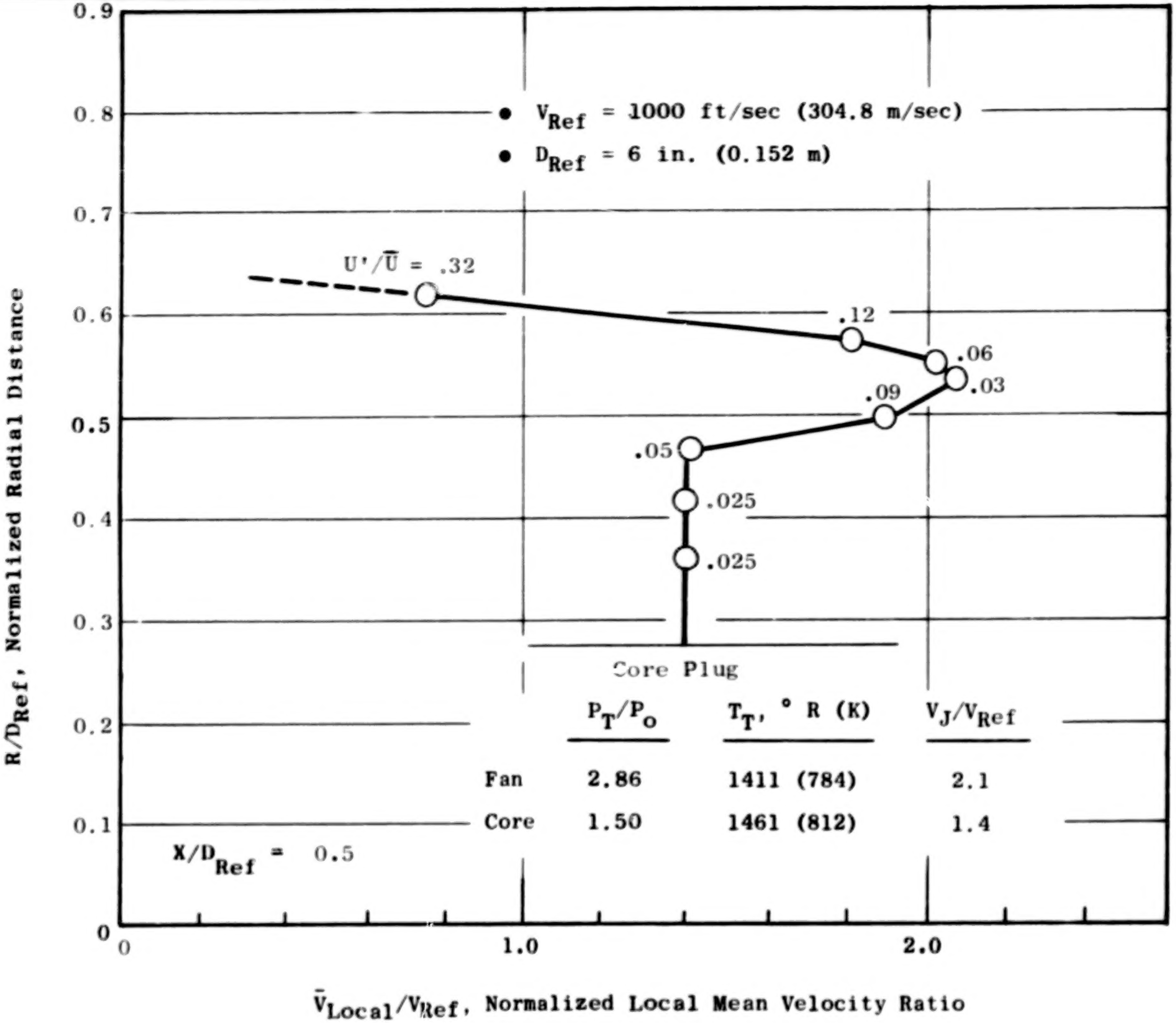

	P_T/P_o	T_T, ° R (K)	V_J/V_{Ref}
Fan	2.86	1411 (784)	2.1
Core	1.50	1461 (812)	1.4

Figure 160. Laser Velocimeter Velocity Profile and Turbulence Measurement; Unsuppressed Coannular Nozzle with Plug (Model 7) at X/D_{Ref} = 0.5.

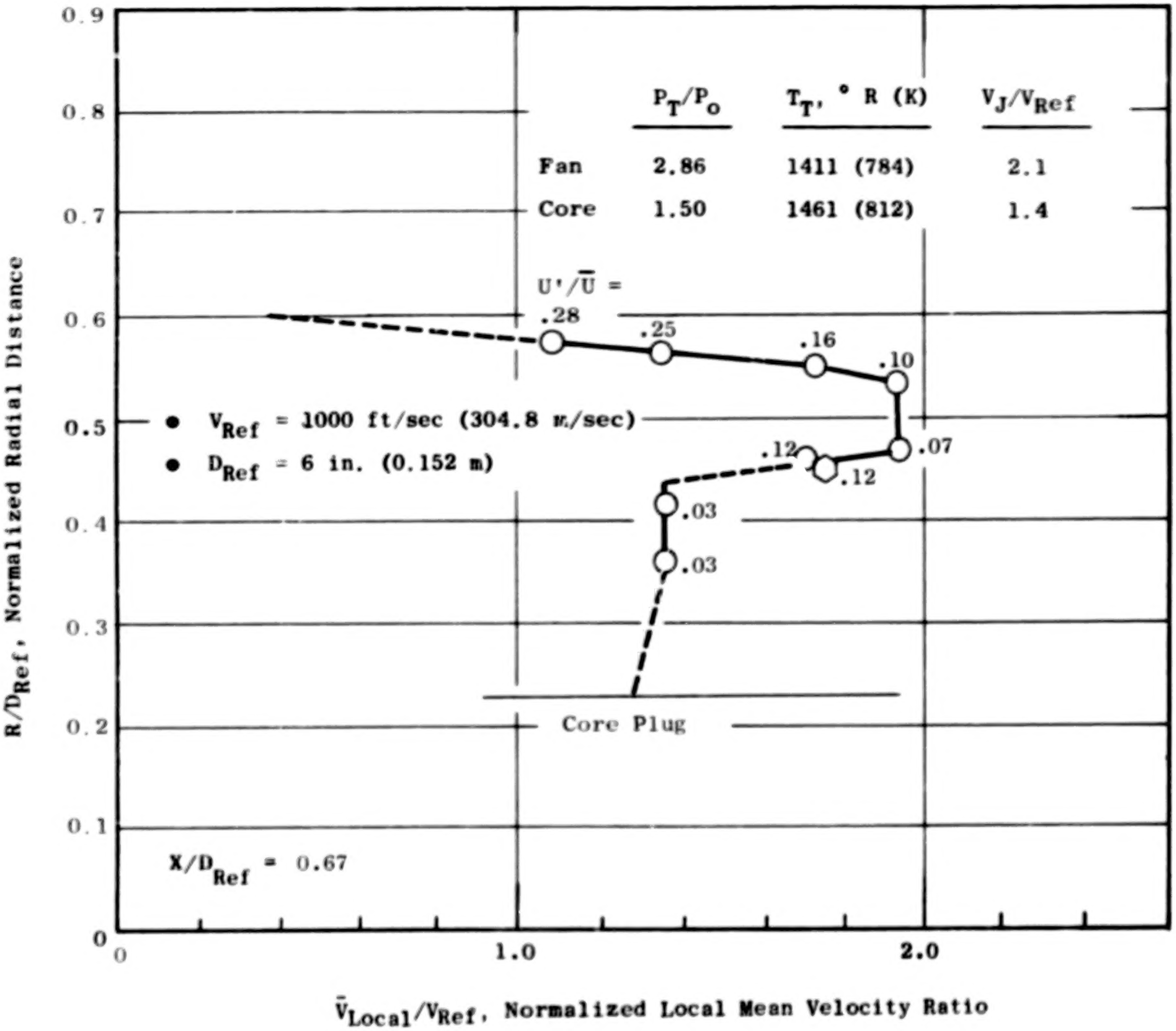

	P_T/P_o	T_T, ° R (K)	V_J/V_{Ref}
Fan	2.86	1411 (784)	2.1
Core	1.50	1461 (812)	1.4

Figure 161. Laser Velocimeter Velocity Profile and Turbulence Measurement; Unsuppressed Coannular Nozzle with Plug (Model 7) at X/D_{Ref} = 0.67.

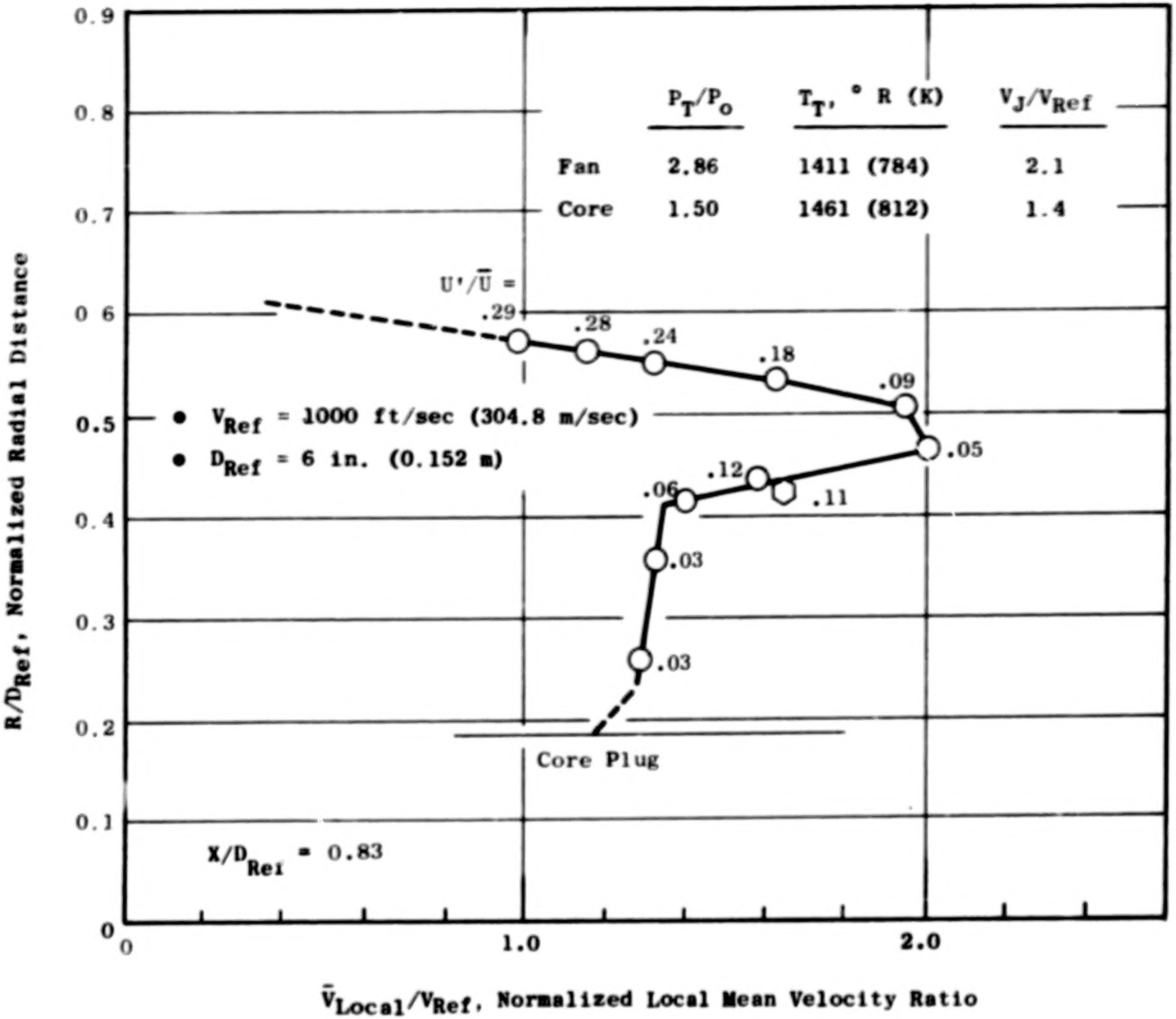

Figure 162. Laser Velocimeter Velocity Profile and Turbulence Measurement; Unsuppressed Coannular Nozzle with Plug (Model 7) at X/D_{Ref} = 0.83.

257

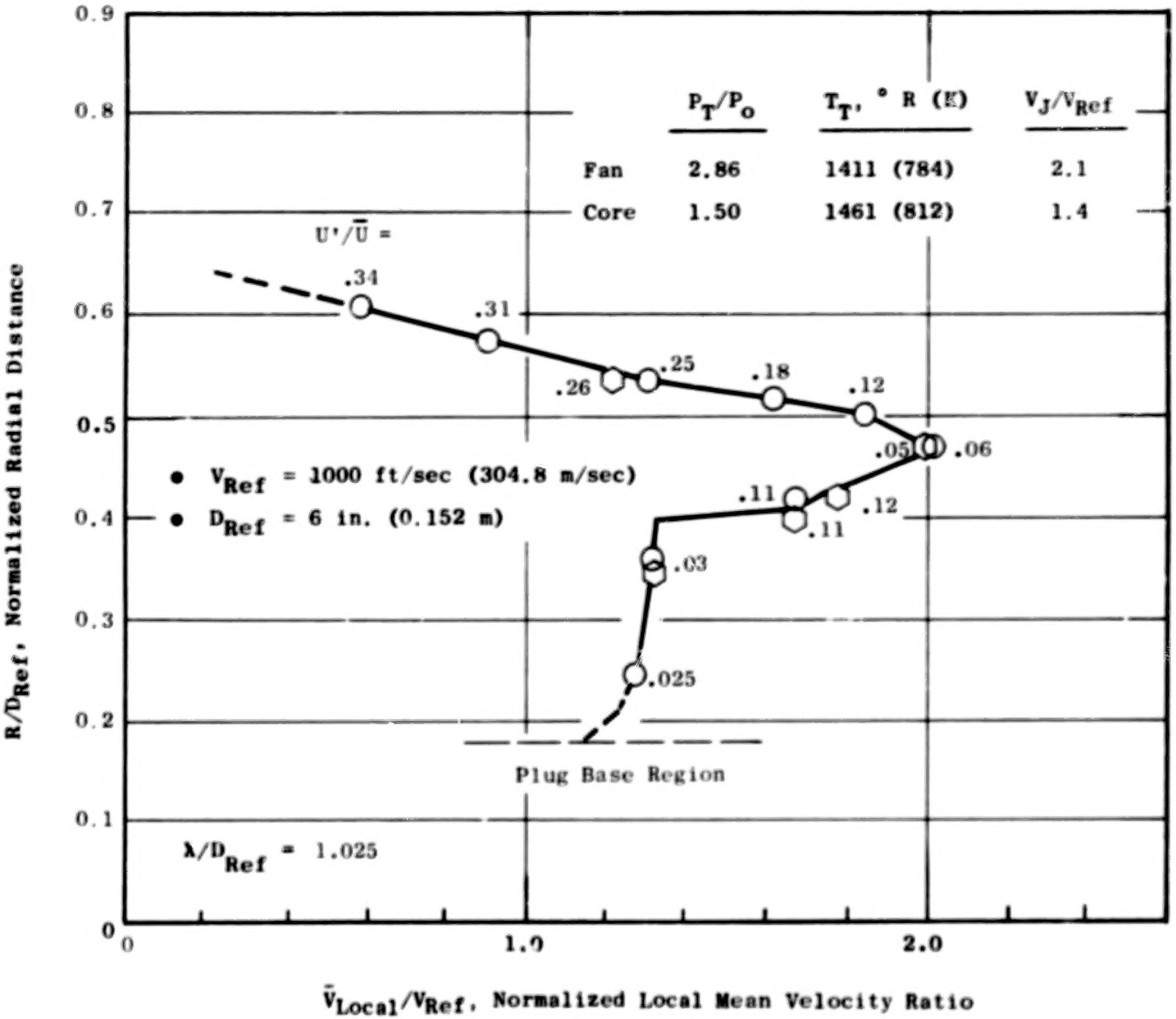

Figure 163. Laser Velocimeter Velocity Profile and Turbulence Measurement; Unsuppressed Coannular Nozzle with Plug (Model 7) at X/D_{Ref} = 1.025.

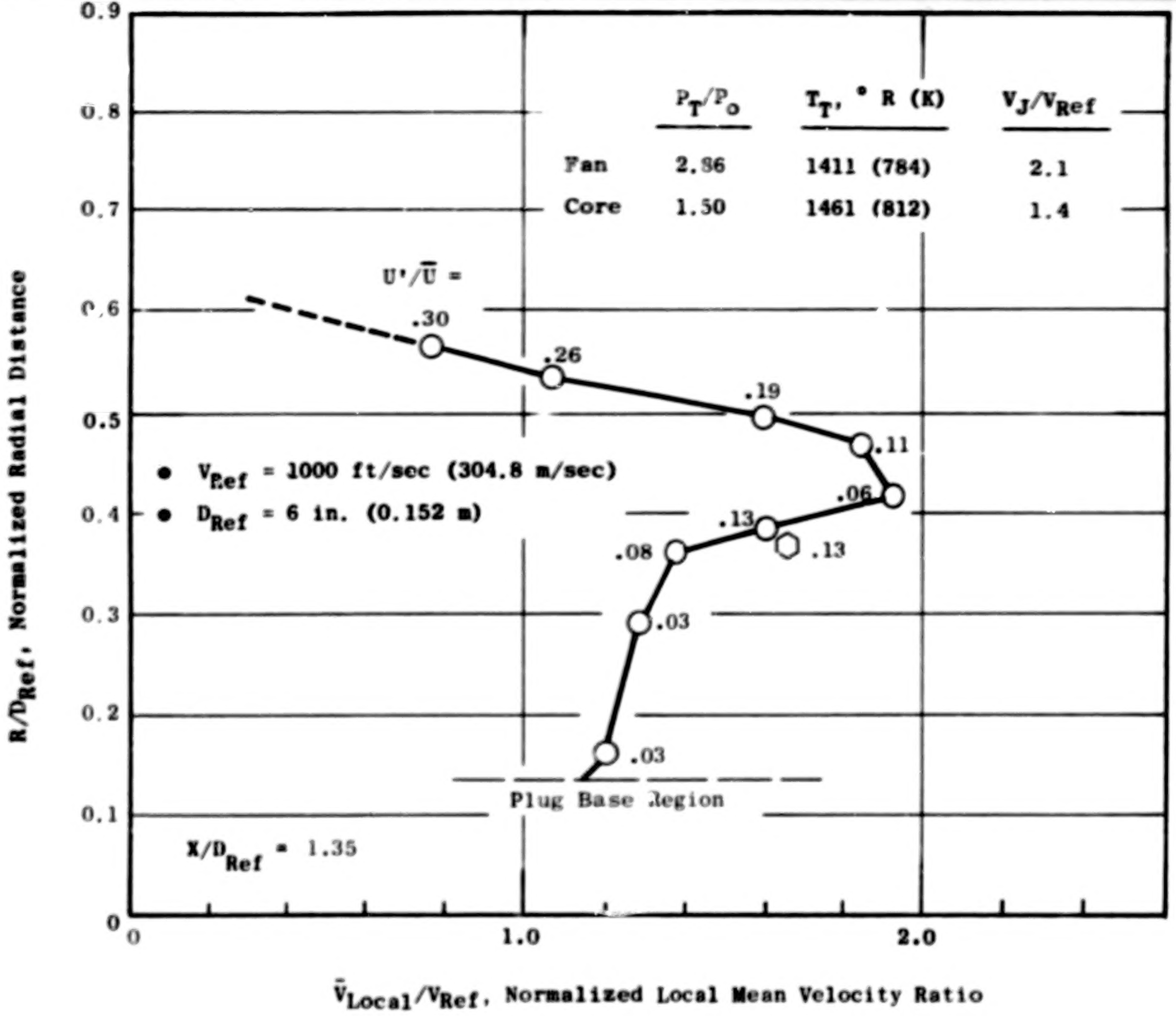

Figure 164. Laser Velocimeter Velocity Profile and Turbulence Measurement; Unsuppressed Coannular Nozzle with Plug (Model 7) at X/D_{Ref} = 1.35.

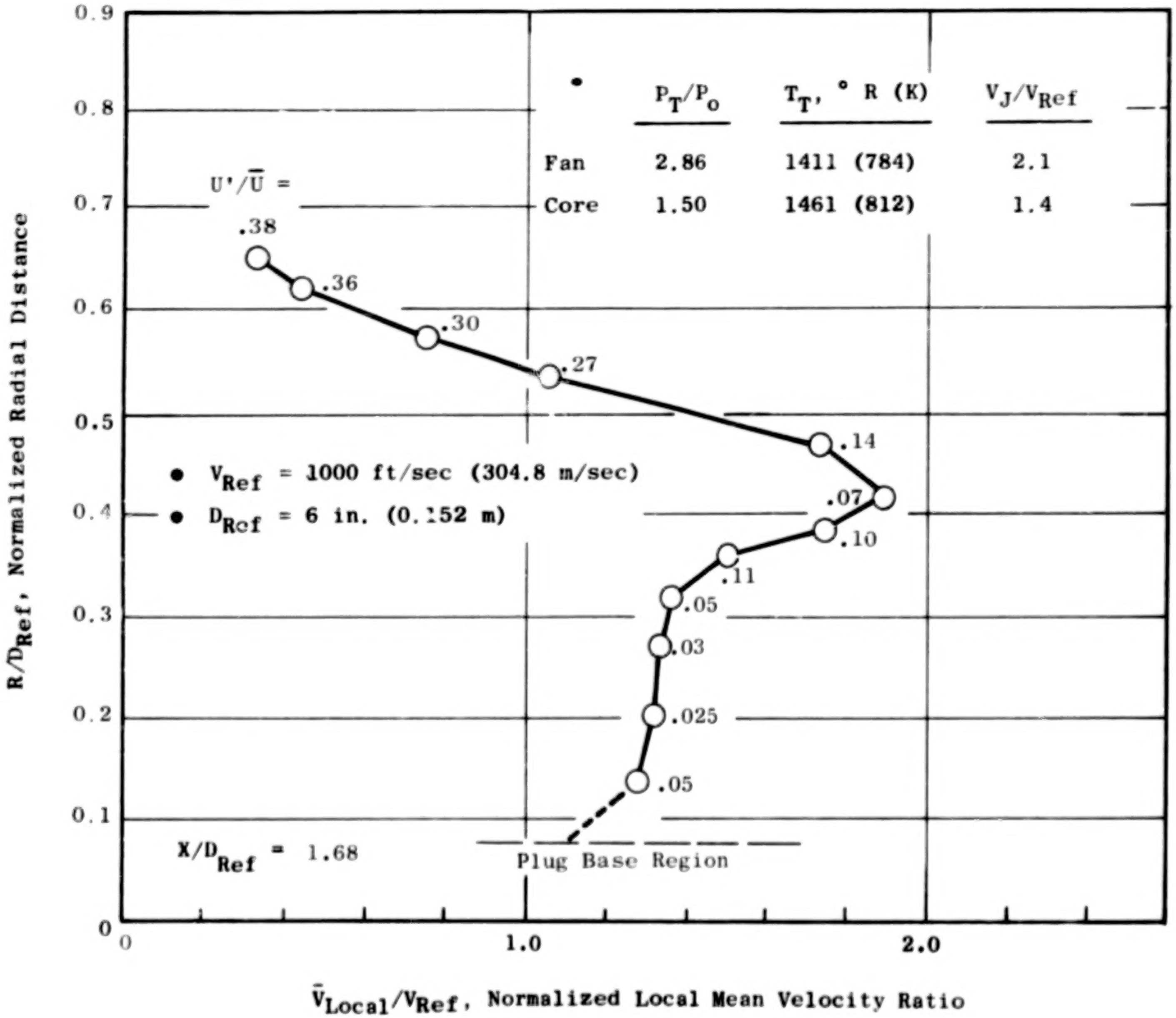

Figure 165. Laser Velocimeter Velocity Profile and Turbulence Measurement; Unsuppressed Coannular Nozzle with Plug (Model 7) at X/D$_{Ref}$ = 1.68.

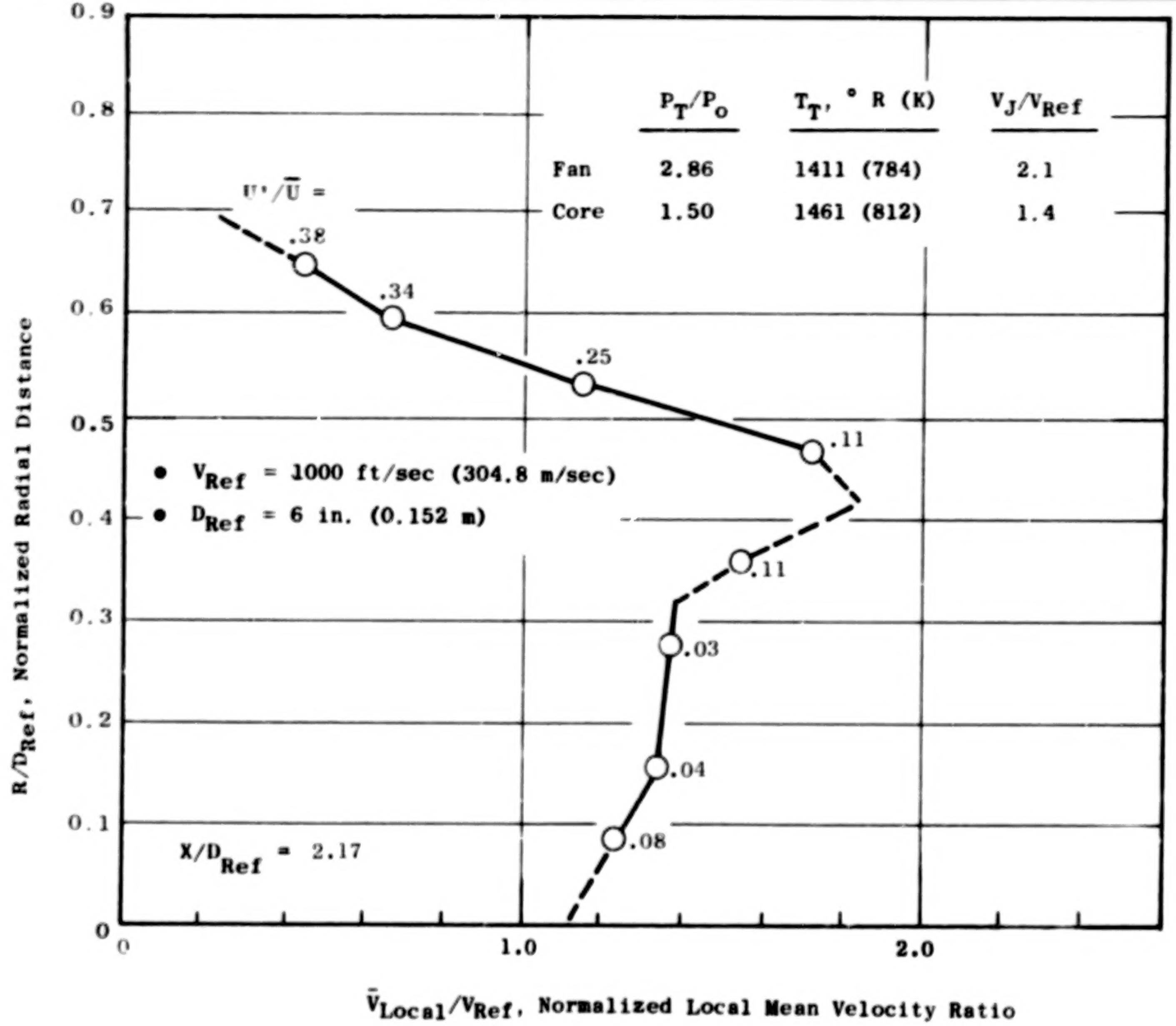

Figure 166. Laser Velocimeter Velocity Profile and Turbulence Measurement; Unsuppressed Coannular Nozzle with Plug (Model 7) at X/D_{Ref} = 2.17.

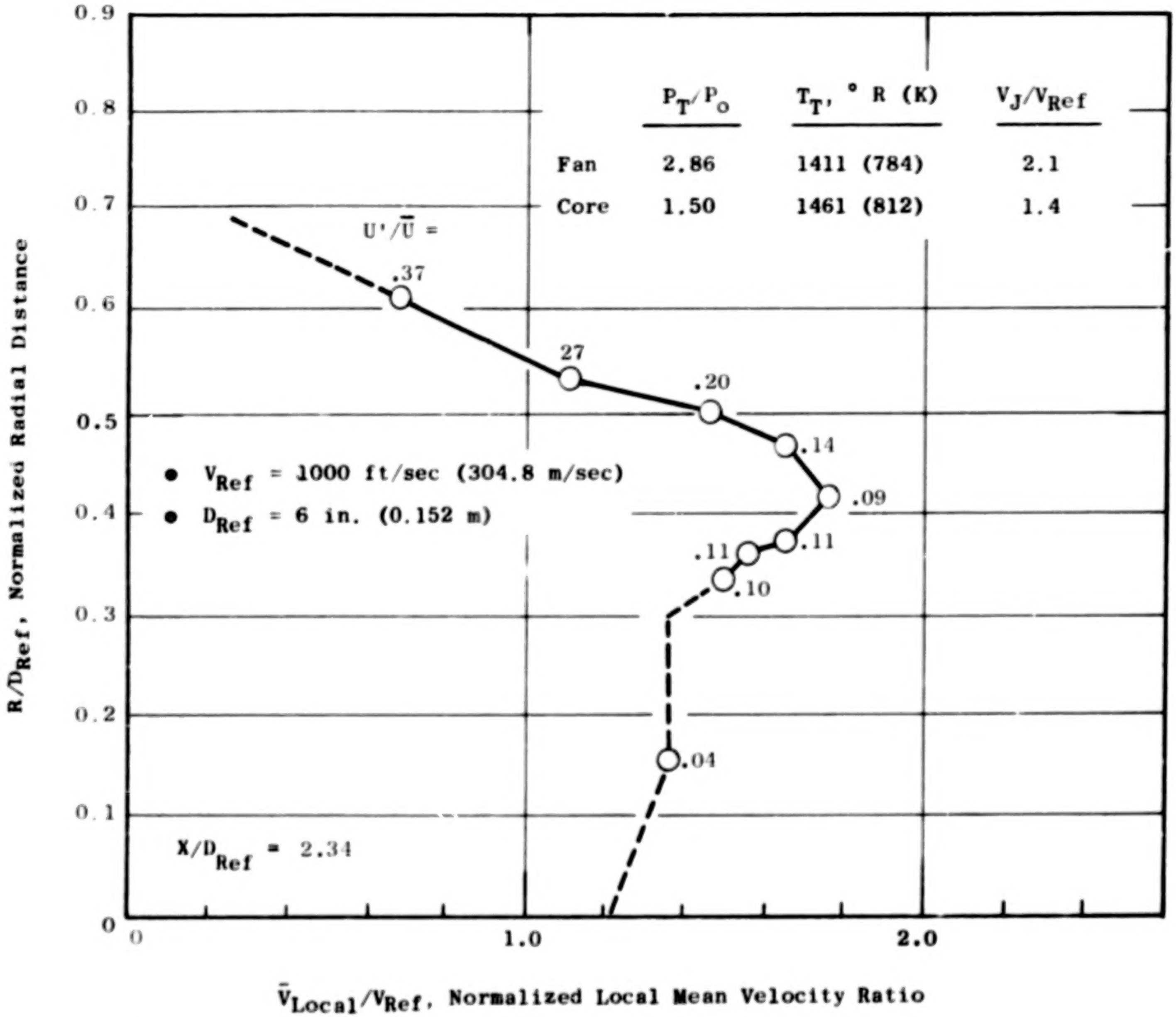

Figure 167. Laser Velocimeter Velocity Profile and Turbulence Measurement; Unsuppressed Coannular Nozzle with Plug (Model 7) at X/D_{Ref} = 2.34.

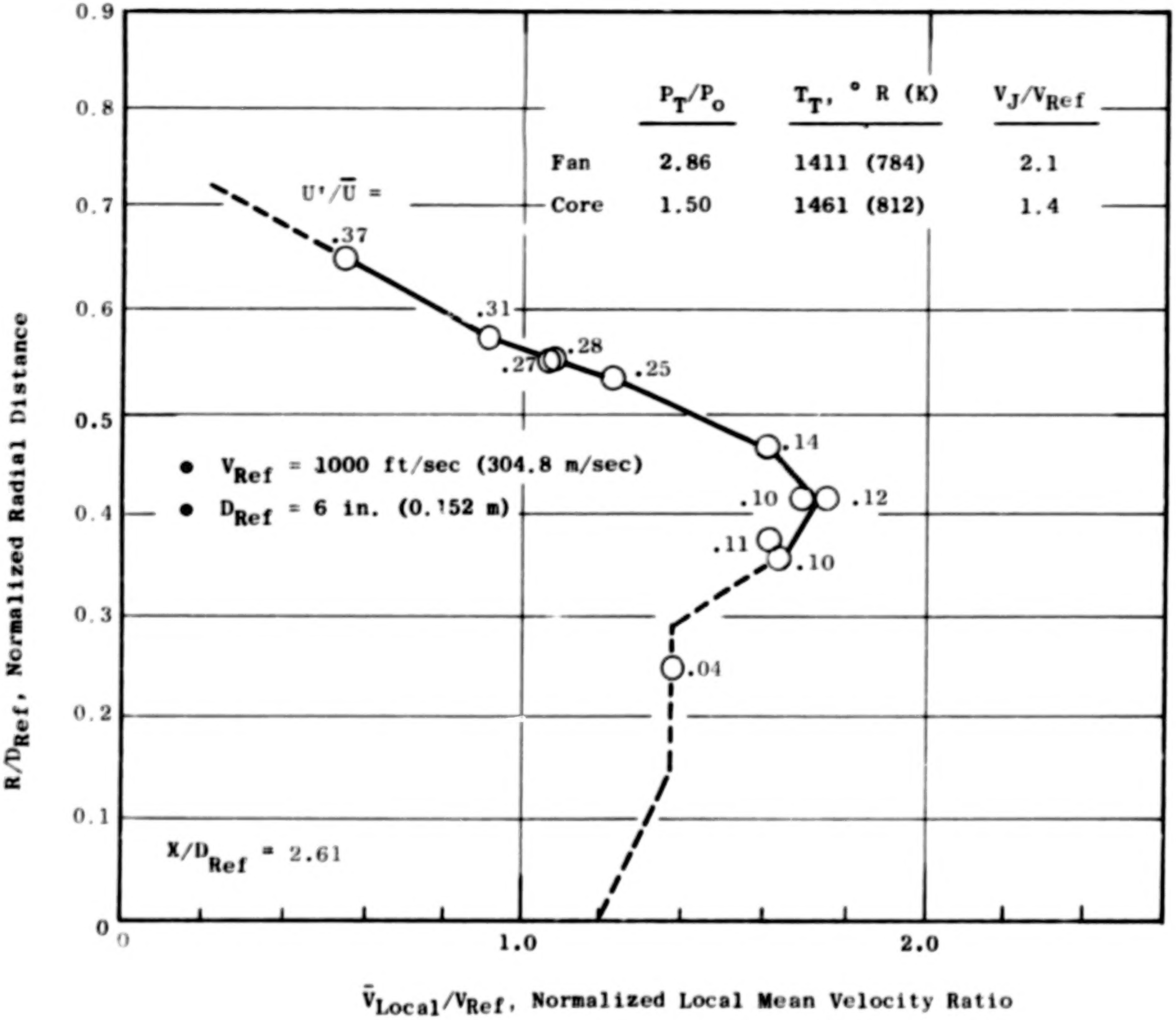

Figure 168. Laser Velocimeter Velocity Profile and Turbulence Measurement; Unsuppressed Coannular Nozzle with Plug (Model 7) at X/D_{Ref} = 2.61.

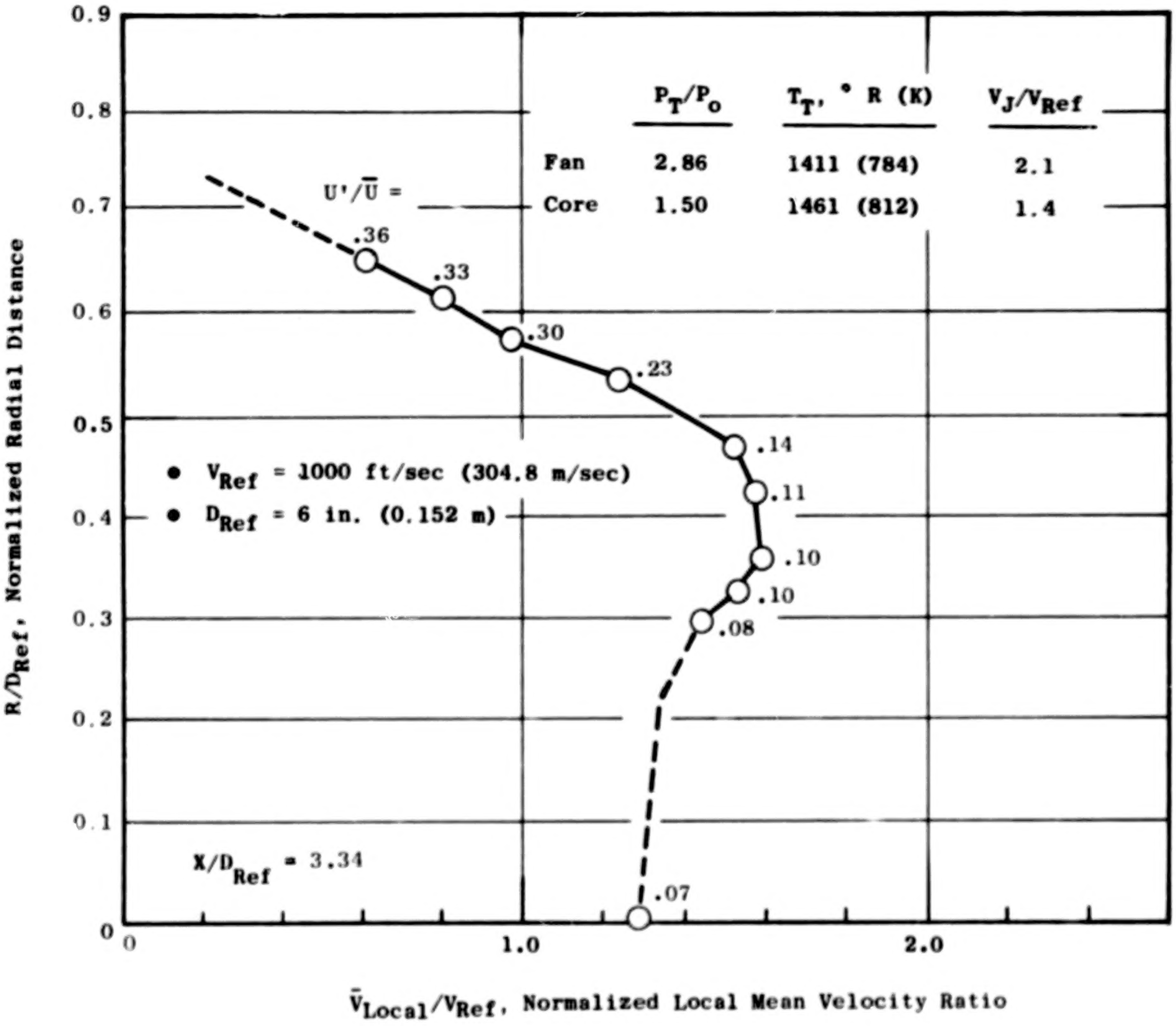

Figure 169. Laser Velocimeter Velocity Profile and Turbulence Measurement; Unsuppressed Coannular Nozzle with Plug (Model 7) at X/D$_{Ref}$ = 3.34

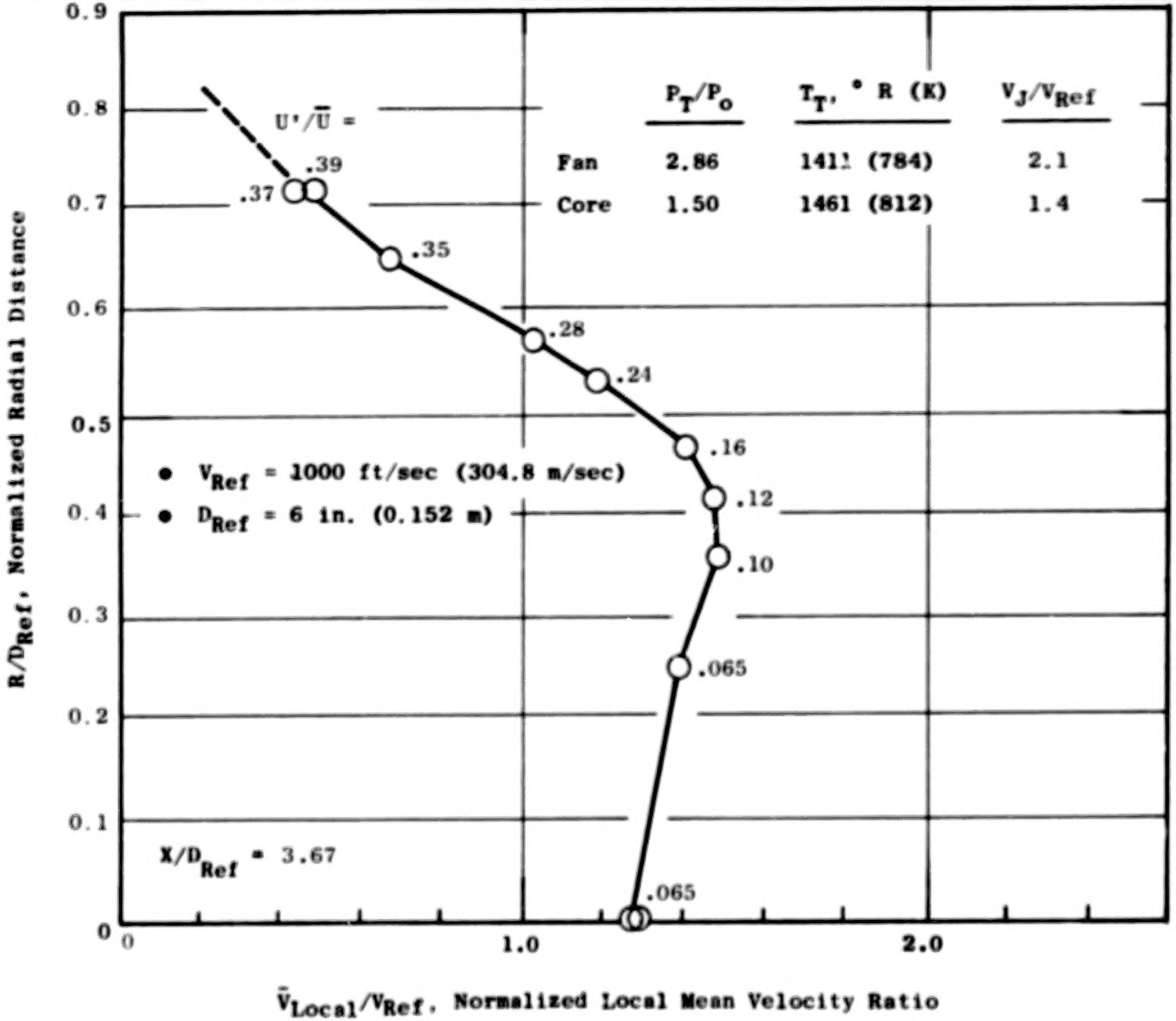

Figure 170. Laser Velocimeter Velocity Profile and Turbulence Measurement; Unsuppressed Coannular Nozzle with Plug (Model 7) at X/D_{Ref} = 3.67.

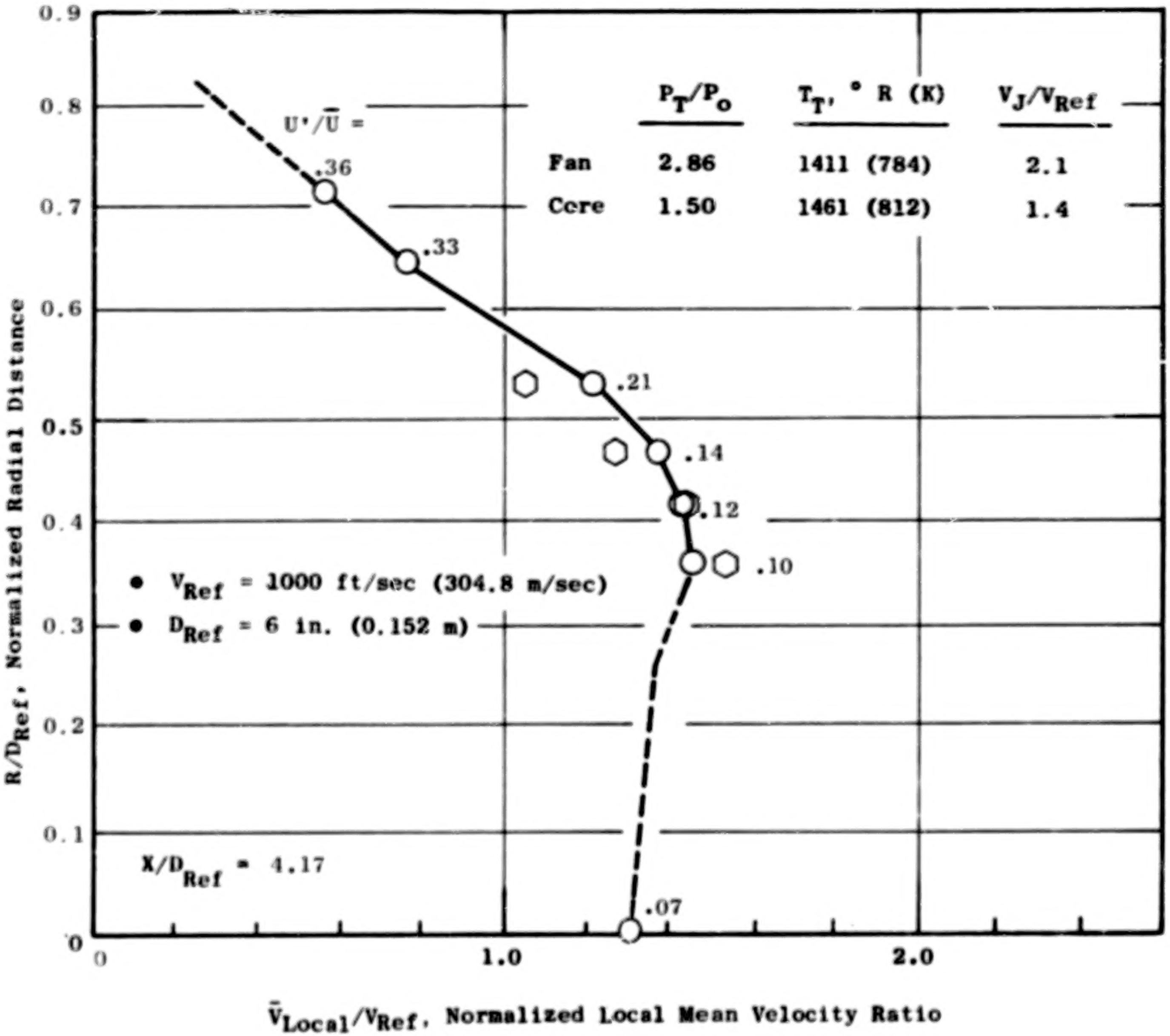

Figure 171. Laser Velocimeter Velocity Profile and Turbulence Measurement; Unsuppressed Coannular Nozzle with Plug (Model 7) at X/D_{Ref} = 4.17.

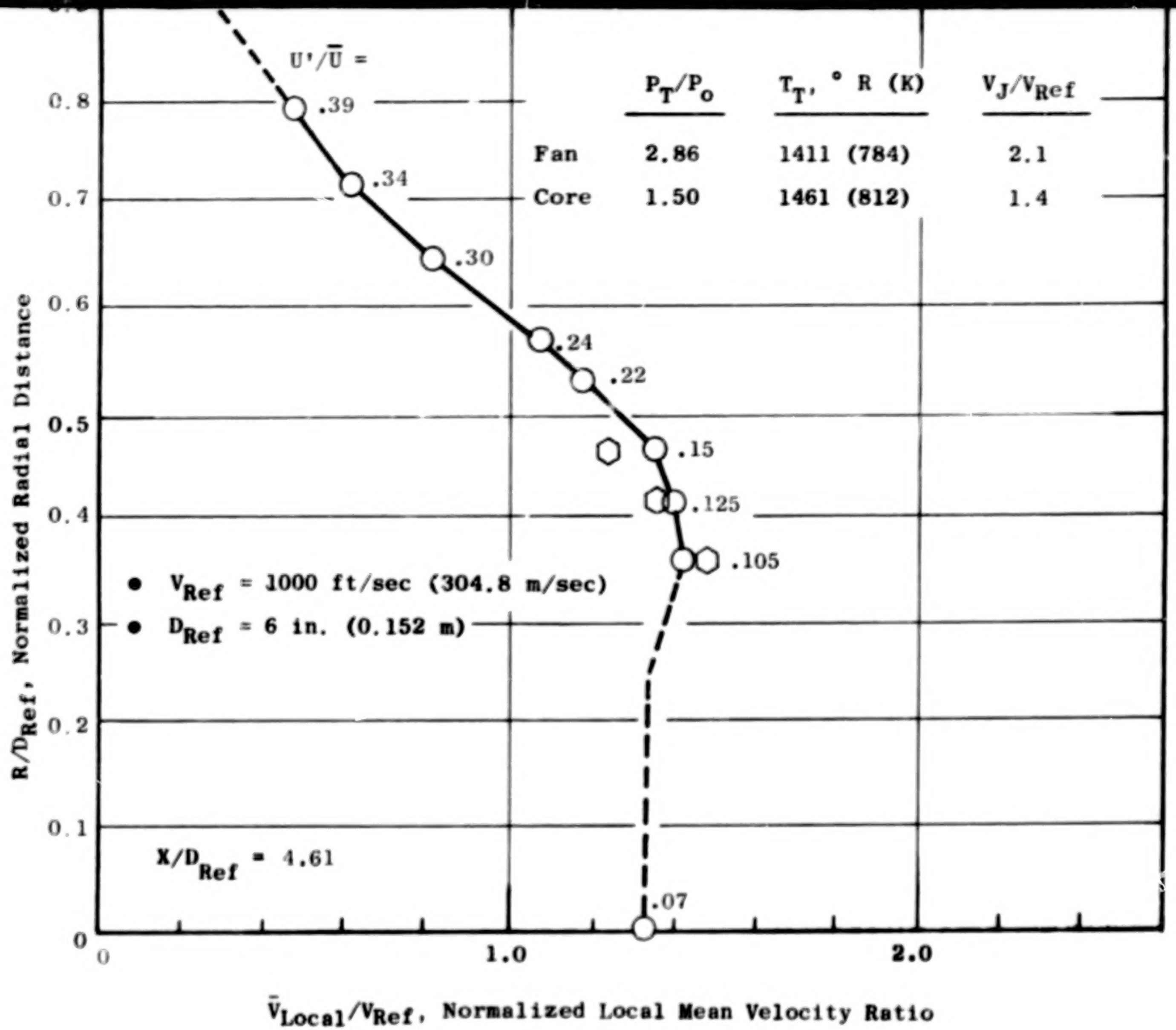

	P_T/P_o	T_T, ° R (K)	V_J/V_{Ref}
Fan	2.86	1411 (784)	2.1
Core	1.50	1461 (812)	1.4

Figure 172. Laser Velocimeter Velocity Profile and Turbulence Measurement; Unsuppressed Coannular Nozzle with Plug (Model 7) at X/D_{Ref} = 4.61.

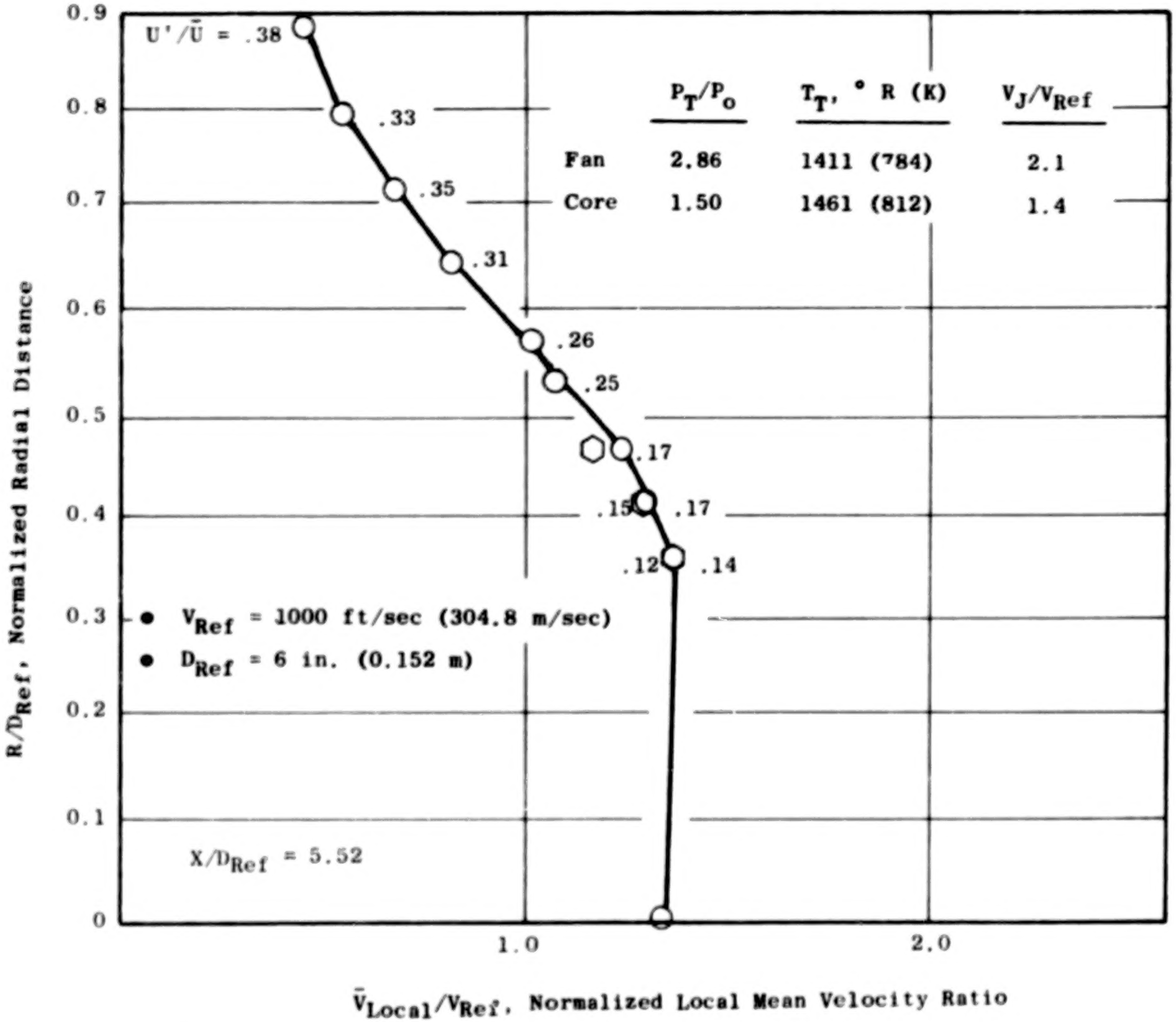

Figure 173. Laser Velocimeter Velocity Profile and Turbulence Measurement; Unsuppressed Coannular Nozzle with Plug (Model 7) at X/D_{Ref} = 5.52.

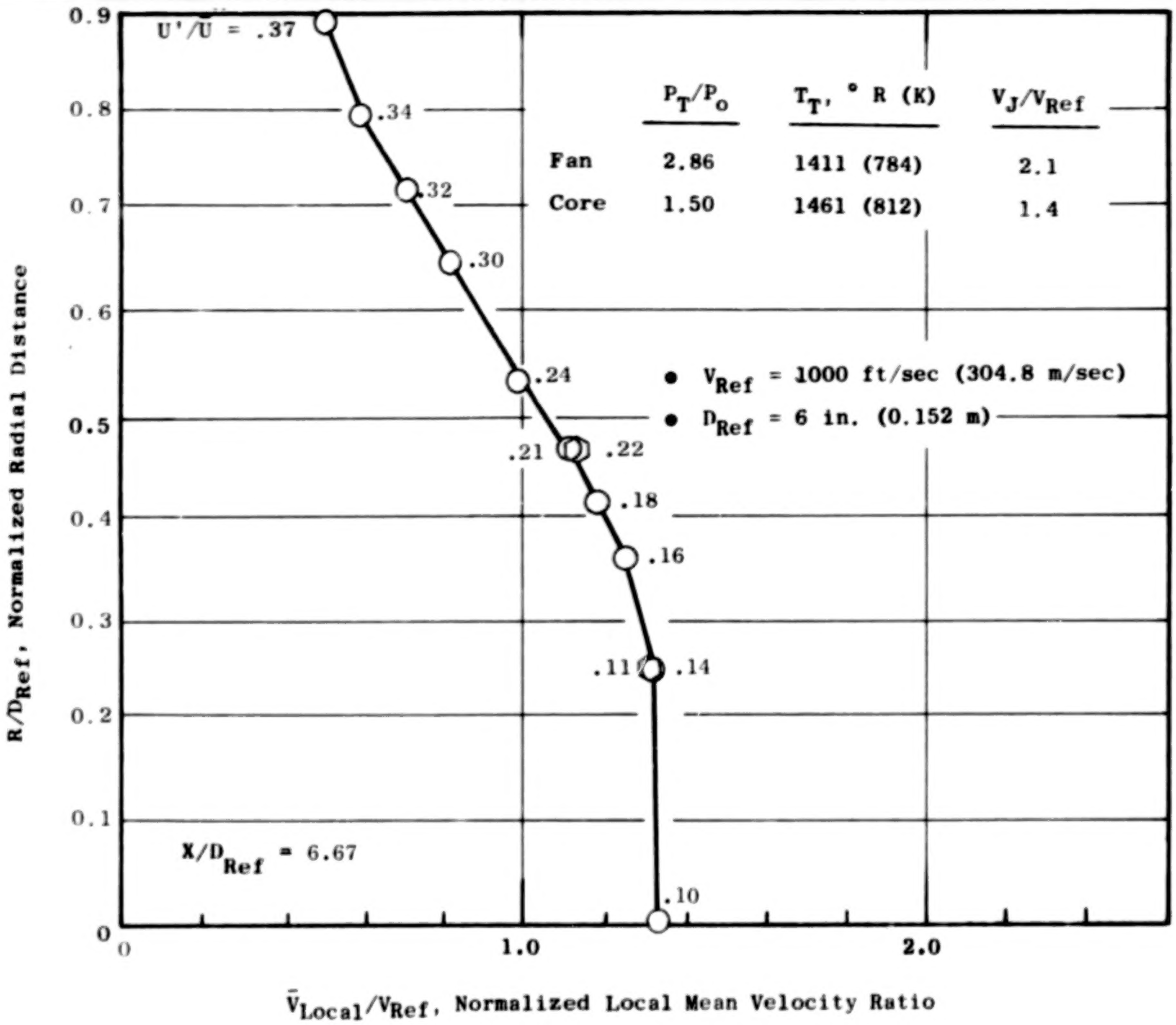

Figure 174. Laser Velocimeter Velocity Profile and Turbulence Measurement; Unsuppressed Coannular Nozzle with Plug (Model 7) at X/D_{Ref} = 6.67.

APPENDIX G

MODEL 7 AXIAL-VELOCITY PROFILES WITH NO CORE FLOW

Laser velocimeter measurements of axial-velocity profiles for the unsuppressed coannular nozzle with plug (Model 7) with the fan stream flowing and the core set for no flow* are presented in Figures 175 through 189 for the following conditions:

	P_T/P_o	T_T, ° R (K)	V_J, ft/sec (m/sec)
Fan	2.86	1411 (784)	2100 (640.5)
Core	1.0	Ambient	0

---

*Although the core was set for no flow, it was found that the core-stream valve was opened slightly while maniplulating the fan stream. The estimated leakage was about 10% of the outer (fan) stream weight flow.

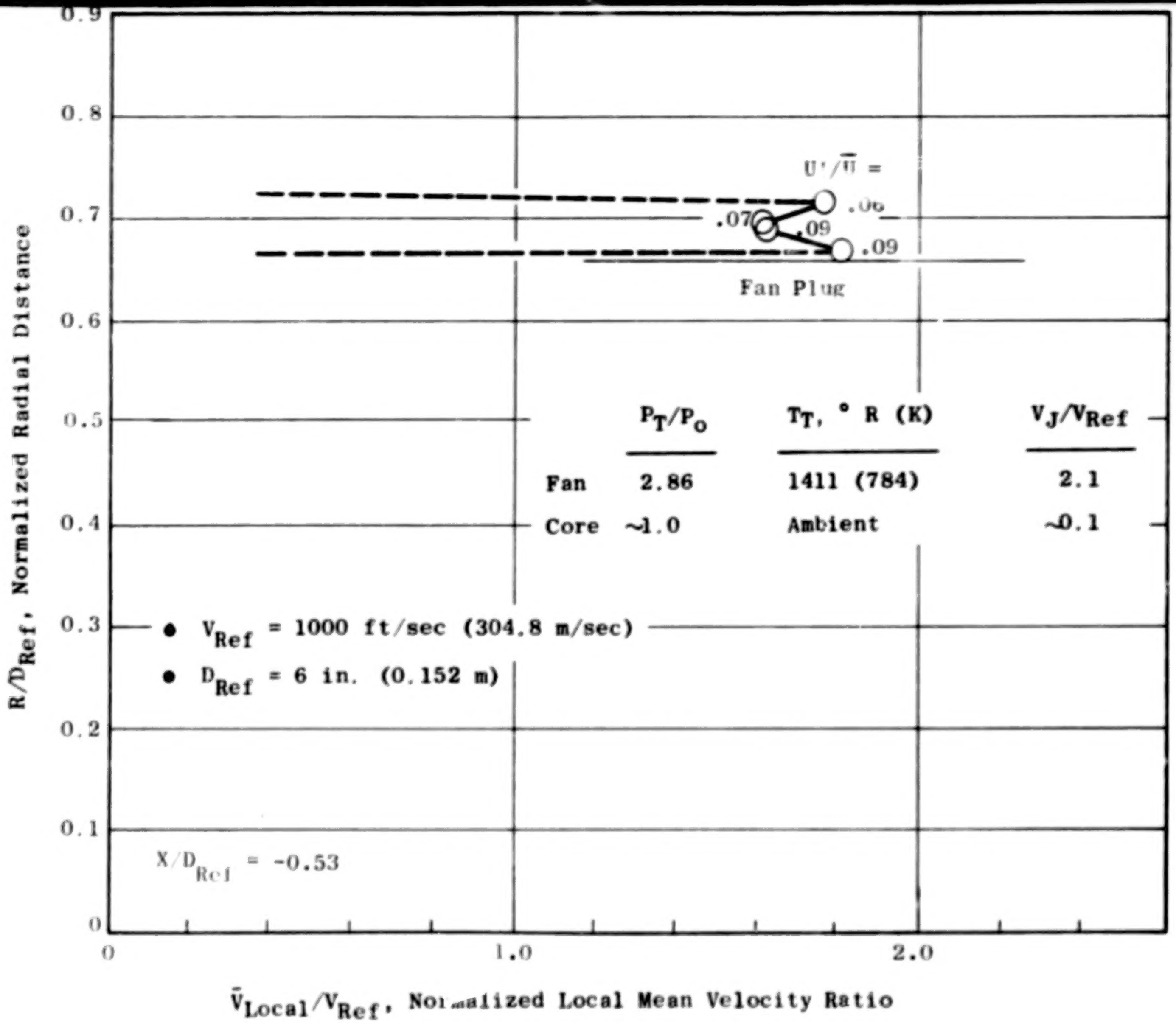

Figure 175. Laser Velocimeter Velocity Profile and Turbulence Measurement for the Unsuppressed Coannular Nozzle with Plug (Model 7) (Fan Stream Flowing, Core Stream Set for No Flow); X/D_{Ref} = -0.53.

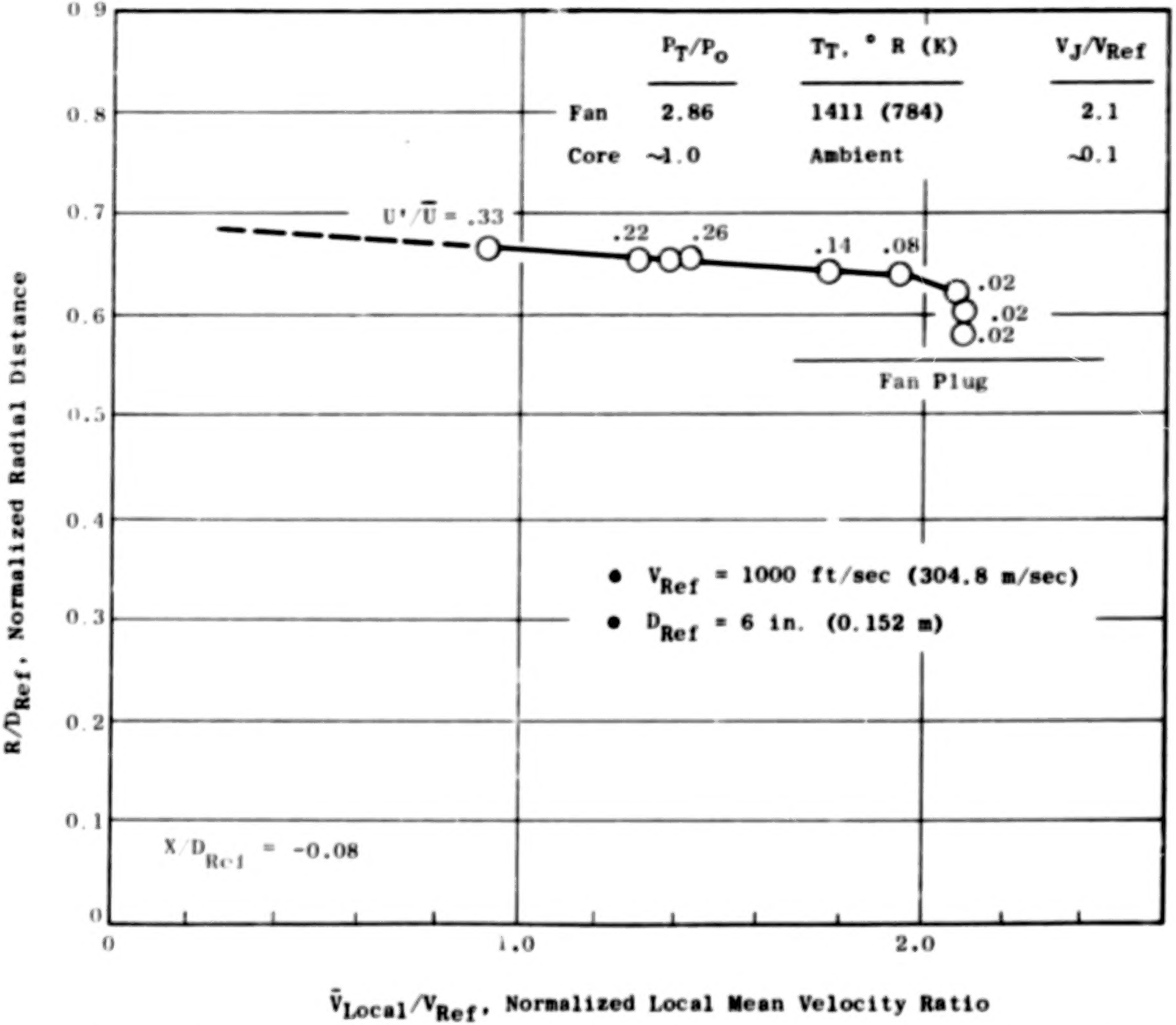

Figure 176. Laser Velocimeter Velocity Profile and Turbulence Measurement for the Unsuppressed Coannular Nozzle with Plug (Model 7) (Fan Stream Flowing, Core Stream Set for No Flow); X/D_{Ref} = -0.08.

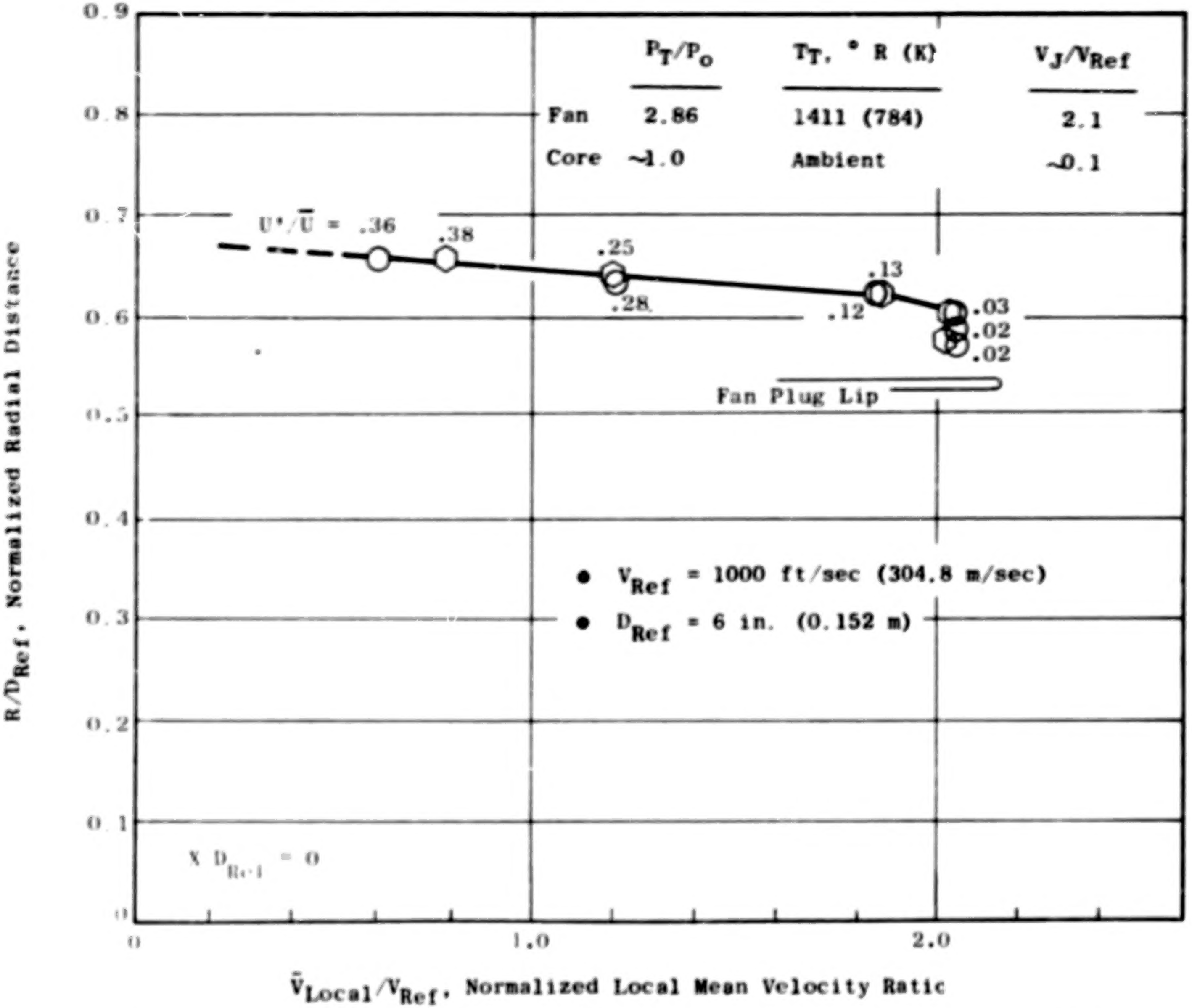

Figure 177. Laser Velocimeter Velocity Profile and Turbulence Measurement for the Unsuppressed Coannular Nozzle with Plug (Model 7) (Fan Stream Flowing, Core Stream Set for No Flow); $X/D_{Ref} = 0$.

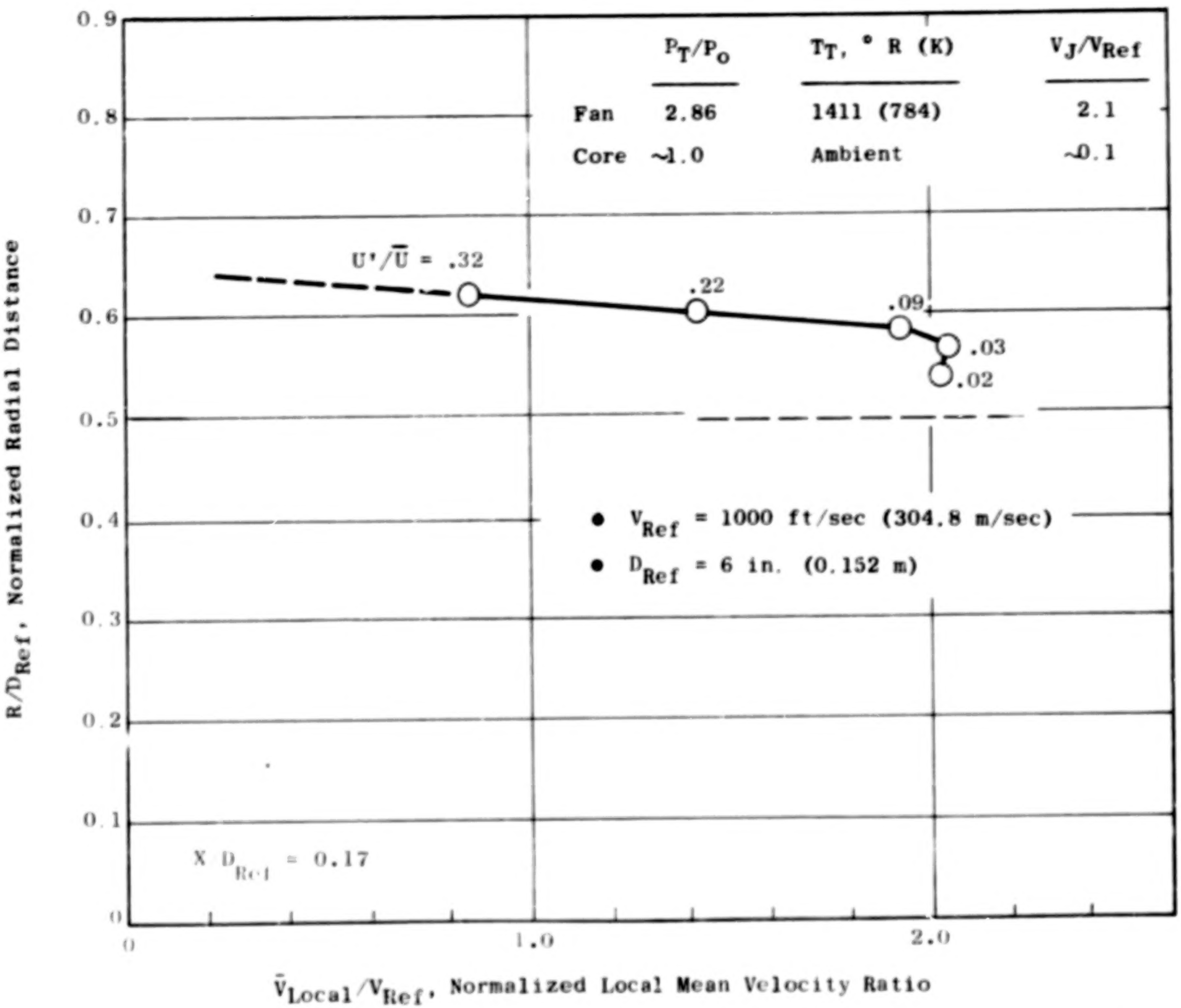

Figure 178. Laser Velocimeter Velocity Profile and Turbulence Measurement for the Unsuppressed Coannular Nozzle with Plug (Model 7) (Fan Stream Flowing, Core Stream Set for No Flow); X/D_{Ref} = 0.17.

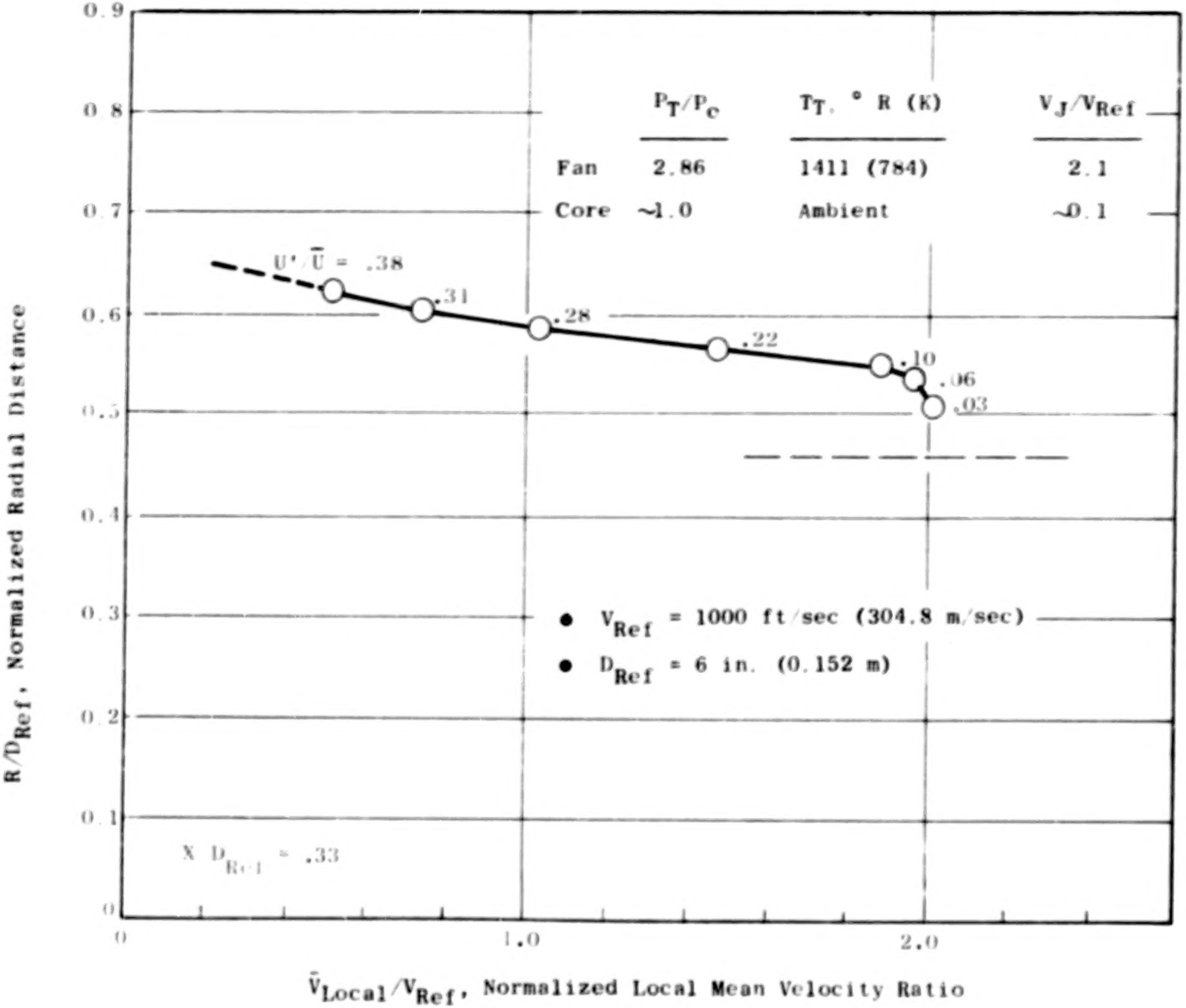

Figure 179. Laser Velocimeter Velocity Profile and Turbulence Measurement for the Unsuppressed Coannular Nozzle with Plug (Model 7) (Fan Stream Flowing, Core Stream Set for No Flow); X/D_{Ref} = 0.33.

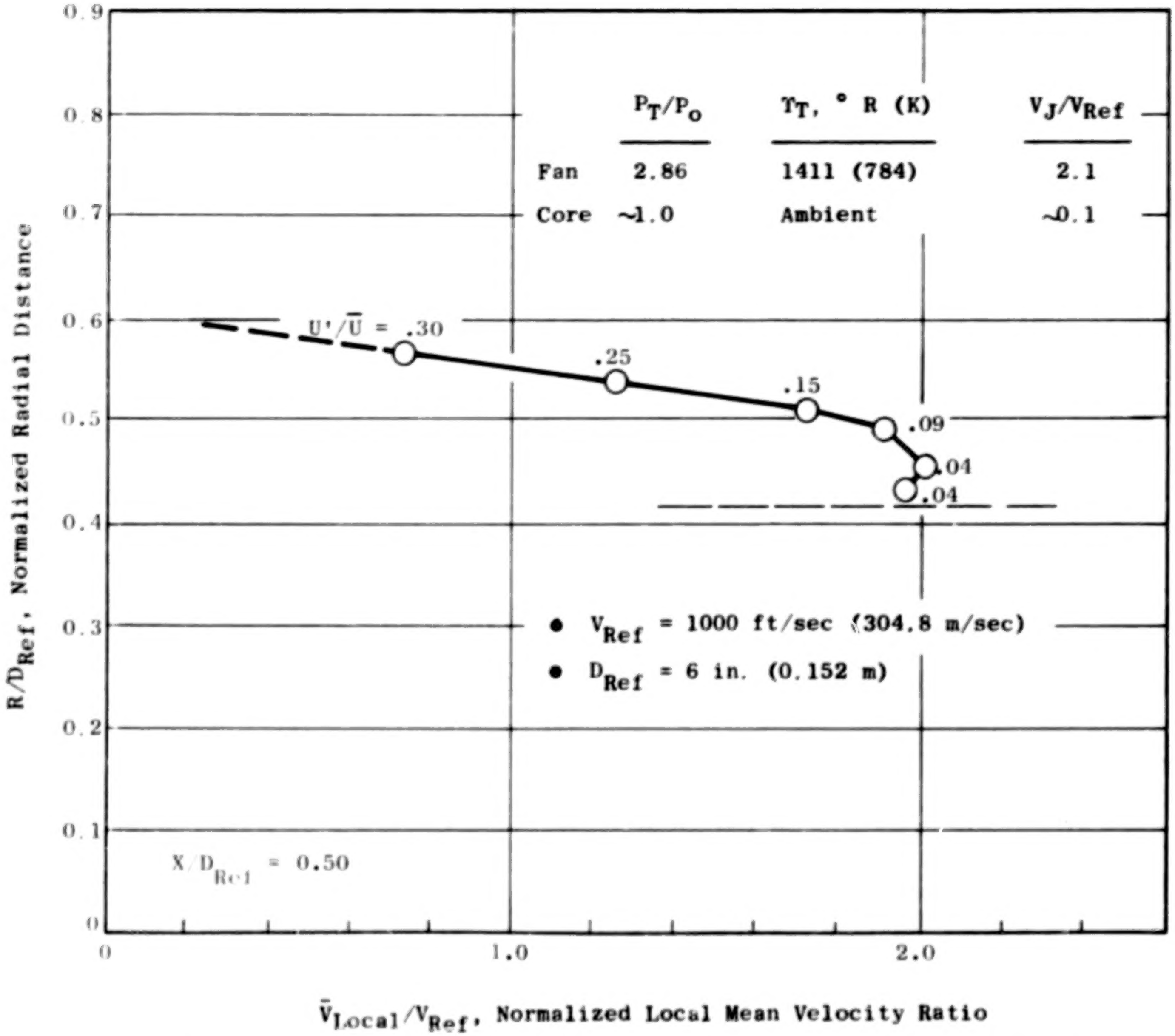

Figure 180. Laser Velocimeter Velocity Profile and Turbulence Measurement for the Unsuppressed Coannular Nozzle with Plug (Model 7) (Fan Stream Flowing, Core Stream Set for No Flow); X/D_{Ref} = 0.50.

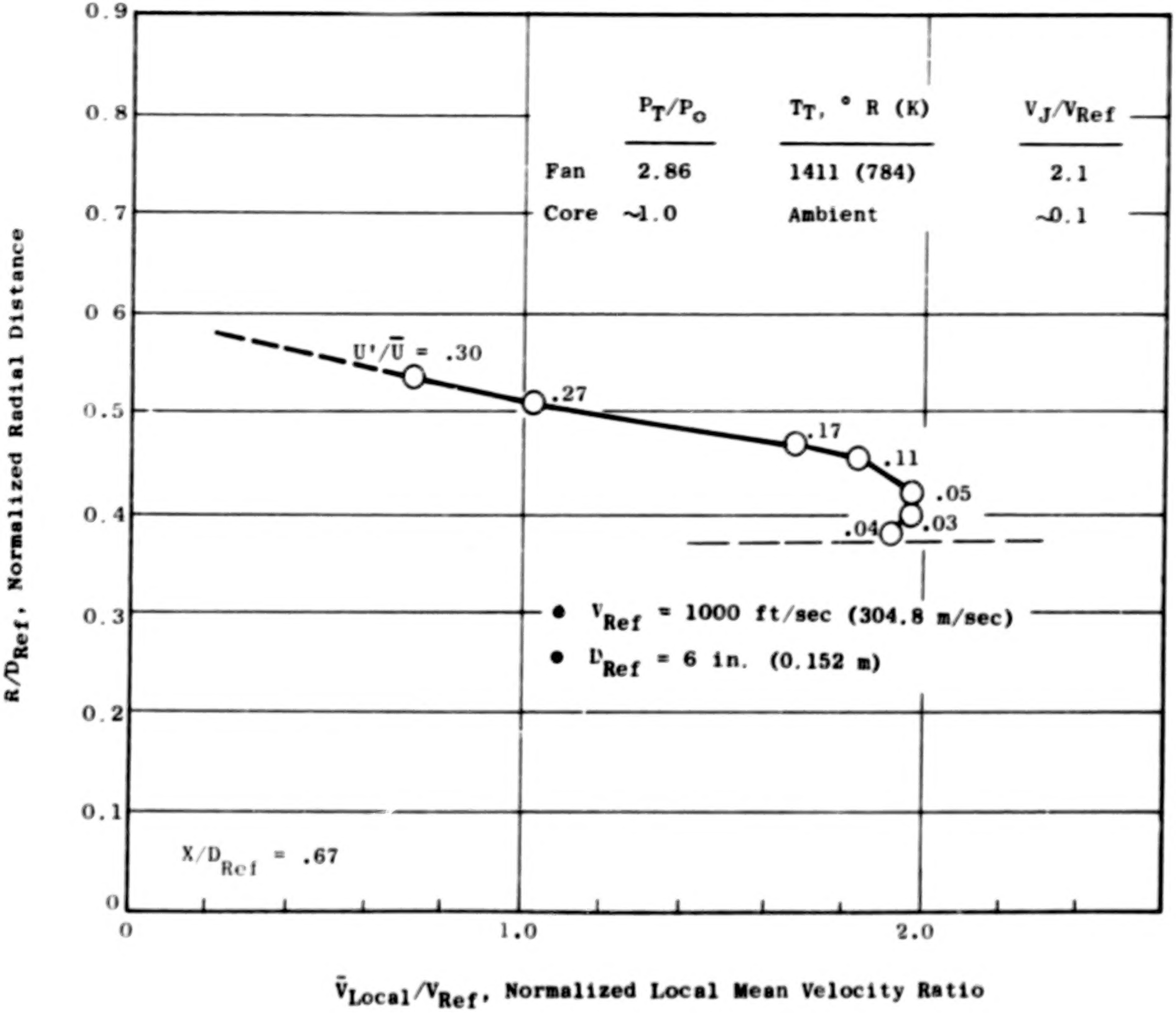

Figure 181. Laser Velocimeter Velocity Profile and Turbulence Measurement for the Unsuppressed Coannular Nozzle with Plug (Model 7) (Fan Stream Flowing, Core Stream Set for No Flow); X/D_{Ref} = 0.67.

277

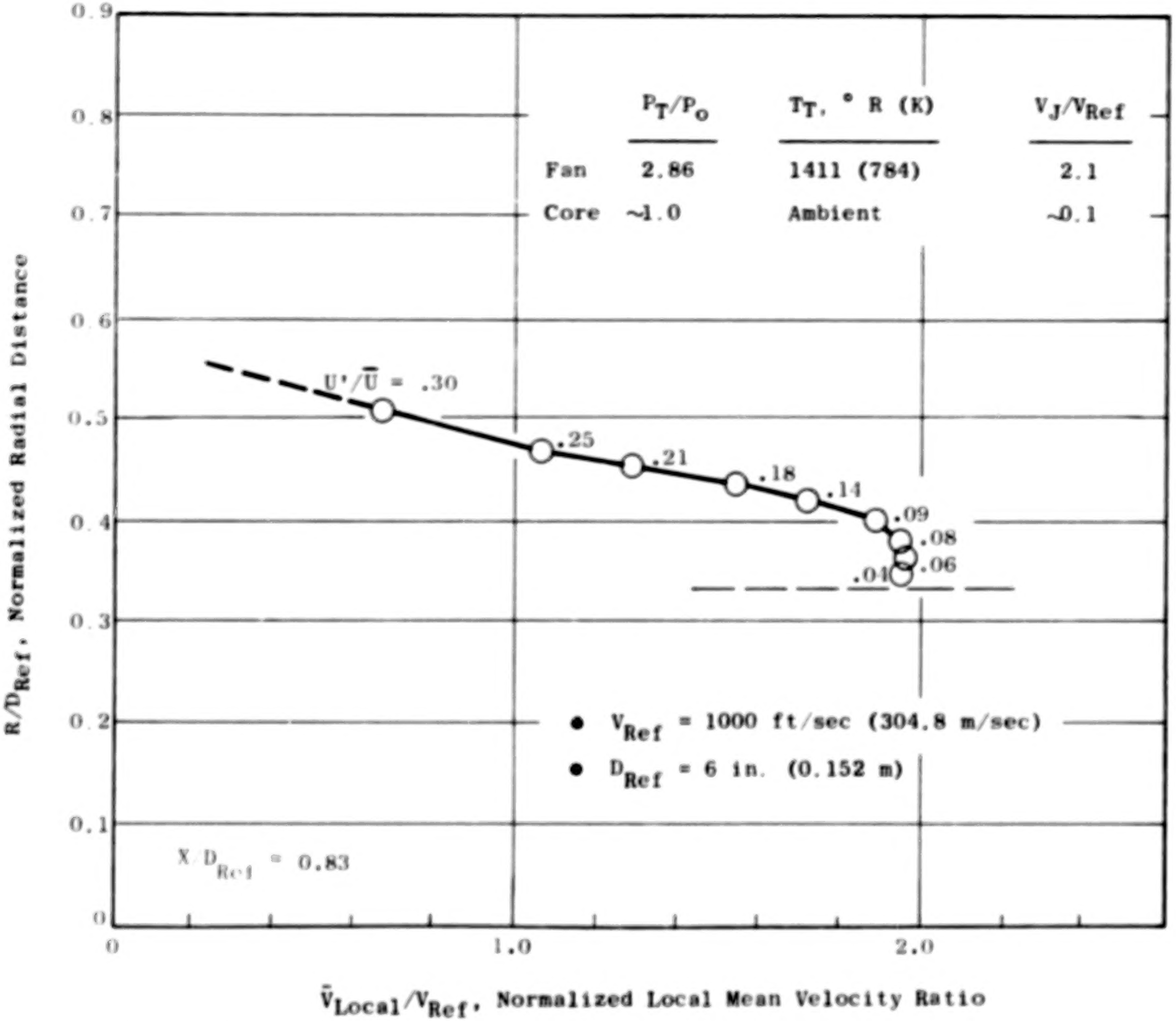

Figure 182. Laser Velocimeter Velocity Profile and Turbulence Measurement for the Unsuppressed Coannular Nozzle with Plug (Model 7) (Fan Stream Flowing, Core Stream Set for No Flow); X/D_{Ref} = 0.83.

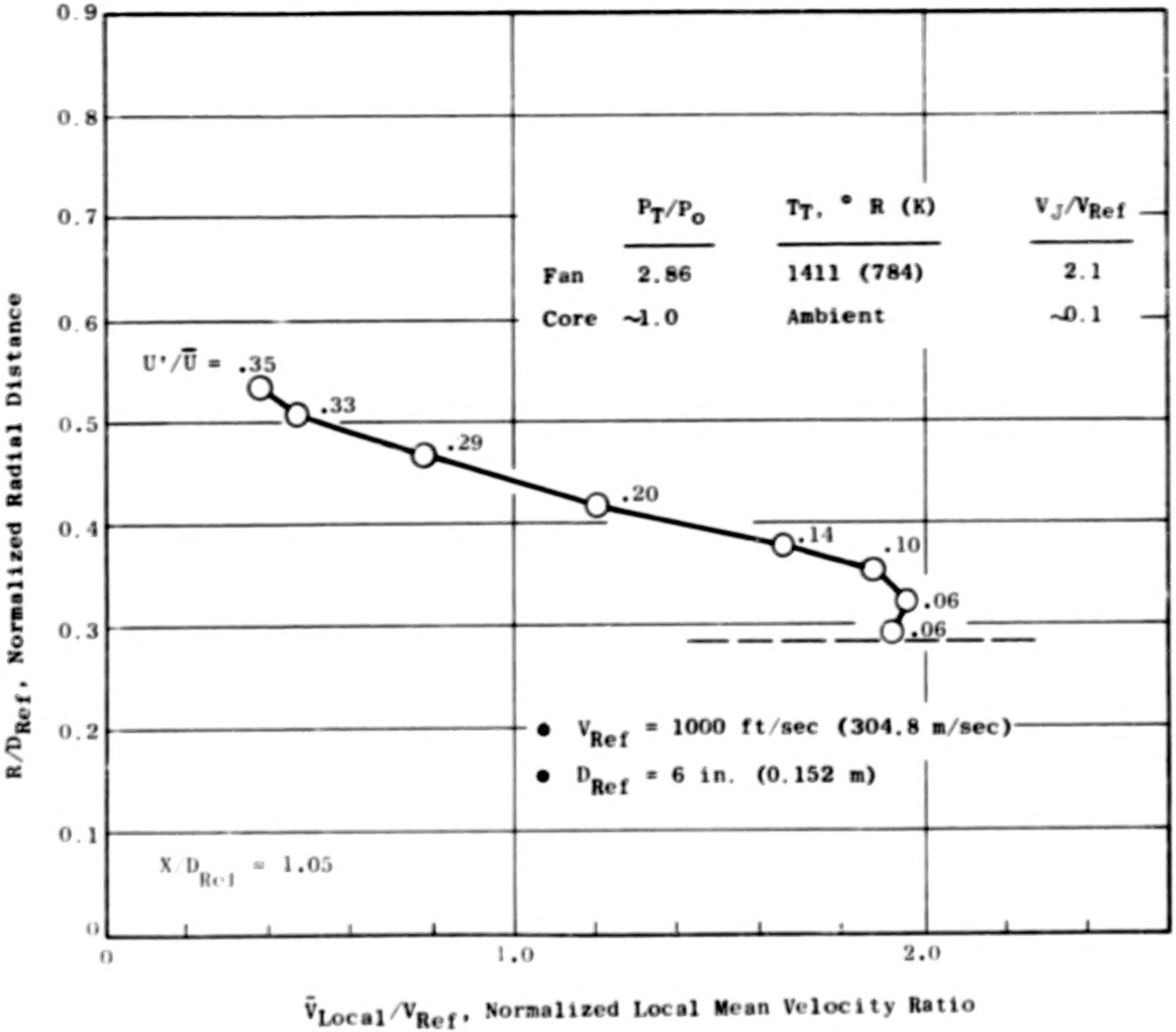

Figure 183. Laser Velocimeter Velocity Profile and Turbulence Measurement for the Unsuppressed Coannular Nozzle with Plug (Model 7) (Fan Stream Flowing, Core Stream Set for No Flow); $X/D_{Ref} = 1.05$.

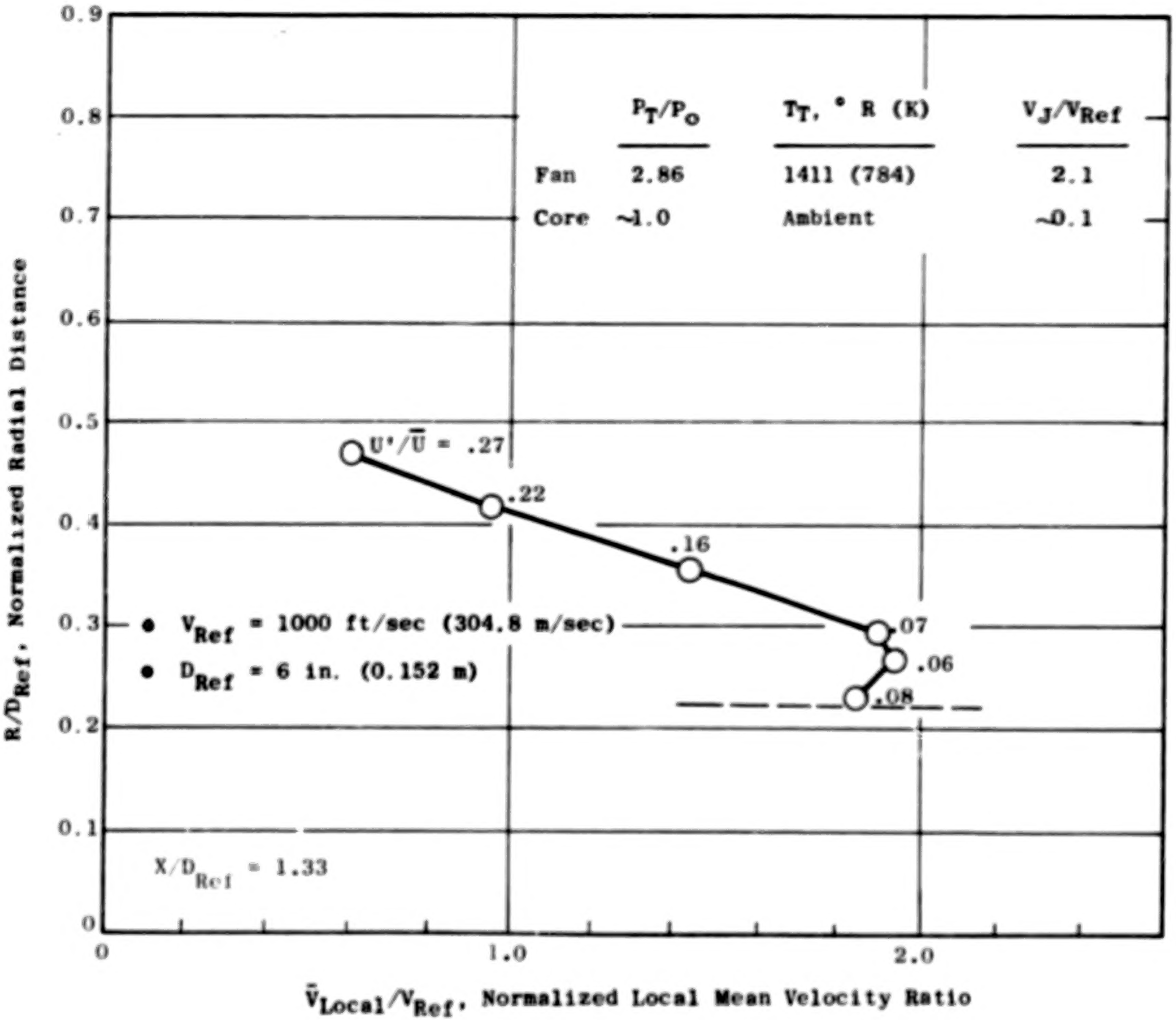

Figure 184. Laser Velocimeter Velocity Profile and Turbulence Measurement for the Unsuppressed Coannular Nozzle with Plug (Model 7) (Fan Stream Flowing, Core Stream Set for No Flow); X/D_{Ref} = 1.33.

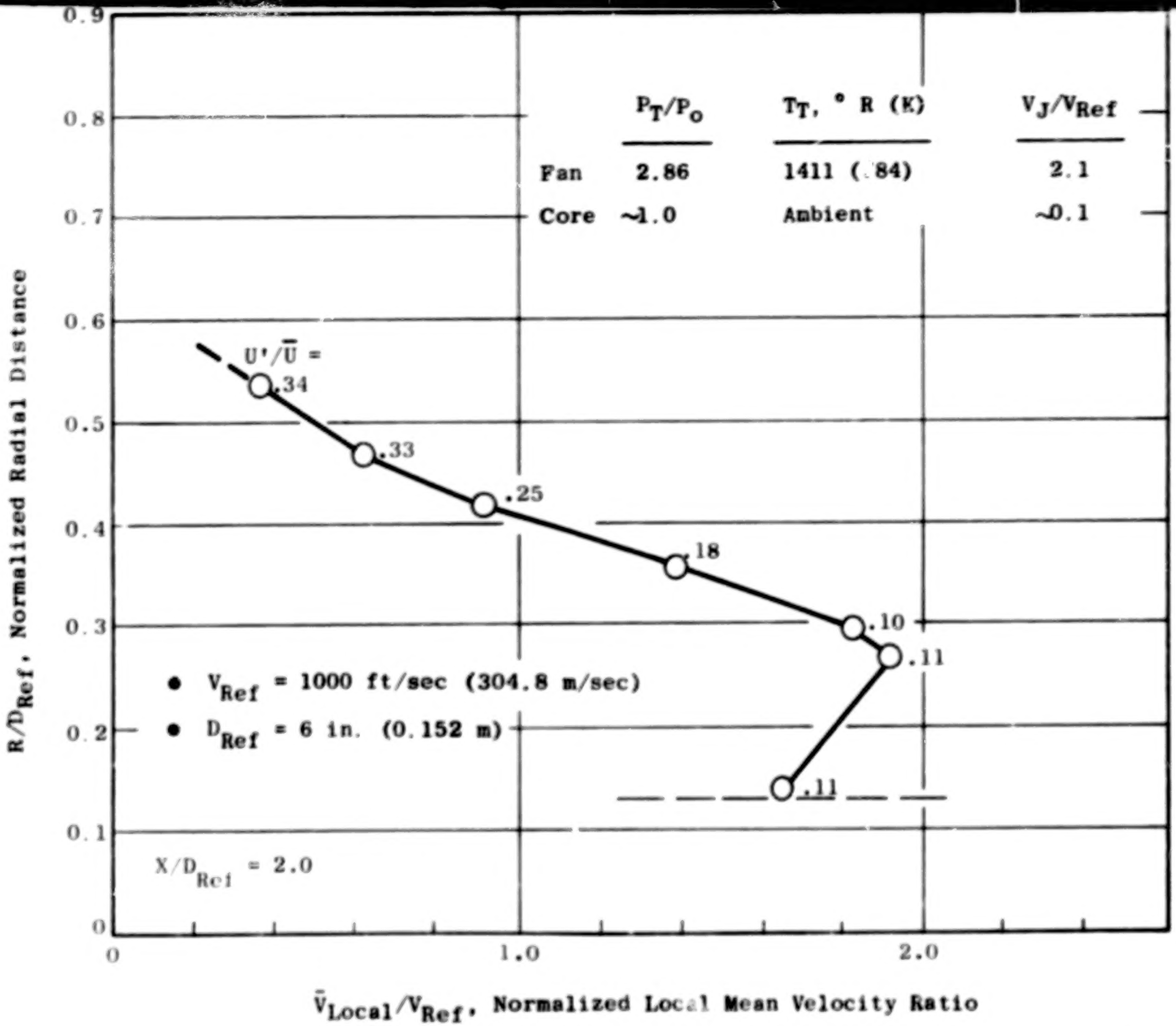

Figure 185. Laser Velocimeter Velocity Profile and Turbulence Measurement for the Unsuppressed Coannular Nozzle with Plug (Model 7) (Fan Stream Flowing, Core Stream Set for No Flow); $X/D_{Ref} = 2.0$.

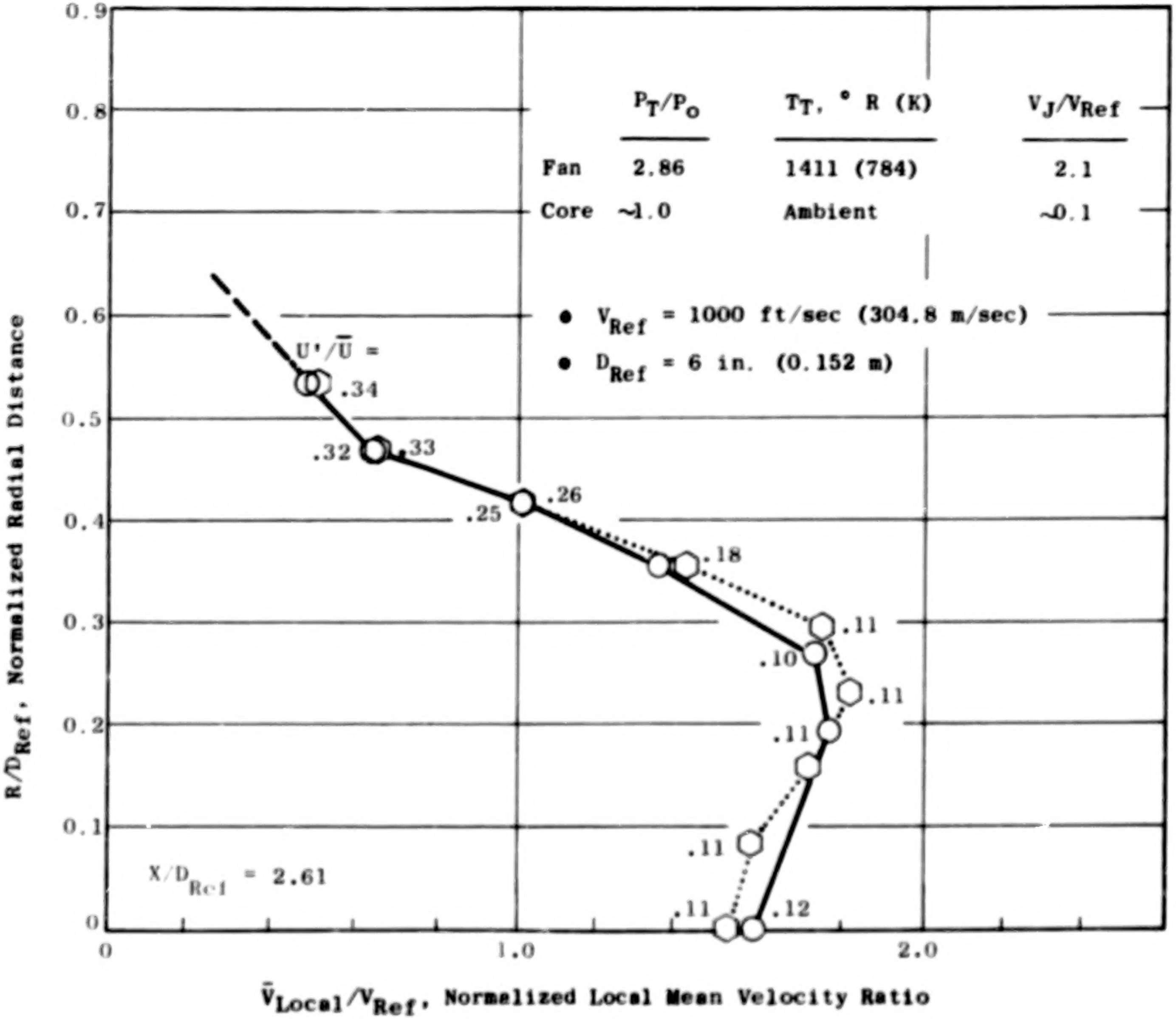

Figure 186. Laser Velocimeter Velocity Profile and Turbulence Measurement for the Unsuppressed Coannular Nozzle with Plug (Model 7) (Fan Stream Flowing, Core Stream Set for No Flow); X/D_{Ref} = 2.61.

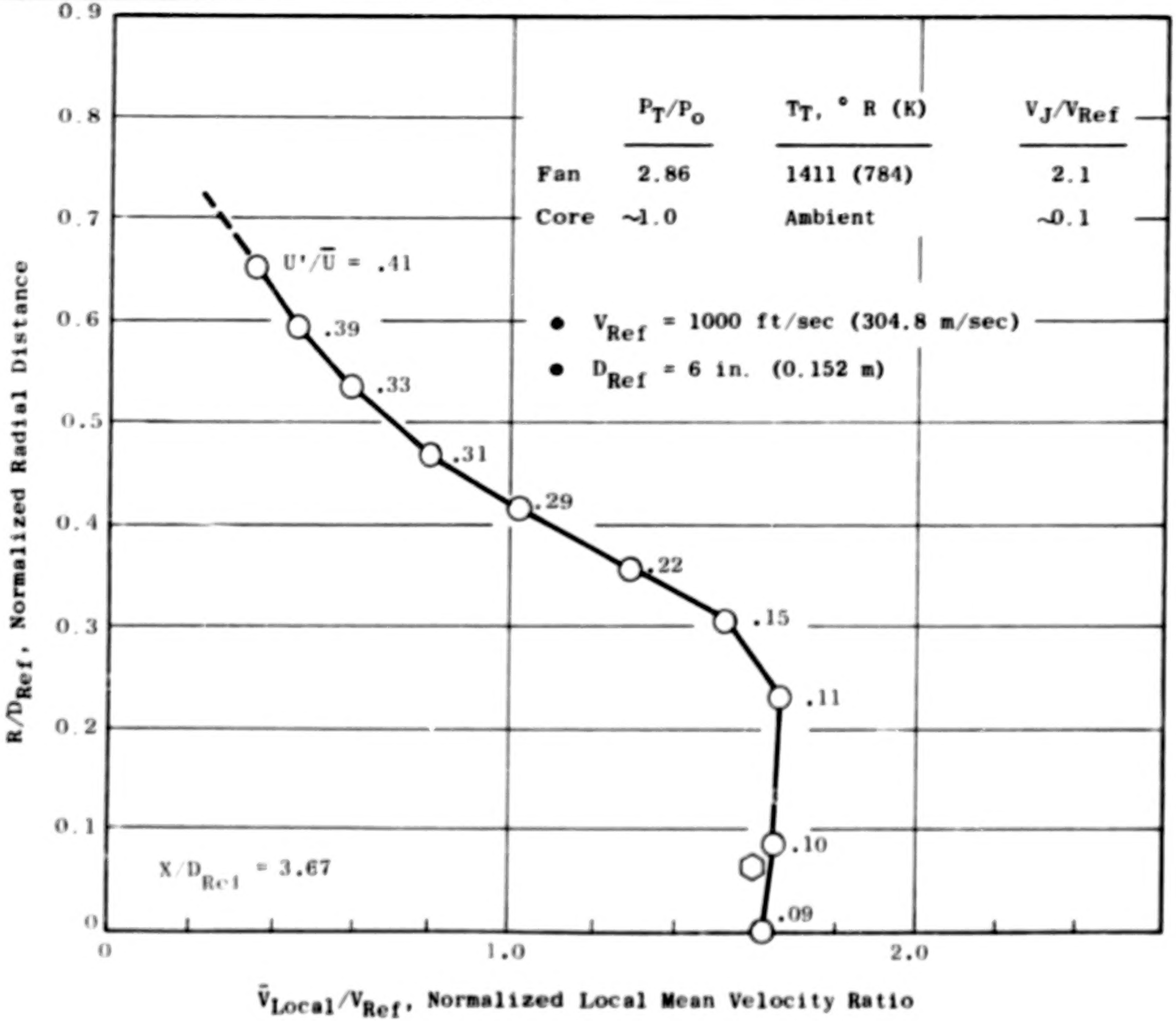

Figure 187. Laser Velocimeter Velocity Profile and Turbulence Measurement for the Unsuppressed Coannular Nozzle with Plug (Model 7) (Fan Stream Flowing, Core Stream Set for No Flow); $X/D_{Ref} = 3.67$.

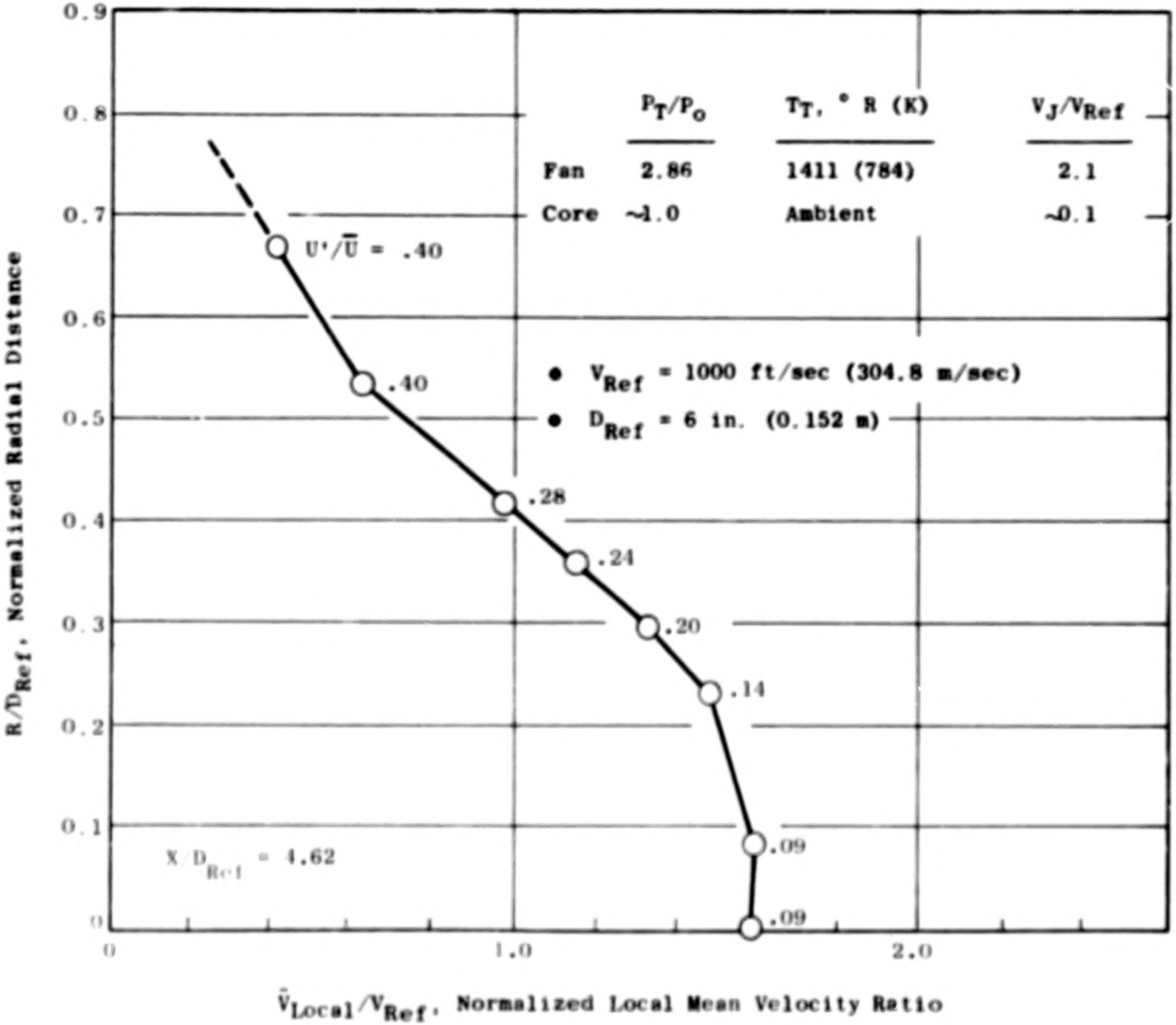

Figure 188. Laser Velocimeter Velocity Profile and Turbulence Measurement for the Unsuppressed Coannular Nozzle with Plug (Model 7) (Fan Stream Flowing, Core Stream Set for No Flow); X/D_{Ref} = 4.61.

	P_T/P_o	T_T, ° R (K)	V_J/V_{Ref}
Fan	2.86	1411 (784)	2.1
Core	~1.0	Ambient	~0.1

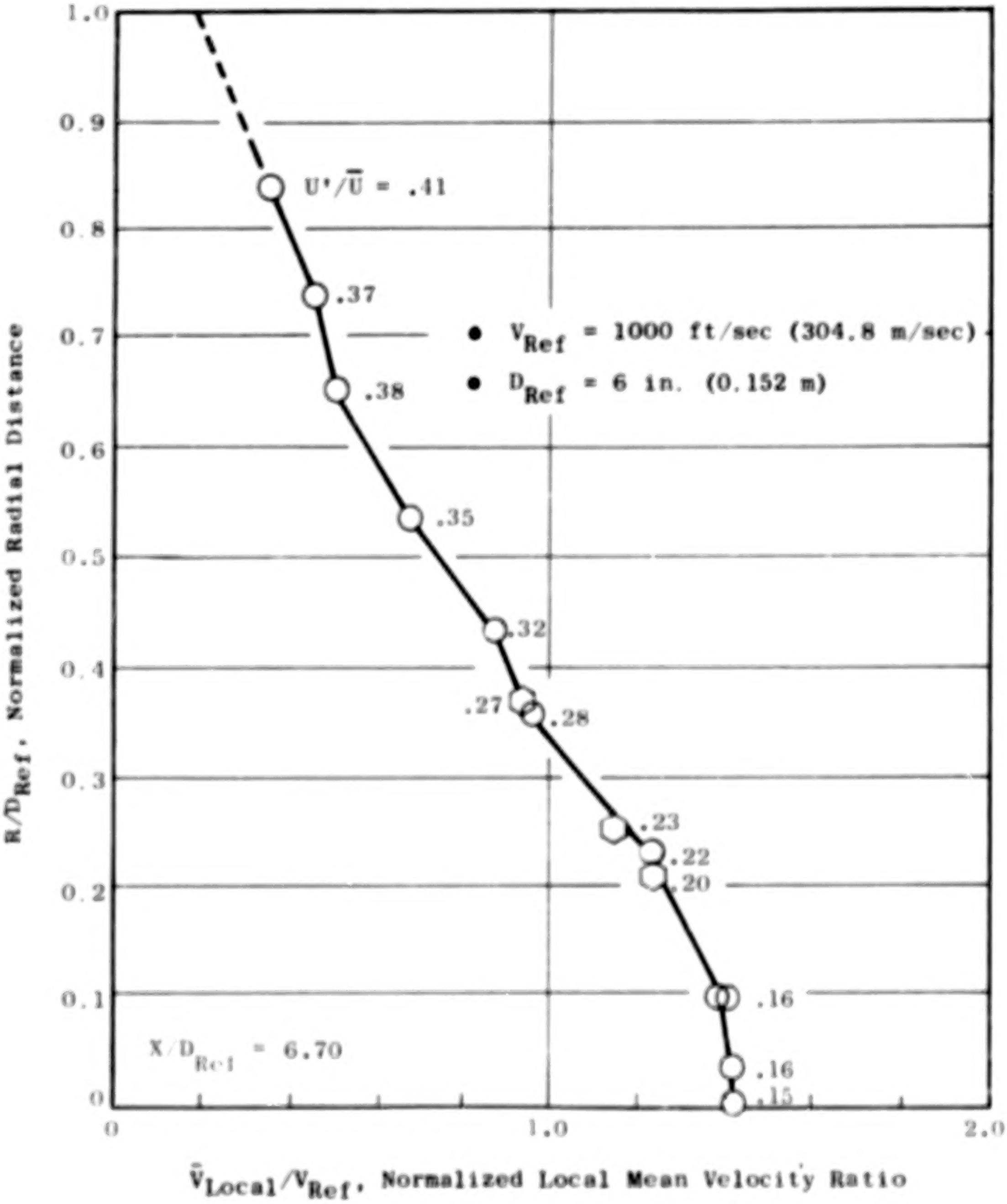

Figure 189. Laser Velocimeter Velocity Profile and Turbulence Measurement for the Unsuppressed Coannular Nozzle with Plug (Model 7) (Fan Stream Flowing, Core Stream Set for No Flow); X/D_{Ref} = 6.70.

APPENDIX H

MODEL 7 AXIAL-VELOCITY PROFILES WITH NO FAN FLOW

Laser velocimeter measurements of axial-velocity profiles for the unsuppressed coannular nozzle with plug (Model 7) with the core stream flowing and the fan stream set for no flow are presented in Figures 190 through 197 for the following conditions.

	P_T/P_o	T_T, ° R (K)	V_J, ft/sec (m/sec)
Fan	1.0	Ambient	0
Core	1.5	1411 (784)	1400 (427)

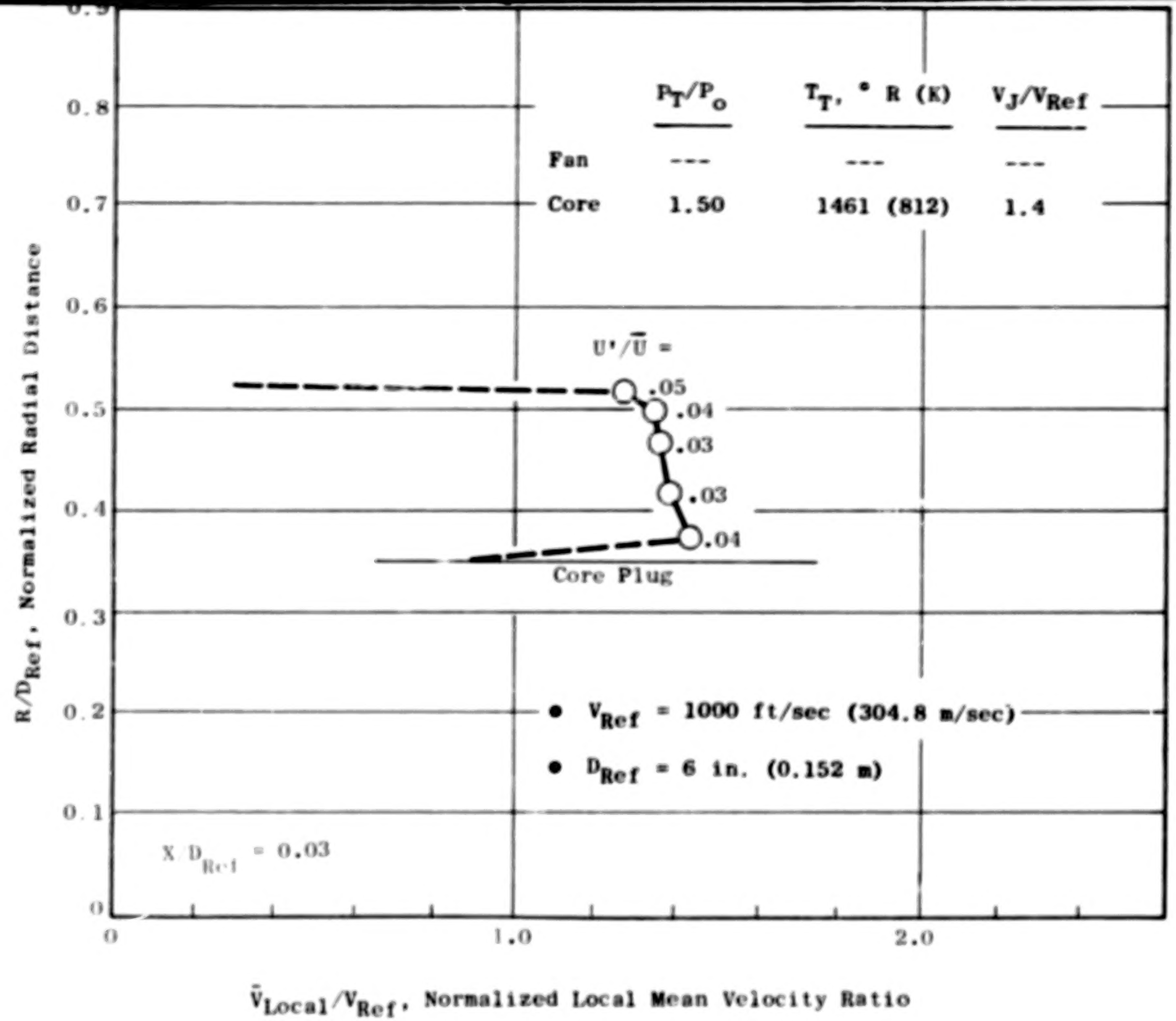

Figure 190. Laser Velocimeter Velocity Profile and Turbulence Measurement for the Unsuppressed Coannular Nozzle with Plug (Model 7) (Core Stream Flowing, Fan Stream Set for No Flow); X/D_{Ref} = 0.03.

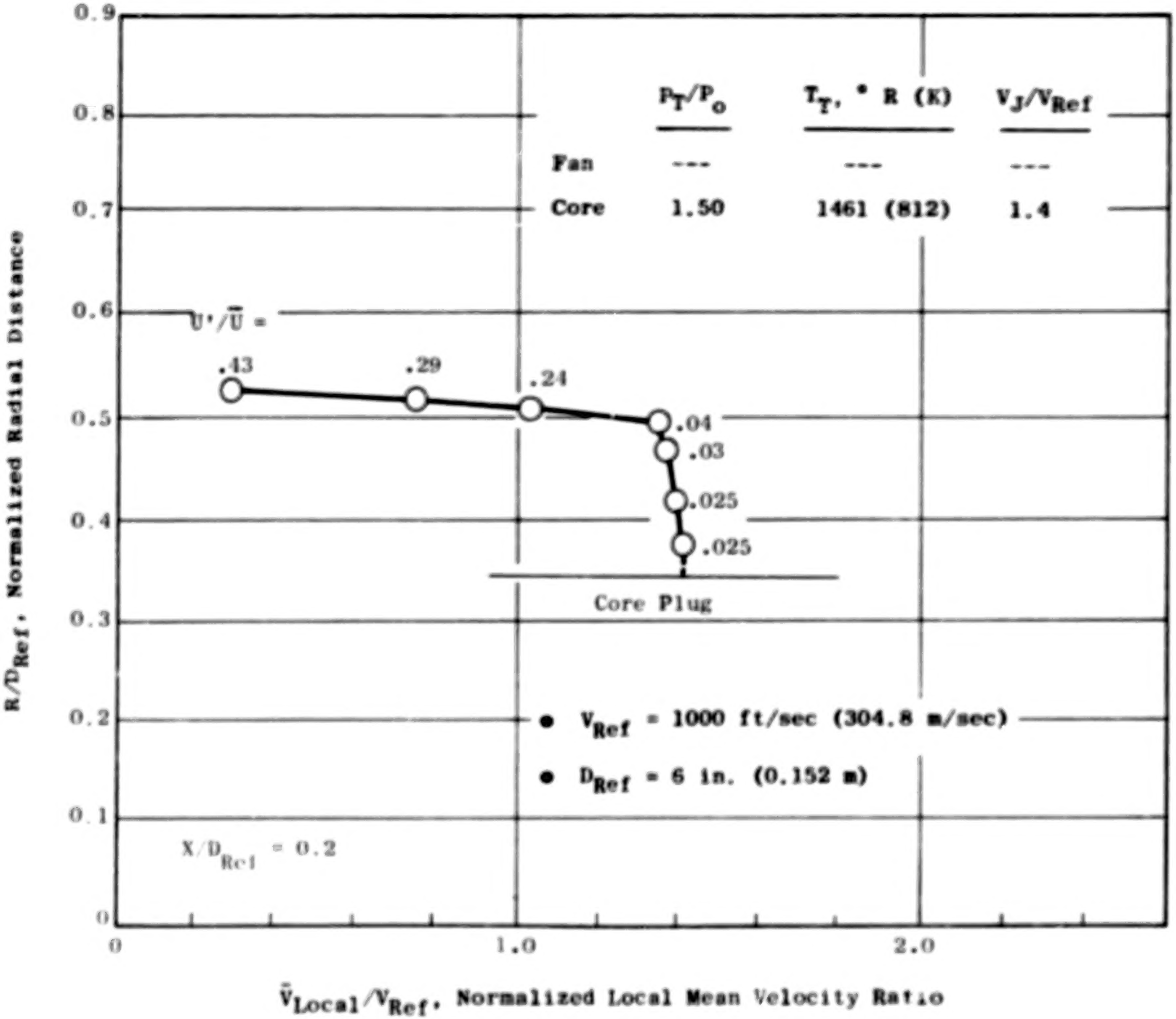

Figure 191. Laser Velocimeter Velocity Profile and Turbulence Measurement for the Unsuppressed Coannular Nozzle with Plug (Model 7) (Core Stream Flowing, Fan Stream Set for No Flow); $X/D_{Ref} = 0.2$.

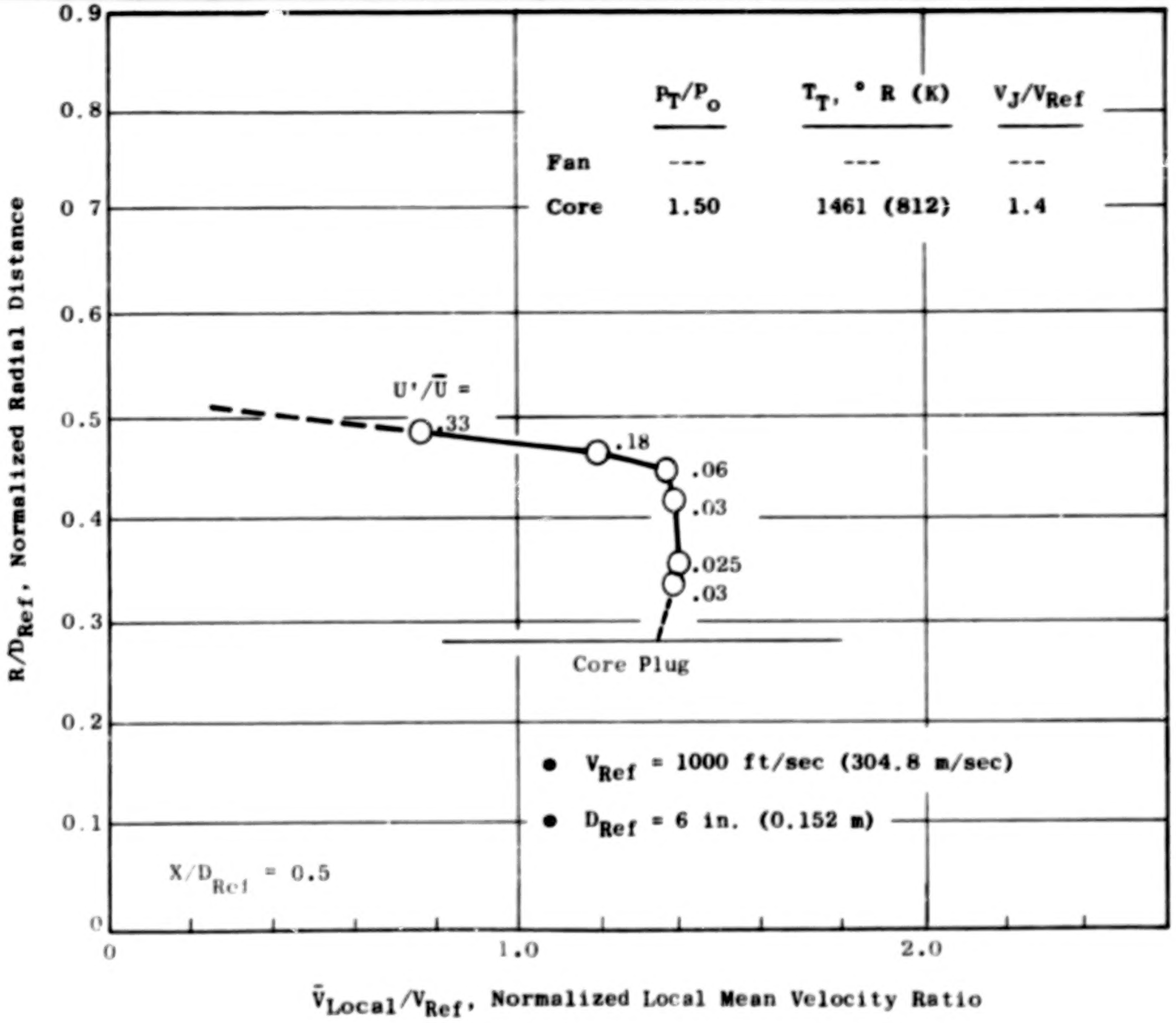

Figure 192. Laser Velocimeter Velocity Profile and Turbulence Measurement for the Unsuppressed Coannular Nozzle with Plug (Model 7) (Core Stream Flowing, Fan Stream Set for No Flow); X/D_{Ref} = 0.5.

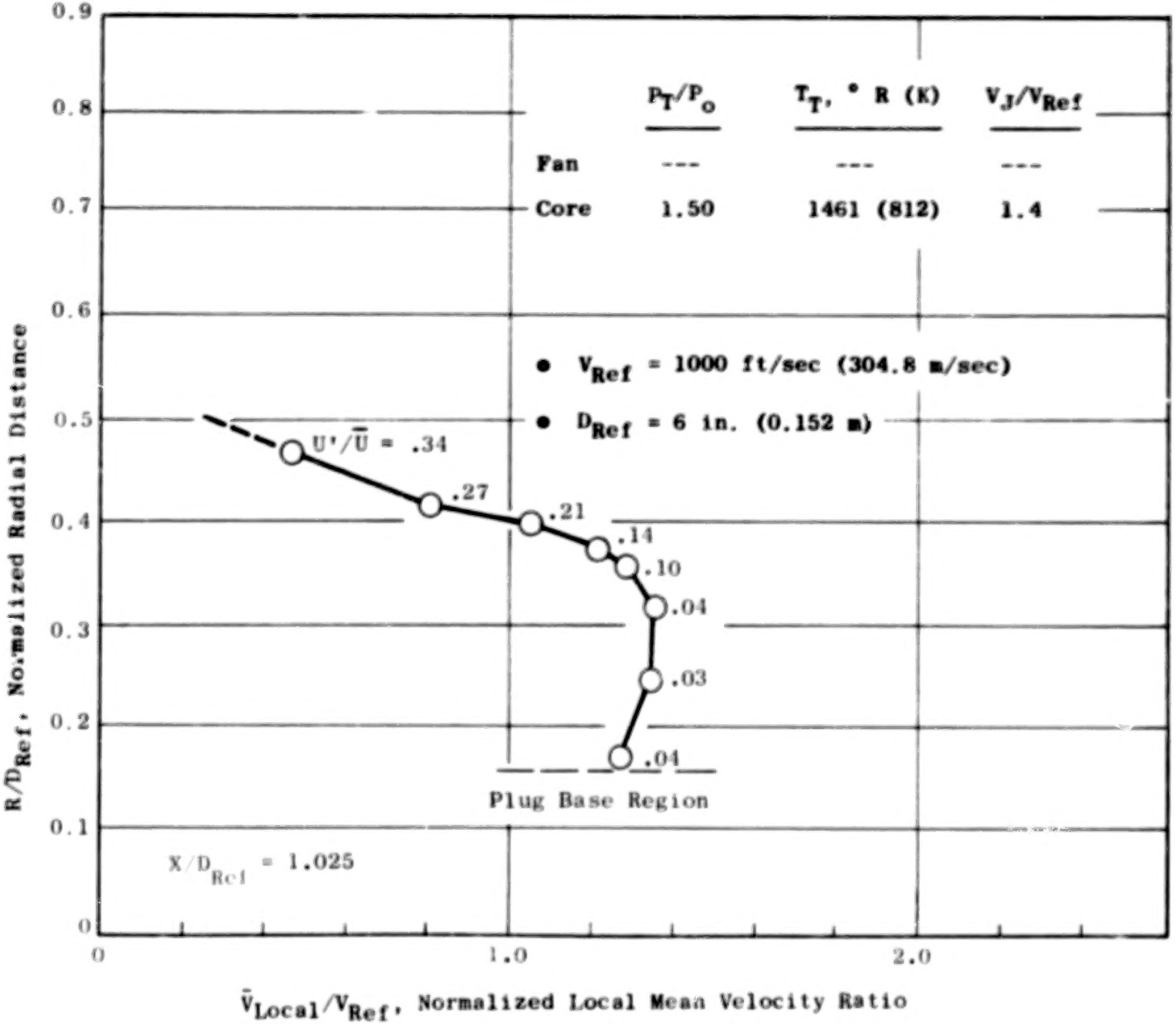

Figure 193. Laser Velocimeter Velocity Profile and Turbulence Measurement for the Unsuppressed Coannular Nozzle with Plug (Model 7) (Core Stream Flowing, Fan Stream Set for No Flow); X/D_{Ref} = 1.025.

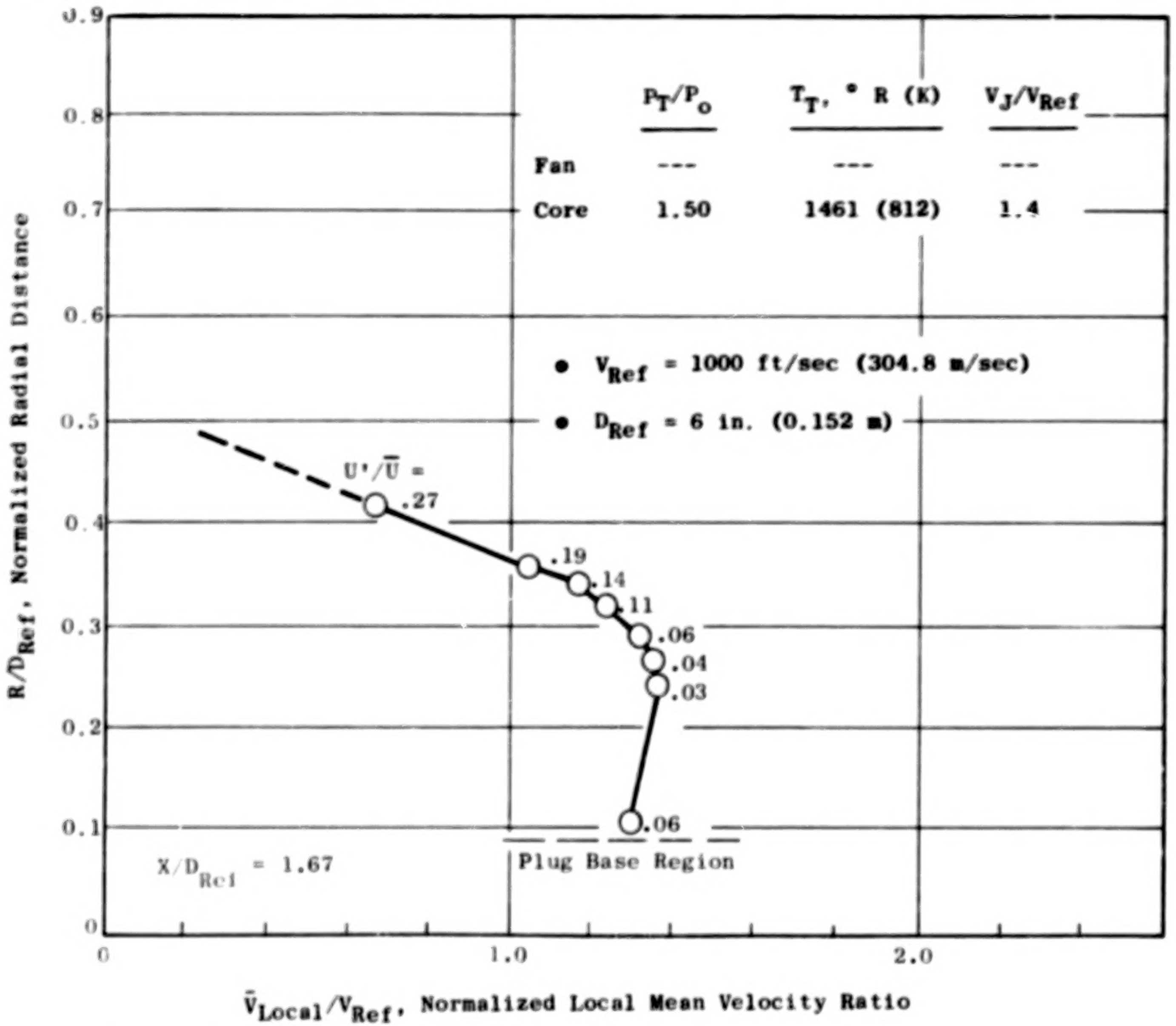

Figure 194. Laser Velocimeter Velocity Profile and Turbulence Measurement for the Unsuppressed Coannular Nozzle with Plug (Model 7) (Core Stream Flowing, Fan Stream Set for No Flow); X/D_{Ref} = 1.67.

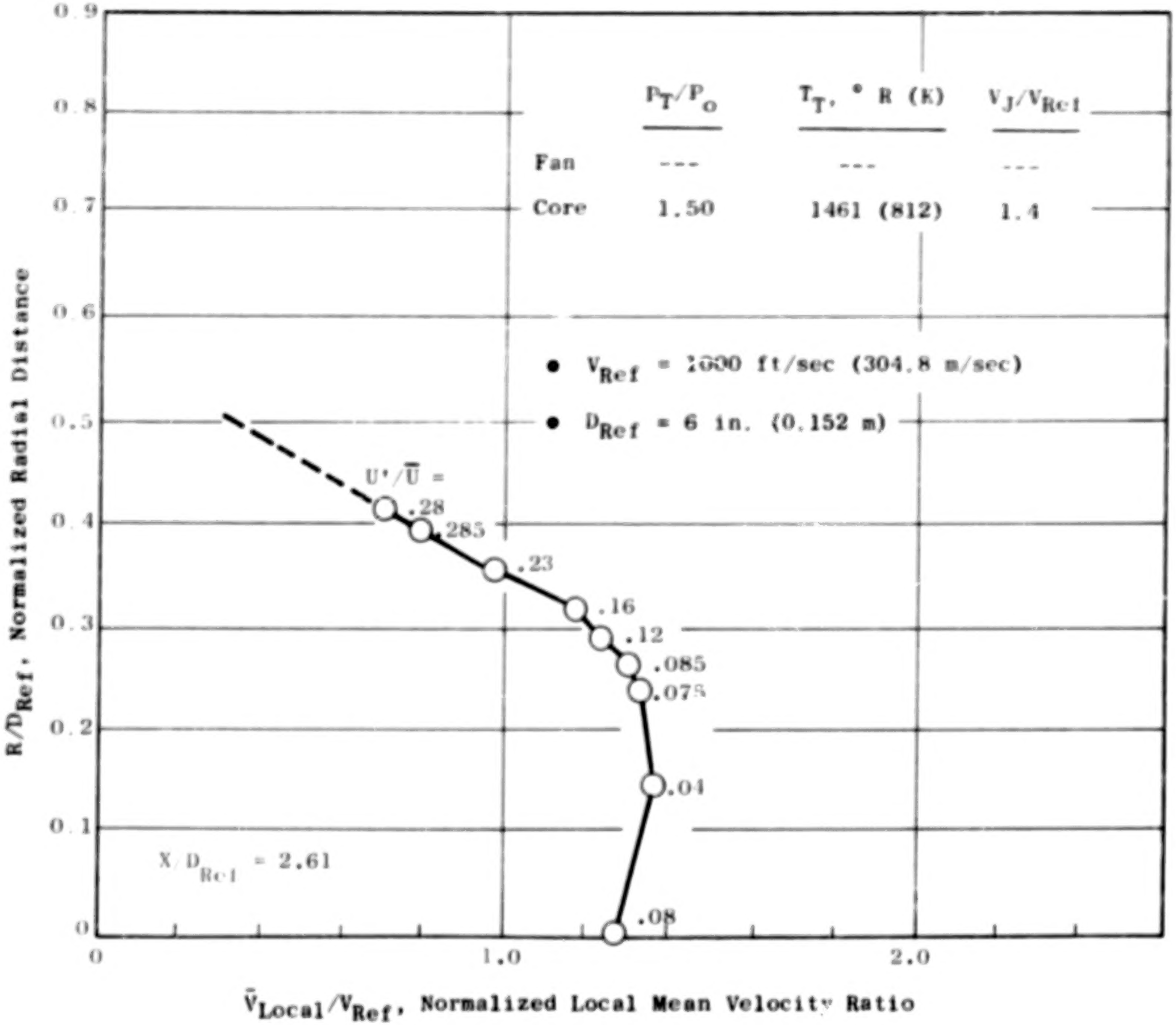

Figure 195. Laser Velocimeter Velocity Profile and Turbulence Measurement for the Unsuppressed Coannular Nozzle with Plug (Model 7) (Core Stream Flowing, Fan Stream Set for No Flow); X/D_{Ref} = 2.61.

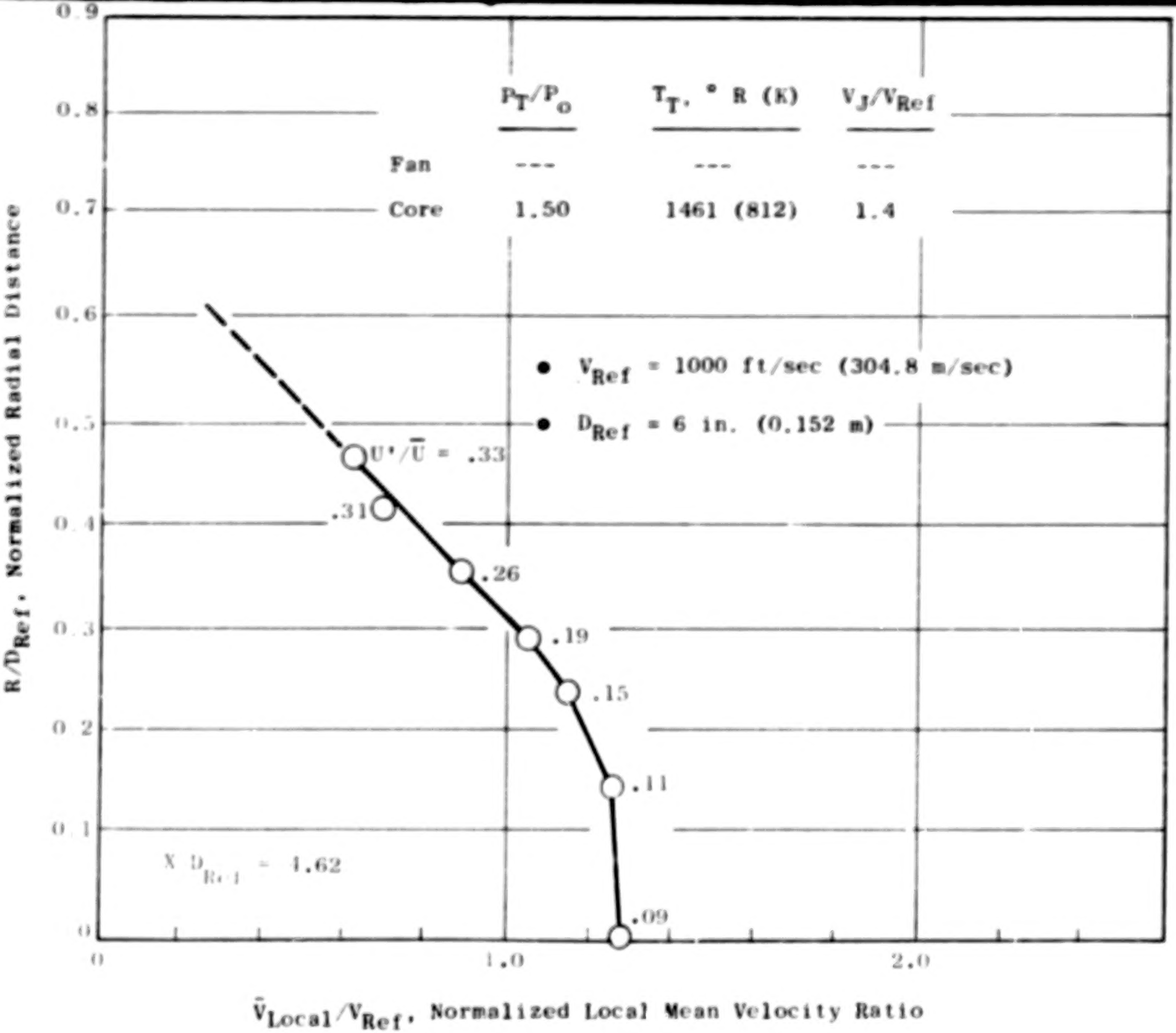

Figure 196. Laser Velocimeter Velocity Profile and Turbulence Measurement for the Unsuppressed Coannular Nozzle with Plug (Model 7) (Core Stream Flowing, Fan Stream Set for No Flow); X/D_{Ref} = 4.62.

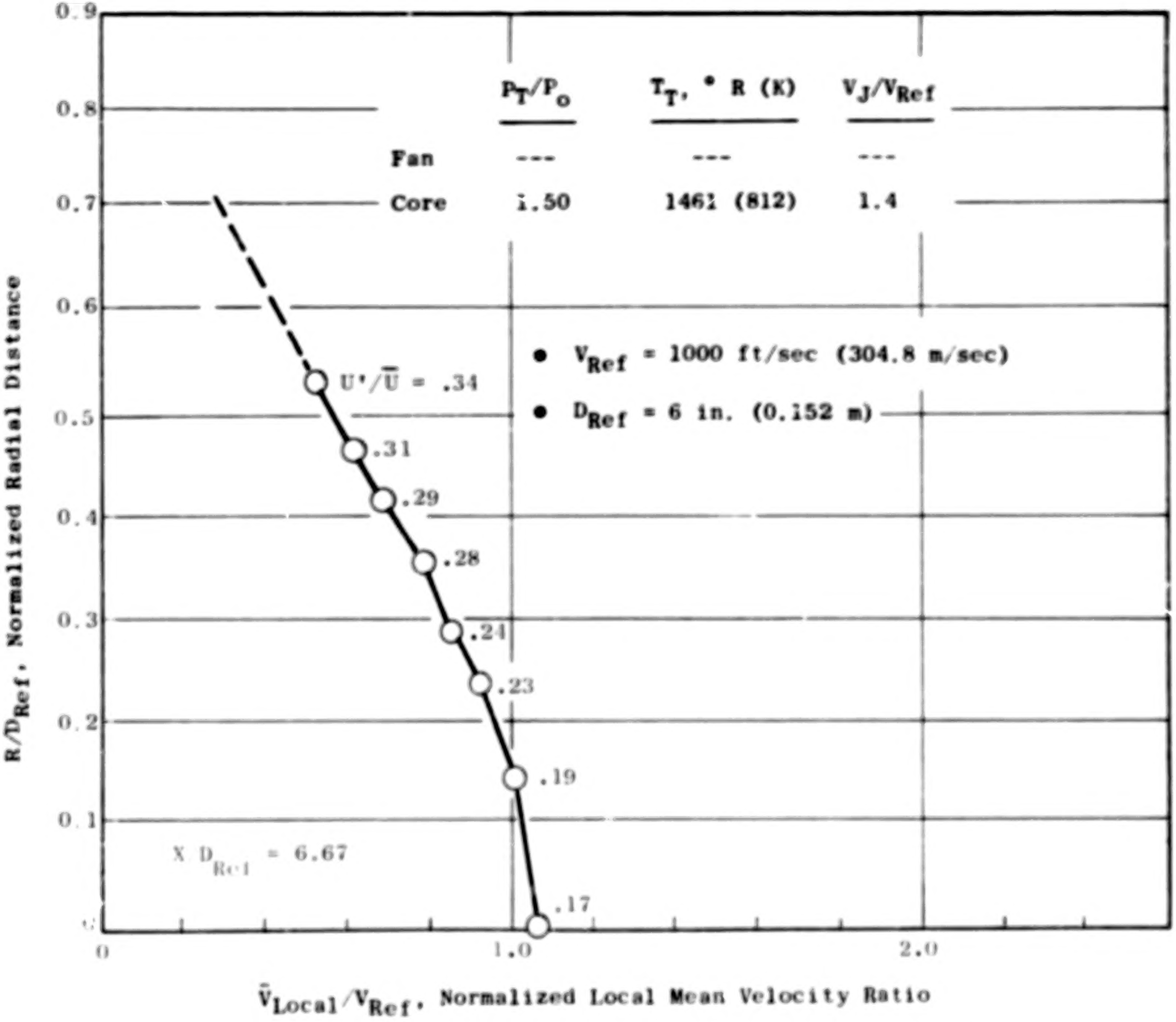

Figure 197. Laser Velocimeter Velocity Profile and Turbulence Measurement for the Unsuppressed Coannular Nozzle with Plug (Model 7) (Core Stream Flowing, Fan Stream Set for No Flow); $X/D_{Ref} = 6.67$.

APPENDIX I

MODEL 1 AXIAL-VELOCITY PROFILES

Laser velocimeter measurements of axial-velocity profiles for the multichute fan-suppressor nozzle (Model 1) are presented in Figures 198 through 204 for the two following sets of conditions:

	P_T/P_o	T_T, °R (K)	V_J, ft/sec (m/sec)	
Fan	1.64	775 (431)	1120	(341)
Core	1.50	1461 (812)	1400	(426)
Fan	3.90	1962 (1090)	2800	(853)
Core	1.50	1461 (812)	1400	(426)

TABLE OF CONTENTS

Section Page

1.0 SUMMARY 1 1/C1

2.0 INTRODUCTION 3 1/C3

3.0 TEST APPARATUS AND PROCEDURES 5 1/C5

3.1 FACILITIES 5 1/C5

3.1.1 General Electric Jet Engine Noise Outdoor Test Stand (JENOTS) Description 6 1/C6
3.1.1.1 Acoustic Arena 6 1/C6
3.1.1.2 Coannular-Flow System 6 1/C6
3.1.1.3 Coannular Frame Section 10 1/C12
3.1.1.4 Plenum Instrumentation Section 10 1/C12
3.1.1.5 Facility Acoustic Validation 12 1/C14
3.1.2 FluiDyne Aerodynamic-Performance Test Facility Description 12 1/C14

3.2 JENOTS INSTRUMENTATION SYSTEMS 16 1/D5

3.2.1 Acoustic Instrumentation Systems 16 1/D5
3.2.2 Laser Velocimeter System 18 1/D8
3.2.2.1 General Arrangement 18 1/D8
3.2.2.2 LV Actuator and Seeding 21 1/D13
3.2.2.3 Signal Processing and Recording 21 1/D13

3.3 DATA REDUCTION METHODS 21 1/D13

3.3.1 Acoustic Data Reduction 22 1/D14
3.3.1.1 JENOTS Data Reduction Systems 22 1/D14
3.3.1.2 Air-Attenuation Corrections 22 1/D14
3.3.1.3 Data-Scaling Procedure 30 1/E12
3.3.1.4 Data Corrections to a Free-Field Environment 30 1/E12
3.3.1.5 Power Level Calculation 30 1/E12
3.3.1.6 Acoustic Measurement Errors, Electronic Noise Floor 30 1/E12
3.3.2 Laser Velocimeter Data Reduction 33 1/F3
3.3.2.1 Basic Idea for LV rms Measurements 33 1/F3
3.3.2.2 The Histogram 36 1/F6
3.3.2.3 Mean Velocity 36 1/F6
3.3.2.4 Turbulent Velocity 37 1/F7
3.3.2.5 Statistical Errors for LV Mean and Turbulent Velocity Measurements 37 1/F7

TABLE OF CONTENTS (continued)

Section Page

3.3.3 Aerodynamic-Performance Test Data Reduction 37 1/F7
3.3.3.1 Flow Rates 39 1/F9
3.3.3.2 Discharge Coefficients 39 1/F9
3.3.3.3 Nozzle Throat 39 1/F9
3.3.3.4 Thrust Coefficient 40 1/F10
3.3.3.5 FluiDyne Force Balance Calibration 40 1/F10
3.3.3.6 Pressure and Temperature Data 41 1/F11
3.3.3.7 Data Quality 41 1/F11

4.0 MODEL DESCRIPTION AND DEFINITION OF TEST MATRICES 44 1/F14

4.1 MODEL DESIGN - SYSTEM EVOLUTION 44 1/F14
4.2 DESCRIPTION OF TEST MODELS 48 1/G6
4.3 ACOUSTIC TEST MATRIX 52 1/G12
4.4 LASER VELOCIMETER TEST MATRIX 56 2/A7
4.5 AERODYNAMIC-PERFORMANCE TEST MATRIX 61 2/B1
4.6 DATA SECTION 61 2/B1

5.0 DISCUSSION OF ACOUSTIC TEST RESULTS 63 2/B3

5.1 ESTABLISHMENT OF GROUND RULES FOR ACOUSTIC COMPARISONS AND DATA ILLUSTRATIONS 63 2/B3

5.1.1 Synthesized Baseline 63 2/B3
5.1.2 Average Conical Nozzle Noise Baseline 64 2/B4
5.1.3 Density Normalization and Presentation of Results 64 2/B4
5.1.3.1 Density Normalization Factors 64 2/B4
5.1.3.2 Presentation of Results 70 2/B13

5.2 UNSUPPRESSED COANNULAR NOZZLES 71 2/B14

5.2.1 High Core-Flow Test Results 71 2/B14
5.2.1.1 Overall Power Level Test Results 71 2/B14
5.2.1.2 Power Spectra Test Results 71 2/B14
5.2.1.3 Perceived Noise Level Test Results 71 2/B14
5.2.1.4 Perceived Noise Level Directivity Test Results 75 2/C6
5.2.1.5 Sound Pressure Level Spectra Test Results 75 2/C6
5.2.2 Low Core-Flow Test Results 75 2/C6
5.2.3 Acoustic Correlations 84 2/D5
5.2.4 Summary Remarks 84 2/D5

5.3 MULTIELEMENT FAN-SUPPRESSOR NOZZLES 88 2/D11

5.3.1 High Core Flow Test Results 88 2/D11
5.3.1.1 Overall Power Level Test Results 88 2/D11
5.3.1.2 Power Spectra Test Results 97 2/E11

TABLE OF CONTENTS (continued)

Section Page

5.3.1.3 Perceived Noise Level Test Results 97 2/E11
5.3.1.4 Sound Pressure Level Spectra Test Results 98 2/E12
5.3.2 Low Core-Flow Test Results 98 2/E12
5.3.3 Comparisons with Unsuppressed Coannular Nozzles 98 2/E12
5.3.4 Summary Remarks 104 2/F9

5.4 MULTIELEMENT FAN-SUPPRESSOR NOZZLES WITH EJECTORS 104 2/F9

5.4.1 Hardwall Ejector Effects 107 2/F12
5.4.1.1 Overall Power Level Test Results 107 2/F12
5.4.1.2 Power Spectra Test Results 107 2/F12
5.4.1.3 Perceived Noise Level Test Results 107 2/F12
5.4.1.4 Sound Pressure Level Test Results 111 2/G2
5.4.2 Treated Ejector Effects 111 2/G2
5.4.2.1 Overall Power Level Test Results 111 2/G2
5.4.2.2 Power Spectra Test Results 115 2/G6
5.4.2.3 Perceived Noise Level Test Results 115 2/G6
5.4.2.4 Sound Pressure Level Test Results 120 2/G11
5.4.3 Inlet Lip Geometry Effects on the Hardwall Ejector 120 2/G11
5.4.3.1 Power Level Test Results 120 2/G11
5.4.3.2 Perceived Noise Level Test Results 124 3/A8
5.4.3.3 Sound Pressure Level Test Results 124 3/A8
5.4.4 Summary Remarks 124 3/A8

5.5 EVALUATION OF A PARTIAL MECHANICAL SHIELD 130 3/B1

5.5.1 Perceived Noise Level Test Results 130 3/B1
5.5.2 Sound Pressure Level Spectra Results 134 3/B6
5.5.3 Summary Remarks 134 3/B6

6.0 DISCUSSION OF AERODYNAMIC-PERFORMANCE TEST RESULTS 140 3/C1

6.1 THRUST COEFFICIENTS 140 3/C1

6.1.1 Unsuppressed Coannular Nozzle with Plug 140 3/C1
6.1.2 Multichute Fan-Suppressor Nozzle 143 3/C5
6.1.3 Multichute Fan-Suppressor Nozzle with Hardwall Ejector with Sharp Lip 143 3/C5
6.1.4 Multitube Fan-Suppressor Nozzle 150 3/C12
6.1.5 Multitube Fan-Suppressor Nozzle with Hardwall Ejector with Sharp Lip 150 3/C12

6.2 EFFECT OF HOT EXHAUST FLOW ON THE THRUST COEFFICIENT OF THE MULTITUBE FAN-SUPPRESSOR NOZZLE WITH HARDWALL EJECTOR WITH SHARP LIP 156 3/D7

TABLE OF CONTENTS (continued)

Section Page

6.3 FLOW COEFFICIENTS 161 3/D14

6.3.1 Unsuppressed Coannular Nozzle with Plug 161 3/D14
6.3.2 Multichute Fan-Suppressor Nozzle 165 3/E6
6.3.3 Multichute Fan-Suppressor Nozzle with Hardwall Ejector with Sharp Lip 165 3/E6
6.3.4 Multitube Fan-Suppressor Nozzle 169 3/E10
6.3.5 Multitube Fan-Suppressor Nozzle with Hardwall Ejector with Sharp Lip 169 3/E10

7.0 DISCUSSION OF LASER VELOCIMETER TEST RESULTS 173 3/E14

7.1 LASER VELOCIMETER PLUME MEASUREMENTS FOR THE UNSUPPRESSED COANNULAR NOZZLE WITH PLUG 173 3/E14

7.1.1 Axial Mean-Velocity Distributions 173 3/E14
7.1.2 Mean-Velocity, Radial-Profile Distributions 176 3/F5
7.1.3 Axial Turbulent-Velocity, Radial-Profile Distributions 176 3/F5

7.2 LASER VELOCIMETER PLUME MEASUREMENTS FOR THE FAN-SUPPRESSED NOZZLES 176 3/F5

7.2.1 Axial Mean-Velocity Distributions 176 3/F5
7.2.2 Mean- and Turbulent-Velocity, Radial-Profile Distributions 180 3/F12
7.2.2.1 Multichute Fan Suppressor 180 3/F12
7.2.2.2 Multitube Fan Suppressor 180 3/F12

7.3 SUMMARY OF OBSERVATIONS 180 3/F12

8.0 DISCUSSION OF ACOUSTIC/AERODYNAMIC-PERFORMANCE CORRELATIONS 186 3/G8

8.1 EVALUATION OF NOISE CANDIDATES FOR DUCT-BURNING TURBOFAN ENGINES 186 3/G8
8.2 LOW CORE-FLOW COMPARISONS 191 4/A6

9.0 CONCLUSIONS AND RECOMMENDATIONS 196 4/A12

9.1 CONCLUSIONS 196 4/A12
9.2 RECOMMENDATIONS 197 4/A13

TABLE OF CONTENTS (concluded)

Section	Page	
APPENDIX A - GENERAL ELECTRIC AIR-ATTENUATION MODEL	199	4/B1
APPENDIX B - POWER LEVEL CALCULATION PROCEDURE	210	4/C1
APPENDIX C - DETAILED DESCRIPTION OF TEST MODELS	214	4/C5
APPENDIX D - ACOUSTIC TEST MATRIX FOR ALL DBTF MODELS AND EXAMPLE DATA PRINT OUT SHEETS	221	4/D3
APPENDIX E - FAN PLUG PRESSURE DISTRIBUTIONS FOR AERODYNAMIC MODEL 5	240	4/F13
APPENDIX F - MODEL 7 AXIAL-VELOCITY PROFILES	249	5/A8
APPENDIX G - MODEL 7 AXIAL-VELOCITY PROFILES WITH NO CORE FLOW	270	5/D7
APPENDIX H - MODEL 7 AXIAL-VELOCITY PROFILES WITH NO FAN FLOW	286	5/F10
APPENDIX I - MODEL 1 AXIAL-VELOCITY PROFILES	295	5/G13
APPENDIX J - MODEL 2 AXIAL-VELOCITY PROFILES	303	6/B6
APPENDIX K - NOMENCLATURE	313	6/C11
REFERENCES	317	6/D1

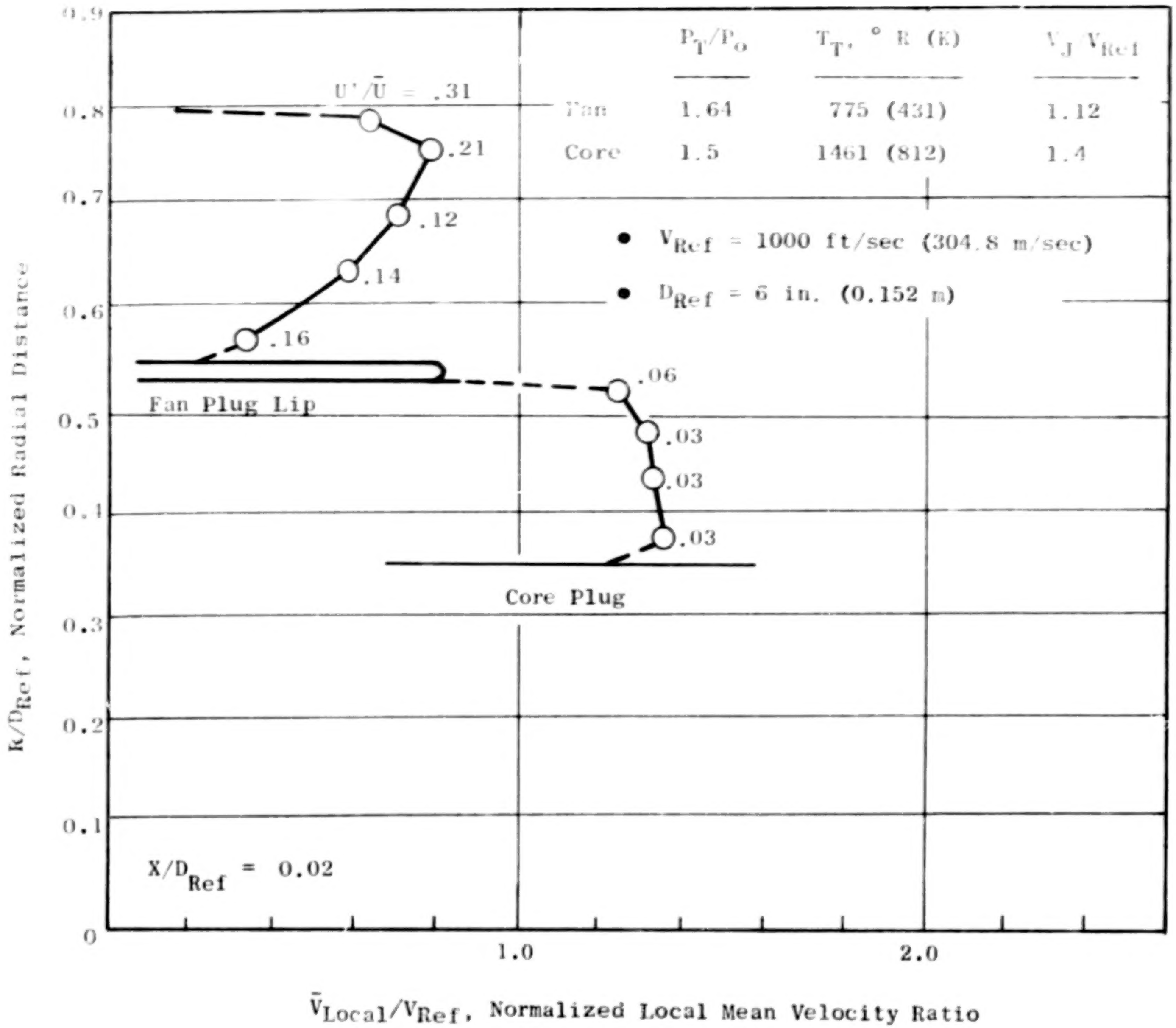

	P_T/P_o	T_T, ° R (K)	V_J/V_{Ref}
Fan	1.64	775 (431)	1.12
Core	1.5	1461 (812)	1.4

Figure 198. Laser Velocimeter Velocity Profile and Turbulence Measurements for the Multichute Fan Suppressor Nozzle (Model 1) at X/D_{Ref} = 0.02.

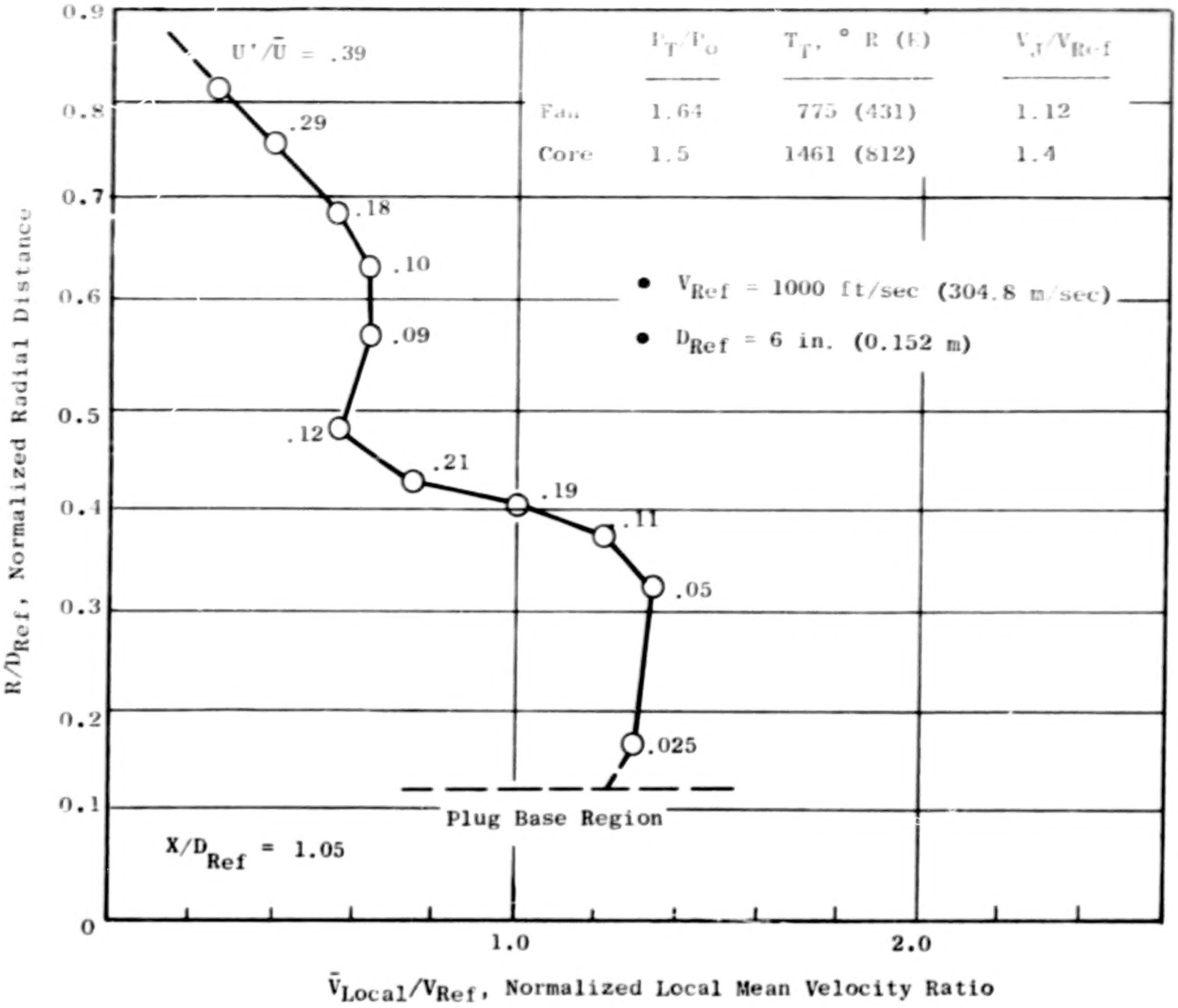

Figure 199. Laser Velocimeter Velocity Profile and Turbulence Measurements for the Multichute Fan Suppressor Nozzle (Model 1) at X/D_{Ref} = 1.05.

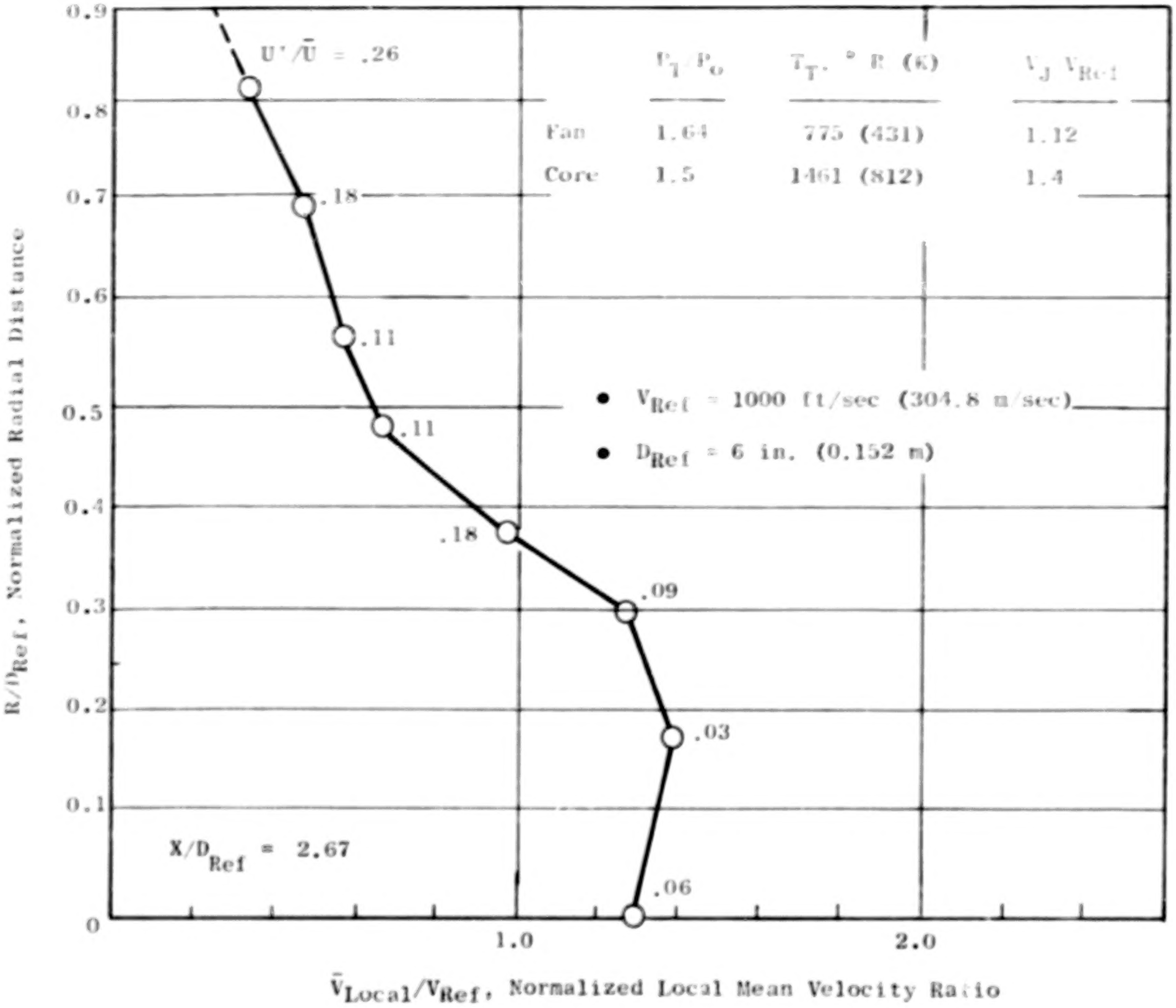

Figure 200. Laser Velocimeter Velocity Profile and Turbulence Measurements for the Multichute Fan Suppressor Nozzle (Model 1) at X/D_{Ref} = 2.67.

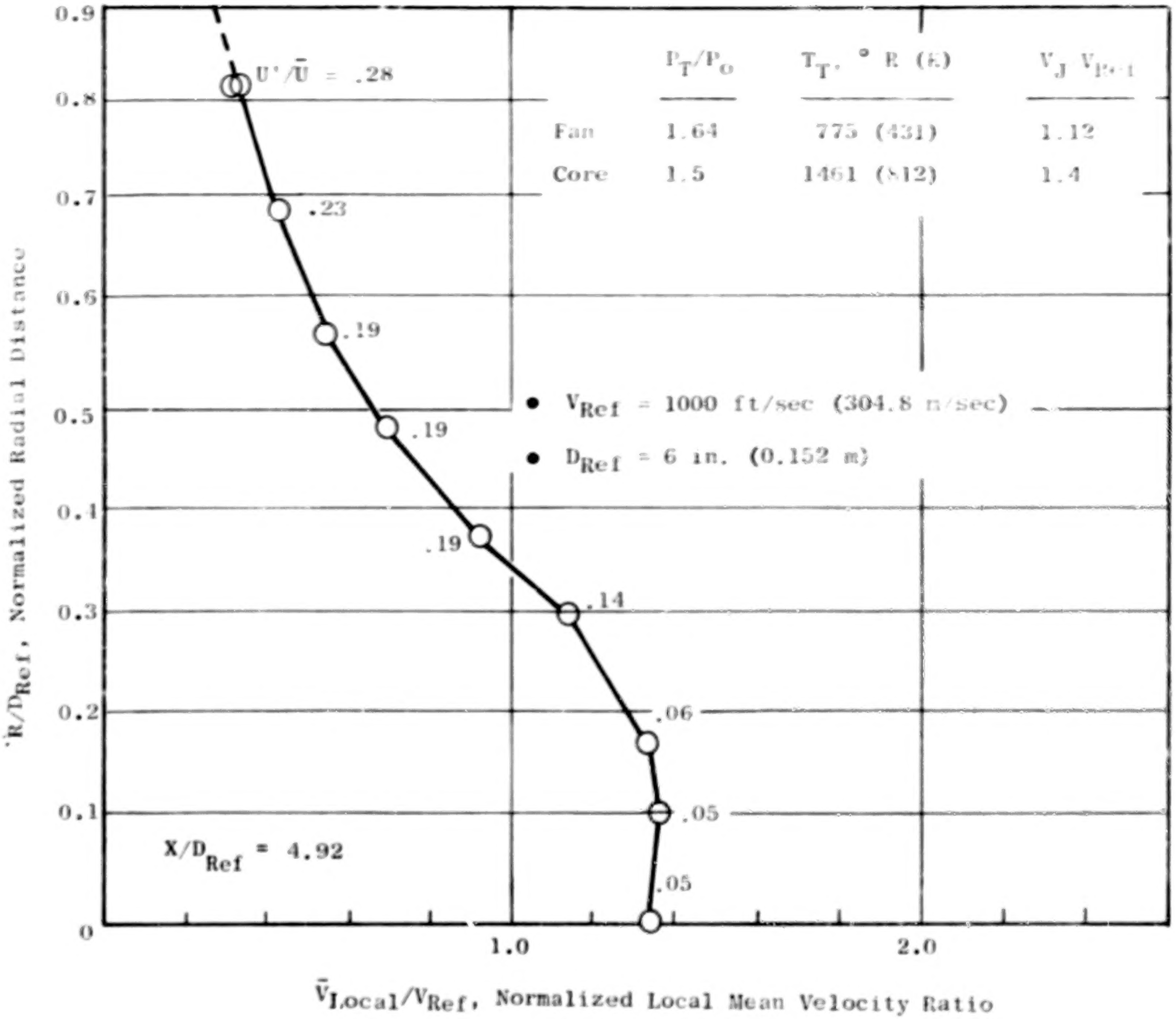

Figure 201. Laser Velocimeter Velocity Profile and Turbulence Measurements for the Multichute Fan Suppressor Nozzle (Model 1) at X/D_{Ref} = 4.92.

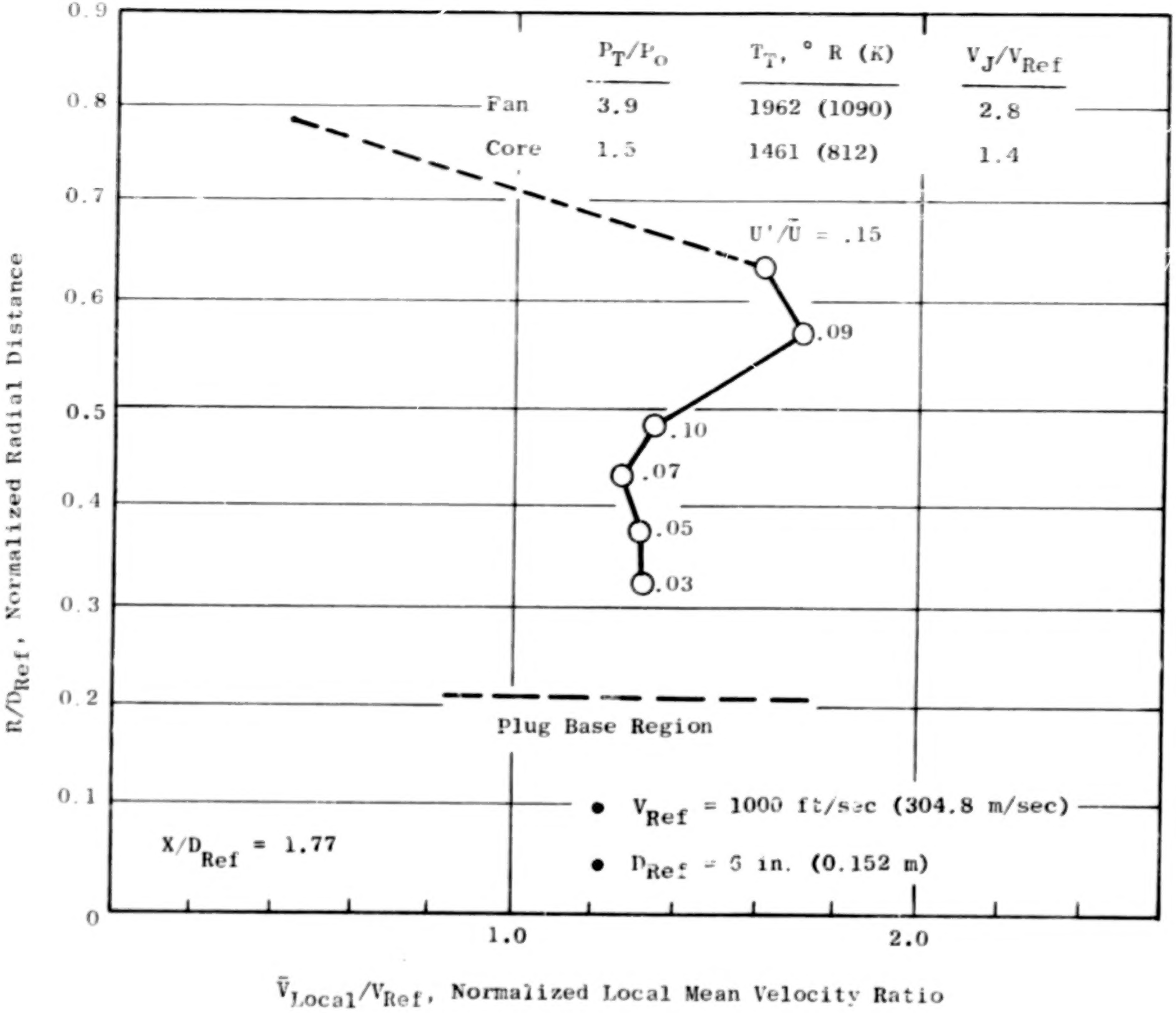

Figure 202. Laser Velocimeter Velocity Profile and Turbulence Measurements for the Multichute Fan Suppressor Nozzle (Model 1) at X/D_{Ref} = 1.77.

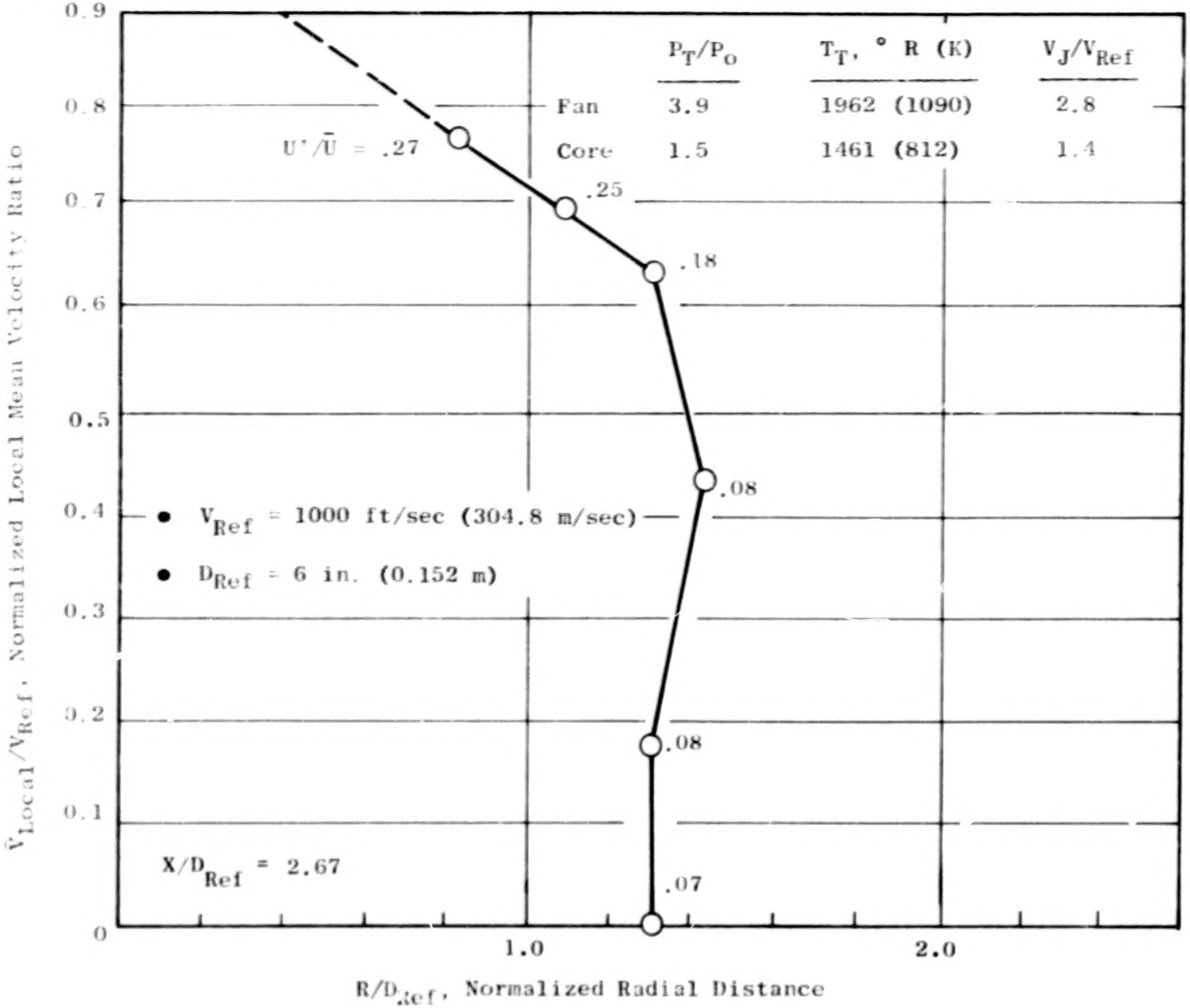

Figure 03, Laser Velocimeter Velocity Profile and Turbulence Measurements for the Multichute Fan Suppressor Nozzle (Model 1) at X/D_{Ref} = 2.67.

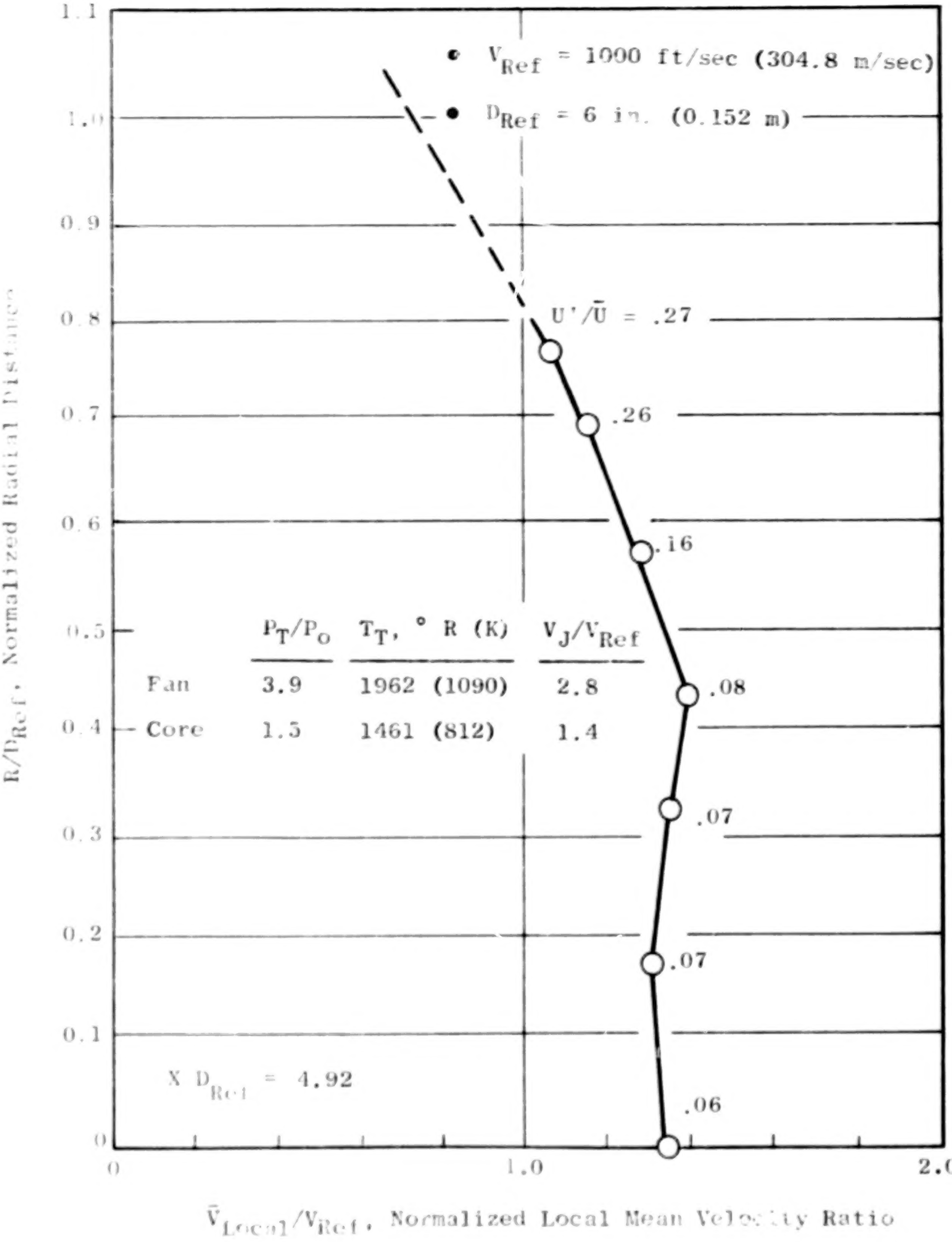

	P_T/P_o	T_T, ° R (K)	V_J/V_{Ref}
Fan	3.9	1962 (1090)	2.8
Core	1.5	1461 (812)	1.4

Figure 204. Laser Velocimeter Velocity Profile and Turbulence Measurements for the Multichute Fan Suppressor Nozzle (Model 1) at X/D_{Ref} = 4.92.

APPENDIX J

MODEL 2 AXIAL-VELOCITY PROFILES

Laser velocimeter measurements of axial-velocity profiles for the multi-tube fan-suppressor nozzle (Model 2) are presented in Figures 205 through 213 for the two following sets of conditions:

	P_T/P_o	T_T, °R (K)	V_J, ft/sec	(m/sec)
Fan	1.64	774 (431)	1120	(341)
Core	1.50	1461 (812)	1400	(426)
Fan	3.90	1962 (1090)	2800	(853)
Core	1.50	1461 (812)	1400	(426)

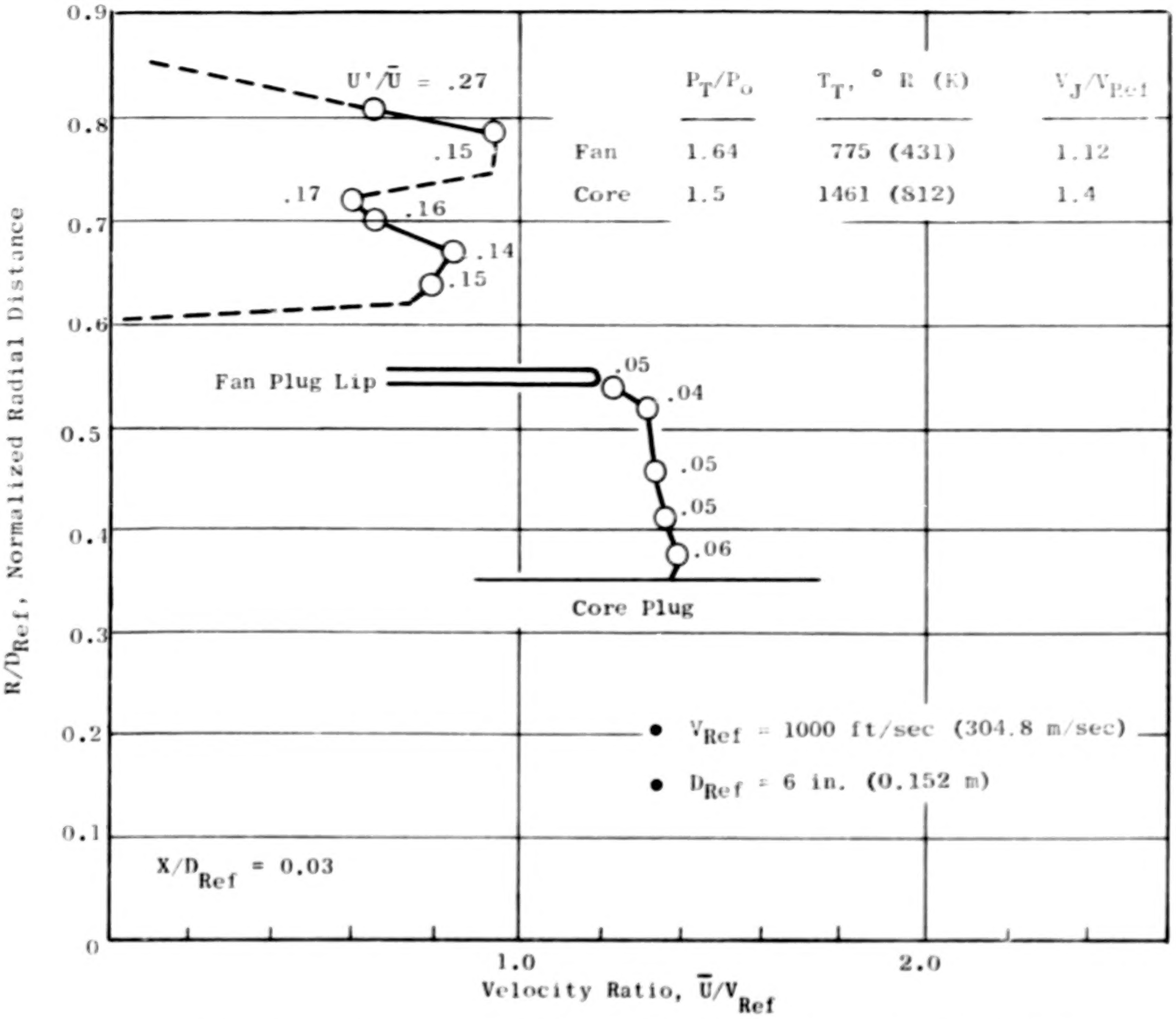

Figure 205. Laser Velocimeter Velocity Profile and Turbulence Measurements for the Multitube Fan Suppressor Nozzle (Model 2) at X/D_{Ref} = 0.03.

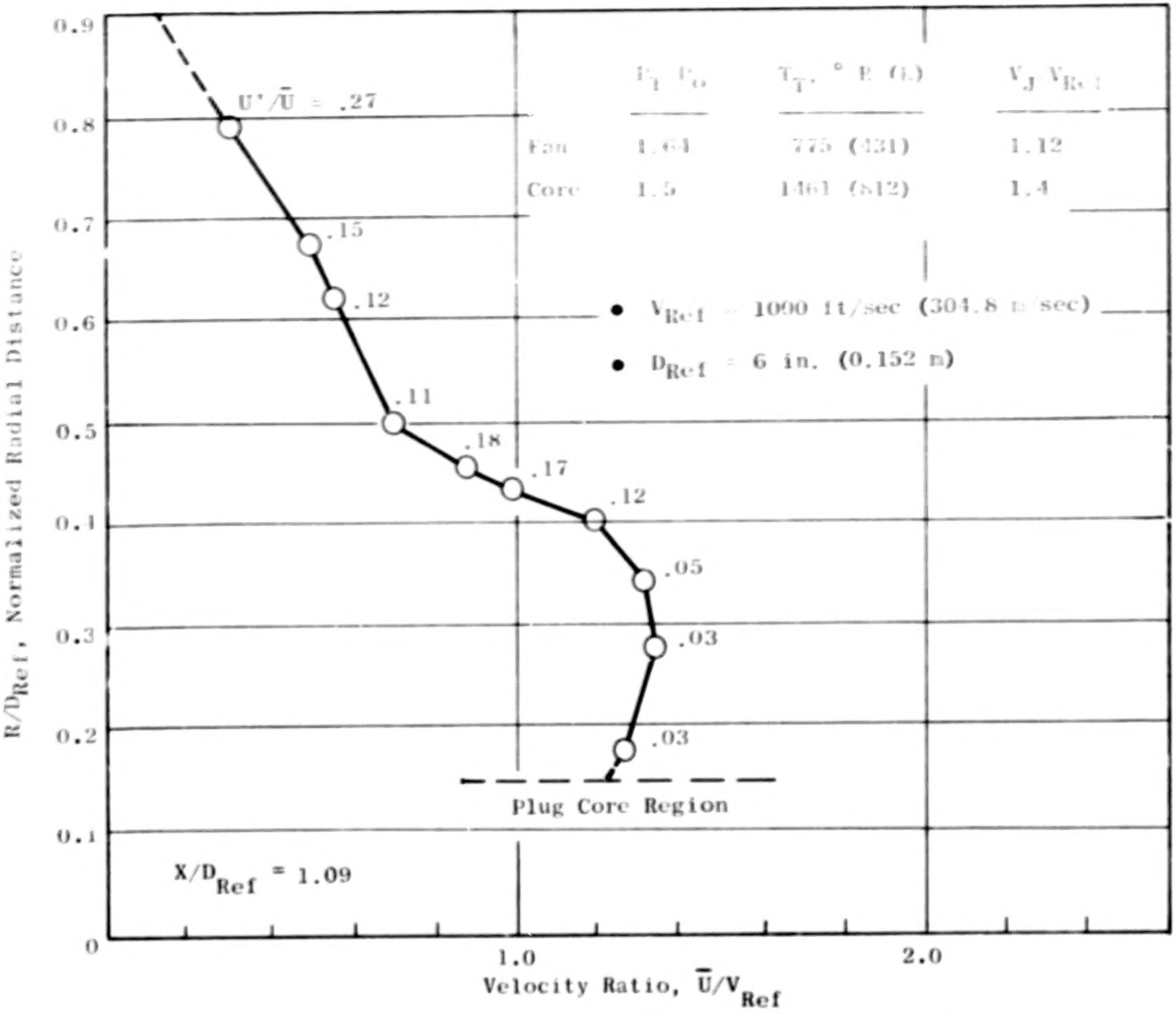

Figure 206. Laser Velocimeter Velocity Profile and Turbulence Measurements for the Multitube Fan Suppressor Nozzle (Model 2) at X/D_{Ref} = 1.09.

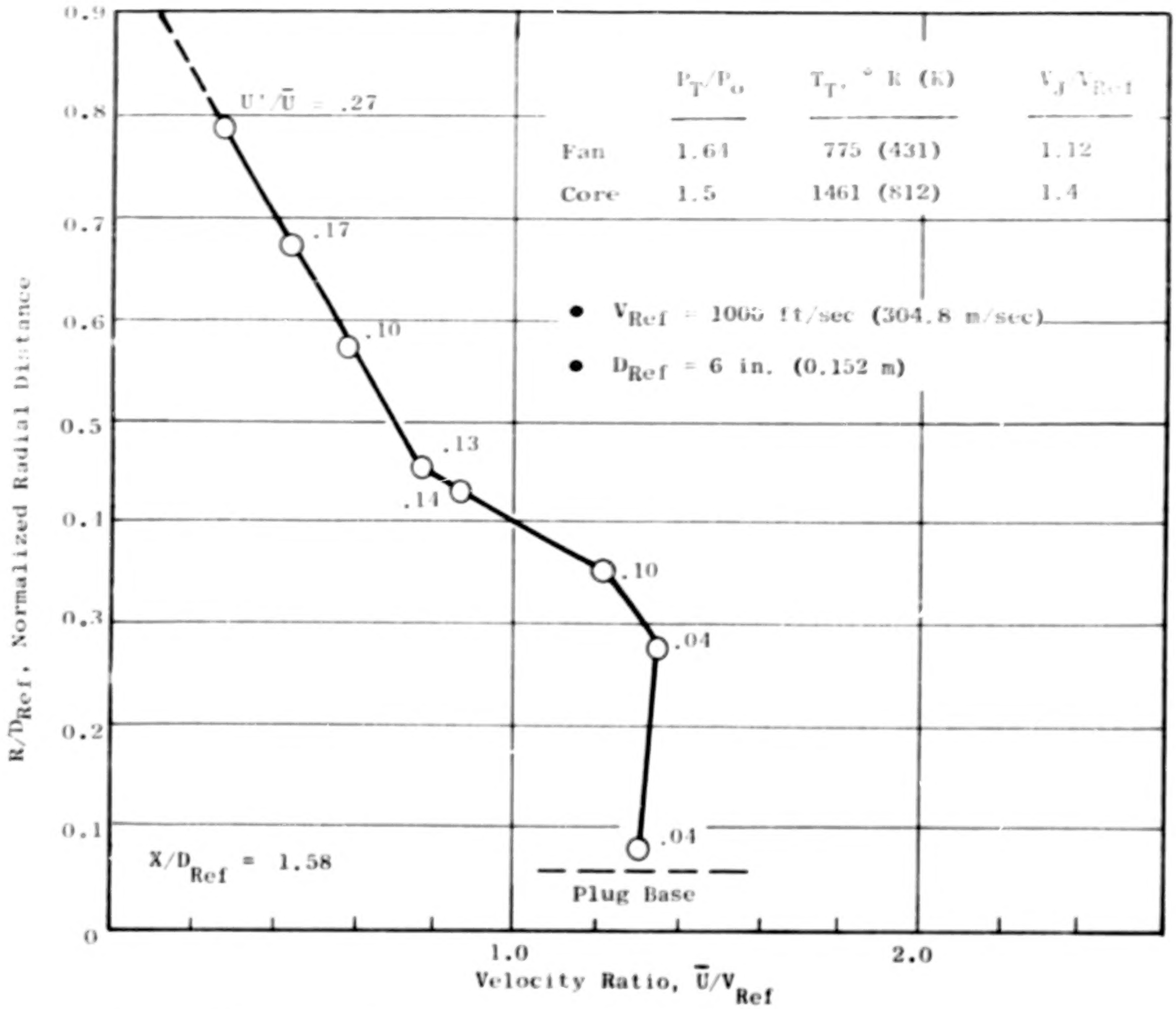

	P_T/P_o	T_T, °R (K)	V_J/V_{Ref}
Fan	1.64	775 (431)	1.12
Core	1.5	1461 (812)	1.4

- V_{Ref} = 1000 ft/sec (304.8 m/sec)
- D_{Ref} = 6 in. (0.152 m)

Figure 207. Laser Velocimeter Velocity Profile and Turbulence Measurements for the Multitube Fan Suppressor Nozzle (Model 2) at X/D_{Ref} = 1.58.

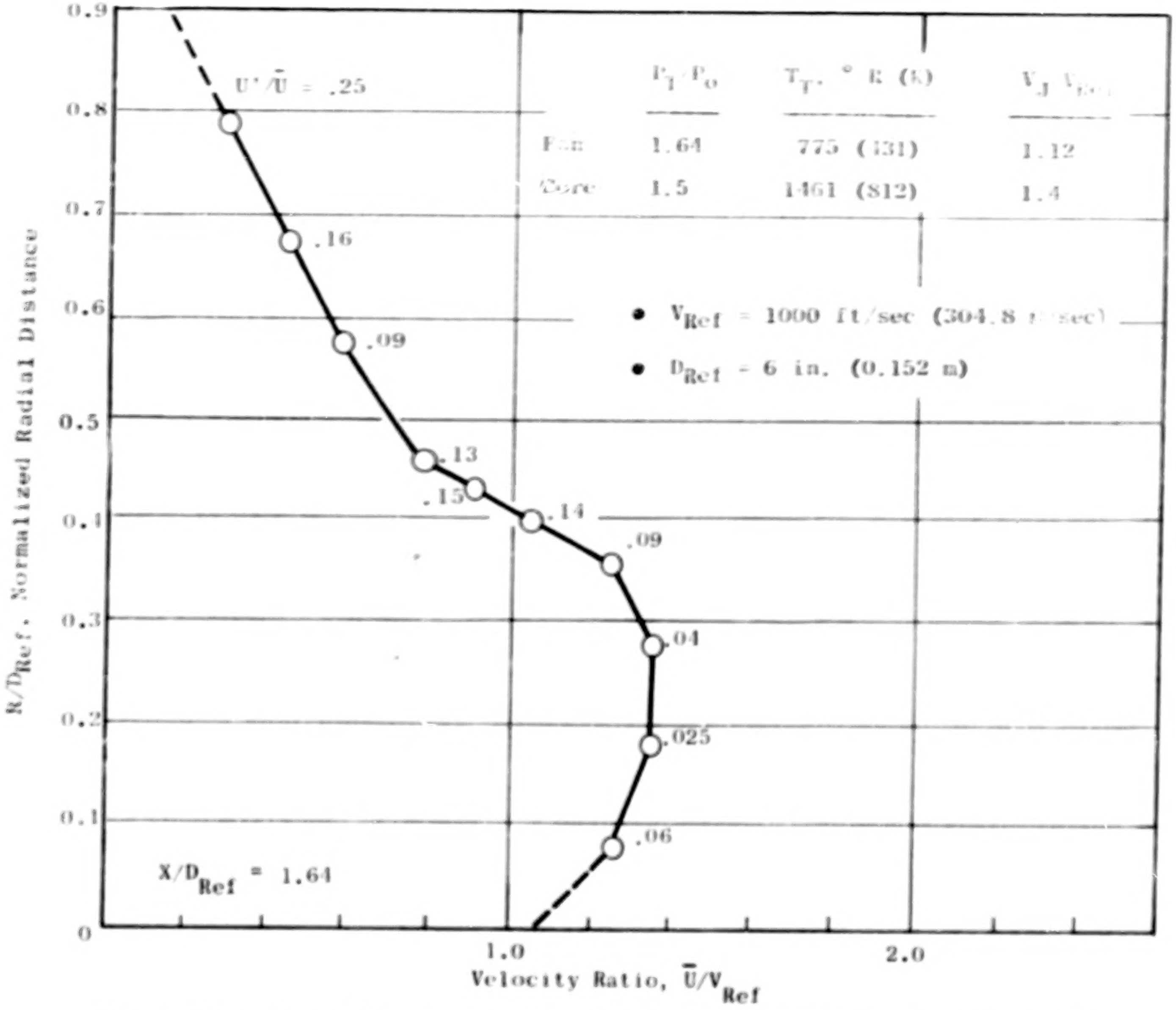

Figure 208. Laser Velocimeter Velocity Profile and Turbulence Measurements for the Multitube Fan Suppressor Nozzle (Model 2) at X/D_{Ref} = 1.64.

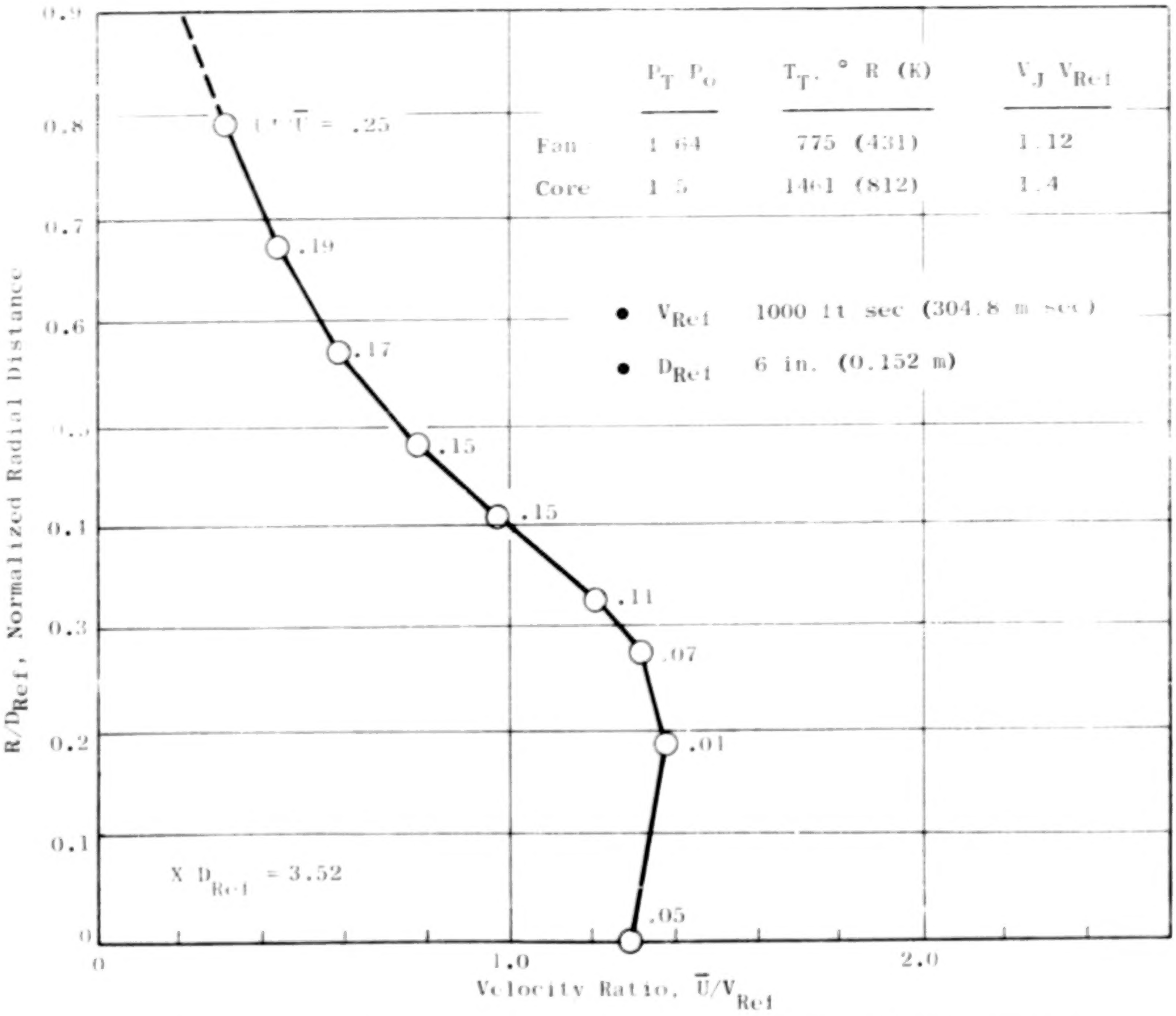

Figure 209. **Laser Velocimeter Velocity Profile and Turbulence Measurements for the Multitube Fan Suppressor Nozzle (Model 2) at X/D_{Ref} = 3.52.**

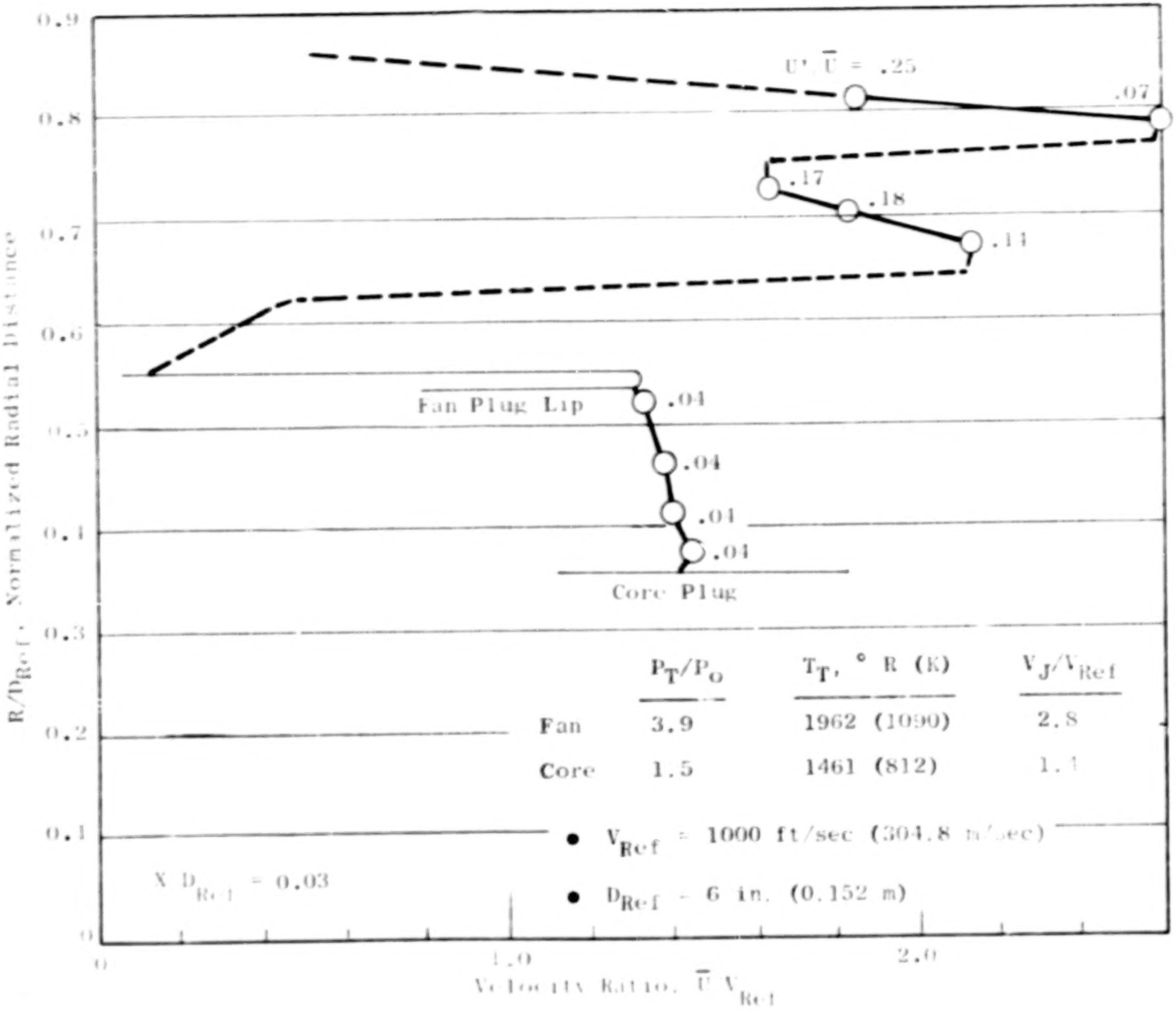

Figure 210. Laser Velocimeter Velocity Profile and Turbulence Measurements for the Multitube Fan Suppressor Nozzle (Model 2) at X/D_{Ref} = 0.03.

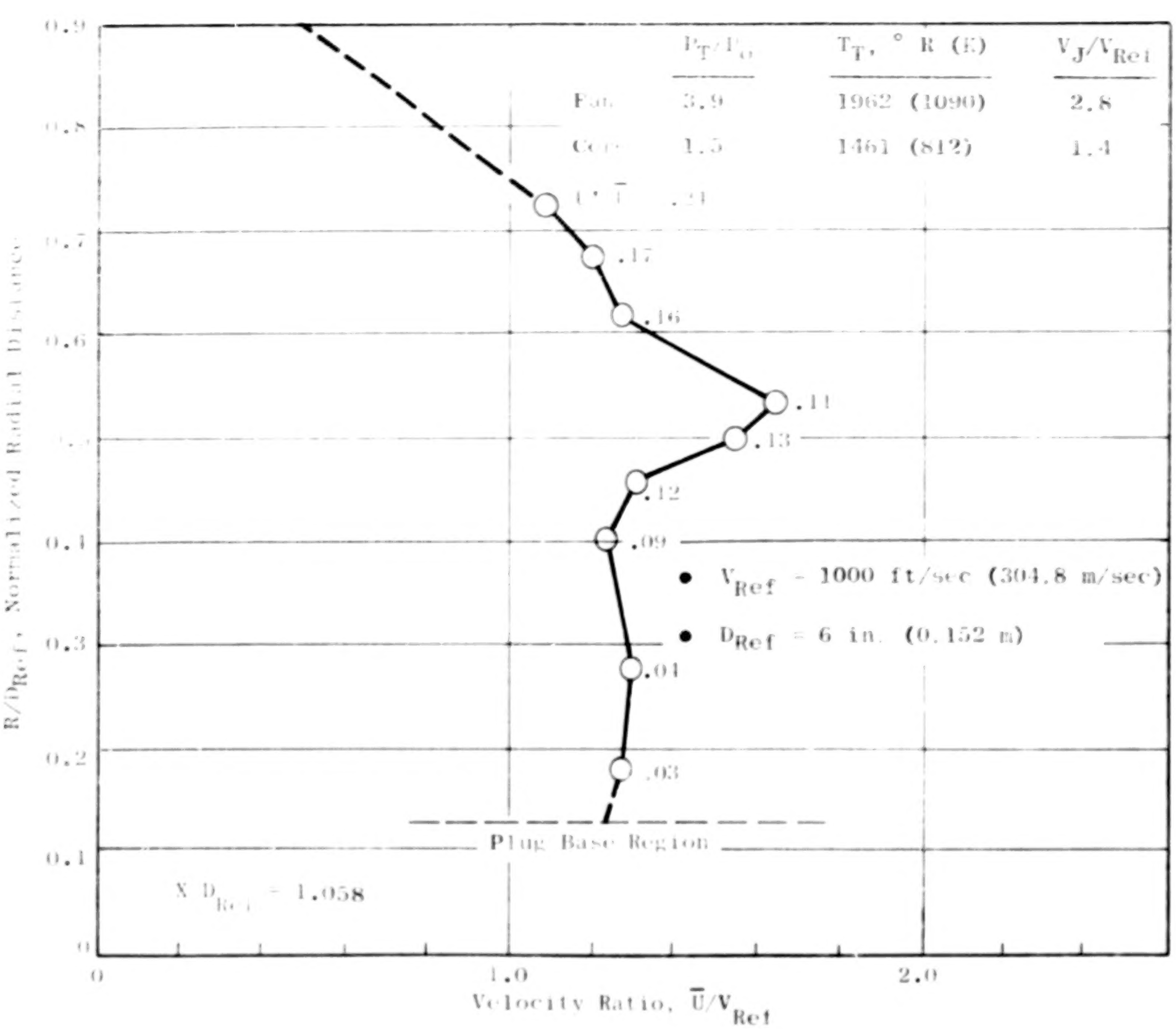

Figure 211. Laser Velocimeter Velocity Profile and Turbulence Measurements for the Multitube Fan Suppressor Nozzle (Model 2) at X/D_{Ref} = 1.058.

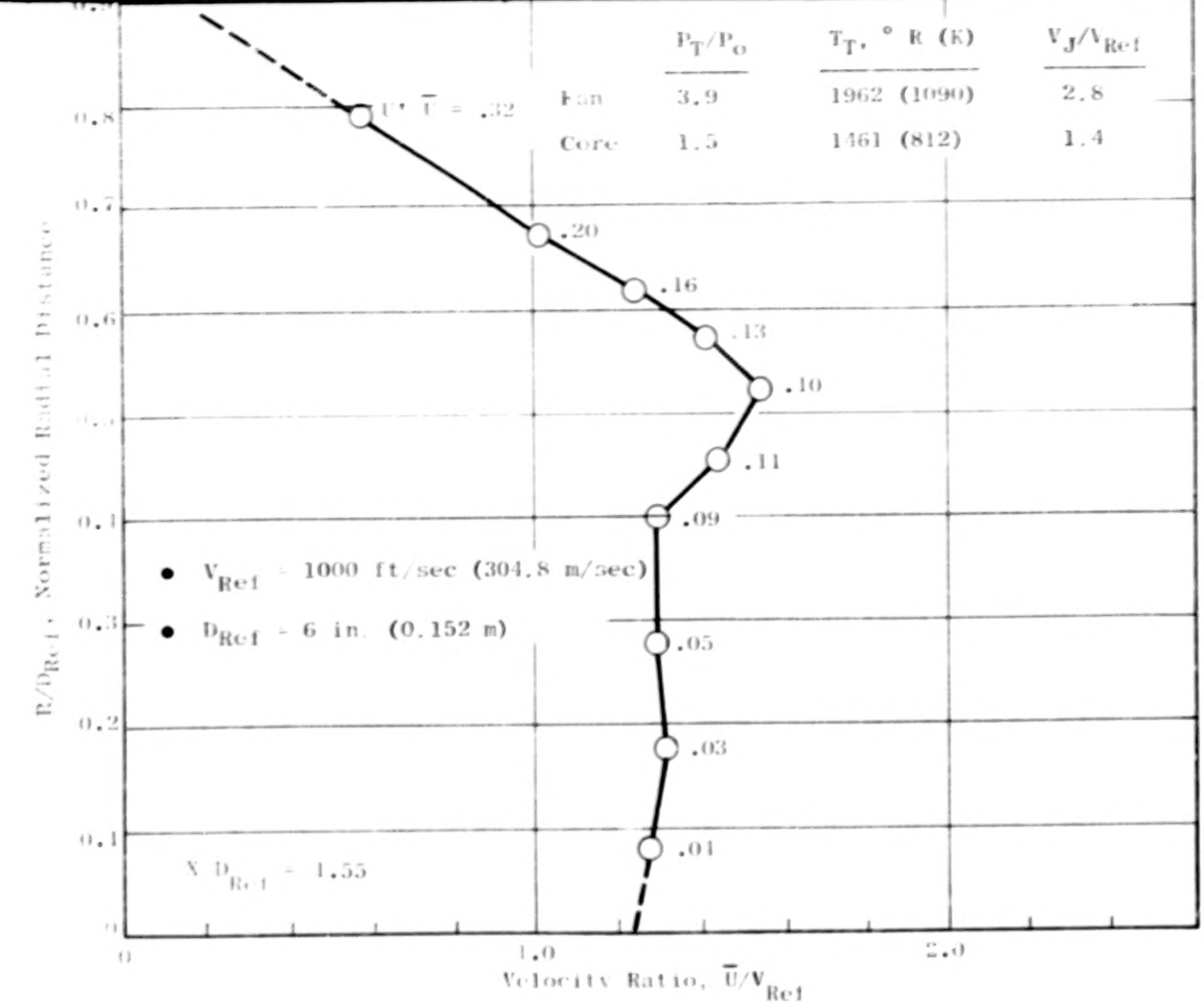

Figure 212. Laser Velocimeter Velocity Profile and Turbulence Measurements for the Multitube Fan Suppressor Nozzle (Model 2) at X/D_{Ref} = 1.55.

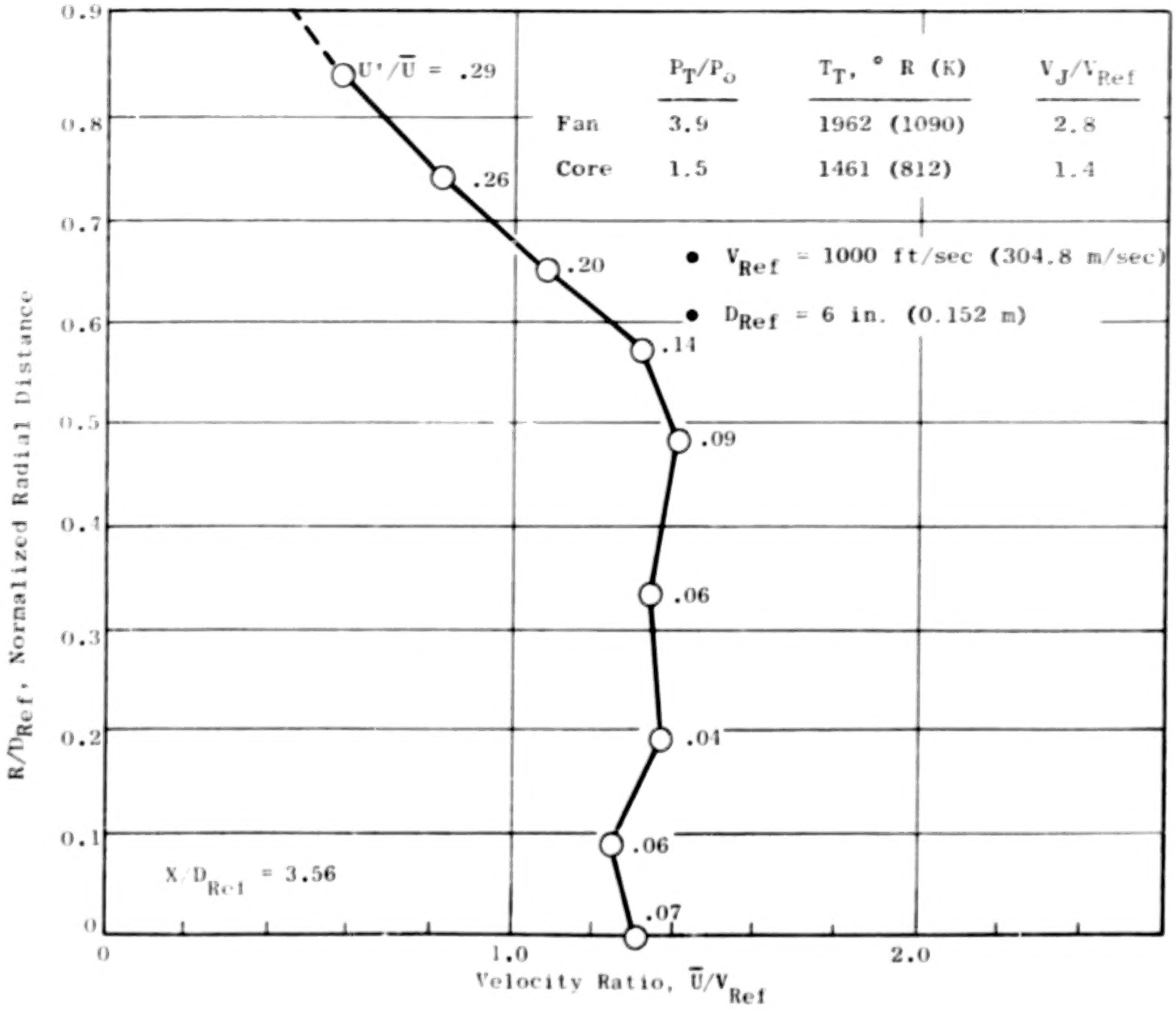

Figure 213. Laser Velocimeter Velocity Profile and Turbulence Measurements for the Multitube Fan Suppressor Nozzle (Model 2) at X/D_{Ref} = 3.56.

APPENDIX K

NOMENCLATURE

A	Cross-sectional area
AR	Area ratio (fan/core)
BPR	Bypass ratio (fan/core)
c	Acoustic velocity
C/D	Convergent/divergent
C_D	Discharge coefficient
CDR	Comprehensive data report
C_T	Thrust coefficient
C_x	Axial force balance readout, counts
D or d	Diameter
DI	Directivity index
EGA	Extra ground attenuation
EPNL	Effective perceived noise level
F	Stream thrust
f	Dimensionless stream thrust
g	Acceleration of gravity
G	Real-gas, stream-thrust correction factor
H	Nozzle thrust axial component
H_x	Axial balance force
I.D.	Inside diameter
K	Critical weight-flow parameter
k_i	Number of velocity samples in the i-th class interval

K_x	Axial force balance calibration factor
L	Applied calibration load
LV	Laser velocimeter
M	Mach number
m	Mass flow rate
N	Total number of velocity samples in the histogram
NOAPWL	Normalized overall power level
NPNL	Normalized perceived noise level
OAPWL	Overall power level
OASPL	Overall sound pressure level
O.D.	Outside diameter
P	Pressure
P_o or P_0	Ambient static pressure
P_R	Pressure ratio
PNL	Perceived noise level
PWL	Acoustic power level, dB re: 10^{-13} watt
Q	Balance force
R	Radius
r	Radial distance
rms	Root mean square
R_N	Reynolds number
S_N	Strouhal number
SPL	Sound pressure level, dB re: 2×10^{-5} N/m^2
T	Temperature
u'	Turbulence velocity (rms) as measured by a laser velocimeter

V	Velocity
V	Local mean velocity, axial, as measured by a laser velocimeter
V_J	Ideal jet velocity
$V(t)$	Measured time-dependent laser velocimeter velocity
V_i	Velocity increment for histograms
VR	Velocity ratio
$\dot{W}$	Nozzle weight flow
X	Axial distance
y	Distance from wall
α	Air attenuation
β	Bypass Ratio
γ	Ratio of specific heats
Δ	Incremental quantity
θ	Angle, relative to inlet axis
ρ	Density
ρ_{ISA}	Density at international standard atmospheric conditions
σ	Boundary layer thickness

Subscripts

c	Core stream flow
e	Exit
f	Fan stream flow
i	Ideal
J or j	Jet Parameter
mean	Mean value
Ref	Value at reference conditions, reference parameter

S	Static
T	Total
t	Throat
w	Wall
0 or o	Ambient
1	ASME meter throat (core flow)
2	Flexible seal (core flow)
4	ASME meter throat (fan flow)
5	Flexible seal (fan flow)
∞	Freestream

Superscripts

*	Sonic condition
ω	Jet density exponent

REFERENCES

1. R.G. Hoch, J.P. Duponchel, B.J. Cocking and W.D. Bryce, "Studies of the Influence of Density on Jet Noise," - Journal of Sound and Vibration, 28 (4), 649-668, 173.

2. Benzakein, M.J. and Knott, P.R., "Supersonic Jet Exhaust Noise" AFAPL-TR-82-52, August, 1972.

3. Knott, P.R. et.al., "Supersonic Jet Exhaust Noise Investigation," AFAPL-TR-76-68 July 1, 1976

4. Anon, "Standard Values of Atmospheric Absorption as a Function of Temperature and Humidity for Use in Evaluating Aircraft Flyover Noise," SAE ARP 866, 1964.

5. Ibid. Proposed Revision to SAE ARP 866, October 1973.

6. Harris, C.M., "Absorption of Sound in Air in the Audio-Frequency Range," JASA Volume 35, 1963.

7. Knesner, H.O., "Interpretation of the Anomalous Sound Absorption in Air and Oxygen in Terms of Molecular Collisions, "JASA Volume 5, 1933.

8. Fogg, R.G. "Internal Memorandum" General Electric Aircraft Engine Group, Cinn., Ohio, December 1973.

9. Evans, L.B., Bass, H.E. and Sutherland, L.C., "Atmospheric Absorption of Sound: Theoretical Predictions," 5 (Part 2) Journal of Acoustic Society of America, Volume 51, 1972.

10. Bass, H.E., Bauer, H.J. and Evans, L.B., "Atmospheric Absorption of Sound; Analytical Expression," Journal of Acoustic Society of America, Volume 52, 5 (Part 2), 1972.

11. SAE AIR 876 "Jet Noise Predictions," July, 1965.

12. SAE AIR 1327 "Acoustic Effects Produced by a Reflecting Plane," October, 1973.

13. [illegible], J.C. et.al., "High Velocity Jet Noise Source Location and Reduction - Task 1. Activation of Facilities and Validation of Source Location Techniques." Draft Report No. FAA-RD-76-79, 1 November, 1976.

14. Siegfried, W.C. and Kuchar, A.P., "A Standard for Exhaust Nozzle Tests." General Electric ESAD Technical Brief 71006. April 6, 1971.

15. "Advanced Supersonic Propulsion System Technology Study - Task 3 Final Report," NASA Contract NAS3-16950, May, 1973.

16. R. Lee and E.B. Smith, "Experimental Investigation of Noise Radiated by Concentric Jets," General Electric Report No. R57AFT381, April, 1957.

17. R. Benham, "Investigation of New Concepts for the Suppression of Jet Noise," Naval Air Propulsion Test Center Report No. AED-1897, February, 1969.

18. C.D. Simcox, et. al., "SST Technology Follow-On Program - Phase I, A Summary of the SST Jet Noise Suppression Test Program," Boeing Company Report No. FAA-SS-[illegible]-1, February 1972.

1. Report No.
NASA CR-2966

2. Government Accession No.

3. Recipient's Catalog No.

4. Title and Subtitle
ACOUSTIC TESTS OF DUCT-BURNING TURBOFAN JET NOISE SIMULATION

5. Report Date
July 1978

6. Performing Organization Code

7. Author(s)
P. R. Knott, E. J. Stringas, J. F. Brausch, P. S. Staid, P. H. Heck, and D. Latham

8. Performing Organization Report No.
R77AEG524

10. Work Unit No.

9. Performing Organization Name and Address
General Electric Company
Aircraft Engine Group
Cincinnati, Ohio 45215

11. Contract or Grant No.
NAS3-18008

13. Type of Report and Period Covered
Contractor Report

12. Sponsoring Agency Name and Address
National Aeronautics and Space Administration
Washington, D.C. 20546

14. Sponsoring Agency Code

15. Supplementary Notes
Final report. Project Manager, Orlando A. Gutierrez, V/STOL and Noise Division, NASA Lewis Research Center, Cleveland, Ohio 44135.

16. Abstract

This report summarizes the results of a static acoustic and aerodynamic performance, model-scale test program on coannular unsuppressed and multielement fan-suppressed nozzle configurations. The nozzle configurations are applicable to dual-stream exhaust systems where the high velocity and high temperature stream is on the outside. In all, eleven dual-stream nozzles were tested. The results of the static acoustic tests showed a very beneficial interaction effect. When the measured noise levels were compared with the predicted noise levels of two independent but equivalent conical nozzle flow streams, noise reductions for the unsuppressed coannular nozzles were of the order of 10 PNdB; high levels of suppression (8 PNdB) were still maintained even when only a small amount of core stream flow was used. The multielement fan-suppressed coannular nozzle tests showed 15 PNdB noise reductions and up to 18 PNdB noise reductions when a treated ejector was added. The static aerodynamic performance tests showed that the unsuppressed coannular plug nozzles obtained gross thrust coefficients of 0.972, with 1.2 to 1.7 percent lower levels for the multielement fan-suppressed coannular flow nozzles. For the first time anywhere, laser velocimeter velocity profile measurements were made on these types of nozzle configurations and with supersonic heated flow condition. Measurements showed that a very rapid decay in the mean velocity occurs for the nozzles tested. The rapid decay of velocity is associated with the high radius ratio designs of the fan streams and may be phenomenologically associated with a reduction in the turbulent mixing noise and in part with the overall observed jet noise reduction. All the detailed acoustic data obtained under this program are presented in the companion comprehensive data report, NASA CR-135236.

17. Key Words (Suggested by Author(s))
Supersonic jet noise; Noise suppression; Duct-burning turbofan; Variable-cycle engine; Acoustic tests; Aerodynamic performance tests; Ejectors, hardwall; Ejectors, treated; Laser velocimeter; Multielement fan suppressors

18. Distribution Statement
Unclassified - unlimited
STAR Category 01

19. Security Classif. (of this report)	20. Security Classif. (of this page)	21. No. of Pages	22. Price*
Unclassified	Unclassified	345	A15

NASA-Langley, 1978

90

50

END

DEC 11 1978